TISSUE ENGINEERING AND CELL THERAPY FOR CARTILAGE RESTORATION

EDITED BY: Tiago Lazzaretti Fernandes, Daniela Franco Bueno, Kazunori Shimomura, Zhenxing Shao and Andreas H. Gomoll

PUBLISHED IN: Frontiers in Cell and Developmental Biology

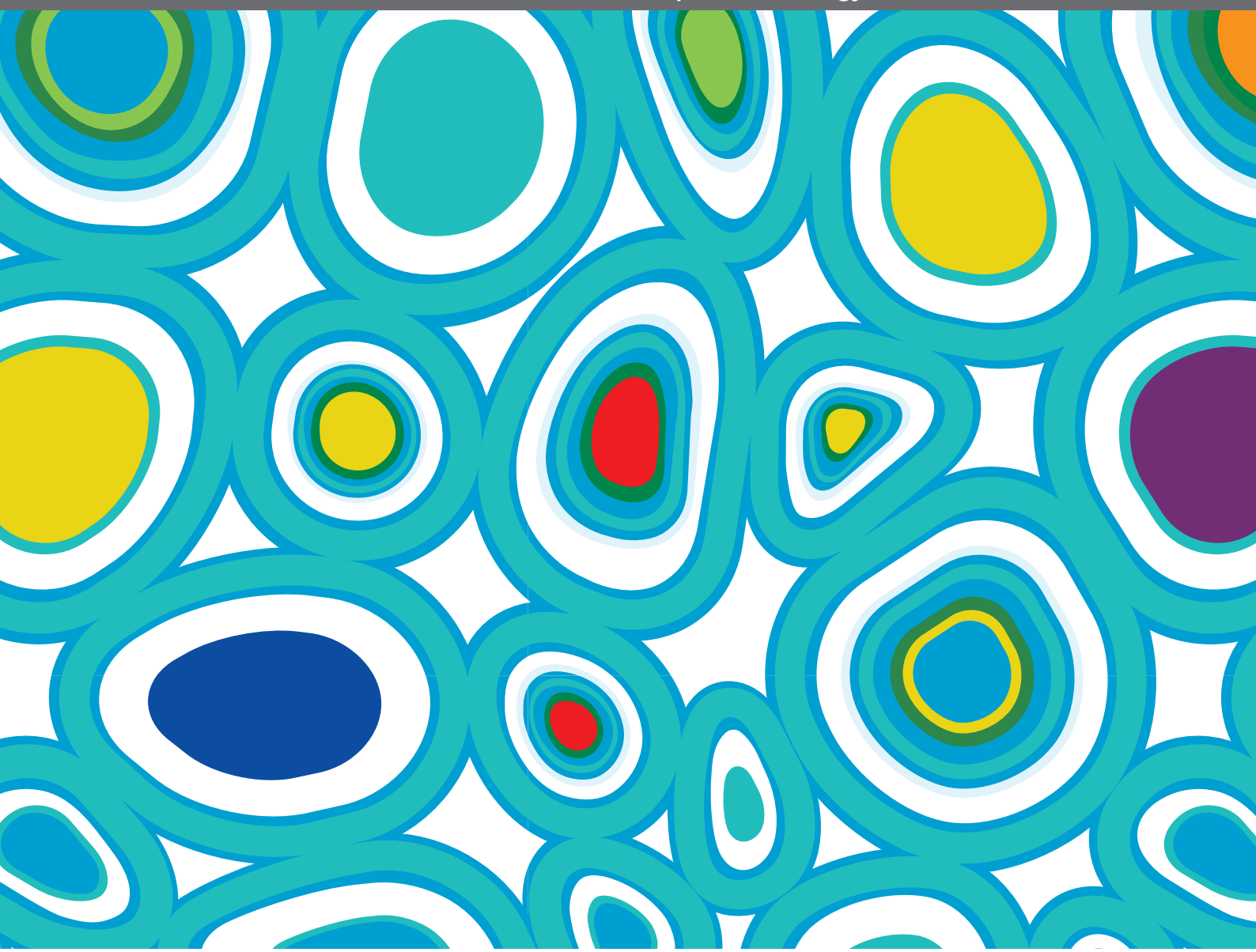

frontiers Research Topics

ISSN 1664-8714
ISBN 978-2-83250-145-0
DOI 10.3389/978-2-83250-145-0

About Frontiers

Frontiers is more than just an open-access publisher of scholarly articles: it is a pioneering approach to the world of academia, radically improving the way scholarly research is managed. The grand vision of Frontiers is a world where all people have an equal opportunity to seek, share and generate knowledge. Frontiers provides immediate and permanent online open access to all its publications, but this alone is not enough to realize our grand goals.

Frontiers Journal Series

The Frontiers Journal Series is a multi-tier and interdisciplinary set of open-access, online journals, promising a paradigm shift from the current review, selection and dissemination processes in academic publishing. All Frontiers journals are driven by researchers for researchers; therefore, they constitute a service to the scholarly community. At the same time, the Frontiers Journal Series operates on a revolutionary invention, the tiered publishing system, initially addressing specific communities of scholars, and gradually climbing up to broader public understanding, thus serving the interests of the lay society, too.

Dedication to Quality

Each Frontiers article is a landmark of the highest quality, thanks to genuinely collaborative interactions between authors and review editors, who include some of the world's best academicians. Research must be certified by peers before entering a stream of knowledge that may eventually reach the public - and shape society; therefore, Frontiers only applies the most rigorous and unbiased reviews.
Frontiers revolutionizes research publishing by freely delivering the most outstanding research, evaluated with no bias from both the academic and social point of view. By applying the most advanced information technologies, Frontiers is catapulting scholarly publishing into a new generation.

What are Frontiers Research Topics?

Frontiers Research Topics are very popular trademarks of the Frontiers Journals Series: they are collections of at least ten articles, all centered on a particular subject. With their unique mix of varied contributions from Original Research to Review Articles, Frontiers Research Topics unify the most influential researchers, the latest key findings and historical advances in a hot research area! Find out more on how to host your own Frontiers Research Topic or contribute to one as an author by contacting the Frontiers Editorial Office: frontiersin.org/about/contact

TISSUE ENGINEERING AND CELL THERAPY FOR CARTILAGE RESTORATION

Topic Editors:
Tiago Lazzaretti Fernandes, University of São Paulo, Brazil
Daniela Franco Bueno, Hospital Sirio Libanes, Brazil
Kazunori Shimomura, Osaka University, Japan
Zhenxing Shao, Peking University Third Hospital, China
Andreas H. Gomoll, Hospital for Special Surgery, United States

Citation: Fernandes, T. L., Bueno, D. F., Shimomura, K., Shao, Z., Gomoll, A. H., eds. (2022). Tissue Engineering and Cell Therapy for Cartilage Restoration. Lausanne: Frontiers Media SA. doi: 10.3389/978-2-83250-145-0

Table of Contents

frontiers | Frontiers in Cell and Developmental Biology

EDITORIAL
published: 01 July 2022
doi: 10.3389/fcell.2022.947588

Editorial: Tissue Engineering and Cell Therapy for Cartilage Restoration

Tiago Lazzaretti Fernandes[1,2]*, *Daniela Franco Bueno*[2], *Kazunori Shimomura*[3], *Zhenxing Shao*[4] and *Andreas H. Gomoll*[5]

[1]Sports Medicine Division, Institute of Orthopedics and Traumatology, Hospital das Clínicas, Faculdade de Medicina, Universidade de São Paulo, São Paulo, Brazil, [2]Hospital Sírio-Libanês, São Paulo, Brazil, [3]Department of Orthopaedic Surgery, Osaka University Graduate School of Medicine, Suita, Japan, [4]Institute of Sports Medicine, Peking University Third Hospital, Beijing, China, [5]Department of Orthopaedic Surgery, Hospital for Special Surgery, New York, NY, United States

Keywords: tissue engineering, cell therapy, cartilage restoration, innovation, stem cells, cartilage, osteoarthritis

Editorial on the Research Topic

Tissue Engineering and Cell Therapy for Cartilage Restoration

Articular cartilage is a connective tissue consisting of two phases: a solid composed of collagen, proteoglycans, proteins, and chondrocytes, and a liquid made up of water and electrolytes. It can be divided into four zones (superficial, middle, deep and calcified), each presenting a different cellular organization, collagen fiber architecture and depth (Hernandez et al., 2000; Meyers and Chawla, 2008; Sophia Fox et al., 2009). These structures and components establish the properties of cartilage, in terms of stiffness, elasticity and other important aspects for its characterization.

It is known that articular cartilage is an avascular tissue with little cellularity, making it difficult to heal. As a consequence, cartilage injuries can generate several complications for the individual, such as loss of mobility, degeneration and osteoarthritis (OA), directly affecting the quality of life. Not to mention that it represents an economic burden (Fernandes et al., 2018; Fernandes et al., 2020).

Current procedures that seek to repair chondral tissue are microfracture stimulation, autograft and osteochondral allograft, and cellular implant therapies based on tissue engineering principles. Cell therapies and regenerative techniques are important and there are two main examples: autologous chondrocyte implantation (ACI) and mesenchymal stromal cells (MSCs). MSCs have received considerable research attention, due to ease of collection, ability to proliferate and differentiate cells, non-rejection by the patient, and paracrine effect on local cellular machinery (Ando et al., 2007; Shimomura et al., 2015).

This Research Topic aimed to widening the knowledge on the strategies being used for articular cartilage regeneration, describing the state-of-the-art and exploring the innovative approaches in cartilage restoration field. This issue currently includes 14 articles related to different innovative propositions associated with cartilage injuries.

In **Table 1**, a summary and the innovative aspects of each article are presented.

Stem-cell-based and gene-enhanced tissue engineered cartilage is promising in the treatment of cartilaginous pathologies, especially traumatic cartilage defects (Bishop et al., 2017; Pirraco et al., 2018; Wang et al., 2019). Bone morphogenetic protein 2 (BMP2) triggers hypertrophic differentiation after chondrogenic differentiation of MSCs, which blocked the further application of BMP2-mediated cartilage tissue engineering. Dai et al. investigated the function of LncRNA H19 (H19) in BMP2, finding out that H19 regulates BMP2-mediated hypertrophic differentiation of MSCs by promoting the phosphorylation of Runx2, that maturates chondrocytes. H19 may play a role in cartilage differentiation, cartilage phenotype maintaining, and cartilage hypertrophic differentiation. They evaluated nine types of porcine tissue through a simple standard decellularization protocol.

At present, tissue engineering and regenerative medicine have focused on extracellular matrices (ECMs) to function as a natural scaffold (Harrison et al., 2014). Hanai et al. found that a soluble

OPEN ACCESS

Edited and reviewed by:
Atsushi Asakura,
University of Minnesota Twin Cities, United States

***Correspondence:**
Tiago Lazzaretti Fernandes
tiagot86@hotmail.com

Received: *18 May 2022*
Accepted: *06 June 2022*
Published: *01 July 2022*

Citation:
Fernandes TL, Bueno DF, Shimomura K, Shao Z and Gomoll AH (2022) Editorial: Tissue Engineering and Cell Therapy for Cartilage Restoration. Front. Cell Dev. Biol. 10:947588. doi: 10.3389/fcell.2022.947588

TABLE 1 | Innovative contribution of the articles published in Research Topic Tissue Engineering and Cell Therapy for Cartilage Restoration.

Authors	Title	Innovative aspect
Dai et al.	LncRNA H19 Regulates BMP2-Induced Hypertrophic Differentiation of Mesenchymal Stem Cells by Promoting Runx2 Phosphorylation	New mechanism to take into consideration when dealing with cartilage tissue engineering treatment. Regulation function of H19 in hypertrophic differentiation of cartilage
Hanai et al.	Potential of Soluble Decellularized Extracellular Matrix for Musculoskeletal Tissue Engineering – Comparison of Various Mesenchymal Tissues	New musculoskeletal therapy using decellularized ECM derived from mesenchymal tissues. Tissue derived soluble ECMs could be employed to regenerate tissues combined with some appropriate scaffolds seeded with some appropriate stem cells.
Wang et al.	BMSC-derived small extracellular vesicles induce cartilage reconstruction of temporomandibular joint osteoarthritis *via* autotaxin-YAP signaling axis	Novel treatment for Temporomandibular joint osteoarthritis (TMJOA) using BMSC-sEVs for cartilage reconstruction
Tejedor et al.	Pyrroline-5-Carboxylate Reductase 1 Directs the Cartilage Protective and Regenerative Potential of Murphy Roths Large Mouse Mesenchymal Stem Cells	The first evidence that MRL MSCs exhibit enhanced chondrogenic, chondroprotective, and regenerative properties as compared with BL6 MSCs in a Pycr1-dependent manner.
Tejedor et al.	MANF Produced by MRL Mouse-Derived Mesenchymal Stem Cells Is Pro-regenerative and Protects From Osteoarthritis	New therapy using MSC derived from MRL mouse as a cartilage regenerative potential, through their high capacity to release MANF.
Da Cruz et al.	Post-adipose-derived stem cells (ADSC) stimulated by collagen type V (Col V) mitigate the progression of osteoarthritic rabbit articular cartilage	Novel OA treatment: post-ADSC stimulation by Col V treatment increased the repair process in an osteoarthritic rabbit articular cartilage model
Yang et al.	Biofunctionalized structure and ingredient mimicking scaffolds achieving recruitment and chondrogenesis for staged cartilage regeneration	Novel strategy for articular cartilage regeneration: endogenous cell recruitment: growth factor-β3 (TGF-β3)-loaded biomimetic natural scaffold based on demineralized cancellous bone (DCB) and acellular cartilage extracellular matrix (ECM). Great promise for clinically effective *in situ* articular cartilage regeneration.
Li et al.	Autologous Fractionated Adipose Tissue as a Natural Biomaterial and Novel One-Step Stem Cell Therapy for Repairing Articular Cartilage Defects	Novel biomaterial, autologous fractionated adipose tissue (ECM/SVF-gel) to facilitate cartilage injury repair. It's simple, time-sparing, cost-effective, minimally invasive, and enzyme-free preparation process
Mustapich et al.	A Novel Strategy to Enhance Microfracture Treatment With Stromal Cell-Derived Factor-1 in a Rat Model	New strategy that can enhance microfracture procedures and significantly improve the quality of cartilage regeneration in an osteochondral defect. Incorporating SDF-1 into an implantable scaffold yielded a superior quality of cartilage repair when compared with microfracture alone.
Lu et al.	Unfavorable Contribution of a Tissue-Engineering Cartilage Graft to Osteochondral Defect Repair in Young Rabbits	New model for studying treatment of cartilage defects. dECM-based tissue-engineering approach is able to repair adult cartilage defects, but is different for premature tissue.
Jacob et al.	Osteochondral Injury, Management and Tissue Engineering Approaches	Literature review combination on the assessment of different techniques for osteochondral lesions
Li et al.	Cell Interplay in Osteoarthritis	Summary of key cells that might be targets of future therapies for OA.
Najar et al.	Mesenchymal Stromal Cell Immunology for Efficient and Safe Treatment of Osteoarthritis	New strategy involving immunological features for developing MSCs as a therapeutic option for OA with high quality, safety and efficiency standards.
Pachito et al.	Technical Procedures for Preparation and Administration of Platelet-Rich Plasma and Related Products: A Scoping Review	Scoping Review: Combined studies of different methods for each stage of PRP processing, that can be used in different clinical situations of Medicine and Dentistry

decellularized ECM (dECM) for each of the nine tissues harvested exhibited variations in their biochemical characteristics and growth factor distribution. On cell culture, it appeared to promote cell differentiation toward the specified used ECM tissue phenotype and decellularization was successful with reducing cellular components in every tissue. The present results are important in the field of musculoskeletal regeneration therapy, since tissue derived soluble ECMs could be employed to regenerate tissues combined with some appropriate scaffolds seeded with stem cells.

Researching less invasive treatments for Temporomandibular joint osteoarthritis (TMJOA), Wang et al. attempted to analyze the cartilage reconstruction effect of bone marrow MSC-derived small extracellular vesicles (BMSC-sEVs) and showed an increase of the tissue in the cartilage lacuna and hypertrophic cartilage cells in the deep area of the bone under the cartilage, besides higher rates of cell proliferation and migratory activity and alleviated G1 stagnation of the cell cycle of OAsEV which may provide guidance regarding their therapeutic applications as early and minimally invasive therapies for TMJOA.

Comparing Murphy Roths Large (MRL), who possess remarkable capacity to regenerate several musculoskeletal tissues, and BL6 mices regeneration to a ear punch, Tejedor et al. demonstrated that the enhanced regenerative potential of MRL mice is attributed, in part, to their MSCs that exhibit PYCR1-dependent higher glycolytic potential, differentiation capacities, chondroprotective abilities, and regenerative properties than BL6 MSCs, what could be a promising tool in the treatment of OA. Comparing the MSCs of these two mouse species, Tejedor et al. showed that the slow-proliferating MRL MSCs display a higher migration potential than the fast-proliferating BL6 MSC and found that mesencephalic astrocyte derived neurotrophic factor (MANF) was specifically highly produced by MRL MSC as compared to MSC derived from other mouse strains, and that MANF highly produced by MRL MSC contributes to their capacity to tend to reduce the OA score.

To delay the development of OA and promote joint cartilage regeneration, Da Cruz et al. demonstrated that post-adipose-derived stem cells (ADSC) stimulation by type V collagen (Col

V) treatment induced a significant regeneration of cartilage in an osteoarthritic rabbit articular cartilage model suggesting that surgical-induced OA treated with ADSCs stimulated by Col V may prevent the progression of cartilage injury and indicating that ADSCs/Col V may be a therapeutic target for the treatment of osteoarthritis. Also using a defect produced in the articular cartilage of rabbits, Yang et al. developed a staged regeneration strategy that combines endogenous cell recruitment and pro-chondrogenesis approaches for *in situ* articular cartilage regeneration with growth factor (GF)-loaded scaffold who facilitated cell homing, migration, and chondrogenic differentiation and promoted the reconstructive effects of *in vivo* cartilage formation.

Studying the regeneration of defects in articular cartilage, Li et al. used extracellular matrix/stromal vascular fraction gel (ECM/SVF-gel) to evaluate the therapeutic effect of this natural biomaterial on this repair, comparing the control group treated with microfractures to the group with microfractures associated with ECM/SVF-gel, finding that autologous ECM/SVF-gel displays a curative effect on articular cartilage regeneration in a rabbit model, besides being a simple, time-sparing, cost-effective, enzyme-free and minimally invasive preparation process.

Microfracture is one of the most widely used techniques for the repair of articular cartilage. However, microfracture often results in filling of the chondral defect with fibrocartilage, which exhibits poor durability and sub-optimal mechanical properties. Mustapich et al. studied a strategy for enhanced microfracture treatment with stromal cell-derived factor-1 (SDF-1), demonstrating a simple cost-effective one-step process for improving the quality of cartilage defect repair in a rat model of microfracture. In this perspective, Lu et al. found that this approach played a unique role in cartilage resurfacing of adult rabbits despite the fact that self-healing dominates cartilage repair in young rabbits less than 9 months old.

After categorizing treatment options for osteochondral lesions into repair and regenerative techniques, Jacob et al. showed emerging techniques, exploring tissue engineering with new methods of cultures and their results, and stated that for improved chondrogenesis the cells require both growth factors and mechanical forces to bring about more physiological cellular responses. The author demonstrated satisfactory results in the medium-term follow-up with the MaioRegen presenting faster return to sports and a low rate of complication and failure, while the Agili-C showed encouraging results through significant improvement in the assessments.

OA is a multifactorial disease that presupposes local and systemic factors and has multiple pathogenetic mechanisms, which must be considered when exploring new treatment options. Li et al. presented the cells in the joint tissues and their role in OA pathogenesis, the numerous ways these cells communicate, and concluded that application of stem cell-derived EVs in OA treatment is an emerging field in regenerative medicine.

Cartilage tissue engineering has potential for the treatment of cartilage pathologies, providing biomaterials that can be adjuvants to already established treatments to improve the clinical outcome, providing a higher quality regeneration and in the shortest possible time. There are clearly several cellular regulatory pathways involved in the therapeutic effect of MSCs, and the broad cellular and molecular changes that accompany MSC apoptosis, autophagy, and senescence may be essential for their therapeutic effects according to Najar et al. This is an essential understanding of the immunological profile and functions of MSCs as a graft and understanding of the mechanisms involved in the effects of MSCs for better therapeutic targeting.

A treatment widely used in different clinical situations is Platelet-rich plasma (PRP), but universal standardization of procedures for its preparation is still lacking. Pachito et al. reviewed thirty-nine studies focusing on the comparison of PRP to a related product, types of anticoagulants, centrifugation protocols, commercial kits, processing time, methods for activation, and application concomitantly to other substances, finding a great variability embed in each step necessary for the preparation of PRP which may justify the variability of clinical effects of PRP across different clinical trials.

FINAL CONSIDERATIONS

In this editorial, it was possible to discover a large number of innovative aspects, with extremely promising research fields that could change the course of the treatment of OA and other pathologies that affect the articular cartilage. Despite that, the articles have some methodological limitations and further research should be carried out focusing on the difficulties raised, in order to increase the level of evidence, safety and efficacy of the new therapies.

Innovative technologies and discoveries take time to be translated from an idea to clinical practice (Fernandes et al., 2022). Moreover the continuing development of the mentioned studies is of key importance to create collaborative learning and reach research goals for cartilage treatment and, at the end, improve healthcare and patient's quality of life.

AUTHOR CONTRIBUTIONS

All authors listed have made a substantial, direct, and intellectual contribution to the work and approved it for publication. TF wrote the manuscript. DB, KS, ZS, NN, and AG carried out the final review.

ACKNOWLEDGMENTS

We'd like to acknowledge Rafaella Rogatto de Faria and Teófilo Josué Alecrim da Costa for contributing to this manuscript.

REFERENCES

Ando, W., Tateishi, K., Hart, D. A., Katakai, D., Tanaka, Y., Nakata, K., et al. (2007). Cartilage Repair Using an In Vitro Generated Scaffold-free Tissue-Engineered Construct Derived from Porcine Synovial Mesenchymal Stem Cells. *Biomaterials* 28 (36), 5462–5470. doi:10.1016/j.biomaterials.2007.08.030

Bishop, E. S., Mostafa, S., Pakvasa, M., Luu, H. H., Lee, M. J., Wolf, J. M., et al. (2017). 3-D Bioprinting Technologies in Tissue Engineering and Regenerative Medicine: Current and Future Trends. *Genes & Dis.* 4, 185–195. doi:10.1016/j.gendis.2017.10.002

Fernandes, T. L., Cortez De Santanna, J. P., Frisene, I., Gazarini, J. P., Gomes Pinheiro, C. C., Gomoll, A. H., et al. (2020). Systematic Review of Human Dental Pulp Stem Cells for Cartilage Regeneration. *Tissue Eng. Part B Rev.* 26 (1), 1–12. doi:10.1089/ten.teb.2019.0140

Fernandes, T. L., de Faria, R. R., Gonzales, M. A., Sherman, S. L., Goldchmit, S., and Fleury, A. (2022). Innovation in Orthopaedics: Part 2—How to Translate Ideas and Research into Clinical Practice. *Curr. Rev. Musculoskelet. Med.* 15, 150–155. doi:10.1007/s12178-022-09749-4

Fernandes, T. L., Kimura, H. A., Pinheiro, C. C. G., Shimomura, K., Nakamura, N., Ferreira, J. R., et al. (2018). Human Synovial Mesenchymal Stem Cells Good Manufacturing Practices for Articular Cartilage Regeneration. *Tissue Eng. Part C. Methods* 24 (12), 709–716. doi:10.1089/ten.tec.2018.0219

Harrison, R. H., St-Pierre, J.-P., and Stevens, M. M. (2014). Tissue Engineering and Regenerative Medicine: a Year in Review. *Tissue Eng. Part B Rev.* 20, 1–16. doi:10.1089/ten.TEB.2013.0668

Hernandez, A. J., Camanho, G. L., and Amatuzzi, M. M. (2000). Cartilagem Articular e Osteoartrose. *Acta ortop. bras.* 8 (2), 100–104. doi:10.1590/s1413-78522000000200005

Meyers, M. A., and Chawla, K. K. (2008). *Mechanical Behavior of Materials*. 2nd Edn. Cambridge: Cambridge University Press, 137–138. doi:10.1017/CBO9780511810947

Pirraco, R. F., Pirraco, R. P., Oliveira, J. M., Reis, R. L., and Marques, A. P. (2018). Stem Cells for Osteochondral Regeneration. *Adv. Exp. Med. Biol.* 1059, 219–240. doi:10.1007/978-3-319-76735-2_10

Shimomura, K., Ando, W., Moriguchi, Y., Sugita, N., Yasui, Y., Koizumi, K., et al. (2015). Next Generation Mesenchymal Stem Cell (MSC)-based Cartilage Repair Using Scaffold-free Tissue Engineered Constructs Generated with Synovial Mesenchymal Stem Cells. *Cartilage* 6, 13S–29S. doi:10.1177/1947603515571002

Sophia Fox, A. J., Bedi, A., and Rodeo, S. A. (2009). The Basic Science of Articular Cartilage: Structure, Composition, and Function. *Sports Health* 1 (6), 461–468. doi:10.1177/1941738109350438

Wang, A.-T., Feng, Y., Jia, H.-H., Zhao, M., and Yu, H. (2019). Application of Mesenchymal Stem Cell Therapy for the Treatment of Osteoarthritis of the Knee: a Concise Review. *World J. Stem Cells* 11, 222–235. doi:10.4252/wjsc.v11.i4.222

Conflict of Interest: The authors declare that the research was conducted in the absence of any commercial or financial relationships that could be construed as a potential conflict of interest.

Publisher's Note: All claims expressed in this article are solely those of the authors and do not necessarily represent those of their affiliated organizations, or those of the publisher, the editors and the reviewers. Any product that may be evaluated in this article, or claim that may be made by its manufacturer, is not guaranteed or endorsed by the publisher.

frontiers in Cell and Developmental Biology

ORIGINAL RESEARCH
published: 29 July 2020
doi: 10.3389/fcell.2020.00580

LncRNA H19 Regulates BMP2-Induced Hypertrophic Differentiation of Mesenchymal Stem Cells by Promoting Runx2 Phosphorylation

Guangming Dai, Haozhuo Xiao, Chen Zhao, Hong Chen, Junyi Liao and Wei Huang**

Department of Orthopaedic Surgery, The First Affiliated Hospital of Chongqing Medical University, Chongqing, China

OPEN ACCESS

Edited by:
Andreas H. Gomoll, Hospital for Special Surgery, United States

Reviewed by:
Karen Bieback, Heidelberg University, Germany
Mauro Alini, AO Foundation, Switzerland

***Correspondence:**
Junyi Liao
liaojunyi@cqmu.edu.cn
Wei Huang
huangwei68@263.net

Specialty section:
This article was submitted to Stem Cell Research, a section of the journal Frontiers in Cell and Developmental Biology

Received: *11 February 2020*
Accepted: *15 June 2020*
Published: *29 July 2020*

Citation:
Dai G, Xiao H, Zhao C, Chen H, Liao J and Huang W (2020) LncRNA H19 Regulates BMP2-Induced Hypertrophic Differentiation of Mesenchymal Stem Cells by Promoting Runx2 Phosphorylation. Front. Cell Dev. Biol. 8:580. doi: 10.3389/fcell.2020.00580

Objectives: Bone morphogenetic protein 2 (BMP2) triggers hypertrophic differentiation after chondrogenic differentiation of mesenchymal stem cells (MSCs), which blocked the further application of BMP2-mediated cartilage tissue engineering. Here, we investigated the underlying mechanisms of BMP2-mediated hypertrophic differentiation of MSCs.

Materials and Methods: *In vitro* and *in vivo* chondrogenic differentiation models of MSCs were constructed. The expression of H19 in mouse limb was detected by fluorescence *in situ* hybridization (FISH) analysis. Transgenes BMP2, H19 silencing, and overexpression were expressed by adenoviral vectors. Gene expression was determined by reverse transcription and quantitative real-time PCR (RT-qPCR), Western blot, and immunohistochemistry. Correlations between H19 expressions and other parameters were calculated with Spearman's correlation coefficients. The combination of H19 and Runx2 was identified by RNA immunoprecipitation (RIP) analysis.

Results: We identified that H19 expression level was highest in proliferative zone and decreased gradually from prehypertrophic zone to hypertrophic zone in mouse limbs. With the stimulation of BMP2, the highest expression level of H19 was followed after the peak expression level of Sox9; meanwhile, H19 expression levels were positively correlated with chondrogenic differentiation markers, especially in the late stage of BMP2 stimulation, and negatively correlated with hypertrophic differentiation markers. Our further experiments found that silencing H19 promoted BMP2-triggered hypertrophic differentiation through *in vitro* and *in vivo* tests, which indicated the essential role of H19 for maintaining the phenotype of BMP2-induced chondrocytes. In mechanism, we characterized that H19 regulated BMP2-mediated hypertrophic differentiation of MSCs by promoting the phosphorylation of Runx2.

Conclusion: These findings suggested that H19 regulates BMP2-induced hypertrophic differentiation of MSCs by promoting the phosphorylation of Runx2.

Keywords: BMP2, lncRNA H19, MSCs, hypertrophic differentiation, cartilage tissue engineering

INTRODUCTION

Stem-cell-based and gene-enhanced tissue engineered cartilage is promising in the treatment of cartilaginous pathologies, especially traumatic cartilage defects (Bishop et al., 2017; Canadas et al., 2018; Wang et al., 2019). Mesenchymal stem cells (MSCs) hold the potential for osteogenic, chondrogenic, adipogenic differentiation, etc., owing to the fact that MSCs are easy to isolate, stable in expressing exogenous genes, abundant in source, and were identified as ideal seed cells for regenerative medicine (Canadas et al., 2018; Kim et al., 2019; Mamidi et al., 2016; Wang et al., 2019). Therefore, it is essential to guide MSC chondrogenic differentiation for the construction of tissue engineering cartilage.

Bone morphogenetic protein 2 (BMP2), a member of the transforming growth factor beta (TGF-β) superfamily, is characterized as one of the most effective growth factors to induce MSC chondrogenic differentiation (Kovermann et al., 2019; Miyazono et al., 2010; Munsell et al., 2018; Pan et al., 2008; Zhou et al., 2016). However, BMP2 is also known to induce MSC osteogenic differentiation and stimulate hypertrophic differentiation after chondrogenic differentiation, which go against maintaining of BMP2-induced cartilage phenotype (An et al., 2010; Liao et al., 2014; Zhou et al., 2016). Our previous studies found that BMP2 induced MSC chondrogenic differentiation by upregulating the expression of Sox9; as the key transcription factor of chondrogenesis, overexpression of Sox9 potentiated BMP2-mediated chondrogenic differentiation and inhibited BMP2-induced osteogenic differentiation (Liao et al., 2014; Zhou et al., 2016). However, BMP2 triggered hypertrophic differentiation process after chondrogenic differentiation still blocked the further application of BMP2-mediated cartilage engineering (Liao et al., 2014; Nasrabadi et al., 2018; Zhou et al., 2016). Hence, it is important to clarify the mechanisms underlying BMP2-mediated hypertrophic differentiation of MSCs.

With the development of next-generation sequencing technologies, it is confirmed that over 80% of human genome is transcribed; however, only ∼2% of human genome is transcribed into messenger RNA (mRNA), which indicates the pervasiveness of non-coding RNAs (ncRNAs) (Clark et al., 2011; Djebali et al., 2012; Pettersson et al., 2009). Recently, ncRNAs especially long non-coding RNAs (lncRNAs), which are identified as non-protein coding transcripts longer than 200 nucleotides, are characterized as regulatory RNAs and are involved in many physiological and/or pathological processes (Morris and Mattick, 2014; Quinn and Chang, 2016; Sanbonmatsu, 2016). As regulatory RNAs, lncRNAs were reported to serve as competition endogenous RNA (ceRNA), primary microRNA precursor, modular scaffold of histone modification, mRNA decay controller, functional protein regulator, etc. (Cai and Cullen, 2007; Kim and Shiekhattar, 2016; Morris and Mattick, 2014; Qi et al., 2019; Tsai et al., 2010). LncRNA H19 (H19), which was first isolated and reported in 1980s by four different laboratories, was identified as one of the first imprinted genes and lncRNAs (Cai and Cullen, 2007; Gabory et al., 2006; Hao et al., 1993; Liu et al., 2017; Moulton et al., 1994a). In the past several decades, H19 was known to regulate diverse cellular processes, including tumorigenesis, embryo growth, stem cell differentiation, etc. (Gabory et al., 2010; Hao et al., 1993; Liu et al., 2017; Moulton et al., 1994b). Meanwhile, evidence have shown that H19 was involved in MSC chondrogenic differentiation (Dudek et al., 2010; Liu et al., 2017; Pang et al., 2019). Dudek et al. (2010) reported that H19 and H19-encoded miR675 are essential for the production of Col2α. Pang et al. characterized that H19 is indispensable for the cartilage differentiation of stem cells. On the basis of our previous studies (Liao et al., 2017b), we speculated the regulatory function of H19 in BMP2-mediated chondrogenic differentiation of MSCs.

In the present study, we investigated the function of H19 in BMP2-mediated chondrogenic and hypertrophic differentiation of MSCs. We found a peak expression level of H19 after the crest stage of Sox9, and the expression levels of H19 were positively correlated with BMP2-mediated expression levels of chondrogenic differentiation markers, especially in the late stage. Our further experiments found that silencing H19 promoted BMP2-triggered hypertrophic differentiation, which indicated the essential role of H19 for maintaining the phenotype of BMP2-induced chondrocytes. In mechanism, we characterized that H19 can directly bind with Runx2 protein and promote Runx2 phosphorylation, which inhibited the function of Runx2. These findings applied a new version for the understanding of BMP2-mediated hypertrophic differentiation, which is beneficial for the construction of BMP2-mediated cartilage tissue engineering.

MATERIALS AND METHODS

Ethics Statement

All animal protocols were approved by the Ethical Committee of The First Affiliated Hospital of Chongqing Medical University. All surgical operations were done under proper anesthesia; animals were kept in independent cages with standard conditions until it is confirmed that they recovered from anesthesia without pain. At the indicated time points, mice were euthanized by overdose intraperitoneal pentobarbital sodium (Sigma-Aldrich, United States) injection. All efforts were made to minimize the suffering of the animals; the ectopic masses were retrieved from the injection sites of the node mice after confirming that the mice were not breathing, have no heartbeat and with dilated pupils.

Cell Culture and Chemicals

The human embryonic kidney (HEK) 293 and mouse bone marrow MSC C3H10T1/2 cell lines were obtained from the American Type Culture Collection (ATCC, Manassas, VA, United States). Cell lines were preserved in complete Dulbecco's modified Eagle's medium (DMEM, Hyclone, China), supplemented with 10% fetal bovine serum (FBS, Gibco, Australia), 100 U/ml penicillin, and 100 mg/ml streptomycin, maintained at 37°C in a humidified 5% carbon dioxide (CO_2) atmosphere. Unless indicated otherwise, all chemicals were purchased from Sigma-Aldrich or Corning.

Fluorescence *in situ* Hybridization

Fetal mouse limbs at embryonic 14.5 day were harvested, fixed overnight in diethyl pyrocarbonate (DEPC)-treated 4% paraformaldehyde (Servicebio, Wuhan, China), and embedded in paraffin. Then, serial 5-μm-thick sections were obtained and deparaffinized in xylene and rehydrated in graded ethanol and RNase-free deionized Millipore water (Invitrogen, CA, United States). The hybridization was performed as describe previously (Li et al., 2018). Prior to hybridization, tissue sections were pretreated with boiled target retrieval buffer supplied in the RNAscope kit (Invitrogen, CA, United States) for 15 min. Then, sections were hybridized for 3 h at 50°C in a hybridization oven with a mixture containing the hybridization buffer supplied in the kit and the probes for mouse H19 that were synthesized by Ribobio (Guangzhou, China) tagged with Cy3, followed by successive incubations and washing accordingly. Finally, slides were mounted with the antifade mounting media containing 4′,6-diamidino-2-phenylindole (DAPI, Vector Lab, Inc., Burlingame, CA, United States). The microscopy images of the sections were acquired with a fluorescence microscope (Olympus, United States). Cy3 (H19) and DAPI (nuclei) were excited at 561 and 405 nm, respectively. As for the analysis of fluorescence intensity, three high-power field of view were randomly selected in each area, and the optical density value per cells in each field was calculated by ImageJ Pro and calibrated relative to the background of the field. Then, the average cell optical density (by dividing nuclei numbers) of each area was calculated, and figure was drawn by GraphPad Prism software. The sequence of H19 probe is 5′-Cy3/*cagttgccctcagacggagatggacg*/Cy3-3′. H19 positive control for FISH analysis was shown in **Supplementary Figure 1A**.

Construction and Generation of Recombinant Adenoviral Vectors AdBMP2, AdGFP, AdH19, and AdsimH19

Recombinant adenoviruses were generated using AdEasy technology as described previously (Deng et al., 2014; He et al., 1998; Lee et al., 2017; Luo et al., 2007); AdBMP2 was previously characterized (Liao et al., 2014; Zhou et al., 2015; Zhou et al., 2016), and AdGFP was used as a mock virus control. Briefly, the coding region of human BMP2, and the full-length transcript of mouse H19, were PCR amplified and subcloned into an adenoviral shuttle vector and used to generate recombinant adenoviral vectors; recombinant adenoviral vectors containing BMP2 or H19 were subsequently used to generate recombinant adenoviruses in HEK-293 cells. For making AdsimH19, three small interfering RNAs (siRNAs) targeting mouse H19 were simultaneously assembled to an adenoviral shuttle vector using the Gibson Assembly system as described (Deng et al., 2014; Liao et al., 2017b). AdBMP2 also expresses green fluorescent protein (GFP), whereas AdsimH19 expresses red fluorescent protein (RFP) as a marker for monitoring infection efficiency.

Chondrogenic Differentiation of MSCs in Micromass Culture

To induce chondrogenic differentiation, micromass culture was used to mimic the condensation of MSCs as previously described (Liao et al., 2014). C3H10T1/2 cells were seeded at 60% confluence and infected with AdGFP, AdBMP2, or/and AdsimH19. Twenty-four hours after infection, cells were harvested and resuspended in high density ($\sim 10^5$ per 25 μl medium), which were subsequently added at the center of each well in the 12-well plates and then incubated in CO_2 incubator. One hour after incubation, 2–3 ml complete DMEM was added to each well; half medium was replaced every 3 days.

RNA Isolation and RT-qPCR, RT Semiquantitative PCR

Total RNA was isolated with TRIZOL reagent (Invitrogen, CA, United States) according to the manufacturer's instructions and subjected to reverse transcription reactions using PrimeScript RT reagent kit (Takara, Dalian, China). The quantitative PCR analysis was carried out using the CFX96 Real-Time PCR Detection System (Bio-Rad, CA, United States) with SYBR premix Ex Taq II kit (Takara, Dalian, China) according to the manufacturer's instructions. Programs for real-time PCR are as follows: 95°C for 30 s, 95°C for 5 s, and 60°C for 30 s, repeating 40 cycles. Gapdh was used as a reference gene. The melting curves did not detect any non-specific amplification. All sample values were normalized to Gapdh expression by using the $2^{-\Delta\Delta Ct}$ method; primer efficiency correction was done and used to corrected amplification efficiency, Gradient concentration DNA samples were used for the normalization. The PCR primer sequences are listed in **Table 1**.

The semiquantitative PCR was preformed using premix Taq^{TM} (Takara, Dalian, China) kit, with the following programs: 92°C for 3 min for one cycle; 92°C for 30 s, 55°C for 30 s, and 72°C for 30 s, for 35 cycles. Then, PCR products were electrophoresed on 1% agarose gels (Invitrogen, CA, United States) and visualized by UV light.

Western Blot Analysis

Protein extraction was performed by using 2% sodium dodecyl sulfate (SDS) lysis buffer that including 100 mM Tris–HCl, 100 mM β-mercaptoethanol, and protease and phosphatase inhibitors (Roche, United States). Total protein was denatured via boiling and determined using a BCA protein assay kit (Beyotime, Beijing, China). Equivalent amounts of protein were electrophoresed on 5–10% Bis-Tris gels (Life Technologies, MA, United States) and transferred to polyvinylidene fluoride membranes (PVDF, Millipore, MA, United States). Membranes were blocked with 5% skimmed milk for 1 h at room temperature and incubated with primary antibodies to collagen 10α1, MMP13, Runx2, phosphor-Runx2, and β-actin overnight (rabbit anti-collagen 10α1 and MMP13, 1:1,000, Abcam, Cambridge, United States; rabbit anti-Runx2 and β-actin, 1:1,000, Cell Signaling Technology, MA, United States; rabbit antiphosphor-Runx2, 1:1,500, Affinity Biosciences, United States). Following this, the membranes were incubated with corresponding secondary antibody conjugated with horseradish peroxidase (HRP, goat antirabbit secondary antibody, 1:1,000, Cell Signaling Technology, MA, United States). The blots were displayed with Immobilon Western Chemiluminescent HRP Substrate

TABLE 1 | Primer oligonucleotide sequences used for PCR.

Gene	Forward primer (5′–3′)	Reverse primer (5′–3′)
BMP2	ACCAGACTATTGGACACCAG	AATCCTCACATGTCTCTTGG
H19 for RT-qPCR	CAGAGTCCGTGGCCAAGG	CGCCTTCAGTGACTGGCA
H19 for RT-PCR	TATGCCCTAACCGCTCAGTC	AGACACCGATCACTGCTCC
SOX9	AGCTCAACCAGACCCTGAGAA	TCCCAGCAATCGTTACCTTC
Collagen 2α1	CAACACAATCCATTGCGAAC	TCTGCCCAGTTCAGGTCTCT
Aggrecan	TGGCTTCTGGAGACAGGACT	TTCTGCTGTCTGGGTCTCCT
MMP13	CTTTGGCTTAGAGGTGACTGG	AGGCACTCCACATCTTGGTTT
Collagen 10α1	CATGCCTGATGGCTTCATAAA	AAGCAGACACGGGCATACCT
MMP9	TTGACAGCGACAAGAAGTGG	CCCTCAGTGAAGCGGTACAT
Adamts5	CCTGCCCACCCAATGGTAAA	CCACATAGTAGCCTGTGCCC
GAPDH	CTACACTGAGGACCAGGTTGTCT	TTGTCATACCAGGAAATGAGCTT
β-actin	AGCCTCGCCTTTGCCGA	CTGGTGCCTGGGGCG

(Millipore, MA, United States). Relative protein expression was analyzed by Image Lab software using β-actin as control.

Subcutaneous Stem Cell Implantation

The use and care of animals in this study were approved by the Institutional Animal Care and Use Committee. All experimental procedures were carried out in accordance with the approved guidelines. Subcutaneous stem cell implantation procedure was performed as described (Liao et al., 2014; Liao et al., 2017a; Liao et al., 2017b). Briefly, the C3H10T1/2 cells were infected with AdGFP, AdBMP2, and/or AdsimBMP2. Twenty-four hours after infection, cells were collected and resuspended in DMEM at a density of $\sim 2 \times 10^5/\mu l$ (100 μl each injection). The cells were injected subcutaneously into the flanks of athymic nude mice (n = 3/group, female, 5–6 weeks old).

At the indicated time points, animals were euthanized, and the ectopic masses were retrieved from injection sites and subjected to X-ray imaging system with automatic exposure under 45 kV, 500 mA. Then, the masses were fixed in 4% paraformaldehyde (Beyotime, Beijing, China) for 24 h at room temperature, decalcified in 0.5 M ethylenediaminetetraacetic acid (EDTA) at 4°C for 14 days and embedded in paraffin. Serial 5-μm-thick sections were obtained and followed by histological and other specialty staining evaluations.

Histological Evaluation: Hematoxylin and Eosin, and Alcian Blue Staining

Sections were deparaffinized with xylene and rehydrated using graded ethanol. H&E and Alcian blue staining were performed using standard protocol as previously described (Liao et al., 2014; Zhou et al., 2015; Zhou et al., 2016). Briefly, the deparaffinized samples were first subjected to antigen retrieval and fixation. Then, sections were stained with hematoxylin and eosin (H&E) and Alcian blue staining. Histological evaluation was performed with the use of a light microscope (Olympus, Japan).

Immunohistochemistry Assay

Generally, sections were deparaffinized with xylene, rehydrated using graded ethanol, treated with 3% H_2O_2 for 10 min to inhibit endogenous peroxidase activity, boiled in citrate buffer (pH 6.0) for 20 min at 95–100°C, and blocked with normal goat serum. Then, sections were incubated with primary antibody to MMP-13 (Santa Cruz Biotechnology Inc., Texas, United States, 1:300 dilution), Collagen 10α1 (Abcam, Cambridge, United States, 1:200 dilution), Runx2 (Cell signaling Technology, MA, United States, 1:200 dilution), and collagen 1α1 (Abcam, Cambridge, United States, 1:200 dilution) at 4°C overnight. After being washed, the sections were incubated with biotin-labeled secondary antibody for 30 min, followed by incubation with streptavidin–HRP conjugate for 20 min at room temperature. Staining without primary antibody was utilized as negative control (**Supplementary Figure 1B**). All photos were obtained by using a microscope (Olympus, Japan).

RNA Immunoprecipitation Analysis

The RNA immunoprecipitation (RIP) analysis was done as described previously (Kallen et al., 2013; Yuan et al., 2014). C3H10 T1/2 cells were infected with AdH19 or AdGFP. Three days after infection, cells were lysed and subjected to RIP analysis with the use of Magna RIPTM RNA-Binding Protein Immunoprecipitation Kit (Millipore, Bedford, MA, United States) according to the manufacturer's instructions. Briefly, prior to immunoprecipitation, magnetic beads were pretreated with RIP wash buffer supplied in the kit and incubated with Runx2 antibody (Cell Signaling Technology, MA, United States) for 30 min. Then, the magnetic bead-Runx2 composites were incubated with cell lysis supernatant and RIP immunoprecipitation buffer overnight at 4°C followed by successive washing with RIP wash buffer. After treatment with immunoprecipitation, the composites were detached by using proteinase K buffer. After that, the RNA fraction was isolated and subjected to perform qPCR analysis as described above.

Statistical Analysis

All images were obtained by using a microscope (Olympus, Japan) and analyzed by ImageJ Pro. Data were expressed as mean ± standard deviation (SD) and analyzed with SPSS software (Version 21, IBM, United States). A one-way analysis of variance was performed to analyze inter- and intragroup differences when more than two groups were compared. A t test was used to compare between any two groups. The correlations between H19 expression and other parameters were calculated with Spearman's

correlation coefficients. A value of $P < 0.05$ was considered statistically significant.

RESULTS

H19 Expression in Fetal Mouse Limb

To understand the function of H19 during the process of hypertrophic differentiation, we determined the expression of H19 in day 14.5 fetal mouse limb with the use of fluorescence *in situ* hybridization (FISH) technology. As shown in **Figure 1A**, the expression of H19 was highest in the proliferative zone, decreased in the prehypertrophic zone, and in lowest level in the hypertrophic zone in day 14.5 fetal mouse limb (**Figure 1A**, upper panel). Higher magnification (**Figure 1A**, lower panel) and H19-positive cells quantitative analysis (**Figure 1B**) showed the same trend. These results indicate that H19 may play a role in maintaining the phenotype of chondrocytes.

BMP2-Induced H19 Expression and Chondrogenic Differentiation of MSCs in Micromass Culture

To mimic the process of MSCs condensation, C3H10T1/2 cells infected with AdBMP2 or AdGFP were subjected to micromass culture (**Figure 1C**). We first determined mRNA expression level of BMP2, as shown in **Figure 1D**, compared with AdGFP

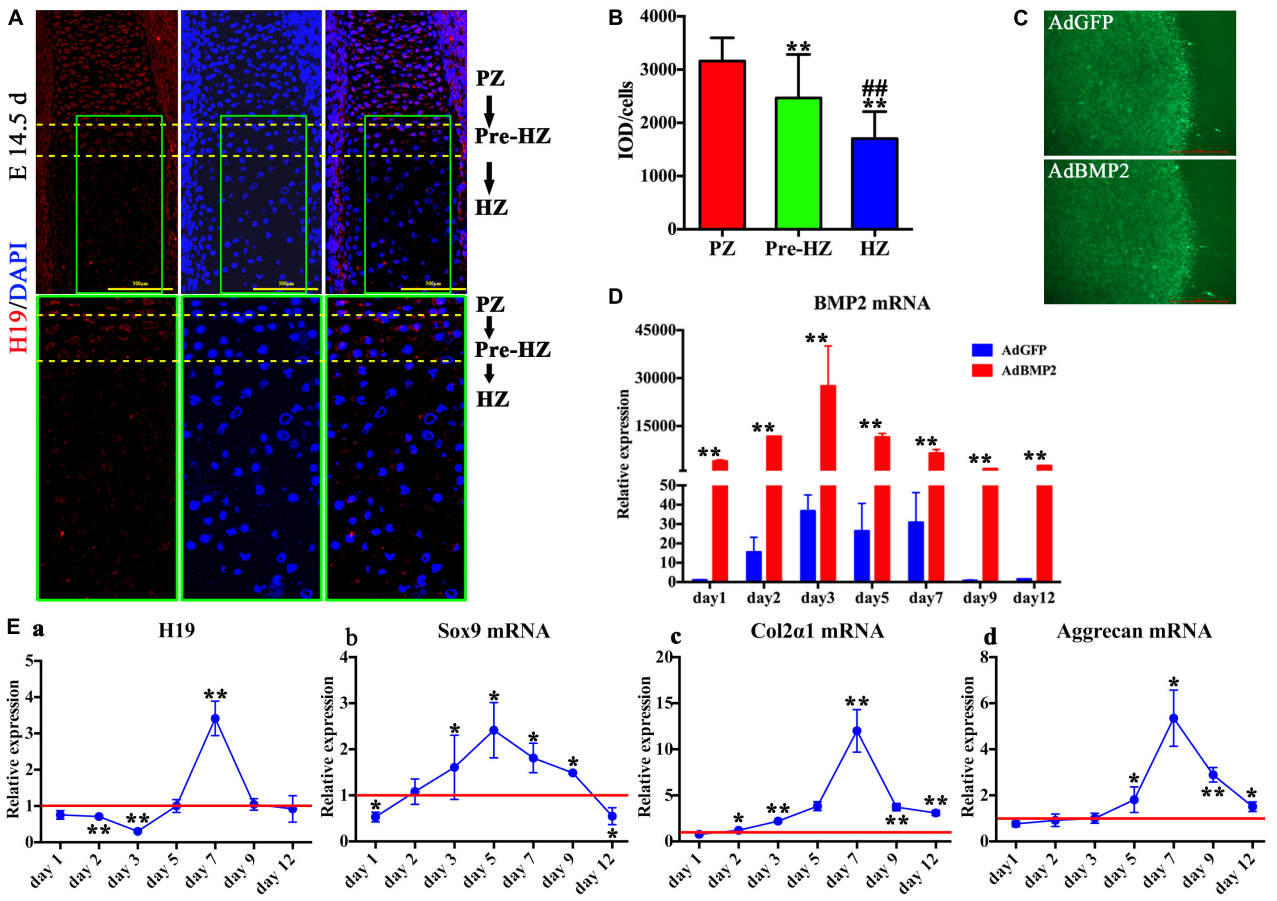

FIGURE 1 | H19 expression in developing endochondral bones and chondrogenic differentiation of mesenchymal stem cells (MSCs) induced by bone morphogenetic protein 2 (BMP2). **(A)** H19 expression in developing endochondral bones. Detection of H19 by fluorescence *in situ* hybridization to sections of the developing radius at E14.5 day. Expression of H19 (Red) is mainly observed in the proliferative zone (PZ), decreased in the prehypertrophic zone (Pre-HZ), and in lowest level in the hypertrophic zone (HZ). Higher magnification images were listed in the lower panel; scale bar = 500 μm. **(B)** Quantitative analysis of positive H19 expression. **(C)** BMP2-induced chondrogenic differentiation of MSCs in micromass culture. C3H10T1/2 cells were infected with AdBMP2 or AdGFP and subjected to micromass culture. Green fluorescent protein (GFP) fluorescence fields were recorded at 3 days after infection, scale bar = 1,000 μm. **(D)** Adenovirus-mediated overexpression of BMP2. The expression level of BMP2 messenger RNA (mRNA) was detected by quantitative PCR (qPCR) from days 1 to 12 after the infection of AdBMP2; AdGFP was used as control. **(E)** BMP2-induced H19 and chondrogenic differentiation markers expression. Relative expression levels of H19 **(a)**, Sox9 mRNA **(b)**, collagen 2α1 mRNA **(c)**, and Aggrecan mRNA **(d)** were detected by reverse transcription and quantitative real-time PCR (RT-qPCR) at a series time (days 1, 2, 3, 5, 7, 9, and 12) with the stimulation of AdBMP2. AdGFP was used as control. The values of AdBMP2/AdGFP were shown (each assay was done in triplicate and/or carried out in three independent experiments at least). "**" and "##" mean $p < 0.01$ compared with PZ and Pre-HZ group, respectively in panel **(B)**; "*" and "**" respectively mean $p < 0.05$ and $p < 0.01$ compared with AdGFP group in panel **(D)** and **(E)**. DAPI, 4′, 6-diamidino-2-phenylindole, PZ, proliferative zone, Pre-HZ, pre-hypertrophic zone, HZ, hypertrophic zone.

group, AdBMP2 dramatically increased the expression of BMP2 from day 1 to 12, which indicated that adenovirus-mediated overexpression of BMP2 was effective and sustained more than 12 days in micromass culture.

Second, we determined BMP2-induced expression of H19. As shown in **Figure 1Ea**, we found that the expression of H19 was downregulated by BMP2 from day 1 to 3, back to the basal level at day 5, then dramatically upregulated at day 7, and finally back to the basal level at days 9 and 12. These results indicated that H19 would function at the medial or late stage of BMP2-mediated MSC chondrogenic differentiation.

In addition, we detected the chondrogenic differentiation marker expression with the stimulation of BMP2. To be consistent with our previous work, we found that the expression level of Sox9 was upregulated by BMP2 from day 2 to 9 and showed a highest level at day 5 (**Figure 1Eb**). Meanwhile, Col2α and Aggrecan expressions decreased gradually from day 1 to 7 and showed a peak level at day 7, then back to the basal level gradually from day 9 to 12 (**Figures 1Ec,d**). Meanwhile, the data demonstrated that the peak expression level of H19 was followed after the crest expression level of Sox9 (**Figure 1E**).

Putting these data together, we infer that H19 may be acting as a regulatory RNA at medial or late stage of BMP2-induced chondrogenic differentiation of MSCs in micromass culture.

BMP2-Induced H19 Expression Is Positively Correlated With Terminal Chondrogenic Differentiation Markers and Negatively Correlated With Hypertrophic Differentiation Markers

To further clarify the relationships between BMP2-induced H19 expression levels and chondrogenic or hypertrophic differentiation markers, correlation analysis was used to analyze the correlation between H19 expression levels and chondrogenic and hypertrophic differentiation markers with the stimulation of BMP2. As for the chondrogenic differentiation markers, on the basis of H19 expression level, we analyzed days 1–5 and days 7–12, respectively. As shown in **Figure 2A**, from days 1 to 5, there was no obvious correlation between H19 expression level and Col2α1 ($r = 0.19$, $P = 0.55$); however, H19 expression levels were positively correlated with key chondrogenic differentiation transcription factor Sox9 expression levels ($r = 0.85$, $P < 0.01$) and chondrogenic marker Aggrecan ($r = 0.63$, $p = 0.03$). What is interesting is that from day 7 to 12 (**Figure 2B**), H19 expression levels were positively correlated with the expression levels of Sox9 ($r = 0.71$, $P = 0.03$), Col2α1 ($r = 0.92$, $P < 0.01$), and Aggrecan ($r = 0.91$, $P < 0.01$). These data highly indicated that H19 might regulate BMP2-induced terminal chondrogenic differentiation.

As for the hypertrophic differentiation markers, we first confirmed that, with the stimulation of BMP2, hypertrophic differentiation markers (MMP13, Adamts5, and Runx2) were significantly upregulated compared with control groups from day 7 to 12 (**Figures 3Aa,Ba,Ca**). Second, correlation analysis exhibited that H19 expression levels were negatively correlated with the expression levels of hypertrophic differentiation markers (MMP13, $r = -0.68$, $P = 0.04$; Adamts5, $r = -0.73$, $P = 0.03$) (**Figure 3B**) and key hypertrophic differentiation transcription factor Runx2 ($r = -0.86$, $P < 0.01$). Taken these data together, we deduced that H19 could play an important role in regulating BMP2-induced hypertrophic differentiation.

Silencing of H19 Promoted BMP2-Induced Hypertrophic Differentiation of MSCs *in vitro* and *in vivo*

To further confirm the role of H19 in BMP2-induced hypertrophic differentiation, we silenced H19 with recombinant adenovirus system and detected the influence of silencing of H19 in BMP2-induced hypertrophic differentiation of MSCs. As for the *in vitro* test, C3H10T1/2 cells infected with AdBMP2, AdBM2 + AdsimH19, and AdGFP were subjected to micromass culture (**Figure 4A**). Relative RNA expression levels of BMP2 and H19 were tested at day 3, as shown in **Figure 4B**. AdsimH19 effectively downregulated the expression levels of H19 in AdGFP and AdBMP2 groups without influence expression levels of BMP2 in AdBMP2 and AdBMP2 + AdSimH19 groups. Then, hypertrophic differentiation markers were determined by RT-qPCR and Western blot. As shown in **Figures 4C,D**, we found that silencing H19 upregulated BMP2-induced Col10α1 and MMP13 expression from day 7 to 12 at genetic level (**Figure 4C**); meanwhile, the same trend was found at protein level (**Figures 4Da,b**).

Using our previously established stem cell implantation assay (Liao et al., 2017a; Zhou et al., 2016), we injected C3H10T1/2 cells infected with AdGFP, AdBMP2, and/or AdsimH19 at the same infection ratio subcutaneously into the flanks of athymic nude (nu/nu) mice for 3 weeks. The cells transduced with AdGFP or AdsimH19 alone failed to form any detectable masses (data not shown). As shown in **Figure 5A**, there was no obvious morphological differences between the masses formed in the AdBMP2 and AdBMP2 + AdSimH19 group (**Figures 5Aa,b**). While the osseous composition in the AdBMP2 + AdSimH19 group was much more than that in the AdBMP2 group through X-ray testing (**Figure 5Ac**). On histological examination (**Figure 5B**), masses formed in the AdBMP2 group showed obvious chondrocytes and cartilaginous matrix. However, except the chondrocytes and cartilaginous matrix, the masses formed in the AdBMP2 + AdSimH19 group formed obvious trabeculae combined with bone-marrow-like tissues. The Alcian blue staining exhibited that there were less cartilaginous matrix and more hypertrophic chondrocytes formation in the AdBMP2 + AdSimH19 group compared with the AdBMP2 group. In quantitative analysis, we found that in the AdBMP2 group, there were significantly more undifferentiated MSCs (UM) and chondrocytes compared with the AdBMP2 + AdSimH19 group. Moreover, there was significantly more trabecular bone formation in the AdBMP2 + AdSimH19 group compared with AdBMP2 group (**Figure 5C**).

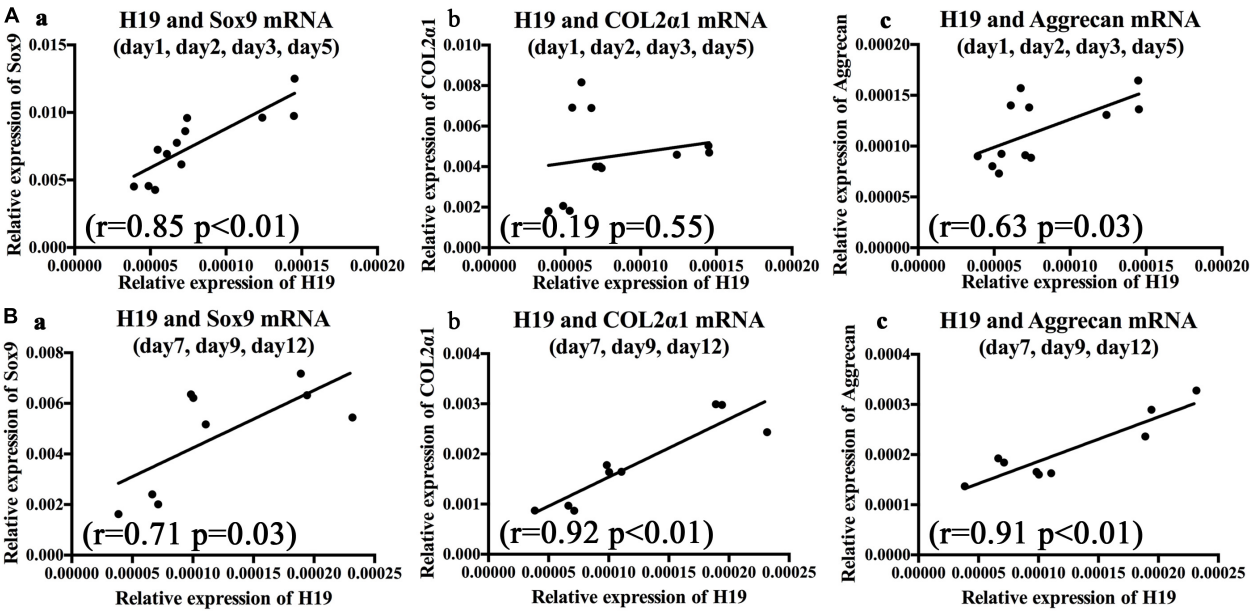

FIGURE 2 | Bone morphogenetic protein 2 (BMP2)-induced H19 expression is positively correlated with terminal chondrogenic differentiation markers. The correlations between BMP2-induced H19 expression and Sox9 messenger RNA (mRNA), collagen 2α1 mRNA, and Aggrecan mRNA were analyzed from day 1 to 5 and day 7 to 12, respectively, with Spearman's correlation coefficients, *r* means correlation coefficients. **(A)** During the early stage of BMP2's stimulation (days 1–5) Sox9 ($r = 0.85$, $p < 0.01$) **(a)** and Aggrecan ($r = 0.63$, $p = 0.03$) **(c)** expression levels were positively corelated with H19 expression level; however, Col2α ($r = 0.19$, $p = 0.55$) **(b)** expression levels were not significantly correlated with H19 expression levels. **(B)** In the late stage of BMP2's stimulation (days 7–12) Sox9 mRNA ($r = 0.71$, $p = 0.03$) **(a)**, Col2α mRNA ($r = 0.92$, $p < 0.01$) **(b)**, and Aggrecan mRNA ($r = 0.91$, $p < 0.01$) **(c)** expression levels were positively corelated with H19 expression levels. Each assay was done in triplicate and/or carried out in three independent experiments at least; mean value of each independent experiment was shown.

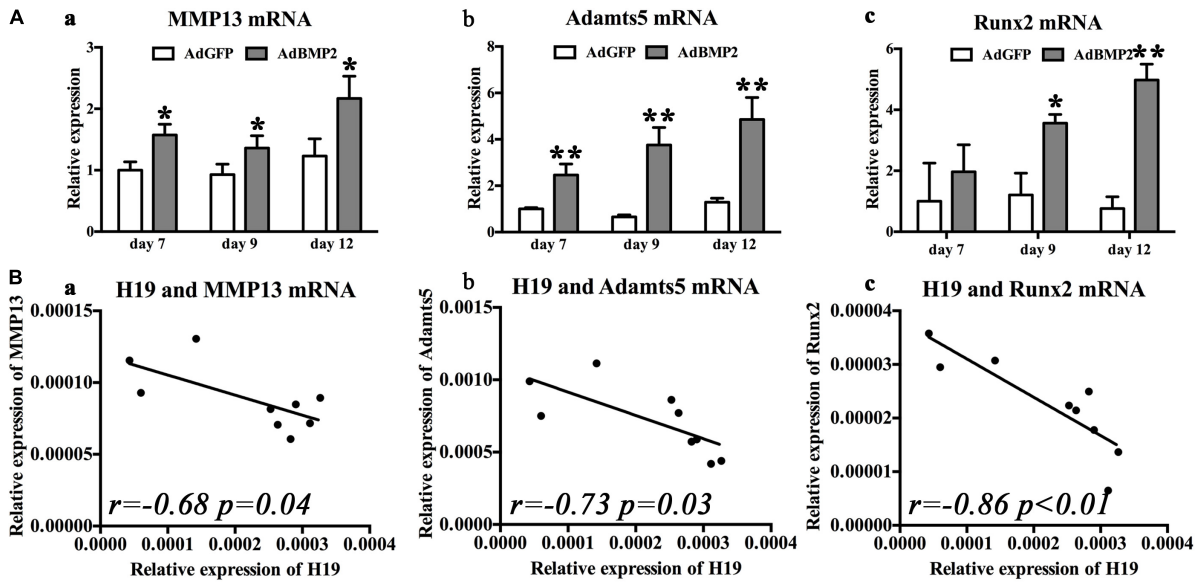

FIGURE 3 | Bone morphogenetic protein 2 (BMP2) induced H19 expression is negatively correlated with hypertrophic differentiation markers. **(A)** BMP2-induced hypertrophic differentiation of mesenchymal stem cells (MSCs). Quantitative PCR (qPCR) analysis of MMP13 **(a)**, Adamts5 **(b)**, and Runx2 **(c)** messenger RNA (mRNA) expression levels at days 7, 9, and 12 with the stimulation of AdBMP2; AdGFP was used as control. **(B)** The correlations between BMP2-induced H19 expression level and hypertrophic differentiation markers expression levels. The correlations between H19 expression levels of MMP13 ($r = -0.68$, $p = 0.04$) **(a)**, Adamts5 ($r = 0.73$, $p = 0.03$) **(b)**, and Runx2 ($r = -0.86$, $p < 0.01$) **(c)** mRNA expression levels at days 7, 9, and 12 were calculated with Spearman's correlation coefficients. "*" and "**" respectively mean $p < 0.05$ and $p < 0.01$ compared with AdGFP group; *r* means correlation coefficients. Each assay was done in triplicate and/or carried out in three independent experiments at least.

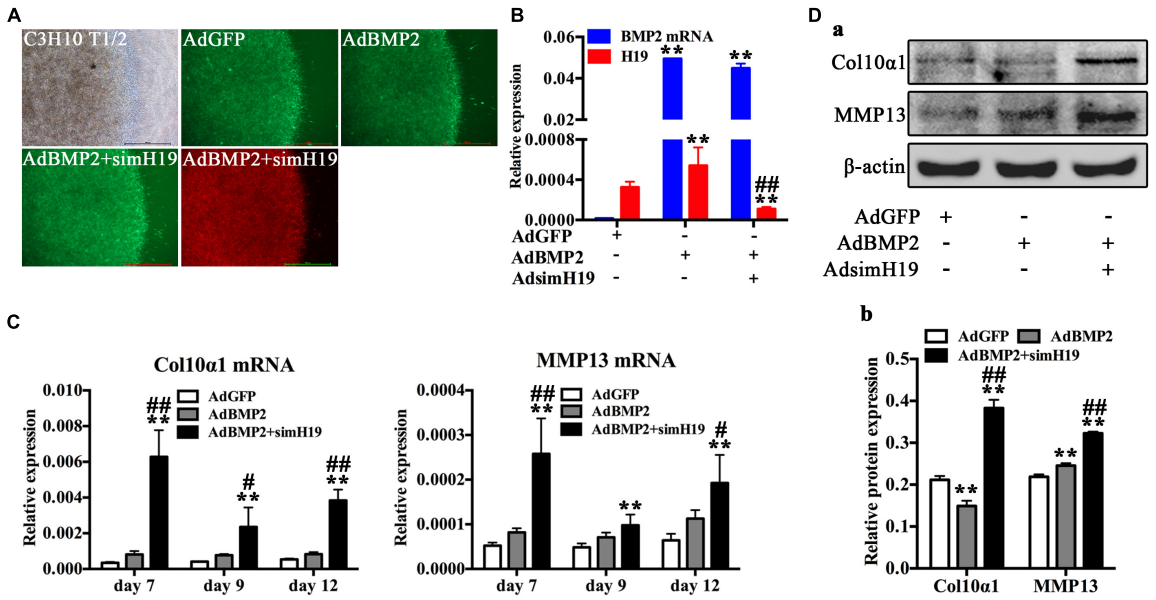

FIGURE 4 | Silencing of H19 promoted bone morphogenetic protein 2 (BMP2)-induced hypertrophic differentiation of mesenchymal stem cells (MSCs) *in vitro*. **(A)** C3H10T1/2 cells infected with AdGFP, AdBMP2, AdBMP2, and AdsimH19 were subjected to micromass culture. Bright field, GFP (AdGFP, AdBMP2) and RFP (AdsimH19) fluorescence fields were recorded at day 3 after infection; the fluorescence indicated high efficiency in single or combination infection, scale bar = 1,000 μm. **(B)** Effective knockdown of mouse H19 expression. The expression level of H19 and BMP2 messenger RNA (mRNA) at day 3 in different groups were detected by reverse transcription and quantitative real-time PCR (RT-qPCR); AdsimH19 silences the expression of H19 without influencing the expression of BMP2. All samples were normalized with the reference gene Gapdh. Each assay condition was done in triplicate. **(C)** Silencing H19 promoted BMP2-induced collagen 10α1 and MMP13 mRNA expression. Subconfluent MSCs were infected with AdBMP9 or AdGFP and/or AdsimH19 and subjected to micromass culture. At the indicated time points, total RNA was isolated and subjected to qPCR analysis using primers for mouse collagen 10α1 and MMP13; each assay condition was done in triplicate. **(D)** Silencing H19 promoted BMP2-induced collagen 10α1 and MMP13 protein expression. Western blot for the expression of collagen 10α1 and MMP13 were conducted at day 7 after transduction of indicated recombinant adenoviruses **(a)**. Relative protein expression was analyzed by Image Lab software using β-actin as control **(b)**. "*" and "**" respectively mean $p < 0.05$ and $p < 0.01$ compared with AdGFP group; "#" and "##" respectively mean $p < 0.05$ and $p < 0.01$ compared with AdBMP2 group. Each assay was done in triplicate and/or carried out in three independent experiments at least; representative results are shown.

The immunohistochemical staining was also utilized to confirm the influence of silencing of H19 in BMP2-induced hypertrophic differentiation *in vivo* (**Figure 5D**). We detected that Col10α1 and MMP13 expression in the AdBMP2 group were less and weakened compared with that in the AdBMP2 + AdSimH19 group (**Figures 5Da–d,a'–d'**). As the key transcription factor for hypertrophic differentiation, Runx2 expression in AdBMP2 group was also less and weakened compared with the AdBMP2 + AdSimH19 group through immunohistochemical staining (**Figures 5De,f,e',f'**). The same trend was found through quantitative analysis (**Figure 5E**). These data further confirmed that silencing of H19 promoted BMP2-induced hypertrophic differentiation of MSCs *in vivo*.

H19 Regulate BMP2-Induced Hypertrophic Differentiation of MSCs by Promoting the Phosphorylation of Runx2

As Runx2 is the key transcription factor of BMP2-mediated hypertrophic differentiation of MSCs (Jonason et al., 2009; Liao et al., 2014; Takeda et al., 2001; Ueta et al., 2001; Zhou et al., 2016), we hypothesized that H19 may regulate BMP2-induced hypertrophic differentiation by targeting Runx2. Using RIP analysis, we further analyzed the posttranscriptional regulation of H19 on the phosphorylation of Runx2. The process of RIP analysis is listed in **Figure 6A**. Briefly, MSCs (C3H10T1/2) infected with adenovirus expression H19 were cultured in micromass; 3 days after infection, cells were lysed and mixed with anti-Runx2 tagged beads. After immunoprecipitation, proteinase K was used for the enzymolysis of protein and RNA; then, total RNA was extracted and purified from the specific RNA protein mixture and subjected to RT-qPCR after to analyze the combination of Runx2 and H19. As shown in **Figure 6B, before** and **after** anti-Runx2-tagged beads extraction, Western blot analysis of Runx2 yielded expected products; immunoglobulin G (IgG) was used as control. RT-qPCR analysis showed that, compared with the IgG group, the expression of H19 in the RIP group was significantly higher, and β-actin was used as control (**Figure 6C**). RT-qPCR products analysis yielded expected products (**Figure 6D**).

These data strongly suggested the combination of H19 and Runx2; however, how H19 regulates the function of Runx2 is still not clear. As posttranslational modification, especially phosphorylation is one important regulatory mechanism of Runx2 activity, and phosphorylated Runx2 downregulated Runx2 activity and further inhibited Runx2-mediated differentiation (Jonason et al., 2009). Thus, we further ask if H19 influences the phosphorylation of Runx2. As shown in **Figure 6Ea**,

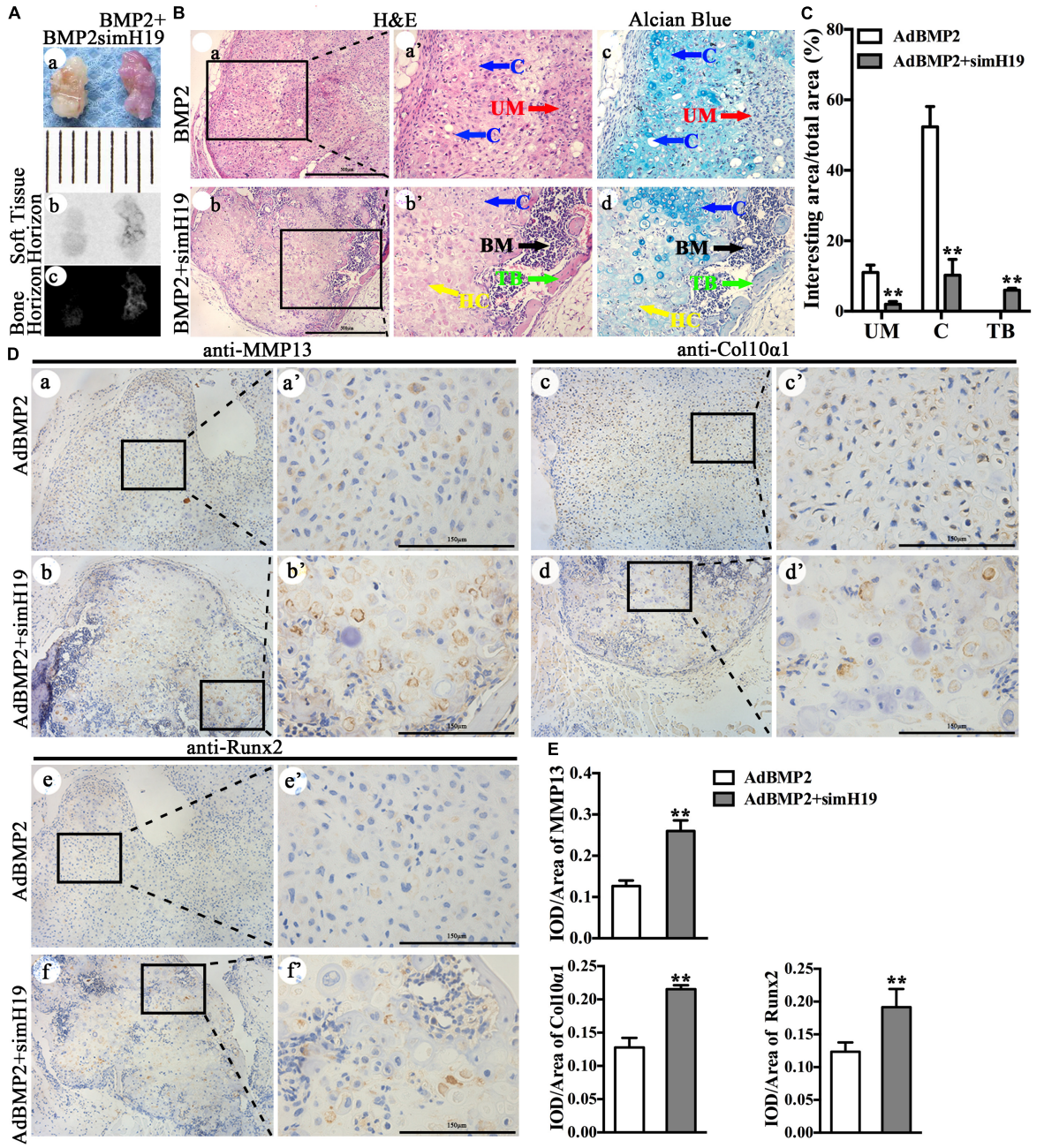

FIGURE 5 | Silencing of H19 promoted bone morphogenetic protein 2 (BMP2)-induced hypertrophic differentiation of mesenchymal stem cells (MSCs) *in vivo*. **(A)** C3H10T1/2 cells infected with AdGFP, AdBMP2, and/or AdsimH19 at the same infection ratio were injected subcutaneously into the flanks of athymic nude (nu/nu) mice for 3 weeks. There was no obvious differences in the morphological phenotype between the cartilaginous/bony masses formed in the AdBMP2 and AdBMP2 + AdSimH19 groups **(a)**, scale = 1 mm; the soft tissue horizon of the masses did not show and obvious difference between AdBMP2 and AdBMP2 + AdSimH19 groups through X-ray testing **(b)**, while the osseous composition in the AdBMP2 + AdSimH19 group was much more than that in the AdBMP2 group through X-ray testing **(c)**. **(B)** On histological examination, masses formed in the AdBMP2 group showed obvious chondrocytes and cartilaginous matrix **(a)**; however, except the chondrocytes and cartilaginous matrix, the masses formed in the AdBMP2 + AdSimH19 group formed obvious trabeculae combined with bone marrow like tissues **(b)**, which indicated the endochondral ossification. At higher magnification, H&E and the Alcian blue staining exhibited less cartilaginous matrix, more hypertrophic chondrocytes, and bone trabecular formation in the AdBMP2 + AdSimH19 group **(b',c")** compared with the AdBMP2 group **(a',a")**, scale bar = 500 μm. **(C)** Quantitative analysis of undifferentiated MSCs, chondrocytes, and trabecular bone. ImageJ was used to quantitatively analyze undifferentiated MSCs, chondrocytes, and trabecular bone. There were significantly more undifferentiated MSCs, more chondrocytes, and less trabecular bone formation in the AdBMP2 group compared with that in the AdBMP2 + AdSimH19 group. **(D)** The immunohistochemical staining was utilized to confirm the influence of silencing of H19 in BMP2-induced hypertrophic differentiation *in vivo*. The expression of Col10α1, MMP13, and Runx2 in the AdBMP2 group were less and weaken compared with the AdBMP2 + AdSimH19 group **(a,b,c,d,e,f; a',b',c',d',e',f')**. **(E)** Quantitative analysis of positive stained area. Integral optical density/area (IOD/Area) was calculated with Image Pro Plus software. Scale bar = 150 μm. UM, undifferentiated MSCs; C, chondrocytes; TB, trabecular bone. $^{**}p < 0.01$ compared with AdBMP2 group. Each assay was done in triplicate and/or carried out in three independent experiments at least; representative results are shown.

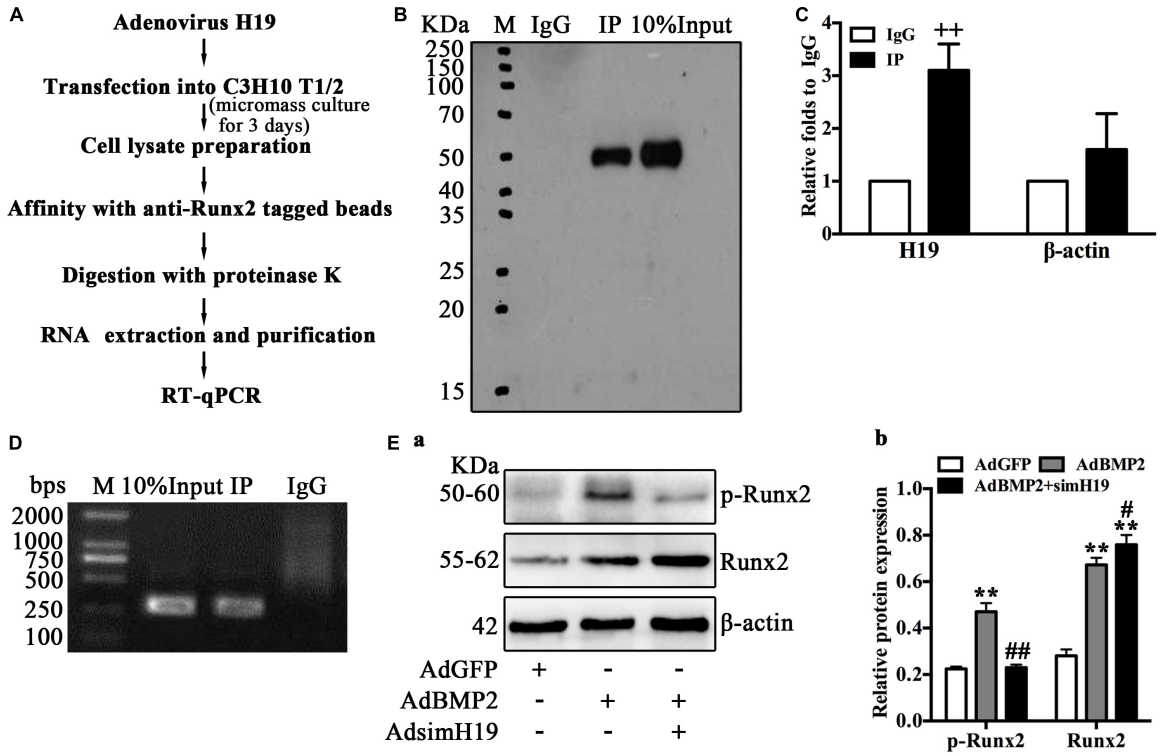

FIGURE 6 | H19 regulates bone morphogenetic protein 2 (BMP2)-induced hypertrophic differentiation of mesenchymal stem cells (MSCs) by promoting the phosphorylation of Runx2. **(A)** Schematic outline of purification of H19-associated ribonucleoprotein (RNPs) and RNA component identification. Briefly, RNA immunoprecipitation (RIP) was performed with mouse monoclonal anti-RUNX2 or preimmune immunoglobulin G (IgG) from extracts of C3H10 T1/2 cells infected with adenovirus expression H19 for 3 days. After immunoprecipitation, proteinase K was used for the enzymolysis of protein and RNA; then, total RNA was extracted, followed by reverse transcription and quantitative real-time PCR (RT-qPCR) and semiquantitative RT-PCR to analyze the combination. **(B)** Immunoprecipitation using anti-RUNX2 or IgG followed by Western blot analysis using a rabbit monoclonal anti-RUNX2. In addition, 10% input was loaded; molecular markers in kDa are on the left. **(C)** H19 levels in immunoprecipitates were determined by RT-qPCR. The levels of H19 and β-actin RNA are presented as fold enrichment in anti-RUNX2 relative to IgG immunoprecipitates. **(D)** Semiquantitative RT-PCR reaction was also used to detect H19 levels in immunoprecipitates, and the PCR products were resolved on 1% agarose gel. **(E)** To assay the posttranscriptional regulation of H19 on Runx2, Western blotting analysis of RUNX2 and phosphorylated RUNX2 expression were performed using a rabbit monoclonal antiphosphorylated RUNX2 (top) and rabbit monoclonal anti-RUNX2 (middle). In bottom, the β-actin was used as control. Molecular markers in kDa are on the left. Western blotting results were quantitatively analyzed by Image Lab software using β-actin as control **(b)** "*" and "**" respectively mean $p < 0.05$ and $p < 0.01$ compared with AdGFP group; "#" and "##" respectively mean $p < 0.05$ and $p < 0.01$ compared with AdBMP2 group; "++" means $p < 0.01$ compared with IgG group. Numbers are mean ± SD ($n = 3$).

BMP2 upregulated total Runx2 and phosphorylated Runx2. However, BMP2 induced upregulation of total Runx2 and was potentiated by silencing H19, and phosphorylated Runx2 was downregulated dramatically by silencing H19, which indicated that the phosphorylation of Runx2 was blocked with the silencing of H19. Quantitative analysis of the protein band confirmed this trend (**Figure 6Eb**). This phenomenon indicated that H19 was essential for the phosphorylation of Runx2. Taking these data together, we strongly speculate that H19-mediated phosphorylation of Runx2 regulated BMP2-induced hypertrophic differentiation of MSCs.

DISCUSSION

Cartilage tissue engineering is potential for the treatment of cartilage pathologies. BMP2 holds the potential to induce MSC chondrogenic differentiation. However, after the chondrocyte formation, BMP2 also stimulates hypertrophic differentiation, which blocks the construction of BMP2-mediated tissue engineering cartilage (Liao et al., 2014; Zhou et al., 2016). Hence, clarifying the mechanisms of BMP2-induced hypertrophic differentiation of MSCs is essential for further application of BMP2-mediated chondrogenic differentiation of MSCs. In the present study, we clarified that physiological expression level of H19 is essential for the phenotype maintaining of BMP2-induced chondrocytes of MSCs. Inhibiting of H19 promotes BMP2-mediated hypertrophic differentiation of MSCs; the mechanisms underlying these processes may be that H19 promotes the phosphorylation of Runx2, which blocks the function of Runx2. These findings applied a version for further construction of BMP2-mediated cartilage tissue engineering.

H19 is a maternal long non-coding RNA in the H19-IGF2 imprint locus, which is abundantly expressed during embryonic development and significantly downregulated after birth (Gabory et al., 2006; Gabory et al., 2009; Gabory et al.,

2010; Liu et al., 2017). Although the H19-IGF2 imprinting mechanism has been well clarified (Gabory et al., 2006; Liu et al., 2017), the regulatory functions and mechanisms of H19 in physical and pathological processes are still nebulous. More recently, H19 regulating stem cells differentiation were reported several times. Huang et al. (2016) found that H19 inhibits MSC adipocyte differentiation through epigenetic modulation of histone deacetylases, which indicates that sufficient expression of H19 is necessary to keep MSC osteogenic differentiation. Similarly Liang et al. (2016) characterized that H19 is essential for the osteogenic differentiation of MSCs; overexpression of H19 would accelerate the activation of Wnt/β-catenin pathway and further promote osteoblast differentiation. What is more, Huang et al. (2015) identified H19–miR675–TGF-β1–Smad3–HDAC pathway regulates human bone marrow mesenchymal stem cell (hMSC) osteogenic differentiation, which indicates the prodifferentiation effect of H19. What is interesting is that Dudek et al. (2010) found that the expression of H19 is regulated by key chondrogenic differentiation transcription factor Sox9, and type II collagen expression is regulated by H19-encoded miR675. These researches highly suggested the regulation function of H19 during the process of MSC osteogenic and/or chondrogenic differentiation. What is more, Pang et al. (2019) identified the regulatory function of H19 during MSCs cartilage differentiation. Hence, we focus on the regulatory functions of H19 in BMP2-mediated chondrogenic differentiation of MSCs. We first identified that H19 expression level was relatively high in the proliferative area of mice limb and downregulated in the hypertrophic area of mice limb, which further confirmed the potential role of H19 in promoting cartilage formation. Second, we identified that, with the stimulation of BMP2, peak expression level of H19 was followed after the crest expression of Sox9, which was consistent with the previous study (Dudek et al., 2010). Our further analysis demonstrated that H19 expression level not only positively correlated with the expression level of Sox9 and chondrogenic differentiation markers (Col2α1 and Aggrecan) in the late stage of BMP2 stimulation but also negatively correlated with the expression level of hypertrophic differentiation markers (MMP13, Adamts5, and Runx2). These data indicate that H19 may also function in BMP2-stimulated hypertrophic differentiation, and this hypothesis was identified by our further *in vitro* and *in vivo* tests. To the best of our knowledge, this is the first time to report the regulation function of H19 in hypertrophic differentiation of cartilage. Taken the previous studies and this study together (Dudek et al., 2010; Pang et al., 2019), we deduce that H19 may play a role in cartilage differentiation, cartilage phenotype maintaining, and cartilage hypertrophic differentiation. Hence, appropriate expression level of H19 is essential for the construction of MSC-based cartilage engineering.

Recombinant human bone morphogenetic protein 2 (rhBMP-2) has been approved for treating acute, open tibial shaft fractures and spinal fusion by the Food and Drug Administration (FDA) (Woo, 2013). Our previous work also identified BMP2-induced chondrogenic differentiation of MSCs. However, the mechanisms underlying BMP2-mediated hypertrophic differentiation are far from being clarified. Hypertrophic differentiation following with endochondral ossification is a consecutive process (Hata et al., 2017). In the present study, we first proved that silencing H19 upregulated hypertrophic differentiation markers expression. Second, we confirmed that silencing H19 facilitated BMP2-mediated hypertrophic differentiation and subsequently potentiated BMP2-induced trabecular and bone-marrow-like tissue formation *in vivo*. These data suggested that BMP2-mediated hypertrophic differentiation was regulated by H19. On the other hand, as the key transcription factor of hypertrophic differentiation, Runx2 promotes the maturity of chondrocytes and subsequently regulates hypertrophic differentiation (Jonason et al., 2009; Takeda et al., 2001; Ueta et al., 2001). Hence, clarifying the regulating relation between Runx2 and H19 is extremely urgent for further understanding the mechanisms underlying BMP2-induced hypertrophic differentiation of MSCs. Here, we identified that silencing H19 upregulated the expression of total Runx2 protein level but diminished phosphorylated Runx2 protein level. These results indicated the posttranscriptional regulation function of H19 on Runx2 phosphorylation.

As a novel and effective modulator, H19 was reported to regulate physical and pathological processes in different ways (Zhang et al., 2017). Except as a transregulator of a group of coexpressed genes belonging to the imprinted gene network (Gabory et al., 2010; Lee et al., 2015; Ripoche et al., 1997), H19 also encodes highly reserved microRNA miR675 with exon-1 (Keniry et al., 2012; Raveh et al., 2015; Steck et al., 2012). Meanwhile, lncRNAH19 and miR675 regulate specific biological processes synergistically (Dudek et al., 2010; Muller et al., 2019; Steck et al., 2012). In addition, H19 was identified as a ceRNA that sponged microRNAs and then regulate gene function. For example, H19 antagonizing let-7 microRNA family members (Cao et al., 2019; Kallen et al., 2013), miR-93-5p (Li et al., 2019), miR-17-5p (Liu et al., 2016), miR-107 (Qian et al., 2018), etc. was reported, respectively. Our previous work also found that H19 regulated the expression of microRNAs, which targets Notch signaling pathway (Liao et al., 2017b). What is more, H19 can act as a molecular scaffold to bind with mRNA, then regulate the decay of mRNA (Giovarelli et al., 2014). As for the posttranscriptional regulation, H19 can act as a modular scaffold of histone modification complexes (Tsai et al., 2010). In this study, we inferred the regulation of H19 on the function of Runx2 and first confirmed the combination of H19 and Runx2 through RIP analysis. Then, we identified that silencing H19 could downregulate the phosphorylation of Runx2, which would promote the function of Runx2. Hence, we deduced that H19-mediated phosphorylation of Runx2 regulated BMP2-induced hypertrophic differentiation of MSCs. As an exotic lncRNA, H19 antisense named 91H RNA also reported to play an important role in modulating H19-Igf2 expression, although the exact mechanism remains to be fully understood (Berteaux et al., 2008; Tran et al., 2012). Hence, it is important to further investigate the function of 91H RNA during the process of BMP2-mediated hypertrophic differentiation of MSCs. In addition, on the basis of the current study, it is reasonable to speculate that overexpression of H19 may be beneficial for BMP2-mediated cartilage tissue engineering, which was indicated

by Pang et al. (2019). However, as a multifunctional lncRNA, H19 may affect BMP2-mediated chondrogenic differentiation of MSCs and hypertrophic differentiation of cartilage by one or more other mechanisms, such as CeRNA mechanism. Therefore, further *in vivo* cartilage repair test is necessary for identifying the potential of overexpression of H19 for cartilage defect repairing.

In summary, clarifying the mechanisms of hypertrophic differentiation is essential for the construction of BMP2-mediated cartilage tissue engineering. Although several studies have been carried out, the details in regulating BMP2-stimulated hypertrophic differentiation are far from being illuminated. Here, in the aspect of lncRNA, we identified the posttranscriptional regulating function of H19 on Runx2-mediated hypertrophic differentiation, which should be helpful for further construction of BMP2-mediated cartilage engineering.

DATA AVAILABILITY STATEMENT

All datasets generated for this study are included in the article/**Supplementary Material**.

ETHICS STATEMENT

The animal study was reviewed and approved by the Ethical Committee of The First Affiliated Hospital of Chongqing Medical University.

AUTHOR CONTRIBUTIONS

WH and JL conceived and designed the experiments. GD, JL, HX, and CZ performed the experiments and collected the data. JL, WH, and HC analyzed the data. JL and WH contributed the reagents, materials, and analysis tools. JL, WH, and GD wrote the manuscript. All authors read and approved the manuscript.

FUNDING

The reported work was supported by the National Natural Science Foundation of China (NSFC) (nos. 81371972, 81572142, and 81972069). This project was also supported by the Natural Science Foundation of Chongqing Science and Technology Commission (nos. cstc2018jcyjAX0088 and cstc2017shmsA0787), Major Project of Chongqing Health and Family Planning Commission (no. 2015-1-12), Cultivating Program of The First Affiliated Hospital of Chongqing Medical University (no. 2018PYJJ-11), and Pre-NSFC research program of Chongqing Medical University. JL was a recipient of the Predoctoral Fellowship from the China Scholarship Council, the Graduate Research and Innovation Project from Chongqing Education Commission, and the Outstanding Predoctorate Research Fellowship from Chongqing Medical University (no. CYB15098). Funding sources were not involved in the study design, in the collection, analysis, and interpretation of data; in writing of the report; and in the decision to submit the paper for publication.

ACKNOWLEDGMENTS

We would like to thank Molecular Oncology Laboratory, Medical Center, The University of Chicago, for the use of AdBMP2, AdH19, AdsimH19, and AdGFP.

SUPPLEMENTARY MATERIAL

The Supplementary Material for this article can be found online at: https://www.frontiersin.org/articles/10.3389/fcell.2020.00580/full#supplementary-material

FIGURE S1 | (A) FISH analysis positive control. **(B)** Negative control of IHC.

REFERENCES

An, C., Cheng, Y., Yuan, Q., and Li, J. (2010). IGF-1 and BMP-2 induces differentiation of adipose-derived mesenchymal stem cells into chondrocytes-like cells. *Ann. Biomed. Eng.* 38, 1647–1654. doi: 10.1007/s10439-009-9892-x

Berteaux, N., Aptel, N., Cathala, G., Genton, C., Coll, J., Daccache, A., et al. (2008). A novel H19 antisense RNA overexpressed in breast cancer contributes to paternal IGF2 expression. *Mol. Cell. Biol.* 28, 6731–6745. doi: 10.1128/mcb.02103-07

Bishop, E. S., Mostafa, S., Pakvasa, M., Luu, H. H., Lee, M. J., Wolf, J. M., et al. (2017). 3-D bioprinting technologies in tissue engineering and regenerative medicine: current and future trends. *Genes Dis.* 4, 185–195. doi: 10.1016/j.gendis.2017.10.002

Cai, X., and Cullen, B. R. (2007). The imprinted H19 noncoding RNA is a primary microRNA precursor. *RNA* 13, 313–316. doi: 10.1261/rna.351707

Canadas, R. F., Pirraco, R. P., Oliveira, J. M., Reis, R. L., and Marques, A. P. (2018). Stem cells for osteochondral regeneration. *Adv. Exp. Med. Biol.* 1059, 219–240. doi: 10.1007/978-3-319-76735-2_10

Cao, L., Zhang, Z., Li, Y., Zhao, P., and Chen, Y. (2019). LncRNA H19/miR-let-7 axis participates in the regulation of ox-LDL-induced endothelial cell injury via targeting periostin. *Intern. Immunopharmacol.* 72, 496–503. doi: 10.1016/j.intimp.2019.04.042

Clark, M. B., Amaral, P. P., Schlesinger, F. J., Dinger, M. E., Taft, R. J., Rinn, J. L., et al. (2011). The reality of pervasive transcription. *PLoS Biol.* 9:e1000625. doi: 10.1371/journal.pbio.1000625

Deng, F., Chen, X., Liao, Z., Yan, Z., Wang, Z., Deng, Y., et al. (2014). A simplified and versatile system for the simultaneous expression of multiple siRNAs in mammalian cells using Gibson DNA Assembly. *PLoS One* 9:e113064. doi: 10.1371/journal.pbio.113064

Djebali, S., Davis, C. A., Merkel, A., Dobin, A., Lassmann, T., Mortazavi, A., et al. (2012). Landscape of transcription in human cells. *Nature* 489, 101–108.

Dudek, K. A., Lafont, J. E., Martinez-Sanchez, A., and Murphy, C. L. (2010). Type II collagen expression is regulated by tissue-specific miR-675 in human articular chondrocytes. *J. Biol. Chem.* 285, 24381–24387. doi: 10.1074/jbc.m110.111328

Gabory, A., Jammes, H., and Dandolo, L. (2010). The H19 locus: role of an imprinted non-coding RNA in growth and development. *Bioessays* 32, 473–480. doi: 10.1002/bies.200900170

Gabory, A., Ripoche, M. A., Digarcher, A. Le, Watrin, F., Ziyyat, A., Forne, T., et al. (2009). H19 acts as a trans regulator of the imprinted gene network controlling growth in mice. *Development* 136, 3413–3421. doi: 10.1242/dev.036061

Gabory, A., Ripoche, M. A., Yoshimizu, T., and Dandolo, L. (2006). The H19 gene: regulation and function of a non-coding RNA. *Cytogenet. Genome Res.* 113, 188–193. doi: 10.1159/000090831

Giovarelli, M., Bucci, G., Ramos, A., Bordo, D., Wilusz, C. J., Chen, C. Y., et al. (2014). H19 long noncoding RNA controls the mRNA decay promoting function of KSRP. *Proc. Natl. Acad. Sci. U.S.A.* 111, E5023–E5028.

Hao, Y., Crenshaw, T., Moulton, T., Newcomb, E., and Tycko, B. (1993). Tumour-suppressor activity of H19 RNA. *Nature* 365, 764–767. doi: 10.1038/365764a0

Hata, K., Takahata, Y., Murakami, T., and Nishimura, R. (2017). Transcriptional network controlling endochondral ossification. *J. Bone Metab.* 24, 75–82.

He, T. C., Zhou, S., da Costa, L. T., Yu, J., Kinzler, K. W., and Vogelstein, B. (1998). A simplified system for generating recombinant adenoviruses. *Proc. Natl. Acad. Sci. U.S.A.* 95, 2509–2514. doi: 10.1073/pnas.95.5.2509

Huang, Y., Zheng, Y., Jia, L., and Li, W. (2015). Long noncoding RNA H19 promotes osteoblast differentiation via TGF-beta1/Smad3/HDAC signaling pathway by deriving miR-675. *Stem Cells* 33, 3481–3492. doi: 10.1002/stem.2225

Huang, Y., Zheng, Y., Jin, C., Li, X., Jia, L., and Li, W. (2016). Long non-coding RNA H19 inhibits adipocyte differentiation of bone marrow mesenchymal stem cells through epigenetic modulation of histone deacetylases. *Sci. Rep.* 6:28897.

Jonason, J. H., Xiao, G., Zhang, M., Xing, L., and Chen, D. (2009). Post-translational regulation of Runx2 in bone and cartilage. *J. Dent. Res.* 88, 693–703. doi: 10.1177/0022034509341629

Kallen, A. N., Zhou, X. B., Xu, J., Qiao, C., Ma, J., Yan, L., et al. (2013). The imprinted H19 lncRNA antagonizes let-7 microRNAs. *Mol. Cell* 52, 101–112. doi: 10.1016/j.molcel.2013.08.027

Keniry, A., Oxley, D., Monnier, P., Kyba, M., Dandolo, L., Smits, G., et al. (2012). The H19 lincRNA is a developmental reservoir of miR-675 that suppresses growth and Igf1r. *Nat. Cell Biol.* 14, 659–665. doi: 10.1038/ncb2521

Kim, H., Yang, G., Park, J., Choi, J., Kang, E., and Lee, B. K. (2019). Therapeutic effect of mesenchymal stem cells derived from human umbilical cord in rabbit temporomandibular joint model of osteoarthritis. *Sci. Rep.* 9:13854.

Kim, T. K., and Shiekhattar, R. (2016). Diverse regulatory interactions of long noncoding RNAs. *Curr. Opin. Genet. Dev.* 36, 73–82. doi: 10.1016/j.gde.2016.03.014

Kovermann, N. J., Basoli, V., Della Bella, E., Alini, M., Lischer, C., Schmal, H., et al. (2019). BMP2 and TGF-beta cooperate differently during synovial-derived stem-cell chondrogenesis in a dexamethasone-dependent manner. *Cells* 8:636. doi: 10.3390/cells8060636

Lee, C. S., Bishop, E. S., Zhang, R., Yu, X., Farina, E. M., Yan, S., et al. (2017). Delivery: potential applications for gene and cell-based therapies in the new era of personalized medicine. *Genes Dis.* 4, 43–63. doi: 10.1016/j.gendis.2017.04.001

Lee, D. F., Su, J., Kim, H. S., Chang, B., Papatsenko, D., Zhao, R., et al. (2015). Modeling familial cancer with induced pluripotent stem cells. *Cell* 161, 240–254.

Li, D. Y., Busch, A., Jin, H., Chernogubova, E., Pelisek, J., Karlsson, J., et al. (2018). H19 induces abdominal aortic aneurysm development and progression. *Circulation* 138, 1551–1568.

Li, J. P., Xiang, Y., Fan, L. J., Yao, A., Li, H., and Liao, X. H. (2019). Long noncoding RNA H19 competitively binds miR-93-5p to regulate STAT3 expression in breast cancer. *J. Cell. Biochem.* 120, 3137–3148. doi: 10.1002/jcb.27578

Liang, W. C., Fu, W. M., Wang, Y. B., Sun, Y. X., Xu, L. L., Wong, C. W., et al. (2016). H19 activates Wnt signaling and promotes osteoblast differentiation by functioning as a competing endogenous RNA. *Sci. Rep.* 6:20121.

Liao, J., Hu, N., Zhou, N., Lin, L., Zhao, C., Yi, S., et al. (2014). Sox9 potentiates BMP2-induced chondrogenic differentiation and inhibits BMP2-induced osteogenic differentiation. *PLoS One* 9:e89025. doi: 10.1371/journal.pbio.89025

Liao, J., Wei, Q., Zou, Y., Fan, J., Song, D., Cui, J., et al. (2017a). Augments BMP9-induced bone formation by promoting the osteogenesis-angiogenesis coupling process in mesenchymal stem cells (MSCs). *Cell. Physiol. Biochem.* 41, 1905–1923. doi: 10.1159/000471945

Liao, J., Yu, X., Hu, X., Fan, J., Wang, J., Zhang, Z., et al. (2017b). lncRNA H19 mediates BMP9-induced osteogenic differentiation of mesenchymal stem cells (MSCs) through notch signaling. *Oncotarget* 8, 53581–53601. doi: 10.18632/oncotarget.18655

Liu, L., Yang, J., Zhu, X., Li, D., Lv, Z., and Zhang, X. (2016). Long noncoding RNA H19 competitively binds miR-17-5p to regulate YES1 expression in thyroid cancer. *FEBS J.* 283, 2326–2339. doi: 10.1111/febs.13741

Liu, Y., Li, G., and Zhang, J. F. (2017). The role of long non-coding RNA H19 in musculoskeletal system: a new player in an old game. *Exper. Cell Res.* 360, 61–65. doi: 10.1016/j.yexcr.2017.09.007

Luo, J., Deng, Z. L., Luo, X., Tang, N., Song, W. X., Chen, J., et al. (2007). A protocol for rapid generation of recombinant adenoviruses using the AdEasy system. *Nat. Protoc.* 2, 1236–1247. doi: 10.1038/nprot.2007.135

Mamidi, M. K., Das, A. K., Zakaria, Z., and Bhonde, R. (2016). Mesenchymal stromal cells for cartilage repair in osteoarthritis. *Osteoarthr. Cartil.* 24, 1307–1316. doi: 10.1016/j.joca.2016.03.003

Miyazono, K., Kamiya, Y., and Morikawa, M. (2010). Bone morphogenetic protein receptors and signal transduction. *J. Biochem.* 147, 35–51. doi: 10.1093/jb/mvp148

Morris, K. V., and Mattick, J. S. (2014). The rise of regulatory RNA. *Nat. Rev. Genet.* 15, 423–437. doi: 10.1038/nrg3722

Moulton, T., Crenshaw, T., Hao, Y., Moosikasuwan, J., Lin, N., Dembitzer, F., et al. (1994a). Epigenetic changes encompassing the IGF2H19 locus associated with relaxation of IGF2 imprinting and silencing of H19 in Wilms tumor. *Proc. Natl. Acad. Sci. U.S.A.* 92, 2159–2163. doi: 10.1073/pnas.92.6.2159

Moulton, T., Crenshaw, T., Hao, Y., Moosikasuwan, J., Lin, N., Dembitzer, F., et al. (1994b). Epigenetic lesions at the H19 locus in Wilms' tumour patients. *Nat. Genet.* 7, 440–447. doi: 10.1038/ng0794-440

Muller, V., Oliveira-Ferrer, L., Steinbach, B., Pantel, K., and Schwarzenbach, H. (2019). Interplay of lncRNA H19/miR-675 and lncRNA NEAT1/miR-204 in breast cancer. *Mol. Oncol.* 13, 1137–1149. doi: 10.1002/1878-0261.12472

Munsell, E. V., Kurpad, D. S., Freeman, T. A., and Sullivan, M. O. (2018). Histone-targeted gene transfer of bone morphogenetic protein-2 enhances mesenchymal stem cell chondrogenic differentiation. *Acta Biomater.* 71, 156–167. doi: 10.1016/j.actbio.2018.02.021

Nasrabadi, D., Rezaeiani, S., Eslaminejad, M. B., and Shabani, A. (2018). Improved protocol for chondrogenic differentiation of bone marrow derived mesenchymal stem cells -effect of PTHrP and FGF-2 on TGFbeta1/BMP2-induced chondrocytes hypertrophy. *Stem Cell Rev.* 14, 755–766. doi: 10.1007/s12015-018-9816-y

Pan, Q., Yu, Y., Chen, Q., Li, C., Wu, H., Wan, Y., et al. (2008). Sox9, a key transcription factor of bone morphogenetic protein-2-induced chondrogenesis, is activated through BMP pathway and a CCAAT box in the proximal promoter. *J. Cell. Physiol.* 217, 228–241. doi: 10.1002/jcp.21496

Pang, H. L., Zhao, Q. Q., Ma, Y., Song, Y. L., Min, J., Lu, J. R., et al. (2019). Long noncoding RNA H19 participates in the regulation of adipose-derived stem cells cartilage differentiation. *Stem Cells Int.* 2019:2139814.

Pettersson, E., Lundeberg, J., and Ahmadian, A. (2009). Generations of sequencing technologies. *Genomics* 93, 105–111. doi: 10.1016/j.ygeno.2008.10.003

Qi, D., Wang, M., and Yu, F. (2019). Knockdown of lncRNA-H19 inhibits cell viability, migration and invasion while promotes apoptosis via microRNA-143/RUNX2 axis in retinoblastoma. *Biomed. Pharmacother.* 109, 798–805. doi: 10.1016/j.biopha.2018.10.096

Qian, B., Wang, D. M., Gu, X. S., Zhou, K., Wu, J., Zhang, C. Y., et al. (2018). LncRNA H19 serves as a ceRNA and participates in non-small cell lung cancer development by regulating microRNA-107. *Eur. Rev. Med. Pharmacol. Sci.* 22, 5946–5953.

Quinn, J. J., and Chang, H. Y. (2016). Unique features of long non-coding RNA biogenesis and function. *Nat. Rev. Genet.* 17, 47–62. doi: 10.1038/nrg.2015.10

Raveh, E., Matouk, I. J., Gilon, M., and Hochberg, A. (2015). The H19 Long non-coding RNA in cancer initiation, progression and metastasis - a proposed unifying theory. *Mol. Cancer* 14:184.

Ripoche, M. A., Kress, C., Poirier, F., and Dandolo, L. (1997). Deletion of the H19 transcription unit reveals the existence of a putative imprinting control element. *Genes Dev.* 11, 1596–1604. doi: 10.1101/gad.11.12.1596

Sanbonmatsu, K. Y. (2016). Towards structural classification of long non-coding RNAs. *Biochim. Biophys. Acta* 1859, 41–45. doi: 10.1016/j.bbagrm.2015.09.011

Steck, E., Boeuf, S., Gabler, J., Werth, N., Schnatzer, P., Diederichs, S., et al. (2012). Regulation of H19 and its encoded microRNA-675 in osteoarthritis and under anabolic and catabolic in vitro conditions. *J. Mol. Med.* 90, 1185–1195. doi: 10.1007/s00109-012-0895-y

Takeda, S., Bonnamy, J. P., Owen, M. J., Ducy, P., and Karsenty, G. (2001). Continuous expression of Cbfa1 in nonhypertrophic chondrocytes uncovers its ability to induce hypertrophic chondrocyte differentiation and partially rescues Cbfa1-deficient mice. *Genes Dev.* 15, 467–481. doi: 10.1101/gad.845101

Tran, V. G., Court, F., Duputie, A., Antoine, E., Aptel, N., Milligan, L., et al. (2012). H19 antisense RNA can up-regulate Igf2 transcription by activation of a novel promoter in mouse myoblasts. *PLoS One* 7:e37923. doi: 10.1371/journal.pbio.37923

Tsai, M. C., Manor, O., Wan, Y., Mosammaparast, N., Wang, J. K., Lan, F., et al. (2010). Long noncoding RNA as modular scaffold of histone modification complexes. *Science* 329, 689–693. doi: 10.1126/science.1192002

Ueta, C., Iwamoto, M., Kanatani, N., Yoshida, C., Liu, Y., Enomoto-Iwamoto, M., et al. (2001). Skeletal malformations caused by overexpression of Cbfa1 or its dominant negative form in chondrocytes. *J. Cell Biol.* 153, 87–100. doi: 10.1083/jcb.153.1.87

Wang, A. T., Feng, Y., Jia, H. H., Zhao, M., and Yu, H. (2019). Application of mesenchymal stem cell therapy for the treatment of osteoarthritis of the knee: a concise review. *World J. Stem Cells* 11, 222–235. doi: 10.4252/wjsc.v11.i4.222

Woo, E. J. (2013). Adverse events after recombinant human BMP2 in nonspinal orthopaedic procedures. *Clin. Orthop. Relat. Res.* 471, 1707–1711. doi: 10.1007/s11999-012-2684-x

Yuan, J.-H., Yang, F., Wang, F., Ma, J.-Z., Guo, Y.-J., Tao, Q.-F., et al. (2014). RNA activated by TGF-β promotes the invasion-metastasis cascade in hepatocellular carcinoma. *Cancer Cell* 25, 666–681. doi: 10.1016/j.ccr.2014.03.010

Zhang, L., Zhou, Y., Huang, T., Cheng, A. S., Yu, J., Kang, W., et al. (2017). The interplay of LncRNA-H19 and its binding partners in physiological process and gastric carcinogenesis. *Intern. J. Mol. Sci.* 18:450. doi: 10.3390/ijms18020450

Zhou, N., Hu, N., Liao, J. Y., Lin, L. B., Zhao, C., Si, W. K., et al. (2015). HIF-1alpha as a regulator of BMP2-induced chondrogenic differentiation, osteogenic differentiation, and endochondral ossification in stem cells. *Cell. Physiol. Biochem.* 36, 44–60. doi: 10.1159/000374052

Zhou, N., Li, Q., Lin, X., Hu, N., Liao, J. Y., Lin, L. B., et al. (2016). BMP2 induces chondrogenic differentiation, osteogenic differentiation and endochondral ossification in stem cells. *Cell Tissue Res.* 366, 101–111. doi: 10.1007/s00441-016-2403-0

Conflict of Interest: The authors declare that the research was conducted in the absence of any commercial or financial relationships that could be construed as a potential conflict of interest.

frontiers in Cell and Developmental Biology

ORIGINAL RESEARCH
published: 31 July 2020
doi: 10.3389/fcell.2020.00694

Autologous Fractionated Adipose Tissue as a Natural Biomaterial and Novel One-Step Stem Cell Therapy for Repairing Articular Cartilage Defects

Qi Li, Fengyuan Zhao, Zong Li, Xiaoning Duan, Jin Cheng, Jiahao Zhang, Xin Fu, Jiying Zhang, Zhenxing Shao, Qinwei Guo, Xiaoqing Hu and Yingfang Ao**

Institute of Sports Medicine, Beijing Key Laboratory of Sports Injuries, Peking University Third Hospital, Beijing, China

OPEN ACCESS

Edited by:
Katiucia Batista Silva Paiva, University of São Paulo, Brazil

Reviewed by:
Francesco De Francesco, Azienda Ospedaliero Universitaria Ospedali Riuniti, Italy
Ming Pei, West Virginia University, United States
Michael Doran, Queensland University of Technology, Australia

***Correspondence:**
Yingfang Ao
aoyingfang@163.com
Xiaoqing Hu
huxiaoqingbd01@sina.com

Specialty section:
This article was submitted to Stem Cell Research, a section of the journal Frontiers in Cell and Developmental Biology

Received: *02 April 2020*
Accepted: *08 July 2020*
Published: *31 July 2020*

Citation:
Li Q, Zhao F, Li Z, Duan X, Cheng J, Zhang J, Fu X, Zhang J, Shao Z, Guo Q, Hu X and Ao Y (2020) Autologous Fractionated Adipose Tissue as a Natural Biomaterial and Novel One-Step Stem Cell Therapy for Repairing Articular Cartilage Defects. Front. Cell Dev. Biol. 8:694. doi: 10.3389/fcell.2020.00694

Articular cartilage damage remains a tough challenge for clinicians. Stem cells have emerged promising biologics in regenerative medicine. Previous research has widely demonstrated that adipose-derived mesenchymal stem cells (ADSCs) can promote cartilage repair due to their multipotency. However, enzymatic isolation and monolayer expansion of ADSCs decrease their differentiation potential and limit their clinical application. Here, a novel adipose tissue-derived product, extracellular matrix/stromal vascular fraction gel (ECM/SVF-gel), was obtained by simple mechanical shifting and centrifugation to separate the fat oil and concentrate the effective constituents. This study aimed to evaluate the therapeutic effect of this natural biomaterial on the repair of articular cartilage defects. Scanning electron microscopy showed that the fibrous structure in the ECM/SVF-gel was preserved. ADSCs sprouted from the ECM/SVF-gel were characterized by their ability of differentiation into chondrocytes, osteoblasts, and adipocytes. In a rabbit model, critical-sized cartilage defects (diameter, 4 mm; depth, 1.5 mm) were created and treated with microfracture (MF) or a combination of autologous ECM/SVF-gel injection. The knee joints were evaluated at 6 and 12 weeks through magnetic resonance imaging, macroscopic observation, histology, and immunohistochemistry. The International Cartilage Repair Society score and histological score were significantly higher in the ECM/SVF-gel group than those in the MF-treated group. The ECM/SVF-gel distinctly improved cartilage regeneration, integration with surrounding normal cartilage, and the expression of hyaline cartilage marker, type II collagen, in comparison with the MF treatment alone. Overall, the ready-to-use ECM/SVF-gel is a promising therapeutic strategy to facilitate articular cartilage regeneration. Moreover, due to the simple, time-sparing, cost-effective, enzyme-free, and minimally invasive preparation process, this gel provides a valuable alternative to stem cell-based therapy for clinical translation.

Keywords: adipose tissue, stem cell, stromal vascular fraction, cartilage regeneration, natural biomaterial

INTRODUCTION

Articular cartilage defects in the knee joint are a common clinical problem, which can result in severe pain, joint swelling, substantial reduction in mobility, further joint deterioration, and progression towards osteoarthritis (Dai et al., 2014; Kwon et al., 2019). Due to its avascular and aneural nature with low cellularity, articular cartilage is difficult to self-heal. The current clinical and pre-clinical strategies for cartilage tissue regeneration mainly include microfracture (MF), autologous chondrocyte implantation (ACI), stem cell therapy, autologous cartilage chip (ACC), allograft cartilage, and scaffold-based tissue engineering techniques (Makris et al., 2015). However, each treatment has some limitations. The clinical outcomes of MF and ACI in a large number of cases show that the fibrocartilage tissue formed and its biomechanical properties are inferior to those of native articular cartilage (Bianchi et al., 2019). Cell-based therapy including ACI and stem cell implantation consists of two stages: primary cell culture and *ex vivo* expansion for a large quantity, and the implantation procedure. Furthermore, dedifferentiation and senescence during cell expansion, high costs, long wait times, and two-stage operation limit their wide clinical use. ACC and allografts such as the recently reported particulate juvenile allograft cartilage, have been proven to have a good repair effect; however, donor-site complications or tissue source are major limitations (Ao et al., 2019). To date, none of these treatments are able to fully restore injured articular cartilage (Wang X. et al., 2019).

In the past two decades, mesenchymal stem cells (MSCs) have been considered one of the most promising treatments for cartilage injuries due to their self-renewal capability, high plasticity, and immunosuppressive, anti-inflammatory action, and multipotent differentiation ability into selected lineages including chondrocytes (Kondo et al., 2019). First described in 2001, MSCs derived from adipose (ADSCs) were found to be superior candidate due to their easy acquisition and good regenerative effect (Cui et al., 2009). Recently, a cohort study demonstrated comparable clinical outcomes of the stromal vascular fraction (SVF) isolated from adipose tissue without primary culture and further expansion, with ADSCs for the treatment of knee osteoarthritis (Yokota et al., 2019). Since 2006, the US FDA has promulgated regulations to prevent the risk of transmitting contamination or genetic damage from stem cells (Halme and Kessler, 2006). Preparation of both ADSCs and SVF requires the process of exogenous enzymatic digestion, increasing the potential risk of infection and requiring a rigorous approval process before clinical application. Therefore, an enzyme-free method with minimal manipulation for ADSCs or SVF needs to be developed. Actually, adipose tissue is a source of stem cells niche (Berry et al., 2016), and provides a native scaffold consisting of extracellular matrix (ECM) elements that support structural architecture and biological function (Yu et al., 2013). Based on this principle, researchers have developed nanofat from lipoaspirate grafting between two syringes, and micro-fragmented adipose tissue from a commercial device kit. Recently, these have shown attractive potential in regenerative medicine including promotion of wound healing (Yao et al., 2017; Lonardi et al., 2019), improving ischemic flap survival (Zhang et al., 2018), and remolding bone tissue formation (Guerrero et al., 2018). However, it is still unclear whether autologous fractionated adipose tissue can provide new treatment options to repair articular cartilage defects.

In this study, autologous adipose tissue was mechanically processed and centrifuged to form a novel ready-to-use ECM/SVF-gel with a short preparation time without enzymatic digestion, additional cell expansion, or other complex manipulations. The ECM/SVF-gel could provide a three-dimensional ECM environment as well as intrinsic ADSCs for the regeneration of hyaline-like cartilage. To the best of our knowledge, this is the first attempt to investigate autologous fractionated adipose tissue with a novel and simple enzyme-free technique for cartilage tissue engineering. We hypothesized that the ECM/SVF-gel would promote cartilage repair compared to the conventional MF treatment alone.

MATERIALS AND METHODS

Animals

This study was approved by the Peking University Biomedical Ethics Committee. All animals were purchased from Peking University Animal Administration Center and all procedures were performed according to the guidelines for the Care and Use of Laboratory Animals (National Academies Press, National Institutes of Health Publication No. 85-23, revised 1996). Adult male New Zealand white rabbits weighing 2.7–3.2 kg (5–6 months) were housed individually with free access to diet and activities.

ECM/SVF-Gel Preparation

The ECM/SVF-gel was prepared as described previously, with some modifications (Yao et al., 2017). Briefly, rabbits were anesthetized by isoflurane inhalation. Their inguinal area was shaved and prepared for aseptic surgery. In total, approximately 5 mL of inguinal adipose tissue was collected and finely minced using ophthalmic scissors. Minced fat tissue was then transferred to two10-mL syringes connected by a Luer-Lock connector with an internal diameter of 2 mm. After mechanical shifting for 90 times, the emulsified fat was filtered to remove the connective tissue remnants and was centrifuged at 2000 × *g* for 3 min. The sticky mixture below the oil layer was defined as the ECM/SVF-gel and was collected for further use.

Rheological Test

To verify the physical properties of the ECM/SVF-gel, rheological test was carried out on a rheometer (HAAKE MARS III, Thermo Fisher Scientific, Karlsruhe, Germany). The storage modulus G′ and loss modulus G″ of the ECM/SVF-gel were measured through frequency sweep analysis. The frequency range was set from 0.1 to 10 Hz at 20 Pa. Three batches of samples were performed with an average of triplicate measurements in each data point.

Cartilage Defect Model

The cartilage defect model was established as previously described (Shi et al., 2017). The left or right knee joints of thirty rabbits were randomly treated with MF (MF group) or combined with autologous ECM/SVF-gel injection (ECM/SVF-gel group). The MF group served as the control group because MF currently is the most commonly used treatment strategy for cartilage injury (Man et al., 2016). For the ECM/SVF-gel group, the autologous ECM/SVF-gel was prepared as described above. Then, an incision was made on the knee from the lateral side under aseptic conditions and the joint was exposed after the patella was dislocated. Then, a cylindrical defect (4-mm diameter, 1.5-mm depth) was created on the trochlear groove of the distal femur using corneal trephine. Afterwards, standard MF treatment or a combination of 0.1 mL autologous ECM/SVF-gel injection was performed at the defect site. Three MF holes (diameter 0.8 mm, depth 2 mm) were performed and evenly distributed within the defect. Finally, the joint was closed with a suture; penicillin was administered intramuscularly for 3 days to avoid infection. All rabbits were kept in their individual cages with free access to food and water before they were sacrificed at 6 weeks or 12 weeks post-operation.

Cell Culture and Multilineage Differentiation

The ECM/SVF-gel was allowed to attach to 25 cm^2 culture flasks containing Minimum Essential Medium-alpha (Gibco, Grand Island, NY, United States) supplemented with 10% fetal bovine serum and 1% penicillin/streptomycin (100 units/ml penicillin and 100 μg/ml streptomycin). The culture flasks were maintained at 37°C in a humidified incubator containing 5% CO_2 with the culture medium changed every 3 days. When the cells reached 90% confluence, they were harvested for multi-lineage differentiation assays including adipogenesis, osteogenesis, and chondrogenesis as described previously (Hu et al., 2015). Briefly, ADSCs were seeded in a 6-well plate at a density of 1.0×10^5 cells/well with adipogenic or osteogenic differentiation medium (Cyagen Biosciences, Guangzhou, China). After three weeks of culture, Oil red O staining and Alizarin red staining were performed to assess adipogenesis and osteogenesis, respectively. For chondrogenesis, micromass culture was performed. Cell suspension droplets (5 μL, with 1.0×10^7 cells/mL) were pipetted in the center of a 24-well plate. After allowing to attach for 4 h, chondrogenic differentiation medium (Cyagen Biosciences) was carefully added and changed once every 3 days. Alcian blue staining was then performed to assess the glycosaminoglycan formation after a 21-day chondrogenic induction.

Flow Cytometry

Cell surface antigen markers was detected by flow cytometry. Briefly, cells were harvested with 0.25% trypsin, centrifuged at 300 × *g* for 5 min, and then incubated with CD29 (Milliopre, MAB1951F, Bedford, MA, United States), CD90 (Abcam, ab226, Cambridge, United Kingdom), CD105 (GeneTex, GTX11415, Irvine, CA, United States), CD34 (eBioscience, MA1-22646, Carlsbad, CA, United States), and CD45 (eBioscience, MHCD4501) for 1 h, respectively. Fluorescence was detected by a FACSVerse flow cytometer (BD Biosciences, San Jose, CA, United States). Data acquisition and analysis were performed using the FlowJo software (Tree Star, Ashland, OR, United States) (Li Q. et al., 2019).

Scanning Electron Microscopy (SEM)

Morphological characteristics of the ECM/SVF-gel were examined using SEM. Briefly, specimens were fixed with 4% glutaraldehyde and post-fixed in 1% osmium tetroxide for 2 h at 4°C. After dehydration in a gradient series of ethanol, samples were sputter-coated with a 5-nm layer of gold in a high-vacuum gold sputter coater, and were then examined using a JSM-7900F scanning electron microscope (JEOL, Tokyo, Japan).

Magnetic Resonance Imaging (MRI)

At 6 and 12 weeks post-surgery, knee samples from each group underwent MRI analysis. All examinations were performed with a Siemens TIM Trio 3.0 T (T) MRI scanner (Siemens, Erlangen, Germany) using a small animal-specific coil. Morphological characteristics of neo-cartilage were evaluated under optimized imaging parameters (**Supplementary Table S1**) as described previously (Huang et al., 2014).

Gross Observation

The distal portion of the femurs in each group was carefully dissected and photographed after MRI scanning. The gross morphology was blindly evaluated by 2 observers. Semiquantitative analysis was then performed based on the degree of defect repair, integration with border zone, and macroscopic appearance (**Supplementary Table S2**) according to the International Cartilage Repair Society (ICRS) scoring system (van den Borne et al., 2007).

Histological Evaluation

At different time points, the repaired knees (n = 5 in each group) were harvested and fixed in 10% neutral buffered formalin for 48 h. Subsequently, whole specimens were demineralized in a decalcifying solution (ZSGB-BIO, Beijing, China) for two weeks. The decalcified specimens were then trimmed, dehydrated in a graded ethanol series, and embedded in paraffin. Serial sections of 5-μm thickness were cut and stained with hematoxylin and eosin (H&E) and toluidine blue (TB). Immunohistochemistry analysis was performed using antibodies against type II collagen (Invitrogen, MA5-13026, Carlsbad, CA, United States), type I collagen (Sigma-Aldrich, C2456, St. Louis, MO, United States), and type X collagen (Abcam, ab49945). A modified scoring system (**Supplementary Table S3**) was used to assess the histological repair outcomes of articular cartilage defects (Wakitani et al., 1994). Histological evaluation was performed by the same 2 observers in a blinded manner.

Nanoindentation Assessment of Repaired Cartilage

Biomechanical properties of regenerated tissues were evaluated using nanoindentation tests at 12 weeks (n = 5 in each group) post-operatively as described in previous reports (Man et al., 2016; Meng et al., 2017). The samples were isolated from the central area of repaired tissues and normal cartilage, and were kept hydrated with phosphate buffered saline solution at room temperature. The specimens were then examined using the TI 950 TriboIndenter In-Situ Nanomechanical Test System (Hysitron Inc., Minneapolis, MN, United States) using a conospherical diamond probe tip. Each indentation was force-controlled to a maximum indentation depth of 500 nm. The load procedure was applied to each specimen with loading (5 s), hold (2 s), and unloading (5 s).

Statistical Analysis

Data are expressed as the mean ± standard deviation (SD). Analyses were performed using the SPSS 22.0 software. Statistical significance ($P < 0.05$) was calculated using unpaired two-tailed Student's t-tests (two groups) or one-way ANOVA (homogeneity of variance, three groups).

RESULTS

Preparation and Characterization of ECM/SVF-gel

After mincing, shifting and centrifugation, the adipose tissue was divided into three layers: the upper oil phase, the middle ECM/SVF-gel, and the lower aqueous phase (**Figure 1A**). Compared to the minced adipose tissue, ECM/SVF-gel formed a jellylike gel with a smooth texture. The ECM/SVF-gel was transferred to a 1-mL syringe and could be easily injected the letters "PKU" shape through a 27-gauge needle (**Figure 1B** and **Supplementary Video**), indicating a good injectable property in the final product. Scanning electron microscopy was conducted to observe alterations in the ECM structure after the mechanical shifting process. The minced adipose showed an intact structure, whereas the ECM/SVF-gel had loose and porous extracellular fibers (**Figure 1C**). Gel usually has a typical characteristic that the storage modulus G′ is higher than the loss modulus G″, while the solution has the opposite property. Then, we performed rheological test to assess the physical properties of the ECM/SVF-gel. Our data showed that the storage modulus G′ was higher compared with the loss modulus G″ in the ECM/SVF-gel (**Figure 1D**), indicating its gel property.

Multilineage Differentiation Potential and Surface Marker of ECM/SVF-Gel Derived ADSCs

The ADSCs isolated from ECM/SVF-gel were cultured for 7–14 days and representative cells were photographed by light microscopy. These cells showed a typical spindle-shaped morphology (**Figure 2A**). To verify whether these ADSCs possessed of multipotential differentiation capability, cells were, respectively, incubated in chondrogenic, osteogenic, and adipogenic medium. Positive results of Alcian blue, Alizarin red, and Oil Red O staining demonstrated that ADSCs successfully differentiated into chondrocytes (**Figure 2B**), osteocytes (**Figure 2C**), and adipocytes (**Figure 2D**), respectively. The results of flow cytometry analysis demonstrated that MSCs positive phenotypic markers of CD29 (97.3%), CD90 (98.7%) and CD105 (99.7%) were overexpressed, whereas the hematopoietic antigen CD34 (1.3%) and the leukocyte common antigen CD45 (1.2%) were negatively expressed (**Figure 2E**).

MRI Observations of Repaired Knees

As shown in **Figure 3A**, high-resolution MRI images demonstrated that the defects in the MF group were poorly filled at 6 weeks postoperatively, whereas those in the ECM/SVF-gel group were almost completely filled with a smooth surface, though not up to the joint surface. At 12 weeks, the injuries in the MF group were irregularly filled with a rough surface. In contrast, uniform and complete filling of cartilage repair was observed in the ECM/SVF-gel group. Furthermore, the signal intensity of the repaired tissue in the ECM/SVF-gel group was similar to that of the adjacent normal cartilage (**Figure 3B**). Collectively, the MRI results indicate that the ECM/SVF-gel had a better effect of cartilage repair compared to the traditional MF treatment that is widely used in the clinic.

Gross Evaluation of Cartilage Repair

No complications were observed in any of the animals. At 6 weeks after surgery, the defects in the MF group were filled with a few blood clot-like tissues, whereas the filling in the ECM/SVF-gel group was more complete and uniform. The boundaries of the repaired sites were still obvious in both groups at 6 weeks (**Figure 4A**). At 12 weeks, the regenerated tissue in the MF group showed a rough surface and recognizable margin. However, in the ECM/SVF-gel group, newly regenerated tissue with a smooth surface showed integration with the surrounding area and had a color and texture similar to normal cartilage, indicating the formation of hyaline cartilage-like tissue (**Figure 4B** and **Supplementary Figure S1**). These findings suggest that the ECM/SVF-gel may effectively promote the filling of cartilage defects and facilitate neo-cartilage regeneration.

The ICRS scoring results were consistent with the macroscopic evaluations. As shown in **Figure 4C**, ICRS scores of the 6-week repaired tissues in the ECM/SVF-gel group (7.20 ± 1.3) were significant higher ($P < 0.05$) than those in the MF group (5.2 ± 0.8). The difference in the scores between the MF group (7.4 ± 1.1) and the ECM/SVF-gel group (9.8 ± 1.3) was significant ($P < 0.05$) at 12 weeks post-surgery, demonstrating that the repaired tissues of the ECM/SVF-gel group were considered as nearly normal (grade II) according to the ICRS overall assessment (**Supplementary Table S2**).

Histological Assessment of Cartilage Repair

Hematoxylin and eosin (H&E) staining was performed to evaluate the general repair effects between the two groups

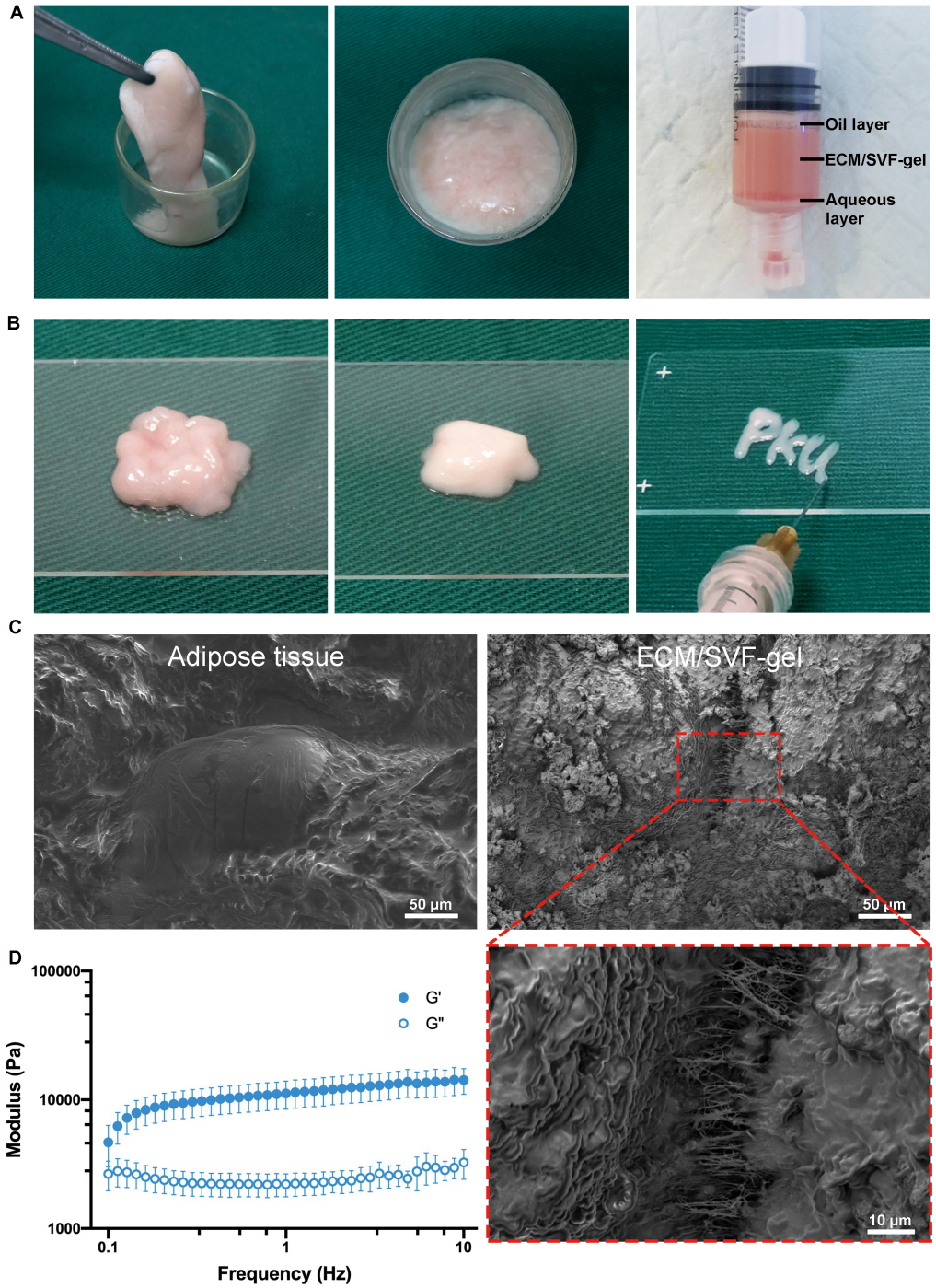

FIGURE 1 | Preparation and morphologic characteristics of the ECM/SVF-gel. **(A)** Rabbit adipose tissue was sufficiently minced. After shifting and centrifugation, the ECM/SVF-gel was in the middle layer. **(B)** Micrographic appearance of minced fat and ECM/SVF-gel. The ECM/SVF-gel could be injected easily through a 27G needle. **(C)** Scanning electron microscopy showed that minced adipose tissue maintained an intact structure, whereas the ECM/SVF-gel had loose and porous extracellular fibers. **(D)** Rheological test for the ECM/SVF-gel (n = 3).

(**Figure 5A**). At 6 weeks post-surgery, the defect in the MF group was poorly filled, with fibrous tissue and a distinct boundary between the normal cartilage and regenerated tissue. However, the defect in the ECM/SVF-gel group was generally filled, and the margin between the normal cartilage and repaired tissue was unclear. At 12 weeks post-surgery, the defect in the MF group was filled with disordered fibrous tissue, and the surface of the repaired tissue was lower than that of

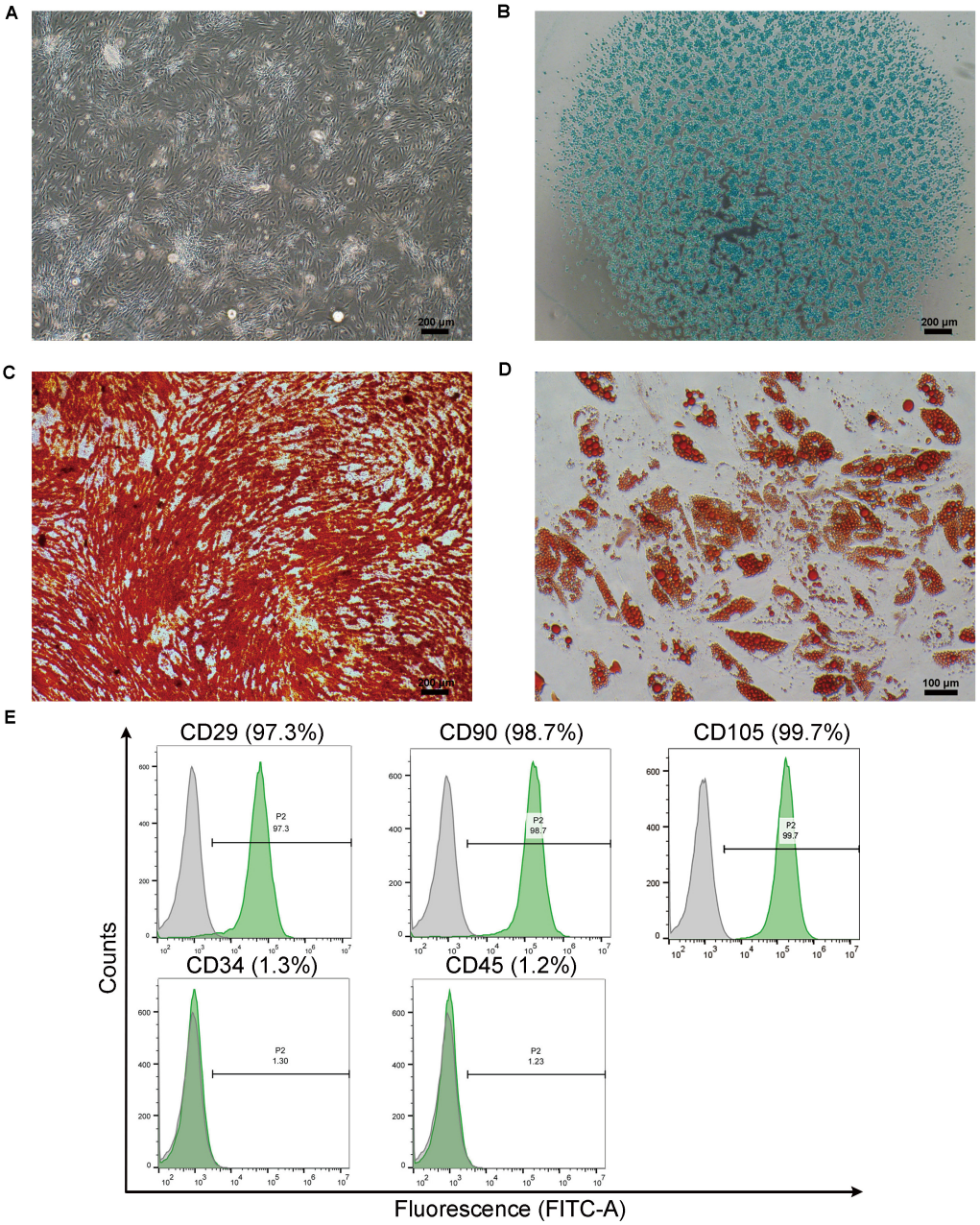

FIGURE 2 | Multi-lineage differentiation of cultured ADSCs migrated from the ECM/SVF-gel. **(A)** Cultured primary ADSCs from the ECM/SVF-gel exhibited a typical spindle shape morphology. **(B)** Chondrogenic, **(C)** osteogenic, and **(D)** adipogenic differentiation of ADSCs was induced and determined by Alcian blue staining for glycosaminoglycans, Alizarin red staining for matrix mineralization, and Oil Red O staining for intracellular lipid droplets, respectively. Scale bars: **(A–C)** = 200 μm; **(D)** = 100 μm. **(E)** Flow cytometry analysis of surface marker on ADSCs from the ECM/SVF-gel.

the adjacent normal cartilage, which showed a degenerative architecture. In contrast, in the ECM/SVF-gel group, the reparative tissue was more similar to the surrounding host cartilage, and highly organized chondrocyte-like cells were observed (**Supplementary Figure S2**).

Further, toluidine blue staining was performed to assess the content of glycosaminoglycan, an important component of the cartilage matrix (**Figure 5B**). In the MF group, weak staining was observed at 6 weeks and 12 weeks post-operation, which indicated poor glycosaminoglycan deposition. After 12 weeks of surgery, the regenerated tissue in the ECM/SVF-gel group displayed strong positive and uniform staining, which was similar to the surrounding normal cartilage (**Supplementary Figure S3**).

A modified scoring system was used to measure the histological outcomes of cartilage repair (**Figure 5C**). Consistent with the results shown above, the ECM/SVF-gel group had

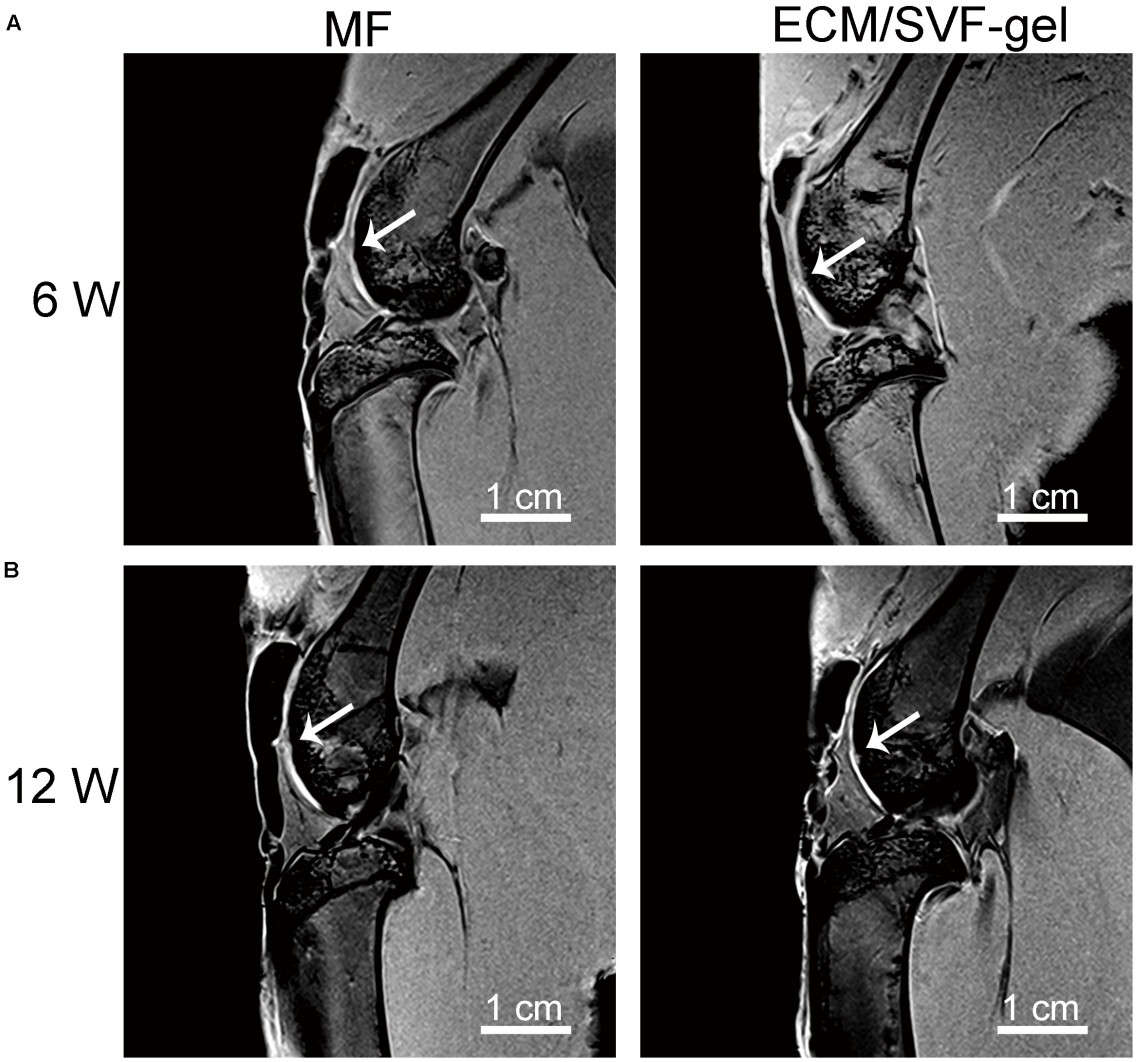

FIGURE 3 | High-resolution MRI of repaired knees. Representative MRI images at 6 weeks **(A)** and 12 weeks **(B)** post-operation. White arrow, repaired sites of articular cartilage; scale bars = 1 cm.

significantly higher ($P < 0.05$) histological scores compared with the MF group at 6 weeks (7.4 ± 1.1 *vs.* 5.6 ± 0.9) and 12 weeks (10.2 ± 0.8 *vs.* 8.4 ± 1.1).

Cartilage-specific type II collagen (COL II) was detected by immunohistochemistry to assess the quality of cartilage repair. As shown in **Figure 6A** and **Supplementary Figure S4**, COL II expression was observed in the regenerated tissue of both the MF and ECM/SVF-gel groups. At both 6 and 12 weeks after surgery, COL II expression from cells in the ECM/SVF-gel group was higher than that in the MF group, which confirmed the results of H&E and toluidine blue staining. Immunohistochemistry for COL I (**Figure 6B** and **Supplementary Figure S5**) was also performed to evaluate the extent of fibrocartilage in the regenerated tissue. In the MF group, the expression of COL I was predominated, suggesting that the main generated component was fibrocartilage. However, the expression of type I collagen was not significant in the ECM/SVF-gel group, indicating the formation of hyaline-like cartilage. Hypertrophy of chondrocytes could disturb articular cartilage regeneration. We further detected hypertrophic marker COL X by immunohistochemistry (**Figure 6C** and **Supplementary Figure S6**). The results showed that COL X was slightly stained in both group, and remained no obvious difference compared with the surrounding normal cartilage. Taken together, these findings demonstrated that the ECM/SVF-gel had a better reparative effect on cartilage defects, and that the newly regenerated tissue is closer to normal cartilage.

Biomechanical Properties of Repaired Cartilage

At 12 weeks post-surgery, nanoindentation was performed to evaluate the biomechanical properties of the reparative tissue. According to the load-displacement curves (**Figure 7A**),

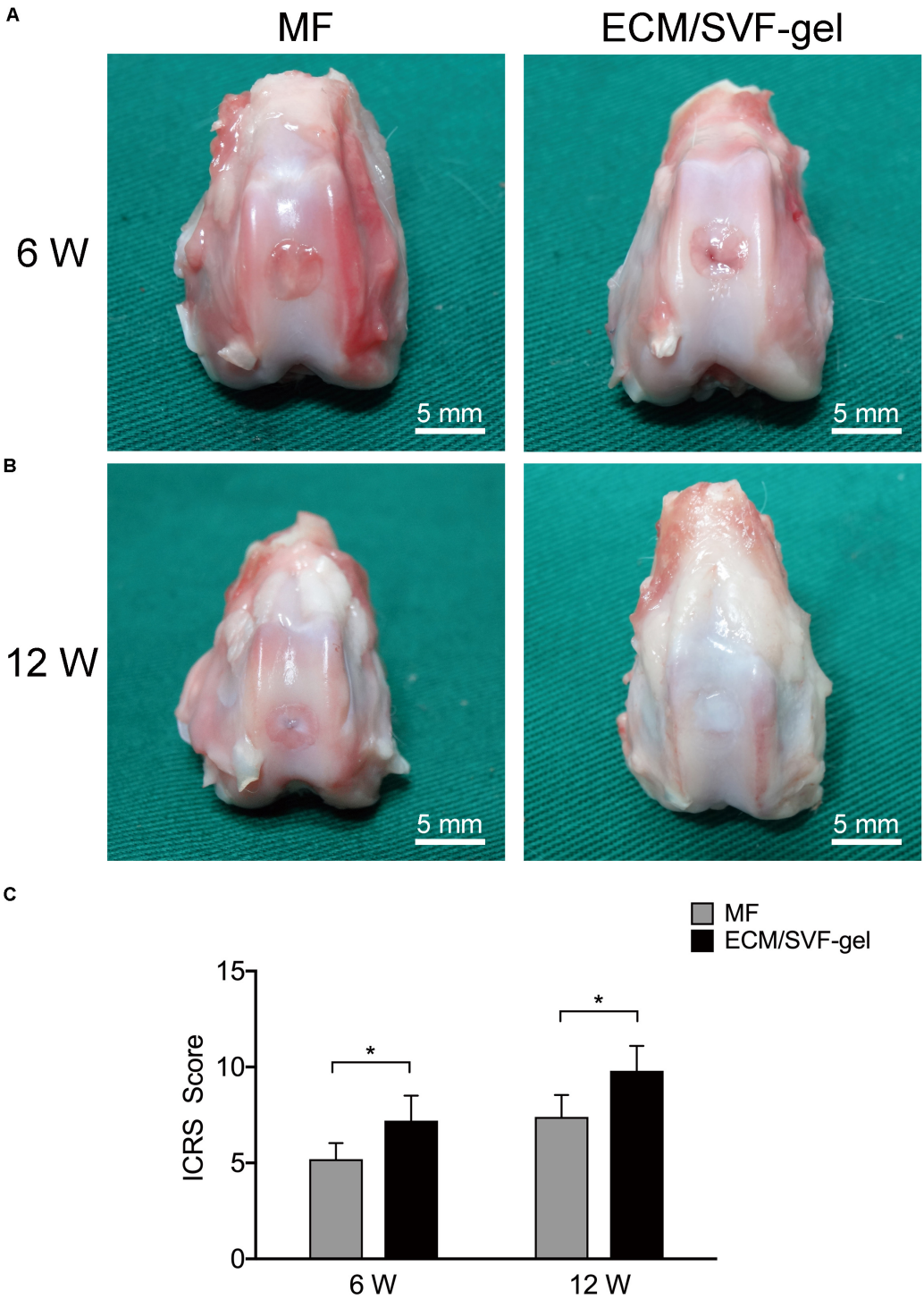

FIGURE 4 | Macroscopic evaluation and ICRS score. **(A)** At 6 weeks and **(B)** 12 weeks, repaired knees were observed and photographed. Scale bars = 5 mm. **(C)** ICRS gross scoring of cartilage repair. Results are presented as the mean ± SD; $n = 5$; $^*p < 0.05$.

reduced modulus and hardness were calculated. Normal cartilage displayed the highest reduced modulus, followed by the ECM/SVF-gel group and the lowest in the MF group (**Figure 7B**). A similar result can be seen in the assessment of hardness (**Figure 7C**), although there is no statistical difference between the MF and ECM/SVF-gel groups. These data indicate that the ECM/SVF-gel facilitates better biomechanical properties in the repaired tissue.

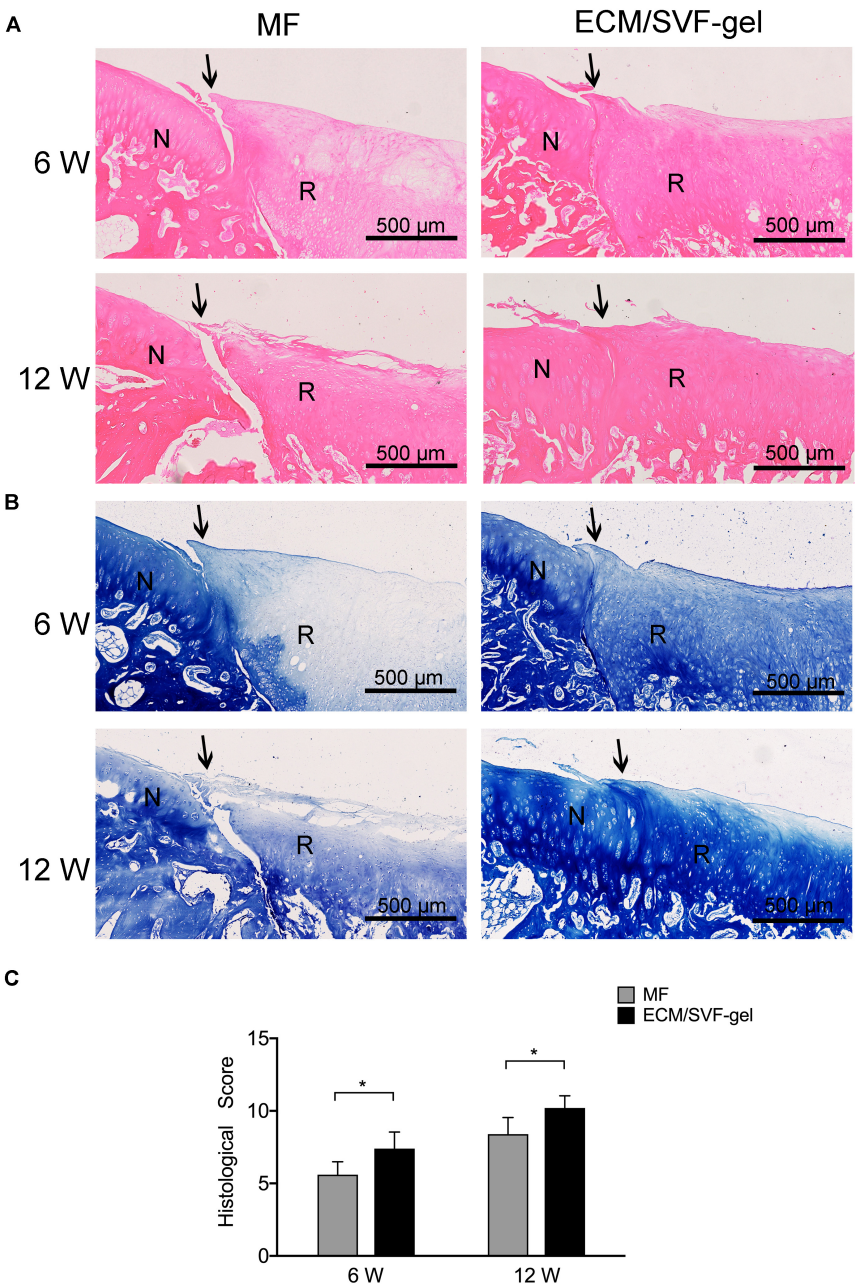

FIGURE 5 | Histological assessment of repaired cartilage. **(A)** Hematoxylin and eosin staining. N, normal cartilage; R, repair cartilage; the arrows indicate the margins of the normal cartilage and repaired cartilage. **(B)** Toluidine blue staining. **(C)** Histological scores for repaired knees. Data are presented as the mean ± SD; $n = 5$; $^*P < 0.05$.

DISCUSSION

This study investigated a novel strategy of ready-to-use autologous fractionated adipose tissue named ECM/SVF-gel, and its therapeutic potential as a scaffolding material and novel stem cell-based approach for articular cartilage restoration.

Due to its poor intrinsic healing capacity, damage to the articular cartilage is difficult to cure fully and may induce osteoarthritis, which is predicted to affect more than 67 million people by 2030, leading to costs of more than $3 billion annually in the United States (Madry et al., 2019). There is thus an urgent need to explore new treatment options. In the present study, mechanical grafting was used to disrupt adipose tissue, and centrifugation was performed to remove the released oil and to further increase the density of ECM fibers and stem cells. SEM demonstrated successful concentration of ECM fibers in the ECM/SVF-gel, which could thus provide a scaffolding biomaterial with the microenvironment required for MSCs

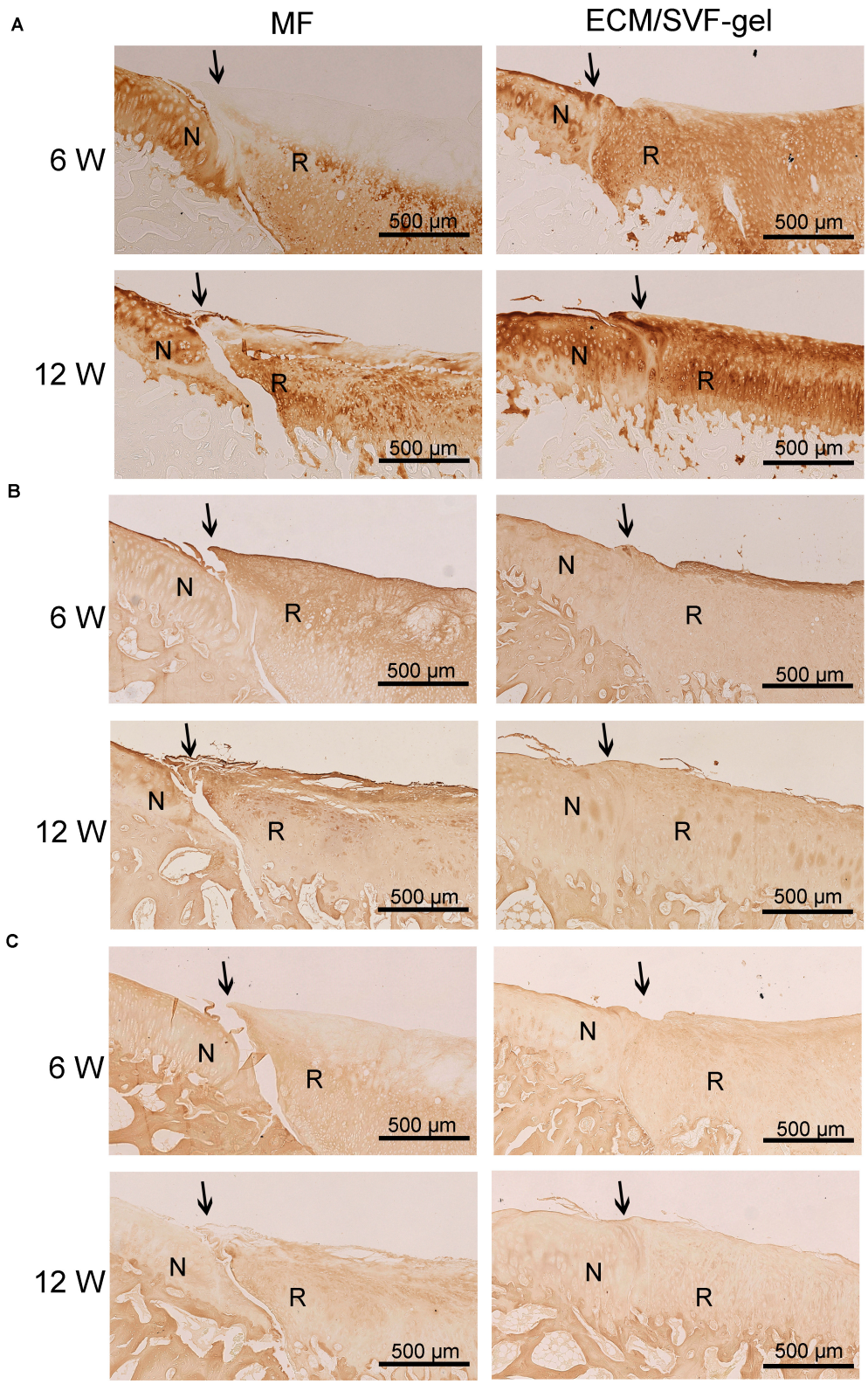

FIGURE 6 | Immunohistochemistry for regenerated tissue. **(A)** COL II, **(B)** COL I, and **(C)** COL X of specimens in each group were detected at 6 and 12 weeks after surgery. N, normal cartilage; R, repair cartilage; the arrows indicate the margins of the normal cartilage and repaired cartilage.

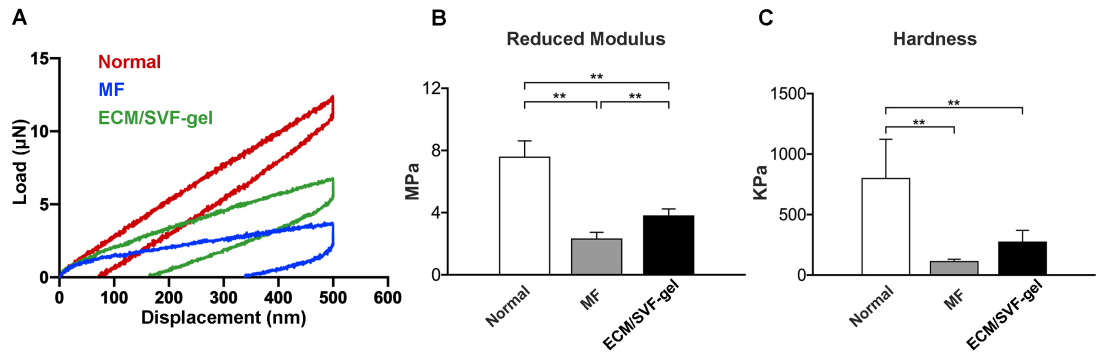

FIGURE 7 | Biomechanical properties of repaired cartilage at 12 weeks post-surgery. **(A)** Typical load-displacement curves obtained with the repaired tissues were compared with those from native cartilage. **(B)** Reduced modulus and **(C)** hardness in each group. Data are presented as the mean ± SD; $n = 5$; $^{**}P < 0.01$.

renewal and differentiation. Consistent with previous studies, we found that ADSCs isolated from ECM/SVF-gel could proliferate and differentiate into various lineages (Zhang et al., 2018; Wang J. et al., 2019), demonstrating that the ECM/SVF-gel preserved the stem cells within adipose tissue. Therefore, the ECM/SVF-gel has attractive prospects as a natural scaffolding biomaterial and stem cell carrier to promote cartilage regeneration. When it comes to the naming of ECM/SVF-gel, we are based on the following reasons. First, the ECM fibers are concentrated and verified by SEM. Second, this method is an enzyme-free approach to isolated SVF cells, which are already demonstrated by some studies (Sun et al., 2017; Yao et al., 2017), and ADSCs isolated in this study are a subset of SVF. Third, gel property is demonstrated by rheological data that the storage modulus G′ was higher than the loss modulus G″. Finally, similar nomenclature has also been reported in other studies (Feng et al., 2019; Wang J. et al., 2019).

To identify the effect on cartilage repair *in vivo*, we injected autologous ECM/SVF-gel into a rabbit cartilage defect model. According to the imaging studies, macroscopic observation and histological examination, the ECM/SVF-gel suggested a superior hyaline-like neo-cartilage restoration compared with the MF treatment alone. Cell migration from adjacent donor cartilage is a key factor driving the process of integration (Pabbruwe et al., 2009). Recently, fragmented adipose tissue was found to significantly accelerated chondrocyte migration into the wound area (Xu et al., 2019), indicating that natural fat derived biomaterials (e.g., ECM/SVF-gel) could recruit chondrocytes to the defect region from the adjacent normal cartilage and promote integration between the repair tissue and surrounding native cartilage. A preclinical study reported that among 130 dogs with spontaneous osteoarthritis, 98% had improved owners' scores after 6 months with a single injection of fat extract (Zeira et al., 2018). Moreover, there is evidence that fragmented adipose tissue can promote cell proliferation and maintain the stemness of progenitor cells (Randelli et al., 2016). In another study, Desando and colleagues demonstrated that mechanically fragmented adipose tissue-based biomaterials were beneficial for cartilage regeneration due to their trophic activity and the wound-healing activity of CD-163^{+} cells contained in its niche (Desando et al., 2019).

Articular cartilage serves as a cushion to protect the joint from mechanical stresses and strains. Biomechanical performance is a key index for evaluating cartilage tissue engineering (Panadero et al., 2016). In the present work, both reduced modulus and hardness were higher in the ECM/SVF-gel group than those in the MF group; however, they did not reach the levels in normal cartilage. One possible reason is that the observation period of 12 weeks is not long enough to achieve complete healing of the articular cartilage, which needs to be considered in future studies. In addition, although difficult to manage in animal experiments, post-operative rehabilitation is a critical component of the treatment process in the biomechanical recovery of cartilage lesions for patients (Mithoefer et al., 2012).

When it comes to traditional stem cell therapies, cell suspensions show poor adhesion to joints and are easily lost to areas outside the injury site, thereby reducing the effectiveness of treatment. Therefore, it may often be necessary to rely on synthetic bio-scaffolds to promote the cell adhesion or recruitment of seed cells to achieve better repair results (Malda et al., 2019). In ECM/SVF-gels, the preserved natural microenvironment and ADSCs may play a different role when compared with the direct delivery of cell suspensions or combination with other synthetic biomaterials. Meanwhile, during the process of mechanically processing adipose tissues and centrifugation, the final product could be enriched with growth factors and other components such as extracellular vesicles (Xu et al., 2019), which can stimulate tissue regeneration. It is possible that the ECM/SVF-gel facilitates cartilage repair more so through its material characteristics, rather than through its cellular characteristics. Previous studies demonstrated that gels could be used to stabilize the blood clot that forms during microfracture (Hoemann et al., 2007). For example, BST-CarGel (Smith&Nephew) or chitosan gels have been successfully used to stabilize microfracture blood clots in animal models and humans, leading to improved cartilage tissue repair (Stanish et al., 2013; Shive et al., 2015; Méthot et al., 2016; Mohan et al., 2017). The ECM/SVF-gel may stabilize the clot formed by cells that seep from the bone marrow into the defect site, thereby facilitating cartilage repair. Future studies could use cell tracing to determine if the repaired cartilage tissue was

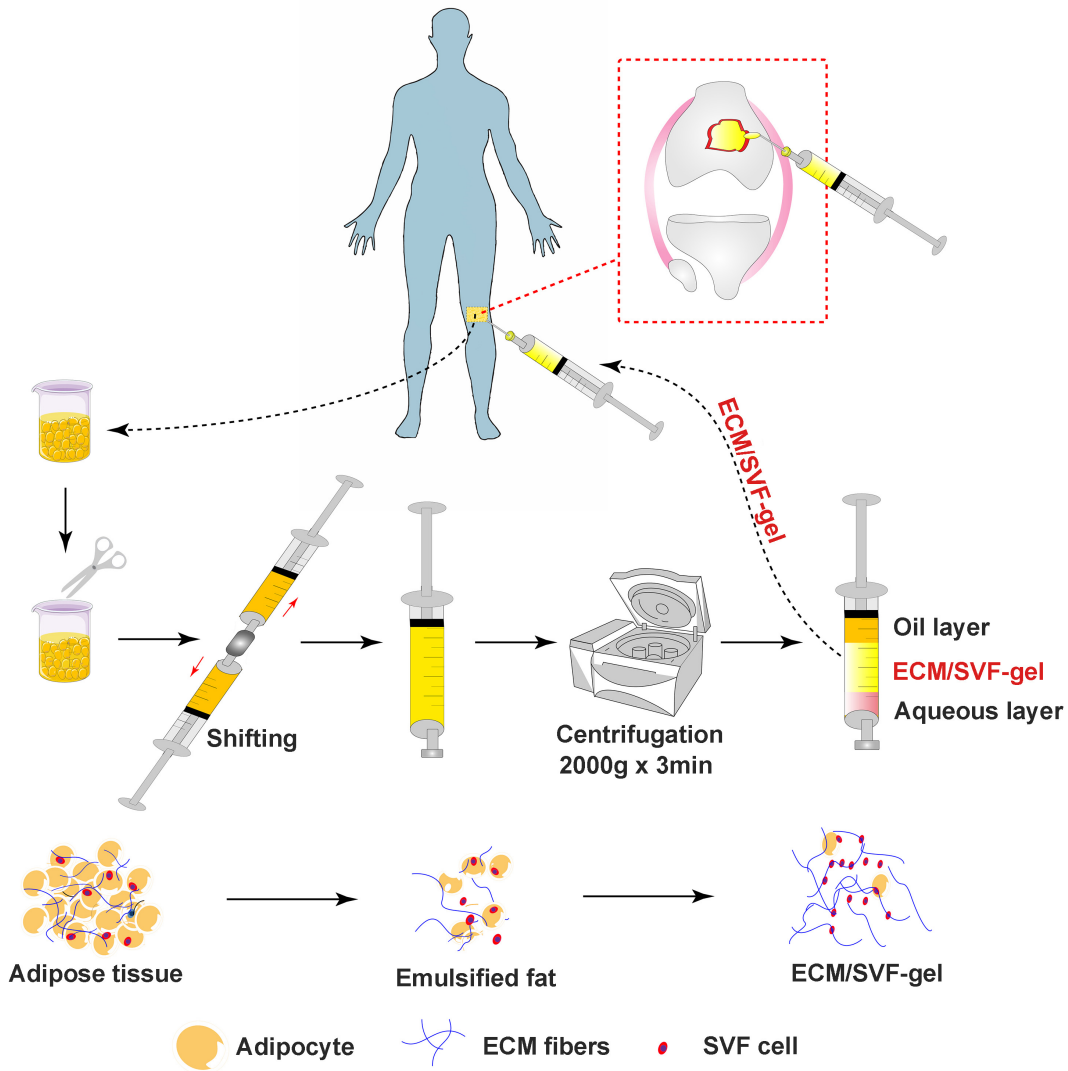

FIGURE 8 | Overview of the clinical application of ECV/SVF-gel for cartilage restoration.

derived from cells contained within the ECM/SVF-gel, or if the repair tissue was derived from other cell sources within the host animal. Furthermore, fragmented fat tissue as a natural biomaterial for efficient drug delivery, improved the local drug concentration and prolonged its therapeutic activity (Alessandri et al., 2019), indicating that our ECM/SCF-gel may act as a self-controlled drug release system of intrinsic growth factors to promote cartilage repair. Different from scaffold-based ADSCs treatment (Li X. et al., 2019), this strategy allows overcoming the limitations associated with the enzymatic isolation of SVF cells from adipose tissue and the expansion of ADSCs, as well as the complex process of scaffold fabrication. In addition, a recent study reported that after cryopreservation at −20°C for 3 months without a cryoprotectant, the mechanically processed fat product SVF gel from human lipoaspirate maintained ECM integrity and ADSC viability as well as their multipotency (Feng et al., 2019).

For clinical application, the adipose tissue for ECM/SVF-gel preparation can be sourced from the infrapatellar fat pad of the synovial joint environment or subcutaneous adipose tissue. In clinical practice, during arthroscopic surgery for articular cartilage repair, in order to expose a clear operation field, the infrapatellar fat pad often needs to be removed. Thus, the donor fat is obtained during the debridement process, which is also in line with the fundamental principles of minimally invasive arthroscopic surgery. Moreover, adjacent to the operative knee area, subcutaneous fat around the inner thigh is another choice for surgeons. In addition, liposuction, a technique that has been used for decades in plastic surgery with a very low incidence of major complications, provides an alternative choice of autologous adipose tissue. Some clinicians have recommended the autologous adipose tissue transplantation should be considered for the treatment of delamination and 1st and 2nd degree chondral lesions (Jannelli and Fontana, 2017);

however, the exact indication and dose management require additional research in the future.

This study is not without limitations. First, a study with a large animal model and a relatively long observation period beyond 12 weeks needs to be performed in future. As mentioned above, from the perspective of clinical application, the infrapatellar fat pad collected during arthroscopic surgery is the best choice, which also truly meets the one-step procedure. In this study, limited by the small volume of the synovial infrapatellar fat pad in rabbits, we adopted inguinal adipose tissue. Although there may be some differences in the fat from different sites, our strategy was found effective for cartilage repair. In future research, we will consider using larger animals such as pigs for confirming these results. Second, rabbits with fully skeletal maturity should be used in chondral restoration, because the relatively young rabbits used in this study have stronger healing capabilities and may promote better repair results. Third, we did not compare the ECM/SVF-gel with traditional stem cell therapy such as ADSCs injection or SVF transplantation, for cartilage regeneration. Finally, the underlying molecular mechanism of cartilage repair needs to be investigated further.

In conclusion, we innovatively propose that application of autologous fractionated adipose tissue (ECM/SVF-gel) could facilitate cartilage injury repair. The ECM/SVF-gel is a minimally manipulated adipose tissue extract that retains the ECM and stem cells after mechanical processing and centrifugation. The results show that the autologous ECM/SVF-gel displays a curative effect on articular cartilage regeneration in a rabbit model. Considering its simple, time-sparing, cost-effective, minimally invasive, and enzyme-free preparation process, this gel may provide a novel concept in the repair of articular cartilage injury (**Figure 8**). More importantly, the paradigm opens an attractive clinical insight in the potential use of stem cell therapy in regenerative medicine.

DATA AVAILABILITY STATEMENT

The raw data supporting the conclusions of this article will be made available by the authors, without undue reservation, to any qualified researcher.

ETHICS STATEMENT

The animal study was reviewed and approved by Peking University Biomedical Ethics Committee.

AUTHOR CONTRIBUTIONS

YA, XH, and QL conceived the project and designed the experiments. QL, FZ, ZL, XD, JYZ, XF, and JHZ performed the experiments. QL, JC, ZS, and QG collected and analyzed the data. QL wrote the manuscript. YA and XH reviewed the manuscript and supervised the project. All authors contributed to the article and approved the submitted version.

FUNDING

This project was supported by the Beijing Municipal Science and Technology Commission (No. Z171100001017085), the National Natural Science Foundation of China (Nos. 81672212, 81672153, and 81902205), and the Beijing Municipal Natural Science Foundation (Nos. 7171014 and 7182175).

ACKNOWLEDGMENTS

We thank Li Chen, Xiaotong Yu, and Yan Song (Peking University Third Hospital, Beijing) for the technical help of histologic staining, and Luzheng Xu (Peking University Health Science Center, Beijing) for the assistance of MRI performing. We also thank Kuo Zhang and Haiming Sun (Peking University Health Science Center, Beijing) for the support of animal care.

SUPPLEMENTARY MATERIAL

The Supplementary Material for this article can be found online at: https://www.frontiersin.org/articles/10.3389/fcell.2020.00694/full#supplementary-material

REFERENCES

Alessandri, G., Cocce, V., Pastorino, F., Paroni, R., Dei Cas, M., Restelli, F., et al. (2019). Microfragmented human fat tissue is a natural scaffold for drug delivery: potential application in cancer chemotherapy. *J. Control Release* 302, 2–18. doi: 10.1016/j.jconrel.2019.03.016

Ao, Y., Li, Z., You, Q., Zhang, C., Yang, L., and Duan, X. (2019). The use of particulated juvenile allograft cartilage for the repair of porcine articular cartilage defects. *Am. J. Sports Med.* 47, 2308–2315. doi: 10.1177/0363546519856346

Berry, D. C., Jiang, Y. W., and Graff', J. M. (2016). Emerging roles of adipose progenitor cells in tissue development, homeostasis, expansion and thermogenesis. *Trends Endocrinol. Metabol.* 27, 574–585. doi: 10.1016/j.tem.2016.05.001

Bianchi, V. J., Lee, A., Anderson, J., Parreno, J., Theodoropoulos, J., Backstein, D., et al. (2019). Redifferentiated chondrocytes in fibrin gel for the repair of articular cartilage lesions. *Am. J. Sports Med.* 47, 2348–2359. doi: 10.1177/0363546519857571

Cui, L., Wu, Y., Cen, L., Zhou, H., Yin, S., Liu, G., et al. (2009). Repair of articular cartilage defect in non-weight bearing areas using adipose derived stem cells loaded polyglycolic acid mesh. *Biomaterials* 30, 2683–2693. doi: 10.1016/j.biomaterials.2009.01.045

Dai, L., He, Z., Zhang, X., Hu, X., Yuan, L., Qiang, M., et al. (2014). One-step repair for cartilage defects in a rabbit model: a technique combining the perforated decalcified cortical-cancellous bone matrix scaffold with microfracture. *Am. J. Sports Med.* 42, 583–591. doi: 10.1177/0363546513518415

Desando, G., Bartolotti, I., Martini, L., Giavaresi, G., Nicoli Aldini, N., Fini, M., et al. (2019). Regenerative features of adipose tissue for osteoarthritis treatment in a rabbit model: enzymatic digestion versus mechanical disruption. *Int. J. Mol. Sci.* 20:2636. doi: 10.3390/ijms20112636

Feng, J., Hu, W., Fanai, M. L., Zhu, S., Wang, J., Cai, J., et al. (2019). Mechanical process prior to cryopreservation of lipoaspirates maintains extracellular matrix integrity and cell viability: evaluation of the retention and regenerative potential of cryopreserved fat-derived product after fat grafting. *Stem Cell Res. Ther.* 10:283. doi: 10.1186/s13287-019-1395-6

Guerrero, J., Pigeot, S., Müller, J., Schaefer, D. J., Martin, I., and Scherberich, A. (2018). Fractionated human adipose tissue as a native biomaterial for the generation of a bone organ by endochondral ossification. *Acta Biomater.* 77, 142–154. doi: 10.1016/j.actbio.2018.07.004

Halme, D. G., and Kessler, D. A. (2006). FDA regulation of stem-cell-based therapies. *N. Engl. J. Med.* 355, 1730–1735. doi: 10.1056/NEJMhpr063086

Hoemann, C. D., Sun, J., McKee, M. D., Chevrier, A., Rossomacha, E., Rivard, G. E., et al. (2007). Chitosan-glycerol phosphate/blood implants elicit hyaline cartilage repair integrated with porous subchondral bone in microdrilled rabbit defects. *Osteoarthr. Cartil.* 15, 78–89. doi: 10.1016/j.joca.2006.06.015

Hu, X., Zhu, J., Li, X., Zhang, X., Meng, Q., Yuan, L., et al. (2015). Dextran-coated fluorapatite crystals doped with Yb3(/Ho3(for labeling and tracking chondrogenic differentiation of bone marrow mesenchymal stem cells in vitro and in vivo. *Biomaterials* 52, 441–451. doi: 10.1016/j.biomaterials.2015.02.050

Huang, H., Zhang, X., Hu, X., Shao, Z., Zhu, J., Dai, L., et al. (2014). A functional biphasic biomaterial homing mesenchymal stem cells for in vivo cartilage regeneration. *Biomaterials* 35, 9608–9619. doi: 10.1016/j.biomaterials.2014.08.020

Jannelli, E., and Fontana, A. (2017). Arthroscopic treatment of chondral defects in the hip: AMIC, MACI, microfragmented adipose tissue transplantation (MATT) and other options. *Sicot J.* 3:43. doi: 10.1051/sicotj/2017029

Kondo, S., Nakagawa, Y., Mizuno, M., Katagiri, K., Tsuji, K., Kiuchi, S., et al. (2019). Transplantation of aggregates of autologous synovial mesenchymal stem cells for treatment of cartilage defects in the femoral condyle and the femoral groove in microminipigs. *Am. J. Sports Med.* 47, 2338–2347. doi: 10.1177/0363546519859855

Kwon, H., Brown, W. E., Lee, C. A., Wang, D., Paschos, N., Hu, J. C., et al. (2019). Surgical and tissue engineering strategies for articular cartilage and meniscus repair. *Nat. Rev. Rheumatol.* 15, 550–570. doi: 10.1038/s41584-019-0255-1

Li, Q., Qin, Z. L., Chen, B., An, Y., Nie, F. F., Yang, X., et al. (2019). "Mitochondrial dysfunction and morphological abnormality in keloid fibroblasts," in *Advances in Wound Care* (New Rochelle, NY: Ann Liebert, Inc., publishers), doi: 10.1089/wound.2019.0988

Li, X., Guo, W., Zha, K., Jing, X., Wang, M., Zhang, Y., et al. (2019). Enrichment of CD146+ adipose-derived stem cells in combination with articular cartilage extracellular matrix scaffold promotes cartilage regeneration. *Theranostics* 9, 5105–5121. doi: 10.7150/thno.33904

Lonardi, R., Leone, N., Gennai, S., Trevisi Borsari, G., Covic, T., and Silingardi, R. (2019). Autologous micro-fragmented adipose tissue for the treatment of diabetic foot minor amputations: a randomized controlled single-center clinical trial (MiFrAADiF). *Stem Cell Res. Ther.* 10:223. doi: 10.1186/s13287-019-1328-4

Madry, H., Gao, L., Rey-Rico, A., Venkatesan, J. K., Müller-Brandt, K., Cai, X., et al. (2019). Thermosensitive hydrogel based on PEO-PPO-PEO poloxamers for a controlled in situ release of recombinant adeno-associated viral vectors for effective gene therapy of cartilage defects. *Adv. Mater.* 32:1906508. doi: 10.1002/adma.201906508

Makris, E. A., Gomoll, A. H., Malizos, K. N., Hu, J. C., and Athanasiou, K. A. (2015). Repair and tissue engineering techniques for articular cartilage. *Nat Rev Rheumatol* 11, 21–34. doi: 10.1038/nrrheum.2014.157

Malda, J., Groll, J., and van Weeren, P. R. (2019). Rethinking articular cartilage regeneration based on a 250-year-old statement. *Nat. Rev. Rheumatol.* 15, 571–572. doi: 10.1038/s41584-019-0278-7

Man, Z., Hu, X., Liu, Z., Huang, H., Meng, Q., Zhang, X., et al. (2016). Transplantation of allogenic chondrocytes with chitosan hydrogel-demineralized bone matrix hybrid scaffold to repair rabbit cartilage injury. *Biomaterials* 108, 157–167. doi: 10.1016/j.biomaterials.2016.09.002

Meng, Q., Hu, X., Huang, H., Liu, Z., Yuan, L., Shao, Z., et al. (2017). Microfracture combined with functional pig peritoneum-derived acellular matrix for cartilage repair in rabbit models. *Acta Biomater* 53, 279–292. doi: 10.1016/j.actbio.2017.01.055

Méthot, S., Changoor, A., Tran-Khanh, N., Hoemann, C. D., Stanish, W. D., Restrepo, A., et al. (2016). Osteochondral biopsy analysis demonstrates that BST-CarGel treatment improves structural and cellular characteristics of cartilage repair tissue compared with microfracture. *Cartilage* 7, 16–28. doi: 10.1177/1947603515595837

Mithoefer, K., Hambly, K., Logerstedt, D., Ricci, M., Silvers, H., and Della Villa, S. (2012). Current concepts for rehabilitation and return to sport after knee articular cartilage repair in the athlete. *J. Orthop Sports Phys. Ther.* 42, 254–273. doi: 10.2519/jospt.2012.3665

Mohan, N., Mohanan, P. V., Sabareeswaran, A., and Nair, P. (2017). Chitosan-hyaluronic acid hydrogel for cartilage repair. *Int. J. Biol. Macromol.* 104(Pt B), 1936–1945. doi: 10.1016/j.ijbiomac.2017.03.142

Pabbruwe, M. B., Esfandiari, E., Kafienah, W., Tarlton, J. F., and Hollander, A. P. (2009). Induction of cartilage integration by a chondrocyte/collagen-scaffold implant. *Biomaterials* 30, 4277–4286. doi: 10.1016/j.biomaterials.2009.02.052

Panadero, J. A., Lanceros-Mendez, S., and Ribelles, J. L. (2016). Differentiation of mesenchymal stem cells for cartilage tissue engineering: individual and synergetic effects of three-dimensional environment and mechanical loading. *Acta Biomater.* 33, 1–12. doi: 10.1016/j.actbio.2016.01.037

Randelli, P., Menon, A., Ragone, V., Creo, P., Bergante, S., Randelli, F., et al. (2016). Lipogems product treatment increases the proliferation rate of human tendon stem cells without affecting their stemness and differentiation capability. *Stem Cells Int.* 2016:4373410. doi: 10.1155/2016/4373410

Shi, W. L., Sun, M. Y., Hu, X. Q., Ren, B., Cheng, J., Li, C. X., et al. (2017). Structurally and functionally optimized silk-fibroin-gelatin scaffold using 3D printing to repair cartilage injury in vitro and in vivo. *Adv. Mater.* 29:1701089. doi: 10.1002/adma.201701089

Shive, M. S., Stanish, W. D., McCormack, R., Forriol, F., Mohtadi, N., Pelet, S., et al. (2015). BST-CarGel (R) treatment maintains cartilage repair superiority over microfracture at 5 years in a multicenter randomized controlled trial. *Cartilage* 6, 62–72. doi: 10.1177/1947603514562064

Stanish, W. D., McCormack, R., Forriol, F., Mohtadi, N., Pelet, S., Desnoyers, J., et al. (2013). Novel scaffold-based BST-CarGel treatment results in superior cartilage repair compared with microfracture in a randomized controlled trial. *J. Bone Joint Surg. Am.* 95, 1640–1650. doi: 10.2106/jbjs.L.01345

Sun, M., He, Y., Zhou, T., Zhang, P., Gao, J., and Lu, F. (2017). Adipose extracellular matrix/stromal vascular fraction gel secretes angiogenic factors and enhances skin wound healing in a murine model. *Biomed. Res. Int.* 2017:3105780. doi: 10.1155/2017/3105780

van den Borne, M. P., Raijmakers, N. J., Vanlauwe, J., Victor, J., de Jong, S. N., Bellemans, J., et al. (2007). International cartilage repair society (ICRS) and oswestry macroscopic cartilage evaluation scores validated for use in autologous chondrocyte implantation (ACI) and microfracture. *Osteoarthr. Cartil.* 15, 1397–1402. doi: 10.1016/j.joca.2007.05.005

Wakitani, S., Goto, T., Pineda, S. J., Young, R. G., Mansour, J. M., Caplan, A. I., et al. (1994). Mesenchymal cell-based repair of large, full-thickness defects of articular cartilage. *J. Bone Joint Surg. Am.* 76, 579–592. doi: 10.2106/00004623-199404000-00013

Wang, J., Liao, Y., Xia, J., Wang, Z., Mo, X., Feng, J., et al. (2019). Mechanical micronization of lipoaspirates for the treatment of hypertrophic scars. *Stem Cell Res. Ther.* 10:42. doi: 10.1186/s13287-019-1140-1

Wang, X., Song, X., Li, T., Chen, J., Cheng, G., Yang, L., et al. (2019). Aptamer-functionalized bioscaffold enhances cartilage repair by improving stem cell recruitment in osteochondral defects of rabbit knees. *Am. J. Sports Med.* 47, 2316–2326. doi: 10.1177/0363546519856355

Xu, T., Yu, X., Yang, Q., Liu, X., Fang, J., and Dai, X. (2019). Autologous micro-fragmented adipose tissue as stem cell-based natural scaffold for cartilage defect repair. *Cell Transpl.* 28, 1709–1720. doi: 10.1177/0963689719880527

Yao, Y., Dong, Z., Liao, Y., Zhang, P., Ma, J., Gao, J., et al. (2017). Adipose extracellular matrix/stromal vascular fraction gel: a novel adipose tissue-derived injectable for stem cell therapy. *Plast Reconstr. Surg.* 139, 867–879. doi: 10.1097/PRS.0000000000003214

Yokota, N., Hattori, M., Ohtsuru, T., Otsuji, M., Lyman, S., Shimomura, K., et al. (2019). Comparative clinical outcomes after intra-articular injection with adipose-derived cultured stem cells or noncultured stromal vascular fraction for the treatment of knee osteoarthritis. *Am. J. Sports Med.* 47, 2577–2583. doi: 10.1177/0363546519864359

Yu, C., Bianco, J., Brown, C., Fuetterer, L., Watkins, J. F., Samani, A., et al. (2013). Porous decellularized adipose tissue foams for soft tissue regeneration. *Biomaterials* 34, 3290–3302. doi: 10.1016/j.biomaterials.2013.01.056

Zeira, O., Scaccia, S., Pettinari, L., Ghezzi, E., Asiag, N., Martinelli, L., et al. (2018). Intra-articular administration of autologous micro-fragmented adipose tissue in dogs with spontaneous osteoarthritis: safety, feasibility, and clinical outcomes. *Stem Cells Transl. Med.* 7, 819–828. doi: 10.1002/sctm.18-0020

Zhang, P., Feng, J., Liao, Y., Cai, J., Zhou, T., Sun, M., et al. (2018). Ischemic flap survival improvement by composition-selective fat grafting with novel adipose tissue derived product - stromal vascular fraction gel. *Biochem. Biophys. Res. Commun.* 495, 2249–2256. doi: 10.1016/j.bbrc.2017.11.196

Conflict of Interest: The authors declare that the research was conducted in the absence of any commercial or financial relationships that could be construed as a potential conflict of interest.

frontiers in Cell and Developmental Biology

REVIEW
published: 22 September 2020
doi: 10.3389/fcell.2020.567813

Mesenchymal Stromal Cell Immunology for Efficient and Safe Treatment of Osteoarthritis

*Mehdi Najar, Johanne Martel-Pelletier, Jean-Pierre Pelletier and Hassan Fahmi**

Osteoarthritis Research Unit, University of Montreal Hospital Research Center, Department of Medicine, University of Montreal, Montreal, QC, Canada

Mesenchymal stem cell (MSC) therapy represents a promising approach for the treatment of osteoarthritis (OA). MSCs can be readily isolated from multiple sources and expanded *ex vivo* for possible clinical application. They possess a unique immunological profile and regulatory machinery that underline their therapeutic effects. They also have the capacity to sense the changes within the tissue environment to display the adequate response. Indeed, there is a close interaction between MSCs and the host cells. Accordingly, MSCs demonstrate encouraging results for a variety of diseases including OA. However, their effectiveness needs to be improved. In this review, we selected to discuss the importance of the immunological features of MSCs, including the type of transplantation and the immune and blood compatibility. It is important to consider MSC immune evasive rather than immune privileged. We also highlighted some of the actions/mechanisms that are displayed during tissue healing including the response of MSCs to injury signals, their interaction with the immune system, and the impact of their lifespan. Finally, we briefly summarized the results of clinical studies reporting on the application of MSCs for the treatment of OA. The research field of MSCs is inspiring and innovative but requires more knowledge about the immunobiological properties of these cells. A better understanding of these features will be key for developing a safe and efficient medicinal product for clinical use in OA.

Keywords: mesenchymal stromal cells, therapeutic effects, immunity, tissue repair, safety, efficiency

OPEN ACCESS

Edited by:
Tiago Lazzaretti Fernandes, University of São Paulo, Brazil

Reviewed by:
Lucienne A. Vonk, CO.DON AG, Germany
Mariane Tami Amano, Hospital Sirio Libanes, Brazil

***Correspondence:**
Hassan Fahmi
h.fahmi@umontreal.ca

Specialty section:
This article was submitted to Stem Cell Research, a section of the journal Frontiers in Cell and Developmental Biology

Received: *30 May 2020*
Accepted: *24 August 2020*
Published: *22 September 2020*

Citation:
Najar M, Martel-Pelletier J, Pelletier J-P and Fahmi H (2020) Mesenchymal Stromal Cell Immunology for Efficient and Safe Treatment of Osteoarthritis. Front. Cell Dev. Biol. 8:567813. doi: 10.3389/fcell.2020.567813

INTRODUCTION

Recent advances in stem cell research have highlighted the role played by these cells and their environment in tissue homeostasis. Several resources of cells can be used to restore the damaged tissue, such as resident stem cells, multipotent adult progenitor cells or embryonic stem cells (Sánchez et al., 2012). As a cell-based therapy product, stem cells have created great hope among the medical field due to their therapeutic potential. However, there are ethical and safety concerns regarding the clinical use of human embryonic stem cells (hESC) and induced pluripotent stem cells (iPSC) (Volarevic et al., 2018). As relatively free from ethical concerns and safer, mesenchymal stem cell (MSCs) are a valuable alternative for cell-based therapy. Their ease of isolation and high *ex vivo* expansion potential have allowed a broad use of MSCs (Bianco et al., 2008).

Mesenchymal stem cells display a specific immunological profile and functions allowing them to efficiently down-regulate immunoinflammatory events and to promote tissue regeneration. In case

of tissue injury, local tissue precursor cells with immunomodulatory capacities were described to be recruited and activated (Hoogduijn, 2015).

Initially, the therapeutic effects of MSCs were thought to be mediated based on their multilineage differentiation ability that enabled them to replace damaged cells in injured tissue. Nonetheless, the capacity of MSCs to transdifferentiate into *tissue*-specific cell types *in vivo* has not been fully confirmed. This is because it is hard to track MSCs after transplantation due to the lack of reliable MSC-specific markers *in vivo*. Subsequent findings indicate that MSCs promote tissue repair through the production of a myriad of trophic factors, including growth factors, chemokines, cytokines and anti-oxidants, rather than direct differentiation and cell replacement (Becerra et al., 2011; Damia et al., 2018; Harrell et al., 2019b; Jimenez-Puerta et al., 2020).

This has prompted the development of numerous preclinical studies as well as clinical trials that demonstrated promising therapeutic results (Noronha et al., 2019). In some cases, the benefits of MSCs are not satisfactory and need to be improved (Andrzejewska et al., 2019; Rendra et al., 2020).

In this review, we mainly focused on the biological effects of MSCs upon their transplantation. We described the characteristics of the transplantation, the immune and blood compatibility, which are relevant for the therapy outcome. Following transplantation, MSCs modulate the local tissue homeostasis and immune responses (Nolta et al., 2020). It should be noted that MSCs do not need to migrate to injured tissue in order to exert their regenerative and immunomodulatory effects. For instance, intraperitoneal injection of allogenic MSCs reduced the severity of cartilage and bone damage in collagen-induced arthritis independently of MSC migration to the joints (Augello et al., 2007). Similarly, Swart et al. (2015) showed in a mouse model of proteoglycan-induced arthritis that intraarticular injection of MSCs ameliorates systemic responses independently of their capacity to migrate from the site of injection. These data suggest that MSCs may exert their beneficial effects on distant tissues, likely via extracellular vesicles.

A clear identification of the crosstalk between MSCs and the immune cells present within the tissue environment as well as their role during tissue repair is required. We therefore reported on the latest advances regarding the main functions and mechanisms of action of MSCs, considering the influence of the tissue microenvironment. In particular, we focused on the cellular and molecular changes that may affect MSCs (i.e., cell death) and contribute to these therapeutic effects. Improving our understanding of the immunological profile and therapeutic effects of MSCs will help to develop a safe, feasible, and efficient cell-therapy strategy.

THE CHARACTERISTICS OF THE TRANSPLANTATION

The transplantation of therapeutic cells depends on both donor and recipient specificities to guide the selection of a suitable graft. Several parameters including the type of transplantation (i.e., autologous, allogeneic, and xenogeneic), the route of cell delivery as well as the blood and immune compatibility of the cellular product should be examined before performing the therapy (Patrikoski et al., 2019).

TABLE 1 | Cell surface positive and negative markers of human MSCs as derived from Samsonraj et al. (2017).

Positive markers	Negative markers
CD105	CD45
CD73	CD34
CD90	CD14
HLA-ABC	CD11
CD10	CD79
CD13	CD19
CD29	HLA-DR
CD44	CD40
CD49	CD80L
CD54	CD80
CD166	CD86

Surface Phenotype of MSCs

The International Society for Cell Therapy (ISCT) has defined MSCs with a minimal set of three standard criteria: (a) adherence to plastic under standard culture conditions, (b) expression of CD105, CD73, and CD90, and lack expression of CD45, CD34, CD14 or CD11b, CD79α, or CD19, and HLA-DR surface molecules, and (c) differentiation into osteoblasts, adipocytes, and chondrocytes *in vitro* (Dominici et al., 2006).

However, these markers are not specific to undifferentiated MSCs and are also detected in other cell types such as fibroblasts and smooth muscle cells (Samsonraj et al., 2017). In addition, MSCs are a heterogeneous population of cells with varying degrees of self-renewal capacity and differentiation potential. Therefore, other surface antigens including CD10, CD13, CD29, CD44, CD49, CD54, and CD166 (Samsonraj et al., 2017) are also used considered as MSC markers (**Table 1**). Recently, the ISCT recommended that the acronym MSCs should be accompanied by tissue-source origin which would feature tissue-specific properties (Viswanathan et al., 2019).

The Immunological Profile of MSCs

The immunologic profile of MSCs has revealed that they express low levels of major histocompatibility complex (MHC) class I molecules. They do not express MHC class II molecules and co-stimulatory molecules CD40, CD80 and CD86, which participate in T cell activation.

This particular immunophenotypic profile allows MSCs to escape immune surveillance and promotes their hypoimmunogenic or immune privileged status. MSCs do not elicit a proliferative response when cocultured with allogeneic T cells *in vitro*. However, some studies reported that MSCs may express these molecules and lose their hypoimmunogenic/immune privileged state. For example, treatment with interferon gamma (IFNγ), which represents an inflammatory environment, induces the expression of MHC

class II molecules and increases the expression of MHC class I molecules (Romieu-Mourez et al., 2007; Van Megen et al., 2019).

As mentioned previously, MSCs typically do not express HLA-DR, an MHC class II molecule which plays important roles in allograft rejection. However, MScs may express these molecules during cell expansion (Grau-Vorster et al., 2019) and thus fail to meet all the ISCT's requirements for MSCs. MSCs were also reported to express HLA-DR after differentiation. For instance, Ryan et al. (2014) demonstrated that chondrogenically differentiated MSCs express HLA-DR. Chondrogenic MSCs induce the proliferation of both CD4 and CD8 cells and increase susceptibility to cytotoxic lysis by allospecific T cells. Moreover, they lose their immunosuppressive properties as evidenced by their inability to prevent T cell proliferation. Subcutaneous implantation of chondrogenically differentiated MSCs increased the infiltration of mononuclear phagocytes and the generation of anti-donor IgG2 antibodies (Ryan et al., 2014). This raises the concern that after differentiation or transplantation, MSCs trigger immune responses, which may hamper their therapeutic efficacy. Further studies are clearly needed to determine the impact of HLA-DR expression in chondrogenically differentiated MSCs on their therapeutic efficacy in OA.

Blood Compatibility of MSCs

The ABO blood group is one of the major immunogenic barriers hampering tissue transplantation into immunocompetent hosts. Indeed, incompatible blood group antigens are highly immunogenic and can cause graft rejections. Such issues may be instrumental in better defining their therapeutic potential in clinical trials. MSCs do not present carbohydrate- and protein-based membrane structures that are defined as blood group antigens. Moreover, MSCs do not upregulate ABO blood group antigens after inflammatory challenge or *in vitro* differentiation confirming that their therapeutic efficacy is not altered by immunogenic blood group antigens (Schäfer et al., 2011).

Selection of Autologous or Allogeneic Transplantation

For cell therapy purposes, the use of *in vitro*-expanded autologous or allogeneic cell populations is possible. In autologous transplantation, the cells are collected from the patient's own tissues, which does not require human leucocyte antigen (HLA) matching therefore avoiding immunological complications (Champlin, 2003). However, allogeneic transplants between two genetically different individuals may be associated with some difficulties (Liras, 2010). Indeed, the graft type of MSCs is a key determinant for the success of the therapy because it is closely linked to the immune response that may be elicited by the recipient. While most of these clinical and preclinical trials utilized autologous MSCs, a significant number of studies examined the feasibility of allogeneic or even xenogeneic MSC transplantation (Lin et al., 2012).

The use of autologous MSCs is time-consuming and costly with additional drawbacks such as donor site morbidity and quality issues in patients with comorbidities or advanced age whose MSCs may have reduced therapeutic efficacy. In contrast, allogeneic MSCs appear to be one of the most promising candidates for therapeutic applications because it provides "off-the-shelf" cellular therapy (Wang et al., 2019). Consequently, understanding their interactions with the recipient's immune system is crucial for their successful clinical application (Kot et al., 2019). Importantly, evidence from currently completed and ongoing clinical trials demonstrate that allogeneic MSC transplantation is safe and seems to cause no major side effects to the patient (Kot et al., 2019). For instance, the POSEIDON clinical trial provided evidence that allogenic MSCs display superior efficacy to autologous MSCs in the treatment of non-ischemic dilated cardiomyopathy (Hare et al., 2017). Interestingly, allogenic MSCs were shown to promote cartilage regeneration and improve the symptoms of OA in two recent clinical trials (Vega et al., 2015; de Windt et al., 2017).

Transplantation of xenogenic MSCs is often unsuccessful due to irreconcilable interspecies differences. There is phylogenetic distinction based on differences in the key mediators of the immunosuppressive effects of MSCs (Su et al., 2014). Moreover, differences in cytokine signaling might lead to failure of MSC activation and therefore to therapeutic misinterpretation or lack of *in vivo* efficient effect. Thus, interspecies incompatibilities from preclinical data should be taken into consideration before translation to clinical trial (Lohan et al., 2018). Overall, the characterization of a functional population of MSCs with a specific profile and function may ultimately influence the choice between autologous or allogeneic transplantation.

The Delivery Route of MSCs

Depending on the clinical purposes, MSCs are administered differently, either systemically infused, locally injected, or locally applied in a cell-carrier glue (de Windt et al., 2017). The optimal cell delivery technique should provide the most regenerative benefit with the lowest side effects. The most common routes of MSC transplantation outside tissue engineering-based methods are by intravenous or intra-arterial infusion, or by direct intra-tissue injection (Kurtz, 2008). Local transplantation deposits MSC in spatial proximity to the lesion, i.e., intraarticularly in the case of OA. Systemic administration routes are favored but require the targeted extravasation of the circulating MSCs at the site of injury. Transplanted MSCs can indeed leave the blood flow and transmigrate through the endothelial barrier, and reach the lesion site (Nitzsche et al., 2017).

THE THERAPEUTIC EFFECTS OF MSCs

The beneficial effects of MSCs rely mostly on their capacity to sense tissue injury, and consequently to display several coordinated therapeutic actions. Through their regulatory and trophic factors, MSCs attenuate detrimental immune response, remove pathogens, and promote the functions of local cells (Harrell et al., 2019a). We highlighted hereafter some relevant elements that contribute to the therapeutic process of MSCs.

The Process of Tissue Injury and Healing

The physiological response to tissue damage involves three consecutive and coordinated phases: inflammatory, reparative, and remodeling. During this process, the inflammatory/immunological status (defined as the nature of immune cells as well as the types and concentrations of present cytokines) varies considerably (Wang et al., 2014). During the first phase of healing, there is a predominance of proinflammatory signals which decrease in the reparative and remodeling phases (wound healing period). The prevalence of proinflammatory mediators induce the recruitment of inflammatory cells (such as neutrophils, monocyte, and platelets). Monocytes/macrophages play the leading role in innate immunity and tissue homeostasis. These cells accumulate in site of injury and are actively involved in tissue repair (Wallace et al., 2012). Then, the infiltrated neutrophils begin to undergo apoptosis, which causes macrophages to shift toward an anti-inflammatory phenotype (wound-healing subset).

MSCs Are Environmentally Responsive

The dynamic flux in the immune microenvironment is essential to facilitate the migration and proliferation of therapeutic cells to repair and regenerate tissue (Toh et al., 2018). Depending on the signals sensed by MSCs, they can migrate and home within a specific tissue. Indeed, MSCs are sensitive to shifts in the local milieu as they harbor a panel of receptors activating various signaling pathways (Paladino et al., 2019). We have previously shown that MSCs express several relevant receptors, such as the receptor for advanced glycation end-products (RAGE), C-type lectin receptors (CLRs, including DECTIN-1, DECTIN-2 and MINCLE), leukotriene B4 (LTB4) receptors (BLT1 and BLT2) and cysteinyl leukotriene (CysLTs) receptors (CYSLTR1 and CYSLTR2) (Najar et al., 2018). These receptors, known for their role in the regulation of inflammatory and immunological responses, were significantly modulated following MSC exposure to inflammatory signals. It is now recognized that the functions of MSCs are not constitutive but induced during their presence in the injured site (Kaundal et al., 2018). This plasticity in their properties allows MSCs to acquire specific phenotypes and functions.

Mobilization and Homing of MSCs

Mesenchymal stem cells reside in their tissue in normal physiological conditions but seem to have the capacity to be mobilized in response to signals produced by injured tissues. These signals may have a role in determining the function of MSCs, e.g., in the promotion of pathogen clearance or the modulation of the inflammation. In response to local environmental cues, MSCs start circulating, proliferate, and migrate from their niche to the injury site. The homing of MSCs is based on a multistep model involving (1) initial tethering by selectins, (2) activation by cytokines, (3) arrest by integrins, (4) diapedesis or transmigration using matrix remodelers, and (5) extravascular migration toward chemokine gradients (Ullah et al., 2019). MSC migration *in vitro* can be induced by different growth factors and chemokines and is enhanced by the pro-inflammatory cytokine tumor necrosis factor alpha TNF-α (Ponte et al., 2007), suggesting that the mobilization of MSCs and their subsequent homing to injured tissues may depend on the systemic and local inflammatory state. Moreover, under injury conditions, endothelial cells are activated and express docking molecules such as CD106 and CD62E (E-selectin). Their ligands, CD49d/CD29 (integrin α4/β1) and CD44, respectively, are expressed by MSCs and are important for their homing and docking (Rüster et al., 2006). In line with this, we have shown that the expression of adhesion molecules by MSCs are tightly regulated and differentially modulated depending on the cell environment. Specifically, we found that an inflammatory or infectious environment, as well as an activated immune response lead to a significant increase of CD54 (intercellular adhesion molecule 1) and CD58 (lymphocyte function-associated antigen 3) expression (Najar et al., 2010). These data were further corroborated by the evidence that damage/inflammatory mediators initiate a cascade of endothelial and leukocyte/MSC adhesion and motility responses relevant to the repair process (Nitzsche et al., 2017). These findings indicate that the homing and adhesion of MSCs are substantially sensitive to the local environment with the injured tissue and are therefore decisive for their therapeutic functions.

MSC-Mediated Cell Empowerment

Initially, the popular appeal as cell-based therapy was based on the *in vitro* multilineage potential of MSCs. Indeed, the tissue repair capability of MSCs was thought to be consecutive to their local differentiation into functional cells to replace the damaged cells. However, there is no *in vivo* evidence that these cells exert their regenerative effects through engraftment and differentiation into target cells (Ayala-Cuellar et al., 2019). In addition, the lack of standardized methods for their isolation, expansion, and identification does not allow to define terminally differentiated and functionally mature populations (Nombela-Arrieta et al., 2011). It has been demonstrated that the multipotency of MSCs is not a pivotal aspect of cell therapy, and thus primarily referred to their paracrine function as a major activity in tissue repair (Drela et al., 2019). In fact, the tissue−specific resident cells of the patient are actively involved in tissue regeneration and repair. These processes are stimulated by the bioactive factors secreted by the exogenously supplied MSCs, rather than by direct differentiation of MSCs (Prockop, 2007). Consequently, upon arrival at damaged tissue, MSCs are believed to exert their regenerative and repair effects by cell "empowerment" rather than by cell replacement. It is likely that MSCs regulate the local environment during tissue repair and provide a good "soil" for tissue regeneration.

It is increasingly recognized that the local environment with it stromal and immunological components (both cellular and molecular) are significantly important for the success of the therapy (Li H. et al., 2019). Indeed, the therapeutic effect of MSCs is mainly a combination of immunomodulation and local cell "empowerment" (Wang et al., 2014). The inhibition of local inflammation and immune responses (immunomodulation) by MSCs establishes a favorable environment to initiate tissue regeneration through empowering the activities of local

tissue stem/progenitor cells. A concerted action of secreted factors by MSCs will induce tissue repair through promoting angiogenesis, remodeling of the extracellular matrix, stimulating the proliferation and differentiation of progenitor/resident cells, and the recruitment of endogenous stem cells to the site of engraftment (Qi et al., 2018). Moreover, several studies underline bioactive exchanges, including ions, nucleic acids, proteins, and organelles transferred from MSCs to stressed cells, thereby improving cell survival and/or renewal in damaged or diseased tissues (Naji et al., 2019).

The Antimicrobial Activity of MSCs

Tissue injury may be also accompanied by infection due to pathogen invasion which may delay the healing process. In this context, MSCs were shown to have strong antimicrobial activities exerted through indirect and direct mechanisms. Most of the data on the antimicrobial properties of MSCs have been obtained from *in vitro* studies with bacteria, although little data exist about the effect of MSCs on viruses, fungi, and parasites. For instance, MSC administration to dogs with spontaneous chronic multi-resistant wound infections led to bacterial clearance and wound healing (Johnson et al., 2017). These effects are partially mediated by the secretion of antimicrobial peptides and proteins (AMPs) (Alcayaga-Miranda et al., 2017). Depending on the tissue origin of MSCs, several AMPs such as cathelicidins (e.g., LL-37), β-defensins (hBD-1, hBD-2, and hBD-3), hepcidin, or lipocalin families (e.g., Lcn2) have been described. These AMPs represent the major arm of the innate immunity and play important roles in initiating inflammation and further immune responses. Moreover, they participate in wound repair by stimulating the expression of cytokines and chemokines involved in the recruitment of immune cells and tissue progenitors (Chow et al., 2020).

Therapeutic Effects of MSCs in OA

Mesenchymal stem cells have been used for the treatment of OA based on their chondrogenic potential or their ability to promote cartilage repair through stimulation of endogenous cells and immunomodulation. In addition MSCs have significant paracrine activity, whereby they secrete a wide array of growth factors, cytokines, and chemokines that mediate various effects on chondrocytes including stimulation of proliferation, autophagy, and ECM synthesis (anabolic activity), as well as the inhibition of apoptosis, senescence, and the production of pro-inflammatory and catabolic factors (**Figure 1**) (for reviews, see references Damia et al., 2018; Harrell et al., 2019b).

In recent years, an increasing number of studies have suggested that the beneficial effects of MSCs are primarily mediated by extracellular vesicles (EVs), particularly exosomes. Cosenza et al. (2017) showed that the treatment of murine OA-like chondrocytes with BM-MSC-derived exosomes promoted anabolic activities (type II collagen and aggrecan), inhibited catabolic (MMP-13 and ADAMT-5) and inflammatory (iNOS) responses, and protected from apoptosis. Using a collagenase-induced OA mouse model, they reported that intraarticular injection of BM-MSC-derived exosomes prevented both cartilage and bone damage. Qi et al. (2019) demonstrated that treatment of rabbit chondrocytes with BM-MSC-derived exosomes prevented IL-1-induced apoptosis, likely via inhibition of the p38 and ERK MAPKs and activation of the Akt pathway. Inhibition of apoptosis by MS-MSC-derived exosomes was also reported in rat chondrocytes (Zhu et al., 2018). More recently, He et al. (2020) evaluated the effect of BM-MSC-derived exosomes on inflammatory and catabolic responses *in vitro* and on the progression of OA in a rat model of the disease. They found that treatment with exosomes diminished the inhibitory effect of IL-1 on the proliferation, migration, and anabolic activity of chondrocytes. Accordingly, *in vivo* studies revealed that administration of exosomes was protective *in vivo*, likely via increased anabolic responses and reduced catabolic responses in the joints (He et al., 2020).

AT-MSC-derived exosomes were also reported to have chondroprotective properties. Treatment of human OA chondrocytes with AT-MSC-derived exosomes decreased IL-1-induced production of numerous inflammatory and catabolic mediators including TNF-α, IL-6, PGE2, NO and MMP13, whereas the production of the anti-inflammatory cytokine IL-10 and type II collagen were enhanced (Tofiño-Vian et al., 2018). The expression of COX-2 and mPGES1 were also down-regulated. These changes were likely due to reduced activity of NF-kB and AP-1. Similarly, Zhao et al. (2020) reported that AT-MSC-derived exosomes displayed chondroprotective and anti-inflammatory properties. They found that co-culture of AT-MSC-derived exosomes with activated synovial fibroblasts reduced the expression of IL-6 and TNF-α, whereas the expression of IL-10 was enhanced. Co-culture with chondrocytes protected from H_2O_2-induced apoptosis. Interestingly, treatment with exosomes stimulated chondrogenesis and increased the expression of chondrogenic markers, such as collagen type II and β-catenin (Zhao et al., 2020). More recently, it was evidenced that human AT-MSC-derived EVs increased human OA chondrocyte proliferation and migration, enhanced type II collagen synthesis, and reduced IL-1-mediated expression of key catabolic enzymes, MMP-1, MMP-3, MMP-13, and ADAMTS-5 (Woo et al., 2020). Further *in vivo* studies indicated intraarticular injection of AT-MSC-derived EVs attenuated cartilage degradation and synovial inflammation in both monosodium iodoacetate-induced OA in rats and destabilization of the medial meniscus (DMM)-induced OA in mice (Woo et al., 2020).

In addition to bone marrow and adipose tissue, exosomes isolated from other sources such as embryonic stem cells have also shown beneficial effects in cartilage repair and OA. For instance, Zhang et al. (2016) demonstrate that human embryonic MSC-derived exosomes promote cartilage repair and regeneration in a rat model of osteochondral defects. After 12 weeks, exosome-treated defects displayed complete recovery of hyaline cartilage characterized by regular biosynthesis and deposition of type II collagen and glycosaminoglycan (GAG). Using a mouse model of instability-induced OA, Wang and colleagues showed that human embryonic MSC prevented cartilage erosion and the expression of ADAMTS-5, a key enzyme in cartilage degradation. Moreover, *in vitro* experiments revealed that treatment with MSC-derived exosomes

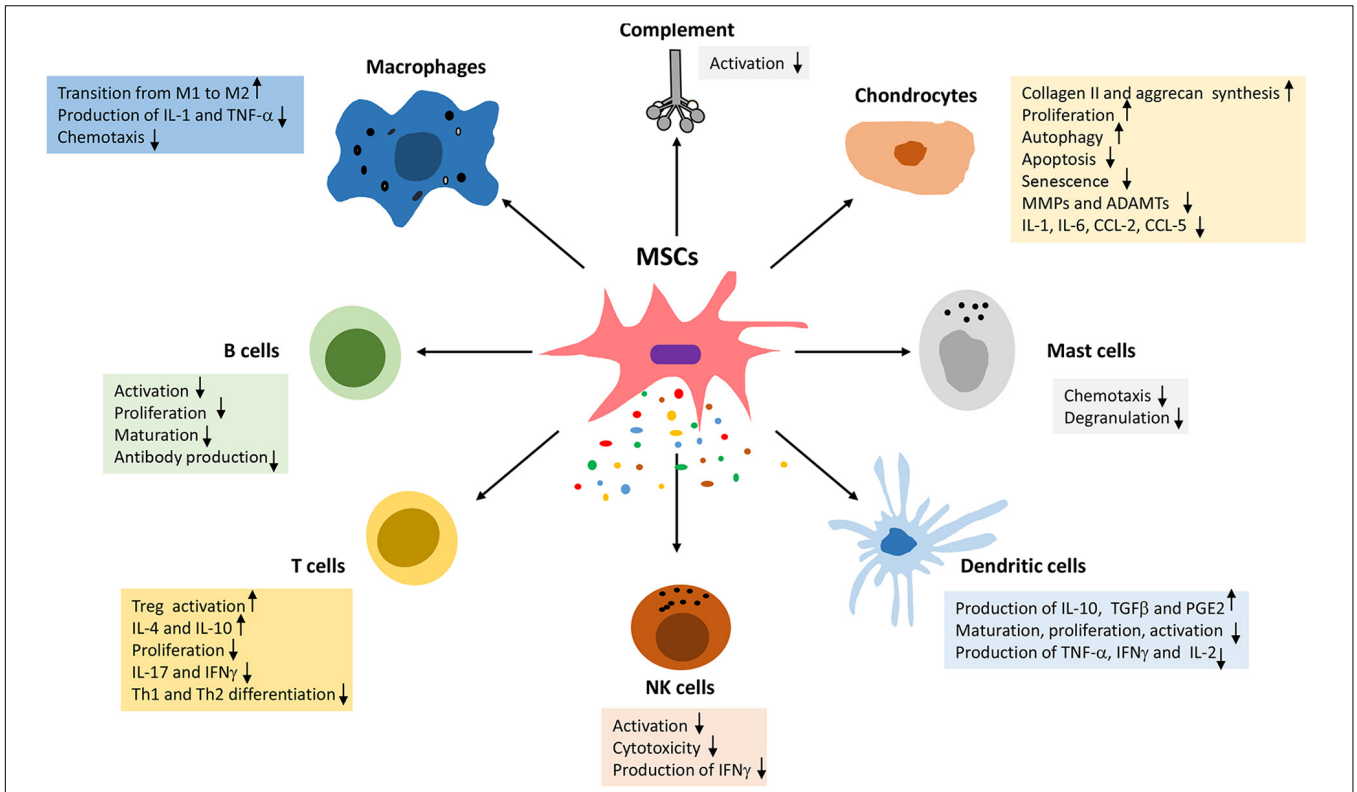

FIGURE 1 | Immunomodulatory effects of MSCs in osteoarthritis.

preserved chondrocyte phenotype upon treatment with IL-1β (Wang et al., 2017).

IMMUNOREGULATION AS A KEY MECHANISM IN TISSUE REPAIR

As previously evoked, MSCs promote tissue repair and regeneration through cell-empowerment and favoring an immune tolerogenic environment. Indeed, MSCs are not immune cells but regulatory progenitors with strong immunomodulatory properties. They can interact with different types of immune cells, leading to reciprocal interplay and modulation (Nemeth, 2014). MSC-mediated immunomodulation operates through a synergy of cell contact-dependent mechanisms and release of soluble factors (Li Y. et al., 2019). These pathways, as it will be highlighted below, cooperate to create a tolerogenic environment suitable for tissue regeneration.

Recruitment of Regulatory Immune Cells

Mesenchymal stem cells can interact with various types of immune cells, including T cells, B cells, natural killer (NK) cells, macrophages, dendritic cells, neutrophils, and monocytes (Leyendecker et al., 2018a). After these interactions, several features linked to immune response such as activation, proliferation and functions of immune cells are modulated by MSCs. We and others have reported that several regulatory immune cells such as Treg, Breg, NKreg, M1/M2, and DCreg are generated from both the innate and adaptive responses following contact with MSCs (Najar et al., 2016). These regulatory cells accumulate within the tissue of interest and regulate the local immune environment to facilitate the tissue repair.

Production of Immunoregulatory Mediators

Both direct cell–cell contact (membrane bounded proteins and receptors) and secretion of regulatory mediators can underline the immunomodulatory effects of MSCs. The secretome of MSCs is composed of cytokines, chemokines, and trophic factors that can be released in the extracellular milieu or within EVs (Zhou et al., 2019). Many mediators were shown to contribute to the therapeutic effects of MSCs including transforming growth factor (TGF)-β1, hepatocyte growth factor (HGF), prostaglandin E2 (PGE_2), indoleamine 2,3-dioxygenase (IDO), nitric oxide (NO), leukemia inhibitory factor (LIF), HLA-G, heme oxygenase-1 (HO-1), insulin growth factor (IGF)/IGF-binding protein (BP) system, TNF-a-stimulated gene 6 (TSG-6), metalloproteinases (MMP-2; MMP-9), TIMP-2 tissue inhibitor of metalloproteinases (TIMP-2; TIMP-3) and chemokine (C-C motif) ligand 2 and 5 (CCL2; CCL5), interleukin (IL)-10, IL-6, semaphorins, galectins, CD200/CD200R, erythropoietin-producing hepatocellular (Eph) receptor tyrosine kinase-B/Eph family receptor interacting proteins (ephrin)-B, glycoprotein

A repetitions predominant (GARP), and purinergic signaling (Damia et al., 2018; Harrell et al., 2019b).

IL-10, a pleiotropic immunomodulatory cytokine, modulates both the innate and adaptive immune systems. Interestingly, several regulatory factors produced by MSCs, such as HGF, TSG-6, PGE2, IDO, HLA-G, and LIF, closely interact with IL-10 to establish a tolerogenic milieu suitable for T-cell inhibition. In addition, there are several interplays between IL-10 and these factors including reciprocal positive feedback loops. IL-10 seems to be primarily derived from immune cells, in particular T cells, and demonstrates an increased level during interactions with MSCs. In this context, we demonstrated that the IL-10/CD210 axis is critical during immunomodulation by inducing proliferative and molecular changes within the immune cells (Najar et al., 2015). Recently, a dose-dependent transfer of mitochondria (MitoT) by MSCs was suggested to promote Treg differentiation, which may rescue target organs from tissue damage and inflammatory response (Court et al., 2020). Additional mediators including lipids, messenger RNAs (mRNAs) and microRNAs (miRNAs) can also contribute to the therapeutic effects of MSCs through their pro-angiogenic, antifibrotic, antiapoptotic or anti-inflammatory properties (Pers et al., 2018a).

Regulation of Metabolic Pathways

There is a close link between the metabolism of immune cells and their biological features. Several metabolic pathways are considered as important actors for regulating immune responses. Indeed, immune cell activation, differentiation, and function require specific energetic and biosynthetic demands (Patel et al., 2019). Metabolic fitness has been shown to be crucial for supporting the major shift from quiescent to active immune cells and for tuning the immune response. Recent studies have shed new light on the role of the end products of metabolism such as lactate, acetate, and adenosine triphosphate (ATP) (Degauque et al., 2018). Such products are likely to participate to tissue and immune homeostasis and are therefore important during transplantation. Intracellular ATP is well-known as the energy source driving cell survival, proliferation, and metabolic function (Pearce and Pearce, 2013). However, under tissue stress, ATP can be released from cells into the extracellular environment. In that sense, MSCs were shown to modulate the immune response by a dynamic ATP hydrolysis (Burr and Parekkadan, 2019). ATP was shown to promote the immunosuppressive properties of MSCs via upregulation of IDO expression (Lotfi et al., 2018). It is noteworthy that, the level of ATP should be well controlled since uncontrolled levels can affect several cellular features and functions. In the case of human endometrium MSCs, ATP was shown to induce cell cycle arrest, alter the proliferative and migration capacity and therefore could affect their regenerative potential (Semenova et al., 2020).

Adenosine (ADO) is a nucleoside with pleiotropic functions, which acts as an intracellular and extracellular mediator of multiple biological processes, including immune responses. It is considered as a common path for MSCs and Treg-mediated immunosuppression (De Oliveira Bravo et al., 2016). In fact, the production of adenosine constitutes a mechanism used by both cell types to control the immune response particularly in the inflammatory environment. To produce ADO, ATP is hydrolyzed to 5′-AMP and ADP by the ectonucleotidase CD39. ADP is further hydrolyzed to ADO by the second ectonucleotidase CD73. Although CD73 is one of the main and highly expressed markers within MSCs, the expression and modulation of CD39 by MSCs has also been confirmed (Kerkelä, 2017). Whereas MSCs from different tissues exhibit many common characteristics, their biological activity and some markers are different and depend on their tissue of origin. Changes in the expression profile of certain markers is also dependent on the environment surrounding MSCs (Kozlowska et al., 2019). Current data indicate that MSCs exhibit different sensitivity to purinergic ligands as well as a distinct activity and expression profiles of ectonucleotidases than mature cells. MSCs may abundantly produce ADO in contrast to other progenitor cells (Jeske et al., 2020). The adenosinergic pathway emerges as a key mechanism by which MSCs exert hemostatic and immunomodulatory functions. Depending on the CD73/adenosine pathway, MSCs inhibited platelet activation and aggregation (Netsch et al., 2018), altered T-cell activation (Chen et al., 2016), and reduced NK cell activity (Yan et al., 2019). Of note, NK cells interacting with MSCs may acquire the expression of external nucleotide CD73. These new CD73−positive NK cells can regulate the function of resting NK cells in either an autocrine or paracrine manner. Intriguingly, the inhibition of CD39 and CD73 ectonucleotidases enhanced the mobilization of MSCs by decreasing the extracellular level of adenosine, which may influence the therapeutic outcomes (Adamiak et al., 2019). The heterogeneity in CD73 expression and its catalytic products may have distinct modulatory effects on the local immune response. This statement may explain the differences observed during tissue regenerative cell-based therapy (Tan et al., 2019).

Overall, it is important to consider and revise the influence of immunometabolism on the therapeutic process of MSCs. This will improve our understanding of the immunobiology of MSCs as well as their therapeutic efficacy.

Immunomodulatory Properties/Effects of MSCs in OA

Osteoarthritis has long been considered a "wear and tear" disease culminating in cartilage loss, but it is now widely accepted that inflammation plays a key role in its pathogenesis. The inflammatory cycle of OA is thought to result from interactions between the immune system and local tissue degradation products. Accumulating clinical evidence recognizes synovial inflammation (synovitis) as a characteristic of OA (Robinson et al., 2016). It is present in about half of the patients with OA and has been shown to correlate with the severity of knee OA symptoms, particularly pain (Hill et al., 2007) and with cartilage damage severity (Ayral et al., 2005).

In OA, synovial membranes are infiltrated with various immune cells predominantly monocytes/macrophages followed by T cells. Mast cells, NK cells, dendritic cells, B cells and granulocytes have also been identified in OA synovium. This

topic has been more comprehensively reviewed elsewhere (van den Bosch et al., 2020).

MSCs have significant immunomodulatory capacity and can suppress all immune cells involved in the development and progression of OA (**Figure 1**). MSCs can promote macrophage transition from the IL-1 and TNF-α producing pro-inflammatory M1 phenotype to the IL-10, IL-RA, and TGF-β producing anti-inflammatory and pro-chondrogenic phenotype (Fernandes et al., 2020). The effect of MSCs on macrophage polarization are mediated via TNFα-stimulated gene/protein 6 (TSG-6), prostaglandin E2 (PGE2) and indoleamine 2,3-dioxygenase (IDO) (Fernandes et al., 2020).

Mesenchymal stem cells, can suppress the proliferation and function of CD4+ and CD8+ T cells and promote the proliferation of immunosuppressive T regulatory cells (Luque-Campos et al., 2019). Moreover, MSCs prevent most functions of NK cells including cytotoxicity, cytokine and granzyme B secretion (Luque-Campos et al., 2019). MSCs were also shown to inhibit the proliferation of autoreactive B cells (de Castro et al., 2019). The proliferation, maturation, and antigen-presenting function of dendritic cells (DC) are also suppressed by MSCs (Spaggiari et al., 2009). Moreover, MSCs suppress numerous functions of mast cells including degranulation, cytokine production and chemotaxis (Brown et al., 2011). Further studies showed that MSC inhibit activation of the complement system (Tu et al., 2010), which plays a central role in the pathophysiology of OA.

Last but not least, MSCs or exosomes may induce their protective effects in OA by modulating chondrocyte functions. Specifically, MSCs were reported to prevent several inflammatory and catabolic events in chondrocytes and cartilage explants (Harrell et al., 2019b). Reports also showed that MSCs enhance chondrocyte proliferation, autophagy and the synthesis of cartilage extracellular matrix (Harrell et al., 2019b).

CELL DEATH AS A COMPONENT OF MSC IMMUNOMODULATORY PROPERTIES

Once transplanted, MSCs may face a harsh microenvironment such as hypoxia, oxidative stress, damage signals, inflammatory, and immunological reactions. Such environments may blunt their engraftment, viability, and functionality indicating that there are further mechanisms by which MSCs repair tissue. It appears that the secretome is only one part of MSC effects, as the viability of MSCs does not appear to be a prerequisite for some of their therapeutic effects (Naji et al., 2019). Different cellular and molecular alterations underlining distinct cell death modes are observed during tissue regeneration (Liu et al., 2018).

Apoptosis

Apoptotic MSCs have been shown to participate in the tissue repair process and immunomodulation (Weiss and Dahlke, 2019). These findings are in keeping with the "dying stem cell hypothesis" stating that the apoptosis of MSCs causes a modulation of the local immune response with a down-regulation of the innate and adaptive immunity (Thum et al., 2005). Usually, apoptosis is an immunologically quiescent process dependent on normal numbers of apoptotic cells (ACs) and rapid clearance by professional and non-professional phagocytes within the injured tissue. MSCs were reported to directly phagocyte ACs, therefore increasing their PGE_2 production, which contributes to MSC-based immunotherapeutic effects (Zhang et al., 2019). In turn, under certain conditions, living MSCs may be subject to perforin-induced apoptosis through recipient cytotoxic cells (CTL or NK cells). Apoptotic MSCs could then face phagocytosis by host-innate immune cells (monocytes/macrophages). Thus, the roles of both "being eaten" and "eating others" appear to be implicated in the immunomodulation mechanisms of MSCs (Zhang et al., 2019). Indeed, apoptotic, metabolically inactivated, or even fragmented MSCs have been shown to possess an immunomodulatory potential as well (Weiss and Dahlke, 2019). After phagocytosis of MSCs, monocytes are polarized toward an immunoregulatory M2 phenotype and redistributed systemically. This mechanism may explain how MSCs with reduced life induce long lasting immunomodulatory effects (Weiss et al., 2019).

Mesenchymal stem cell efferocytosis (phagocytic clearance of apoptotic cells) has also been reported to contribute to their immunomodulatory effects (Piraghaj et al., 2018). Apoptotic MSCs release "find-me" signals that recruit macrophages which recognize "eat-me" signals such as phosphatidylserine (PtS). This recognition triggers an actin-mediated cytoskeletal rearrangement that enables engulfment of the apoptotic MSCs by macrophages. Efferocytosis culminates by the clearance of the dying/dead cells and their toxic components as well as the expression of immune tolerance factors (Galipeau and Sensébé, 2018). Recently, MSCs have been demonstrated to harness macrophage derived amphiregulin (AREG) to maintain tissue homeostasis after injury. By increasing the secretion of AREG in a phagocytosis-dependent manner, MSC-primed macrophages allowed immunosuppression through the promotion of regulatory T (Treg) (Ko et al., 2020).

Complement Mediated Cell Death

In addition to its role in the innate immune system, the complement pathway can contribute to tissue repair at different levels (Schraufstatter et al., 2015). The complement cascade may stimulate the phagocytosis of pathogens and damaged cells but also the recruitment of stem and progenitor cells to the site of injury. In parallel, it promotes inflammation and adaptive immune response as well as activation of cell death pathway. There is an interplay between the complement-mediated cell lysis and distinct cell death pathways (Fishelson et al., 2001). Activation of the terminal pathway of the complement system leads to insertion of terminal complement complexes (C5b-9) into the cell membrane, which may induce apoptosis via a caspase-dependent pathway. Apoptosis as a consequence of complement-mediated cell damage may provide an explanation for the presence of apoptosis in inflammatory processes, for instance in hyperacute xenograft rejection (Nauta et al., 2002). The complement system has been shown to interact with MSCs and to differentially influence some of their biological features (Schraufstatter et al., 2009). Accumulating evidence suggests that

molecules of the innate immune system, including complement components and pentraxins, have a role in the recognition and clearance of apoptotic cells (Nauta et al., 2003). In a complement-activated environment, MSCs are injured following formation of membrane attack complexes (MACs), which may be linked to the rapid clearance of systemically circulating MSCs after infusion (Li and Lin, 2012). Moreover, complement-mediated opsonization has a pivotal role in immune tolerance by recognition and uptake of apoptotic cells and modulation of cytokine release (Jin and He, 2017). It was reported that complement activity, by binding to MSCs, promotes their phagocytosis by monocytes, which may shift into M2-healing subsets thus contributing to establishing a tolerogenic environment (Gavin et al., 2019). Intriguingly, MSCs have been shown to express complement inhibitor proteins CD46, CD55, CD59, and Factor H suggesting that they are partially protected from the lytic activity of complement (Tu et al., 2010). Indeed, BM-MSCs have been reported to express the receptors for anaphylatoxins C3a and C5a which are highly present within inflamed and injured tissues. Such expression was linked to homing of MSCs to site of injury, resistance to oxidative stress and apoptosis as well as inhibition of immune response (Le Blanc and Davies, 2015). Despite the rapid clearance of MSCs after systemic infusion, a favorable therapeutic effect is still observed. It is possible that complement activation by promoting monocyte phagocytosis of MSCs, participates in tissue repair.

Autophagy

The therapeutic potential of MSCs may also be linked to autophagy. Autophagy is a highly conserved cellular process that degrades modified, surplus, or harmful cytoplasmic components by sequestering them in autophagosomes, which then fuses with the lysosome for degradation. As a major intracellular degradation and recycling pathway, autophagy is crucial for maintaining cellular homeostasis, as well as for remodeling during normal development (Chen et al., 2018). MSCs may modulate autophagy of tissue-resident and recruited cells (target cells) involved in disease pathogenesis. MSCs can affect autophagy of immune cells involved in injury by reducing their survival, proliferation, and function and favoring the resolution of inflammation. In addition, MSCs can affect autophagy in endogenous adult or progenitor cells, promoting their survival, proliferation and differentiation and thus supporting the restoration of functional tissue (Ceccariglia et al., 2020). Stress signals or pharmacological agents can also modulate autophagy in MSCs. All these types of autophagy may affect MSC functions and have an impact on the therapeutic potential (either directly or indirectly) by influencing survival, vascularization, immunomodulation, and cell differentiation (Jakovljevic et al., 2018).

Senescence

Successful MSC therapy needs a prolonged and large-scale cell culture which may lead to cell senescence. Administration of senescent MSCs may result in an inefficient therapeutic issue (Li et al., 2017). Therefore, it is of utmost importance to enhance our knowledge of the aging process and methods to detect cell senescence in order to overcome this challenge. Senescence is a cellular response to stress limiting proliferation of damaged and aged cells. It is involved not only in pathological processes but also in physiological mechanisms like aging, tissue repair, and homeostasis (Neri and Borzì, 2020). Several factors such as DNA damage, telomere shortening, oncogenic insults, metabolic stress, epigenetic changes, and mitochondrial dysfunction might induce senescence (Neri and Borzì, 2020). Aging of MSCs (both *in vivo* and *in vitro*) can affect distinct properties of MSCs such as self-renewal, proliferation, differentiation, and immunomodulation thus possibly compromising their therapeutic effect (Chen et al., 2018). A recent study indicated that aging significantly altered distinct biological characteristics of MSCs, with old MSCs displaying reduced proliferation, differentiation potential, immunoregulatory, and secretory ability (Yang et al., 2020).

THE THERAPEUTIC EFFECT OF MSCs DEPENDS ON THEIR ORIGIN

Since their first isolation BM, other alternative tissue sources of MSCs were identified. Because of this diversity, it is important to define MSCs and recognize the inherit differences between these sources (Le Blanc and Davies, 2018). The accessibility, frequency, and properties of MSCs may thus differ, requiring more attention in the choice of the source of MSCs (Busser et al., 2015). Moreover, it is essential to find non-invasive cell sources to avoid donor site morbidity (Pinheiro et al., 2019). In addition to BM, MSCs have also been isolated from adipose tissue, synovial membrane, fetal tissues, and dental pulp (Leyendecker et al., 2018b). MSCs from different tissue sources may share similar phenotypes and proliferation properties, but show distinct transcriptome and cytokine profiles (Meng et al., 2019). Indeed, these MSCs may present unique gene expression pattern that reflects an advantage in terms of biological activities (Alhattab et al., 2019). Several differentially expressed genes were identified among these types of MSCs playing roles in immunomodulation, angiogenesis, wound healing, apoptosis, and chemotaxis (Barrett et al., 2019). These specific signaling pathways suggest that MSCs preserve different functional potentials according to their origin (Najar et al., 2019). For example, synovial and infrapatellar fat pad-derived stem cells present improved proliferative and survival potential in comparison to BM (Fernandes et al., 2018). Wharton's jelly of the human umbilical cord (WJ-MSCs) were shown to display distinct immunomodulatory and pro-regenerative transcriptional signature compared to BM-MSCs (Donders et al., 2018). WJ-MSCs may thus be considered as potent tolerogenic tools to modulate local immune response in support type regenerative medicine approaches (Corsello et al., 2019). Of note, MSCs are a composite of cell progenitors at different states of lineage commitment and cellular aging (O'Connor, 2019). Recently, several types of oral MSCs have been described as immunomodulatory masters because of their ability to interact with an inflammatory microenvironment and to exert a multitude of immunological actions (Zhou et al., 2020). Moreover, several distinct subpopulations of MSCs with differentially expressed genes related to proliferation,

development, and inflammation response were observed in WJ-MSCs (Sun et al., 2020). These subpopulations of MSCs may display distinct tissue repair effects, and therefore represent relevant sources for specific therapeutic applications.

CLINICAL TRIALS USING MSCs FOR THE TREATMENT OF KNEE OA

The use of MSCs in the treatment of OA is an expanding and growing area of research, and several studies have reported on the clinical efficacy of MSCs in OA. As stated above, MSCs can be isolated from many different tissues; however, BM- and *adipose tissue-derived MSCs* are the two most commonly used types of MSCs in OA therapy.

Orozco et al. (2013) studied 12 patients with knee OA who received an intraarticular injection of autologous expanded BM-derived MSCs (40×10^6 cells). These patients had Kellgren-Lawrence grade II-IV. They reported that patients had significant improvements in patient reported outcome measures, including visual analog scale (VAS), and the Western Ontario and McMaster Universities Arthritis Index (WOMAC) pain scores at 12 months. Patients also had improved quality of life as assessed by the 36-item Short Form *Health Survey* (*SF-36*). Magnetic resonance imaging (MRI) quantitative T2 mapping revealed an improvement of cartilage quality and a decrease of poor cartilage areas (Orozco et al., 2013). These improvements were maintained at 2 years (Orozco et al., 2014).

In a 5-year follow-up study, Davatchi and colleagues investigated the effects of transplanting autologous BM-MSCs in four patients with moderate to severe knee OA. At 6 months post-injection, three patients had improved functions as assessed by reduced walking distance to onset of pain. The number of stairs they could climb and the pain on the VAS were improved for all four patients. Then, they observed a progressive gradual deterioration, but at 5 years the outcomes were still better than at baseline, suggesting a protective role of BM-MSCs compared to untreated controls (Davatchi et al., 2011, 2016). It is noteworthy that this study only included four patients making it difficult to draw firm conclusions.

Lamo-Espinosa and colleagues tested the efficacy of two doses (10 or 100×10^6 cells) of autologous BM-derived MSC in combination with hyaluronic acid (HA) in a randomized controlled clinical trial. Thirty patients with OA (Kellgren–Lawrence grades II–IV) were enrolled with a follow-up period of 12 months. Patients who received BM-MSC showed improvement in WOMAC and VAS pain scores. Accordingly, the range of motion was also improved. Interestingly, radiological and MRI analyses revealed that only high dose treated-patients had significant improvement in cartilage thickness (Lamo-Espinosa et al., 2016). The observed clinical and functional improvement of knee OA was sustained after a follow up of 4 years.

In a similar study Soler et al. (2016), evaluated the effect of autologous BM-MSCs (40.9×10^6 cells) in 15 OA patients (Kellgren–Lawrence grades II–III). Outcomes assessed included VAS for pain, algofunctional Health Assessment Questionnaire, Quality of Life (QoL) SF-36 questionnaire, Lequesne functional index, WOMAC score, and cartilage structure. The authors reported improvements in pain and function, and noted signs of cartilage regeneration at 12 months, which were maintained for 4 years (Soler et al., 2016).

Administration of allogenic MSCs also led to significant improvements in knee OA. In a randomized controlled trial, Vega and colleagues compared the efficacy of allogenic BM-MSCs (40×10^6 cells) to HA in 30 patients. Outcomes analyzed included pain, disability, quality of life and cartilage quality. Compared to HA-treated patients, allogeneic-BM-MSC-treated patients showed improvement in pain and function. Additionally, there was a significant decrease in poor cartilage areas in MSC-treated patients (Vega et al., 2015). The therapeutic effect of observed in this trial was smaller than those reported for autologous MSCs. Further studies comparing the efficacy of autologous with allogenic BM-MSC in the same clinical trial are needed to confirm these findings.

In a randomized, double-blind, controlled trial, Gupta et al. (2016) evaluated the efficacy of different doses of allogenic BM-MSCs (25, 50, 75, or 150×10^6 cells) in 60 OA patients. Outcomes including VAS, WOMAC, intermittent and constant OA pain (ICOAP), and cartilage structure were evaluated at regular intervals for 12 months. All subjective outcomes tended to improve in participants who received MSCs, with the 25×10^6 dose being the most effective. However, MRI evaluation revealed no perceptible change in cartilage structure and integrity (Gupta et al., 2016).

More recently, Chahal et al. (2019), treated 12 patients with escalating doses of autologous BM-MSCs (1, 10, or 50×10^6 cells). There was an overall improvement in pain, symptom, quality of life, and stiffness scores. Best clinical and radiological responses were obtained in patients who received the high dose MSC. Interestingly, the synovial levels of monocytes/macrophages and IL-12 were decreased after MSCs administration. In addition, MSC-treated patients displayed lower cartilage catabolic biomarkers, suggesting a chondroprotective effect of MSCs (Chahal et al., 2019).

Adipose tissue-derived MSCs (AT-MSCs) have also been shown to have beneficial effects in the treatment of OA (Jo et al., 2014; Pers et al., 2016, 2018b). Pers and colleagues evaluated the impact of three doses of AT-MSCs (2, 10, or 50×10^6 cells) in 18 OA patients. The parameters assessed were pain and function. They reported that participants who received low dose of MSCs had the best response in terms of pain and function (Pers et al., 2016). A later study by the same group found that injection of AT-MSCs in the knee triggers a systemic long-lasting immune modulation involving an increase in the percentage of $CD4^+CD25^{high}CD127^{low}FOXP3^+$ regulatory T cells and $CD24^{high}CD38^{high}$ transitional B cells (Pers et al., 2018b).

In a distinct study using similar number of patients, Jo et al. (2014) tested the efficacy of increasing doses of AT-MSCs (10, 50, or 100×10^6 cells). Outcomes included pain, function and cartilage structure. Treatment with either dose improved all algofunctional indices and structural outcomes but statistical significance was reached only with the high dose of MSCs (Jo et al., 2014). It should be noted that the clinical improvement

does not last longer and started to decline within 2 years following treatment.

CONCLUSION AND PERSPECTIVES

The utilization of MSCs in the treatment of OA is a promising avenue. There are clearly several cellular regulatory pathways involved in the therapeutic effect of MSCs. These pathways cooperate to promote cartilage regeneration and an anti-inflammatory environment. Moreover, the broad cellular and molecular changes that accompany MSC apoptosis, autophagy, and senescence may be essential for their therapeutic effects. Identifying the function and mode of action of these different cell death pathways will help in improving the efficacy of MSCs in the treatment of OA. From our point of view, two important steps need to be developed to guarantee a successful anti-OA therapeutic strategy based on MSCs:

The first step is the understanding of the immunological profile and functions of MSCs as a graft. This would allow to match the adequate needs with the right response. Accordingly, we must find specific immunological signatures that identify these specific therapeutic progenitors.

The second step is the understanding of the mechanisms involved in the effects of MSCs for better therapeutic targeting. We should well-understand the tissue injury environment and mechanisms of the recipient that may critically influence the beneficial effects of MSCs.

Collectively, all these features are relevant for developing MSCs as a therapeutic option for OA with high quality, safety and efficiency standards.

AUTHOR CONTRIBUTIONS

All authors listed have made a substantial, direct and intellectual contribution to the work, and approved it for publication.

FUNDING

This work was supported by *La Chaire en Arthrose de l'Université de Montréal*, Montreal, QC, Canada.

ACKNOWLEDGMENTS

We warmly thank Dr. Laurence Lagneaux for fruitful discussions and constant support.

REFERENCES

Adamiak, M., Bujko, K., Brzezniakiewicz-Janus, K., Kucia, M., Ratajczak, J., and Ratajczak, M. Z. (2019). The inhibition of CD39 and CD73 cell surface ectonucleotidases by small molecular inhibitors enhances the mobilization of bone marrow residing stem cells by decreasing the extracellular level of adenosine. *Stem Cell Rev. Rep.* 15, 892–899. doi: 10.1007/s12015-019-09918-y

Alcayaga-Miranda, F., Cuenca, J., and Khoury, M. (2017). Antimicrobial activity of mesenchymal stem cells: current status and new perspectives of antimicrobial peptide-based therapies. *Front. Immunol.* 8:339. doi: 10.3389/fimmu.2017.00339

Alhattab, D., Jamali, F., Ali, D., Hammad, H., Adwan, S., Rahmeh, R., et al. (2019). An insight into the whole transcriptome profile of four tissue-specific human mesenchymal stem cells. *Regen. Med.* 14, 841–865. doi: 10.2217/rme-2018-0137

Andrzejewska, A., Lukomska, B., and Janowski, M. (2019). Concise review: mesenchymal stem cells: from roots to boost. *Stem Cells* 37, 855–864. doi: 10.1002/stem.3016

Augello, A., Tasso, R., Negrini, S. M., Cancedda, R., and Pennesi, G. (2007). Cell therapy using allogeneic bone marrow mesenchymal stem cells prevents tissue damage in collagen-induced arthritis. *Arthritis Rheum.* 56, 1175–1186. doi: 10.1002/art.22511

Ayala-Cuellar, A. P., Kang, J. H., Jeung, E. B., and Choi, K. C. (2019). Roles of mesenchymal stem cells in tissue regeneration and immunomodulation. *Biomol. Ther.* 27, 25–33. doi: 10.4062/biomolther.2017.260

Ayral, X., Pickering, E. H., Woodworth, T. G., Mackillop, N., and Dougados, M. (2005). Synovitis: a potential predictive factor of structural progression of medial tibiofemoral knee osteoarthritis – results of a 1 year longitudinal arthroscopic study in 422 patients. *Osteoarthr. Cartil.* 13, 361–367. doi: 10.1016/j.joca.2005.01.005

Barrett, A. N., Fong, C. Y., Subramanian, A., Liu, W., Feng, Y., Choolani, M., et al. (2019). Human Wharton's jelly mesenchymal stem cells show unique gene expression compared with bone marrow mesenchymal stem cells using single-cell RNA-sequencing. *Stem Cells Dev.* 28, 196–211. doi: 10.1089/scd.2018.0132

Becerra, J., Santos-Ruiz, L., Andrades, J. A., and Marí-Beffa, M. (2011). The stem cell niche should be a key issue for cell therapy in regenerative medicine. *Stem Cell Rev. Rep.* 7, 248–255. doi: 10.1007/s12015-010-9195-5

Bianco, P., Robey, P. G., and Simmons, P. J. (2008). Mesenchymal stem cells: revisiting history, concepts, and assays. *Cell Stem Cell* 2, 313–319. doi: 10.1016/j.stem.2008.03.002

Brown, J. M., Nemeth, K., Kushnir-Sukhov, N. M., Metcalfe, D. D., and Mezey, E. (2011). Bone marrow stromal cells inhibit mast cell function via a COX2-dependent mechanism. *Clin. Exp. Allergy* 41, 526–534. doi: 10.1111/j.1365-2222.2010.03685.x

Burr, A., and Parekkadan, B. (2019). Kinetics of MSC-based enzyme therapy for immunoregulation. *J. Transl. Med.* 17:263. doi: 10.1186/s12967-019-2000-6

Busser, H., Najar, M., Raicevic, G., Pieters, K., Pombo, R. V., Philippart, P., et al. (2015). Isolation and characterization of human mesenchymal stromal cell subpopulations: comparison of bone marrow and adipose tissue. *Stem Cells Dev.* 24, 2142–2157. doi: 10.1089/scd.2015.0172

Ceccariglia, S., Cargnoni, A., Silini, A. R., and Parolini, O. (2020). Autophagy: a potential key contributor to the therapeutic action of mesenchymal stem cells. *Autophagy* 16, 28–37. doi: 10.1080/15548627.2019.1630223

Chahal, J., Gomez-Aristizabal, A., Shestopaloff, K., Bhatt, S., Chaboureau, A., Fazio, A., et al. (2019). Bone marrow mesenchymal stromal cell treatment in patients with osteoarthritis results in overall improvement in pain and symptoms and reduces synovial inflammation. *Stem Cells Transl. Med.* 8, 746–757. doi: 10.1002/sctm.18-0183

Champlin, R. (2003). "Selection of autologous or allogeneic transplantation," in *Holland-Frei Cancer Medicine*, eds D. W. Kufe, R. E. Pollock, R. R. Weichselbaum, R. C. Bast, T. S. Gansler, J. F. Holland, et al. (Hamilton, ON: BC Decker).

Chen, X., He, Y., and Lu, F. (2018). Autophagy in stem cell biology: a perspective on stem cell self-renewal and differentiation. *Stem Cells Int.* 2018:9131397. doi: 10.1155/2018/9131397

Chen, X., Shao, H., Zhi, Y., Xiao, Q., Su, C., Dong, L., et al. (2016). CD73 pathway contributes to the immunosuppressive ability of mesenchymal stem cells in intraocular autoimmune responses. *Stem Cells Dev.* 25, 337–346. doi: 10.1089/scd.2015.0227

Chow, L., Johnson, V., Impastato, R., Coy, J., Strumpf, A., and Dow, S. (2020). Antibacterial activity of human mesenchymal stem cells mediated directly by constitutively secreted factors and indirectly by activation of innate immune effector cells. *Stem Cells Transl. Med.* 9, 235–249. doi: 10.1002/sctm.19-0092

Corsello, T., Amico, G., Corrao, S., Anzalone, R., Timoneri, F., Lo Iacono, M., et al. (2019). Wharton's jelly mesenchymal stromal cells from human umbilical cord: a close-up on immunomodulatory molecules featured in situ and in vitro. *Stem Cell Rev. Rep.* 15, 900–918. doi: 10.1007/s12015-019-09907-1

Cosenza, S., Ruiz, M., Toupet, K., Jorgensen, C., and Noel, D. (2017). Mesenchymal stem cells derived exosomes and microparticles protect cartilage and bone from degradation in osteoarthritis. *Sci. Rep.* 7:16214. doi: 10.1038/s41598-017-15376-8

Court, A. C., Le-Gatt, A., Luz-Crawford, P., Parra, E., Aliaga-Tobar, V., Bátiz, L. F., et al. (2020). Mitochondrial transfer from MSCs to T cells induces Treg differentiation and restricts inflammatory response. *Embo Rep.* 21:e48052. doi: 10.15252/embr.201948052

Damia, E., Chicharro, D., Lopez, S., Cuervo, B., Rubio, M., Sopena, J. J., et al. (2018). Adipose-derived mesenchymal stem cells: are they a good therapeutic strategy for osteoarthritis? *Int. J. Mol. Sci.* 19:1926. doi: 10.3390/ijms19071926

Davatchi, F., Abdollahi, B. S., Mohyeddin, M., Shahram, F., and Nikbin, B. (2011). Mesenchymal stem cell therapy for knee osteoarthritis. Preliminary report of four patients. *Int. J. Rheum. Dis.* 14, 211–215. doi: 10.1111/j.1756-185X.2011.01599.x

Davatchi, F., Sadeghi Abdollahi, B., Mohyeddin, M., and Nikbin, B. (2016). Mesenchymal stem cell therapy for knee osteoarthritis: 5 years follow-up of three patients. *Int. J. Rheum. Dis.* 19, 219–225. doi: 10.1111/1756-185X.12670

de Castro, L. L., Lopes-Pacheco, M., Weiss, D. J., Cruz, F. F., and Rocco, P. R. M. (2019). Current understanding of the immunosuppressive properties of mesenchymal stromal cells. *J. Mol. Med.* 97, 605–618. doi: 10.1007/s00109-019-01776-y

De Oliveira Bravo, M., Carvalho, J. L., and Saldanha-Araujo, F. (2016). Adenosine production: a common path for mesenchymal stem-cell and regulatory T-cell-mediated immunosuppression. *Purinergic Signal.* 12, 595–609. doi: 10.1007/s11302-016-9529-0

de Windt, T. S., Vonk, L. A., Slaper-Cortenbach, I. C. M., Nizak, R., van Rijen, M. H. P., and Saris, D. B. F. (2017). Allogeneic MSCs and recycled autologous chondrons mixed in a one-stage cartilage cell transplantion: a first-in-man trial in 35 patients. *Stem Cells* 35, 1984–1993. doi: 10.1002/stem.2657

Degauque, N., Brosseau, C., and Brouard, S. (2018). Regulation of the immune response by the inflammatory metabolic microenvironment in the context of allotransplantation. *Front. Immunol.* 9:1465. doi: 10.3389/fimmu.2018.01465

Dominici, M., Le Blanc, K., Mueller, I., Slaper-Cortenbach, I., Marini, F., Krause, D., et al. (2006). Minimal criteria for defining multipotent mesenchymal stromal cells. The international society for cellular therapy position statement. *Cytotherapy* 8, 315–317. doi: 10.1080/14653240600855905

Donders, R., Bogie, J. F. J., Ravanidis, S., Gervois, P., Vanheusden, M., Marée, R., et al. (2018). Human Wharton's jelly-derived stem cells display a distinct immunomodulatory and proregenerative transcriptional signature compared to bone marrow-derived stem cells. *Stem Cells Dev.* 27, 65–84. doi: 10.1089/scd.2017.0029

Drela, K., Stanaszek, L., Nowakowski, A., Kuczynska, Z., and Lukomska, B. (2019). Experimental strategies of mesenchymal stem cell propagation: adverse events and potential risk of functional changes. *Stem Cells Int.* 2019:7012692. doi: 10.1155/2019/7012692

Fernandes, T. L., Gomoll, A. H., Lattermann, C., Hernandez, A. J., Bueno, D. F., and Amano, M. T. (2020). Macrophage: a potential target on cartilage regeneration. *Front. Immunol.* 11:111. doi: 10.3389/fimmu.2020.00111

Fernandes, T. L., Kimura, H. A., Pinheiro, C. C. G., Shimomura, K., Nakamura, N., Ferreira, J. R., et al. (2018). Human synovial mesenchymal stem cells good manufacturing practices for articular cartilage regeneration. *Tissue Eng. Part C Methods* 24, 709–716. doi: 10.1089/ten.TEC.2018.0219

Fishelson, Z., Attali, G., and Mevorach, D. (2001). Complement and apoptosis. *Mol. Immunol.* 38, 207–219. doi: 10.1016/s0161-5890(01)00055-4

Galipeau, J., and Sensébé, L. (2018). Mesenchymal stromal cells: clinical challenges and therapeutic opportunities. *Cell Stem Cell* 22, 824–833. doi: 10.1016/j.stem.2018.05.004

Gavin, C., Meinke, S., Heldring, N., Heck, K. A., Achour, A., Iacobaeus, E., et al. (2019). The complement system is essential for the phagocytosis of mesenchymal stromal cells by monocytes. *Front. Immunol.* 10:2249. doi: 10.3389/fimmu.2019.02249

Grau-Vorster, M., Laitinen, A., Nystedt, J., and Vives, J. (2019). HLA-DR expression in clinical-grade bone marrow-derived multipotent mesenchymal stromal cells: a two-site study. *Stem Cell Res. Ther.* 10:164. doi: 10.1186/s13287-019-1279-9

Gupta, P. K., Chullikana, A., Rengasamy, M., Shetty, N., Pandey, V., Agarwal, V., et al. (2016). Efficacy and safety of adult human bone marrow-derived, cultured, pooled, allogeneic mesenchymal stromal cells (Stempeucel(R)): preclinical and clinical trial in osteoarthritis of the knee joint. *Arthritis Res. Ther.* 18:301. doi: 10.1186/s13075-016-1195-7

Hare, J. M., DiFede, D. L., Rieger, A. C., Florea, V., Landin, A. M., El-Khorazaty, J., et al. (2017). Randomized comparison of allogeneic versus autologous mesenchymal stem cells for nonischemic dilated cardiomyopathy: POSEIDON-DCM trial. *J. Am. Coll. Cardiol.* 69, 526–537. doi: 10.1016/j.jacc.2016.11.009

Harrell, C. R., Jankovic, M. G., Fellabaum, C., Volarevic, A., Djonov, V., Arsenijevic, A., et al. (2019a). Molecular mechanisms responsible for anti-inflammatory and immunosuppressive effects of mesenchymal stem cell-derived factors. *Adv. Exp. Med. Biol.* 1084, 187–206. doi: 10.1007/5584_2018_306

Harrell, C. R., Markovic, B. S., Fellabaum, C., Arsenijevic, A., and Volarevic, V. (2019b). Mesenchymal stem cell-based therapy of osteoarthritis: current knowledge and future perspectives. *Biomed. Pharmacother.* 109, 2318–2326. doi: 10.1016/j.biopha.2018.11.099

He, L., He, T., Xing, J., Zhou, Q., Fan, L., Liu, C., et al. (2020). Bone marrow mesenchymal stem cell-derived exosomes protect cartilage damage and relieve knee osteoarthritis pain in a rat model of osteoarthritis. *Stem Cell Res. Ther.* 11:276. doi: 10.1186/s13287-020-01781-w

Hill, C. L., Hunter, D. J., Niu, J., Clancy, M., Guermazi, A., Genant, H., et al. (2007). Synovitis detected on magnetic resonance imaging and its relation to pain and cartilage loss in knee osteoarthritis. *Ann. Rheum. Dis.* 66, 1599–1603. doi: 10.1136/ard.2006.067470

Hoogduijn, M. J. (2015). Are mesenchymal stromal cells immune cells? *Arthritis Res. Ther.* 17:88. doi: 10.1186/s13075-015-0596-3

Jakovljevic, J., Harrell, C. R., Fellabaum, C., Arsenijevic, A., Jovicic, N., and Volarevic, V. (2018). Modulation of autophagy as new approach in mesenchymal stem cell-based therapy. *Biomed. Pharmacother.* 104, 404–410. doi: 10.1016/j.biopha.2018.05.061

Jeske, S. S., Theodoraki, M. N., Boelke, E., Laban, S., Brunner, C., Rotter, N., et al. (2020). Adenosine production in mesenchymal stromal cells in relation to their developmental status. *HNO* 68, 87–93. doi: 10.1007/s00106-019-00805-z

Jimenez-Puerta, G. J., Marchal, J. A., López-Ruiz, E., and Gálvez-Martín, P. (2020). Role of mesenchymal stromal cells as therapeutic agents: potential mechanisms of action and implications in their clinical use. *J. Clin. Med.* 9:445. doi: 10.3390/jcm9020445

Jin, J., and He, S. (2017). The complement system is also important in immunogenic cell death. *Nat. Rev. Immunol.* 17:143. doi: 10.1038/nri.2016.142

Jo, C. H., Lee, Y. G., Shin, W. H., Kim, H., Chai, J. W., Jeong, E. C., et al. (2014). Intra-articular injection of mesenchymal stem cells for the treatment of osteoarthritis of the knee: a proof-of-concept clinical trial. *Stem Cells* 32, 1254–1266. doi: 10.1002/stem.1634

Johnson, V., Webb, T., Norman, A., Coy, J., Kurihara, J., Regan, D., et al. (2017). Activated mesenchymal stem cells interact with antibiotics and host innate immune responses to control chronic bacterial infections. *Sci. Rep.* 7:9575. doi: 10.1038/s41598-017-08311-4

Kaundal, U., Bagai, U., and Rakha, A. (2018). Immunomodulatory plasticity of mesenchymal stem cells: a potential key to successful solid organ transplantation. *J. Transl. Med.* 16:31. doi: 10.1186/s12967-018-1403-0

Kerkelä, E. (2017). Reply: adenosine producing mesenchymal stromal cells. *Stem Cells* 35, 1649–1650. doi: 10.1002/stem.2531

Ko, J. H., Kim, H. J., Jeong, H. J., Lee, H. J., and Oh, J. Y. (2020). Mesenchymal stem and stromal cells harness macrophage-derived amphiregulin to maintain tissue homeostasis. *Cell Rep.* 30, 3806.e6–3820.e6. doi: 10.1016/j.celrep.2020.02.062

Kot, M., Baj-Krzyworzeka, M., Szatanek, R., Musiał-Wysocka, A., Suda-Szczurek, M., and Majka, M. (2019). The importance of HLA assessment in "Off-the-Shelf" allogeneic mesenchymal stem cells based-therapies. *Int. J. Mol. Sci.* 20:5680. doi: 10.3390/ijms20225680

Kozlowska, U., Krawczenko, A., Futoma, K., Jurek, T., Rorat, M., Patrzalek, D., et al. (2019). Similarities and differences between mesenchymal stem/progenitor cells derived from various human tissues. *World J. Stem Cells* 11, 347–374. doi: 10.4252/wjsc.v11.i6.347

Kurtz, A. (2008). Mesenchymal stem cell delivery routes and fate. *Int. J. Stem Cells* 1, 1–7. doi: 10.15283/ijsc.2008.1.1.1

Lamo-Espinosa, J. M., Mora, G., Blanco, J. F., Granero-Molto, F., Nunez-Cordoba, J. M., Sanchez-Echenique, C., et al. (2016). Intra-articular injection of two different doses of autologous bone marrow mesenchymal stem cells versus hyaluronic acid in the treatment of knee osteoarthritis: multicenter randomized controlled clinical trial (phase I/II). *J. Transl. Med.* 14:246. doi: 10.1186/s12967-016-0998-2

Le Blanc, K., and Davies, L. C. (2015). Mesenchymal stromal cells and the innate immune response. *Immunol. Lett.* 168, 140–146. doi: 10.1016/j.imlet.2015.05.004

Le Blanc, K., and Davies, L. C. (2018). MSCs-cells with many sides. *Cytotherapy* 20, 273–278. doi: 10.1016/j.jcyt.2018.01.009

Leyendecker, A. Jr., Pinheiro, C. C. G., Amano, M. T., and Bueno, D. F. (2018a). The use of human mesenchymal stem cells as therapeutic agents for the in vivo treatment of immune-related diseases: a systematic review. *Front. Immunol.* 9:2056. doi: 10.3389/fimmu.2018.02056

Leyendecker, A. Jr., Pinheiro, C. C. G., Fernandes, T. L., and Bueno, D. F. (2018b). The use of human dental pulp stem cells for in vivo bone tissue engineering: a systematic review. *J. Tissue Eng.* 9:2041731417752766. doi: 10.1177/2041731417752766

Li, H., Shen, S., Fu, H., Wang, Z., Li, X., Sui, X., et al. (2019). Immunomodulatory functions of mesenchymal stem cells in tissue engineering. *Stem Cells Int.* 2019:9671206. doi: 10.1155/2019/9671206

Li, Y., Zhang, D., Xu, L., Dong, L., Zheng, J., Lin, Y., et al. (2019). Cell-cell contact with proinflammatory macrophages enhances the immunotherapeutic effect of mesenchymal stem cells in two abortion models. *Cell. Mol. Immunol.* 16, 908–920. doi: 10.1038/s41423-019-0204-6

Li, Y., and Lin, F. (2012). Mesenchymal stem cells are injured by complement after their contact with serum. *Blood* 120, 3436–3443. doi: 10.1182/blood-2012-03-420612

Li, Y., Wu, Q., Wang, Y., Li, L., Bu, H., and Bao, J. (2017). Senescence of mesenchymal stem cells (Review). *Int. J. Mol. Med.* 39, 775–782. doi: 10.3892/ijmm.2017.2912

Lin, C. S., Lin, G., and Lue, T. F. (2012). Allogeneic and xenogeneic transplantation of adipose-derived stem cells in immunocompetent recipients without immunosuppressants. *Stem Cells Dev.* 21, 2770–2778. doi: 10.1089/scd.2012.0176

Liras, A. (2010). Future research and therapeutic applications of human stem cells: general, regulatory, and bioethical aspects. *J. Transl. Med.* 8:131. doi: 10.1186/1479-5876-8-131

Liu, X., Yang, W., Guan, Z., Yu, W., Fan, B., Xu, N., et al. (2018). There are only four basic modes of cell death, although there are many ad-hoc variants adapted to different situations. *Cell Biosci.* 8:6. doi: 10.1186/s13578-018-0206-6

Lohan, P., Treacy, O., Morcos, M., Donohoe, E., O'Donoghue, Y., Ryan, A. E., et al. (2018). Interspecies incompatibilities limit the immunomodulatory effect of human mesenchymal stromal cells in the rat. *Stem Cells* 36, 1210–1215. doi: 10.1002/stem.2840

Lotfi, R., Steppe, L., Hang, R., Rojewski, M., Massold, M., Jahrsdörfer, B., et al. (2018). ATP promotes immunosuppressive capacities of mesenchymal stromal cells by enhancing the expression of indoleamine dioxygenase. *Immun. Inflamm. Dis.* 6, 448–455. doi: 10.1002/iid3.236

Luque-Campos, N., Contreras-Lopez, R. A., Jose Paredes-Martinez, M., Torres, M. J., Bahraoui, S., Wei, M., et al. (2019). Mesenchymal stem cells improve rheumatoid arthritis progression by controlling memory t cell response. *Front. Immunol.* 10:798. doi: 10.3389/fimmu.2019.00798

Meng, X., Sun, B., and Xiao, Z. (2019). Comparison in transcriptome and cytokine profiles of mesenchymal stem cells from human umbilical cord and cord blood. *Gene* 696, 10–20. doi: 10.1016/j.gene.2019.02.017

Najar, M., Bouhtit, F., Melki, R., Afif, H., Hamal, A., Fahmi, H., et al. (2019). Mesenchymal stromal cell-based therapy: new perspectives and challenges. *J. Clin. Med.* 8:626. doi: 10.3390/jcm8050626

Najar, M., Fayyad-Kazan, M., Raicevic, G., Fayyad-Kazan, H., Meuleman, N., Bron, D., et al. (2018). Advanced glycation end- products-, C-type lectin- and cysteinyl/ leukotriene-receptors in distinct mesenchymal stromal cell populations: differential transcriptional profiles in response to inflammation. *Cell J.* 20, 250–258. doi: 10.22074/cellj.2018.5104

Najar, M., Raicevic, G., Fayyad-Kazan, H., Bron, D., Toungouz, M., and Lagneaux, L. (2016). Mesenchymal stromal cells and immunomodulation: a gathering of regulatory immune cells. *Cytotherapy* 18, 160–171. doi: 10.1016/j.jcyt.2015.10.011

Najar, M., Raicevic, G., Fayyad-Kazan, H., De Bruyn, C., Bron, D., Toungouz, M., et al. (2015). Bone marrow mesenchymal stromal cells induce proliferative, cytokinic and molecular changes during the T cell response: the importance of the IL-10/CD210 axis. *Stem Cell Rev. Rep.* 11, 442–452. doi: 10.1007/s12015-014-9567-3

Najar, M., Raicevic, G., Id Boufker, H., Stamatopoulos, B., De Bruyn, C., Meuleman, N., et al. (2010). Modulated expression of adhesion molecules and galectin-1: role during mesenchymal stromal cell immunoregulatory functions. *Exp. Hematol.* 38, 922–932. doi: 10.1016/j.exphem.2010.05.007

Naji, A., Favier, B., Deschaseaux, F., Rouas-Freiss, N., Eitoku, M., and Suganuma, N. (2019). Mesenchymal stem/stromal cell function in modulating cell death. *Stem Cell Res. Ther.* 10:56. doi: 10.1186/s13287-019-1158-4

Nauta, A. J., Daha, M. R., Tijsma, O., Van de Water, B., Tedesco, F., and Roos, A. (2002). The membrane attack complex of complement induces caspase activation and apoptosis. *Eur. J. Immunol.* 32, 783–792. doi: 10.1002/1521-4141(200203)32:3<783::aid-immu783<3.0.co;2-q

Nauta, A. J., Daha, M. R., Van Kooten, C., and Roos, A. (2003). Recognition and clearance of apoptotic cells: a role for complement and pentraxins. *Trends Immunol.* 24, 148–154. doi: 10.1016/s1471-4906(03)00030-9

Nemeth, K. (2014). Mesenchymal stem cell therapy for immune-modulation: the donor, the recipient, and the drugs in-between. *Exp. Dermatol.* 23, 625–628. doi: 10.1111/exd.12459

Neri, S., and Borzì, R. M. (2020). Molecular mechanisms contributing to mesenchymal stromal cell aging. *Biomolecules* 10:340. doi: 10.3390/biom10020340

Netsch, P., Elvers-Hornung, S., Uhlig, S., Klüter, H., Huck, V., Kirschhöfer, F., et al. (2018). Human mesenchymal stromal cells inhibit platelet activation and aggregation involving CD73-converted adenosine. *Stem Cell Res. Ther.* 9:184. doi: 10.1186/s13287-018-0936-8

Nitzsche, F., Müller, C., Lukomska, B., Jolkkonen, J., Deten, A., and Boltze, J. (2017). Concise review: MSC adhesion cascade-insights into homing and transendothelial migration. *Stem Cells* 35, 1446–1460. doi: 10.1002/stem.2614

Nolta, J. A., Galipeau, J., and Phinney, D. G. (2020). Improving mesenchymal stem/stromal cell potency and survival: proceedings from the International Society of Cell Therapy (ISCT) MSC preconference held in May 2018, Palais des Congrès de Montréal, organized by the ISCT MSC scientific committee. *Cytotherapy* 22, 123–126. doi: 10.1016/j.jcyt.2020.01.004

Nombela-Arrieta, C., Ritz, J., and Silberstein, L. E. (2011). The elusive nature and function of mesenchymal stem cells. *Nat. Rev. Mol. Cell Biol.* 12, 126–131. doi: 10.1038/nrm3049

Noronha, N. C., Mizukami, A., Caliári-Oliveira, C., Cominal, J. G., Rocha, J. L. M., Covas, D. T., et al. (2019). Priming approaches to improve the efficacy of mesenchymal stromal cell-based therapies. *Stem Cell Res. Ther.* 10:131. doi: 10.1186/s13287-019-1224-y

O'Connor, K. C. (2019). Molecular profiles of cell-to-cell variation in the regenerative potential of mesenchymal stromal cells. *Stem Cells Int.* 2019:5924878. doi: 10.1155/2019/5924878

Orozco, L., Munar, A., Soler, R., Alberca, M., Soler, F., Huguet, M., et al. (2013). Treatment of knee osteoarthritis with autologous mesenchymal stem cells: a pilot study. *Transplantation* 95, 1535–1541. doi: 10.1097/TP.0b013e318291a2da

Orozco, L., Munar, A., Soler, R., Alberca, M., Soler, F., Huguet, M., et al. (2014). Treatment of knee osteoarthritis with autologous mesenchymal stem cells: two-year follow-up results. *Transplantation* 97, e66–e68. doi: 10.1097/TP.0000000000000167

Paladino, F. V., De Moraes Rodrigues, J., Da Silva, A., and Goldberg, A. C. (2019). The immunomodulatory potential of Wharton's jelly mesenchymal stem/stromal cells. *Stem Cells Int.* 2019:3548917. doi: 10.1155/2019/3548917

Patel, C. H., Leone, R. D., Horton, M. R., and Powell, J. D. (2019). Targeting metabolism to regulate immune responses in autoimmunity and cancer. *Nat. Rev. Drug Discov.* 18, 669–688. doi: 10.1038/s41573-019-0032-5

Patrikoski, M., Mannerström, B., and Miettinen, S. (2019). Perspectives for clinical translation of adipose stromal/stem cells. *Stem Cells Int.* 2019:5858247. doi: 10.1155/2019/5858247

Pearce, E. L., and Pearce, E. J. (2013). Metabolic pathways in immune cell activation and quiescence. *Immunity* 38, 633–643. doi: 10.1016/j.immuni.2013.04.005

Pers, Y. M., Maumus, M., Bony, C., Jorgensen, C., and Noël, D. (2018a). Contribution of microRNAs to the immunosuppressive function of mesenchymal stem cells. *Biochimie* 155, 109–118. doi: 10.1016/j.biochi.2018.07.001

Pers, Y. M., Quentin, J., Feirreira, R., Espinoza, F., Abdellaoui, N., Erkilic, N., et al. (2018b). Injection of adipose-derived stromal cells in the knee of patients with severe osteoarthritis has a systemic effect and promotes an anti-inflammatory phenotype of circulating immune cells. *Theranostics* 8, 5519–5528. doi: 10.7150/thno.27674

Pers, Y. M., Rackwitz, L., Ferreira, R., Pullig, O., Delfour, C., Barry, F., et al. (2016). Adipose mesenchymal stromal cell-based therapy for severe osteoarthritis of the knee: a Phase I dose-escalation trial. *Stem Cells Transl. Med.* 5, 847–856. doi: 10.5966/sctm.2015-2245

Pinheiro, C. C. G., Leyendecker Junior, A., Tanikawa, D. Y. S., Ferreira, J. R. M., Jarrahy, R., and Bueno, D. F. (2019). Is there a noninvasive source of MSCs isolated with GMP methods with better osteogenic potential? *Stem Cells Int.* 2019:7951696. doi: 10.1155/2019/7951696

Piraghaj, M. G., Soudi, S., Ghanbarian, H., Bolandi, Z., Namaki, S., and Hashemi, S. M. (2018). Effect of efferocytosis of apoptotic mesenchymal stem cells (MSCs) on C57BL/6 peritoneal macrophages function. *Life Sci.* 212, 203–212. doi: 10.1016/j.lfs.2018.09.052

Ponte, A. L., Marais, E., Gallay, N., Langonné, A., Delorme, B., Hérault, O., et al. (2007). The in vitro migration capacity of human bone marrow mesenchymal stem cells: comparison of chemokine and growth factor chemotactic activities. *Stem Cells* 25, 1737–1745. doi: 10.1634/stemcells.2007-0054

Prockop, D. J. (2007). "Stemness" does not explain the repair of many tissues by mesenchymal stem/multipotent stromal cells (MSCs). *Clin. Pharmacol. Ther.* 82, 241–243. doi: 10.1038/sj.clpt.6100313

Qi, H., Liu, D. P., Xiao, D. W., Tian, D. C., Su, Y. W., and Jin, S. F. (2019). Exosomes derived from mesenchymal stem cells inhibit mitochondrial dysfunction-induced apoptosis of chondrocytes via p38, ERK, and Akt pathways. *In Vitro Cell Dev. Biol. Anim.* 55, 203–210. doi: 10.1007/s11626-019-00330-x

Qi, K., Li, N., Zhang, Z., and Melino, G. (2018). Tissue regeneration: the crosstalk between mesenchymal stem cells and immune response. *Cell. Immunol.* 326, 86–93. doi: 10.1016/j.cellimm.2017.11.010

Rendra, E., Scaccia, E., and Bieback, K. (2020). Recent advances in understanding mesenchymal stromal cells. *F1000Res.* 9:F1000 Faculty Rev-1156. doi: 10.12688/f1000research.21862.1

Robinson, W. H., Lepus, C. M., Wang, Q., Raghu, H., Mao, R., Lindstrom, T. M., et al. (2016). Low-grade inflammation as a key mediator of the pathogenesis of osteoarthritis. *Nat. Rev. Rheumatol.* 12, 580–592. doi: 10.1038/nrrheum.2016.136

Romieu-Mourez, R., Francois, M., Boivin, M. N., Stagg, J., and Galipeau, J. (2007). Regulation of MHC class II expression and antigen processing in murine and human mesenchymal stromal cells by IFN-gamma, TGF-beta, and cell density. *J. Immunol.* 179, 1549–1558. doi: 10.4049/jimmunol.179.3.1549

Rüster, B., Göttig, S., Ludwig, R. J., Bistrian, R., Müller, S., Seifried, E., et al. (2006). Mesenchymal stem cells display coordinated rolling and adhesion behavior on endothelial cells. *Blood* 108, 3938–3944. doi: 10.1182/blood-2006-05-025098

Ryan, A. E., Lohan, P., O'Flynn, L., Treacy, O., Chen, X., Coleman, C., et al. (2014). Chondrogenic differentiation increases antidonor immune response to allogeneic mesenchymal stem cell transplantation. *Mol. Ther.* 22, 655–667. doi: 10.1038/mt.2013.261

Samsonraj, R. M., Raghunath, M., Nurcombe, V., Hui, J. H., van Wijnen, A. J., and Cool, S. M. (2017). Concise review: multifaceted characterization of human mesenchymal stem cells for use in regenerative medicine. *Stem Cells Transl. Med.* 6, 2173–2185. doi: 10.1002/sctm.17-0129

Sánchez, A., Schimmang, T., and García-Sancho, J. (2012). Cell and tissue therapy in regenerative medicine. *Adv. Exp. Med. Biol.* 741, 89–102. doi: 10.1007/978-1-4614-2098-9_7

Schäfer, R., Schnaidt, M., Klaffschenkel, R. A., Siegel, G., Schüle, M., Rädlein, M. A., et al. (2011). Expression of blood group genes by mesenchymal stem cells. *Br. J. Haematol.* 153, 520–528. doi: 10.1111/j.1365-2141.2011.08652.x

Schraufstatter, I. U., Discipio, R. G., Zhao, M., and Khaldoyanidi, S. K. (2009). C3a and C5a are chemotactic factors for human mesenchymal stem cells, which cause prolonged ERK1/2 phosphorylation. *J. Immunol.* 182, 3827–3836. doi: 10.4049/jimmunol.0803055

Schraufstatter, I. U., Khaldoyanidi, S. K., and DiScipio, R. G. (2015). Complement activation in the context of stem cells and tissue repair. *World J. Stem Cells* 7, 1090–1108. doi: 10.4252/wjsc.v7.i8.1090

Semenova, S., Shatrova, A., Vassilieva, I., Shamatova, M., Pugovkina, N., and Negulyaev, Y. (2020). Adenosine-5'-triphosphate suppresses proliferation and migration capacity of human endometrial stem cells. *J. Cell. Mol. Med.* 24, 4580–4588. doi: 10.1111/jcmm.15115

Soler, R., Orozco, L., Munar, A., Huguet, M., Lopez, R., Vives, J., et al. (2016). Final results of a phase I-II trial using ex vivo expanded autologous Mesenchymal Stromal Cells for the treatment of osteoarthritis of the knee confirming safety and suggesting cartilage regeneration. *Knee* 23, 647–654. doi: 10.1016/j.knee.2015.08.013

Spaggiari, G. M., Abdelrazik, H., Becchetti, F., and Moretta, L. (2009). MSCs inhibit monocyte-derived DC maturation and function by selectively interfering with the generation of immature DCs: central role of MSC-derived prostaglandin E2. *Blood* 113, 6576–6583. doi: 10.1182/blood-2009-02-203943

Su, J., Chen, X., Huang, Y., Li, W., Li, J., Cao, K., et al. (2014). Phylogenetic distinction of iNOS and IDO function in mesenchymal stem cell-mediated immunosuppression in mammalian species. *Cell Death Differ.* 21, 388–396. doi: 10.1038/cdd.2013.149

Sun, C., Wang, L., Wang, H., Huang, T., Yao, W., Li, J., et al. (2020). Single-cell RNA-seq highlights heterogeneity in human primary Wharton's jelly mesenchymal stem/stromal cells cultured in vitro. *Stem Cell Res. Ther.* 11:149. doi: 10.1186/s13287-020-01660-4

Swart, J. F., de Roock, S., Hofhuis, F. M., Rozemuller, H., van den Broek, T., Moerer, P., et al. (2015). Mesenchymal stem cell therapy in proteoglycan induced arthritis. *Ann. Rheum. Dis.* 74, 769–777. doi: 10.1136/annrheumdis-2013-204147

Tan, K., Zhu, H., Zhang, J., Ouyang, W., Tang, J., Zhang, Y., et al. (2019). CD73 expression on mesenchymal stem cells dictates the reparative properties via its anti-inflammatory activity. *Stem Cells Int.* 2019, 8717694. doi: 10.1155/2019/8717694

Thum, T., Bauersachs, J., Poole-Wilson, P. A., Volk, H. D., and Anker, S. D. (2005). The dying stem cell hypothesis: immune modulation as a novel mechanism for progenitor cell therapy in cardiac muscle. *J. Am. Coll. Cardiol.* 46, 1799–1802. doi: 10.1016/j.jacc.2005.07.053

Tofiño-Vian, M., Guillen, M. I., Perez Del, Caz, M. D., Silvestre, A., and Alcaraz, M. J. (2018). Microvesicles from human adipose tissue-derived mesenchymal stem cells as a new protective strategy in osteoarthritic chondrocytes. *Cell Physiol. Biochem* 47, 11–25. doi: 10.1159/000489739

Toh, W. S., Zhang, B., Lai, R. C., and Lim, S. K. (2018). Immune regulatory targets of mesenchymal stromal cell exosomes/small extracellular vesicles in tissue regeneration. *Cytotherapy* 20, 1419–1426. doi: 10.1016/j.jcyt.2018.09.008

Tu, Z., Li, Q., Bu, H., and Lin, F. (2010). Mesenchymal stem cells inhibit complement activation by secreting factor H. *Stem Cells Dev.* 19, 1803–1809. doi: 10.1089/scd.2009.0418

Ullah, M., Liu, D. D., and Thakor, A. S. (2019). Mesenchymal stromal cell homing: mechanisms and strategies for improvement. *iScience* 15, 421–438. doi: 10.1016/j.isci.2019.05.004

van den Bosch, M. H. J., van Lent, P., and van der Kraan, P. M. (2020). Identifying effector molecules, cells, and cytokines of innate immunity in OA. *Osteoarthr. Cartil.* 28, 532–543. doi: 10.1016/j.joca.2020.01.016

Van Megen, K. M., Van 't Wout, E. J. T., Motta, J. L., Dekker, B., Nikolic, T., and Roep, B. O. (2019). Activated mesenchymal stromal cells process and present antigens regulating adaptive immunity. *Front. Immunol.* 10:694. doi: 10.3389/fimmu.2019.00694

Vega, A., Martin-Ferrero, M. A., Del Canto, F., Alberca, M., Garcia, V., Munar, A., et al. (2015). Treatment of knee osteoarthritis with allogeneic bone marrow mesenchymal stem cells: a randomized controlled trial. *Transplantation* 99, 1681–1690. doi: 10.1097/TP.0000000000000678

Viswanathan, S., Shi, Y., Galipeau, J., Krampera, M., Leblanc, K., Martin, I., et al. (2019). Mesenchymal stem versus stromal cells: international society for cell & gene therapy (ISCT®) mesenchymal stromal cell committee position statement on nomenclature. *Cytotherapy* 21, 1019–1024. doi: 10.1016/j.jcyt.2019.08.002

Volarevic, V., Markovic, B. S., Gazdic, M., Volarevic, A., Jovicic, N., Arsenijevic, N., et al. (2018). Ethical and safety issues of stem cell-based therapy. *Int. J. Med. Sci.* 15, 36–45. doi: 10.7150/ijms.21666

Wallace, J. L., Ferraz, J. G. P., and Muscara, M. N. (2012). Hydrogen sulfide: an endogenous mediator of resolution of inflammation and injury. *Antioxid. Redox Signal.* 17, 58–67. doi: 10.1089/ars.2011.4351

Wang, Y., Chen, X., Cao, W., and Shi, Y. (2014). Plasticity of mesenchymal stem cells in immunomodulation: pathological and therapeutic implications. *Nat. Immunol.* 15, 1009–1016. doi: 10.1038/ni.3002

Wang, Y., Yu, D., Liu, Z., Zhou, F., Dai, J., Wu, B., et al. (2017). Exosomes from embryonic mesenchymal stem cells alleviate osteoarthritis through balancing synthesis and degradation of cartilage extracellular matrix. *Stem Cell Res. Ther.* 8:189. doi: 10.1186/s13287-017-0632-0

Wang, Y., Tian, M., Wang, F., Heng, B. C., Zhou, J., Cai, Z., et al. (2019). Understanding the immunological mechanisms of mesenchymal stem cells in allogeneic transplantation: from the aspect of major histocompatibility complex class I. *Stem Cells Dev.* 28, 1141–1150. doi: 10.1089/scd.2018.0256

Weiss, A. R. R., and Dahlke, M. H. (2019). Immunomodulation by mesenchymal stem cells (MSCs): mechanisms of action of living, apoptotic, and dead MSCs. *Front. Immunol.* 10:1191. doi: 10.3389/fimmu.2019.01191

Weiss, D. J., English, K., Krasnodembskaya, A., Isaza-Correa, J. M., Hawthorne, I. J., and Mahon, B. P. (2019). The necrobiology of mesenchymal stromal cells affects therapeutic efficacy. *Front. Immunol.* 10:1228. doi: 10.3389/fimmu.2019.01228

Woo, C. H., Kim, H. K., Jung, G. Y., Jung, Y. J., Lee, K. S., Yun, Y. E., et al. (2020). Small extracellular vesicles from human adipose-derived stem cells attenuate cartilage degeneration. *J Extracell Vesicles* 9:1735249. doi: 10.1080/20013078.2020.1735249

Yan, F., Liu, O., Zhang, H., Zhou, Y., Zhou, D., Zhou, Z., et al. (2019). Human dental pulp stem cells regulate allogeneic NK cells' function via induction of anti-inflammatory purinergic signalling in activated NK cells. *Cell Prolif.* 52:e12595. doi: 10.1111/cpr.12595

Yang, M., Lin, J., Tang, J., Chen, Z., Qian, X., Gao, W. Q., et al. (2020). Decreased immunomodulatory and secretory capability of aging human umbilical cord mesenchymal stem cells in vitro. *Biochem. Biophys. Res. Commun.* 525, 633–638. doi: 10.1016/j.bbrc.2020.02.125

Zhang, S., Chu, W. C., Lai, R. C., Lim, S. K., Hui, J. H., and Toh, W. S. (2016). Exosomes derived from human embryonic mesenchymal stem cells promote osteochondral regeneration. *Osteoarthr. Cartil.* 24, 2135–2140. doi: 10.1016/j.joca.2016.06.022

Zhang, Z., Huang, S., Wu, S., Qi, J., Li, W., Liu, S., et al. (2019). Clearance of apoptotic cells by mesenchymal stem cells contributes to immunosuppression via PGE2. *EBioMedicine* 45, 341–350. doi: 10.1016/j.ebiom.2019.06.016

Zhao, C., Chen, J. Y., Peng, W. M., Yuan, B., Bi, Q., and Xu, Y. J. (2020). Exosomes from adiposederived stem cells promote chondrogenesis and suppress inflammation by upregulating miR145 and miR221. *Mol. Med. Rep.* 21, 1881–1889. doi: 10.3892/mmr.2020.10982

Zhou, L. L., Liu, W., Wu, Y. M., Sun, W. L., Dörfer, C. E., and El-Sayed, K. M. F. (2020). Oral mesenchymal stem/progenitor cells: the immunomodulatory masters. *Stem Cells Int.* 2020:1327405. doi: 10.1155/2020/1327405

Zhou, Y., Yamamoto, Y., Xiao, Z., and Ochiya, T. (2019). The immunomodulatory functions of mesenchymal stromal/stem cells mediated via paracrine activity. *J. Clin. Med.* 8:1025. doi: 10.3390/jcm8071025

Zhu, H., Ji, J., Fu, T., Yang, J., and Gu, Z. (2018). The effect of exosomes from bone marrow mesenchymal stem cells on osteoarthritis. *Ann. Rheum. Dis.* 77:893. doi: 10.1136/annrheumdis-2020-eular.6040

Conflict of Interest: The authors declare that the research was conducted in the absence of any commercial or financial relationships that could be construed as a potential conflict of interest.

frontiers in Cell and Developmental Biology

ORIGINAL RESEARCH
published: 29 October 2020
doi: 10.3389/fcell.2020.595518

Unfavorable Contribution of a Tissue-Engineering Cartilage Graft to Osteochondral Defect Repair in Young Rabbits

Zhihua Lu[1,2], Sheng Zhou[1], Justin Vaida[1], Gongming Gao[1], Amanda Stewart[1], Joshua Parenti[1], Lianqi Yan[2] and Ming Pei[1,3]**

[1] Stem Cell and Tissue Engineering Laboratory, Department of Orthopaedics, West Virginia University, Morgantown, WV, United States, [2] Department of Orthopedics, Clinical Medical College of Yangzhou University, Subei People's Hospital of Jiangsu Province, Yangzhou, China, [3] WVU Cancer Institute, Robert C. Byrd Health Sciences Center, West Virginia University, Morgantown, WV, United States

OPEN ACCESS

Edited by:
Zhenxing Shao, Peking University Third Hospital, China

Reviewed by:
Hang Lin, University of Pittsburgh, United States
Gianandrea Pasquinelli, University of Bologna, Italy

***Correspondence:**
Lianqi Yan
yanlianqi@126.com
Ming Pei
mpei@hsc.wvu.edu
orcid.org/0000-0001-5710-3578

Specialty section:
This article was submitted to Stem Cell Research, a section of the journal Frontiers in Cell and Developmental Biology

Received: *16 August 2020*
Accepted: *12 October 2020*
Published: *29 October 2020*

Citation:
Lu Z, Zhou S, Vaida J, Gao G, Stewart A, Parenti J, Yan L and Pei M (2020) Unfavorable Contribution of a Tissue-Engineering Cartilage Graft to Osteochondral Defect Repair in Young Rabbits. Front. Cell Dev. Biol. 8:595518. doi: 10.3389/fcell.2020.595518

A stem cell-based tissue-engineering approach is a promising strategy for treatment of cartilage defects. However, there are conflicting data in the feasibility of using this approach in young recipients. A young rabbit model with an average age of 7.7 months old was used to evaluate the effect of a tissue-engineering approach on the treatment of osteochondral defects. Following *in vitro* evaluation of proliferation and chondrogenic capacity of infrapatellar fat pad-derived stem cells (IPFSCs) after expansion on either tissue culture plastic (TCP) or decellularized extracellular matrix (dECM), a premature tissue construct engineered from pretreated IPFSCs was used to repair osteochondral defects in young rabbits. We found that dECM expanded IPFSCs exhibited higher proliferation and chondrogenic differentiation compared to TCP expanded cells in both pellet and tissue construct culture systems. Six weeks after creation of bilateral osteochondral defects in the femoral trochlear groove of rabbits, the Empty group (left untreated) had the best cartilage resurfacing with the highest score in Modified O'Driscoll Scale (MODS) than the other groups; however, this score had no significant difference compared to that of 15-week samples, indicating that young rabbits stop growing cartilage once they reach 9 months old. Interestingly, implantation of premature tissue constructs from both dECM and TCP groups exhibited significantly improved cartilage repair at 15 weeks compared to those at six weeks (about 9 months old), indicating that a tissue-engineering approach is able to repair adult cartilage defects. We also found that implanted pre-labeled cells in premature tissue constructs were undetectable in resurfaced cartilage at both time points. This study suggests that young rabbits (less than 9 months old) might respond differently to the classical tissue-engineering approach that is considered as a potential treatment for cartilage defects in adult rabbits.

Keywords: young rabbit, osteochondral defect, tissue engineering, decellularized extracellular matrix, infrapatellar fat pad-derived stem cell

INTRODUCTION

Articular cartilage holds a limited capacity for self-healing due to a shortage of blood supply. Several surgical methods are available for the treatment of cartilage damage, including arthroscopic debridement, microfracture, and osteochondral transplantation; (Willers et al., 2003) however, none can consistently reproduce normal hyaline cartilage (Smith et al., 2005). As an alternative treatment, stem cell-based tissue engineering has been validated as a promising approach to reconstitute cartilage defects (Nukavarapu and Dorcemus, 2013). Seed cells and scaffolds are two important parameters for the success of a tissue-engineering strategy. Increasing data indicate the advantages of infrapatellar fat pad (IPFP)-derived stem cells (IPFSCs) as a stem cell source due to strong proliferation capacities and multilineage differentiation potentials, particularly for cartilage engineering and regeneration (Sun et al., 2018; Wang T. et al., 2020). Among the candidate scaffold materials, polylactic-co-glycolic acid (PLGA) is one of the most widely used biodegradable polymers, owing to its prominent advantages such as maneuverability of degradation rates and outstanding processability (Uematsu et al., 2005). Therefore, in this study, IPFSCs were chosen as seed cells to grow on PLGA scaffolds.

Cell expansion on a two-dimensional (2D) culture substrate often causes stem cell senescence (Li and Pei, 2012). Evidence indicates that decellularized extracellular matrix (dECM), a three-dimensional (3D) culture system, can efficiently rejuvenate expanded stem cells in both proliferation and chondrogenic differentiation (Li and Pei, 2010; Pei et al., 2011; Pei, 2017). A previous report successfully utilized dECM expanded synovium-derived stem cells in the treatment of partial-thickness cartilage defects in a minipig model *via* intraarticular injection (Pei et al., 2013). Given that a stem cell-based tissue-engineering approach exhibits a promising strategy to overcome the challenge of tissue defects in elderly recipients, (Uematsu et al., 2005; Han et al., 2008) there are few reports available to determine the feasibility of this approach in cartilage repair in young recipients, considering that older transplant recipients exhibited differently from young recipients in some biological aspects such as in immunosenescence (Colvin et al., 2017). Moreover, there is no consensus on skeletally mature rabbit age with a range from four to nine months old (Masoud et al., 1986; Wei et al., 1997; Wei and Messner, 1999; Rudert, 2002; Reinholz et al., 2004; Hoemann et al., 2007; Hunziker et al., 2007; Pei et al., 2009; Isaksson et al., 2010). In this study, a rabbit model (between 7.5–8 months old) considered as skeletally mature (Masoud et al., 1986; Gilsanz et al., 1988; Newman et al., 1995) was used to evaluate whether articular cartilage became mature and whether a tissue-engineering approach benefited the treatment of osteochondral defects. We hypothesized that a young rabbit (less than 9 months old) does not have mature cartilage and may not respond to a tissue-engineering approach for cartilage repair the same as an adult rabbit does.

MATERIALS AND METHODS

Experimental Design

Following isolation of IPFSCs from rabbit IPFP, both *in vitro* and *in vivo* studies were designed (**Figure 1**). In the *in vitro* study (**Figure 2**), IPFSCs were evaluated in cell proliferation and chondrogenic differentiation (3D culture systems - both pellets and PLGA tissue constructs) by comparing the influence of (1) dECM expansion with tissue culture plastic (TCP) as a control and (2) lentivirus transduction with non-transduction as a control. In the *in vivo* study (**Figures 3–8**), after creation of osteochondral defects, four groups were designed: Empty group (left untreated), PLGA group (filled with PLGA alone), TCP group (filled with 20-day-cartilage grafts using TCP expanded IPFSCs), and dECM group (filled with 20-day-cartilage grafts using dECM expanded IPFSCs). Histological evaluation was quantified for cartilage resurfacing of osteochondral defects (**Tables 1–3**) and implanted cells were tracked using both immunofluorescence microscopy and immunohistochemical staining for green fluorescence protein (GFP) (**Figure 8**).

IPFSC Isolation and Culture

This animal study was approved by the Institutional Animal Care and Use Committee. Infrapatellar fat pads from four New Zealand White (NZW) rabbits were used to collect stem cells (IPFSCs) after a sequential digestion using 0.1% trypsin (Roche, Indianapolis, IN) for 30 min and 0.1% collagenase P (Roche) for 2 h to release cells. The stemness of IPFSCs was characterized in both human (He and Pei, 2013; Pizzute et al., 2016; Wang et al., 2019; Wang Y. M. et al., 2020) and rabbit donors (Wang T. et al., 2020). The pooled IPFSCs were cultured in growth medium [Minimum Essential Medium–Alpha Modification (αMEM) containing 10% fetal bovine serum (FBS), 100 U/mL penicillin, 100 μg/mL streptomycin, and 0.25 μg/mL fungizone (Invitrogen, Carlsbad, CA)] at 37°C in a humidified 21% O_2 and 5% CO_2 incubator. The medium was changed every three days.

IPFSC Labeling

Passage 2 rabbit IPFSCs were transduced with lentivirus carrying GFP in the presence of 4 μg/mL of protamine sulfate (MilliporeSigma, Burlington, MA). Twenty-four hours later, the medium was replaced with αMEM with 10% FBS and 2 μg/mL of puromycin (MilliporeSigma) for cell screening. Passage 5 rabbit IPFSCs labeled with GFP were collected for the *in vivo* study.

dECM Preparation

dECM was prepared by following a protocol described in a previous report (Li and Pei, 2018). Briefly, TCP was treated with 0.2% gelatin (MilliporeSigma), 1% glutaraldehyde (MilliporeSigma), and 1 M ethanolamine (MilliporeSigma). Passage 2 IPFSCs at 100% confluence on pre-coated TCP were treated with 250 μM of L-ascorbic acid phosphate (Wako Chemicals, Richmond, VA) for seven days (Pizzute et al., 2016) followed by an incubation with extraction buffer (0.5% Triton X-100 containing 20 mM ammonium

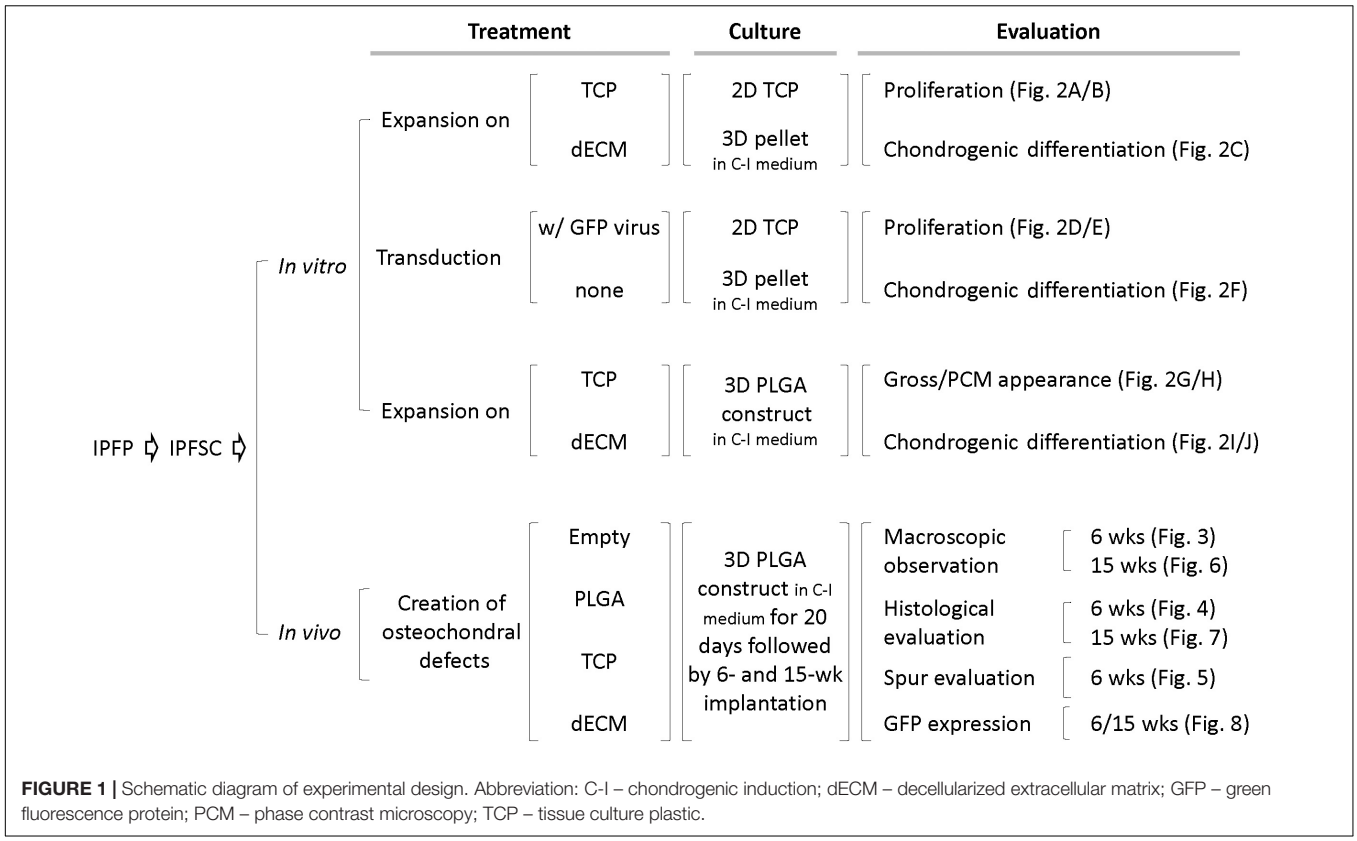

FIGURE 1 | Schematic diagram of experimental design. Abbreviation: C-I – chondrogenic induction; dECM – decellularized extracellular matrix; GFP – green fluorescence protein; PCM – phase contrast microscopy; TCP – tissue culture plastic.

hydroxide). After cells were removed, dECM was stored in phosphate buffered solution (PBS) containing 100 U/mL penicillin, 100 μg/mL streptomycin, and 0.25 μg/mL fungizone at 4°C until use.

Three Experiments Were Designed as Follows

1) **A comparison of dECM and TCP expanded IPFSCs in proliferation and chondrogenic differentiation:** Passage 5 IPFSCs were expanded on TCP and dECM for one passage followed by a 30-day chondrogenic induction in a pellet culture system. Cell morphology and relative 5-Ethynyl-2′-deoxyuridine (EdU) incorporation were evaluated for proliferation capacity. A serum-free chondrogenic medium consisted of high-glucose Dulbecco's modified Eagle's medium, 100 nM dexamethasone, 40 μg/mL proline, 0.1 mM L-ascorbic acid-2-phosphate, 100 U/mL penicillin, 100 μg/mL streptomycin, 0.25 μg/mL fungizone, and 1 × ITS^{TM} Premix (Corning, Bedford, MA) with the addition of 10 ng/mL transforming growth factor beta3 (TGF-β3; PeproTech, Rocky Hill, NJ). Real-time quantitative PCR (RT-qPCR) analysis was used to assess mRNA levels of chondrogenic markers [*SOX9* (SRY-box 9), *ACAN* (aggrecan), and *COL2A1* (type II collagen alpha I chain)] in expanded cells and chondrogenic pellets (day 0, 14, and 30).

Following our previously published methods, (Pei et al., 2002a,b) 1.3 × 10^6 cells from either TCP or dECM expansion were seeded on one 5 mm diameter × 2 mm thickness PLGA mesh (Synthecon, Houston, TX) in a spinner flask. After incubation for 72 h to allow cell attachment, the cell-scaffold constructs were transferred into six-well plates and cultured in a serum-free chondrogenic medium in a standard incubator (5% CO_2 and 21% O_2) for ten days and subsequently in a hypoxia incubator (5% CO_2 and 5% O_2) for ten days (Li et al., 2011; Galeano-Garces et al., 2017). Constructs were harvested at day 20 for chondrogenic evaluation [*SOX9*, *ACAN*, *COL2A1*, and *COL10A1* (type X collagen alpha1)] using RT-qPCR analyses.

Cell proliferation was evaluated using the Click-iT^{TM} EdU Alexa Fluor^{TM} 647 Flow Cytometry Assay Kit (Invitrogen). IPFSCs (5 × 10^5) were incubated with 10 μM EdU for 18 h followed by staining as per manufacturer's protocol. Briefly, cells were incubated with Click-iT^{TM} fixative for 15 min in the dark followed by washing with 1% bovine serum albumin (BSA)-PBS and then resuspended in 1 × Click-iT^{TM} saponin-based permeabilization buffer. Following staining in labeling cocktail for 30 min, cells were analyzed with a FACS Calibur (BD Biosciences, San Jose, CA) and data analyzed using FCS Express software package (*De Novo* Software, Pasadena, CA).

For RT-qPCR, total RNA was extracted from tissue constructs (n = 4) using TRIzol® (Life Technologies, Carlsbad, CA) as per manufacturer's protocol. Subsequently, cDNA was synthesized

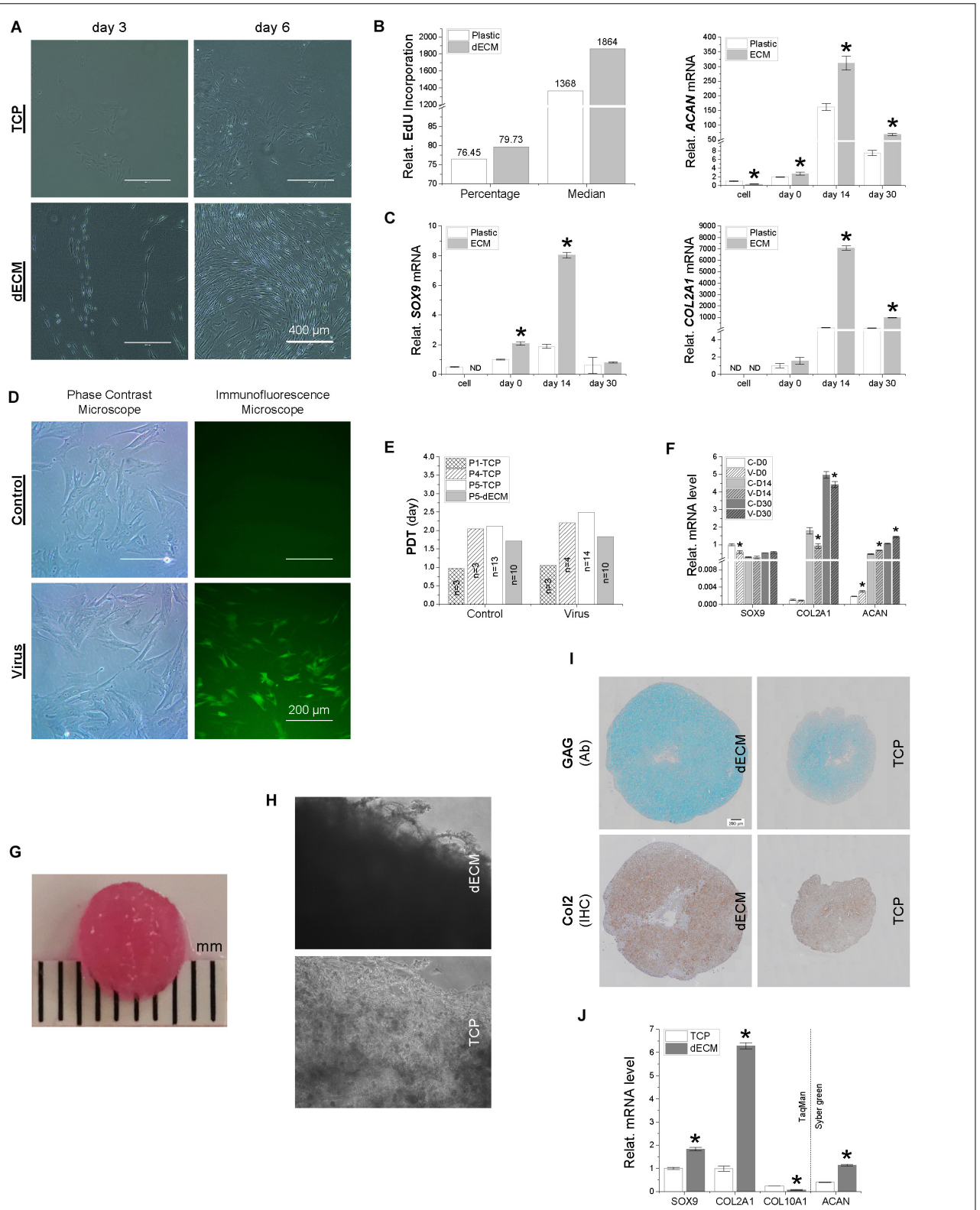

FIGURE 2 | A comparison of IPFSCs and their capacity for proliferation and chondrogenic differentiation following expansion on either dECM or TCP **(A–C)** and with or without lentivirus transduction **(D–F)** as well as of premature tissue constructs seeded with 2.2 × 10^6 IPFSCs after expansion on dECM or TCP **(G–K)**. **(A)** Cell morphology of IPFSCs after 3- and 6-day culture on either dECM or TCP; Scale bar: 400 μm; **(B)** relative EdU incorporation of dECM or TCP expanded

(Continued)

FIGURE 2 | Continued

IPFSCs (5×10^5) measured by flow cytometry, and **(C)** RT-qPCR evaluation of expression level of chondrogenic marker genes (*SOX9*, *ACAN*, and *COL2A1*) in dECM or TCP expanded IPFSCs ($n = 4$) after 30-day chondrogenic induction in a pellet culture system. *$p < 0.05$ as compared to the control group (TCP). **(D)** Transduction efficiency in puromycin screened IPFSCs visualized by immunofluorescence and phase contrast microscopy; Scale bar: 200 μm; **(E)** population doubling time (PDT) in IPFSCs with or without transduction following dECM and TCP expansion; and **(F)** expression of chondrogenic marker genes (*SOX9*, *ACAN*, and *COL2A1*) *via* RT-qPCR in IPFSCs ($n = 4$) with ("V") or without ("C") transduction after 30-day chondrogenic induction in a pellet culture system. *$p < 0.05$ as compared to the control group (non-virus transduction). **(G)** A representative photo of a two-week tissue construct; **(H)** phase contrast microscopy of 20-day tissue constructs (dECM or TCP expanded IPFSCs grown on PLGA mesh); **(I)** histological evaluation of 20-day tissue constructs using Alcian blue staining (Ab) for sulfated GAGs and immunohistochemical staining (IHC) for type II collagen; Scale bar: 200 μm; **(J)** expression of chondrogenic marker genes (*SOX9*, *ACAN*, *COL2A1*, and *COL10A1*) *via* RT-qPCR analysis in dECM or TCP expanded IPFSCs ($n = 4$) after 20-day chondrogenic induction in six-well plates. *$p < 0.05$ as compared to the control group (TCP).

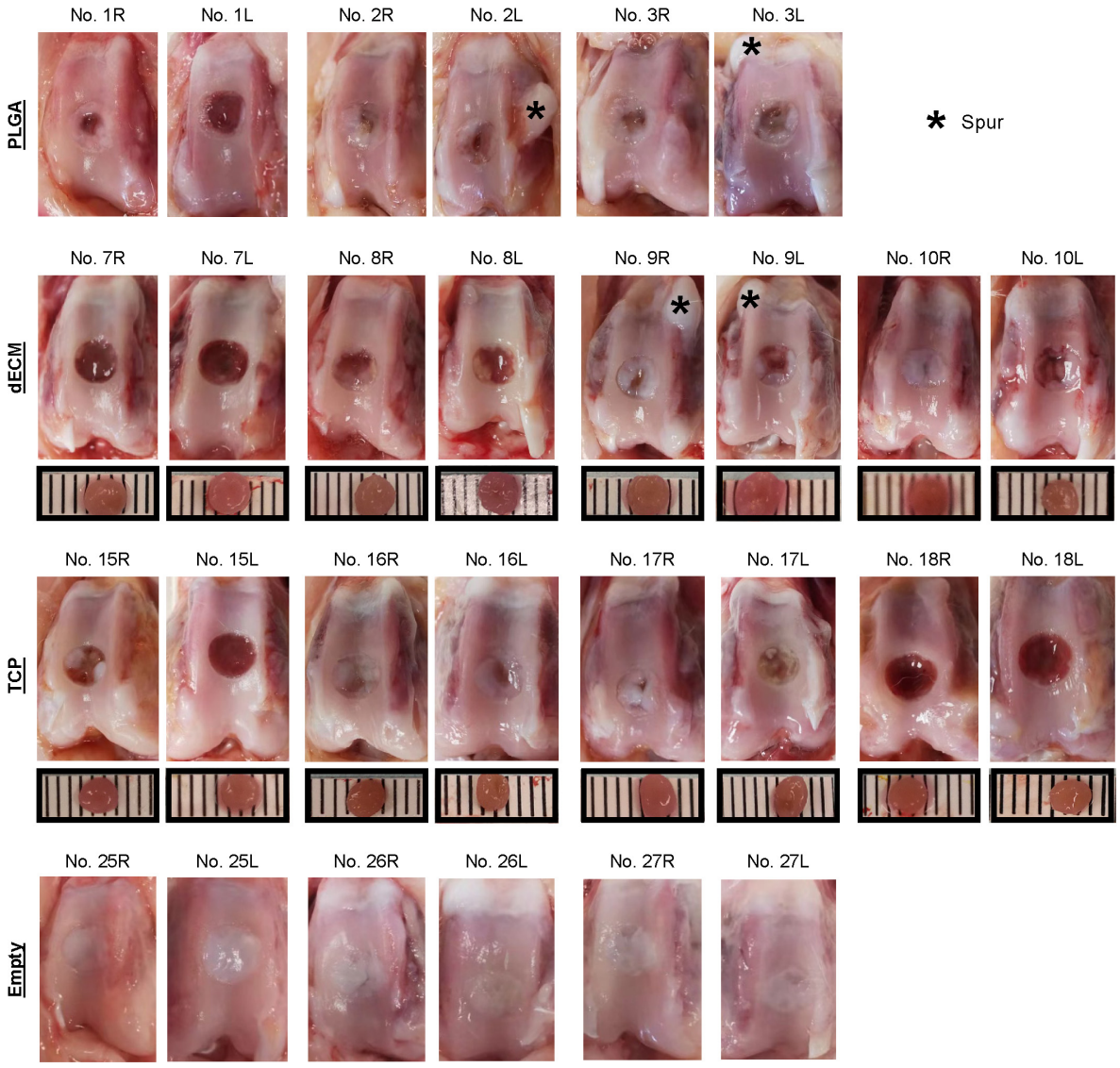

FIGURE 3 | Macroscopic observation of six-week osteochondral defects repaired with PLGA mesh alone (PLGA; $n = 3$ rabbits/6 knees), tissue constructs developed from dECM expanded IPFSCs (dECM; $n = 4$ rabbits/8 knees) or TCP expanded cells (TCP; $n = 4$ rabbits/8 knees), or left untreated (Empty; $n = 3$ rabbits/6 knees). Scale bar: 1 mm.

from mRNA by reverse transcriptase using a High-Capacity cDNA Archive Kit (Thermo Fisher Scientific, Waltham, MA). Primers of the chondrogenic marker gene [*ACAN* (forward GCTACGGAGACAAGGATGAGTTC and reverse CGTAAAAGACCTCACCCTCCAT)] and endogenous control gene *GAPDH* (glyceraldehyde-3-phosphate dehydrogenase;

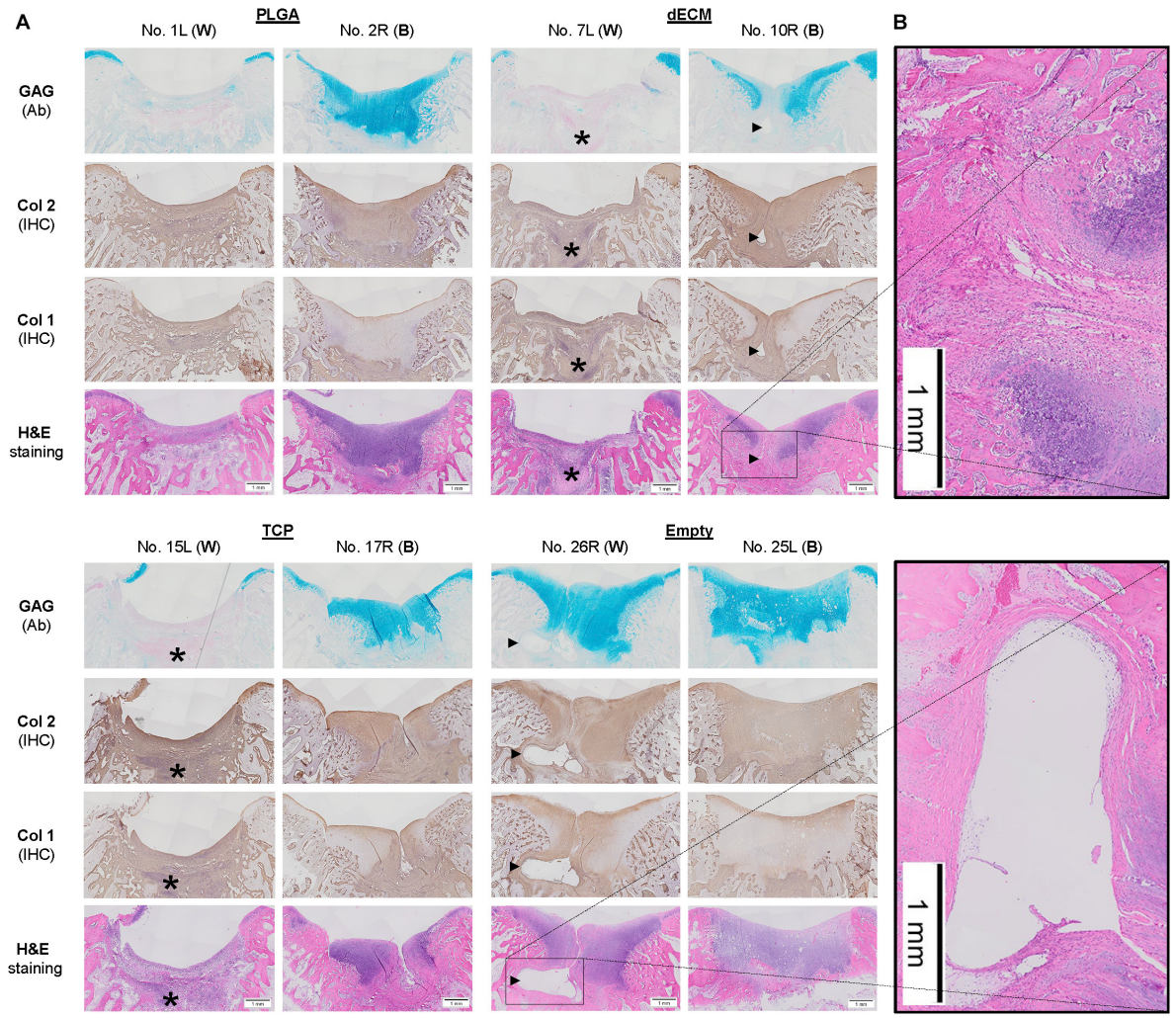

FIGURE 4 | Histological evaluation of six-week osteochondral defects repaired with PLGA mesh alone (PLGA; *n* = 6 knees), tissue constructs developed from dECM expanded IPFSCs (dECM; *n* = 8 knees) or TCP expanded cells (TCP; *n* = 8 knees), or left untreated (Empty; *n* = 6 knees) using Alcian blue staining (Ab) for sulfated GAGs, H&E staining for the intact tidemark, and immunohistochemical staining (IHC) for types I and II collagen (Col 1 and Col 2). **(A)** Two representative cartilage resurfacings were chosen from each group to serve as the best repair ("B") including rabbit No. 2R/10R/17R/25L or the worst repair ("W") including rabbit No. 1L/7L/15L/26R. Arrows (▶) indicate location of subchondral bone cysts and the asterisk (*) indicates mononuclear cells. **(B)** Bone cysts were shown at higher magnification in H&E staining. Scale bar: 1 mm.

forward TTCCACGGCACGGTCAAGGC and reverse GGGCAC CAGCATCACCCCAC) were designed by Integrated DNA Technologies (IDT, Coralville, IA) as a SYBR® green gene expression assay using their PCR primer design tool. Primers for chondrogenic-related genes [*SOX9* (Assay ID Oc04096872_m1), *COL2A1* (Assay ID Oc03396132_g1), and *COL10A1* (Assay ID Oc04097225_s1)] were used in a TaqMan® gene expression assay from Applied Biosystems (Foster City, CA). RT-qPCR was performed using the iCycler iQ™ Multicolor RT-PCR Detection.

2) **A comparison of IPFSCs with or without lentivirus transduction in proliferation and chondrogenic differentiation:** Passage 5 IPFSCs with or without transduction of lentivirus vector carrying GFP (pRSC-SFFV-Luciferase-E2A-Puro-E2A-GFP-wpre) were evaluated for potential influence of viral transduction on cell proliferation and chondrogenic capacity. Immunofluorescence microscopy was used to demonstrate successful transduction following puromycin screening. TCP expanded IPFSCs with or without transduction were counted in T175 TCP (n = 3∼14) using a hemocytometer from passage 1 to 5 along with dECM expanded cells at passage 5 with or without transduction. Cell population doubling time (PDT) was then calculated as "PDT = T*log (2)/[log (N_1) – log (N_0)]", where T represents incubation time, N_1 for harvesting cell number, and N_0 for plating cell number. Expanded IPFSCs (4×10^5 cells) with or without transduction at passage 5 were pelleted by centrifugation in a 15-ml polypropylene tube at 1200 revolutions per

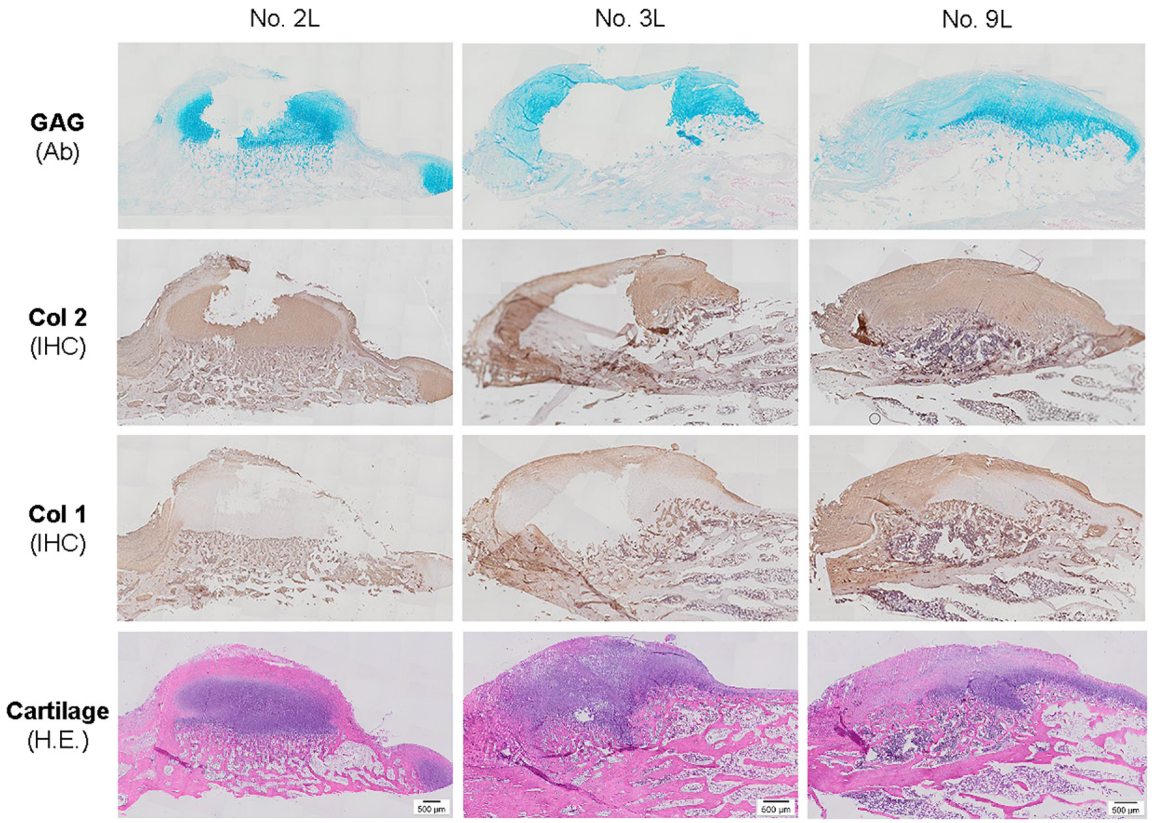

FIGURE 5 | Histological evaluation of bone spurs in 6-week cartilage resurfacing using Alcian blue staining (Ab) for sulfated GAGs, H&E staining for cartilage tissue and immunohistochemical staining (IHC) for types I and II collagen (Col 1 and Col 2). Scale bar: 500 μm.

minute for 7 min. Following overnight incubation (day 0 samples), pellets were grown in a serum-free chondrogenic medium for up to 30 days. Pellets were harvested at day 0, 14, and 30 for evaluation of chondrogenic marker genes (*SOX9*, *COL2A1*, and *ACAN*) *via* RT-qPCR.

3) **Using GFP-labeled IPFSCs with or without dECM expansion to develop premature tissue constructs to repair osteochondral defects in young rabbits**. GFP-labeled passage 6 IPFSCs (2.2×10^6 cells) with or without dECM expansion were seeded in 5 mm diameter × 2 mm thickness PLGA mesh in a spinner flask for three days, (Pei et al., 2002a,b) followed by culture in six-well plates in the presence of serum-free chondrogenic induction medium in a standard incubator (5% CO_2 and 21% O_2) for ten days and subsequently in a hypoxia incubator (5% CO_2 and 5% O_2) for ten days (Li et al., 2011; Galeano-Garces et al., 2017). After observation with immunofluorescence microscopy to confirm the presence of a GFP signal, 20-day tissue constructs developed from either dECM or TCP expanded IPFSCs were used to repair osteochondral defects in young rabbits.

Young NZW rabbits (n = 28, female, 2.5–4 kg, 235.2 ± 2.7 days with an average age of 7.7-months) (Envigo Global Services Inc., Denver, PA) were used in this study. Anesthesia was induced with an intramuscular injection with 5 mg/kg xylazine (Phoenix Pharmaceutical, St. Joseph, MO) and 35 mg/kg ketamine (Phoenix Pharmaceutical) and maintained with isofluorane. The patella was dislocated laterally and a 4.76 mm diameter × 2 mm depth osteochondral defect was created in the patellar groove of the femur in both knees using a custom designed hand drill with a depth stop. Four groups were designated: defects treated with premature tissue constructs developed by either dECM or TCP expanded cells (the dECM group and the TCP group, respectively) (n = 16 knees/8 rabbits/group), and PLGA scaffold only (the PLGA group) or left untreated (the Empty group) (n = 12 knee/6 rabbits/group). Six weeks and 15 weeks postoperatively, rabbits in each group were euthanized for gross observation and histologic evaluation for cartilage resurfacing.

For macroscopic evaluation, once both knee joints were opened, the defect area of the patellar groove was photographed, and gross examination was performed. Femoral condyles were dissected followed by fixation in 4% paraformaldehyde in PBS at 4°C for three days. Each specimen was decalcified by incubation in 15% ethylenediaminetetraacetic acid (EDTA)/0.1% paraformaldehyde solution for six weeks. A 5-μm thick section of the grafted area in the coronal plane was stained using Alcian blue (counterstained with fast red) for sulfated

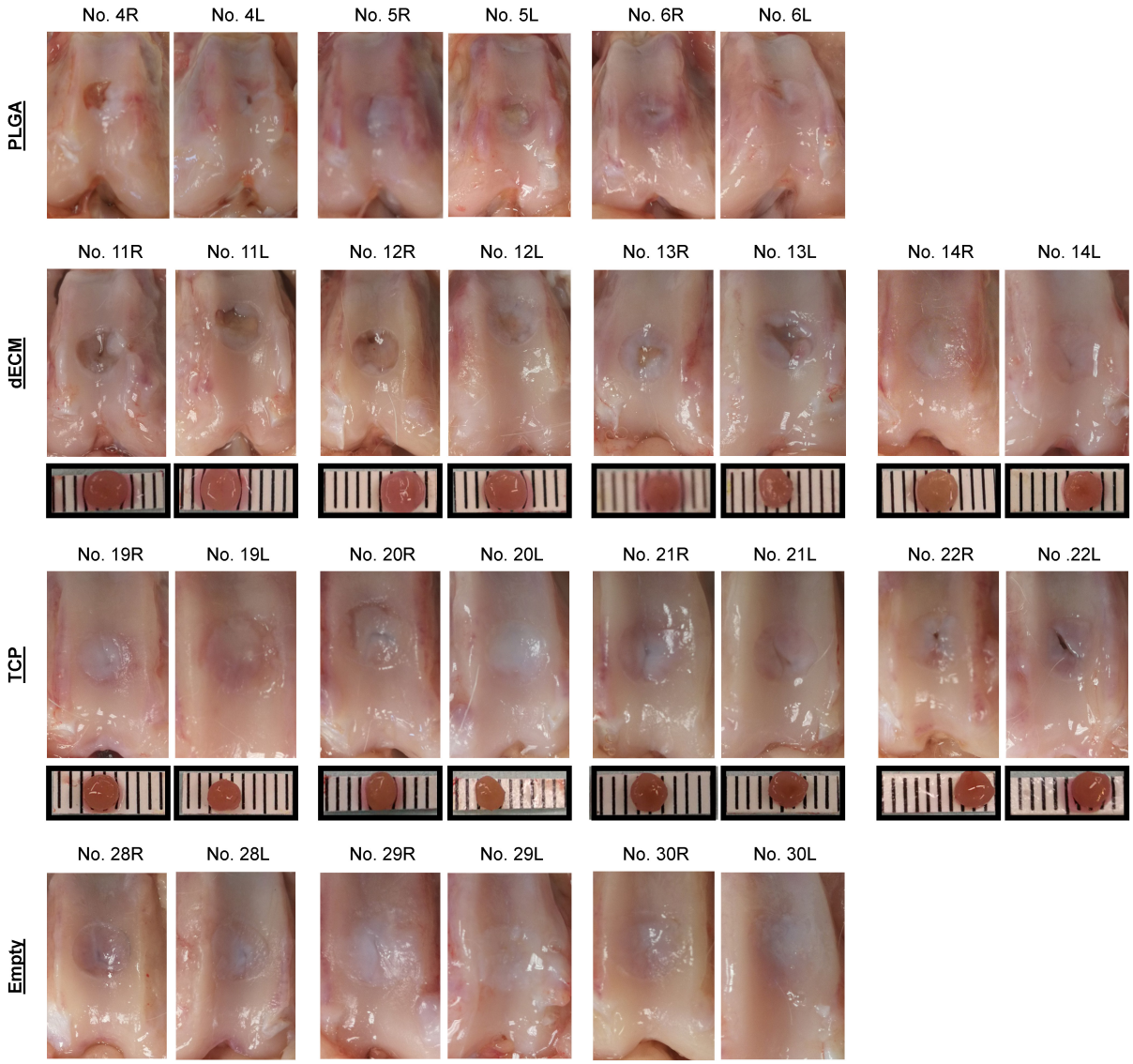

FIGURE 6 | Macroscopic observation of 15-week osteochondral defects repaired with PLGA mesh alone (PLGA; *n* = 3 rabbits/6 knees), tissue constructs developed from dECM expanded IPFSCs (dECM; *n* = 4 rabbits/8 knees) or TCP expanded cells (TCP; *n* = 4 rabbits/8 knees), or left untreated (Empty; *n* = 3 rabbits/6 knees). Scale bar: 1 mm.

glycosaminoglycans (GAGs) and hematoxylin-eosin staining (H&E) for identification of the intact tidemark line that separates calcified and non-calcified cartilaginous matrix. For immunohistochemical analysis, 1% hydrogen peroxide (H_2O_2) in methanol was used to inactivate endogenous peroxidase activity. Sections were digested with 2 mg/mL hyaluronidase for 30 min followed by overnight incubation at 4°C with monoclonal mouse antibodies against type I collagen (MilliporeSigma) and type II collagen (Developmental Studies Hybridoma Bank, Iowa City, IA). Sections for GFP detection were treated with citrate unmasking solution for 20 min followed by overnight incubation at 4°C with a monoclonal mouse antibody against GFP (4B10, Cell Signaling Technology, Danvers, MA). After extensive washing with PBS, sections were incubated with a secondary antibody for 30 min at room temperature. Immunostaining conducted with Vectastain® ABC reagent (Vector Laboratories, Burlingame, CA) was followed by 3,30-diaminobenzidine (DAB) staining and counterstaining was performed with hematoxylin (Vector Laboratories). Tissue sections were graded by four experts blinded to group assignment using a Modified O'Driscoll Scale (MODS) (**Table 1**; O'Driscoll et al., 1986; Rutgers et al., 2010; Barron et al., 2015).

Statistical Analysis

Results from RT-qPCR and histological scoring are presented as mean ± standard error of the mean; the *t*-test was used to assess data between two groups. All statistical analyses were performed

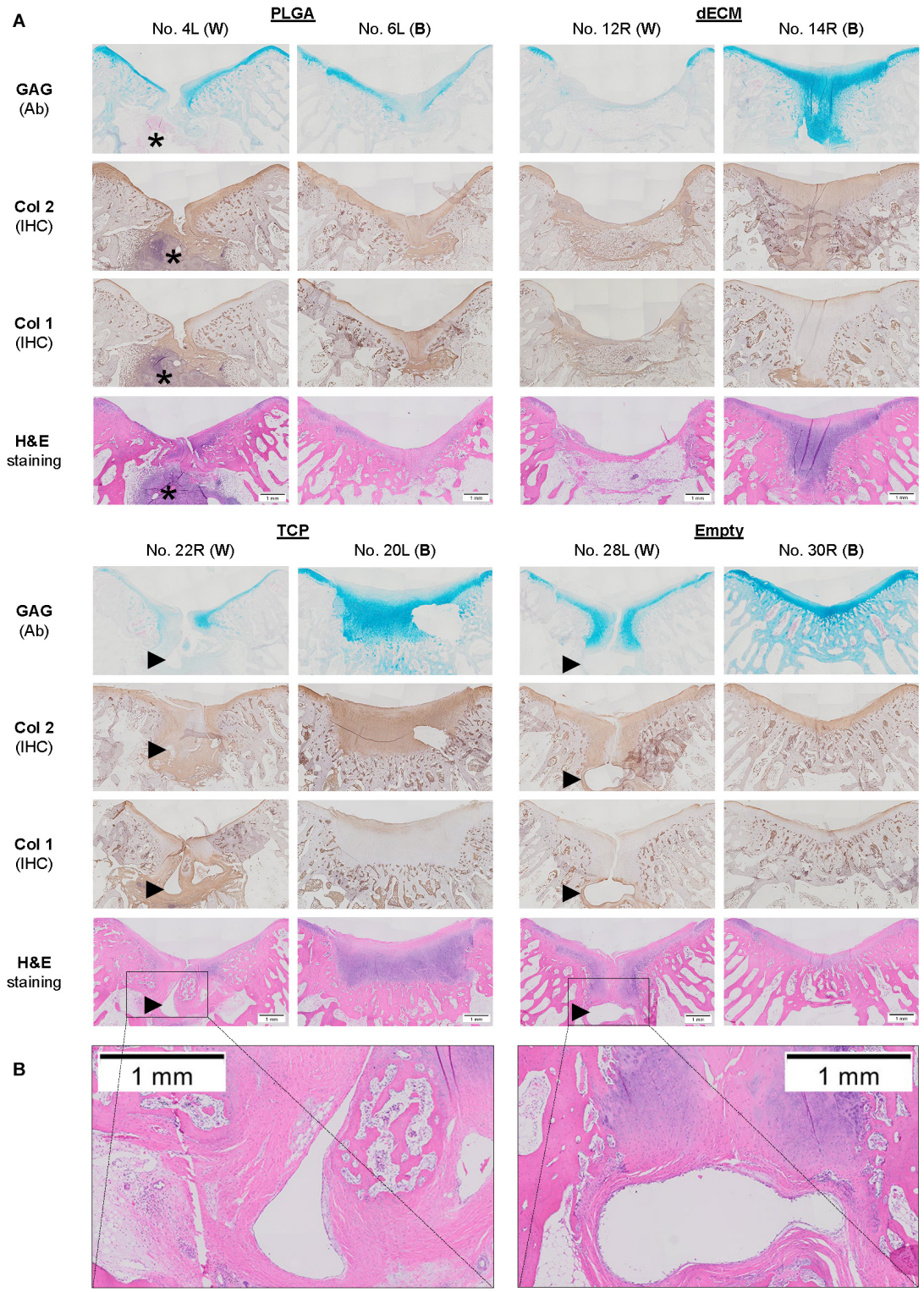

FIGURE 7 | Histological evaluation of 15-week osteochondral defects repaired with PLGA mesh alone (PLGA; *n* = 6 knees), tissue constructs developed from dECM expanded IPFSCs (dECM; *n* = 8 knees) or TCP expanded cells (TCP; *n* = 8 knees), or left untreated (Empty; *n* = 6 knees) using Alcian blue staining (Ab) for sulfated GAGs, H&E staining for the intact tidemark, and immunohistochemical staining (IHC) for types I and II collagen (Col 1 and Col 2). **(A)** Two representative cartilage resurfacings were chosen from each group to serve as the best repair ("B") including rabbit No. 6L/14R/20L/30R or the worst repair ("W") including rabbit No. 4L/12R/22R/28L. Arrows (▶ indicate location of subchondral bone cysts and the asterisk (*) indicates inflammatory cells. **(B)** Bone cysts were shown at higher magnification in H&E staining. Scale bar: 1 mm.

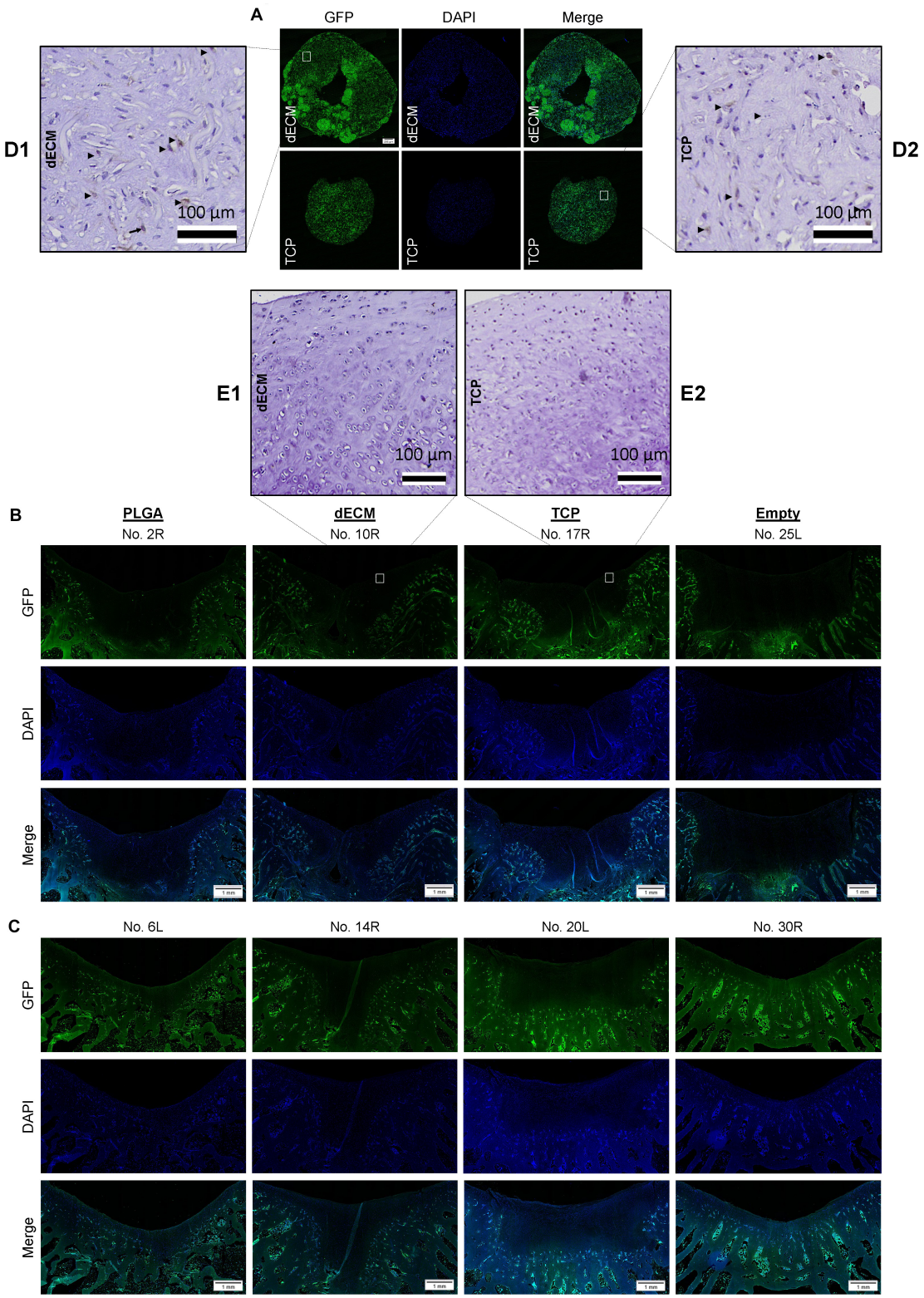

FIGURE 8 | Track of implanted cells labeled with GFP signal. Immunofluorescence of GFP expression in *in vitro* tissue constructs (Scale bar: 200 µm) from either dECM or TCP expanded IPFSCs **(A)**, and six-week (**(B)** and 15-week **(C)** osteochondral defects repaired with PLGA mesh alone (PLGA; $n = 6$ knees), tissue constructs developed from dECM expanded IPFSCs (dECM; $n = 8$ knees) or TCP expanded cells (TCP; $n = 8$ knees), or left untreated (Empty; $n = 6$ knees) (Scale bar: 1 mm). DAPI served as a counterstain. Immunohistochemical staining using monoclonal antibody showed positive staining (Arrows; ▶) for *in vitro* tissue constructs **(D)** but negative staining for *in vivo* resurfacing cartilage from the tissue construct groups **(E)**. Scale bar: 100 µm. Hematoxylin served as a counterstain.

TABLE 1 | Modified O'Driscoll histological scoring system.

Category	Score
I: Percentage of repair tissue that is hyaline cartilage	
100–125%	6
80–100%	8
60–80%	6
40–60%	4
20–40%	2
0–20%	0
II: Articular surface continuity	
Continuous and smooth	2
Continuous but rough	1
Discontinuous	0
III: Tidemark	
Present	2
Incomplete (degenerative, vessel crossing)	1
Absent	0
IV: Thickness of repair tissue compared to host cartilage	
121–150% of normal cartilage	1
81–120% of normal cartilage	2
51–80% of normal cartilage	1
0–50% of normal cartilage	0
V: Integration of cartilage	
Complete (integrated at both sides)	2
Partial	1
Poor (not integrated at both sides)	0
VI: Degenerated changes in repair tissue	
Normal cellularity	2
Slight to moderate hypocellularity or hypercellularity	1
Severe hypocellularity or hypercellularity	0
VII: Degenerative changes in adjacent cartilage	
Normal cellularity, no clusters, no fibrillations	3
Normal cellularity, mild clusters, superficial fibrillations	2
Mild or moderate changes in cellularity, moderate fibrillations	1
Severe changes in cellularity, severe fibrillations	0
VIII: Chondrocyte clustering	
No clusters	2
<25% of the cells	1
25–100% of the cells	0
Total	**Max. 23**

with SPSS 13.0 statistical software (SPSS, Inc., Chicago, IL); $p < 0.05$ was considered statistically significant.

RESULTS

dECM Expanded IPFSCs Exhibited Superior Capacity in Proliferation and Chondrogenic Differentiation

To determine whether dECM expansion could rejuvenate IPFSCs' proliferation and chondrogenic differentiation, IPFSCs were grown on dECM and TCP for one passage followed by chondrogenic induction in a pellet culture system. We found that IPFSCs grown on dECM exhibited a glistening profile and were arranged in the direction of matrix fibers below; in contrast, IPFSCs grown on TCP were larger in size and arranged in a disorderly fashion (**Figure 2A**). EdU incorporation data showed that dECM expanded IPFSCs had a 4.3% increase in percentage and 36.3% increase in median compared to TCP expanded cells (**Figure 2B**). After chondrogenic induction, we found that dECM expanded IPFSCs exhibited significantly higher expression levels of chondrogenic marker genes (**Figure 2C**), including *SOX9*, *ACAN*, and *COL2A1*, than the corresponding TCP group in a time-dependent manner for up to 14 days despite a drop in the expression of these genes at 30 days.

TABLE 2 | Adaptive reactions in cartilage resurfacing.

Group	Category			
	Bone cyst		*Mononuclear cells*	
6 weeks	**No.**	**Ratio**	**No.**	**Ratio**
PLGA	3L	1/6	–	–
dECM	10R	1/8	7L/7R/8L/8R	4/8
TCP	17R	1/8	15L/15R/18L/18R	4/8
EMPTY	26R	1/6	–	–
15 weeks				
PLGA	4L/5R	2/6	4L	1/6
dECM	28L/28R	2/8	12L	1/8
TCP	20R/21L/21R/22L/22R	5/8	–	–
EMPTY	28L/28R	2/6	–	–

Transduction of Lentivirus Showed a Limited Influence on IPFSCs' Stem Cell Properties

To determine whether lentivirus transduction affected IPFSCs' proliferation and chondrogenic induction, IPFSCs were transduced with lentivirus carrying GFP followed by screening with puromycin to remove non-transduced cells (**Figure 2D**). PDT data showed comparable proliferation capacity in the IPFSCs with or without lentivirus transduction at passages 1, 4, and 5 following TCP expansion and at passage 5 following dECM expansion (**Figure 2E**). RT-qPCR data showed that, during chondrogenic induction, IPFSCs with or without lentivirus transduction had a comparable expression level of *SOX9* despite an increase of *ACAN* and a decrease of *COL2A1* in those with lentivirus transduction (**Figure 2F**).

dECM Expanded IPFSCs Developed Better Premature Cartilage Tissue Constructs Than TCP Expanded Cells

Both dECM and TCP expanded IPFSCs (2.2 million each) were dynamically seeded into PLGA mesh scaffold (5 mm diameter × 2 mm thickness) in a spinner flask system. A representative tissue construct is shown in **Figure 2G**. Three weeks after chondrogenic induction, under microscopy, the tissue constructs seeded with dECM expanded cells appeared thicker, with cells settled on the fibers of PLGA mesh, whereas those grown with TCP expanded cells were thinner, indicating

TABLE 3 | Six-week and 15-week cartilage resurfacing graded by MODS.

Group	Category								Total score
	I	II	III	IV	V	VI	VII	VIII	
6 weeks									
PLGA	3.33	0.50	0.17	1.17	1.67	0.50	2.33	1.00	10.67 ± 5.82
dECM	2.00	0.50	-	-	1.50	0.63	2.25	0.88	7.75 ± 3.49
TCP	2.25	0.50	0.13	0.50	1.63	0.75	2.00	1.00	8.75 ± 4.83
EMPTY	7.67	2.00	1.00	1.00	1.83	2.00	2.00	1.00	18.50 ± 0.84
15 weeks									
PLGA	5.33	1.00	0.83	1.83	1.50	1.83	1.67	1.00	15.00 ± 3.35
dECM	3.75	1.38	0.50	1.13	2.00	1.25	2.00	1.00	13.00 ± 5.61
TCP	5.50	1.25	0.63	1.13	1.75	1.13	2.00	1.00	14.38 ± 3.81
EMPTY	7.67	1.83	1.17	1.67	1.83	1.33	2.00	1.00	18.50 ± 1.38

greater cell density in the dECM group than the TCP group (**Figure 2H**). Histology data showed that, following three-week chondrogenic induction, dECM expanded IPFSCs yielded tissue constructs with a larger size and higher intensity of sulfated GAGs as stained by Alcian blue (Ab) and type II collagen (Col 2) immunostained by monoclonal antibody (**Figure 2I**). These observations were further supported by RT-qPCR, as tissue constructs made by dECM expanded cells had higher expression levels of chondrogenic marker genes *SOX9*, *COL2A1*, and *ACAN* than the TCP group; interestingly, the dECM group had less expression of the hypertrophic marker gene *COL10A1* (**Figure 2J**).

Early Stage Evidence of Cartilage Resurfacing Using Different Approaches

Premature tissue constructs from the dECM and TCP groups were used to fill in the defects with implantation of PLGA scaffold alone and the defect left untreated as controls. Six weeks after implantation, defects left untreated (the Empty group) exhibited the best cartilage regeneration with glistening, smooth, and whitish neotissue in most joint samples; however, in other groups, some defects remained uncovered or were partially covered with neotissue, showing a donor-dependent manner of cartilage regeneration. The best and worst examples of healed defects on both sides of the dECM group were exhibited by rabbit No. 10 and No. 7, respectively (**Figure 3**). Greatest healing of defects in the TCP group was found in rabbit Nos. 16 and 17, whereas healing was more limited in rabbit Nos. 15 and 18 (**Figure 3**). Despite lack of inflammatory signs in synovial tissue in all six-week groups, we found subchondral bone cysts in all groups and mononuclear cells in some groups (**Table 2**) as well as subchondral bone spurs in some rabbit joints, including rabbits Nos. 2 and 3 (left side) in the PLGA group and rabbit No. 9 in the dECM group (both left and right sides**; Figure 3**).

The above-mentioned morphological appearance of six-week cartilage resurfacing was further confirmed by histology and immunostaining (**Figure 4**). Most defects in the Empty group were filled with regenerated tissue having integrated at both sides and intensive staining of Alcian blue for sulfated GAGs and immunostaining for type II collagen as well as less staining of type I collagen located primarily on the surface of the neotissue, indicative of a mature articular cartilage (for example, in rabbit No. 25 on the left side). Bone spurs that were composed of regenerated tissue stained positively for sulfated GAGs and type II collagen, indicating the presence of hyaline cartilage, covered with a tissue stained positively for types I and II collagen, indicative of fibrocartilage (**Figure 5**). However, we also found subchondral bone cysts in some joints (No. 26, right side), which likely formed *via* an extension of regenerated cartilage; the wall of cysts expressed both types I and II collagen but not sulfated GAGs, suggestive of fibrocartilage. The other groups included the "best" healing of osteochondral defects such as rabbit No. 2 (right side) in the PLGA group, No. 10 (right side) in the dECM group, and No. 17 (right side) in the TCP group. The "worst" healing of osteochondral defects was found in rabbit No. 1 (left side) in the PLGA group, No. 7 (left side) in the dECM group, and No. 15 (left side) in the TCP group. The MODS scores ("Empty" *versus* "PLGA", $p = 0.009$; "Empty" *versus* "dECM", $p = 0.000$; and "Empty" versus "TCP", $p = 0.000$) (**Table 3**) support the above observation, indicating that the Empty group outperformed the other implantation groups in cartilage resurfacing.

Late Stage Evidence of Cartilage Resurfacing Using Different Approaches

The Empty group exhibited superior cartilage healing as compared to all other groups (**Figure 6**), which was supported by their MODS scores ("Empty" vs. "PLGA", $p = 0.039$; "Empty" vs. "dECM", $p = 0.038$; and "Empty" vs. "TCP", $p = 0.028$) (**Table 3**). Compared to those of six-week rabbit joints, cartilage regeneration in the 15-week joints of the Empty group did not have a significant change; however, other groups at 15 weeks had greatly improved in osteochondral defect repairs, particularly for the dECM and TCP groups which had implantation of tissue constructs (**Figures 6**, **7**).

There were no signs of inflammation or bone spurs in 15-week joints in any group. Compared to six-week cartilage resurfacing, we found more bone cysts in each group and mononuclear cells surrounding regenerated tissue in some groups (**Table 2**), particularly in rabbit No. 4 (left side) in the PLGA group (**Figure 7**). The MODS score of cartilage resurfacing with tissue

constructs (dECM and TCP groups) exhibited a significant increase at 15 weeks compared to that at six weeks ($p = 0.041$ and $p = 0.022$, respectively) (**Table 3**).

Tracking of Implanted Cells Labeled With GFP

Under immunofluorescence microscopy, GFP expression in both *in vitro* tissue constructs was maintained from expanded IPFSCs after lentivirus transduction and puromycin screening (**Figure 8A**). However, GFP expression in the regenerated cartilage tissue was undetectable in all groups at both six-week (**Figure 8B**) and 15-week time points (**Figure 8C**), indicating that implanted IPFSCs might not be directly involved in cartilage resurfacing. In order to exclude the influence of decalcification on the immunofluorescence signal, an immunohistochemical staining was conducted using a monoclonal antibody against GFP. The result confirmed immunofluorescence data (**Figures 8A–C**) – positive staining in *in vitro* tissue construct samples (**Figure 8D**) but not in *in vivo* resurfacing cartilage from the tissue construct groups (**Figure 8E**).

DISCUSSION

The goal of this study was to assess the feasibility of using a dECM-mediated-tissue engineering approach to treat osteochondral defects in young rabbits. Interestingly, we found that the Empty group (with defects left untreated) exhibited superior cartilage resurfacing at both six weeks and 15 weeks compared to the PLGA, TCP, and dECM groups. In addition, the MODS score of 15-week cartilage resurfacing in the Empty group had no significant change compared to that of six-week samples, indicating that 7.7-month-old rabbits still had a strong capacity to self-heal cartilage defects up to six weeks until 9 months of age (7.7 months + 6 weeks) by which time the rabbits had lost this ability. Consistent with a previous report, (He et al., 2009) despite the excellent chondrogenic capacity and less hypertrophy of dECM expanded IPFSCs evaluated *in vitro*, tissue constructs developed by dECM expanded cells failed to show an advantage for cartilage resurfacing over those from TCP expanded cells. However, the MODS scoring data indicated that cartilage resurfacing was significantly improved in both tissue construct groups at 15 weeks compared to those at six weeks, suggesting that a tissue-engineering approach plays a unique role in cartilage resurfacing of adult rabbits despite the fact that self-healing dominates cartilage repair in young rabbits less than 9 months old. Although the implanted cells were pre-labeled with GFP, no positive staining was detectable in the resurfaced cartilage from both six-week and 15-week osteochondral defects, suggesting that the implanted cells might not be directly involved in cartilage resurfacing.

As a conventionally used animal model, the rabbit has a strong ability for spontaneous cartilage repair, (Chu et al., 2010; Anderson et al., 2014) which implies the chondrocytes' capacity in proliferation and deposition of functional matrix in the absence of vascular elements (Dell'Accio and Vincent, 2010). Therefore, it is important to choose rabbits with minimized self-healing capacity for a cartilage regeneration study. NZW rabbits' skeletal maturity is reported to occur between four and six months, (Reinholz et al., 2004; Hunziker et al., 2007) but some groups believe rabbits become skeletally mature between six and nine months of age (Rudert, 2002; Isaksson et al., 2010) or between seven and eight months of age, (Masoud et al., 1986) with an age of eight months and above, (Wei et al., 1997; Wei and Messner, 1999; Pei et al., 2009) or with an age of nine months or more (Hoemann et al., 2007). The finding in this study indicates there is no further growth of cartilage when rabbits reach nine months old, the age when a young rabbit becomes an adult (Laber-Laird et al., 1996), which might be attributed to cartilage maturation, meeting the guidelines recommended by the International Cartilage Regeneration & Joint Preservation Society (ICRS), as opposed to skeletal maturity (Hurtig et al., 2011). Cartilage maturation is defined by an intact tidemark that is the calcified cartilage layer and complete subchondral bone plate with minimized vascularization (Müller-Gerbl, 1998; Madry et al., 2010). Given a 3-mm diameter cartilage lesion defined as the critical sized defect in a rabbit knee model, in this study, 4.76 mm diameter × 2 mm depth osteochondral defects that did not penetrate subchondral bone in the Empty group were filled with a neotissue with intensive expression of sulfated GAGs and type II collagen but less expression of type I collagen, indicative of a hyaline articular cartilage. These findings are in contrast to fibrocartilage with inferior mechanical properties as reported in the Empty group by Barron et al. Barron and coworkers reported that type I collagen was evident throughout the neotissue along with type II collagen, (Barron et al., 2015) likely contributed by bone marrow stomal cells released from penetrating subchondral bone through a 3-mm-depth cartilage defect model (Wei and Messner, 1999).

Some researchers think articular cartilage is immunoprivileged because of cartilage's avascular and dense ECM; however, this view has been questioned by antigenic evidence of chondrocytes and associated ECM, (Revell and Athanasiou, 2009; Arzi et al., 2015). As shown by the cartilage resurfacing joint samples in the PLGA group, implant materials evoked a robust and constant inflammatory response evidenced by the presence of a large number of mononuclear cells surrounding subchondral bone at 15 weeks postoperatively. However, there was no sign of immune rejection observed during tissue harvesting. This finding confirmed the view that the recipient could reject a xenogeneic but not allogeneic implant (Pei et al., 2009, 2010; Arzi et al., 2015). Increasing evidence shows that the discrepancy exists in response to foreign implants between young and old recipients due to the changed local matrix microenvironment (Lynch and Pei, 2014; Brown et al., 2017). For example, Hachim et al. (2017) reported that, compared to eight-week-old mice, 18-month-old mice exhibited significant differences in macrophage polarization during the early phase of implantation and delayed resolution of the host response. Colvin et al. (2017) demonstrated that older transplant recipients exhibited reduced frequency of acute allograft rejection due to immunosenescence. The above-mentioned evidence might partially explain why implant groups were not better in cartilage

resurfacing than the Empty group (left untreated), at least in the earlier time points assessed in this study, such as six weeks and 15 weeks.

Abnormal reactions during cartilage resurfacing include, but are not limited to, osteophytes, bone cysts, and synovial tissue inflammation (Hoemann et al., 2011). In this study, we did not observe synovial tissue inflammation, but both osteophytes and bone cysts existed in some groups at some time points. In animal models, subchondral bone cysts can appear following the treatment of cartilage repair, (Benazzo et al., 2008; Getgood et al., 2012) suggesting abnormal biological remodeling (Henderson et al., 2003) resulting from unusual mechanobiology (Von Rechenberg et al., 2003; Pallante-Kichura et al., 2013). Different from previous findings that bone cysts were only observed in the Empty group but not in the cell-free or cell-seeded scaffold groups (Barron et al., 2015) and that bone cysts occurred in the implantation with either collagen-GAG or PLGA scaffold, (Getgood et al., 2012) we found that subchondral bone cysts existed in all groups at both time points; however, cartilage resurfacing at 15 weeks postoperatively had more bone cysts than the earlier time point at six weeks. Since both time points designed for observation were still in the early phase of cartilage resurfacing, the wall of bone cysts was characterized as fibrocartilage, which positively stained for both types I and II collagen but was negative for sulfated GAG. This finding is in contrast to previous reports in which mature bone cysts were surrounded by bone tissue (Chen et al., 2011; Pallante-Kichura et al., 2013).

Potential mechanisms underlying the role of mesenchymal stromal/stem cells in cartilage repair include two viewpoints, *via* direct (chondrogenic differentiation) and/or indirect (secretion of paracrine factors) strategies (Meirelles Lda et al., 2009; Toh et al., 2014). Previous studies indicated that only a small fraction of labeled cells traceable in the repair tissue originated from the implanted cells (Grande et al., 1989; Dell'Accio et al., 2003; Tatebe et al., 2005; Blanke et al., 2009). In this study, we were unable to trace at either six-weeks or 15-weeks postoperatively using both immunofluorescence microscopy and immunohistochemical staining for GFP signal, indicating that trophic factors released by the implanted cells might contribute to cartilage resurfacing rather than direct differentiation. In comparison to defects at six and 15 weeks, both tissue construct groups exhibited a significant improvement in cartilage resurfacing indicting that the impact of implanted cells on reparative cells might dominate osteochondral defect repair and play a more critical role than the implanted cells themselves (Muschler et al., 2010).

Taken together, in this study, young NZW rabbits (around 7.7 months old) exhibited a strong ability for simultaneous cartilage regeneration until nine months of age. Compared to TCP expanded IPFSCs, dECM expanded cells presented a robust chondrogenic capacity under *in vitro* induction in both pellet and tissue construct cultures, but this advantage was not reflected in cartilage resurfacing of osteochondral defects in young rabbits. Interestingly, both tissue construct groups displayed improved cartilage resurfacing in a time-dependent manner, indicating that a tissue-engineering cartilage graft can facilitate osteochondral defect repair in adult rabbits, in which the untreated group did not have improvement. In the future, the dECM-based tissue-engineering approach will be further explored to treat osteochondral defects in models utilizing older animals, including adult and elderly rabbits with mature cartilage.

DATA AVAILABILITY STATEMENT

The raw data supporting the conclusions of this article will be made available by the authors, without undue reservation.

ETHICS STATEMENT

The animal study was reviewed and approved by WVU IACUC committee.

AUTHOR CONTRIBUTIONS

ZL performed collection and assembly of data, data analysis and interpretation, manuscript writing, and final approval. SZ, JV, AS, and JP performed collection of data and final approval of manuscript. GG performed data analysis and interpretation and final approval of manuscript. LY performed data analysis and interpretation, final approval of manuscript, and financial support. MP performed conception and design, data analysis and interpretation, manuscript writing and final approval, and financial support. All authors contributed to the article and approved the submitted version.

ACKNOWLEDGMENTS

We thank Suzanne Danley for editing the manuscript. This work was supported by Research Grants from the Musculoskeletal Transplant Foundation (MTF) and the National Institutes of Health (1R01AR067747-01A1). We also would like to acknowledge the WVU Flow Cytometry and Microscope Imaging Facility and the grants that support these facility, TME CoBRE grant P20GM121322, and WV-INBRE grant P20 GM103434 and P30GM103488.

REFERENCES

Anderson, J. A., Little, D., Toth, A. P., Moorman, C. T. III, Tucker, B. S., Ciccotti, M. G., et al. (2014). Stem cell therapies for knee cartilage repair: the current status of preclinical and clinical studies. *Am. J. Sports Med.* 42, 2253–2261. doi: 10.1177/0363546513508744

Arzi, B., DuRaine, G. D., Lee, C. A., Huey, D. J., Borjesson, D. L., Murphy, B. G., et al. (2015). Cartilage immunoprivilege depends on donor source

and lesion location. *Acta Biomater.* 23, 72–81. doi: 10.1016/j.actbio.2015.05.025

Barron, V., Merghani, K., Shaw, G., Coleman, C. M., Hayes, J. S., Ansboro, S., et al. (2015). Evaluation of cartilage repair by mesenchymal stem cells seeded on a PEOT/PBT scaffold in an osteochondral defect. *Ann. Biomed. Eng.* 43, 2069–2082. doi: 10.1007/s10439-015-1246-2

Benazzo, F., Cadossi, M., Cavani, F., Fini, M., Giavaresi, G., Setti, S., et al. (2008). Cartilage repair with osteochondral autografts in sheep: effect of biophysical stimulation with pulsed electromagnetic fields. *J. Orthop. Res.* 26, 631–642. doi: 10.1002/jor.20530

Blanke, M., Carl, H. D., Klinger, P., Swoboda, B., Hennig, F., and Gelse, K. (2009). Transplanted chondrocytes inhibit endochondral ossification within cartilage repair tissue. *Calcif Tissue Int.* 85, 421–433. doi: 10.1007/s00223-009-9288-9

Brown, B. N., Haschak, M. J., Lopresti, S. T., and Stahl, E. C. (2017). Effects of age-related shifts in cellular function and local microenvironment upon the innate immune response to implants. *Semin. Immunol.* 29, 24–32. doi: 10.1016/j.smim.2017.05.001

Chen, H., Chevrier, A., Hoemann, C. D., Sun, J., Ouyang, W., and Buschmann, M. D. (2011). Characterization of subchondral bone repair for marrow-stimulated chondral defects and its relationship to articular cartilage resurfacing. *Am. J. Sports Med.* 39, 1731–1740. doi: 10.1177/0363546511403282

Chu, C. R., Szczodry, M., and Bruno, S. (2010). Animal models for cartilage regeneration and repair. *Tissue Eng. Part B Rev.* 16, 105–115. doi: 10.1089/ten.teb.2009.0452

Colvin, M. M., Smith, C. A., Tullius, S. G., and Goldstein, D. R. (2017). Aging and the immune response to organ transplantation. *J. Clin. Invest.* 127, 2523–2529. doi: 10.1172/jci90601

Dell'Accio, F., Vanlauwe, J., Bellemans, J., Neys, J., De Bari, C., and Luyten, F. P. (2003). Expanded phenotypically stable chondrocytes persist in the repair tissue and contribute to cartilage matrix formation and structural integration in a goat model of autologous chondrocyte implantation. *J. Orthop Res.* 21, 123–131. doi: 10.1016/s0736-0266(02)00090-6

Dell'Accio, F., and Vincent, T. L. (2010). Joint surface defects: clinical course and cellular response in spontaneous and experimental lesions. *Eur. Cell Mater.* 20, 210–217. doi: 10.22203/ecm.v020a17

Galeano-Garces, C., Camilleri, E. T., Riester, S. M., Dudakovic, A., Larson, D. R., Qu, W., et al. (2017). Molecular validation of chondrogenic differentiation and hypoxia responsiveness of platelet-Lysate expanded adipose tissue-derived human mesenchymal stromal cells. *Cartilage* 8, 283–299. doi: 10.1177/1947603516659344

Getgood, A. M., Kew, S. J., Brooks, R., Aberman, H., Simon, T., Lynn, A. K., et al. (2012). Evaluation of early-stage osteochondral defect repair using a biphasic scaffold based on a collagen glycosaminoglycan biopolymer in a caprine model. *Knee* 19, 422–430. doi: 10.1016/j.knee.2011.03.011

Gilsanz, V., Roe, T. F., Gibbens, D. T., Schulz, E. E., Carlson, M. E., Gonzalez, O., et al. (1988). Effect of sex steroids on peak bone density of growing rabbits. *Am. J. Physiol.* 255, E416–E421.

Grande, D. A., Pitman, M. I., Peterson, L., Menche, D., and Klein, M. (1989). The repair of experimentally produced defects in rabbit articular cartilage by autologous chondrocyte transplantation. *J. Orthop Res.* 7, 208–218. doi: 10.1002/jor.1100070208

Hachim, D., Wang, N., Lopresti, S. T., Stahl, E. C., Umeda, Y. U., Rege, R. D., et al. (2017). Effects of aging upon the host response to implants. *J. Biomed. Mater. Res. A* 105, 1281–1292. doi: 10.1002/jbm.a.36013

Han, S. H., Kim, Y. H., Park, M. S., Kim, I. A., Shin, J. W., Yang, W. I., et al. (2008). Histological and biomechanical properties of regenerated articular cartilage using chondrogenic bone marrow stromal cells with a PLGA scaffold in vivo. *J. Biomed. Mat. Res. Part A.* 87A, 850–861. doi: 10.1002/jbm.a.31828

He, F., Chen, X., and Pei, M. (2009). Reconstruction of an in vitro tissue-specific microenvironment to rejuvenate synovium-derived stem cells for cartilage tissue engineering. *Tissue Eng. Part A.* 15, 3809–3821. doi: 10.1089/ten.tea.2009.0188

He, F., and Pei, M. (2013). Extracellular matrix enhances differentiation of adipose stem cells from infrapatellar fat pad toward chondrogenesis. *J. Tissue Eng. Regen. Med.* 7, 73–84. doi: 10.1002/term.505

Henderson, I. J., Tuy, B., Connell, D., Oakes, B., and Hettwer, W. H. (2003). Prospective clinical study of autologous chondrocyte implantation and correlation with MRI at three and 12 months. *J. Bone Joint Surg. Br.* 85B, 1060–1066. doi: 10.1302/0301-620x.85b7.13782

Hoemann, C., Kandel, R., Roberts, S., Saris, D. B., Creemers, L., Mainil-Varlet, P., et al. (2011). International Cartilage Repair Society (ICRS) recommended guidelines for histological endpoints for cartilage repair studies in animal models and clinical trials. *Cartilage* 2, 153–172. doi: 10.1177/1947603510397535

Hoemann, C. D., Sun, J., McKee, M. D., Chevrier, A., Rossomacha, E., Rivard, G. E., et al. (2007). Chitosan-glycerol phosphate/blood implants elicit hyaline cartilage repair integrated with porous subchondral bone in microdrilled rabbit defects. *Osteoarthritis Cartilage* 15, 78–89. doi: 10.1016/j.joca.2006.06.015

Hunziker, E. B., Kapfinger, E., and Geiss, J. (2007). The structural architecture of adult mammalian articular cartilage evolves by a synchronized process of tissue resorption and neoformation during postnatal development. *Osteoarthritis Cartilage* 15, 403–413. doi: 10.1016/j.joca.2006.09.010

Hurtig, M. B., Buschmann, M. D., Fortier, L. A., Hoemann, C. D., Hunziker, E. B., Jurvelin, J. S., et al. (2011). Preclinical studies for cartilage repair: recommendations from the International Cartilage Repair Society. *Cartilage* 2, 137–152. doi: 10.1177/1947603511401905

Isaksson, H., Harjula, T., Koistinen, A., Iivarinen, J., Seppänen, K., Arokoski, J. P., et al. (2010). Collagen and mineral deposition in rabbit cortical bone during maturation and growth: effects on tissue properties. *J. Orthop Res.* 28, 1626–1633. doi: 10.1002/jor.21186

Laber-Laird, K., Flecknell, P., and Swindle, M. (1996). *Handbook of Rodent and Rabbit Medicine*. Oxford: Butterworth-heinemann.

Li, J., and Pei, M. (2010). Optimization of an in vitro three-dimensional microenvironment to reprogram synovium-derived stem cells for cartilage tissue engineering. *Tissue Eng. Part A* 17, 703–712. doi: 10.1089/ten.tea.2010.0339

Li, J., and Pei, M. A. (2018). Protocol to prepare decellularized stem cell matrix for rejuvenation of cell expansion and cartilage regeneration. *Methods Mol. Biol.* 1577, 147–154. doi: 10.1007/7651_2017_27

Li, J. T., He, F., and Pei, M. (2011). Creation of an in vitro microenvironment to enhance human fetal synovium-derived stem cell chondrogenesis. *Cell Tissue Res.* 345, 357–365. doi: 10.1007/s00441-011-1212-8

Li, J. T., and Pei, M. (2012). Cell senescence: a challenge in cartilage engineering and regeneration. *Tissue Eng. Part B* 18, 270–287. doi: 10.1089/ten.teb.2011.0583

Lynch, K., and Pei, M. (2014). Age associated communication between cells and matrix: a potential impact on stem cell-based tissue regeneration strategies. *Organogenesis* 10, 289–298. doi: 10.4161/15476278.2014.970089

Madry, H., van Dijk, C. N., and Mueller-Gerbl, M. (2010). The basic science of the subchondral bone. *Knee Surg. Sports Traumatol. Arthrosc.* 18, 419–433. doi: 10.1007/s00167-010-1054-z

Masoud, I., Shapiro, F., and Moses, A. (1986). Tibial epiphyseal development: a cross-sectional histologic and histomorphometric study in the New Zealand white rabbit. *J. Orthop Res.* 4, 212–220. doi: 10.1002/jor.1100040210

Meirelles Lda, S., Fontes, A. M., Covas, D. T., and Caplan, A. I. (2009). Mechanisms involved in the therapeutic properties of mesenchymal stem cells. *Cytokine Growth Factor Rev.* 20, 419–427. doi: 10.1016/j.cytogfr.2009.10.002

Müller-Gerbl, M. (1998). The subchondral bone plate. *Adv. Anat. Embryol. Cell Biol.* 141, 1–134. doi: 10.1007/978-3-642-72019-2_1

Muschler, G. F., Raut, V. P., Patterson, T. E., Wenke, J. C., and Hollinger, J. O. (2010). The design and use of animal models for translational research in bone tissue engineering and regenerative medicine. *Tissue Eng. Part B Rev.* 16, 123–145. doi: 10.1089/ten.teb.2009.0658

Newman, E., Turner, A. S., and Wark, J. D. (1995). The potential of sheep for the study of osteopenia: current status and comparison with other animal models. *Bone* 16, 277–284.

Nukavarapu, S. P., and Dorcemus, D. L. (2013). Osteochondral tissue engineering: Current strategies and challenges. *Biotechnol. Adv.* 31, 706–721. doi: 10.1016/j.biotechadv.2012.11.004

O'Driscoll, S. W., Keeley, F. W., and Salter, R. B. (1986). The chondrogenic potential of free autogenous periosteal grafts for biological resurfacing of major full-thickness defects in joint surfaces under the influence of continuous passive motion. An experimental investigation in the rabbit. *J. Bone Joint Surg. Am.* 68, 1017–1035. doi: 10.2106/00004623-198668070-00008

Pallante-Kichura, A. L., Cory, E., Bugbee, W. D., and Sah, R. L. (2013). Bone cysts after osteochondral allograft repair of cartilage defects in goats suggest

abnormal interaction between subchondral bone and overlying synovial joint tissues. *Bone* 57, 259–268. doi: 10.1016/j.bone.2013.08.011

Pei, M. (2017). Environmental preconditioning rejuvenates stem cells' chondrogenic potential. *Biomaterials* 117, 10–23. doi: 10.1016/j.biomaterials.2016.11.049

Pei, M., He, F., Boyce, B. M., and Kish, V. L. (2009). Repair of full-thickness femoral condyle cartilage defects using allogeneic synovial cell-engineered tissue constructs. *Osteoarthritis Cartilage* 17, 714–722. doi: 10.1016/j.joca.2008.11.017

Pei, M., He, F., Li, J., Tidwell, J. E., Jones, A. C., and McDonough, E. B. (2013). Repair of large animal partial-thickness cartilage defects through intraarticular injection of matrix-rejuvenated synovium-derived stem cells. *Tissue Eng. Part A* 19, 1144–1154. doi: 10.1089/ten.tea.2012.0351

Pei, M., He, F., and Wei, L. (2011). Three-dimensional cell expansion substrate for cartilage tissue engineering and regeneration: a comparison in decellularized matrix deposited by synovium-derived stem cells and chondrocytes. *J. Tissue Sci Eng* 2:2.

Pei, M., Seidel, J., Vunjak-Novakovic, G., and Freed, L. E. (2002a). Growth factors for sequential cellular de- and redifferentiation in tissue engineering. *Biochem. Biophys. Res. Commun.* 294, 149–154. doi: 10.1016/s0006-291x(02)00439-4

Pei, M., Solchaga, L. A., Seidel, J., Zeng, L., Vunjak-Novakovic, G., Caplan, A. I., et al. (2002b). Bioreactors mediate the effectiveness of tissue engineering scaffolds. *FASEB J.* 16, 1691–1694. doi: 10.1096/fj.02-0083fje

Pei, M., Yan, Z., Shoukry, M., and Boyce, B. M. (2010). Failure of xenoimplantation using porcine synovium-derived stem cell-based cartilage tissue constructs for the repair of rabbit osteochondral defects. *J. Orthop. Res.* 28, 1064–1070. doi: 10.1002/jor.21096

Pizzute, T., Zhang, Y., He, F., and Pei, M. (2016). Ascorbate-dependent impact on cell-derived matrix in modulation of stiffness and rejuvenation of infrapatellar fat derived stem cells toward chondrogenesis. *Biomed. Mater.* 11:045009. doi: 10.1088/1748-6041/11/4/045009

Reinholz, G. G., Lu, L., Saris, D. B., Yaszemski, M. J., and O'Driscoll, S. W. (2004). Animal models for cartilage reconstruction. *Biomaterials* 25, 1511–1521. doi: 10.1016/s0142-9612(03)00498-8

Revell, C. M., and Athanasiou, K. A. (2009). Success rates and immunologic responses of autogenic, allogenic, and xenogenic treatments to repair articular cartilage defects. *Tissue Eng. Part B Rev* 15, 1–15. doi: 10.1089/ten.teb.2008.0189

Rudert, M. (2002). Histological evaluation of osteochondral defects: consideration of animal models with emphasis on the rabbit, experimental setup, follow-up and applied methods. *Cells Tissues Organs* 171, 229–240. doi: 10.1159/000063125

Rutgers, M., van Pelt, M. J., Dhert, W. J., Creemers, L. B., and Saris, D. B. (2010). Evaluation of histological scoring systems for tissue-engineered, repaired and osteoarthritic cartilage. *Osteoarthritis Cartilage* 18, 12–23. doi: 10.1016/j.joca.2009.08.009

Smith, G. D., Knutsen, G., and Richardson, J. B. (2005). A clinical review of cartilage repair techniques. *J. Bone Joint Surg. Br.* 87, 445–449.

Sun, Y., Chen, S., and Pei, M. (2018). Comparative advantages of infrapatellar fat pad: an emerging stem cell source for regenerative medicine. *Rheumatology* 57, 2072–2086. doi: 10.1093/rheumatology/kex487

Tatebe, M., Nakamura, R., Kagami, H., Okada, K., and Ueda, M. (2005). Differentiation of transplanted mesenchymal stem cells in a large osteochondral defect in rabbit. *Cytotherapy* 7, 520–530. doi: 10.1080/14653240500361350

Toh, W. S., Foldager, C. B., Pei, M., and Hui, J. H. (2014). Advances in mesenchymal stem cell-based strategies for cartilage repair and regeneration. *Stem. Cell Rev. Rep.* 10, 686–696. doi: 10.1007/s12015-014-9526-z

Uematsu, K., Hattori, K., Ishimoto, Y., Yamauchi, J., Habata, T., Takakura, Y., et al. (2005). Cartilage regeneration using mesenchymal stem cells and a three-dimensional poly-lactic-glycolic acid (PLGA) scaffold. *Biomaterials.* 26, 4273–4279. doi: 10.1016/j.biomaterials.2004.10.037

Von Rechenberg, B., Akens, M. K., Nadler, D., Bittmann, P., Zlinszky, K., Kutter, A., et al. (2003). Changes in subchondral bone in cartilage resurfacing–an experimental study in sheep using different types of osteochondral grafts. *Osteoarthritis Cartilage* 11, 265–277. doi: 10.1016/s1063-4584(03)00006-2

Wang, T., Hill, R. C., Dzieciatkowska, M., Zhu, L., Infante, A. M., Hu, G., et al. (2020). Site-dependent lineage preference of adipose stem cells. *Front. Cell Dev. Biol.* 8:237.

Wang, Y. M., Fu, Y. W., Yan, Z. Q., Zhang, X. B., and Pei, M. (2019). Impact of fibronectin knockout on proliferation and differentiation of human infrapatellar fat pad-derived stem cells. *Front. Bioeng. Biotechnol.* 7:321.

Wang, Y. M., Hu, G. Q., Hill, R. C., Dzieciatkowska, M., Hansen, K. C., Zhang, X. B., et al. (2020). Matrix reverses immortalization-mediated stem cell fate determination. *Biomaterials* 265:120387. doi: 10.1016/j.biomaterials.2020.120387

Wei, X., Gao, J., and Messner, K. (1997). Maturation-dependent repair of untreated osteochondral defects in the rabbit knee joint. *J. Biomed. Mater Res.* 34, 63–72. doi: 10.1002/(sici)1097-4636(199701)34:1<63::aid-jbm9>3.0.co;2-l

Wei, X., and Messner, K. (1999). Maturation-dependent durability of spontaneous cartilage repair in rabbit knee joint. *J. Biomed. Mater. Res.* 46, 539–548. doi: 10.1002/(sici)1097-4636(19990915)46:4<539::aid-jbm12>3.0.co;2-s

Willers, C., Wood, D. J., and Zheng, M. H. (2003). A current review on the biology and treatment of articular cartilage defects (Part I & Part II). *J. Musculoskelet Res.* 7, 157–181. doi: 10.1142/s0218957703001125

Conflict of Interest: The authors declare that the research was conducted in the absence of any commercial or financial relationships that could be construed as a potential conflict of interest.

frontiers in Cell and Developmental Biology

REVIEW
published: 04 November 2020
doi: 10.3389/fcell.2020.580868

Osteochondral Injury, Management and Tissue Engineering Approaches

George Jacob[1,2], *Kazunori Shimomura*[1] *and Norimasa Nakamura*[3,4]*

[1] Department of Orthopedic Surgery, Osaka University Graduate School of Medicine, Osaka, Japan, [2] Department of Orthopedics, Tejasvini Hospital, Mangalore, India, [3] Institute for Medical Science in Sports, Osaka Health Science University, Osaka, Japan, [4] Global Center for Medical Engineering and Informatics, Osaka University, Osaka, Japan

Osteochondral lesions (OL) are a common clinical problem for orthopedic surgeons worldwide and are associated with multiple clinical scenarios ranging from trauma to osteonecrosis. OL vary from chondral lesions in that they involve the subchondral bone and chondral surface, making their management more complex than an isolated chondral injury. Subchondral bone involvement allows for a natural healing response from the body as marrow elements are able to come into contact with the defect site. However, this repair is inadequate resulting in fibrous scar tissue. The second differentiating feature of OL is that damage to the subchondral bone has deleterious effects on the mechanical strength and nutritive capabilities to the chondral joint surface. The clinical solution must, therefore, address both the articular cartilage as well as the subchondral bone beneath it to restore and preserve joint health. Both cartilage and subchondral bone have distinctive functional requirements and therefore their physical and biological characteristics are very much dissimilar, yet they must work together as one unit for ideal joint functioning. In the past, the obvious solution was autologous graft transfer, where an osteochondral bone plug was harvested from a non-weight bearing portion of the joint and implanted into the defect site. Allografts have been utilized similarly to eliminate the donor site morbidity associated with autologous techniques and overall results have been good but both techniques have their drawbacks and limitations. Tissue engineering has thus been an attractive option to create multiphasic scaffolds and implants. Biphasic and triphasic implants have been under explored and have both a chondral and subchondral component with an interface between the two to deliver an implant which is biocompatible and emulates the osteochondral unit as a whole. It has been a challenge to develop such implants and many manufacturing techniques have been utilized to bring together two unalike materials and combine them with cellular therapies. We summarize the functions of the osteochondral unit and describe the currently available management techniques under study.

Keywords: osteochondral repair, Tissue Engineering and Regenerative Medicine, articular cartilage, multiphasic scaffold, Mesenchymal stem cell

OPEN ACCESS

Edited by:
Takashi Nakamura,
Tohoku University, Japan

Reviewed by:
Susanne Grässel,
University of Regensburg, Germany
Ke Xue,
Shanghai Jiao Tong University, China
Salvatore Rinaldi,
Istituto Rinaldi Fontani, Italy

***Correspondence:**
Norimasa Nakamura
norimasa.nakamura@ohsu.ac.jp

Specialty section:
This article was submitted to Stem Cell Research, a section of the journal Frontiers in Cell and Developmental Biology

Received: *07 July 2020*
Accepted: *22 September 2020*
Published: *04 November 2020*

Citation:
Jacob G, Shimomura K and Nakamura N (2020) Osteochondral Injury, Management and Tissue Engineering Approaches. Front. Cell Dev. Biol. 8:580868. doi: 10.3389/fcell.2020.580868

INTRODUCTION

Osteochondral lesions (OL) are a morphological finding as a result of an acute trauma or occur due to osteochondritis dissecans, osteoarthritis (OA), subchondral insufficiency fractures or osteonecrosis (Gorbachova et al., 2018). OLs pose a difficult clinical situation for joint preservation surgeons as they extend beyond the articular cartilage into the subchondral bone and marrow

(Gorbachova et al., 2018). The additional injury to the underlying structural support system along with the articular cartilage demands a more comprehensive clinical solution.

Due to the avascular nature of cartilage tissue, it is beyond the reach of reparative growth factors and cells, therefore not fortunate to follow normal tissue injury response (Temenoff and Mikos, 2000; Sophia Fox et al., 2009). The natural healing of OLs vary from that of chondral lesions due to their subchondral extension resulting in spontaneous cellular repair (Charalambous, 2014). This natural response leads to the formation of unsatisfactory fibrocartilage and the articular surface degenerates over time (Ochi et al., 2001) progressing toward OA. OL treatment strategies must aim to address both the subchondral bone and chondral surface above it (Gomoll et al., 2010). Current techniques include autologous chondrocyte implantation (ACI), osteochondral grafting and a combination of ACI and grafting, depending on the lesion. More recent treatments have employed tissue engineering and stem cell therapies using biphasic and triphasic scaffolds to provide effective osteochondral repair. We aim to focus on the osteochondral unit, its management and new emerging technologies for OL treatment.

ANATOMY OF CARTILAGE AND SUBCHONDRAL BONE

The osteochondral unit consists of a articular chondral component and a deeper subchondral bone component (Madry et al., 2010). Cartilage is composed mainly of a dense extracellular matrix (ECM) made up of water, type II collagen, and proteoglycans (Buckwalter and Mankin, 1997; Keeney and Pandit, 2009). Within the cartilage tissue lies specialized cells known as chondrocytes (Sophia Fox et al., 2009). Cartilage is distinct in that it is completely devoid of blood vessels, lymphatics, and nerves (Buckwalter and Mankin, 1997; Sofat et al., 2011). It is divided into four zones, the superficial, the middle, the deep, and the calcified cartilage zone. Each zone having a unique cell orientation, collagen fiber arrangement and ECM composition allowing it to fulfill different biomechanical functions. For example, the superficial zone serves to protect the deeper zones from shear forces while the deeper zones are better arranged to counter compressive forces (Sophia Fox et al., 2009).

The deepest tissue of the osteochondral unit is the subchondral bone. Bone consists mainly of hydroxyapatite (HA) and type I collagen which contribute to the strength and stiffness of bone tissue (Yang and Temenoff, 2009; Arvidson et al., 2011). The subchondral bone region consists of thick plates joined together to form a subchondral bone plate below which is the subarticular spongiosa (Lopa and Madry, 2014). Separating the cartilage tissue and the bone is a complex junction known as the osteochondral junction also referred to by some authors as the chondro-osseous junction. It consists of the deepest zone of uncalcified cartilage, the tidemark, a layer of calcified cartilage, a thin line known as the cement line and beyond this the subchondral bone (Lyons et al., 2006). It is the tidemark that separates the non-calcified and calcified layer of cartilage from each other as a histologic wavy boundary up to 10 μm in thickness (Gannon and Sokoloff, 1999). Calcified cartilage has a lower mechanical strength than the bone below it (Mente and Lewis, 1994), however, a few unique features aid in better integration between the two layers (Nooeaid et al., 2012). Such as prolonged extensions of uncalcified cartilage extending through the calcified layer to abut the subchondral bone but not beyond it (Hunter et al., 2009). Also, the wavy nature of the tidemark and its vertically oriented fibers (Oegema et al., 1997). The junction is not impermeable (Madry et al., 2010) and a large number of arteries, veins, and nerves (Pan et al., 2009) send branches through minute canals within the subchondral plate into the calcified cartilage. This is the route by which nutrients are brought to the articular cartilage and a homeostatic environment maintained. In the setting of OA, there is the loss of articular cartilage, subchondral thickening, and formation of osteophytes (Haverkamp et al., 2011; Loeser et al., 2012) leading to loss of the normal biochemical and biomechanical processes **Figure 1**. Illustrates the cross-sectional anatomy of the osteochondral unit.

BIOMECHANICS OF THE OSTEOCHONDRAL UNIT

The osteochondral unit performs several functions with each layer of the tissue having a specific and some overlapping roles. The chondral and subchondral tissues are separated by a chondro-osseous junction allowing them to work together to help the entire osteochondral unit accomplish its responsibilities in maintaining healthy joint homeostasis (Lyons et al., 2006).

The chondral layer being the most superficial layer of the osteochondral unit is subjected to a greater number of force vectors. As with most of the osteochondral unit, the chondral layer must withstand compressive forces but in addition to this, it must also counter friction and shear forces generated cyclically during normal joint articulation. Chondral tissue is best described as being biphasic as it demonstrated features of both a fluid and solid phase substance. Water and inorganic ions such as sodium, potassium, calcium and chloride are responsible for its fluid phase and ECM for its solid phase (Sophia Fox et al., 2009). With the presence of negatively charged proteoglycans (Ghadially, 1981) and the porous permeable ECM (Mow et al., 1984; Ateshian et al., 1997), interstitial fluids can move in and out of the tissue with the increasing and decreasing joint forces (Maroudas and Bullough, 1968; Mow et al., 1984; Frank and Grodzinsky, 1987). This summarizes the flow-dependent mechanism which allows for the chondral tissue to exhibit a biphasic viscoelastic behavior (Mow et al., 1980). The flow independent mechanism is brought about by the viscoelastic behavior of the collagen-proteoglycan matrix (Hayes and Bodine, 1978; Woo et al., 1987). As the forces increase on the chondral tissue the tissue becomes stiffer and more resistant to the forces applied due to these mechanisms.

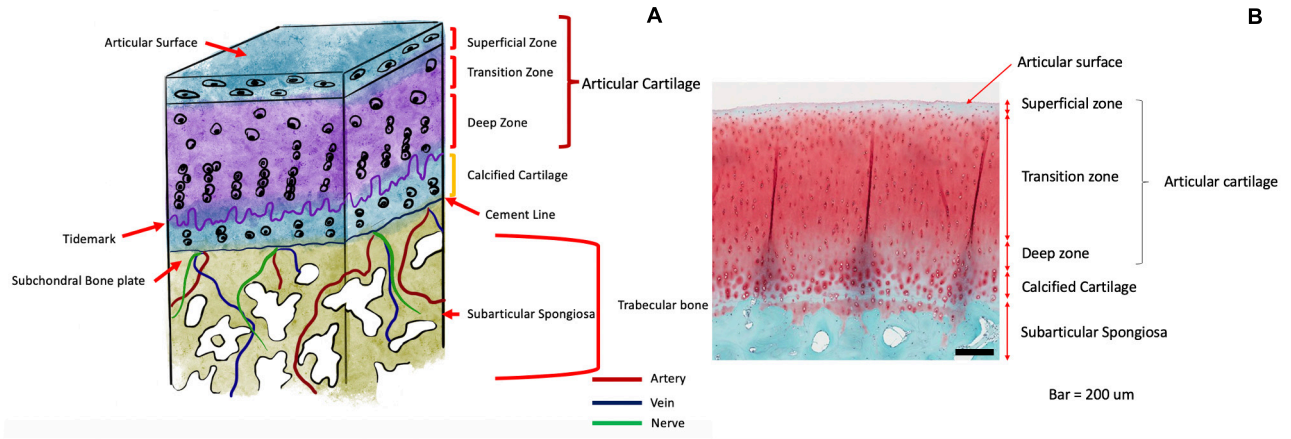

FIGURE 1 | (A) Schematic Illustration of the anatomy of the osteochondral unit. **(B)** Histologic image of the osteochondral unit.

The osteochondral junction is an integral region in the osteochondral unit allowing for communication between the lower subchondral bone and the upper chondral surface. This region encompasses arteries, nerves, and veins that extend from the subchondral bone up to the calcified cartilage, where nutrient exchange is facilitated (Honner and Thompson, 1971). It is also responsible for mineralization, directing cells into various types of chondrocytes. The calcified cartilage layer interdigitates with the subchondral bone and contains chondrocytes embedded within a mineralized ECM. These features help in giving it a high stiffness to anchor the cartilage to the subchondral bone below (Mente and Lewis, 1994).

The subchondral bone consists of impermeable compact bone with many penetrating vascular canals allowing it to play a role in both strength and nutrition to the tissues above it (Duncan et al., 1987; Aigner and Dudhia, 1997; Imhof et al., 2000). Sensory neurons innervate the subchondral bone region and provide nociception (Lepage et al., 2019). The deeper layers of the subchondral bone consist of trabecular bone which can absorb and dissipate the forces applied across the joint (Stewart and Kawcak, 2018) **Figure 2**. Summarizes the various specific roles of each layer of the osteochondral unit.

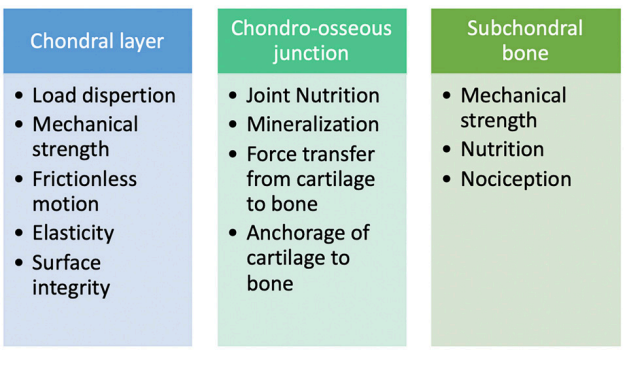

FIGURE 2 | List of functional roles each layer of the osteochondral unit performs.

DIAGNOSIS OF AN OSTEOCHONDRAL LESION

Clinical diagnosis of an OL can be elusive, when relying purely on patient complaints and clinical examination. Common complaints may or may not include an episode of trauma, however, there usually will be complaints of pain, swelling, crepitus, and possible history of knee locking. An examination may reveal joint line tenderness depending on the OL location and with associated injuries special meniscal and ligament tests may be positive. Older clinical tests for OLs such as Wilson's test seem to not be of diagnostic value (Conrad and Stanitski, 2003).

Radiological diagnosis of an OL can be done by X-ray and computed tomography, but magnetic resonance imaging (MRI) has shown to be more useful especially in earlier stages of OL development. It can also detect earlier subchondral bone changes predisposing to OLs (Gorbachova et al., 2018). Thus, MRI with cartilage mapping software and sequences are the gold standard for radiologic evaluation of joint surfaces (Lepage et al., 2019). MRI has an important advantage over arthroscopy in that the status of the subchondral can be studied. MRI is also non-invasive and functions without the need of ionizing radiation and therefore well suited for OL evaluation. MRI studies allow for determination of lesion size, location, presence of bone marrow lesions, fracture lines, and subchondral plate deformities. These features can be used to make a diagnosis of the primary causes of the OL. Newer less invasive diagnostic arthroscopic techniques are being introduced and may be a useful tool in the outpatient clinic such as needle arthroscopy (McMillan et al., 2017) but can still only visualize the superficial chondral surface. It is also important to note that the clinical symptoms of an OL and diagnostic imaging may not correlate (Guermazi et al., 2012) making treatment decisions less straightforward. Additionally, it is important to diagnose the cause and chronicity of an OL. Acute traumatic lesions are a simpler clinical scenario while

older more chronic lesions result in global degeneration of the involved joint. This eventually results in negative biochemical and biomechanical changes in the joint where most repair and regenerative treatments are no longer options and patients may have to consider other treatments such as arthroplasty.

REPAIR TECHNIQUES

Osteochondral Fragment Fixation

In certain acute traumatic OLs, there may be a large osteochondral fragment present within the joint that can be reduced and fixed back into the defect site. This is usually limited by the time from injury and the integrity and size of the fragment. Numerous fixation techniques have been described such as screws (Thomson, 1987; Herring et al., 2019), metal/bioabsorbable pins (Hirsch and Boman, 1998; Gkiokas et al., 2012), fibrin glue (Jeuken et al., 2019), and sutures (Vogel et al., 2020). Satisfactory osteochondral fragment union rates have been reported for each technique but there are some disadvantages and complications associated with each method (Gkiokas et al., 2012; Barrett et al., 2016; Herring et al., 2019) such as the requirement for second stage implant removal, tissue reactions, delayed degradation, and subchondral remodeling (Pascual-Garrido et al., 2009; Millington et al., 2010). Newer suture techniques have been described aiming to reduce the tissue reaction, implant footprint and requirement for implant removal (Vogel et al., 2020). Fixation in the case of a large acute osteochondral fragment should always be considered as the first option of treatment for an OL.

Osteochondral Autologous Graft Transfer

Osteochondral autograft transfer (OAT) has been a popular technique since its first introduction by Matsusue et al. (1993). Here healthy articular cartilage and it's underlying subchondral bone is harvested as a cylindrical plug, usually from the non-weight bearing region of the femoral trochlea. This cylinder is contoured to match the lesion site allowing for repair with smooth, healthy, mature, hyaline cartilage. The procedure can also be performed using a combination of multiple smaller diameter cylinders known as mosaicplasty. The advantages and disadvantages of OAT are summarized in **Table 1**. OAT has proven to be an attractive option in knee joint preservation surgery demonstrating good clinical outcomes and long term results, especially in lesions smaller than 2 cm^2 (Gudas et al., 2012; Ulstein et al., 2014; Lynch et al., 2015; Pareek et al., 2016; Richter et al., 2016; Solheim et al., 2018). There is no difference in outcomes based on lesion location when assessing lesions on the femur, however, Bentley et al did report inferior outcomes when treating patellar lesions (Bentley et al., 2003). The main limitation for larger lesions is the amount of tissue required from the donor site and greater amounts of donor tissue lead to possibly increased donor site morbidity. It is in situations where larger amounts of donor tissue where a surgeon may have to resort to allogeneic graft options. A summary of the advantages and disadvantages of OATS can be found in **Table 1**.

Osteochondral Allograft Transplant

Osteochondral Allograft Transplant (OCA) is a popular technique used especially when dealing with larger OLs where an allograft is used for lesion restoration. This has all the advantages of OATS but with the added advantage of no donor site morbidity. OCA grafts can be fresh, fresh frozen or cryopreserved each having its effect on the chondrogenic viability of the cells within the graft. There is convincing data that patients tolerate allografting to the chondral component of the graft tissue with no immune response (Langer and Gross, 1974). This cannot be said for the subchondral and bony component which does elicit a strong immune response that increases with the size of graft tissue (Kandel et al., 1985; Stevenson et al., 1996). Patient selection is an important consideration in OCA transplantation and results have been superior in younger active patients (Krych et al., 2017; Nielsen et al., 2017). Factors such as age, sex, body mass index, and overall physical fitness play an important role in the prognosis of OCA (Sherman et al., 2014). OCA can be used for lesions >2 cm^2 where marrow stimulation has been shown to have poor results. Over 2 cm^2 cell-based techniques and OAT are options but cell-based techniques do not address subchondral bone pathologies and OAT has donor site morbidity. Therefore, OCA is indicated in lesions greater than 2 cm^2 where autologous donor tissue is unavailable or insufficient. The indications of OCA have even extended to include the femoral hemicondyle, entire condyle, and even tibial plateau depending on the patient's requirement (McCulloch et al., 2007; Williams et al., 2007; Levy et al., 2013). A summary of the advantages and disadvantages of OCA can be found in **Table 2**.

REGENERATIVE TECHNIQUES

Osteochondral unit regeneration is challenging owing to its complex anatomy and demanding functions. Both the chondral and subchondral layers must be regenerated for the regenerate to resemble native cartilage (Schek et al., 2004; Kon et al., 2011;

TABLE 1 | Summary of the advantages and disadvantages of OATS.

Advantages	Disadvantages
Mature hyaline cartilage	Limited quantity
No chance of immune response	Donor site morbidity
Immediate fill of lesion	Possibly >1 surgical site
No graft availability concerns	Limited lesion size
Addresses subchondral and chondral layer	

TABLE 2 | Summary of the advantages and disadvantages of OCA.

Advantages	Disadvantages
Mature hyaline cartilage	Immunogenicity concerns
No limit to size of donor graft	Banked tissue therefore less cell viability
Immediate fill of lesion	Difficult to procure and store
Addresses subchondral and chondral layer	Additional expense
No donor site morbidity	Possible graft size mismatching

Orth et al., 2013). In addition, both layers should integrate with the surrounding cartilage and bone tissue. Attempts have been made by developing biphasic scaffolds that have an osseous layer providing rigid, structural support incorporated to a more bioactive chondral layer into which cells may be seeded. It has been postulated that a triphasic scaffold with an intermediate layer between the chondral and bone layers would be beneficial and emulate the tidemark found in a native osteochondral unit (Marquass et al., 2010; Longley et al., 2018). This intermediate layer would have to mimic the osteochondral junction containing intricate networks of arteries and nerves with no currently available faultless biomaterial. Finally, the subchondral region would have to promote bony ingrowth from the surrounding tissue and have a low elastic modulus, providing strength to the entire construct. **Figure 3** outlines the ideal requirements of a regenerated osteochondral unit.

Cells

As mentioned earlier a regenerative osteochondral implant must be bioactive and the most important factor to achieve this is the addition of a cells. Various cell sources have been studied and employed such as embryonic stem cells (ESCs) and MSCs. MSCs have remained more popular given the ethical obstacles associated with ESCs (Lo and Parham, 2009). MSCs have been derived from a variety of tissues such as bone marrow (Mafi, 2011), adipose (Berebichez-Fridman et al., 2017), synovium (Sakaguchi et al., 2005), periosteum (de Mara et al., 2011), muscle (Jackson et al., 2010), dental pulp (Pierdomenico et al., 2005), and many more. More recently the discovery of the induced pluripotent stem cell (iPS cell) has made available a more easily accessible cell source with superior differentiation and proliferative potential (Takahashi and Yamanaka, 2006; Yu et al., 2007). Embryonic and induced pluripotent stem cells can differentiate into any of the three germ layers therefore along with having limitless proliferative potential and superior differentiation capacity they both pose a risk of teratoma formation (Tsumaki et al., 2015; Chijimatsu et al., 2017). Each MSC source has its own advantages and disadvantages. Concerning cell number harvest, adipose has shown the greatest yield while bone marrow the least (Baer and Geiger, 2012; Chahla et al., 2016). Synovium has demonstrated to have the most superior osteogenic and chondrogenic differentiation capacity compared to bone marrow and adipose, however, requires expansion when used in clinical applications (Sakaguchi et al., 2005). The high MSC yield in adipose tissue is beneficial as *in vitro* expansion has shown to have negative effects on cell homing (Sohni and Verfaillie, 2013).

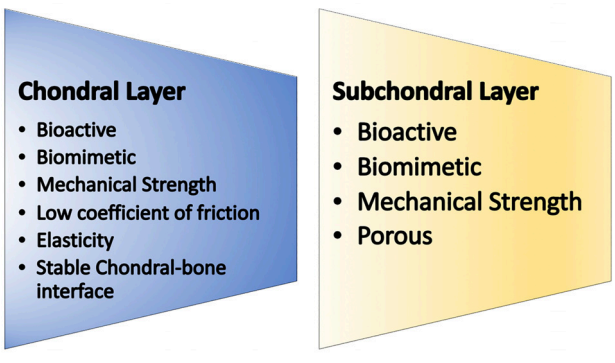

FIGURE 3 | The ideal osteochondral unit.

Cells have been incorporated with tissue engineering for osteochondral regeneration with various techniques investigated till date. In the past, an autologous biopsy of chondrocytes and osteoblasts from the patient done during ACI was the most popular solution as obtaining the cells was easier, however, this did not result in sufficient cell numbers. At the expense of expanding the cells to increase the numbers in primary culture, the cells undergo dedifferentiation and lose their chondrogenic phenotype (Benya and Shaffer, 1982; Stewart et al., 2000; Schnabel et al., 2002; Darling and Athanasiou, 2005). Though ACI has been further improved over the years with the addition of collagen membranes and scaffolds, there is still no evidence that it is superior to other cartilage repair techniques (Samsudin and Kamarul, 2016). ACI also includes the higher cost of two surgeries and donor site morbidity. MSC therapies provide a solution in terms of not requiring a autologous articular cartilage biopsy along with providing pluripotent MSCs which are unlike already differentiated chondrocytes. MSCs can be be differentiated into chondrocytes by first isolating them from any of the aforementioned sources (Sundelacruz and Kaplan, 2009; Mafi, 2011; Nooeaid et al., 2012) or can be co-cultured with chondrocytes. This has shown to help maintain chondrocyte phenotype and characteristics (Hubka et al., 2014). It is worth mentioning that iPS cells have been studied for cartilage culture and maybe a promising source of stem cell going forward (Ko et al., 2014;Tsumaki et al., 2015). The most important advantage of using MSCs is that they are bioactive and therefore offer better incorporation with the body and can influence and mediate biological processes effectively. The cells exhibit paracrine functions (Hocking and Gibran, 2010; Barry and Murphy, 2013) which promote cell growth and have anti-inflammatory roles (Johnstone et al., 1998; Freyria and Mallein-Gerin, 2012; Ruiz et al., 2016). MSCs also stimulate endogenous cell recruitment and are involved with immunomodulation as well as secrete exosomes (Kanazawa et al., 2011; Zhang et al., 2020). MSC therapies are, however, considerably expensive and time consuming therefore acellular techniques are being explored (Dhollander et al., 2012; Joshi et al., 2012) though most preclinical data is in favor of cell-seeded scaffolds with a subchondral osteoinductive scaffold (Lopa and Madry, 2014). MSC treatments do, however, remain costly.

Growth Factors

Growth factors are the most bioactive part of a regenerative process in that they control and initiate a host of cellular mechanisms which lead to superior chondrogenesis and cell proliferation. The most often utilized growth factors for

chondrogenic differentiation are those in the TGF- β superfamily. This consists of bone morphogenic proteins (BMP-2,4,6, 7), cartilage-derived morphogenic proteins (CDMP-1,2), and transforming growth factor beta-1 (TGF-β). These factors are especially useful to stimulate chondrogenic differentiation, reverse dedifferentiation and encourage the production of ECM an essential component of chondral tissue. They also have an overall inhibitory effect on catabolic processes mediated by Interleukin-1,6,8 and matrix metalloproteinases (MMP; Salgado et al., 2004; Fortier et al., 2011; Re'Em et al., 2012; Tuan et al., 2013). Fibroblast growth factor (FGF) -2 and 18 play a prominent role in chondrogenic differentiation and seem to have different actions on MSCs and chondrocytes. FGF-2 and FGF-18 promote anabolic and reduce catabolic cell pathways which in turn lead to increased proteoglycan (PG) synthesis in MSCs (Cuevas et al., 1988; Stewart et al., 2007; Fortier et al., 2011). However, pre-clinical data has suggested FGF-2 to have deleterious effects on chondrocyte proliferation especially in higher doses by upregulation of MMP and reducing PG synthesis and increasing inflammation (Tuan et al., 2013). On the other hand FGF-18 has shown to promote chondrocyte proliferation (Ellsworth et al., 2002; Ellman et al., 2008). FGF-2 and TGF-β have been noted to work together to enhance cartilage ECM formation under culture conditions of chondrogenic cells and are essential for cartilage homeostasis (Huang et al., 2018). The FGF family does have a prominent effect on MSCs though possibly not as beneficial to chondrocyte metabolism. Another growth factor involved in cartilage synthesis is insulin-like growth factor (IGF-1) which supports the roles of TGF- β and BMP-7 and upregulates anabolic mechanisms and downregulates catabolism in the cells. IGF-1 has shown to promote chondrogenic differentiation in MSCs in a synergistic manner alongside TGF-β and BMP-7 (Loeser et al., 2003; Zhou et al., 2016). It has been noted that with decreased IGF-1 there is reduction in chondrocyte number and proteoglycan synthesis (Wei et al., 2017). Platelet derived growth factor (PGDF) is another growth factor which has a role in increasing chondrocyte proliferation and proteoglycan synthesis. PGDF has also shown to reduce IL- β1 levels which are known to cause chondral degradation (Schmidt et al., 2006).

Platelet rich plasma (PRP), autologous conditioned plasma and bone marrow concentrate are considered to be abundant in growth factors and have been used in clinical practice (Jacob et al., 2017). These therapies are manufactured by concentrating blood or bone marrow aspirate using a centrifugation process or specific company system to concentrate native growth factors present in the sample. As there are multiple types of growth factors with varying functional roles being concentrated in these injections both growth factors that promote chondrocyte metabolism and inhibit it are being concentrated (Rutgers et al., 2010). Literature has reported these blood derived products to not be beneficial in promoting chondrogenic differentiation of MSCs (Rutgers et al., 2010; Liou et al., 2018), however, some other studies have shown benefit (Frisbie et al., 2007; Mishra et al., 2009). The advantage of such therapies is the easy availability of autologous growth factors but the major disadvantage is the lack of standardization and determination of exact factor concentrations (Chahla et al., 2017).

Emerging Techniques

Newer cell culture methods have been explored aiming to alter the cell microenvironment to improve cell differentiation and result in better quality regenerate synthesis (Vats et al., 2006). Three dimensional MSC cultures and scaffolding techniques have shown to be effective in improving cell proliferation (Estes and Guilak, 2011). High density cultures techniques such as micro mass and pellet cultures have demonstrated superior chondrocyte differentiation as the three-dimensional nature of the culture simulates a similar microenvironment to that of tissue during embryogenesis (Pelttari et al., 2008; Zhang et al., 2010). Other explored culture techniques have involved varying hydrostatic pressures, the addition of mechanical loading and use of low oxygen tensions. These variations can be brought about to the cell culture by using bioreactors aiming to replicate physiologic *in vivo* conditions. Various designs of bioreactors have been manufactured to produced compressive forces, shear forces and even dynamic cyclic loading of the cell culture (Angele et al., 2004; Campbell et al., 2006; Chen et al., 2018). Applying cyclical increasing hydrostatic pressures on MSC cultures has shown to enhance the production of cartilage matrix even in the absence of chondrogenic growth factors (Miyanishi et al., 2006; Puetzer et al., 2013). A large number of studies have reported improved chondrogenesis in cultures exposed to mechanical loading with dynamic, shear or compression forces (Huang et al., 2004; Mouw et al., 2007; Waldman et al., 2007; Villanueva et al., 2009). This emulates joint reaction forces and the additional mechanical stimulation on the chondrocytes results in better chondrogenic differentiation and matrix production. With this evidence it is reasonable to say that for improved chondrogenesis the cells require both growth factors and mechanical forces to bring about more physiological cellular responses.

SCAFFOLDS

Chondral Layer

Synthetic polymers or natural biomaterial-based scaffolds are generally utilized for constructing the chondral component of the osteochondral unit. Though, recent reports have utilized scaffold-free implants as well. Because natural-based polymers are fabricated from materials that make up typical natural cellular environments, they may be ideal for cell proliferation with a reduced possibility of unfavorable reactions. Natural polymers may additionally be able to enhance cell proliferation and guide cellular differentiation to more desirable results (Mano and Reis, 2007; Nooeaid et al., 2012). In the process of procuring biocompatibility through these scaffolds they may lack mechanical vigor (Nooeaid et al., 2012). Commonly employed materials include chitosan, collagen, hyaluronic acid, and bio-based polymers (Shimomura et al., 2014b).

Bio-degradable synthetic scaffolds include poly (glycolic acid), poly (L-lactic acid), poly (D, L-lactic-co-glycolic acid), poly (caprolactone), and poly (ethylene glycol). These are superior to natural scaffolds in that their mechanical strength and crystallinity can be varied during manufacture along with the rate at which they undergo degradation (Gunatillake et al., 2003; Kundu et al., 2013). Furthermore, with newer techniques such as electrospinning and 3D printing, scaffold porosity, and shape are easily modifiable and constructed based on the requirement (Woodfield et al., 2005; Li et al., 2007; Thorvaldsson et al., 2008; Duan et al., 2014; Zhou et al., 2018). The major drawback of synthetic scaffolds is their poor bioactivity owing to their hydrophobic surfaces hindering cellular attachment (Bhattarai et al., 2006; Lee et al., 2006). These scaffolds may also be combined with growth factors (Morille et al., 2013; Reyes et al., 2014) and materials such as silica and alkalis to improve their bioactivity (Peña et al., 2006; Buchtová et al., 2013).

Extracellular matrix can provide a form of scaffolding to an osteochondral repair by providing some form of tissue architectural structure as well as bio signaling (Sutherland et al., 2015). Using chemical or physical methods cartilage ECM can be decellularized and then used to facilitate chondrogenic differentiation of MSCs (Cheng et al., 2009; Sutherland et al., 2015). Another method similar to an ECM is the use of a cell-derived matrix such as tissue-engineered construct (TEC) derived from synovial MSCs (Ando et al., 2007). TEC has favorable properties of being superiorly bioactive and highly adherent to the surrounding cartilage matrix. Combining TEC with HA and beta-tricalcium phosphate has been studied in animal models and shown favorable outcomes of OL repairs with the HA combination demonstrating better results (Shimomura et al., 2014a, 2017).

Bioceramics encompass both osteoconductive and bioresorbable properties which are favorable in the scenario of an osteochondral repair. To increase the elastic modulus of bioceramics, polymers have been combined with them and have shown encouraging cartilage regenerative results (Xue et al., 2010; Lv and Yu, 2015). Bioactive ions such as lithium, manganese, zinc, and silicon have also been under recent study to improve the bioactivity of the implants and shown promising results (Deng et al., 2017, 2019).

Subchondral Layer

As mentioned earlier the subchondral bone is responsible for providing compressive strength to the osteochondral unit and has a low elastic modulus. Currently available materials that meet this requirement include metals, bioglass, and bioceramics (Kon et al., 2010; Chen et al., 2011; Zhang et al., 2013; Deng et al., 2017). Metallic compounds are inert and therefore have been popular in orthopedic surgery, however, for integration they must possess a basic level of bioactivity. This led to coating metals with HA and calcium phosphate thereby promoting better implant integration but not addressing the degradation of the material. Magnesium base alloys are now being studied as they possess adequate mechanical strength, bioactivity, and degradation (Yang et al., 2018). Overall, wear particle release and corrosion remain a limitation when using metallic materials (Sonny Bal et al., 2010).

Ceramics and bioglass possess excellent osteoconductive and inductive properties which allow them to bond well to the adjacent host bone (Tamai et al., 2005; Martin et al., 2007). These materials are, however, brittle and can fracture under mechanical loading (Nooeaid et al., 2012; Deng et al., 2019). By modifying the porosity of ceramics, their biodegradability can be effectively altered and titrated to the desired rate. Porosity and mechanical strength are inversely related and the addition of biodegradable polymers can help solve this problem (Miao et al., 2008; Ren et al., 2008). The integration of these subchondral substitution materials with a chondral natural or synthetic polymers, e.g., collagen, hyaluronic acid, poly (glycolic acid) can together manufacture an osteochondral unit with materials that satasify the functions of both the chondral and subchondral layers.

CLINICAL RESULTS OF OSTEOCHONDRAL IMPLANTS

Clinical data utilizing multiphasic osteochondral implants is sparse along with the fact that only three such osteochondral implants have been used. These are MaioRegen (Fin-Cermica Faenza SpA), TruFit (Smith and Nephew, Andover, MA, United States) and more recently Agili-C (Cartilheal Ltd, Kfar Sava, Israel). MaioRegen and TruFit have been studied and reported further than Agili- C and clinical trial results for Agili-C are awaited.

Recently, D'Ambrosi et al. (2019) published a systematic review on the results of MaioRegen. MaioRegen being a triphasic scaffold aims to closely resemble the osteochondral unit. 471 patients were included in the review with a mean follow up of 24 months. 15 out of the included 16 studies were level IV and only one was a comparative level III study. The included lesions were all ICRS grade III and IV excluding two studies which included spontaneous osteonecrosis of the knee and Kellgren-Lawrence grade III OA. Clinical outcome scores at 24 months demonstrated significant improvement in thirteen studies with only one study reporting no difference. Histological analysis was reported by only two studies and indicated no residual scaffold with a strong presence of type II collagen and proteoglycan content. This reveals that the implant resorption and regenerative tissue response is adequate. Complications included 2 partial implant detachments, 2 cases of graft hypertrophy, and 52 patients reported minor complications such as joint stiffness and swelling. There were 16 failures in this systematic review. On the whole, the results of MaioRegen have been favorable with good clinical results and a low complication rate, however, the included studies were of a low level of evidence and as a result, they could not conclude that MaioRegen was superior to other treatments till better randomized trials were performed.

TruFit is a biphasic acellular synthetic scaffold mainly composed of a polylactide-coglycolide copolymer for the chondral region and calcium sulfate for the bone region. TruFit has shown to have a clinical benefit at 12 months of follow up but two studies reported worsening on longer follow up as reported by a systematic review in 2015 (Verhaegen et al., 2015). The main complication reported with use of the TruFit implant was

TABLE 3 | Summarizes the clinical studies using multiphasic scaffolds.

Author/Year	Type of study	Patient number	Implant specifics/ company	First clinical trial	Lesion size/cm^2	Follow up/months	Results
D'Ambrosi et al., 2019	Systematic review	471	MaioRegen Triphasic C: Coll I B: 70%HA-30% Coll I 30%HA-70%Coll I /Finceramica, Italy	2011–2016	3.6 ± 0.85	24	Satisfactory mid-term follow-up results and quicker return to sports. Low complication and failure rates.
Verhaegen et al., 2015	Systematic review	130	TruFit Biphasic C: PGA, PLGA, surfactant B: Ca Sulfate /Smith & Nephew, United States	2010–1015	N/A	12	No evidence for TruFit being superior or equal to other techniques. Longer follow ups result in poorer outcomes. Subchondral integration is inferior with bone cysts reported. Chondral regenerate contains fibroblastic tissue.
Kon et al., 2014	Case report	1	Agili-C Biphasic C: Modified aragonite + HA B: Aragonite /CartiHeal (2009) Ltd, Israel	2015–2020	2	24	MRI: Good tissue integration. Regenerate resembled hyaline cartilage. VAS, Lysholm. Tegner, IKDC scores significantly improved with excellent outcomes

the failure of bony ingrowth and fissured lesions in the surface of the chondral regenerate at 24 months. Few studies reporting histology also showed the presence of subchondral cysts and fibrous cartilage, but it should be noted these were biopsies performed in patients that required revision (Dhollander et al., 2012; Joshi et al., 2012). TruFit being a synthetic scaffold appears to have issues with biodegradability and integration and therefore needs to be further improved before further clinical application (Verhaegen et al., 2015).

A more recent developed synthetic osteochondral implant is Agili-C which has a chondral phase made up of modified aragonite with hyaluronic acid and a bone phase of calcium carbonate. Only one clinical case report is published with most results of the Agili-C implant being in pre-clinical studies. Pre-clinical studies have shown excellent cell recruitment and biocompatibility of the materials (Kon et al., 2014, 2015; Chubinskaya et al., 2019). Kon et al recently reported the use of a hemicondylar aragonite implant in a caprine model. At 12 months follow up they found the implant promoted good chondral and subchondral regeneration, excellent integration and no adverse effects (Gomoll, 2020; Kon et al., 2020). In the clinical case study, a 47-year-old male patient underwent an osteochondral repair with Agili-C and reported significant improvement in functional outcome scores. Radiographic studies at 24 months indicated hyaline cartilage regeneration over the entire defect and good bone integration. Sequential radiography suggested the entire implant degraded and was substituted for cartilage and bone by creeping substitution. Results of the Agili-C implant are encouraging, and a randomized clinical trial has been underway. Hopefully, in the near future, these results will be available to better evaluate and make recommendation guidelines for the use of Agili-C **Table 3**. Summarizes the clinical studies using multiphasic scaffolds.

FUTURE DIRECTION

As several of the proposed strategies to treat OLs remains in experimental and pre-clinical phases, it is difficult to predict which will prove most useful in the clinical management of OLs. We see popular chondral substitutes being derived from polymers and ECMS while the subchondral materials frequently used are ceramics, bioglass, and metals. These materials seeded with stem cells, growth factors, different culture methods or bioactive ions show encouraging results with the most effective combination of these yet to be determined. Clinical recommendations for the use of osteochondral implants are awaited pending further well-designed trials. The present literature reports encouraging results but in the interim osteochondral fragment fixation, OATs and OCA remain techniques with respectable outcomes so long as their specific indications and limitations are noted.

AUTHOR CONTRIBUTIONS

GJ wrote the first draft of the manuscript. KS and NN edited the manuscript. All authors contributed to manuscript revision, read and approved the submitted version.

FUNDING

This work was supported by a Health and Labor Sciences Research grant from the Ministry of Health, Labor, and Welfare of Japan (to NN); a grant from the New Energy and Industrial Technology Development Organization, Japan (to NN); and a Grant-in-Aid for Scientific Research, Japan Society for the Promotion of Science (to NN and KS).

REFERENCES

Aigner, T., and Dudhia, J. (1997). Phenotypic modulation of chondrocytes as a potential therapeutic target in osteoarthritis: a hypothesis. *Ann. Rheum. Dis.* 56, 287–291. doi: 10.1136/ard.56.5.287

Ando, W., Tateishi, K., Hart, D. A., Katakai, D., Tanaka, Y., Nakata, K., et al. (2007). Cartilage repair using an in vitro generated scaffold-free tissue-engineered construct derived from porcine synovial mesenchymal stem cells. *Biomaterials* 28, 5462–5470. doi: 10.1016/j.biomaterials.2007.08.030

Angele, P., Schumann, D., Angele, M., Kinner, B., Englert, G., Hente, R., et al. (2004). Cyclic, mechanical compression enhances chondrogenesis of mesenchymal progenitor cells in tissue engineering scaffolds. *Biorheology* 41, 335–346.

Arvidson, K., Abdallah, B. M., Applegate, L. A., Baldini, N., Cenni, E., Gomez-Barrena, E., et al. (2011). Bone regeneration and stem cells. *J. Cell. Mol. Med.* 15, 718–746. doi: 10.1111/j.1582-4934.2010.01224.x

Ateshian, G. A., Warden, W. H., Kim, J. J., Grelsamer, R. P., and Mow, V. C. (1997). Finite deformation biphasic material properties of bovine articular cartilage from confined compression experiments. *J. Biomech.* 30, 1157–1164. doi: 10.1016/S0021-9290(97)85606-0

Baer, P. C., and Geiger, H. (2012). Adipose-derived mesenchymal stromal/stem cells: tissue localization, characterization, and heterogeneity. *Stem Cells Int.* 2012:812693. doi: 10.1155/2012/812693

Barrett, I., King, A. H., Riester, S., van Wijnen, A., Levy, B. A., Stuart, M. J., et al. (2016). Internal fixation of unstable osteochondritis dissecans in the skeletally mature knee with metal screws. *Cartilage* 7, 157–162. doi: 10.1177/1947603515622662

Barry, F., and Murphy, M. (2013). Mesenchymal stem cells in joint disease and repair. *Nat. Rev. Rheumatol.* 9, 584–594. doi: 10.1038/nrrheum.2013.109

Bentley, G., Biant, L. C., Carrington, R. W. J., Akmal, M., Goldberg, A., Williams, A. M., et al. (2003). A prospective, randomised comparison of autologous chondrocyte implantation versus mosaicplasty for osteochondral defects in the knee. *J. Bone Jt. Surg. Ser. B* 85, 223–230. doi: 10.1302/0301-620X.85B2.13543

Benya, P. D., and Shaffer, J. D. (1982). Dedifferentiated chondrocytes reexpress the differentiated collagen phenotype when cultured in agarose gels. *Cell* 30, 215–224. doi: 10.1016/0092-8674(82)90027-7

Berebichez-Fridman, R., Gómez-García, R., Granados-Montiel, J., Berebichez-Fastlicht, E., Olivos-Meza, A., Granados, J., et al. (2017). The holy grail of orthopedic surgery: mesenchymal stem cells - their current uses and potential applications. *Stem Cells Int.* 2017:2638305. doi: 10.1155/2017/2638305

Bhattarai, S. R., Bhattarai, N., Viswanathamurthi, P., Yi, H. K., Hwang, P. H., and Kim, H. Y. (2006). Hydrophilic nanofibrous structure of polylactide; fabrication and cell affinity. *J. Biomed. Mater. Res. Part A* 78, 247–257. doi: 10.1002/jbm.a.30695

Buchtová, N., Réthoré, G., Boyer, C., Guicheux, J., Rambaud, F., Vallé, K., et al. (2013). Nanocomposite hydrogels for cartilage tissue engineering: Mesoporous silica nanofibers interlinked with siloxane derived polysaccharide. *J. Mater. Sci. Mater. Med.* 24, 1875–1884. doi: 10.1007/s10856-013-4951-0

Buckwalter, J. A., and Mankin, H. J. (1997). Instructional course lectures, the american academy of orthopaedic surgeons - articular cartilage. part i: tissue

design and chondrocyte-matrix interactions*†. *J Bone Jt. Surg. Am.* 79, 600–611. doi: 10.2106/00004623-199704000-00021

Campbell, J. J., Lee, D. A., and Bader, D. L. (2006). Dynamic compressive strain influences chondrogenic gene expression in human mesenchymal stem cells. *Biorheology* 43, 455–470.

Chahla, J., Cinque, M. E., Piuzzi, N. S., Mannava, S., Geeslin, A. G., Murray, I. R., et al. (2017). A call for standardization in platelet-rich plasma preparation protocols and composition reporting. *J. Bone Jt. Surg.* 99, 1769–1779. doi: 10.2106/jbjs.16.01374

Chahla, J., Piuzzi, N. S., Mitchell, J. J., Dean, C. S., Pascual-Garrido, C., LaPrade, R. F., et al. (2016). Intra-articular cellular therapy for osteoarthritis and focal cartilage defects of the knee: a systematic review of the literature and study quality analysis. *J. Bone Jt. Surg. Am.* 98, 1511–1521. doi: 10.2106/JBJS.15.01495

Charalambous, C. P. (2014). Cell origin and differentiation in the repair of full-thickness defects of articular cartilage. *Class. Pap. Orthop.* 75, 377–379. doi: 10.1007/978-1-4471-5451-8_95

Chen, C. H., Kuo, C. Y., and Chen, J. P. (2018). Effect of cyclic dynamic compressive loading on chondrocytes and adipose-derived stem cells co-cultured in highly elastic cryogel scaffolds. *Int. J. Mol. Sci.* 19:370. doi: 10.3390/ijms19020370

Chen, J., Chen, H., Li, P., Diao, H., Zhu, S., Dong, L., et al. (2011). Simultaneous regeneration of articular cartilage and subchondral bone in vivo using MSCs induced by a spatially controlled gene delivery system in bilayered integrated scaffolds. *Biomaterials* 32, 4793–4805. doi: 10.1016/j.biomaterials.2011.03.041

Cheng, N. C., Estes, B. T., Awad, H. A., and Guilak, F. (2009). Chondrogenic differentiation of adipose-derived adult stem cells by a porous scaffold derived from native articular cartilage extracellular matrix. *Tissue Eng. Part A* 15, 231–241. doi: 10.1089/ten.tea.2008.0253

Chijimatsu, R., Ikeya, M., Yasui, Y., Ikeda, Y., Ebina, K., Moriguchi, Y., et al. (2017). Characterization of mesenchymal stem cell-like cells derived from human iPSCs via neural crest development and their application for osteochondral repair. *Stem Cells Int.* 2017:1960965. doi: 10.1155/2017/1960965

Chubinskaya, S., Di Matteo, B., Lovato, L., Iacono, F., Robinson, D., and Kon, E. (2019). Agili-C implant promotes the regenerative capacity of articular cartilage defects in an ex vivo model. *Knee Surg. Sport Traumatol. Arthrosc.* 27, 1953–1964. doi: 10.1007/s00167-018-5263-1

Conrad, J. M., and Stanitski, C. L. (2003). Osteochondritis dissecans: Wilson's sign revisited. *Am. J. Sports Med.* 31, 777–778. doi: 10.1177/03635465030310052301

Cuevas, P., Burgos, J., and Baird, A. (1988). Basic fibroblast growth factor (FGF) promotes cartilage repair in vivo. *Biochem. Biophys. Res. Commun.* 156, 611–618. doi: 10.1016/s0006-291x(88)80887-8

D'Ambrosi, R., Valli, F., De Luca, P., Ursino, N., and Usuelli, F. (2019). MaioRegen osteochondral substitute for the treatment of knee defects: a systematic review of the literature. *J. Clin. Med.* 8:783. doi: 10.3390/jcm8060783

Darling, E. M., and Athanasiou, K. A. (2005). Rapid phenotypic changes in passaged articular chondrocyte subpopulations. *J. Orthop. Res.* 23, 425–432. doi: 10.1016/j.orthres.2004.08.008

de Mara, C. S., Sartori, A. R., Duarte, A. S., Andrade, A. L. L., Pedro, M. A. C., and Coimbra, I. B. (2011). Periosteum as a source of mesenchymal stem cells: The effects of TGF-β3 on chondrogenesis. *Clinics* 66, 487–492. doi: 10.1590/S1807-59322011000300022

Deng, C., Chang, J., and Wu, C. (2019). Bioactive scaffolds for osteochondral regeneration. *J. Orthop. Transl.* 17, 15–25. doi: 10.1016/j.jot.2018.11.006

Deng, C., Yao, Q., Feng, C., Li, J., Wang, L., Cheng, G., et al. (2017). 3D printing of bilineage constructive biomaterials for bone and cartilage regeneration. *Adv. Funct. Mater.* 27:1703117. doi: 10.1002/adfm.201703117

Dhollander, A. A. M., Liekens, K., Almqvist, K. F., Verdonk, R., Lambrecht, S., Elewaut, D., et al. (2012). A pilot study of the use of an osteochondral scaffold plug for cartilage repair in the knee and how to deal with early clinical failures. *Arthrosc. J. Arthrosc. Relat. Surg.* 28, 225–233. doi: 10.1016/j.arthro.2011.07.017

Duan, P., Pan, Z., Cao, L., He, Y., Wang, H., Qu, Z., et al. (2014). The effects of pore size in bilayered poly(lactide-co-glycolide) scaffolds on restoring osteochondral defects in rabbits. *J. Biomed. Mater. Res. Part A* 102, 180–192. doi: 10.1002/jbm.a.34683

Duncan, H., Jundt, J., Riddle, J. M., Pitchford, W., and Christopherson, T. (1987). The tibial subchondral plate. A scanning electron microscopic study. *J. Bone Jt. Surg. Ser. A* 69, 1212–1220. doi: 10.2106/00004623-198769080-00015

Ellman, M. B., An, H. S., Muddasani, P., and Im, H. J. (2008). Biological impact of the fibroblast growth factor family on articular cartilage and intervertebral disc homeostasis. *Gene* 420, 82–89. doi: 10.1016/j.gene.2008.04.019

Ellsworth, J. L., Berry, J., Bukowski, T., Claus, J., Feldhaus, A., Holderman, S., et al. (2002). Fibroblast growth factor-18 is a trophic factor for mature chondrocytes and their progenitors. *Osteoarthr. Cartil.* 10, 308–320. doi: 10.1053/joca.2002.0514

Estes, B. T., and Guilak, F. (2011). Three-dimensional culture systems to induce chondrogenesis of adipose-derived stem cells. *Methods Mol. Biol.* 702, 201–217. doi: 10.1007/978-1-61737-960-4_15

Fortier, L. A., Barker, J. U., Strauss, E. J., McCarrel, T. M., and Cole, B. J. (2011). The role of growth factors in cartilage repair. *Clin. Orthop. Relat. Res.* 469, 2706–2715. doi: 10.1007/s11999-011-1857-3

Frank, E. H., and Grodzinsky, A. J. (1987). Cartilage electromechanics-I. Electrokinetic transduction and the effects of electrolyte pH and ionic strength. *J. Biomech.* 20, 615–627. doi: 10.1016/0021-9290(87)90282-X

Freyria, A. M., and Mallein-Gerin, F. (2012). Chondrocytes or adult stem cells for cartilage repair: the indisputable role of growth factors. *Injury* 43, 259–265. doi: 10.1016/j.injury.2011.05.035

Frisbie, D. D., Kawcak, C. E., Werpy, N. M., Park, R. D., and Mcllwraith, C. W. (2007). Clinical, biochemical, and histologic effects of intra-articular administration of autologous conditioned serum in horses with experimentally induced osteoarthritis. *Am. J. Vet. Res.* 68, 290–296. doi: 10.2460/ajvr.68.3.290

Gannon, F. H., and Sokoloff, L. (1999). Histomorphometry of the aging human patella: histologic criteria and controls. *Osteoarthr. Cartil.* 7, 173–181. doi: 10.1053/joca.1998.0206

Ghadially, F. N. (1981). *Structure and Function of Articular Cartilage*. Philadelphia, PA: Lippincott-Raven.

Gkiokas, A., Morassi, L. G., Kohl, S., Zampakides, C., Megremis, P., and Evangelopoulos, D. S. (2012). Bioabsorbable pins for treatment of osteochondral fractures of the knee after acute patella dislocation in children and young adolescents. *Adv. Orthop.* 2012:249687. doi: 10.1155/2012/249687

Gomoll, A. H. (2020). Aragonite-based implants for Osteochondral Defects Could coral make old goats run again? *Arthrosc. J. Arthrosc. Relat. Surg.* 36, 1895–1896. doi: 10.1016/j.arthro.2020.05.011

Gomoll, A. H., Madry, H., Knutsen, G., van Dijk, N., Seil, R., Brittberg, M., et al. (2010). The subchondral bone in articular cartilage repair: current problems in the surgical management. *Knee Surg Sport Traumatol. Arthrosc.* 18, 434–447. doi: 10.1007/s00167-010-1072-x

Gorbachova, T., Melenevsky, Y., Cohen, M., and Cerniglia, B. W. (2018). Osteochondral lesions of the knee: differentiating the most common entities at MRI. *Radiographics* 38, 1478–1495. doi: 10.1148/rg.2018180044

Gudas, R., Gudaite, A., Pocius, A., Gudiene, A., Ėekanauskas, E., Monastyreckiene, E., et al. (2012). Ten-year follow-up of a prospective, randomized clinical study of mosaic osteochondral autologous transplantation versus microfracture for the treatment of osteochondral defects in the knee joint of athletes. *Am. J. Sports Med.* 40, 2499–2508. doi: 10.1177/0363546512458763

Guermazi, A., Niu, J., Hayashi, D., Roemer, F. W., Englund, M., Neogi, T., et al. (2012). Prevalence of abnormalities in knees detected by MRI in adults without knee osteoarthritis: population based observational study (Framingham Osteoarthritis Study). *BMJ* 345:e5339. doi: 10.1136/bmj.e5339

Gunatillake, P. A., Adhikari, R., and Gadegaard, N. (2003). Biodegradable synthetic polymers for tissue engineering. *Eur. Cells Mater.* 5, 1–16. doi: 10.22203/eCM.v005a01

Haverkamp, D. J., Schiphof, D., Bierma-Zeinstra, S. M., Weinans, H., and Waarsing, J. H. (2011). Variation in joint shape of osteoarthritic knees. *Arthritis Rheum.* 63, 3401–3407. doi: 10.1002/art.30575

Hayes, W. C., and Bodine, A. J. (1978). Flow-independent viscoelastic properties of articular cartilage matrix. *J. Biomech.* 11, 407–419. doi: 10.1016/0021-9290(78)90075-1

Herring, M. J., Knudsen, M. L., and Macalena, J. A. (2019). Open reduction, bone grafting, and internal fixation of osteochondritis dissecans lesion of the knee. *JBJS Essent. Surg. Tech.* 9:e23. doi: 10.2106/jbjs.st.18.00035

Hirsch, G., and Boman, A. (1998). Osteochondral fractures of the knee in children and adolescents - Treatment with open reduction and osteosynthesis using biodegradable pins. *Tech. Orthop.* 13, 139–142. doi: 10.1097/00013611-199806000-00007

Hocking, A. M., and Gibran, N. S. (2010). Mesenchymal stem cells: paracrine signaling and differentiation during cutaneous wound repair. *Exp. Cell Res.* 316, 2213–2219. doi: 10.1016/j.yexcr.2010.05.009

Honner, R., and Thompson, R. C. (1971). The nutritional pathways of articular cartilage. An autoradiographic study in rabbits using 35S injected intravenously. *J. Bone Joint Surg. Am.* 53, 742–748. doi: 10.2106/00004623-197153040-00013

Huang, C.-Y. C., Hagar, K. L., Frost, L. E., Sun, Y., and Cheung, H. S. (2004). Effects of cyclic compressive loading on chondrogenesis of rabbit bone-marrow derived mesenchymal stem cells. *Stem Cells* 22, 313–323. doi: 10.1634/stemcells.22-3-313

Huang, L., Yi, L., Zhang, C., He, Y., Zhou, L., Liu, Y., et al. (2018). Synergistic effects of FGF-18 and TGF- β 3 on the chondrogenesis of human adipose-derived mesenchymal stem cells in the pellet culture. *Stem Cells Int.* doi: 10.1155/2018/7139485

Hubka, K. M., Dahlin, R. L., Meretoja, V. V., Kasper, F. K., and Mikos, A. G. (2014). Enhancing chondrogenic phenotype for cartilage tissue engineering: monoculture and coculture of articular chondrocytes and mesenchymal stem cells. *Tissue Eng. Part B Rev.* 20, 641–654. doi: 10.1089/ten.teb.2014.0034

Hunter, D. J., Buck, R., Vignon, E., Eckstein, F., Brandt, K., Mazzuca, S. A., et al. (2009). Relation of regional articular cartilage morphometry and meniscal position by MRI to joint space width in knee radiographs. *Osteoarthr. Cartil.* 17, 1170–1176. doi: 10.1016/j.joca.2009.04.001

Imhof, H., Sulzbacher, I., Grampp, S., Czerny, C., Youssefzadeh, S., and Kainberger, F. (2000). Subchondral bone and cartilage disease: a rediscovered functional unit. *Invest. Radiol.* 35, 581–588. doi: 10.1097/00004424-200010000-0004

Jackson, W. M., Nesti, L. J., and Tuan, R. S. (2010). Potential therapeutic applications of muscle-derived mesenchymal stem and progenitor cells. *Expert Opin. Biol. Ther.* 10, 505–517. doi: 10.1517/14712591003610606

Jacob, G., Shetty, V., and Shetty, S. (2017). A study assessing intra-articular PRP vs PRP with HMW HA vs PRP with LMW HA in early knee osteoarthritis. *J. Arthrosc. Jt. Surg.* 4, 65–71. doi: 10.1016/j.jajs.2017.08.008

Jeuken, R. M., Vles, G. F., Jansen, E. J. P., Loeffen, D., and Emans, P. J. (2019). The modified hedgehog technique to repair pure chondral shear-off lesions in the pediatric knee. *Cartilage*. doi: 10.1177/1947603519855762 [Epub ahead of print].

Johnstone, B., Hering, T. M., Caplan, A. I., Goldberg, V. M., and Yoo, J. U. (1998). In vitro chondrogenesis of bone marrow-derived mesenchymal progenitor cells. *Exp. Cell Res.* 238, 265–272. doi: 10.1006/excr.1997.3858

Joshi, N., Reverte-Vinaixa, M., Díaz-Ferreiro, E. W., and Domínguez-Oronoz, R. (2012). Synthetic resorbable scaffolds for the treatment of isolated patellofemoral cartilage defects in young patients: magnetic resonance imaging and clinical evaluation. *Am. J. Sports Med.* 40, 1289–1295. doi: 10.1177/0363546512441585

Kanazawa, H., Fujimoto, Y., Teratani, T., Iwasaki, J., Kasahara, N., Negishi, K., et al. (2011). Bone marrow-derived mesenchymal stem cells ameliorate hepatic ischemia reperfusion injury in a rat model. *PLoS One* 6:e19195. doi: 10.1371/journal.pone.0019195

Kandel, R. A., Gross, A. E., Ganel, A., McDermott, A. G., Langer, F., and Pritzker, K. P. (1985). Histopathology of failed osteoarticular shell allografts. *Clin. Orthop. Relat. Res.* 197, 103–110. doi: 10.1097/00003086-198507000-00012

Keeney, M., and Pandit, A. (2009). The osteochondral junction and its repair via bi-phasic tissue engineering scaffolds. *Tissue Eng. Part B Rev.* 15, 55–73. doi: 10.1089/ten.teb.2008.0388

Ko, J. Y., Kim, K. I., Park, S., and Im, G. I. (2014). In vitro chondrogenesis and in vivo repair of osteochondral defect with human induced pluripotent stem cells. *Biomaterials* 35, 3571–3581. doi: 10.1016/j.biomaterials.2014.01.009

Kon, E., Delcogliano, M., Filardo, G., Busacca, M., Di Martino, A., and Marcacci, M. (2011). Novel nano-composite multilayered biomaterial for osteochondral regeneration: a pilot clinical trial. *Am. J. Sports Med.* 39, 1180–1190. doi: 10.1177/0363546510392711

Kon, E., Delcogliano, M., Filardo, G., Fini, M., Giavaresi, G., Francioli, S., et al. (2010). Orderly osteochondral regeneration in a sheep model using a novel nano-composite multilayered biomaterial. *J. Orthop. Res.* 28, 116–124. doi: 10.1002/jor.20958

Kon, E., Filardo, G., Robinson, D., Eisman, J. A., Levy, A., Zaslav, K., et al. (2014). Osteochondral regeneration using a novel aragonite-hyaluronate bi-phasic scaffold in a goat model. *Knee Surg. Sport Traumatol. Arthrosc.* 22, 1452–1464. doi: 10.1007/s00167-013-2467-2

Kon, E., Filardo, G., Shani, J., Altschuler, N., Levy, A., Zaslav, K., et al. (2015). Osteochondral regeneration with a novel aragonite-hyaluronate biphasic scaffold: up to 12-month follow-up study in a goat model. *J. Orthop. Surg. Res.* 10:81. doi: 10.1186/s13018-015-0211-y

Kon, E., Robinson, D., Shani, J., Alves, A., Di Matteo, B., Ashmore, K., et al. (2020). Reconstruction of large osteochondral defects using a hemicondylar aragonite-based implant in a caprine model. *Arthrosc. J. Arthrosc. Relat. Surg.* 36, 1884–1894. doi: 10.1016/j.arthro.2020.02.026

Krych, A. J., Pareek, A., King, A. H., Johnson, N. R., Stuart, M. J., and Williams, R. J. (2017). Return to sport after the surgical management of articular cartilage lesions in the knee: a meta-analysis. *Knee Surg. Sport Traumatol. Arthrosc.* 25, 3186–3196. doi: 10.1007/s00167-016-4262-3

Kundu, J., Pati, F., Hun Jeong, Y., and Cho, D. W. (2013). "Biomaterials for biofabrication of 3D tissue scaffolds," in *Biofabrication: Micro- and Nano-Fabrication, Printing, Patterning and Assemblies*, 23–46. doi: 10.1016/B978-1-4557-2852-7.00002-0

Langer, F., and Gross, A. E. (1974). Immunogenicity of allograft articular cartilage. *J. Bone Jt. Surg. Ser. A* 56, 297–304. doi: 10.2106/00004623-197456020-00007

Lee, E. S., Kwon, M. J., Lee, H., Na, K., and Kim, J. J. (2006). In vitro study of lysozyme in poly(lactide-co-glycolide) microspheres with sucrose acetate isobutyrate. *Eur. J. Pharm. Sci.* 29, 435–441. doi: 10.1016/j.ejps.2006.08.005

Lepage, S. I. M., Robson, N., Gilmore, H., Davis, O., Hooper, A., St John, S., et al. (2019). Beyond cartilage repair: the role of the osteochondral unit in joint health and disease. *Tissue Eng. Part B Rev.* 25, 114–125. doi: 10.1089/ten.teb.2018.0122

Levy, Y. D., Görtz, S., Pulido, P. A., McCauley, J. C., and Bugbee, W. D. (2013). Do fresh osteochondral allografts successfully treat femoral condyle lesions? *Clin. Orthopaed. Relat. Res.* 471, 231–237. doi: 10.1007/s11999-012-2556-4

Li, W. J., Mauck, R. L., Cooper, J. A., Yuan, X., and Tuan, R. S. (2007). Engineering controllable anisotropy in electrospun biodegradable nanofibrous scaffolds for musculoskeletal tissue engineering. *J. Biomech.* 40, 1686–1693. doi: 10.1016/j.jbiomech.2006.09.004

Liou, J. J., Rothrauff, B. B., Alexander, P. G., and Tuan, R. S. (2018). Effect of platelet-rich plasma on chondrogenic differentiation of adipose- and bone marrow-derived mesenchymal stem cells. *Tissue Eng. Part A* 24, 1432–1443. doi: 10.1089/ten.tea.2018.0065

Lo, B., and Parham, L. (2009). Ethical issues in stem cell research. *Endocr. Rev.* 30, 204–213. doi: 10.1210/er.2008-0031

Loeser, R. F., Goldring, S. R., Scanzello, C. R., and Goldring, M. B. (2012). Osteoarthritis: a disease of the joint as an organ. *Arthritis Rheum.* 64, 1697–1707. doi: 10.1002/art.34453

Loeser, R. F., Pacione, C. A., and Chubinskaya, S. (2003). The combination of insulin-like growth factor 1 and osteogenic protein 1 promotes increased survival of and matrix synthesis by normal and osteoarthritic human articular chondrocytes. *Arthritis Rheum.* 48, 2188–2196. doi: 10.1002/art.11209

Longley, R., Ferreira, A. M., and Gentile, P. (2018). Recent approaches to the manufacturing of biomimetic multi-phasic scaffolds for osteochondral regeneration. *Int. J. Mol. Sci.* 19:1755. doi: 10.3390/ijms19061755

Lopa, S., and Madry, H. (2014). Bioinspired scaffolds for osteochondral regeneration. *Tissue Eng. Part A* 20, 2052–2076. doi: 10.1089/ten.tea.2013.0356

Lv, Y. M., and Yu, Q. S. (2015). Repair of articular osteochondral defects of the knee joint using a composite lamellar scaffold. *Bone Jt. Res.* 4, 56–64. doi: 10.1302/2046-3758.44.2000310

Lynch, T. S., Patel, R. M., Benedick, A., Amin, N. H., Jones, M. H., and Miniaci, A. (2015). Systematic review of autogenous osteochondral transplant outcomes. *Arthrosc. J. Arthrosc. Relat. Surg.* 31, 746–754. doi: 10.1016/j.arthro.2014.11.018

Lyons, T. J., McClure, S. F., Stoddart, R. W., and McClure, J. (2006). The normal human chondro-osseous junctional region: evidence for contact of uncalcified cartilage with subchondral bone and marrow spaces. *BMC Musculoskelet. Disord.* 7:52. doi: 10.1186/1471-2474-7-52

Madry, H., van Dijk, C. N., and Mueller-Gerbl, M. (2010). The basic science of the subchondral bone. *Knee Surg. Sport Traumatol. Arthrosc.* 18, 419–433. doi: 10.1007/s00167-010-1054-z

Mafi, R. (2011). Sources of adult mesenchymal stem cells applicable for musculoskeletal applications - a systematic review of the literature. *Open Orthop. J.* 5(Suppl. 2), 242–248. doi: 10.2174/1874325001105010242

Mano, J. F., and Reis, R. L. (2007). Osteochondral defects: present situation and tissue engineering approaches. *J. Tissue Eng. Regen. Med.* 1, 261–273. doi: 10.1002/term.37

Maroudas, A., and Bullough, P. (1968). Permeability of articular cartilage. *Nature* 219, 1260–1261. doi: 10.1038/2191260a0

Marquass, B., Somerson, J. S., Hepp, P., Aigner, T., Schwan, S., Bader, A., et al. (2010). A novel MSC-seeded triphasic construct for the repair of osteochondral defects. *J. Orthop. Res.* 28, 1586–1599. doi: 10.1002/jor.21173

Martin, I., Miot, S., Barbero, A., Jakob, M., and Wendt, D. (2007). Osteochondral tissue engineering. *J. Biomech.* 40, 750–765. doi: 10.1016/j.jbiomech.2006.03.008

Matsusue, Y., Yamamuro, T., and Hama, H. (1993). Arthroscopic multiple osteochondral transplantation to the chondral defect in the knee associated with anterior cruciate ligament disruption. *Arthroscopy* 9, 318–321. doi: 10.1016/S0749-8063(05)80428-1

McCulloch, P. C., Kang, R. W., Sobhy, M. H., Hayden, J. K., and Cole, B. J. (2007). Prospective evaluation of prolonged fresh osteochondral allograft transplantation of the femoral condyle: minimum 2-year follow-up. *Am. J. Sports Med.* 35, 411–420. doi: 10.1177/0363546506295178

McMillan, S., Saini, S., Alyea, E., and Ford, E. (2017). Office-based needle arthroscopy: a standardized diagnostic approach to the knee. *Arthrosc. Tech.* 6, e1119–e1124. doi: 10.1016/j.eats.2017.03.031

Mente, P. L., and Lewis, J. L. (1994). Elastic modulus of calcified cartilage is an order of magnitude less than that of subchondral bone. *J. Orthop. Res.* 12, 637–647. doi: 10.1002/jor.1100120506

Miao, X., Tan, D. M., Li, J., Xiao, Y., and Crawford, R. (2008). Mechanical and biological properties of hydroxyapatite/tricalcium phosphate scaffolds coated with poly(lactic-co-glycolic acid). *Acta Biomater.* 4, 638–645. doi: 10.1016/j.actbio.2007.10.006

Millington, K. L., Shah, J. P., Dahm, D. L., Levy, B. A., and Stuart, M. J. (2010). Bioabsorbable fixation of unstable osteochondritis dissecans lesions. *Am. J. Sports Med.* 38, 2065–2070. doi: 10.1177/0363546510371369

Mishra, A., Tummala, P., King, A., Lee, B., Kraus, M., Tse, V., et al. (2009). Buffered platelet-rich plasma enhances mesenchymal stem cell proliferation and chondrogenic differentiation. *Tissue Eng. Part C Methods* 15, 431–435. doi: 10.1089/ten.tec.2008.0534

Miyanishi, K., Trindade, M. C. D., Lindsey, D. P., Beaupré, G. S., Carter, D. R., Goodman, S. B., et al. (2006). Effects of hydrostatic pressure and transforming growth factor-β3 on adult human mesenchymal stem cell chondrogenesis in vitro. *Tissue Eng.* 12, 1419–1428. doi: 10.1089/ten.2006.12.1419

Morille, M., Van-Thanh, T., Garric, X., Cayon, J., Coudane, J., Noël, D., et al. (2013). New PLGA-P188-PLGA matrix enhances TGF-β3 release from pharmacologically active microcarriers and promotes chondrogenesis of mesenchymal stem cells. *J. Control. Release* 170, 99–110. doi: 10.1016/j.jconrel.2013.04.017

Mouw, J. K., Connelly, J. T., Wilson, C. G., Michael, K. E., and Levenston, M. E. (2007). Dynamic compression regulates the expression and synthesis of chondrocyte-specific matrix molecules in bone marrow stromal cells. *Stem Cells* 25, 655–663. doi: 10.1634/stemcells.2006-0435

Mow, V. C., Holmes, M. H., and Michael Lai, W. (1984). Fluid transport and mechanical properties of articular cartilage: a review. *J. Biomech.* 17, 377–394. doi: 10.1016/0021-9290(84)90031-9

Mow, V. C., Kuei, S. C., Lai, W. M., and Armstrong, C. G. (1980). Biphasic creep and stress relaxation of articular cartilage in compression: theory and experiments. *J. Biomech. Eng.* 102, 73–84. doi: 10.1115/1.3138202

Nielsen, E. S., McCauley, J. C., Pulido, P. A., and Bugbee, W. D. (2017). Return to sport and recreational activity after osteochondral allograft transplantation in the knee. *Am. J. Sports Med.* 45, 1608–1614. doi: 10.1177/0363546517694857

Nooeaid, P., Salih, V., Beier, J. P., and Boccaccini, A. R. (2012). Osteochondral tissue engineering: scaffolds, stem cells and applications. *J. Cell. Mol. Med.* 16, 2247–2270. doi: 10.1111/j.1582-4934.2012.01571.x

Ochi, M., Uchio, Y., Tobita, M., and Kuriwaka, M. (2001). Current concepts in tissue engineering technique for repair of cartilage defect. *Artif. Organs* 25, 172–179. doi: 10.1046/j.1525-1594.2001.025003172.x

Oegema, T. R., Carpenter, R. J., Hofmeister, F., and Thompson, R. C. (1997). The interaction of the zone of calcified cartilage and subchondral bone in osteoarthritis. *Microsc. Res. Tech.* 37, 324–332. doi: 10.1002/(SICI)1097-0029(19970515)37:4<324::AID-JEMT7>3.0.CO;2-K

Orth, P., Meyer, H. L., Goebel, L., Eldracher, M., Ong, M. F., Cucchiarini, M., et al. (2013). Improved repair of chondral and osteochondral defects in the ovine trochlea compared with the medial condyle. *J. Orthop. Res.* 31, 1772–1779. doi: 10.1002/jor.22418

Pan, J., Zhou, X., Li, W., Novotny, J. E., Doty, S. B., and Wang, L. (2009). In situ measurement of transport between subchondral bone and articular cartilage. *J. Orthop. Res.* 27, 1347–1352. doi: 10.1002/jor.20883

Pareek, A., Reardon, P. J., Maak, T. G., Levy, B. A., Stuart, M. J., and Krych, A. J. (2016). Long-term outcomes after osteochondral autograft transfer: a systematic review at mean follow-up of 10.2 years. *Arthrosc. J. Arthrosc. Relat. Surg.* 32, 1174–1184. doi: 10.1016/j.arthro.2015.11.037

Pascual-Garrido, C., Friel, N. A., Kirk, S. S., McNickle, A. G., Bach, B. R., Bush-Joseph, C. A., et al. (2009). Midterm results of surgical treatment for adult osteochondritis dissecans of the knee. *Am. J. Sports Med.* 37(Suppl. 1), 125S–130S. doi: 10.1177/0363546509350833

Pelttari, K., Steck, E., and Richter, W. (2008). The use of mesenchymal stem cells for chondrogenesis. *Injury* 39(Suppl. 1), S58–S65. doi: 10.1016/j.injury.2008.01.038

Peña, J., Corrales, T., Izquierdo-Barba, I., Serrano, M. C., Portolés, M. T., Pagani, R., et al. (2006). Alkaline-treated poly(ε-caprolactone) films: degradation in the presence or absence of fibroblasts. *J. Biomed. Mater. Res. Part A* 76, 788–797. doi: 10.1002/jbm.a.30547

Pierdomenico, L., Bonsi, L., Calvitti, M., Rondelli, D., Arpinati, M., Chirumbolo, G., et al. (2005). Multipotent mesenchymal stem cells with immunosuppressive activity can be easily isolated from dental pulp. *Transplantation* 80, 836–842. doi: 10.1097/01.tp.0000173794.72151.88

Puetzer, J., Williams, J., Gillies, A., Bernacki, S., and Loboa, E. G. (2013). The effects of cyclic hydrostatic pressure on chondrogenesis and viability of human adipose-and bone marrow-derived mesenchymal stem cells in three-dimensional agarose constructs. *Tissue Eng. Part A* 19, 299–306. doi: 10.1089/ten.tea.2012.0015

Re'Em, T., Witte, F., Willbold, E., Ruvinov, E., and Cohen, S. (2012). Simultaneous regeneration of articular cartilage and subchondral bone induced by spatially presented TGF-beta and BMP-4 in a bilayer affinity binding system. *Acta Biomater.* 8, 3283–3293. doi: 10.1016/j.actbio.2012.05.014

Ren, J., Zhao, P., Ren, T., Gu, S., and Pan, K. (2008). Poly (D,L-lactide)/nano-hydroxyapatite composite scaffolds for bone tissue engineering and biocompatibility evaluation. *J. Mater. Sci. Mater. Med.* 19, 1075–1082. doi: 10.1007/s10856-007-3181-8

Reyes, R., Delgado, A., Sánchez, E., Fernández, A., Hernández, A., and Evora, C. (2014). Repair of an osteochondral defect by sustained delivery of BMP-2 or TGFβ1 from a bilayered alginate-PLGA scaffold. *J. Tissue Eng. Regen. Med.* 8, 521–533. doi: 10.1002/term.1549

Richter, D. L., Tanksley, J. A., and Miller, M. D. (2016). Osteochondral autograft transplantation: a review of the surgical technique and outcomes. *Sports Med. Arthrosc.* 24, 74–78. doi: 10.1097/JSA.0000000000000099

Ruiz, M., Cosenza, S., Maumus, M., Jorgensen, C., and Noël, D. (2016). Therapeutic application of mesenchymal stem cells in osteoarthritis. *Exp. Opin. Biol. Ther.* 16, 33–42. doi: 10.1517/14712598.2016.1093108

Rutgers, M., Saris, D. B. F., Dhert, W. J. A., and Creemers, L. B. (2010). Cytokine profile of autologous conditioned serum for treatment of osteoarthritis, in vitro effects on cartilage metabolism and intra-articular levels after injection. *Arthritis Res. Ther.* 12:R114. doi: 10.1186/ar3050

Sakaguchi, Y., Sekiya, I., Yagishita, K., and Muneta, T. (2005). Comparison of human stem cells derived from various mesenchymal tissues: Superiority of synovium as a cell source. *Arthritis Rheum.* 52, 2521–2529. doi: 10.1002/art.21212

Salgado, A. J., Coutinho, O. P., and Reis, R. L. (2004). Bone tissue engineering: State of the art and future trends. *Macromol. Biosci.* 4, 743–765. doi: 10.1002/mabi.200400026

Samsudin, E. Z., and Kamarul, T. (2016). The comparison between the different generations of autologous chondrocyte implantation with other treatment modalities: a systematic review of clinical trials. *Knee Surg. Sport Traumatol. Arthrosc.* 4, 3912–3926. doi: 10.1007/s00167-015-3649-x

Schek, R. M., Taboas, J. M., Segvich, S. J., Hollister, S. J., and Krebsbach, P. H. (2004). Engineered osteochondral grafts using biphasic composite solid free-form fabricated scaffolds. *Tissue Eng.* 10, 1376–1385. doi: 10.1089/ten.2004.10.1376

Schmidt, M. B., Chen, E. H., and Lynch, S. E. (2006). A review of the effects of insulin-like growth factor and platelet derived growth factor on in vivo cartilage healing and repair. *Osteoarthr. Cartil.* 14, 403–412. doi: 10.1016/j.joca.2005.10.011

Schnabel, M., Marlovits, S., Eckhoff, G., Fichtel, I., Gotzen, L., Vécsei, V., et al. (2002). Dedifferentiation-associated changes in morphology and gene expression in primary human articular chondrocytes in cell culture. *Osteoarthr. Cartil.* 10, 62–70. doi: 10.1053/joca.2001.0482

Sherman, S. L., Garrity, J., Bauer, K., Cook, J., Stannard, J., and Bugbee, W. (2014). Fresh osteochondral allograft transplantation for the knee: current concepts. *J. Am. Acad. Orthop. Surg.* 22, 121–133. doi: 10.5435/JAAOS-22-02-121

Shimomura, K., Moriguchi, Y., Ando, W., Nansai, R., Fujie, H., Hart, D. A., et al. (2014a). Osteochondral repair using a scaffold-free tissue-engineered construct derived from synovial mesenchymal stem cells and a hydroxyapatite-based artificial bone. *Tissue Eng. Part A* 20, 2291–2304. doi: 10.1089/ten.tea.2013.0414

Shimomura, K., Moriguchi, Y., Murawski, C. D., Yoshikawa, H., and Nakamura, N. (2014b). Osteochondral tissue engineering with biphasic scaffold: current strategies and techniques. *Tissue Eng. Part B Rev.* 20, 468–476. doi: 10.1089/ten.teb.2013.0543

Shimomura, K., Moriguchi, Y., Nansai, R., Fujie, H., Ando, W., Horibe, S., et al. (2017). Comparison of 2 different formulations of artificial bone for a hybrid implant with a tissue-engineered construct derived from synovial mesenchymal stem cells. *Am. J. Sports Med.* 45, 666–675. doi: 10.1177/0363546516668835

Sofat, N., Ejindu, V., and Kiely, P. (2011). What makes osteoarthritis painful? The evidence for local and central pain processing. *Rheumatology* 50, 2157–2165. doi: 10.1093/rheumatology/ker283

Sohni, A., and Verfaillie, C. M. (2013). Mesenchymal stem cells migration homing and tracking. *Stem Cells Int.* 2013:130763. doi: 10.1155/2013/130763

Solheim, E., Hegna, J., Strand, T., Harlem, T., and Inderhaug, E. (2018). Randomized study of long-term (15-17 years) outcome after microfracture versus mosaicplasty in knee articular cartilage defects. *Am. J. Sports Med.* 46, 826–831. doi: 10.1177/0363546517745281

Sonny Bal, B., Rahaman, M. N., Jayabalan, P., Kuroki, K., Cockrell, M. K., Yao, J. Q., et al. (2010). In vivo outcomes of tissue-engineered osteochondral grafts. *J. Biomed. Mater. Res. Part B Appl. Biomater.* 93, 164–174. doi: 10.1002/jbm.b.31571

Sophia Fox, A. J., Bedi, A., and Rodeo, S. A. (2009). The basic science of articular cartilage: structure, composition, and function. *Sports Health* 1, 461–468. doi: 10.1177/1941738109350438

Stevenson, S., Shaffer, J. W., and Goldberg, V. M. (1996). The humoral response to vascular and nonvascular allografts of bone. *Clin. Orthop. Relat.Res.* 323, 86–95. doi: 10.1097/00003086-199605000-00011

Stewart, A. A., Byron, C. R., Pondenis, H., and Stewart, M. C. (2007). Effect of fibroblast growth factor-2 on equine mesenchymal stem cell monolayer expansion and chondrogenesis. *Am. J. Vet. Res.* 68, 941–945. doi: 10.2460/ajvr.68.9.941

Stewart, H. L., and Kawcak, C. E. (2018). The importance of subchondral bone in the pathophysiology of osteoarthritis. *Front. Vet. Sci.* 5:178. doi: 10.3389/fvets.2018.00178

Stewart, M. C., Saunders, K. M., Burton-Wurster, N., and MacLeod, J. N. (2000). Phenotypic stability of articular chondrocytes in vitro: the effects of culture models, bone morphogenetic protein 2, and serum supplementation. *J. Bone Miner. Res.* 15, 166–174. doi: 10.1359/jbmr.2000.15.1.166

Sundelacruz, S., and Kaplan, D. L. (2009). Stem cell- and scaffold-based tissue engineering approaches to osteochondral regenerative medicine. *Semin. Cell Dev. Biol.* 20, 646–655. doi: 10.1016/j.semcdb.2009.03.017

Sutherland, A. J., Converse, G. L., Hopkins, R. A., and Detamore, M. S. (2015). The bioactivity of cartilage extracellular matrix in articular cartilage regeneration. *Adv. Healthc. Mater.* 4, 29–39. doi: 10.1002/adhm.201400165

Takahashi, K., and Yamanaka, S. (2006). Induction of pluripotent stem cells from mouse embryonic and adult fibroblast cultures by defined factors. *Cell* 126, 663–676. doi: 10.1016/j.cell.2006.07.024

Tamai, N., Myoui, A., Hirao, M., Kaito, T., Ochi, T., Tanaka, J., et al. (2005). A new biotechnology for articular cartilage repair: Subchondral implantation of a composite of interconnected porous hydroxyapatite, synthetic polymer (PLA-PEG), and bone morphogenetic protein-2 (rhBMP-2). *Osteoarthr. Cartil.* 13, 405–417. doi: 10.1016/j.joca.2004.12.014

Temenoff, J. S., and Mikos, A. G. (2000). Review: tissue engineering for regeneration of articular cartilage. *Biomaterials* 21, 431–440. doi: 10.1016/S0142-9612(99)00213-6

Thomson, N. L. (1987). Osteochondritis dissecans and osteochondral fragments managed by Herbert compression screw fixation. *Clin. Orthop. Relat. Res.* 224, 71–78. doi: 10.1097/00003086-198711000-00010

Thorvaldsson, A., Stenhamre, H., Gatenholm, P., and Walkenström, P. (2008). Electrospinning of highly porous scaffolds for cartilage regeneration. *Biomacromolecules* 9, 1044–1049. doi: 10.1021/bm701225a

Tsumaki, N., Okada, M., and Yamashita, A. (2015). iPS cell technologies and cartilage regeneration. *Bone* 70, 48–54. doi: 10.1016/j.bone.2014.07.011

Tuan, R. S., Chen, A. F., and Klatt, B. A. (2013). Cartilage regeneration. *J. Am. Acad. Orthop. Surg.* 21, 303–311. doi: 10.5435/JAAOS-21-05-303

Ulstein, S., Årøen, A., Røtterud, J. H., Løken, S., Engebretsen, L., and Heir, S. (2014). Microfracture technique versus osteochondral autologous transplantation mosaicplasty in patients with articular chondral lesions of the knee: a prospective randomized trial with long-term follow-up. *Knee Surg. Sport Traumatol. Arthrosc.* 22, 1207–1215. doi: 10.1007/s00167-014-2843-6

Vats, A., Bielby, R. C., Tolley, N., Dickinson, S. C., Boccaccini, A. R., Hollander, A. P., et al. (2006). Chondrogenic differentiation of human embryonic stem cells: the effect of the micro-environment. *Tissue Eng.* 12, 1687–1697. doi: 10.1089/ten.2006.12.1687

Verhaegen, J., Clockaerts, S., Van Osch, G. J. V. M., Somville, J., Verdonk, P., and Mertens, P. (2015). TruFit plug for repair of osteochondral defects—where is the evidence? Systematic review of literature. *Cartilage* 6, 12–19. doi: 10.1177/1947603514548890

Villanueva, I., Weigel, C. A., and Bryant, S. J. (2009). Cell-matrix interactions and dynamic mechanical loading influence chondrocyte gene expression and bioactivity in PEG-RGD hydrogels. *Acta Biomater.* 5, 2832–2846. doi: 10.1016/j.actbio.2009.05.039

Vogel, L. A., Fitzsimmons, K. P., and Lee Pace, J. (2020). Osteochondral fracture fixation with fragment preserving suture technique. *Arthrosc. Tech.* 9, e761–e767. doi: 10.1016/j.eats.2020.02.018

Waldman, S. D., Couto, D. C., Grynpas, M. D., Pilliar, R. M., and Kandel, R. A. (2007). Multi-axial mechanical stimulation of tissue engineered cartilage: review. *Eur. Cells Mater.* 13, 66–73; discussion 73–4. doi: 10.22203/ecm.v013a07

Wei, F. Y., Lee, J. K., Wei, L., Qu, F., and Zhang, J. Z. (2017). Correlation of insulin-like growth factor 1 and osteoarthritic cartilage degradation: a spontaneous osteoarthritis in guinea-pig. *Eur. Rev. Med. Pharmacol. Sci.* 21, 4493–4500.

Williams, R. J., Ranawat, A. S., Potter, H. G., Carter, T., and Warren, R. F. (2007). Fresh stored allografts for the treatment of osteochondral defects of the knee. *J. Bone Jt. Surg. Ser. A* 89, 718–726. doi: 10.2106/JBJS.F.00625

Woo, S. L.-Y., Mow, V. C., Lai, W. M., Skalak, R., and Chien, S. (1987). "Biomechanical properties of articular cartilage," in *Handbook of Bioengineering*, eds R. Skalak and S. Chien (New York, NY: McGraw-Hill Book Co), 4.1–4.44.

Woodfield, T. B. F., Van Blitterswijk, C. A., De Wijn, J., Sims, T. J., Hollander, A. P., and Riesle, J. (2005). Polymer scaffolds fabricated with pore-size gradients as a model for studying the zonal organization within tissue-engineered cartilage constructs. *Tissue Eng.* 11, 1297–1311. doi: 10.1089/ten.2005.11.1297

Xue, D., Zheng, Q., Zong, C., Li, Q., Li, H., Qian, S., et al. (2010). Osteochondral repair using porous poly(lactide-co-glycolide)/ nano-hydroxyapatite hybrid scaffolds with undifferentiated mesenchymal stem cells in a rat model. *J. Biomed. Mater. Res. Part A* 94, 259–270. doi: 10.1002/jbm.a.32691

Yang, K., Zhou, C., Fan, H., Fan, Y., Jiang, Q., Song, P., et al. (2018). Bio-functional design, application and trends in metallic biomaterials. *Int. J. Mol. Sci.* 19:24. doi: 10.3390/ijms19010024

Yang, P. J., and Temenoff, J. S. (2009). Engineering orthopedic tissue interfaces. *Tissue Eng. Part B Rev.* 15, 127–141. doi: 10.1089/ten.teb.2008.0371

Yu, J., Vodyanik, M. A., Smuga-Otto, K., Antosiewicz-Bourget, J., Frane, J. L., Tian, S., et al. (2007). Induced pluripotent stem cell lines derived from human somatic cells. *Science* 318, 1917–1920. doi: 10.1126/science.1151526

Zhang, L., Su, P., Xu, C., Yang, J., Yu, W., and Huang, D. (2010). Chondrogenic differentiation of human mesenchymal stem cells: a comparison between micromass and pellet culture systems. *Biotechnol. Lett.* 32, 1339–1346. doi: 10.1007/s10529-010-0293-x

Zhang, S., Hu, B., Liu, W., Wang, P., Lv, X., Chen, S., et al. (2020). Articular cartilage regeneration: The role of endogenous mesenchymal stem/progenitor cell recruitment and migration. *Semin. Arthritis Rheum.* 50, 198–208. doi: 10.1016/j.semarthrit.2019.11.001

Zhang, W., Chen, J., Tao, J., Hu, C., Chen, L., Zhao, H., et al. (2013). The promotion of osteochondral repair by combined intra-articular injection of parathyroid hormone-related protein and implantation of a bi-layer collagen-silk scaffold. *Biomaterials* 34, 6046–6057. doi: 10.1016/j.biomaterials.2013.04.055

Zhou, Q., Li, B., Zhao, J., Pan, W., Xu, J., and Chen, S. (2016). IGF-I induces adipose derived mesenchymal cell chondrogenic differentiation in vitro and enhances chondrogenesis in vivo. *Vitr. Cell. Dev. Biol. Anim.* 52, 356–364. doi: 10.1007/s11626-015-9969-9

Zhou, Y., Chyu, J., and Zumwalt, M. (2018). Recent progress of fabrication of cell scaffold by electrospinning technique for articular cartilage tissue engineering. *Int. J. Biomater.* 2018, doi: 10.1155/2018/1953636

Conflict of Interest: The authors declare that the research was conducted in the absence of any commercial or financial relationships that could be construed as a potential conflict of interest.

frontiers in Cell and Developmental Biology

ORIGINAL RESEARCH
published: 24 November 2020
doi: 10.3389/fcell.2020.581972

Potential of Soluble Decellularized Extracellular Matrix for Musculoskeletal Tissue Engineering – Comparison of Various Mesenchymal Tissues

*Hiroto Hanai[1], George Jacob[1,2], Shinichi Nakagawa[1], Rocky S. Tuan[3,4], Norimasa Nakamura[1,5,6] and Kazunori Shimomura[1]**

[1] Department of Orthopaedic Surgery, Osaka University Graduate School of Medicine, Suita, Japan, [2] Department of Orthopaedics, Tejasvini Hospital, Mangalore, India, [3] Center for Cellular and Molecular Engineering, Department of Orthopaedic Surgery, University of Pittsburgh, Pittsburgh, PA, United States, [4] Institute for Tissue Engineering and Regenerative Medicine, The Chinese University of Hong Kong, Hong Kong, China, [5] Institute for Medical Science in Sports, Osaka Health Science University, Osaka, Japan, [6] Global Center for Medical Engineering and Informatics, Osaka University, Suita, Japan

OPEN ACCESS

Edited by:
Katiucia Batista Silva Paiva, University of São Paulo, Brazil

Reviewed by:
Daniel E. Heath, The University of Melbourne, Australia
Hugo C. Olguín, Pontificia Universidad Católica de Chile, Chile
Ander Abarrategi, CIC biomaGUNE, Spain

***Correspondence:**
Kazunori Shimomura
kazunori-shimomura@umin.net

Specialty section:
This article was submitted to Stem Cell Research, a section of the journal Frontiers in Cell and Developmental Biology

Received: *10 July 2020*
Accepted: *05 November 2020*
Published: *24 November 2020*

Citation:
Hanai H, Jacob G, Nakagawa S, Tuan RS, Nakamura N and Shimomura K (2020) Potential of Soluble Decellularized Extracellular Matrix for Musculoskeletal Tissue Engineering – Comparison of Various Mesenchymal Tissues. Front. Cell Dev. Biol. 8:581972. doi: 10.3389/fcell.2020.581972

Background: It is well studied that preparations of decellularized extracellular matrix (ECM) obtained from mesenchymal tissues can function as biological scaffolds to regenerate injured musculoskeletal tissues. Previously, we reported that soluble decellularized ECMs derived from meniscal tissue demonstrated excellent biocompatibility and produced meniscal regenerate with native meniscal anatomy and biochemical characteristics. We therefore hypothesized that decellularized mesenchymal tissue ECMs from various mesenchymal tissues should exhibit tissue-specific bioactivity. The purpose of this study was to test this hypothesis using porcine tissues, for potential applications in musculoskeletal tissue engineering.

Methods: Nine types of porcine tissue, including cartilage, meniscus, ligament, tendon, muscle, synovium, fat pad, fat, and bone, were decellularized using established methods and solubilized. Although the current trend is to develop tissue specific decellularization protocols, we selected a simple standard protocol across all tissues using Triton X-100 and DNase/RNase after mincing to compare the outcome. The content of sulfated glycosaminoglycan (sGAG) and hydroxyproline were quantified to determine the biochemical composition of each tissue. Along with the concentration of several growth factors, known to be involved in tissue repair and/or maturation, including bFGF, IGF-1, VEGF, and TGF-β1. The effect of soluble ECMs on cell differentiation was explored by combining them with 3D collagen scaffold culturing human synovium derived mesenchymal stem cells (hSMSCs).

Results: The decellularization of each tissue was performed and confirmed both histologically [hematoxylin and eosin (H&E) and 4',6-diamidino-2-phenylindole (DAPI) staining] and on the basis of dsDNA quantification. The content of hydroxyproline of each

tissue was relatively unchanged during the decellularization process when comparing the native and decellularized tissue. Cartilage and meniscus exhibited a significant decrease in sGAG content. The content of hydroxyproline in meniscus-derived ECM was the highest when compared with other tissues, while sGAG content in cartilage was the highest. Interestingly, a tissue-specific composition of most of the growth factors was measured in each soluble decellularized ECM and specific differentiation potential was particularly evident in cartilage, ligament and bone derived ECMs.

Conclusion: In this study, soluble decellularized ECMs exhibited differences based on their tissue of origin and the present results are important going forward in the field of musculoskeletal regeneration therapy.

Keywords: decellularized extracellular matrix, soluble factor, growth factor, mesenchymal tissue, tissue engineering

INTRODUCTION

Musculoskeletal disorders are a prominent clinical problem in today's population especially due to the increasing number of elderly people (Wolff et al., 2002). With age, musculoskeletal tissues degenerate significantly and result in bone fragility, loss of cartilage resilience, reduced ligament elasticity, loss of muscular strength, and fat redistribution, which deter the normal functioning of the bodied tissues (Freemont and Hoyland, 2007). Moreover, it is known that with age the body exhibits reduced healing potential and does not heal spontaneously. It is, therefore, a formidable clinical challenge to treat these disorders, with only a few currently available therapeutic strategies.

At present, tissue engineering and regenerative medicine have focused on extracellular matrices (ECMs) to function as a natural scaffold (Harrison et al., 2014). Such natural ECMs have been preferred as they contain many of the structural and bioactive components providing a natural microenvironment for seeded pluripotent cells used in tissue engineering (Yue, 2014). This overcomes many issues associated with synthetic scaffolds such as biocompatibility and degradability (Chan and Leong, 2008). However, natural tissues are a biological material, which raises concerns of immunologic reactions when transferred. Therefore, to mitigate immunogenic reactions the ECM cellular components must be removed by the process of decellularization (Gilpin and Yang, 2017). Decellularized ECM products of whole tissues have already been applied in clinical practice (Crapo et al., 2011).

While decellularized ECM products of whole tissues retain the ECMs basic morphology such as its biomechanical strength and high bioactive potency, it does have disadvantages such as size- and shape- mismatch and hampered cell infiltration due to its dense collagen structure (Ozasa et al., 2014; Schwarz et al., 2015). Past studies have focused on the soluble factors of decellularized ECMs derived from tendon, meniscus and cartilage and reported soluble factors of each tissue having tissue-specific and in some cases tissue region-specific bioactivity (Zhang et al., 2009; Rothrauff et al., 2017a,b; Shimomura et al., 2017). This indicates that each tissue or region constitutes different growth factors in varying amounts making them more or less ideal for application in the desired engineering of a specific tissue. Soluble factors extracted from each tissue have been thought to have the potential for application in various tissue regeneration therapies as they are effective as well as easy to handle in liquid form. We noted that past studies have only reported and compared two or three types of tissues at a time. Thus, we hypothesized that decellularized ECMs derived from different mesenchymal tissues could exhibit tissue-specific bioactivity. The purpose of this study is to compare the bioactivity of soluble decellularized ECMs obtained from various mesenchymal tissues and reveal the tissue-specific differences to investigate the content of sulfated glycosaminoglycan (sGAG), hydroxyproline and the concentration of several growth factors within each soluble factor of decellularized ECM. Finally, the effect of soluble ECMs on cell differentiation was explored by supplementing them into 3D collagen scaffolds culturing human synovium derived mesenchymal stem cells (hSMSCs) to confirm the bioactivity of each soluble ECM. In turn, these soluble ECMs may be utilized for future applications in musculoskeletal tissue engineering.

MATERIALS AND METHODS

Tissue Decellularization

All experiments were conducted under the standard biosecurity and institutional safety procedures. Nine types of porcine tissues including cartilage, meniscus, ligament, tendon, muscle, synovium, fat pad, fat, and bone were harvested from the hindlimbs of 6–8-week-old pigs procured from a local slaughterhouse (Kasumi-syoji, Ibaraki, Japan) and stored at −20°C until use. After thawing the hindlimbs for preparation of the decellularized ECMs, each tissue fragment was harvested and then minced separately into small pieces. Bone tissue was collected from the anterior cortex of the midshaft of the tibia. For the preparation of decellularized ECMs a previously published protocol established for bovine meniscus and tendon, ECMs was utilized (Shimomura et al., 2017). Briefly, 4 g wet weight of minced tissues was agitated in 40 ml of phosphate-buffered saline (PBS; pH 7.4) containing with 1% Triton X-100 (Sigma-Aldrich,

St. Louis, MO, United States) at 4°C for 3 days. Followed by three washes in PBS at 4°C for 30 min each, pieces of tissues were transferred to 40 ml of Hanks Buffered Salt Solution (HBSS, Thermo Fisher Scientific, Pittsburgh, PA, United States) supplemented with 200 U/ml DNase and 50 U/ml RNase (Worthington, Lakewood, NJ, United States) with continuous agitation at 37°C for 24 h. Finally, pieces of tissues were washed six times in PBS, as above. Decellularized tissues were stored at −20°C until the subsequent experiment. To confirm the complete decellularization, the absence of nuclei on both hematoxylin and eosin (H&E)-stained and 4',6-diamidino-2-phenylindole (DAPI)-stained sections were observed and the content of double-stranded (ds) DNA per dry weight was calculated for each tissue, as described below.

Histology of Native and Decellularized ECMs

Pieces of native and decellularized tissues were fixed in 10% phosphate buffered formalin, serially dehydrated, embedded in paraffin, followed by sectioned (3 μm thickness) with a microtome (REM-710, Yamato Koki, Saitama, Japan). Sample sections were rehydrated and stained with H&E or DAPI (Thermo Fisher Scientific). H&E-stained samples were examined with a slide scanner (Aperio CS2, Leica) while DAPI stained sections were imaged using an inverted fluorescent microscope (Eclipse 90i, Nikon Instruments, Tokyo, Japan) with excitation at 405 nm.

dsDNA Quantification of Native and Decellularized ECMs

After overnight lyophilization to measure dry weight of ECMs, dried samples were digested overnight at 65°C in papain digestion reagent consisted of 0.2 M sodium phosphate buffer (Na_2HPO_4 – NaH_2PO_4, pH 6.4) with 0.1 M sodium acetate, 0.01 M EDTA, disodium salt, 5 mM cysteine HCl, and 0.5 v/v% papain (crystallized suspension, Sigma-Aldrich). The dsDNA content in the supernatant of the papain digested samples was measured, in duplicate, with Quant-iT PicoGreen dsDNA Assay Kit (Thermo Fisher Scientific) using a fluorescence microplate reader (excitation 485 nm, emission 535 nm, SH-9000Lab, Hitachi High-Tech, Tokyo, Japan) according to the manufacturer's instructions.

Biochemical Composition of Native and Decellularized ECMs

To quantify sGAG content the papain digested samples (see above) were treated with a Blyscan Glycosaminoglycan Assay Kit (Biocolor, Carrickfergus, United Kingdom) according to the manufacturer's instructions. Dilutions of the provided bovine tracheal chondroitin 4-sulfate were used to generate a standard curve and the absorbance of each sample was measured, in duplicate, on a spectrophotometer at 656 nm (Multiscan Go, Thermo Fisher Scientific). The hydroxyproline content was determined to be the amount of total collagen as hydroxyproline is present almost exclusively in collagen. This was determined using a modified hydroxyproline assay (Cissell et al., 2017). Briefly, 200 μl of each papain digested sample was hydrolyzed with an equal volume of 4 N NaOH at 95°C overnight, followed by cooling to room temperature. It was then neutralized with 200 μl of 4 N HCl. Subsequently, 100 μl of the neutralized solution was combined with 200 μl chloramine-T solution containing 0.05 M chloramine-T (Nacalai tesque, Kyoto, Japan) in 74% v/v H_2O, 26% v/v 2-propanol, 0.629 M NaOH, 0.140 M citric acid (anhydrous), 0.453 M sodium acetate (trihydrate), and 0.112 M acetic acid and allowed to stand at room temperature for 20 min. The solution was then combined with 200 μl of Ehrlich's solution consisting of 1M p-dimethylaminobenzaldehyde (DMAB, Nacalai tesque) in 30% v/v HCl and 70% v/v 2-propanol and incubated at 65°C for 20 min. 200 μl of each sample was transferred to a clear 96-well plate, in duplicate, and absorbance at 550 nm was read. Serial dilutions of L-hydroxyproline (Wako, Osaka, Japan) was prepared as a standard curve.

Solubilization of Decellularized ECM

A water-soluble fraction of decellularized ECM was extracted by urea solution, as previously described (Shimomura et al., 2017). Briefly, 4 g of wet decellularized ECM was powdered using a Freezer/Mill 6770 (SPEX Sample Prep, Metuchen, NJ, United States) and then agitated in 40 ml of 3 M urea (Sigma-Aldrich) in water at 4°C for 3 days. The suspension was then centrifuged for 20 min at 1,500 g and the supernatant was then transferred to a benzoylated dialysis tube (pore size; 2,000 MWCO, Sigma-Aldrich) and dialyzed against ddH2O for 2 days at 4°C. Water changes were done every 12 h. After removal of urea, the water-soluble ECM was transferred into centrifugal filter tubes (pore size; 3,000 MWCO, Merk Millipore, Billerica, MA, United States) and spin-concentrated approximately 10-fold at 4,000 g for 30 min. Protein concentration was determined by performing a BCA assay (Thermo Fisher Scientific) according to the manufacturer's instructions and the soluble ECMs were stored at −80°C until further use.

SDS-PAGE and Gel Staining

Each urea-extracted sample was suspended in RIPA buffer (Thermo Fisher Scientific). One μg total protein was mixed with a loading buffer (NuPAGE, Thermo Fisher Scientific) and dithiothreitol (DTT) used as a reducing agent and heated for 10 min at 70°C. The protein was loaded into a pre-cast 12-well 4–12% Bis-Tris gel (Thermo Fisher Scientific) and separated by electrophoresis in MOPS running buffer for 35 min at constant 200 V. The gel was stained with Silver Stain MS Kit (Wako) according to the manufacturer's instructions. The stained gel was photographed using a CCD camera gel imaging system (ChemiDoc Touch, Bio-Rad, Hercules, CA, United States).

Growth Factor Analysis of Soluble ECM

The amounts of basic fibroblast growth factor (bFGF), insulin-like growth factor-1 (IGF-1), vascular endothelial growth factor (VEGF), transforming growth factor-β1 (TGF-β1), bone morphogenic protein-2 (BMP-2) and growth differentitaion factor 7 (GDF-7) in the extracted solution were measured by enzyme-linked immunosorbent assay (ELISA) kits for human

purchased from R&D Systems (Minneapolis, MN, United States) for bFGF, IGF-1, VEGF, TGF-β1,and BMP-2, Biocompare (South San Francisco, CA, United States) for GDF-7 according to the manufacturer's instructions. The concentration of growth factor was calculated in 500 μg/ml soluble ECM preparations.

Cell Isolation and Culture

Human synovium derived mesenchymal stem cells were isolated and expanded as previously described (Ando et al., 2007; Koizumi et al., 2016). Synovium was obtained from an 18-year-old male donor who underwent arthroscopic surgery for an anterior crucial ligament reconstruction in accordance with the approvals of the institutional committee for medical ethics. hSMSCs were cultured in growth medium containing high-glucose Dulbecco's Modified Eagle's Medium (DMEM, Nacalai tesque), supplemented with 10% fetal bovine serum (FBS, Sigma-Aldrich) and 1% antibiotic-antimycotic solution (Sigma-Aldrich) at 37°C with humidified 5% CO_2. At 80% confluence, cells were detached with 0.25% trypsin in 1 mM EDTA (Thermo Fisher Scientific) and passaged. All experiments were performed with passage 4 hSMSCs.

3D Culture With Collagen Gel

The hSMSCs were trypsinized from cell culture dishes and embedded in a collagen gel. Eight volumes of Cellmatrix type I-A (Nitta Gelatin, Osaka, Japan) were mixed with both one of 10 × MEM and the reconstitution buffer according to the manufacturer's instructions. hSMSCs were suspended in the collagen mixture at a density of 1.0×10^7 cells/ml of gel, containing a final concentration of either 100 mg/mL of each soluble ECM or the equivalent volume of PBS as a control. Then, 15 μl of collagen mixture containing cells and soluble ECMs were added into 1.5 ml conical tubes. After the gel forming by incubation, 0.5 ml of reduced-serum medium (DMEM with 2% FBS and 1% antibiotics) was added to each tube and changed every 3 days.

Gene Expression Analysis

On culture days 3 and 7 for 3D culture, RNA isolation was preceded by homogenization of samples in Trizol (Thermo Fisher Scientific) and then extracted using a Direct-zol RNA Microprep Kit (Zymo Research, Irvine, CA, United States) according to the manufacturer's protocol. Total RNA was reverse transcribed into complementary DNA through use of the ReverTra Ace qPCR RT Master Mix with gDNA Remover (Toyobo, Osaka, Japan). Quantitative PCR (qPCR) was performed using SYBR Green Master Mix in the Step One Plus real-time PCR system (Thermo Fisher Scientific). Data were normalized to GAPDH and relative expression of each target was calculated according to the $2^{-\Delta\Delta Ct}$ formula. Ten kinds of genes were selected for investigation, including SOX9, ACAN, SCX, TNC, Desmin, PPARG, RUNX2, COL1A1, COL2A1, and COL3A1. The targets and sequences of primers are shown in **Table 1**.

TABLE 1 | Target gene primer sequences for quantitative PCR (qPCR).

Gene		Primer Sequence (5′-3′)	Product Size (bp)
GAPDH	Forward	CAAGGCTGAGAACGGGAAGC	194
	Reverse	AGGGGGCAGAGATGATGACC	
SOX9	Forward	CTGAGCAGCGACGTCATCTC	72
	Reverse	GTTGGGCGGCAGGTACTG	
ACAN	Forward	AGGCAGCGTGATCCTTACC	137
	Reverse	GGCCTCTCCAGTCTCATTCTC	
SCX	Forward	TGCGAATCGCTGTCTTTC	91
	Reverse	GAGAACACCCAGCCCAAA	
TNC	Forward	TTCACTGGAGCTGACTGTGG	223
	Reverse	TAGGGCAGCTCATGTCACTG	
Desmin	Forward	CTGAGCAAAGGGGTTCTGAG	109
	Reverse	ACTTCATGCTGCTGCTGTGT	
PPARG	Forward	GGCTTCATGACAAGGGAGTTTC	74
	Reverse	AACTCAAACTTGGGCTCCATAAAG	
RUNX2	Forward	CAACCACAGAACCACAAGTGCG	196
	Reverse	TGTTTGATGCCATAGTCCCTCC	
COL1A1	Forward	TAAAGGGTCACCGTGGCT	355
	Reverse	CGAACCACATTGGCATCA	
COL2A1	Forward	CGTCCAGATGACCTTCCTACG	122
	Reverse	TGAGCAGGGCCTTCTTGAG	
COL3A1	Forward	CAGCGGTTCTCCAGGCAAGG	179
	Reverse	CTCCAGTGATCCCAGCAATCC	

Statistical Analysis

All quantitative data were reported as mean ± standard deviation (SD). Student's t-test for DNA content or one-way analysis of variance (one-way ANOVA) for growth factor concentration and relative gene expression levels or two-way ANOVA for hydroxyproline and sGAG content followed by Tukey's *post hoc* test or Dunnett's test were performed and analyzed with JMP pro 14.0 (SAS Institute, Cary, NC, United States) and significance was set as $p < 0.05$.

RESULTS

Decellularization of ECMs

The decellularization protocol with Triton X-100 treatment and nuclease enzymes reduced cellular content from every tissue, and this was verified by histology with H&E staining (**Figure 1A**). When compared to native tissues the morphology of the decellularized tissue was reasonably preserved in each tissue. Furthermore, DAPI staining also confirmed the absence of cell nuclei (**Figure 1B**). The DNA content of each decellularized tissue was significantly reduced compared with that of its original tissue (e.g., native vs. decellularized meniscus: 836.9 ± 190.3 ng/mg vs. 12.6 ± 1.7 ng/mg, $p < 0.001$; native vs. decellularized fat pad: 204.1 ± 7.9 ng/mg vs. 40.9 ± 3.8 ng/mg, $p < 0.001$; a similar trend was observed in the rest of the tissues tested; **Figure 2**). This confirmed the successful decellularization of the tissues.

Hydroxyproline and sGAG Content

Hydroxyproline content was quantified by determining the total amount of collagen in the native and decellularized tissue.

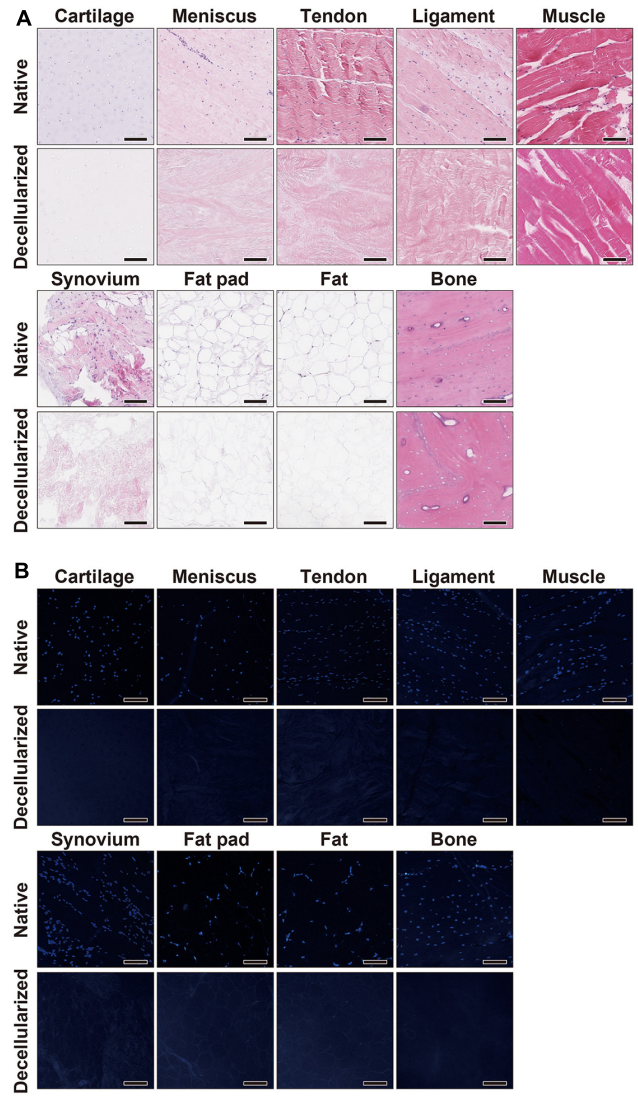

FIGURE 1 | Histological characterization of native and decellularized tissue. **(A)** H&E and **(B)** DAPI staining of each native and decellularized tissue; Scale bar = 100 μm. H&E, hematoxylin and eosin; DAPI, 4',6-diamidino-2-phenylindole.

Per dry weight hydroxyproline content was maintained during the decellularization process and there were no significant differences between native and decellularized tissue (**Figure 3A**). The content of hydroxyproline in the meniscus-derived ECM was the highest (native: 123.6 ± 15.1 μg/mg; decellularized: 125.7 ± 12.4 μg/mg) when compared to other tissues closely followed by that of ligament and tendon tissue (native: 114.1 ± 15.5 μg/mg, $p = 0.99$ and 113.0 ± 19.5 μg/mg, $p = 0.99$; decellularized: 107.6 ± 10.4 μg/mg, $p = 0.57$ and 107.3 ± 18.9 μg/mg, $p = 0.55$, respectively). The difference between the hydroxyproline content of meniscus, tendon and ligament tissue was not significant. When compared to muscle, synovium, fat pad, fat, and bone the hydroxyproline content was significantly higher in meniscus, ligament, tendon, and cartilage tissue ($p < 0.01$). When studying the sGAG content, cartilage tissue demonstrated significantly higher sGAG content than any of the other tissues followed by meniscus and then ligament tissue (Cartilage; native: 302.1 ± 16.6 μg/mg, $p < 0.01$, decellularized: 193.9 ± 16.4 μg/mg, $p < 0.01$. Meniscus; native: 50.6 ± 14.9 μg/mg, $p < 0.01$; decellularized: 28.5 ± 6.2 μg/mg, $p < 0.01$ except for when compared to decellularized ligament, $p = 0.013$; **Figure 3B**). In the decellularization process, cartilage- and meniscus-derived decellularized ECMs significantly lost their sGAG content when compared to that of their native tissue ($p < 0.01$). The remaining seven types of tissues also showed 32–72% loss of the sGAG content but the difference between their native and decellularized state was no significant.

Total Protein and Growth Factor Distribution

SDS-PAGE showed that the urea-extracted protein distribution of each tissue was different, but most samples were enriched for low to moderate molecular weight proteins. Tissues derived from fat pad and fat exhibited less content of protein (**Figure 4A**). ELISA analysis confirmed the presence of various growth factors in the different solubilized decellularized ECMs (**Figure 4B**). The amount of bFGF in cartilage was significantly higher than the other tissues (993.5 ± 51.5 pg/ml, $p < 0.01$), followed by tendon and then muscle. In bone tissue, IGF-1 content was found to be significantly higher than the other studied tissues (4688.1 ± 51.5 pg/ml, $p < 0.01$). VEGF presence in bone and meniscus (1162.0 ± 179.6 pg/ml, 1098.6 ± 20.8 pg/ml, respectively) was significantly greater than the other seven studied tissues, followed by tendon and ligament. The concentration of TGF-β1 in cartilage (498.6 ± 62.8 pg/ml) was significantly higher when compared to other tissues-derived soluble factors, followed by meniscus tissue. Both GDF-7and BMP-2 were not detected in any of the sample preparations.

Gene Expression Profiles During 3D Culturing

Quantitative PCR showed that supplementation with each tissue-derived soluble ECM varied the relative level of some gene expressions on culture days 3 and 7 when compared to the control group (**Figure 5**). The expression of SOX9 was significantly higher on day 3 of culture in tissues including meniscus, synovium, muscle and fat. It was upregulated slightly in the cartilage tissue on day 7 (1.45 ± 0.26 -fold change compared to the control), but there was no significant difference in any groups when compared to the control group. ACAN was significantly higher in the cartilage and meniscus group on day 7 ($p < 0.01$ and $p < 0.05$, respectively). The expression level of COL2A1 was significantly higher in the cartilage group when compared to the control on day 7 ($p < 0.01$). On the other hand, COL1A1 was significantly upregulated in the meniscus tissue on days 3 and 7 ($p < 0.01$). We also noted SCX to be significantly higher in the ligament group on day 3 ($p < 0.01$) and was further upregulated in the ligament and tendon group compared to the control (1.78 ± 1.07 or 1.55 ± 0.75 fold change, respectively) on day 7, but not significantly. TNC was not significantly higher in

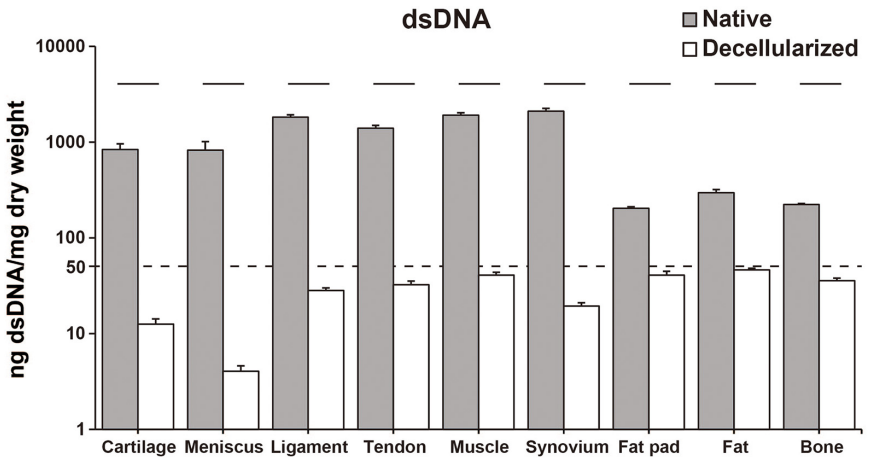

FIGURE 2 | dsDNA content of native and decellularized tissue. *Y*-axis was indicated with logarithmic scale; dotted line at 50 ng/mg is established threshold for sufficient decellularization. $n = 5$ per condition. Lines over bars indicate significant difference between native and decellularized tissue of each region, $p < 0.001$. dsDNA, double stranded DNA.

the ligament and tendon group when compared to the control on days 3 and 7. However, COL3A1 expression was significantly lower in the ligament and tendon group when compared to the control on day 3 ($p < 0.01$) and still lower on day 7, although without significance. Desmin was upregulated in the muscle group on day 7 (1.52 ± 0.14 -fold change compared to the control group) with the tendency of difference ($p = 0.056$). There was no upregulation of expression of PPARG in any group compared to the control. RUNX2 was significantly higher in the cartilage and bone group on day 3 ($p < 0.01$). Taken together, these findings demonstrated that hSMSCs exposed to each tissue-derived soluble ECM in 3D culture exhibited varying gene expression levels that suggested differentiation toward a certain tissue based on the ECM tissue source used may be possible.

DISCUSSION

Our study applied one decellularization protocol to nine types of porcine tissue and compared the differences of biochemical composition in each decellularized tissue and the distributions of several growth factors and bioactivities in each soluble fragment. Our findings revealed that decellularization was successful with minimal disruption to the original tissue morphology. Hydroxyproline content was retained in all of the tissues post the decellularization protocol with some tissue specific variations noted. sGAG content was reduced post decellularization, notably in cartilage and meniscus which contained the highest amount in their native states. Moreover, several growth factors important for cell proliferation, migration and differentiation such as bFGF, IGF-1, VEGF, and TGF-β1 were detected in the tissues in varying amounts and each tissue-derived soluble ECM behaved with dissimilar bioactivity. Further studies will be needed, but soluble decellularized ECMs may be feasible to repair and regenerate injured musculoskeletal tissues and matching the decellularized tissue ECM to the desired tissue regenerate may allow for a more effective tissue engineering method. Thus, our results are important going forward in the field of musculoskeletal regeneration therapy to construct effective tissue specific ECMs.

Tissue ECMs make up the non-cellular components of all tissues and have been shown to provide important signaling for cell migration, proliferation as well as providing an essential physical 3-D scaffolding for the cells. Together these features contribute to the biochemical and biomechanical roles a tissue requires to undergo morphogenesis, differentiation and to maintain a homeostatic environment (Frantz et al., 2010; Vorotnikova et al., 2010; Crapo et al., 2011; Yue, 2014). Due to these advantages, ECMs have been regarded as an ideal scaffold material for tissue engineering especially when engineering an identical tissue (Valentin et al., 2006; Badylak et al., 2009). The native tissues possess genetic cellular material which can elicit harmful immunologic reactions therefore when used in a clinical setting all cellular material must be removed by the process of decellularization (Brown et al., 2009; Nagata et al., 2010; Zhang et al., 2010). To eliminate the cellular components and reduce immune reactions without extensively damaging the ECM, numerous decellularization protocols have been described. The optimal technique for decellularization depends on the structure and tissue cellularity (Petersen et al., 2010; Lehr et al., 2011; Yang et al., 2013). Decellularized ECM products of whole tissues have been already applied in clinical practice (Crapo et al., 2011).

There are still concerns about that the dense collagenous architecture of ECM acting as a barrier for cell infiltration, with cells often localized only to the tissue surface (Ozasa et al., 2014; Schwarz et al., 2015). Moreover, the use of whole decellularized tissues as grafts is limited because of size and shape as well as the immunogenicity elicited between donors and recipients. To overcome these problems while retaining the tissue-specific bioactivity in the ECM, decellularized tissues have been processed into powder form (Almeida et al., 2016; Beck et al., 2016; Rowland et al., 2016) or solubilized with enzymatic (like pepsin) or chaotropic agents (like urea), resulting

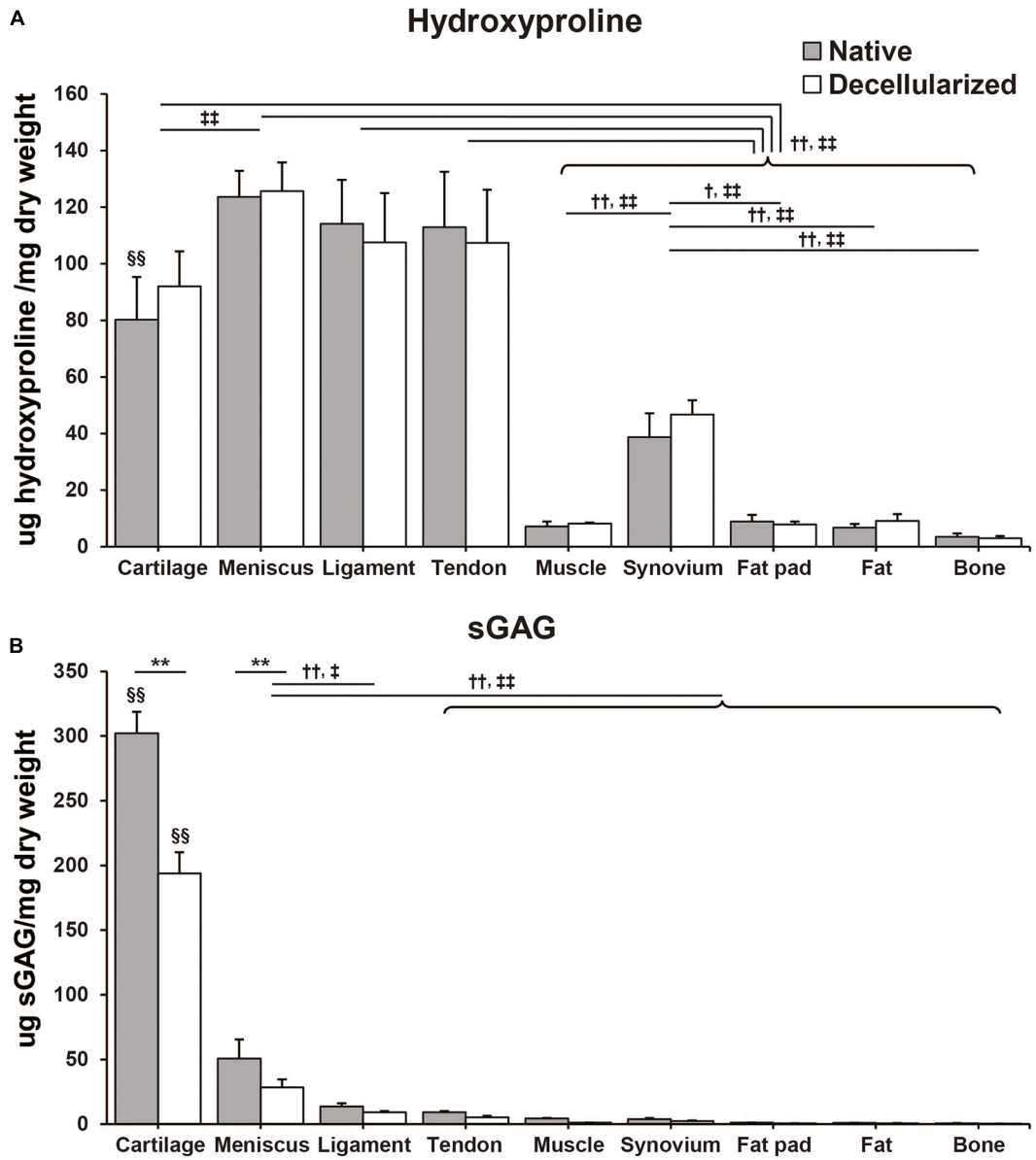

FIGURE 3 | Biochemical composition of native and decellularized tissue. **(A)** Total hydroxyproline and **(B)** total sulfated glycosaminoglycan (sGAG) content in native and decellularized tissue. $n = 5$ per condition. $^{**}p < 0.01$, significant difference between native and decellularized tissue for each step. $^{\dagger}p < 0.05$, $^{\dagger\dagger}p < 0.01$, significant difference between regions in a given native tissue. $^{\ddagger}p < 0.05$, $^{\ddagger\ddagger}p < 0.01$, significant difference between regions in a given decellularized tissue. $^{\S\S}p < 0.01$, significant difference from any other tissues in the same step.

in easy-to-handle solutions (Kwon et al., 2013; Farnebo et al., 2014; Kim et al., 2014; Pati et al., 2014). Urea extracted ECMs are superior to pepsin digested ECMs as they retain several growth factors. These growth factors have been noted to promote tissue-specific cell phenotypes and differentiation, indicating that urea extracted decellularized ECMs possess tissue-specific growth factors (Zhang et al., 2009; Lin et al., 2012; Yang et al., 2013; Rothrauff et al., 2017b). Past studies have only reported and compared two or three types of tissues. Zhang et al. (2009) reported that urea-extracted fractions of decellularized ECM from the skin, skeletal muscle and liver tissues revealed significant differences in adhesion properties, growth rates and promoting tissue-specific differentiation. Rothrauff et al. (2017b) compared cartilage and tendon growth factors and reported promotion of tissue-specific differentiation across multiple cultures and also reported the distributions of various growth factors. Lee et al. (2019) confirmed the decellularization of seven tissues including organs such as liver and heart. They fabricated uniform sized tissue microbeads using them ECM and reported three kinds of tissue-specific microbeads derived from liver, heart and muscle (Lee et al., 2019). These significantly enhanced the viability, lineage specific maturation, and functionality of each type of

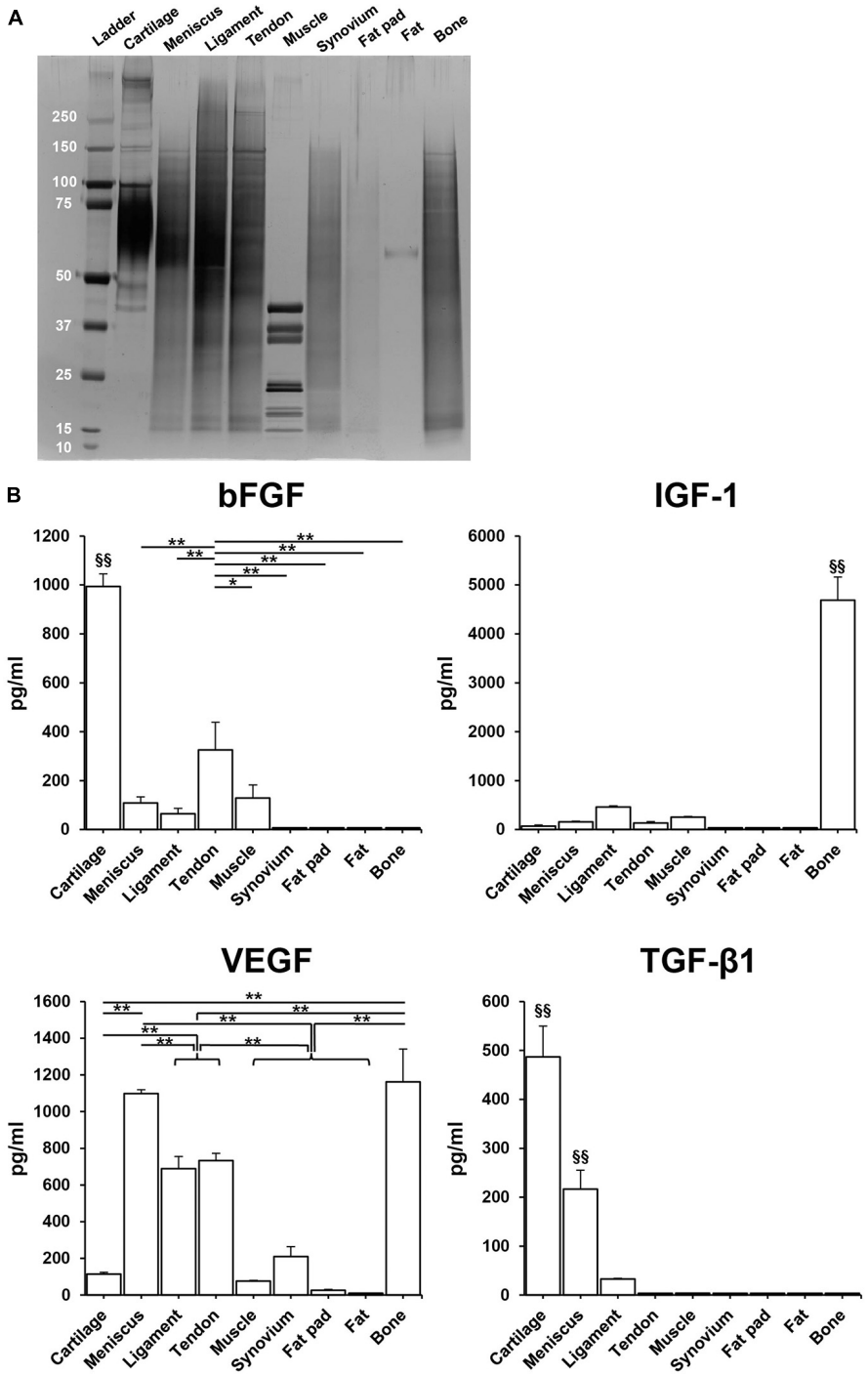

FIGURE 4 | Total protein and human growth factor analysis of soluble decellularized extracellular matrix (ECM) preparations. **(A)** SDS-PAGE analysis of each urea-extracted tissue. **(B)** Growth factor concentrations (pg/ml) in 500 μg/ml soluble ECM preparations. $n = 3$ per condition. $^{*}p < 0.05$, $^{**}p < 0.01$, significant difference from each preparation. §§ $p < 0.01$, significant difference from any other preparations. bFGF, basic fibroblast growth factor; IGF-1, insulin-like growth factor-1; VEGF, vascular endothelial growth factor; TGF-β1, transforming growth factor-β1.

reprogrammed cell, when compared to conventional microbeads from collagen components.

In our present study, the tissue-specific differences of hydroxyproline, sGAG, growth factors and bioactivities in nine types of decellularized porcine mesenchymal tissues including cartilage, meniscus, ligament, tendon, muscle, synovium, fat pad, fat, and bone were investigated. Minimal criteria of successful decellularization was reported as < 50 ng dsDNA/mg ECM

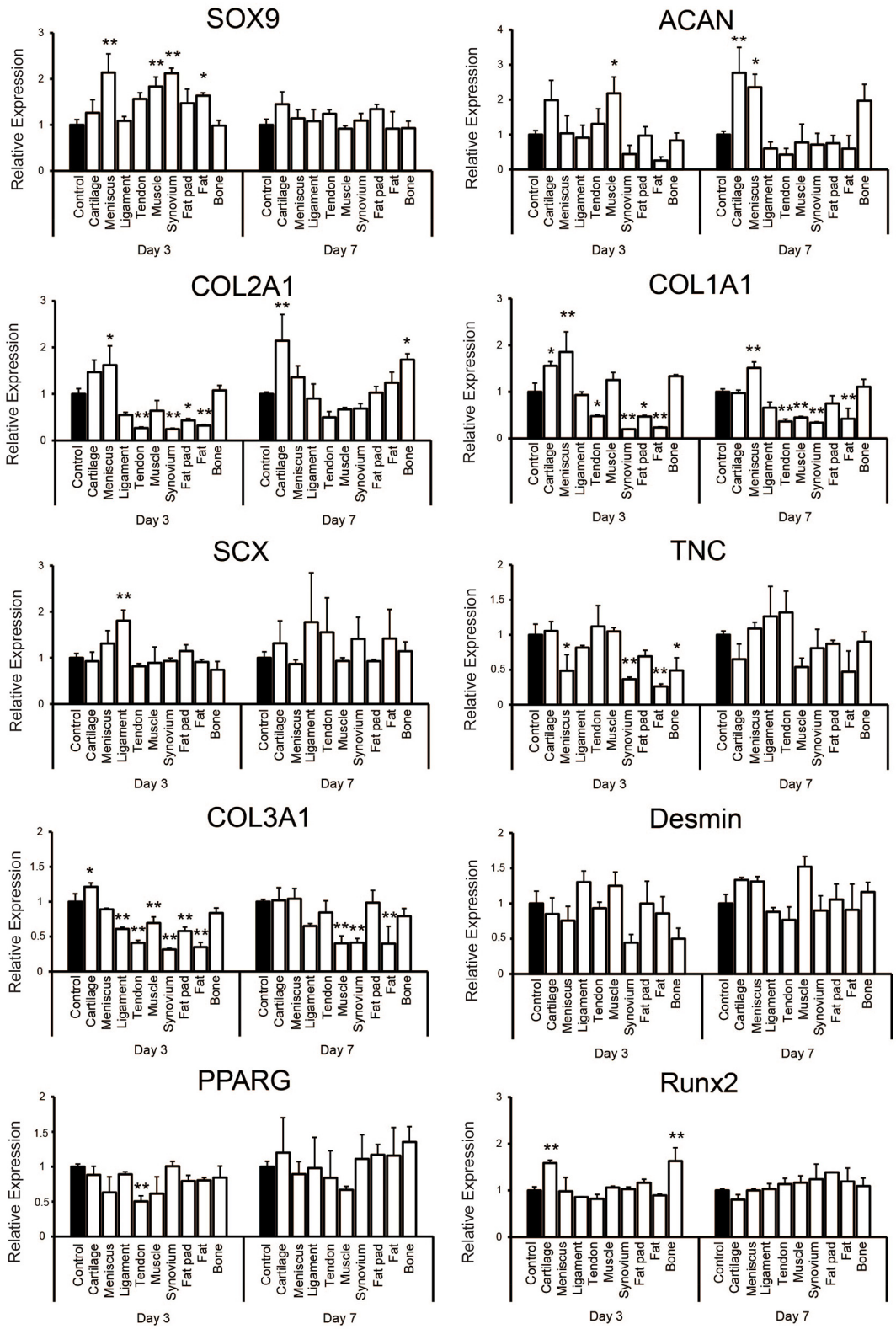

FIGURE 5 | Gene expression analysis of human synovium derived mesenchymal stem cells (hSMSCs) seeded in soluble decellularized extracellular matrix (ECM)-supplemented scaffolds (3D collagen + ECM) on days 3 and 7. Each gene expression level was normalized to GAPDH and showed as relative expression levels compared to the control group of the respective day. $n = 3$ per condition. $^{*}p < 0.05$, $^{**}p < 0.01$, significant difference compared to the control group.

dry weight, < 200 bp DNA fragment length and the lack of visible nuclear material in tissue sections stained with DAPI or H&E (Crapo et al., 2011). The decellularization technique in our present study was previously reported successful for bovine tendon, meniscus and cartilage tissues with significant reduction in DNA content and absence of cellular nuclei by DAPI staining (Yang et al., 2013; Rothrauff et al., 2017a,b; Shimomura et al., 2017). Other tissues were decellularized with a similar protocol based on Triton-X, such as for ligament combined with nucleases (Vavken et al., 2009) or for muscle after 1 h exposure to trypsin/EDTA but without nucleases (Stern et al., 2009). Reisbig et al. (2016) pointed out that decellularized synovium incubated with 1% Triton X-100 followed by DNase had low DNA content and short DNA fragments, but the synovial villous architecture was destroyed and therefore suggested using peracetic acid was better methods. Adipose tissue was decellularized by Triton-X combined with nucleases, but the result was not sufficient reduction of cells or cell fragments (Sano et al., 2014). While Triton-X was exposed for only 16 h in their protocol, the present protocol was for 72 h, which may cause to reduce cell fragments more. Bone tissue were decellularized Triton-X after freeze and thermal shock and followed by incubation with ethanol and then the reduction in DNA content was higher than 90% compared to that of native bone (Gardin et al., 2015). On the other hand, considering that the reduction rate of dsDNA in fat pad, fat or bone tissue is around 80% and the dry weight of them included fat or mineral component, the present method might be not so effective for all tissues. Triton-X could be one of the most standard process for decellularization, but residual DNA may remain present in the tissue (Yang et al., 2017). Therefore, enzymatic treatments are used in the final decellularization step to reduce any residual DNA content. At the same time it is already known that it is not the best process for most tissues and the most effective agents for decellularization of each tissue will depend upon many factors, including the tissue's cellularity, density, lipid content, and thickness (Crapo et al., 2011). For example fatty, amorphous organs and tissues such as adipose tissue typically require the addition of lipid solvents such as alcohols (Flynn, 2010). The optimized tissue-specific decellularized methods which preserve tissue-specific key ECM components for orthopedic tissue engineering can be found in recent comprehensive reviews (Cheng et al., 2014; Mendibil et al., 2020). Considering the effectiveness of decellularization or preservation of the components of each tissue-derived ECM, it might be better to select the appropriate protocol depend on tissue, but a single protocol same as our past study was chosen because we would like to expand our past procedure to the present tissues and compare them.

We noted hydroxyproline content was retained in all of the tissues after the decellularization protocol indicating good retention of collagen content. On the other hand, native meniscus and cartilage tissue had a high amount of sGAG which was significantly reduced after decellularization. The remaining tissues also demonstrated 32–72% reduction in sGAG, however, they did not have a high sGAG content to begin with. The variations in native collagen content can be explained by the functional roles of the tissue and the type and magnitude of stresses applied on them. Eleswarapu et al. (2011) reported hyaline tissue to have high collagen and sGAG content while fibrous tissue such as ligaments and tendons to have high collagen, and low sGAG content. Hyaline tissue experiences a balance of compressive and tensile forces while fibrous tissues mainly experience tensile stresses on locomotion. Another study concluded that baseline muscle collagen content was much lower when compared to the collagen content of dense connective tissues (tendons and aponeuroses) in murine native legs (Binder-Markey et al., 2020). We also noted synovial tissue to possess a reasonable collagen content. In spite of the joint synovial membrane lacking a continuous basement membrane the cells on the surface of the synovial membrane are supported by a loose fibrillary network containing a mixture of fibers derived from Type I and III collagen molecules (Gay et al., 1980). With regard to bone tissue, it's organic matrix contains type I collagen, which constitutes 85–95% of the matrix (Rogers et al., 1952). In our study papain was used as a digestion buffer for each decellularized ECM. It was likely that sGAG and collagen contents could have been underestimated due to the use of a mild digestion which was expected to high amount of insoluble material.

We also studied growth factor contents within the various mesenchymal tissues and key growth factors for cell proliferation, migration and differentiation were detected in varying amounts in each different tissue. bFGF, also known as FGF-2 plays various roles in fibroblast proliferation, migration, angiogenesis but also promotes differentiation (Fujita et al., 2005; Yun et al., 2010). The possible effects of bFGF on myogenesis, adipogenesis, tenogenesis, and osteogenesis along with regeneration of these tissues has been reported (Webb et al., 1997; Kawaguchi et al., 1998; Doukas et al., 2002; Jeong et al., 2010). bFGF is produced by chondrocytes and stored within the ECM (Ellman et al., 2013). It aids in collagen and glycosaminoglycan synthesis and helps maintain stem cells in a undifferentiated state (Shida et al., 2001). Another important growth factor is insulin-like growth factor-I (IGF-I) which plays a crucial role in muscle and bone regeneration (Adams and McCue, 1998; Trippel, 1998; Titan et al., 2019). IGF-I mediates to be largely proliferation and differentiation of satellite cells as well as recruitment of bone marrow stem cells (Musaro et al., 2004; Provenzano et al., 2007). Furthermore, IGF-I is involved in numerous physiologic processes and promotes healing in tissues such as cartilage, skin and tendon (Dahlgren et al., 2002; Zhang et al., 2017). Though literature has determined the potential roles of various growth factors, their tissue-specific distribution is not certain. In our study we found the amount of bFGF to be increased in cartilage tissue, followed by tendon and muscle. However, bFGF content in fat, fat pad, synovium and bone were negligible. IGF-1 content was very high in bone tissue even without demineralization. VEGF is an important angiogenic factor which increases vascular permeability and vascular endothelial cell proliferation (Ferrara, 1999; Turnbull et al., 2018). We expected a high concentration of VEGF in the vascular-rich tissues such as muscle and bone, however, interestingly we noted a high level in the meniscus tissue, while that in muscle was low. The

meniscus has been described to have heterogeneous structure, and possesses a vascularity only in its middle and outer zones (Mauck and Burdick, 2015; Jacob et al., 2019). Porcine menisci has also been described to have increased VEGF content from the inner to the outer zone, explaining why the meniscus tissue expressed a high VEGF concentration (Di Giancamillo et al., 2017). Moreover, as the concentration of growth factor was calculated to per unit protein not per tissue weight in this study, the distributions in soluble factor of each tissue may be different from that we have expected. The final growth factor that we studied was TGF-β1 which is member of a family of numerous ligands essential for development and cell homeostasis (Mao and Mooney, 2015; Kwak and Lee, 2019). TGF-β1 has been frequently employed in tissue engineering to support cell growth, adhesion and proliferation making it essential component for successful regeneration of tissue (Kwak and Lee, 2019). TGF-β1 is particularly abundant in cartilage tissue and helps in promoting matrix synthesis in articular chondrocytes without which the chondrocyte phenotype resemble that of osteoarthritic tissue (Blaney Davidson et al., 2007; Finnson et al., 2012). This is aided by the presence of decorin, biglycan, and chondroitin sulfate which keeps TGF-β1 within the pericellular matrix (Lindahl et al., 2015). Our results also indicate and confirm increased presence of TGF-β1 in cartilage tissue followed by meniscus which does possess cells with chondrocyte-like-morphology (Wilson et al., 2009). Other factors such as GDF-7 and BMP-2 were not found in the tissues though we expected to find a high content of GDF-7 in ligament and tendon tissue and BMP-2 in bone and cartilage (Wolfman et al., 1997). We postulate that either these factors are not present within the tissues or have been not been detected due to our decellularization protocol. Luo et al. (2019) compared various reagents for decellularization of porcine cartilage scaffolds and found the longer the exposure to the decellularizing detergents the less the detected growth factor concentration. The differences of protein distributions in each tissue derived soluble factor were also supported by SDS-PAGE results. The amount of protein factor in fat pad and fat were less than that we expected, which may be caused by less contains of protein in their original tissues or less extraction under the present protocol in such fat-rich tissues and then may result in most of all growth factor could not be detected. Taken together our results suggested that at least 4 kinds of growth factors such as bFGF, IGF-1, VEGF, and TGF-β1 have the tendency of tissue-specific.

To confirm if different tissue-derived soluble ECMs elicited tissue-specific cellular responses, we analyzed their bioactivities by seeding hSMSCs in high density in a 3D collagen gel. As far as the regeneration of musculoskeletal tissues are concerned, SMSCs possess the potential to differentiate into multiple lineages (Fan et al., 2009; Dai et al., 2015; Jacob et al., 2019). Moreover, hSMSCs have already been applied in previous clinical studies in the tissue engineering field (Shimomura et al., 2018). Therefore, hSMSCs were considered to be appropriate to study the differentiation potentials of each soluble ECM. PCR analysis revealed some gene expressions related to each tissue differentiation and maturation showing upregulation in accordance with its origin (**Figure 5**). SOX9, ACAN, or COL2A1, which are known to be chondrogenic differentiation markers, were upregulated mainly when supplemented with cartilage derived ECM. Addition of meniscus-derived ECM showed upregulation of COL1A1, SOX9, and ACAN, which resembles the meniscal fibrous tissue more than cartilage. SCX, a transcription factor specifically detected in tendon precursor cells (Schweitzer et al., 2001), was likely higher in the groups supplemented with ligament and tendon derived soluble ECMs when compared to their controls or other groups. In the tendon and ligament group, the level of TNC and COL3A1 which are tendon and ECM related genes, were not upregulated when compared to the control. Although the method of cell assay was different from our past study, a similar pattern was found in gene expression profiling in the present study (Yang et al., 2013; Rothrauff et al., 2017a,b; Shimomura et al., 2017). We also noted slight upregulation of desmin in the muscle group. Desmin is an MSC marker, but also expressed in mature myotubes (Kadam et al., 2009). Talovic et al. (2019) reported skeletal muscle derived decellularized ECM gelloids supported MSC differentiation toward myogenic tissue. Their results showed the protein of desmin in MSCs on decellularized ECM gelloids was expressed about three times higher than on pure gelatin gelloids (Talovic et al., 2019). Our results also suggest that muscle-derived soluble ECM has the potential to promote myogenic differentiation to about 1.5 higher than the control although in the gene expression. On the contrary, PPARG, which is transcription factor related with adipogenic differentiation, was not upregulated in fat pad and fat groups. This may result in the ineffective preparation of soluble ECM derived from fat pad or fat tissue. Runx2, which is a master transcription gene for osteoblast differentiation was higher in the cartilage and bone group, although no consequent improvement was demonstrated. However, COL1A1, which is also a marker for bone tissue, was not upregulated significantly but demonstrated expression similar to the control group, while other tissues excluding cartilage and meniscus showed reduced expression. The present cell assay was performed under single 3D condition (such as medium, cell source, tensile loading material of scaffold and cell orientation) to compare the potential of each soluble ECMs purely. More definite differences may be observed by culturing the cells for a longer duration with more appropriate culture conditions and method of decellularization and solubilization for each tissue. Considering the enhanced expression of these markers which are specific to each tissue-derived group, we noted soluble ECMs to be highly bioactive and likely act to promote differentiation toward the native ECM tissue source.

In the present study, soluble factors were extracted using urea. Urea is a chaotropic agent that disrupts hydrogen bonding, resulting in the denaturation of proteins and disruption of lipids and protein interactions (Yang et al., 2013). In a previous study, urea-extracted decellularized ECM had higher concentrations of small and moderate molecular weight proteins compared to pepsin-digested decellularized ECM, which consisted primarily of collagen chains (Yang et al., 2013), therefore we applied a urea extraction protocol to the present study. Guanidine

hydrochloride is also known to be effective in extracting heavily cross-linked proteins and proteoglycans from tissues such as tendons or cartilage and applied to other tissues (Vogel and Peters, 2001; Wilson et al., 2010; Barallobre-Barreiro et al., 2017). There is a possibility that a more efficient appropriate decellularization protocol could results in high yield of growth factors with increased bioactivity. To our knowledge, this is the first study to evaluate and compare the biochemical characteristics, growth factor soluble component distribution and bioactivities in nine types of decellularized ECM derived from mesenchymal tissues in the same experiment. In the future such tissue derived soluble ECMs could be employed to regenerate tissues combined with some appropriate scaffolds seeded with some appropriate stem cells. They could be manufactured and delivered as a "bio ink" which would be an efficient natural scaffold solution to print for any defect size and shape matching the recipient site.

Our study is not without limitations in that we didn't confirm the content of elastin, laminin, lipid, or calcium to prescribe the characteristic of each ECM component. It is unclear how the present protocol could affect them. We only assessed a limited number of growth factors from a large possible number within the tissues. Further variations in growth factors are likely and a more detailed analysis would allow us to draw further conclusions. Finally, we assessed the gene expression profile within 1 week and didn't confirm the profiling of their synthesized proteins. This should be the next step in our future research to determine the effects of these ECMs on protein synthesis in cultures of longer duration.

CONCLUSION

In this study, soluble fractions of nine types of porcine tissues were prepared with a same protocol. Decellularization was successful with reducing cellular component in every tissue and the difference of hydroxyproline and sGAG contain in each native and decellularized tissue was revealed. Moreover, the soluble decellularized ECMs of each tissue exhibited variations in their growth factor distribution and on cell culture appeared to promote cell differentiation toward the specified used ECM tissue phenotype.

DATA AVAILABILITY STATEMENT

The original contributions presented in the study are included in the article/supplementary material, further inquiries can be directed to the corresponding author.

ETHICS STATEMENT

The studies involving human participants were reviewed and approved by Osaka University Clinical Research Review Committee. Written informed consent to participate in this study was provided by the participants' legal guardian/next of kin.

AUTHOR CONTRIBUTIONS

HH, GJ, and KS contributed conception and design of the study. HH and SN prepared materials. HH and GJ contributed experimental procedures and wrote sections of the manuscript. HH performed the statistical analysis and wrote the first draft of the manuscript. GJ, RT, NN, and KS edited the manuscript. All authors contributed to manuscript revision, read and approved the submitted version.

FUNDING

This study was supported by a Grant-in-Aid for Young Scientists (A), the Japan Society for the Promotion of Science (Grant Number JP16H06264; to KS), and Grant-in-Aid for Scientific Research (B), the Japan Society for the Promotion of Science (Grant Number JP19H03781; to NN).

ACKNOWLEDGMENTS

The authors would like to thank Fumiko Hirayama, Mari Shinkawa, and Yukiko Eguchi for their technical support, and Center for Medical Research and Education, Graduate School of Medicine, Osaka University for using the device of SH-9000Lab and Chemi Doc Touch.

REFERENCES

Adams, G. R., and McCue, S. A. (1998). Localized infusion of IGF-I results in skeletal muscle hypertrophy in rats. *J. Appl. Physiol.* 84, 1716–1722. doi: 10.1152/jappl.1998.84.5.1716

Almeida, H. V., Eswaramoorthy, R., Cunniffe, G. M., Buckley, C. T., O'brien, F. J., and Kelly, D. J. (2016). Fibrin hydrogels functionalized with cartilage extracellular matrix and incorporating freshly isolated stromal cells as an injectable for cartilage regeneration. *Acta Biomater.* 36, 55–62. doi: 10.1016/j.actbio.2016.03.008

Ando, W., Tateishi, K., Hart, D. A., Katakai, D., Tanaka, Y., Nakata, K., et al. (2007). Cartilage repair using an in vitro generated scaffold-free tissue-engineered construct derived from porcine synovial mesenchymal stem cells. *Biomaterials* 28, 5462–5470. doi: 10.1016/j.biomaterials.2007.08.030

Badylak, S. F., Freytes, D. O., and Gilbert, T. W. (2009). Extracellular matrix as a biological scaffold material: structure and function. *Acta Biomater.* 5, 1–13. doi: 10.1016/j.actbio.2008.09.013

Barallobre-Barreiro, J., Baig, F., Fava, M., Yin, X., and Mayr, M. (2017). Glycoproteomics of the extracellular matrix: a method for intact glycopeptide analysis using mass spectrometry. *J. Vis. Exp.* 2017:e55674. doi: 10.3791/55674

Beck, E. C., Barragan, M., Tadros, M. H., Kiyotake, E. A., Acosta, F. M., Kieweg, S. L., et al. (2016). Chondroinductive hydrogel pastes composed of naturally derived devitalized cartilage. *Ann. Biomed. Eng.* 44, 1863–1880. doi: 10.1007/s10439-015-1547-5

Binder-Markey, B. I., Broda, N. M., and Lieber, R. L. (2020). Intramuscular anatomy drives collagen content variation within and between muscles. *Front. Physiol.* 11:293. doi: 10.3389/fphys.2020.00293

Blaney Davidson, E. N., Van Der Kraan, P. M., and Van Den Berg, W. B. (2007). TGF-beta and osteoarthritis. *Osteoarthrit. Cartil.* 15, 597–604. doi: 10.1016/j.joca.2007.02.005

Brown, B. N., Valentin, J. E., Stewart-Akers, A. M., Mccabe, G. P., and Badylak, S. F. (2009). Macrophage phenotype and remodeling outcomes in response to biologic scaffolds with and without a cellular component. *Biomaterials* 30, 1482–1491. doi: 10.1016/j.biomaterials.2008.11.040

Chan, B. P., and Leong, K. W. (2008). Scaffolding in tissue engineering: general approaches and tissue-specific considerations. *Eur. Spine J.* 17(Suppl. 4), 467–479. doi: 10.1007/s00586-008-0745-3

Cheng, C. W., Solorio, L. D., and Alsberg, E. (2014). Decellularized tissue and cell-derived extracellular matrices as scaffolds for orthopaedic tissue engineering. *Biotechnol. Adv.* 32, 462–484. doi: 10.1016/j.biotechadv.2013.12.012

Cissell, D. D., Link, J. M., Hu, J. C., and Athanasiou, K. A. (2017). A modified hydroxyproline assay based on hydrochloric acid in ehrlich's solution accurately measures tissue collagen content. *Tissue Eng. Part C Methods* 23, 243–250. doi: 10.1089/ten.tec.2017.0018

Crapo, P. M., Gilbert, T. W., and Badylak, S. F. (2011). An overview of tissue and whole organ decellularization processes. *Biomaterials* 32, 3233–3243. doi: 10.1016/j.biomaterials.2011.01.057

Dahlgren, L. A., Van Der Meulen, M. C. H., Bertram, J. E. A., Starrak, G. S., and Nixon, A. J. (2002). Insulin-like growth factor-I improves cellular and molecular aspects of healing in a collagenase-induced model of flexor tendinitis. *J. Orthopaed. Res.* 20, 910–919. doi: 10.1016/s0736-0266(02)00009-8

Dai, L., Hu, X., Zhang, X., Zhu, J., Zhang, J., Fu, X., et al. (2015). Different tenogenic differentiation capacities of different mesenchymal stem cells in the presence of BMP-12. *J. Transl. Med.* 13:200. doi: 10.1186/s12967-015-0560-7

Di Giancamillo, A., Deponti, D., Modina, S., Tessaro, I., Domeneghini, C., and Peretti, G. M. (2017). Age-related modulation of angiogenesis-regulating factors in the swine meniscus. *J. Cell Mol. Med.* 21, 3066–3075. doi: 10.1111/jcmm.13218

Doukas, J., Blease, K., Craig, D., Ma, C., Chandler, L. A., Sosnowski, B. A., et al. (2002). Delivery of FGF genes to wound repair cells enhances arteriogenesis and myogenesis in skeletal muscle. *Mol. Ther.* 5, 517–527. doi: 10.1006/mthe.2002.0579

Eleswarapu, S. V., Responte, D. J., and Athanasiou, K. A. (2011). Tensile properties, collagen content, and crosslinks in connective tissues of the immature knee joint. *PLoS One* 6:e26178. doi: 10.1371/journal.pone.0026178

Ellman, M. B., Yan, D., Ahmadinia, K., Chen, D., An, H. S., and Im, H. J. (2013). Fibroblast growth factor control of cartilage homeostasis. *J. Cell Biochem.* 114, 735–742. doi: 10.1002/jcb.24418

Fan, J., Varshney, R. R., Ren, L., Cai, D., and Wang, D. A. (2009). Synovium-derived mesenchymal stem cells: a new cell source for musculoskeletal regeneration. *Tissue Eng. Part B Rev.* 15, 75–86. doi: 10.1089/ten.teb.2008.0586

Farnebo, S., Woon, C. Y., Schmitt, T., Joubert, L. M., Kim, M., Pham, H., et al. (2014). Design and characterization of an injectable tendon hydrogel: a novel scaffold for guided tissue regeneration in the musculoskeletal system. *Tissue Eng. Part A* 20, 1550–1561. doi: 10.1089/ten.TEA.2013.0207

Ferrara, N. (1999). Role of vascular endothelial growth factor in the regulation of angiogenesis. *Kidney Int.* 56, 794–814. doi: 10.1046/j.1523-1755.1999.00610.x

Finnson, K. W., Chi, Y., Bou-Gharios, G., Leask, A., and Philip, A. (2012). TGF-b signaling in cartilage homeostasis and osteoarthritis. *Front. Biosci.* 4, 251–268. doi: 10.2741/s266

Flynn, L. E. (2010). The use of decellularized adipose tissue to provide an inductive microenvironment for the adipogenic differentiation of human adipose-derived stem cells. *Biomaterials* 31, 4715–4724. doi: 10.1016/j.biomaterials.2010.02.046

Frantz, C., Stewart, K. M., and Weaver, V. M. (2010). The extracellular matrix at a glance. *J. Cell Sci.* 123, 4195–4200. doi: 10.1242/jcs.023820

Freemont, A. J., and Hoyland, J. A. (2007). Morphology, mechanisms and pathology of musculoskeletal ageing. *J. Pathol.* 211, 252–259. doi: 10.1002/path.2097

Fujita, M., Kinoshita, Y., Sato, E., Maeda, H., Ozono, S., Negishi, H., et al. (2005). Proliferation and differentiation of rat bone marrow stromal cells on poly(glycolic acid)-collagen sponge. *Tissue Eng.* 11, 1346–1355. doi: 10.1089/ten.2005.11.1346

Gardin, C., Ricci, S., Ferroni, L., Guazzo, R., Sbricoli, L., De Benedictis, G., et al. (2015). Decellularization and delipidation protocols of bovine bone and pericardium for bone grafting and guided bone regeneration procedures. *PLoS One* 10:e0132344. doi: 10.1371/journal.pone.0132344

Gay, S., Gay, R. E., and Miller, E. F. (1980). The collagens of the joint. *Arthrit. Rheum.* 23, 937–941. doi: 10.1002/art.1780230810

Gilpin, A., and Yang, Y. (2017). Decellularization strategies for regenerative medicine: from processing techniques to applications. *Biomed. Res. Int.* 2017:9831534. doi: 10.1155/2017/9831534

Harrison, R. H., St-Pierre, J. P., and Stevens, M. M. (2014). Tissue engineering and regenerative medicine: a year in review. *Tissue Eng. Part B Rev.* 20, 1–16. doi: 10.1089/ten.TEB.2013.0668

Jacob, G., Shimomura, K., Krych, A. J., and Nakamura, N. (2019). The meniscus tear: a review of stem cell therapies. *Cells* 9:92. doi: 10.3390/cells9010092

Jeong, I., Yu, H. S., Kim, M. K., Jang, J. H., and Kim, H. W. (2010). FGF2-adsorbed macroporous hydroxyapatite bone granules stimulate in vitro osteoblastic gene expression and differentiation. *J. Mater. Sci. Mater. Med.* 21, 1335–1342. doi: 10.1007/s10856-009-3971-2

Kadam, S. S., Patki, S. M., and Bhonde, R. R. (2009). Human Fallopian tube as a novel source of multipotent stem cells with potential for islet neogenesis. *J. Stem Cells Regener. Med.* 5, 37–42. doi: 10.46582/jsrm.0501007

Kawaguchi, N., Toriyama, K., Nicodemou-Lena, E., Inou, K., Torii, S., and Kitagawa, Y. (1998). De novo adipogenesis in mice at the site of injection of basement membrane and basic fibroblast growth factor. *Proc. Natl. Acad. Sci. U.S.A.* 95, 1062–1066. doi: 10.1073/pnas.95.3.1062

Kim, M. Y., Farnebo, S., Woon, C. Y., Schmitt, T., Pham, H., and Chang, J. (2014). Augmentation of tendon healing with an injectable tendon hydrogel in a rat Achilles tendon model. *Plast. Reconstr. Surg.* 133, 645–653. doi: 10.1097/PRS.0000000000000106

Koizumi, K., Ebina, K., Hart, D. A., Hirao, M., Noguchi, T., Sugita, N., et al. (2016). Synovial mesenchymal stem cells from osteo- or rheumatoid arthritis joints exhibit good potential for cartilage repair using a scaffold-free tissue engineering approach. *Osteoarthrit. Cartil.* 24, 1413–1422. doi: 10.1016/j.joca.2016.03.006

Kwak, E. A., and Lee, N. Y. (2019). Synergetic roles of TGF-beta signaling in tissue engineering. *Cytokine* 115, 60–63. doi: 10.1016/j.cyto.2018.12.010

Kwon, J. S., Yoon, S. M., Shim, S. W., Park, J. H., Min, K. J., Oh, H. J., et al. (2013). Injectable extracellular matrix hydrogel developed using porcine articular cartilage. *Int. J. Pharm.* 454, 183–191. doi: 10.1016/j.ijpharm.2013.06.023

Lee, J. S., Roh, Y. H., Choi, Y. S., Jin, Y., Jeon, E. J., Bong, K. W., et al. (2019). Tissue beads: tissue-specific extracellular matrix microbeads to potentiate reprogrammed cell-based therapy. *Adv. Funct. Mater.* 29:1807803. doi: 10.1002/adfm.201807803

Lehr, E. J., Rayat, G. R., Chiu, B., Churchill, T., Mcgann, L. E., Coe, J. Y., et al. (2011). Decellularization reduces immunogenicity of sheep pulmonary artery vascular patches. *J. Thorac. Cardiovasc. Surg.* 141, 1056–1062. doi: 10.1016/j.jtcvs.2010.02.060

Lin, H., Yang, G., Tan, J., and Tuan, R. S. (2012). Influence of decellularized matrix derived from human mesenchymal stem cells on their proliferation, migration and multi-lineage differentiation potential. *Biomaterials* 33, 4480–4489. doi: 10.1016/j.biomaterials.2012.03.012

Lindahl, U., Couchman, J., Kimata, K., and Esko, J. D. (2015). "Proteoglycans and sulfated glycosaminoglycans," in *Essentials of Glycobiology*, 3rd Edn, eds A. Varki, R. D. Cummings, and J. D. Esko (Cold Spring Harbor, NY: Cold Spring Harbor Laboratory Press).

Luo, Z., Bian, Y., Su, W., Shi, L., Li, S., Song, Y., et al. (2019). Comparison of various reagents for preparing a decellularized porcine cartilage scaffold. *Am. J. Transl. Res.* 11, 1417–1427.

Mao, A. S., and Mooney, D. J. (2015). Regenerative medicine: current therapies and future directions. *Proc. Natl. Acad. Sci. U.S.A.* 112, 14452–14459. doi: 10.1073/pnas.1508520112

Mauck, R. L., and Burdick, J. A. (2015). From repair to regeneration: biomaterials to reprogram the meniscus wound microenvironment.

Ann. Biomed. Eng. 43, 529–542. doi: 10.1007/s10439-015-1249-z

Mendibil, U., Ruiz-Hernandez, R., Retegi-Carrion, S., Garcia-Urquia, N., Olalde-Graells, B., and Abarrategi, A. (2020). Tissue-specific decellularization methods: rationale and strategies to achieve regenerative compounds. *Intern. J. Mol. Sci.* 21:5447. doi: 10.3390/ijms21155447

Musaro, A., Giacinti, C., Borsellino, G., Dobrowolny, G., Pelosi, L., Cairns, L., et al. (2004). Stem cell-mediated muscle regeneration is enhanced by local isoform of insulin-like growth factor 1. *Proc. Natl. Acad. Sci. U.S.A.* 101, 1206–1210. doi: 10.1073/pnas.0303792101

Nagata, S., Hanayama, R., and Kawane, K. (2010). Autoimmunity and the clearance of dead cells. *Cell* 140, 619–630. doi: 10.1016/j.cell.2010.02.014

Ozasa, Y., Amadio, P. C., Thoreson, A. R., An, K. N., and Zhao, C. (2014). Repopulation of intrasynovial flexor tendon allograft with bone marrow stromal cells: an ex vivo model. *Tissue Eng. Part A* 20, 566–574. doi: 10.1089/ten.TEA.2013.0284

Pati, F., Jang, J., Ha, D. H., Won Kim, S., Rhie, J. W., Shim, J. H., et al. (2014). Printing three-dimensional tissue analogues with decellularized extracellular matrix bioink. *Nat. Commun.* 5:3935. doi: 10.1038/ncomms4935

Petersen, T. H., Calle, E. A., Zhao, L., Lee, E. J., Gui, L., Raredon, M. B., et al. (2010). Tissue-engineered lungs for in vivo implantation. *Science* 329, 538–541. doi: 10.1126/science.1189345

Provenzano, P. P., Alejandro-Osorio, A. L., Grorud, K. W., Martinez, D. A., Vailas, A. C., Grindeland, R. E., et al. (2007). Systemic administration of IGF-I enhances healing in collagenous extracellular matrices: evaluation of loaded and unloaded ligaments. *BMC Physiol.* 7:2. doi: 10.1186/1472-6793-7-2

Reisbig, N. A., Hussein, H. A., Pinnell, E., and Bertone, A. L. (2016). Comparison of four methods for generating decellularized equine synovial extracellular matrix. *Am. J. Vet. Res.* 77, 1332–1339. doi: 10.2460/ajvr.77.12.1332

Rogers, H. J., Weidmann, S. M., and Parkinson, A. (1952). Studies on the skeletal tissues. II. The collagen content of bones from rabbits, oxen and humans. *Biochem. J.* 50, 537–542. doi: 10.1042/bj0500537

Rothrauff, B. B., Shimomura, K., Gottardi, R., Alexander, P. G., and Tuan, R. S. (2017a). Anatomical region-dependent enhancement of 3-dimensional chondrogenic differentiation of human mesenchymal stem cells by soluble meniscus extracellular matrix. *Acta Biomater.* 49, 140–151. doi: 10.1016/j.actbio.2016.11.046

Rothrauff, B. B., Yang, G., and Tuan, R. S. (2017b). Tissue-specific bioactivity of soluble tendon-derived and cartilage-derived extracellular matrices on adult mesenchymal stem cells. *Stem Cell Res. Ther.* 8:133. doi: 10.1186/s13287-017-0580-8

Rowland, C. R., Colucci, L. A., and Guilak, F. (2016). Fabrication of anatomically-shaped cartilage constructs using decellularized cartilage-derived matrix scaffolds. *Biomaterials* 91, 57–72. doi: 10.1016/j.biomaterials.2016.03.012

Sano, H., Orbay, H., Terashi, H., Hyakusoku, H., and Ogawa, R. (2014). Acellular adipose matrix as a natural scaffold for tissue engineering. *J. Plast. Reconstr. Aesthet. Surg.* 67, 99–106. doi: 10.1016/j.bjps.2013.08.006

Schwarz, S., Elsaesser, A. F., Koerber, L., Goldberg-Bockhorn, E., Seitz, A. M., Bermueller, C., et al. (2015). Processed xenogenic cartilage as innovative biomatrix for cartilage tissue engineering: effects on chondrocyte differentiation and function. *J. Tissue Eng. Regen. Med.* 9, E239–E251. doi: 10.1002/term.1650

Schweitzer, R., Chyung, J. H., Murtaugh, L. C., Brent, A. E., Rosen, V., Olson, E. N., et al. (2001). Analysis of the tendon cell fate using Scleraxis, a specific marker for tendons and ligaments. *Development* 128, 3855–3866.

Shida, J.-I., Jingushi, S., Izumi, T., Ikenoue, T., and Iwamoto, Y. (2001). Basic fibroblast growth factor regulates expression of growth factors in rat epiphyseal chondrocytes. *J. Orthopaed. Res.* 19, 259–264. doi: 10.1016/s0736-0266(00)90009-3

Shimomura, K., Rothrauff, B. B., and Tuan, R. S. (2017). Region-specific effect of the decellularized meniscus extracellular matrix on mesenchymal stem cell-based meniscus tissue engineering. *Am. J. Sports Med.* 45, 604–611. doi: 10.1177/0363546516674184

Shimomura, K., Yasui, Y., Koizumi, K., Chijimatsu, R., Hart, D. A., Yonetani, Y., et al. (2018). First-in-human pilot study of implantation of a scaffold-free tissue-engineered construct generated from autologous synovial mesenchymal stem cells for repair of knee chondral lesions. *Am. J. Sports Med.* 46, 2384–2393. doi: 10.1177/0363546518781825

Stern, M. M., Myers, R. L., Hammam, N., Stern, K. A., Eberli, D., Kritchevsky, S. B., et al. (2009). The influence of extracellular matrix derived from skeletal muscle tissue on the proliferation and differentiation of myogenic progenitor cells ex vivo. *Biomaterials* 30, 2393–2399. doi: 10.1016/j.biomaterials.2008.12.069

Talovic, M., Patel, K., Schwartz, M., Madsen, J., and Garg, K. (2019). Decellularized extracellular matrix gelloids support mesenchymal stem cell growth and function in vitro. *J. Tissue Eng. Regen. Med.* 13, 1830–1842. doi: 10.1002/term.2933

Titan, A. L., Foster, D. S., Chang, J., and Longaker, M. T. (2019). Flexor tendon: development, healing, adhesion formation, and contributing growth factors. *Plast. Reconstr. Surg.* 144, 639e–647e. doi: 10.1097/PRS.0000000000006048

Trippel, S. B. (1998). Potential role of insulinlike growth factors in fracture healing. *Clin. Orthop. Relat. Res.* 355(Suppl.), S301–S313. doi: 10.1097/00003086-199810001-00031

Turnbull, G., Clarke, J., Picard, F., Riches, P., Jia, L., Han, F., et al. (2018). 3D bioactive composite scaffolds for bone tissue engineering. *Bioact. Mater.* 3, 278–314. doi: 10.1016/j.bioactmat.2017.10.001

Valentin, J. E., Badylak, J. S., Mccabe, G. P., and Badylak, S. F. (2006). Extracellular matrix bioscaffolds for orthopaedic applications. A comparative histologic study. *J. Bone Joint. Surg. Am.* 88, 2673–2686. doi: 10.2106/JBJS.E.01008

Vavken, P., Joshi, S., and Murray, M. M. (2009). TRITON-X is most effective among three decellularization agents for ACL tissue engineering. *J. Orthop. Res.* 27, 1612–1618. doi: 10.1002/jor.20932

Vogel, K. G., and Peters, J. A. (2001). Isolation of proteoglycans from tendon. *Methods Mol. Biol.* 171, 9–17. doi: 10.1007/978-3-0348-7545-5_3

Vorotnikova, E., Mcintosh, D., Dewilde, A., Zhang, J., Reing, J. E., Zhang, L., et al. (2010). Extracellular matrix-derived products modulate endothelial and progenitor cell migration and proliferation in vitro and stimulate regenerative healing in vivo. *Matrix Biol.* 29, 690–700. doi: 10.1016/j.matbio.2010.08.007

Webb, S. E., Lee, K. K. H., Tang, M. K., and Ede, D. A. (1997). Fibroblast growth factors 2 and 4 stimulate migration of mouse embryonic limb myogenic cells. *Dev. Dyn.* 209, 206–216. doi: 10.1002/(sici)1097-0177(199706)209:2<206::aid-aja6>3.0.co;2-m

Wilson, C. G., Nishimuta, J. F., and Levenston, M. E. (2009). Chondrocytes and meniscal fibrochondrocytes differentially process aggrecan during de novo extracellular matrix assembly. *Tissue Eng. Part A* 15, 1513–1522. doi: 10.1089/ten.tea.2008.0106

Wilson, R., Diseberg, A. F., Gordon, L., Zivkovic, S., Tatarczuch, L., Mackie, E. J., et al. (2010). Comprehensive profiling of cartilage extracellular matrix formation and maturation using sequential extraction and label-free quantitative proteomics. *Mol. Cell Proteom.* 9, 1296–1313. doi: 10.1074/mcp.M000014-MCP201

Wolff, J. L., Starfield, B., and Anderson, G. (2002). Prevalence, expenditures, and complications of multiple chronic conditions in the elderly. *Arch. Intern. Med.* 162, 2269–2276. doi: 10.1001/archinte.162.20.2269

Wolfman, N. M., Hattersley, G., Cox, K., Celeste, A. J., Nelson, R., Yamaji, N., et al. (1997). Ectopic induction of tendon and ligament in rats by growth and differentiation factors 5, 6, and 7, members of the TGF-beta gene family. *J. Clin. Invest.* 100, 321–330. doi: 10.1172/JCI119537

Yang, G., Rothrauff, B. B., Lin, H., Gottardi, R., Alexander, P. G., and Tuan, R. S. (2013). Enhancement of tenogenic differentiation of human adipose stem cells by tendon-derived extracellular matrix. *Biomaterials* 34, 9295–9306. doi: 10.1016/j.biomaterials.2013.08.054

Yang, Q., Teng, B. H., Wang, L. N., Li, K., Xu, C., Ma, X. L., et al. (2017). Silk fibroin/cartilage extracellular matrix scaffolds with sequential delivery of TGF-beta3 for chondrogenic differentiation of adipose-derived stem cells. *Int. J. Nanomed.* 12, 6721–6733. doi: 10.2147/IJN.S141888

Yue, B. (2014). Biology of the extracellular matrix: an overview. *J. Glaucoma* 23, S20–S23. doi: 10.1097/IJG.0000000000000108

Yun, Y. R., Won, J. E., Jeon, E., Lee, S., Kang, W., Jo, H., et al. (2010). Fibroblast growth factors: biology, function, and application for

tissue regeneration. *J. Tissue Eng.* 2010:218142. doi: 10.4061/2010/218142

Zhang, Q., Raoof, M., Chen, Y., Sumi, Y., Sursal, T., Junger, W., et al. (2010). Circulating mitochondrial DAMPs cause inflammatory responses to injury. *Nature* 464, 104–107. doi: 10.1038/nature08780

Zhang, Y., He, Y., Bharadwaj, S., Hammam, N., Carnagey, K., Myers, R., et al. (2009). Tissue-specific extracellular matrix coatings for the promotion of cell proliferation and maintenance of cell phenotype. *Biomaterials* 30, 4021–4028. doi: 10.1016/j.biomaterials.2009.04.005

Zhang, Z., Li, L., Yang, W., Cao, Y., Shi, Y., Li, X., et al. (2017). The effects of different doses of IGF-1 on cartilage and subchondral bone during the repair of full-thickness articular cartilage defects in rabbits. *Osteoarthrit. Cartil.* 25, 309–320. doi: 10.1016/j.joca.2016.09.010

Conflict of Interest: The authors declare that the research was conducted in the absence of any commercial or financial relationships that could be construed as a potential conflict of interest.

frontiers in Cell and Developmental Biology

REVIEW
published: 11 December 2020
doi: 10.3389/fcell.2020.598816

Technical Procedures for Preparation and Administration of Platelet-Rich Plasma and Related Products: A Scoping Review

Daniela Vianna Pachito[1,2], Ângela Maria Bagattini[1,3], Adriano Marques de Almeida[4], Alfredo Mendrone-Júnior[5] and Rachel Riera[1,6]*

[1] Núcleo de Avaliação de Tecnologias em Saúde, Hospital Sírio-Libanês, São Paulo, Brazil, [2] Fundação Getúlio Vargas, São Paulo, Brazil, [3] Instituto de Patologia Tropical e Saúde Pública, Universidade Federal de Goiás, Goiânia, Brazil, [4] Instituto de Ortopedia e Traumatologia, Hospital das Clínicas, Universidade de São Paulo, São Paulo, Brazil, [5] Fundação Pro Sangue Hemocentro de São Paulo e Laboratório de Processamento Celular, Hospital Sírio Libanês, São Paulo, Brazil, [6] Disciplina de Medicina Baseada em Evidências, Escola Paulista de Medicina, Universidade Federal de São Paulo, São Paulo, Brazil

OPEN ACCESS

Edited by:
Kazunori Shimomura, Osaka University, Japan

Reviewed by:
Pietro Gentile, University of Rome Tor Vergata, Italy
James Wang, StemBios Technologies, Inc., United States
Jose Fabio Lana, Indaiatuba, Brazil

***Correspondence:**
Daniela Vianna Pachito
daniela.vpachito@hsl.org.br; pachito@uol.com.br

Specialty section:
This article was submitted to Stem Cell Research, a section of the journal Frontiers in Cell and Developmental Biology

Received: *25 August 2020*
Accepted: *19 November 2020*
Published: *11 December 2020*

Citation:
Pachito DV, Bagattini ÂM, de Almeida AM, Mendrone-Júnior A and Riera R (2020) Technical Procedures for Preparation and Administration of Platelet-Rich Plasma and Related Products: A Scoping Review. Front. Cell Dev. Biol. 8:598816. doi: 10.3389/fcell.2020.598816

Introduction: Platelet-rich plasma is widely used for different types of clinical situations, but universal standardization of procedures for its preparation is still lacking.

Methods: Scoping review of comparative studies that have assessed at least two alternatives in one or more stages of preparation, storage and/or administration of PRP or its related products. A systematic search was conducted in MEDLINE, Embase, and LILACS. Two authors screened references independently. Data extraction was performed iteratively, and results were presented for each included comparison.

Results: Thirty-nine studies were included after assessing full texts, focusing on the comparison of PRP to a related product, types of anticoagulants, centrifugation protocols, commercial kits, processing time, methods for activation, and application concomitantly to other substances. Only laboratory outcomes were assessed, as platelet, leukocyte and growth factor concentrations.

Conclusion: Results showed great variability related to methods employed in different stages of PRP processing, which may explain the variability observed in clinical trials assessing the efficacy of PRP for different clinical situations.

Keywords: platelet-rich plasma, platelet-rich fibrin, platelet concentrates, growth factors, platelets

INTRODUCTION

Platelet-rich plasma (PRP) has been advocated as a therapeutic option for a vast array of clinical situations in different fields of Medicine and Dentistry (Albanese et al., 2013; Robins, 2017). The therapeutic effects of PRP have been attributed to the supraphysiological concentration of growth factors and cell adhesion molecules (Marx, 2004), ultimately leading to, among other effects, angiogenesis, cell proliferation, deposition of collagen, and mesenchymal stem cell differentiation (Smyth et al., 2013).

Despite the increasing demonstration of its efficacy by previous research (Roselló-Camps et al., 2015; Martinez-Zapata et al., 2016; Sadabad et al., 2016; Li et al., 2017), there is still considerable uncertainty about the characteristics of PRP that may lead to optimal results. Clear recommendations about the ideal concentration of platelets and growth factors are still lacking, although a number of studies suggest a dose-effect relation with a ceiling effect (Giusti et al., 2009). Additionally, other characteristics of PRP still remain object of debate, such as the benefits related to white blood cells in PRP (L-PRP) (Bielecki et al., 2012; Wang et al., 2018b).

The variability of procedures applied for preparing PRP and other related products, including plasma-rich fibrin (PRF), along all stages of preparation, such as centrifugation, activation and types of anticoagulants, challenges a uniform recommendation of standardized procedures (Russell et al., 2013). Different terminologies and classification schemes have been proposed to embrace the diversity of procedures for the preparation of PRP (Ehrenfest et al., 2010, 2014; DeLong et al., 2012; Magalon et al., 2016; Lana et al., 2017), as well as frameworks to allow discrimination and specification of processing quantitative and qualitative standards (Gentile et al., 2020).

From the clinical perspective, the lack of standardization hampers the comparation of results from clinical trials that may had employed different protocols for PRP production. This fact may explain the heterogeneity of results observed in these trials and contributes to the uncertainties related to the clinical effects of PRP (Vos et al., 2014). Additionally, the diversity of methods embedded in PRP preparation defies the delineation of regulatory norms, which, by its turn, may contribute to the permissiveness toward substandard practices.

The objectives of this scoping review were to identify and summarize methods employed for preparation, storage and administration of PRP and its related products, and to identify the gaps of knowledge, following an evidence-based approach.

MATERIALS AND METHODS

Study Design

This scoping review was developed in five stages, namely (i) definition of the research question, (ii) elaboration of search strategies, (iii) assessment of study eligibility, (iv) data extraction, and (v) summary of findings. This methodological framework was first proposed by Arksey (Arksey and Malley, 2005) and later revised by Levac (Levac et al., 2010). The study report was structured in a way to contemplate all items of the PRISMA extension for scoping reviews (PRISMA-ScR) (Tricco et al., 2018). A protocol describing the review methods was *a priori* developed and made available at Open Science Framework (doi: 10.17605/OSF.IO/3WZEP).

Definition of the Research Questions

Research questions were prospectively defined to reflect the aspects susceptible to variability during preparation, storage and administration of PRP. Research questions are presented in **Box 1**. These questions were iteratively expanded during the stage of data extraction.

Search Strategies

Search strategies were applied in MEDLINE (via PubMed), Embase (via Elsevier) and LILACS – (via Biblioteca Virtual em Saúde, BVS), on 23rd November 2018 (**Supplementary Material**). Additionally, reference lists of included studies were hand searched aiming at identifying potentially eligible studies.

Eligibility Criteria, Study Screening and Data Extraction

Inclusion and exclusion criteria were iteratively defined along data extraction, as previously recommended by Arksey and Levac (Arksey and Malley, 2005; Levac et al., 2010; **Table 1**). Different types of primary study designs, such as randomized controlled trials, non-randomized trials and *in vitro* studies were considered for inclusion, provided they had assessed at least two alternatives for any stage of preparation of PRP. Studies conducted before 2000 were not considered for inclusion, given that they might not reflect the current standard of practice due to the fast evolution of the field along the last two decades.

Screening of studies was performed at two stages. At the first stage, titles and abstracts were screened independently by two authors, with resolution of disagreements by consensus. At the second stage, full texts were assessed and confronted against the inclusion and exclusion criteria, as they were iteratively defined. Both stages of study screening were conducted in the Rayyan platform (Ouzzani et al., 2016).

Data Extraction

Data extraction was performed in a Microsoft Excel® spreadsheet (2016). The framework for data extraction was *a priori* defined in a way to reflect the research questions. The final framework was achieved after incorporating relevant aspects.

Summary of Findings

Study screening was documented and presented in a PRISMA flow diagram. Results were presented narratively, grouped by stage of preparation and administration of PRP.

RESULTS

Electronic searches retrieved 2,757 references. Two additional references were additionally identified. After removing duplicates, titles and abstracts of 2,552 references were screened, leading to a selection of 94 studies. Thirty-nine studies were included after the assessment of full texts (**Figure 1**). The list of excluded studies at the full text stage and reasons for exclusion are presented in **Supplementary Material**.

Characteristics of Included Studies

Study Design

One non-randomized clinical trial was included (Alhumaidan et al., 2011). The other included studies

BOX 1 | Predefined research questions.

- Methods for obtaining PRP (e.g., open systems, closed systems).
- Activation methods.
- Centrifugation protocols.
- Methods applied for quality control.

TABLE 1 | Inclusion and exclusion criteria.

Inclusion criteria	Exclusion criteria
• Comparative research that have assessed at least two alternatives in one or more stages of preparation, storage and/or administration of PRP or its related products.	• Studies published in languages other than English, Spanish and Portuguese. • Studies conducted before 2000. • Secondary studies (e.g., systematic reviews, narrative reviews). • Non-comparative studies. • Comparative studies in which quantitative analyzes were not reported. • Animal studies. • PRP for transfusion. • Studies enrolling participants under antiplatelet therapy. • Studies comparing platelet concentrates to other types of blood components.

were *in vitro* controlled studies employing different methods for any one of stage of production of PRP or related products.

Research Questions

Included studies addressed different research questions, namely (i) comparison of PRP to related products; (ii) different commercial kits for PRP processing; (iii) types of anticoagulants; (iv) centrifugation protocols; (v) time for PRP processing; (vi) activation methods; and (vii) combined use with other substances.

Comparisons of Included Studies

PRP compared to other platelet concentrates

Five studies compared the characteristics of PRP to other platelet concentrates (Lachert et al., 2011; Cavallo et al., 2014; Kobayashi et al., 2015; Mariani et al., 2015; Kieb et al., 2017). These studies compared PRP with PRP with leukocytes (L-PRP) (Cavallo et al., 2014; Mariani et al., 2015); powdered PRP (Kieb et al., 2017); and PRF (Kobayashi et al., 2015).

In the study by Cavallo et al. (2014), PRP was compared to L-PRP, regarding the potential of inducing *in vitro* chondrocyte proliferation, concentration of growth factors (GFs) and production of cartilage matrix. L-PRP was demonstrated to present higher concentration of GFs. Both types of platelet concentrate induced chondrocyte proliferation, however PRP was associated with more expressive cell proliferation after seven days of cell culture. PRP-L induced higher levels of genic expression of hyaluronic acid synthase-2.

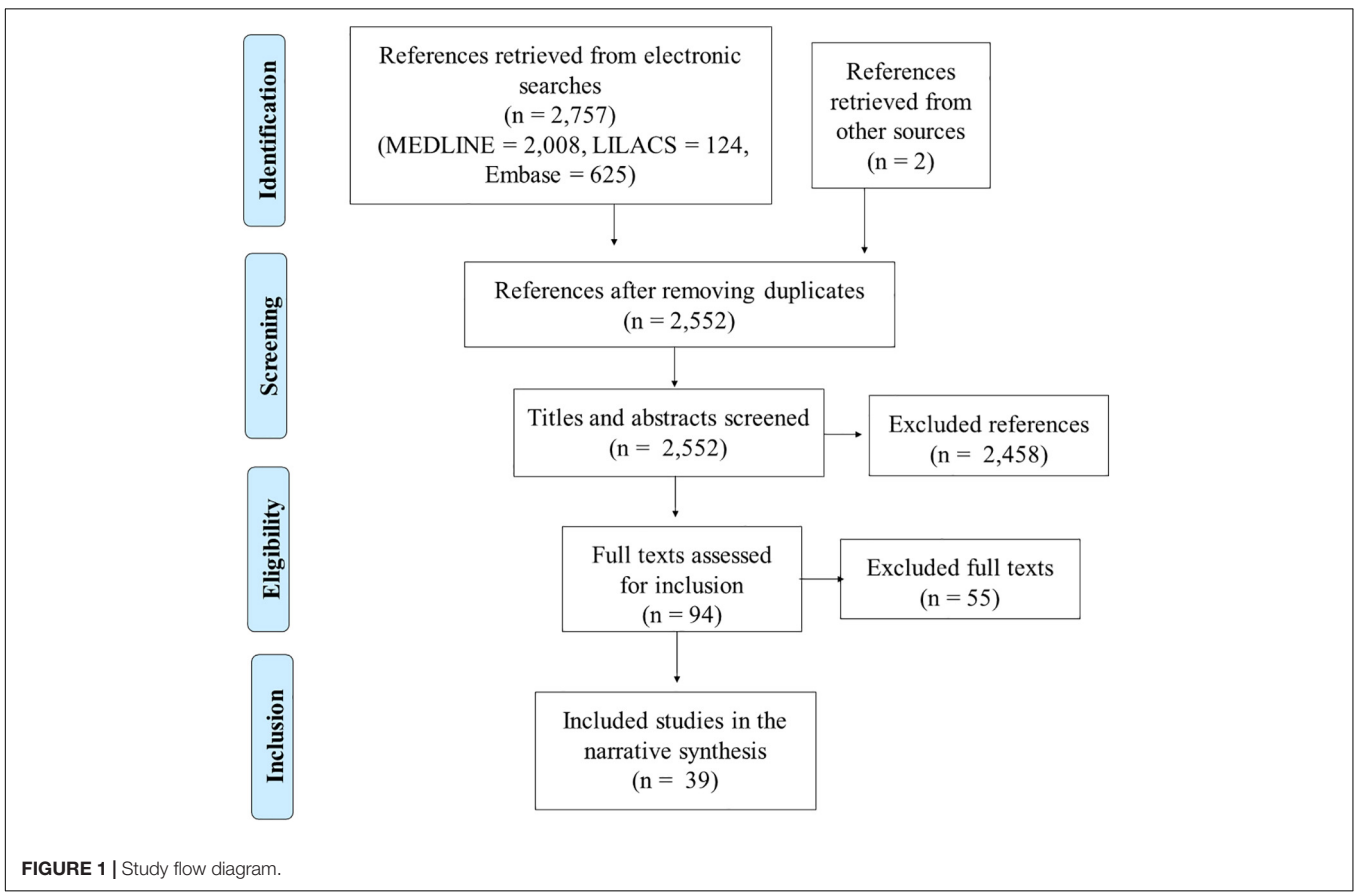

FIGURE 1 | Study flow diagram.

Mariani et al. (2015) compared PRP to L-PRP in relation to antimicrobial properties, after incubation assays with different pathogens. Both types of platelet concentrate inhibited bacterial growth during a four-hour period of incubation.

Kieb et al. (2017) compared PRP to PRP powder. PRP powder was obtained after sequential stages of depuration of cell components, leading to protein concentration of 30 g/ml. Platelet, leukocyte and GF concentrations were assessed. Both PRP and PRP powder presented higher concentration of GFs (VEGF, bFGF, PDGF-AB and TGF-b1), when compared to whole blood. PRP powder showed higher concentrations of these GF, when compared to PRP.

In the study by Kobayashi et al., PRF was compared to PRP in relation to concentration of GF and the angiogenic and healing effects (Kobayashi et al., 2015). Higher concentration of PDGF-BB was observed in PRP. Results for angiogenic GFs (VEGF and DLL1) were deemed inconsistent. The scratch assay showed better responses of healing for PRF. Similarly, PRF was considered superior regarding neovascularization.

Xian et al. (2015) compared the potential to induce keratinocyte and fibroblast differentiation for PRP with different concentrations (10% PRP and 20% PRP). Concentrations of GFs, cell viability and responses to the scratch assay were also assessed. Higher concentrations of HGF and VEGF-a were found in 10% PRP. Other GFs were not detected in neither of the two groups. Cell cultures with 10% PRP presented more abundant keratinocyte proliferation, however, cultures with 20% PRP showed more collagen fibers types I and III.

Comparisons between PRP with different GFs and platelet concentrations

Han et al. (2007) compared PRP with different concentrations of TGF-β1 and PDGF, by assessing its potential to induce proliferation of periodontal ligament cells. The effects on cell proliferation and differentiation occurred following a dose-response gradient, with an ideal concentration of TGF-β1determined to be in the range of 50 to 100 ng/ml. No increments were observed with concentrations higher than 100 ng/ml, suggesting a ceiling effect.

The ideal platelet concentration for activated and non-activated PRP, regarding the potential to induce mesenchymal cell proliferation, was addressed by Wang et al. (2018a) Proliferation cell was increasingly more pronounced for platelet concentration from 200.000/ml to 1.500.000/ml, but with no further increments above 1.500.000/ml, which reinforces the existence of a ceiling effect.

Commercial kits for PRP preparation

Four studies compared the performance of different commercial kits, regarding platelet, leukocytes and GF concentration and platelet activation (Castillo et al., 2011; Magalon et al., 2014; Degen et al., 2017; Fitzpatrick et al., 2017).

Castillo et al. (2011) compared three commercial kits for PRP preparation (MTF Cascade, Arteriocyte Magellan, and Biomet GPS III PRP), in relation to platelet, leukocyte concentrations and to the concentration of PDGF-AB, PDGF-BB, TGF-β1, and VEGF. There was no statistically significant difference in relation to platelet concentration across different types of commercial kits. However, leukocyte concentration was significantly lower for the MTF Cascade system, followed by the Arteriocyte Magellan system. PRP produced by the Biomet GPS III system presented the highest leukocyte concentrations. There were observed differences related to the concentration of PDGF-AB, PDGF-BB, and VEGF, with no differences in TGF-β1 concentration. Arteriocyte Magellan yielded PRP with statistically higher concentrations of PDGF-AB and PDGF-BB, when compared to MTF Cascade. PRP produced by Biomet GPS III presented the highest concentration of VEGF.

The performance of several systems was assessed by Degen et al. Commercial kits that were tested included Arteriocyte Magellan, Biomet GPS III, Arthrex Angel 2% and 7%, Emcyte Genesis CS and Harvest SmartPrep APC + (Degen et al., 2017). Centrifugation protocols varied across different commercial kits, respecting the recommendations of manufacturers. Outcomes assessed included platelet and leukocyte concentration and pH. Overall, there was no significant differences related to platelet concentration, except for the 7% Arthrex Angel system, which led to higher concentrations of platelets than Genesis CS (2,310,000 ± 524,000 vs. 1,129,000 ± 264,000/mm^3). In relation to leukocyte concentration, the observed variability did not reach statistical significance, with the exception of 2% Arthrex Angel, that showed statistically significant differences when compared to GPS III (11,000 ± 4,500 vs 27,300 ± 7,100/mm^3). The pH of PRP obtained with SmartPrep APC + was lower (6.95 ± 0.06) when compared to other systems (≥ 7.26 ± 0.06).

Fitzpatrick compared four commercial systems for PRP production (PS III, Smart-Prep2, Arteriocyte Magellan, and ACP), in relation to platelet and leukocyte concentration, pH and platelet activation (Fitzpatrick et al., 2017). ACP system was associated with lower platelet concentration (1 to 1.7 times basal values), when compared to the PS III, Smart-Prep2 and Arteriocyte Magellan systems, which were associated to increases in platelet concentration in the magnitude of 3 to 6 times of basal values. The only system associated with leukocyte reduction was the ACP system (1,300/mm^3; reduction of 5 to 22 times the basal values). The other systems were associated with increases in the concentration of leukocytes from 3 to 5 times the basal values. Mean pH of end product ranged between 6.59 (SmartPrep) to 7.05 (GPS). Lower levels of pH were associated with ACD-A.

In the study by Magalon et al., five systems were compared, two using a gel separation (SelphylSystem e RegenPRP), and three using centrifugation (Mini GPS III, Arthrex ACP, and the system developed in the laboratory study) (Magalon et al., 2014). Outcomes assessed included platelet, leukocyte and GF (VEGF, PDGF-AB, EGF, and TGF-b1) concentrations, and platelet activation. Mini GPS III System yielded higher platelet concentrations, when compared with the laboratory system, which by its turn was associated with higher platelet concentrations than the Regen PRP and Selphyl Systems. Mini GPS III and Regen PRP systems produced PRP with leukocyte concentration, as oppose to the Selphyl System, and the laboratory system, which led to leukocyte concentrations lower

than basal values. Mini GPS III System was associated with higher concentrations of VEGF and EGF.

Anticoagulant and antiaggregating agents employed during PRP preparation

Amaral et al. (2016) compared PRP obtained with different anticoagulants regarding the potential of inducing proliferation of mesenchymal cells. Anticoagulants employed were EDTA, sodium citrate and ACD-A. Outcomes assessed were platelet and GF (TGF-1 and VEGF) concentrations, mean platelet volume. PRP generated from blood samples collected with EDTA exhibited more platelets, followed by sodium citrate and ACD-A. The number of platelet cells obtained with sodium citrate was 16,3% lower in relation to the EDTA samples, while the number of platelets in ACD-A samples was 23% lower than EDTA and 8% lower than sodium citrate. However, mean platelet volume was higher in EDTA samples, which suggests alterations in platelet morphology and reduced cell viability. Despite these findings, no difference in relation to TGF-1 and VEGF concentrations. Sodium citrate samples were associated with less proliferation of mesenchymal cells.

Two protocols for PRP production were compared by Anitua et al., one called physiological protocol, with less anticoagulants (0.4 mL of trisodium citrate 3,8%) and less intense platelet activation to a conventional protocol (0,9 mL of trisodium citrate 3,8%) (Anitua et al., 2016). Therefore, two interventions were simultaneously applied, preventing estimates for each intervention in separate. Assessed outcomes were platelet concentration, platelet activation, GF concentration (TGFβ1, IGF-1, VEGF, and PDGF-AB), and induction of fibroblast proliferation. Physiological protocol was associated with higher platelet and GF concentration, although exhibiting less platelet activation.

The employ of anticoagulants (ACD-A or heparine), in isolation or combined to the antiaggregant PGE1, was assessed by Fukaya and Ito (2014) Two activation methods were employed (0,5% Triton X and calcium gluconate 8.5%), beyond a control group with no activation. Assessed outcomes included platelet and PDGF-BB concentrations. In relation to platelet concentration, results were inconsistent across different samples, preventing conclusions. Both for inactivated and calcium-gluconate activated PRP, higher PDGF-BB concentrations were obtained with the concomitant utilization of ACD-A and PGE1. Results for PRP activated by Triton X were inconsistent across tested samples.

Kraus et al. (2018) compared ACD-A to sodium citrate, in relation to platelet concentration and morphology, through automatized analysis. The utilization of ACD-A was associated with higher platelet concentration, as well as with evidence of a more intense platelet activation, when compared to the employ of sodium citrate.

Other study compared three different types of EDTA, sodium citrate and ACD-A during PRP production for alopecia treatment in males (Singh, 2018). Platelet concentration and morphology were assessed, however clinical outcomes were not reported. Platelet concentration was higher in ACD-A samples (310%), when compared to EDTA (110%), or sodium citrate (100%) ($p < 0{,}001$). Morphological aspects, such as size, shape and the activation pattern, were more preserved in ACD-A samples.

Methods for activation

Lachert et al. (2011) compared GF concentration in PRP and in platelet gel, before and after thawing. Platelet gel was obtained by activating PRP with thrombin solution. TGF β1 concentration was 7 to 9 times higher in platelet gel. Higher concentrations were obtained after thawing. The same finding was observed in relation to PDGF-AB concentrations.

Lee et al. (2013) compared inactivated PRP to PRP activated by lyophilized thrombin plus calcium chloride. Assessed outcomes were GF (PDGF-AB, PDGF-BB and TGF-β) concentrations. There were no statistically significant differences related to GF concentrations between activated and inactivated PRP.

Vahabi et al. (2017) compared the effects of PRP activated by 10% calcium gluconate to inactivated PRP, in relation to the potential to induce fibroblasts and osteoblasts proliferation *in vitro*. Activated PRP was associated with more intense cell proliferation, with statistically significant results.

In the study by Anitua et al. (2016) two different protocols for PRP production were compared, namely the physiological protocol, employing lower quantities of anticoagulants and activators, and the conventional protocol. Due to the combined employment of interventions, separate estimates for each intervention were not possible. PGRF-Endoret was the activation substance in both study arms, with varying concentrations (20 microl/ml in the physiological protocol and 50 microl/ml in the conventional protocol). The physiological protocol was associated with higher platelet and GF concentrations, but with lower platelet activation.

Sadeghi-Ataabadi et al. (2017) compared different concentrations of calcium chloride (2.5; 5 and 10%) to activate PRP. Authors assessed the properties of the fibrine matrix and the potential to induce fibroblast proliferation. Higher rates of cell adhesion and cell proliferation were obtained with 2.5% calcium chloride. Cultures with PRP activated by 10% calcium chloride presented cells with fusiform morphology and a parallel configuration of stress fibers, while cultures with PRP activated with lower concentrations of calcium chloride showed typical fibroblast cells and stress fibers distributed in a net configuration.

Cavallo et al. (2016) compared 10% calcium chloride, 10% autologous thrombin, calcium chloride plus autologous thrombin, or 10% type I collagen. Assessed outcomes included concentrations of VEGF, TGF-β1 and PDGF-AB. Activation by collagen type I was associated with an overall reduction of GF concentrations. PRP activated by thrombin, calcium chloride plus autologous thrombin, and 10% type I collagen showed an immediate release of PDGF, and a progressive pattern of VEGF release along the period from 15 min to 24 h. Calcium chloride was associated with a progressive release of all GFs, with release starting from 15 min after activation up to 24 h.

Çetinkaya et al. (2016) compared activation by freezing to 10% calcium gluconate. Freezing temperature was −80°C for 24 h. Assessed outcomes included IGF-1, PDGF-BB, and βFGF concentrations. There was statistically significant difference related to PDGF concentration, favoring activation

by freezing. There were no statistically significant differences concerning other GFs.

Thermal methods of activation were compared to activation with thrombin in the study by Du et al. (2018). The thermal protocol consisted in centrifugation under 4oC, with subsequent reheating to 37oC. Assessed outcomes included platelet count, GF (VEGF, PDGF-AB, PDGF-BB, TGF-α, βFGF, EGF and IGF) concentration. Platelet concentration was significantly higher with PRP activated by thermal methods. The pattern of GF release was considered more stable in samples activated with the thermal protocol.

Tunali et al. (2014) compared activation by the employ of titanium tubes to PRP with no activation, having assessed the histological properties of the fibrin net. Titanium activation was associated with larger fibrin nets.

Two studies compared the effects of activated and non-activated PRP on clinical outcomes. In the study conducted by Gentile et al. (2017) one group of participants with androgenetic alopecia were treated with autologous non-activated PRP and the other group was treated with calcium-activated PRP. Both activated and non-activated PRP groups presented increases in epidermal thickness and number of follicles, but concentrations of PDGF-BB, TGF-β1, and VEGF were higher in activated PRP. In Gentile et al. (2020), participants with androgenetic alopecia received activated and non-activated PRP. Short-term results in trichoscopy with non-activated PRP were more expressive than those observed in the activated-PRP group. This difference was statistically significant ($p < 0.01$). Long-term results of hair density also favored non-activated PRP (Gentile and Garcovich, 2020a).

Centrifugation protocols

Single versus double centrifugation. Single centrifugation protocol was compared to double centrifugation for PRP production in the study by Carofino et al. (2012). Single centrifugation protocol consisted in centrifugation under 1,500 rpm for 5 min. Double centrifugation involved a first centrifugation under 1,500 rpm for 5 min, followed by a second centrifugation under 6,300 rpm for 20 min. Centrifugal force was not reported. Assessed outcomes included platelet and leukocyte concentrations. Single protocol resulted in platelet concentration 3.6 times the basal values, while the double protocol resulted in increases of 3.3 times the basal values. Double centrifugation protocol was associated with lower leukocyte concentrations.

Mazzocca et al. (2012) compared three centrifugation protocols, in relation to platelet, leukocyte and GF (VEGF, HGF, IGF-1 and PDGF-AB) concentration and in relation to the potential to induce proliferation of human bone and muscle cells. Protocol 1 consisted in a single centrifugation under 500 rpm for 5 min. Protocol 2 involved a single centrifugation under 3200 rpm for 15 min. Protocol 3 involved two centrifugations, the first under 1500 rpm for 5 min, and the one under 6,300 rpm for 20 min. Centrifugal forces were not reported.

Protocol 2 was associated with higher platelet counts when compared to protocols 1 and 3. There was no statistically significant differences between protocols 1 and 3. Protocol 2 also resulted in the highest leukocyte counts (20,500 ± 6,700/mm^3), while Protocol 1resulted in lowest leukocyte counts (600 ± 300/mm^3). Protocol 3 resulted in intermediate values for leukocyte counts (1,700 ± 1,800/mm^3), with values lower than those in whole blood (5,600 ± 1,700/mm^3). Protocol 2 was the most effective in obtaining higher GF concentrations, with exception of VEGF-A. Protocol 1 was associated to higher concentrations of HGF, IGF-1 and PDGF-AB, in comparison to Protocol 3. Protocol 3 was more effective in inducing osteoblast proliferation, with no differences between Protocols 1 and 2. There was no difference across the three protocols in relation to myocyte or tenocyte proliferation.

Pochini et al. compared a single centrifugation protocol to two commercial kits employing double centrifugation, namely the Magellan and the GPSIII systems, in relation to platelet, leukocyte and GF (FGF-2 e TGF-beta1) concentrations (de Pochini et al., 2016). Both systems are associated with high leukocyte concentrations in the end product. The single centrifugation protocol consisted in applying a centrifugal force of 650 *g* for 8 min. The protocols of double centrifugation were performed as recommended by each manufacturer. The single-centrifugation protocol was associated with higher concentrations of TGF-β1, but with a lower concentration of FGF-2, when compared to both double-centrifugation protocols. The platelet concentrations obtained by the employ of the Magellan system was 2.7 (CI95% 2.11-3.95) times higher than those of samples processed with the GPSIII system. PRP obtained by the employ of the single-centrifugation protocol presented the lowest platelet concentrations. The GPSIII system was associated with the highest leukocyte concentrations, followed by the Magellan system.

Tamimi et al. (2007) compared a single-centrifugation protocol to double centrifugation for the prepare of PRP gel (Tamimi et al., 2007). Single centrifugation protocol consisted in applying 280g (1500 rpm) for seven minutes. The double centrifugation protocol consisted in applying 160 *g* (1300 rpm) for 10 min during the first centrifugation, followed by a second centrifugation of 400 *g* for 10 min. Platelet count and the ultrastructural analysis of PRP gel were assessed. Higher platelet concentrations were observed with the employ of the double-centrifugation protocol (352% of basal values), in comparison with single centrifugation (232% of basal values). However, the double-centrifugation protocol was associated with ultrastructure alterations of PRP gel, with fibrin agglutination.

Three centrifugation protocols for PRP processing were compared in the study by Kutlu et al. (2013) Protocol 1 employed single centrifugation at 43 *g* (1000 rpm) for 10 min. Protocol 2 employed double centrifugation, with the first at 103 g (2400 rpm) for 10 minutes and the second at 230 *g* (3600 rpm) for 15 min. Protocol 3 employed a first centrifugation at 129 *g* (3000 rpm) for three minutes and the second at 129 *g* (3000 rpm) for 13 min. PRP obtained by double-centrifugation protocols (Protocols 2 and 3) were associated with higher platelet concentrations. There was no statistically significant difference between Protocol 2 and 3.

Centrifugal forces. Kececi et al. (2014) employed a double-centrifugation protocol, by varying the centrifugal forces during

the second centrifugation. The first centrifugation was performed at 250 *g* for 10 min. The second centrifugation was performed at 300, 500, 750, 1000, 1500, and 2000 *g* for 10 min. Platelet concentrations increased as centrifugal forces raised from 300 to 2000 *g*. The magnitude of increases was of 1.92, 2.16, 2.80, 3.48, 3.67, and 3.76 times basal values for centrifugal forces of 300, 500, 750, 1000, 1500, and 2000 *g*, respectively.

Ehrenfest et al. compared four commercial centrifuges (original L-PRF centrifuge®, A-PRF 12®, Salvin 1310® and LW -UPD8®) for the processing of L-PRF (Ehrenfest et al., 2018). All samples were centrifuged once at 400 *g* for 12 min. Cell morphology and features of the fibrin matrix were assessed. The PRF obtained with the Intra-Spin® centrifuge showed a highly polymerized fibrin matrix, with thick fibrin fibers and cells presenting physiological morphology. The other centrifuges produced PRF with thinner fibrin fibers, and irregular body cells with reduced dimensions.

In the study by Perez et al. (2014) the effects of varying centrifugal forces in both stages of double-centrifugation protocols were investigated. First centrifugation applied centrifugal forces ranging from 50 to 820 *g* (50, 70, 100, 190, 280, 370, 460, 550, and 820) for 10 min. The second centrifugation applied forces of 200, 400, 800, 1200, and 1600 *g* for 10 min, after a standard first centrifugation at 100 *g* for 10 min. Authors assessed platelet concentrations and platelet integrity. For the first centrifugation, greatest platelet concentrations were observed between 70 to 100 *g*, with decreases being observed above 190 *g*. The recovery rate of leukocytes ranged between 5 to 10%, independently of the centrifugal force applied during the second centrifugation. The most effective protocol for optimizing platelet concentration (5 times the basal values) was the double-centrifugation protocol, at 100 *g* for 10 min during the first centrifugation, followed by a second centrifugation at 400 *g* for 10 min. This protocol was also associated with platelet integrity.

Duration of centrifugation. Eren et al. (2016) compared 10 to 12-minute centrifugation for PRF processing, in relation to GF concentrations and cell composition of the end product. A single-centrifugation protocol at 400 *g* (2660 rpm) for 10 or 12 min was applied. The analyses carried out at 24 and 72 h showed higher concentration of VEGF, in samples obtained with the 12-min centrifugation protocol. The duration of the centrifugation did not influence the concentration of PDGF and TGF-ß or the platelet concentration.

Yin et al. compared double-centrifugation protocols, by applying different durations and forces of centrifugation in both stages (Yin et al., 2017). The assessed outcomes included platelet function and the potential to induce proliferation of mesenchymal cells. First centrifugations were performed at 10 *g* for 15min; 110 *g* for 15min; 130 *g* for 10 min; 130 *g* for 15 min; 160 *g* for 10 min; 160 *g* for 15 min; or 180 *g* for 10 min. Second centrifugation was performed at 80 *g* for 10 min; 180 *g* for 15 min; 250 *g* for 10 min; 250 *g* for 15 min; 450 *g* for 10 min; or 450 *g* for 15 min. Results indicated that a first centrifugation at 160 *g* for 10 min, followed by a second centrifugation at 250 *g* for 15 min led to the highest platelet and GF concentration, with preservation of the platelet function ($P < 0.05$). PRP obtained under these conditions induced more proliferation and migration of mesenchymal cells ($P < 0.05$), but with no impact over cell survival.

Duration of PRP processing time. Abu Kasim and Al-Hassan (2016) compared processing times for PRP produced at room temperature. PRP obtained with an 8-h processing time was compared to samples processed along 24 h. Platelet and leukocyte counts, platelet activation, and pH were assessed. PRP prepared along the 24-h period exhibited lower leukocyte concentrations. Differences in pH were observed, with lower pH for samples prepared in 24 h (pH = 7.3 ± 0,05), when compared to 8-hour samples (pH = 7,4 ± 0,13) ($p < 0.001$). Authors concluded that the differences were not clinically relevant, however no microbiological testing was performed to guarantee lack of contamination.

Storage conditions. The utilization of residual plasma at 20 to 24°C after centrifugation with glucose additive solution at room temperature for storing PRP was evaluated in the study by Alhumaidan et al. (2011). Authors assessed platelet and leukocyte counts, and platelet morphology. There were no differences related to platelet or leukocyte counts. Samples stored in the glucose additive solution presented more physiological morphology, when compared to the storage in residual plasma.

Combined use of PRP and other substances. Carofino et al. (2012) assessed the utilization of PRP in isolation or simultaneously to lidocaine 1%, bupivacaine 0.5%, and methylprednisolone, in relation to the potential to induce tenocyte proliferation (Carofino et al., 2012). All three substances resulted in less tenocyte proliferation (p = 0,05), with more pronounced reductions observed lidocaine and bupivacaine.

The influence of two types of iodinated contrast on the PRP characteristics were assessed in one study, considering that iodinated contrasts are frequently employed to guide intra-articular application of PRP (Dallaudiere et al., 2018). Assessed outcomes were platelet concentration, percentage of platelet aggregation, and platelet activation. Iodinated contrasts employed were Iodixanol and Iopamidol. There were no differences between PRP in isolation to PRP in association with both types of contrasts.

The association of PRP to hyaluronic acid in relation to final TGF-b1 and PDGF-AA concentration was assessed in another study. Release of TGF-b1 and PDGF-AA on the fifth day were greater with PRP combined to hyaluronic acid.

Most important results are synthesized in **Supplementary Table 2**.

DISCUSSION

Our results reflect the great variability embed in each step necessary for the preparation of PRP and related products, from the choice of anticoagulants during blood collection to the use of activation methods.

Studied anticoagulants included EDTA, ACD-A and sodium citrate. The employ of ACD-A was associated

to the preservation of platelet morphology, with no effects on GF concentrations. Sodium citrate was associated with greater induction of proliferation of mesenchymal cells.

Double-centrifugation protocols was associated with higher platelet concentrations and to the decrease of leukocyte concentrations. However, these protocols are associated with lower concentrations of GFs, such as HGF, IGF-1 and PDGF-AB, probably by the loss of GFs contained within leukocytes. For PRP gel, double-centrifugation protocols lead to ultrastructural alterations of the fibrin net and fibrin agglutination.

The duration of the centrifugation time has also been shown to influence the concentration of at least some GFs. Centrifugation at 400 *g* for 12 min seems to be superior to 400 *g* for 10 min, regarding the concentration of VEGF. The same was observed in relation to the centrifugal force. For double-centrifugation protocols, the optimal centrifugal force for the first centrifugation seems to range between 70 to 100 *g*. For the second step, centrifugation at 2000 *g* for 10 min result in a platelet concentration 3.76 times greater than the basal values. When platelet integrity and viability were considered, the optimal centrifugation protocol was at 100 *g* for 10 min for the first centrifugation, followed by a second centrifugation at 400 *g* for 10 min.

Commercial kits currently available for PRP preparation employ different protocols of centrifugation, and therefore, variability in the characteristics of the end product are expected. Indeed, the platelet concentration ranged from 1.7 to 6 times the basal values, across kits from different manufacturers. In relation to the time of PRP processing, one study compared 24-h to 8-h processing time. No differences were observed in relation to platelet concentrations; however, microbiological tests were not performed to ensure the safety of extending the processing time.

Activation of PRP by calcium gluconate 10% was associated with greater potential of inducing osteoblast and fibroblast proliferation, but not to higher platelet or GF concentrations in some studies. Thermal activation seems to be a viable alternative, being associated with higher platelet concentrations, when compared to the activation by calcium gluconate 10%. For PRF processing, the employ of titanium tubes as an activation method was associated to more extensive fibrin net.

Concomitant application of PRP to lidocaine, bupivacaine and methylprednisolone was found to impact the expected biological action of PRP, therefore, caution should be taken when considering the combined use of these substances. The same was not observed with iodinated contrasts, commonly used to guide intra-articular injections, or with hyaluronic acid, that may even have a synergic effect, increasing GF release.

All this variability in PRP processing imposes one further question, related to definition of the ideal characteristics of PRP, in terms of the optimal platelet and GF concentrations. Some of the included studies point to a dose-response effect between the platelet and GF concentrations and the expected biological effects of PRP, with a ceiling effect.

To the best of our knowledge, this is the first attempt to review comparative studies that focused on different methods for each stage of PRP processing. In the systematic review conducted by Gentile et al. focusing on optimal concentration of PRP, results shown that higher concentrations of PRP may be associated with a significant decline in cell proliferation (Gentile and Garcovich, 2020b), which stresses the need for standardization of procedures in this regard. In other systematic review, recently conducted by Chahla et al. (2017) studies in which PRP was used for musculoskeletal conditions were assessed in relation to the reporting of the applied methods for PRP processing or of the composition of the final product. Authors found that only 10% of studies provided a clear description of the preparation protocol and only 16% provided quantitative parameters on the final composition of PRP.

The major limitation of the present study refers to the need of analyzing each step of the production process independently. We acknowledge that PRP production is a sequential process, rather than a combination of independent steps, but a framework to explore all types of results presented in included studies was needed. As most included studies assessed a single step in the process rather than sequential processes, the applied framework was built to reflect how comparative research in the field is being developed. Our scoping review did not embrace all sources of diversity related to the preparation and administration of platelet-rich plasma, but the reason for this was the fact that we did not identify any study comparing different techniques for certain steps of the production process. As our study included only comparative research, it was not possible to present evidence or draw conclusions on questions such as the use of handmade techniques in comparison to use of commercial kits, or the effects of light activation versus other methods of activation. Similarly, we did not find comparative research on the influence of red blood cell or peripheral blood mononuclear cells or on the role of image guidance during the application of platelet concentrates.

Protocols for PRP production should be clearly defined for each stage of processing, in accordance with desired biological effects. All studies included in this review focused on laboratorial outcomes, such as platelet, leukocyte, and GF concentrations, or on the potential to stimulate cell proliferation. The choice of this type of outcome relies on feasibility issues, however, the lack of clinical trials comparing PRP obtained from different methods precludes ultimate conclusions about the definition of best methods for PRP processing, under the perspective of efficacy, effectiveness and safety. This conundrum becomes even more complex, considering the vast universe of clinical situations for which PRP has been used. It is logical to assume that the ideal characteristics of PRP should differ in relation to platelet, leukocyte and GF concentration, for each type of clinical situation.

CONCLUSION

Evidences found in this scoping review showed great variability related to methods for different stages of PRP processing, such as choice of anticoagulants during blood collect, centrifugation protocols, employ of activation methods, among others. This variability may justify the variability of clinical effects of PRP across different clinical trials.

AUTHOR CONTRIBUTIONS

DP, ÂB, and RR developed the study protocol, performed searches, screened references, performed narrative synthesis, and developed the first draft. AA and AM-J participated in the protocol elaboration and revised the manuscript. All authors contributed to the article and approved the submitted version.

FUNDING

Projeto de Apoio ao Desenvolvimento Institucional do Sistema Único de Saúde (PROADI–SUS), Hospital Sírio-Libanês and the Brazilian Ministry of Health

ACKNOWLEDGMENTS

The authors are thankful to João Batista da Silva Júnior and to Christiane da Silva Costa, from ANVISA, for their valuable comments along the conduction of this review.

SUPPLEMENTARY MATERIAL

The Supplementary Material for this article can be found online at: https://www.frontiersin.org/articles/10.3389/fcell.2020.598816/full#supplementary-material

REFERENCES

Abu Kasim, H., and Al-Hassan, F. (2016). Assessment of platelet concentrate prepared from fresh and overnight held whole blood. *Asian J. Pharm. Clin. Res.* 9, 16–20. doi: 10.22159/ajpcr.2016.v9i6.11715

Albanese, A., Licata, M. E., Polizzi, B., and Campisi, G. (2013). Platelet-rich plasma (PRP) in dental and oral surgery: from the wound healing to bone regeneration. *Immun. Ageing* 10:3. doi: 10.1186/1742-4933-10-23

Alhumaidan, H., Cheves, T., Holme, S., and Sweeney, J. D. (2011). Manufacture of pooled platelets in additive solution and storage in an ELX container after an overnight warm temperature hold of platelet-rich plasma. *Am. J. Clin. Pathol.* 136, 638–645. doi: 10.1309/AJCPFD87THDWCSVA

Amaral, R., Silva, N., Haddad, N., Lopes, L., Ferreira, F., Bastos Filho, R., et al. (2016). Platelet-Rich plasma obtained with different anticoagulants and their effect on platelet numbers and mesenchymal stromal cells behavior in vitro. *Stem Cells Int.* 2016:7414036. doi: 10.1155/2016/7414036

Anitua, E., Prado, R., Troya, M., Zalduendo, M., de la Fuente, , M., Pino, A., et al. (2016). Implementation of a more physiological plasma rich in growth factor (PRGF) protocol: anticoagulant removal and reduction in activator concentration. *Platelets* 27, 459–466. doi: 10.3109/09537104.2016.1143921

Arksey, H., and Malley, L. O. (2005). Scoping studies: towards a methodological framework. *Int. J. Soc. Res. Methodol.* 8, 19–32. doi: 10.1080/1364557032000119616

Bielecki, T., Ehrenfest, D. M. D., Everts, P. A., and Wiczkowski, A. (2012). The role of leukocytes from L-PRP / L-PRF in wound healing and immune defense: new perspectives. *Curr. Pharm. Biotechnol.* 13, 1153–1162. doi: 10.2174/138920112800624373

Carofino, B., Chowaniec, D. M., McCarthy, M. B., Bradley, J. P., Delaronde, S., Beitzel, K., et al. (2012). Corticosteroids and local anesthetics decrease positive effects of platelet-rich plasma: an in vitro study on human tendon cells. *Arthroscopy* 28, 711–719. doi: 10.1016/j.arthro.2011.09.013

Castillo, T. N., Pouliot, M. A., Kim, H. J., and Dragoo, J. L. (2011). Comparison of growth factor and platelet concentration from commercial platelet-rich plasma separation systems. *Am. J. Sports Med.* 39, 266–271. doi: 10.1177/0363546510387517

Cavallo, C., Filardo, G., Roffi, A., Kon, E., Marcacci, M., Desando, G., et al. (2014). Platelet-rich plasma to stimulate cartilage healing, which product? a comparative in vitro study. *Osteoarthr. Cartil.* 22:S487. doi: 10.1016/j.joca.2014.02.926

Cavallo, C., Roffi, A., Grigolo, B., Mariani, E., Pratelli, L., and Merli, G. (2016). Platelet-Rich plasma: the choice of activation method affects the release of bioactive molecules. *BioMed. Res. Int.* 2016:6591717. doi: 10.1155/2016/6591717

Çetinkaya, R. A., Eker, I., Yilmaz, S., Ünlü, A., Pekel, A., Sağkan, R. I., et al. (2016). A new method for activating platelets in platelet-rich plasma to use in regenerative medicine: a cycle of freezing and thawing. *Rev. Haematol.* 101:646.

Chahla, J., Cinque, M. E., Piuzzi, N. S., Mannava, S., Geeslin, A. G., Murray, I. R., et al. (2017). A call for standardization in platelet-rich plasma preparation protocols and composition reporting. *J. Bone Jt. Surg.* 99, 1769–1779. doi: 10.2106/JBJS.16.01374

Dallaudiere, B., Crombé, A., Gadeau, A. P., Pesquer, L., Peuchant, A., James, C., et al. (2018). Iodine contrast agents do not influence platelet-rich plasma function at an early time point in vitro. *J. Exp. Orthop.* 5:47. doi: 10.1186/s40634-018-0162-164

de Pochini, A. C., Antonioli, E., Bucci, D. Z., Sardinha, L. R., Andreoli, C. V., Ferretti, M., et al. (2016). Analysis of cytokine profile and growth factors in platelet-rich plasma obtained by open systems and commercial columns. *Einstein (Sao Paulo)* 14, 391–397. doi: 10.1590/S1679-45082016AO3548

Degen, R. M., Bernard, J. A., Oliver, K. S., and Dines, J. S. (2017). Commercial separation systems designed for preparation of platelet-rich plasma yield differences in cellular composition. *HSS J.* 13, 75–80. doi: 10.1007/s11420-016-9519-9513

DeLong, J., Russel, R., and Mazzocca, A. (2012). Platelet-Rich plasma: the PAW classification system. *Arthroscopy* 28, 998–1009. doi: 10.1016/j.arthro.2012.04.148

Du, L., Miao, Y., Li, X., Shi, P., and Hu, Z. (2018). A novel and convenient method for the preparation and activation of prp without any additives: temperature controlled PRP. *Biomed Res. Int.* 2018:1761865. doi: 10.1155/2018/1761865

Ehrenfest, D. M., Pinto, N. R., Pereda, A., Jiménez, P., Corso, M., Del, et al. (2018). The impact of the centrifuge characteristics and centrifugation protocols on the cells, growth factors, and fibrin architecture of a leukocyte- and platelet-rich fibrin (L-PRF) clot and membrane. *Platelets* 29, 171–184. doi: 10.1080/09537104.2017.1293812

Ehrenfest, D. M. D., Andia, I., Zumstein, M. A., Zhang, C., Pinto, N. R., and Bielecki, T. (2014). Classification of platelet concentrates (Platelet-Rich Plasma-PRP. Platelet-Rich Fibrin-PRF) for topical and infiltrative use in orthopedic and sports medicine: current consensus, clinical implications and perspectives. *Muscles. Ligaments Tendons J.* 4, 3–9.

Ehrenfest, D. M. D., Bielecki, T., Del Corso, M., Inchingolo, F., and Sammartino, G. (2010). Shedding light in the controversial terminology for platelet-rich products: platelet-rich plasma (PRP), platelet-rich fibrin (PRF), platelet-leukocyte gel (PLG), preparation rich in growth factors (PRGF), classification and commercial. *J. Biomed. Mater. Res.* 95A, 1280–1282. doi: 10.1002/jbm.a.32894

Eren, G., Gürkan, A., Atmaca, H., Dönmez, A., and Atilla, G. (2016). Effect of centrifugation time on growth factor and MMP release of an experimental

platelet-rich fibrin-type product. *Platelets* 27, 427–432. doi: 10.3109/09537104.2015.1131253

Fitzpatrick, J., Bulsara, M. K., McCrory, P. R., Richardson, M. D., and Zheng, M. H. (2017). Analysis of platelet-rich plasma extraction: variations in platelet and blood components between 4 common commercial kits. *Orthop. J. Sport. Med.* 5:2325967116675272. doi: 10.1177/2325967116675272

Fukaya, M., and Ito, A. (2014). A new economic method for preparing platelet-rich plasma. *Plast. Reconstr. surgery. Glob. open* 2:e162. doi: 10.1097/GOX.0000000000000109

Gentile, P., Calabrese, C., De Angelis, B., Dionisi, L., Pizzicannella, J., Kothari, A., et al. (2020). Impact of the different preparation methods to obtain autologous non-activated platelet-rich plasma (A-PRP) and activated platelet-rich plasma (AA-PRP) in plastic surgery: Wound healing and hair regrowth evaluation. *Int. J. Mol. Sci.* 21:431. doi: 10.3390/ijms21020431

Gentile, P., Cole, J. P., Cole, M. A., Garcovich, S., Bielli, A., Scioli, M. G., et al. (2017). Evaluation of not-activated and activated PRP in hair loss treatment: role of growth factor and cytokine concentrations obtained by different collection systems. *Int. J. Mol. Sci.* 18:408. doi: 10.3390/ijms18020408

Gentile, P., and Garcovich, S. (2020a). Autologous activated platelet-rich plasma (AA-PRP) and non-activated (A-PRP) in hair growth: a retrospective, blinded, randomized evaluation in androgenetic alopecia. *Expert Opin. Biol. Ther.* 20, 327–337. doi: 10.1080/14712598.2020.1724951

Gentile, P., and Garcovich, S. (2020b). Systematic review-The potential implications of different platelet-rich plasma (Prp) concentrations in regenerative medicine for tissue repair. *Int. J. Mol. Sci.* 21:5702. doi: 10.3390/ijms21165702

Giusti, I., Rughetti, A., D'Ascenzo, S., Millimaggi, D., Pavan, A., Dell'Orso, L., et al. (2009). Identification of an optimal concentration of platelet gel for promoting angiogenesis in human endothelial cells. *Transfusion* 49, 771–778. doi: 10.1111/j.1537-2995.2008.02033.x

Han, J., Meng, H. X., Tang, J. M., Li, S. L., Tang, Y., and Chen, Z. B. (2007). The effect of different platelet-rich plasma concentrations on proliferation and differentiation of human periodontal ligament cells in vitro. *Cell Prolif.* 40, 241–252. doi: 10.1111/j.1365-2184.2007.00430.x

Kececi, Y., Ozsu, S., and Bilgir, O. (2014). A cost-effective method for obtaining standard platelet-rich plasma. *Wounds a Compend. Clin. Res. Pract.* 26, 232–238.

Kieb, M., Sander, F., Prinz, C., Adam, S., Mau-Möller, A., Bader, R., et al. (2017). Platelet-Rich plasma powder: a new preparation method for the standardization of growth factor concentrations. *Am. J. Sports Med.* 45, 954–960. doi: 10.1177/0363546516674475

Kobayashi, M., Kawase, T., Okuda, K., Wolff, L. F., and Yoshie, H. (2015). In vitro immunological and biological evaluations of the angiogenic potential of platelet-rich fibrin preparations: a standardized comparison with PRP preparations. *Int. J. Implant Dent.* 1:31. doi: 10.1186/s40729-015-0032-0

Kraus, M., Neeb, H., and Strasser, E. (2018). ACD vs. sodium-citrate as an anticoagulant for platelet rich plasma (PRP) preparation influences the extent of platelet shape change during spreading-quantitative morphometric data from standardized robotic darkfield microscopy. *Hamostaseologie* 38, A66–A67. doi: 10.1055/s00034925

Kutlu, B., Tiğlı Aydın, R. S., Akman, A. C., Gümüşderelioglu, M., and Nohutcu, R. M. (2013). Platelet-rich plasma-loaded chitosan scaffolds: preparation and growth factor release kinetics. *J. Biomed. Mater. Res. B. Appl. Biomater.* 101, 28–35. doi: 10.1002/jbm.b.32806

Lachert, E., Misiak, A., Antoniewicz-Papis, J., Kubis, J., Tomaszewska, A., Janik, K., et al. (2011). Evaluation of the concentration of platelet growth factors in platelet concentrate (PC), the basic component of platelet-gel. *Vox Sang.* 101:47.

Lana, J. F. S. D., Purita, J., Paulus, C., Huber, S. C., Rodrigues, B. L., Rodrigues, A. A., et al. (2017). Contributions for classification of platelet rich plasma - proposal of a new classification: MARSPILL. *Regen. Med.* 12, 565–574. doi: 10.2217/rme-2017-0042

Lee, J. W., Kwon, O. H., Kim, T. K., Cho, Y. K., Choi, K. Y., Chung, H. Y., et al. (2013). Platelet-rich plasma: quantitative assessment of growth factor levels and comparative analysis of activated and inactivated groups. *Arch. Plast. Surg.* 40, 530–535. doi: 10.5999/aps.2013.40.5.530

Levac, D., Colquhoun, H., and O'Brien, K. K. (2010). Scoping studies: advancing the methodology. *Implement. Sci.* 5:69. doi: 10.1186/1748-5908-5-69

Li, F.-X., Li, Y., Qiao, C.-W., Zhu, J., Chen, J., and Zhang, P.-Y. (2017). Topical use of platelet-rich plasma can improve the clinical outcomes after total knee arthroplasty: a systematic review and meta-analysis of 1316 patients. *Int. J. Surg.* 38, 109–116. doi: 10.1016/j.ijsu.2016.12.013

Magalon, J., Bausset, O., Serratrice, N., Giraudo, L., Aboudou, H., Veran, J., et al. (2014). Characterization and comparison of 5 platelet-rich plasma preparations in a single-donor model. *Arthroscopy* 30, 629–638. doi: 10.1016/j.arthro.2014.02.020

Magalon, J., Chateau, A. L., Bertrand, B., Louis, M. L., Silvestre, A., Giraudo, L., et al. (2016). DEPA classification: a proposal for standardising PRP use and a retrospective application of available devices. *BMJ Open Sport Exerc. Med.* 2:e000060. doi: 10.1136/bmjsem-2015-000060

Mariani, E., Canella, V., Berlingeri, A., Bielli, A., Cattini, L., Landini, M. P., et al. (2015). Leukocyte presence does not increase microbicidal activity of platelet-rich plasma in vitro. *BMC Microbiol.* 15:149. doi: 10.1186/s12866-015-0482-489

Martinez-Zapata, M. J., Martí-Carvajal, A. J., Solà, I., Expósito, J. A., Bolíbar, I., Rodríguez, L., et al. (2016). Autologous platelet-rich plasma for treating chronic wounds. *Cochrane Database Syst. Rev.* 25:CD006899. doi: 10.1002/14651858.CD006899.pub3

Marx, R. E. (2004). Platelet-Rich plasma: evidence to support its use. *J. Oral. Maxillofac. Surg.* 62, 489–496. doi: 10.1016/j.joms.2003.12.003

Mazzocca, A. D., McCarthy, M. B. R., Chowaniec, D. M., Cote, M. P., Romeo, A. A., Bradley, J. P., et al. (2012). Platelet-rich plasma differs according to preparation method and human variability. *J. Bone Joint Surg. Am.* 94, 308–316. doi: 10.2106/JBJS.K.00430

Ouzzani, M., Hammady, H., Fedorowicz, Z., Elmagarmid, A., Chalmers, T., Smith, H., et al. (2016). Rayyan—a web and mobile app for systematic reviews. *Syst. Rev.* 5:210. doi: 10.1186/s13643-016-0384-384

Perez, A. G. M., Lana, J. F. S. D., Rodrigues, A. A., Luzo, A. C. M., Belangero, W. D., and Santana, M. H. A. (2014). Relevant aspects of centrifugation step in the preparation of platelet-rich plasma. *ISRN Hematol.* 2014:176060. doi: 10.1155/2014/176060

Robins, R. J. (2017). Platelet rich plasma: current indications and use in orthopaedic care. *Med. Res. Arch.* 5, 1–17. doi: 10.18103/mra.v5i6.1293

Roselló-Camps, À, Monje, A., Lin, G.-H., Khoshkam, V., Chávez-Gatty, M., Wang, H.-L., et al. (2015). Platelet-rich plasma for periodontal regeneration in the treatment of intrabony defects: a meta-analysis on prospective clinical trials. *Oral Surg. Oral Med. Oral Pathol. Oral Radiol.* 120, 562–574. doi: 10.1016/j.oooo.2015.06.035

Russell, R. P., Apostolakos, J., Hirose, T., Cote, M. P., and Mazzocca, A. D. (2013). Variability of platelet-rich plasma preparations. *Sports Med. Arthrosc.* 21, 186–190. doi: 10.1097/JSA.0000000000000007

Sadabad, H. N., Behzadifar, M., Arasteh, F., Behzadifar, M., and Dehghan, H. R. (2016). Efficacy of platelet-rich plasma versus hyaluronic acid for treatment of knee osteoarthritis: a systematic review and meta-analysis. *Electron. physician* 8, 2115–2122. doi: 10.19082/2115

Sadeghi-Ataabadi, M., Mostafavi-Pour, Z., Vojdani, Z., Sani, M., Latifi, M., and Talaei-Khozani, T. (2017). Fabrication and characterization of platelet-rich plasma scaffolds for tissue engineering applications. *Mater. Sci. Eng. C. Mater. Biol. Appl.* 71, 372–380. doi: 10.1016/j.msec.2016.10.001

Singh, S. (2018). Comparative (quantitative and qualitative) analysis of three different reagents for preparation of platelet-rich plasma for hair rejuvenation. *J. Cutan. Aesthet. Surg.* 11:127. doi: 10.4103/jcas.jcas_108_18

Smyth, N., Murawski, C., Fortier, L., Cole, B., and Kennedy, J. (2013). Platelet-Rich plasma in the pathologic processes of cartilage: review of basic science evidence. *Arthroscopy* 29, 1399–1409. doi: 10.1016/j.arthro.2013.03.004

Tamimi, F. M., Montalvo, S., Tresguerres, I., and Blanco Jerez, L. (2007). A comparative study of 2 methods for obtaining platelet-rich plasma. *J. Oral Maxillofac. Surg.* 65, 1084–1093. doi: 10.1016/j.joms.2006.09.012

Tricco, A. C., Lillie, E., Zarin, W., O'Brien, K. K., Colquhoun, H., Levac, D., et al. (2018). PRISMA extension for scoping reviews (PRISMA-ScR): checklist and explanationThe PRISMA-ScR statement. *Ann. Intern. Med.* 169, 467–473. doi: 10.7326/M18-0850

Tunalı, M., Özdemir, H., Küçükodacı, Z., Akman, S., Yaprak, E., Toker, H., et al. (2014). A novel platelet concentrate: titanium-prepared platelet-rich fibrin. *Biomed Res. Int.* 2014:209548. doi: 10.1155/2014/209548

Vahabi, S., Yadegari, Z., and Mohammad-Rahimi, H. (2017). Comparison of the effect of activated or non-activated PRP in various concentrations on osteoblast and fibroblast cell line proliferation. *Cell Tissue Bank.* 18, 347–353. doi: 10.1007/s10561-017-9640-9647

Vos, R., Windt, J., Weir, A., de Vos, R.-J., Windt, J., and Weir, A. (2014). Strong evidence against platelet-rich plasma injections for chronic lateral epicondylar tendinopathy: a systematic review. *Br. J. Sports Med.* 48, 952–956. doi: 10.1136/bjsports-2013-093281

Wang, K., Li, Z., Li, J., Liao, W., Qin, Y., Zhang, N., et al. (2018a). Optimization of the platelet-rich plasma concentration for mesenchymal stem cell applications. *Tissue Eng. Part A* 25, 333–351. doi: 10.1089/ten.tea.2018.0091

Wang, S., Fan, W., Jia, J., Ma, L., Yu, J., and Wang, C. (2018b). Is exclusion of leukocytes from platelet-rich plasma (PRP) a better choice for early intervertebral disc regeneration? *Stem Cell Res. Ther.* 9:199. doi: 10.1186/s13287-018-0937-937

Xian, L. J., Chowdhury, S. R., Bin Saim, A., and Idrus, R. B. H. (2015). Concentration-dependent effect of platelet-rich plasma on keratinocyte and fibroblast wound healing. *Cytotherapy* 17, 293–300. doi: 10.1016/j.jcyt.2014.10.005

Yin, W., Xu, H., Sheng, J., Zhu, Z., Jin, D., Hsu, P., et al. (2017). Optimization of pure platelet-rich plasma preparation: a comparative study of pure platelet-rich plasma obtained using different centrifugal conditions in a single-donor model. *Exp. Ther. Med.* 14, 2060–2070. doi: 10.3892/etm.2017.4726

Conflict of Interest: The authors declare that the research was conducted in the absence of any commercial or financial relationships that could be construed as a potential conflict of interest.

frontiers in Cell and Developmental Biology

ORIGINAL RESEARCH
published: 04 February 2021
doi: 10.3389/fcell.2020.595932

A Novel Strategy to Enhance Microfracture Treatment With Stromal Cell-Derived Factor-1 in a Rat Model

Taylor Mustapich[1], John Schwartz[1], Pablo Palacios[1], Haixiang Liang[1], Nicholas Sgaglione[2] and Daniel A. Grande[1,2]*

[1] Orthopaedic Research Laboratory, Feinstein Institutes for Medical Research, Northwell Health, Manhasset, NY, United States, [2] Department of Orthopaedic Surgery, Northwell Health, New Hyde Park, NY, United States

Background: Microfracture is one of the most widely used techniques for the repair of articular cartilage. However, microfracture often results in filling of the chondral defect with fibrocartilage, which exhibits poor durability and sub-optimal mechanical properties. Stromal cell-derived factor-1 (SDF-1) is a potent chemoattractant for mesenchymal stem cells (MSCs) and is expressed at high levels in bone marrow adjacent to developing cartilage during endochondral bone formation. Integrating SDF-1 into an implantable collagen scaffold may provide a chondro-conductive and chondro-inductive milieu *via* chemotaxis of MSCs and promotion of chondrogenic differentiation, facilitating more robust hyaline cartilage formation following microfracture.

Objective: This work aimed to confirm the chemoattractive properties of SDF-1 *in vitro* and develop a one-step method for incorporating SDF-1 *in vivo* to enhance cartilage repair using a rat osteochondral defect model.

Methods: Bone marrow-derived MSCs (BMSCs) were harvested from the femurs of Sprague–Dawley rats and cultured in low-glucose Dulbecco's modified Eagle's medium containing 10% fetal bovine serum, with the medium changed every 3 days. Passage 1 MSCs were analyzed by flow cytometry with an S3 Cell Sorter (Bio-Rad). *In vitro* cell migration assays were performed on MSCs by labeling cells with carboxyfluorescein diacetate, succinimidyl ester (CFDA-SE; Bio-Rad). For the microfracture model, a 1.6-mm-diameter osteochondral defect was created in the femoral trochleae of 20 Sprague–Dawley rats bilaterally until bone marrow spillage was seen under saline irrigation. One knee was chosen at random to receive implantation of the scaffold, and the contralateral knee was left unfilled as an empty control. Type I collagen scaffolds (Kensey Nash) were coated with either gelatin only or gelatin and SDF-1 using a dip coating process. The rats received implantation of either a gelatin-only scaffold (N = 10) or gelatin-and-SDF-1 scaffold (N = 10) at the site of the microfracture. Femurs were collected for histological analyses at 4- and 8-week time points post-operatively, and sections were stained with Safranin O/Fast Green. The samples were graded blindly by two observers using the Modified O'Driscoll score, a validated scoring system for chondral repair. A minimum of 10 separate grading scores were made per sample

OPEN ACCESS

Edited by:
Tiago Lazzaretti Fernandes, University of São Paulo, Brazil

Reviewed by:
David Arthur Hart, University of Calgary, Canada
Pedro Debieux, Albert Einstein Israelite Hospital, Brazil

****Correspondence:***
Taylor Mustapich
taylor.mustapich@einsteinmed.org

Specialty section:
This article was submitted to Stem Cell Research, a section of the journal Frontiers in Cell and Developmental Biology

Received: *18 August 2020*
Accepted: *31 December 2020*
Published: *04 February 2021*

Citation:
Mustapich T, Schwartz J, Palacios P, Liang H, Sgaglione N and Grande DA (2021) A Novel Strategy to Enhance Microfracture Treatment With Stromal Cell-Derived Factor-1 in a Rat Model. Front. Cell Dev. Biol. 8:595932. doi: 10.3389/fcell.2020.595932

and averaged. Quantitative comparisons of cell migration *in vitro* were performed with one-way ANOVA. Cartilage repair *in vivo* was also compared among groups with one-way ANOVA, and the results were presented as mean ± standard deviation, with *P*-values < 0.05 considered as statistically significant.

Results: MSC migration showed a dose–response relationship with SDF-1, with an optimal dosage for chemotaxis between 10 and 100 ng/ml. After scaffold implantation, the SDF-1-treated group demonstrated complete filling of the cartilage defect with mature cartilage tissue, exhibiting strong proteoglycan content, smooth borders, and good incorporation into marginal cartilage. Modified O'Driscoll scores after 8 weeks showed a significant improvement of cartilage repair in the SDF-1 group relative to the empty control group ($P < 0.01$), with a trend toward improvement when compared with the gelatin-only-scaffold group ($P < 0.1$). No significant differences in scores were found between the empty defect group and gelatin-only group.

Conclusion: In this study, we demonstrated a simple method for improving the quality of cartilage defect repair in a rat model of microfracture. We confirmed the chemotactic properties of SDF-1 on rat MSCs and found an optimized dosage range for chemotaxis between 10 and 100 ng/ml. Furthermore, we demonstrated a strategy to incorporate SDF-1 into gelatin–collagen I scaffolds *in vivo* at the site of an osteochondral defect. SDF-1-treated defects displayed robust hyaline cartilage resurfacing of the defect with minimal fibrous tissue, in contrast to the empty control group. The results of the *in vitro* and *in vivo* studies together suggest that SDF-1-mediated signaling may significantly improve the quality of cartilage regeneration in an osteochondral defect.

Keywords: osteoarthritis-therapies < cartilage, subchondral arthroplasty, tissue scaffolds, mesenchymal stem cell, microfracture (MFX), stromal cell derived factor-1 (CXCL12), bone marrow stem cell-based therapy

INTRODUCTION

While the etiology of joint degeneration and osteoarthritis occurs at the molecular, cellular, and tissue level, current treatments of isolated chondral defects are primarily surgical (Furman et al., 2006; Daher et al., 2009; Anderson et al., 2011). Regeneration of hyaline cartilage is limited by the lack of chondral vascularity, diminishing the recruitment of renewable cells to the site of injury (Csaki et al., 2008; Fong et al., 2011). Thus, penetration of the subchondral bone with techniques such as microfracture emerged and served to recruit mesenchymal stem cells (MSCs) from the bone marrow to infiltrate the overlying chondral lesion. However, long-term durability was inadequate, as the native hyaline cartilage was repaired with fibrocartilage consisting of primarily type I collagen, which is prone to rapid degeneration and less adaptable than its hyaline counterpart (Mithoefer et al., 2009; Gomoll and Minas, 2014; Richter et al., 2016). It is thought that microfracture alone does not recruit a sufficient amount of reparative cells and growth factors to promote adequate native tissue repair (Richter, 2009). One potential therapeutic strategy to augment the chondrogenic milieu following microfracture is by incorporating homing factors into cell-free scaffolds to promote the recruitment of MSCs to the site of injury (Mishima and Lotz, 2008; Chanda et al., 2010; Fong et al., 2011; Eseonu and De Bari, 2015; Truong et al., 2017; Lu et al., 2018).

Stromal cell-derived factor-1 (SDF-1) is a potent chemoattractant for MSCs and has associations with bone repair (Hwang et al., 2015; Liu et al., 2015). SDF-1 attracts MSCs to the site of bone fractures and is expressed in marrow adjacent to developing cartilage during endochondral bone formation (Wei et al., 2010; Murata et al., 2012; Toupadakis et al., 2012). In addition, the receptor for SDF-1, C-X-C chemokine receptor type 4 (CXCR4), plays a significant role in chondrocyte differentiation and proliferation (Mazzetti et al., 2004). Integrating SDF-1 into an implantable collagen scaffold may improve the quality of cartilage repair by recruiting MSCs from the underlying bone marrow and promoting a chondroinductive milieu. We seek to evaluate a novel method of improving the quality of chondral repair following microfracture by incorporating SDF-1 into an implantable, cell-free scaffold and directly comparing it to microfracture alone.

MATERIALS AND METHODS

Preparation of BMSCs

Rat bone marrow-derived MSCs (BMSCs) were isolated from the femurs of Sprague–Dawley rats as previously described (Haynesworth et al., 1992). Briefly, the femurs were harvested using an aseptic technique. After removing the soft tissue and

periosteum, the bones were cut using a bone rongeur. Bone marrow was washed out with low-glucose Dulbecco's modified Eagle's medium (Fisher Scientific, Pittsburgh, PA, United States) containing 10% fetal bovine serum (Fisher Scientific, Pittsburgh, PA, United States) using a syringe. The bone marrow was then mixed with medium and cultured at 37°C with 5% CO_2 in an incubator, with the medium changed every 3 days.

Flow Cytometry Study

Rat BMSCs at passage 1 were detached from the cell culture flask by Accutase (Innovative Cell Technologies, San Diego, CA, United States). After washing with phosphate-buffered saline (PBS), the cells were stained with antibodies against CD45 (AbD Serotec, Raleigh, NC, United States), CD73 (BD Biosciences, San Jose, CA, United States), CD90 (BioLegend, San Diego, CA, United States), and CD106 (BioLegend, San Diego, CA, United States). The stained cells were analyzed by flow cytometry with an S3 Cell Sorter (Bio-Rad, Hercules, CA, United States).

In vitro Cell Migration Assay

Rat BMSCs at passage 1 were serum-starved for 2 h at 37°C. A 24-well plate was loaded with Transwell inserts (8.0 μm in pore size; Fisher Scientific, Pittsburgh, PA, United States). The lower chambers contained 600 μl of either serum-free medium (negative control), medium with serum (positive control), or SDF-1 (1, 10, or 100 ng/ml; R&D Systems, Minneapolis, MN, United States). Each condition was set up in triplicate. The serum-starved BMSCs (105 cells/well) were loaded on the upper chamber and incubated at 37°C for 4 h. The membranes were fixed with formalin for 10 min and washed with PBS before staining with Wright–Giemsa. The migrated cells were counted under a light microscope (×400), with 30 random fields analyzed per membrane. The results are represented as the average number of migrated cells counted per ×400 magnification field.

For morphological observation, BMSCs were labeled with carboxyfluorescein diacetate, succinimidyl ester (CFDA-SE; Bio-Rad, Hercules, CA, United States) following the manufacturer's instructions prior to loading on Transwell inserts. Fluorescence blocking inserts were used; thus, fluorescence was visible only when cells migrated to the observation side of the membrane.

Scaffold Preparation

Type I collagen was selected as the scaffold biomaterial given its proven safety and biocompatibility profile and widespread availability, making it an ideal agent for translation into clinical application (Tampieri et al., 2008; Kon et al., 2010). Collagen I scaffolds (Kensey Nash, Exton, PA, United States) were coated with either gelatin only (control) or gelatin and SDF-1 using a dip coating process previously described (Dines et al., 2007, 2011; Uggen et al., 2010; Cummings et al., 2012). Briefly, gelatin was prepared by heating a 10% (wt) solution of medical-grade soluble bovine collagen (Semed-S, Kensey-Nash, Exton PA) to 80°C for 10 min, followed by incubation at 37°C. SDF-1 (50 ng/ml) was reconstituted in 10 mM HCl and mixed with the gelatin at a ratio of 2:1 (gelatin/SDF). Collagen scaffolds were pre-treated in 70% EtOH for 10 min, washed with PBS, and then dip-coated in the gelatin solution at 37°C for 30 min with gentle agitation. The scaffolds were removed from the solution and air-dried overnight in a sterile laminar flow hood.

Surgical Procedure

The usage of animals in this study was approved by the Institutional Animal Care and Use Committee of Feinstein Institutes for Medical Research. A medial parapatellar approach to the knee joint was performed bilaterally in Sprague–Dawley rats (N = 20; weight, 500 g). A 1.6-mm-diameter full-thickness osteochondral defect was created in each femoral trochlea until bone marrow spillage was visualized under saline irrigation as a model of microfracture. One knee was chosen at random with a coin toss to receive scaffold implantation (1.8 mm in diameter, 1.5 mm in thickness) and the contralateral knee served as an empty control. The rats received implantation of a scaffold dip-coated either with gelatin only (N = 10) or with gelatin and SDF-1 (N = 10). Femurs were collected for histological analysis at 4- and 8-week time points post-operatively, with the endpoints defined based upon current literature (Lee and Im, 2012; Dahlin et al., 2014; Mahmoud et al., 2017; Hayashi et al., 2018).

Histological Evaluation

The distal femurs were dissected free of soft tissue and fixed in 10% Millonig's buffered formalin (Fisher Scientific, Pittsburgh, PA, United States). The samples were decalcified with formic acid decalcification solution (Fisher Scientific, Pittsburgh, PA, United States) for 5 days with shaking, then embedded in paraffin, and cut in the coronal plane (5 μm in thickness). Serial sections were cut at 100-μm intervals through an area approximately 30% of the total surface area of the defect. The sections were mounted and stained with Safranin-O/Fast Green. The samples were graded blindly by two observers using the Modified O'Driscoll Score, a validated scoring system for chondral repair (Qi et al., 2014). A minimum of 10 separate grading scores were made per sample and averaged.

Statistical Analyses

The samples were tested for normality using the Shapiro–Wilk test. Quantitative comparisons of cell migration *in vitro* were performed with one-way ANOVA. The results are presented as mean ± standard deviation, with P-values less than 0.05 considered as statistically significant. Cartilage repair *in vivo* was compared among groups with one-way ANOVA. The results are presented as mean ± standard deviation, with P-values less than 0.05 considered as statistically significant.

RESULTS

Flow Cytometric Characteristics of Rat BMSCs

Bone marrow-derived MSCs at passage 1 were 43% CD90-positive and 21% CD45-negative. Among the CD45-negative cells, 95% were CD90-positive, 19% of CD45-negative cells were positive for both CD90 and CD106, and 38% of CD45-negative cells were positive for both CD90 and CD73 (**Figure 1**).

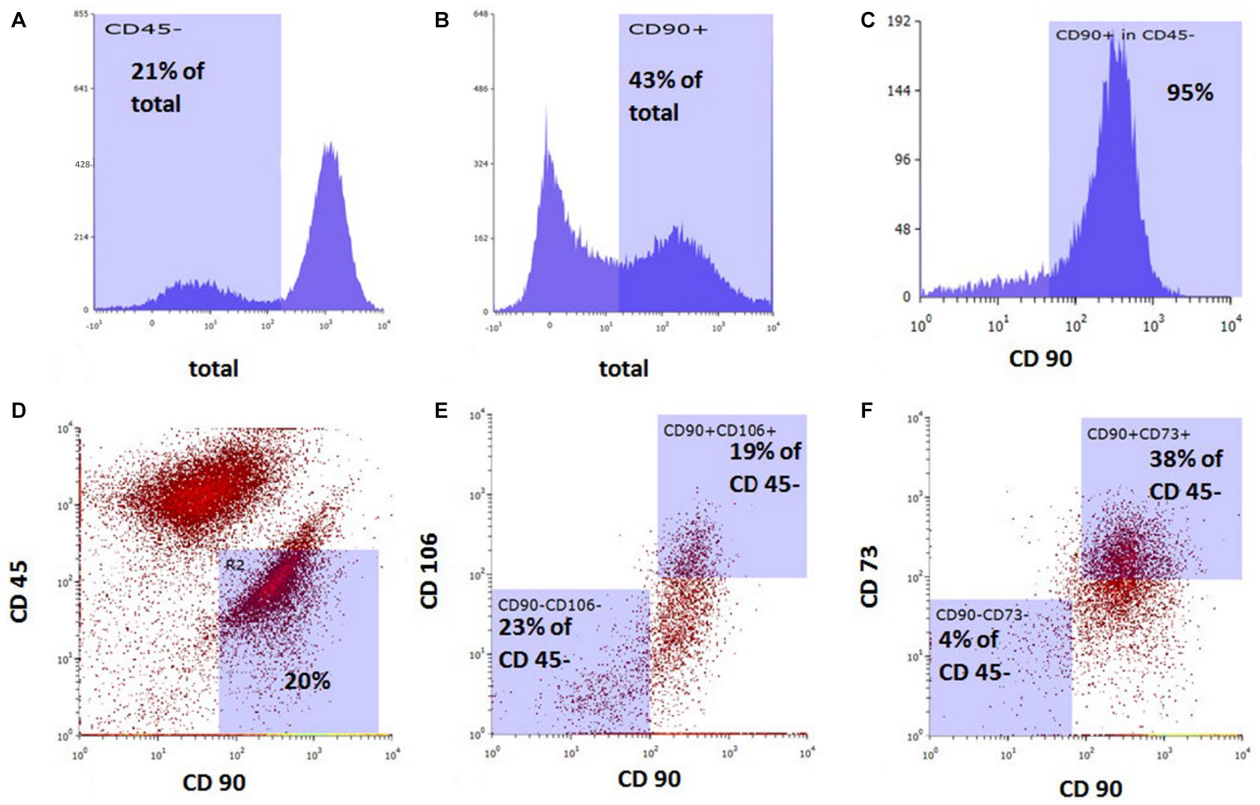

FIGURE 1 | Flow cytometric analysis of rat bone marrow-derived mesenchymal stem cells prior to *in vitro* cell migration studies. Cell population stained with **(A)** anti-CD45, **(B)** anti-CD90, and **(C)** anti-CD90 among CD45-negative cells. Dot plot of combined staining for **(D)** CD45 and CD90, **(E)** CD106 and CD90 among CD45-negative population, and **(F)** CD73 and CD90 among CD45-negative population.

In vitro Cell Migration

Chemoattraction of BMSCs by SDF-1 was tested with the Transwell culture system *in vitro*. After 4 h in culture, the CFDA-SE-stained cells were found to have migrated in great quantities toward the SDF-1-containing chamber (100 ng/ml). Morphologically, these cells were round and larger than the pore size (**Figure 2A**).

To determine the optimal dosage of SDF-1 for chemoattraction of BMSCs, SDF-1 was added to the Transwell system at concentrations of 1, 10, and 100 ng/ml. Cell migration was increased significantly from the control group at both 10 ng/ml (28 ± 3 *vs.* 74 ± 25 cells/×400 field, respectively; $P = 0.04$) and 100 ng/ml (79 ± 22 cells/×400 field; $P = 0.04$) concentrations of SDF-1, which is consistent with previous literature (**Figure 2B**) (Ji et al., 2013). Cell migration did not differ significantly between the control group and the SDF-1 group containing 1 ng/ml (33 ± 14 cells/×400 field; $P = 0.56$).

In vivo Cartilage Repair

No post-operative complications were noted throughout the study period. SDF-1-treated defects showed complete filling of mature cartilage tissue with strong proteoglycan content, smooth borders, and substantial incorporation into surrounding cartilage (**Figures 3A–C**). Modified O'Driscoll scores at 4 weeks post-operatively showed a trend toward improvement in cartilage repair quality in the SDF-1 group relative to the empty control group (13 ± 8 *vs.* 3 ± 1; $P = 0.07$); however, the difference was not statistically significant. No significant difference in cartilage repair quality was found at 4 weeks post-operatively between the SDF-1 group and the gelatin-only group (8 ± 5; $P = 0.26$). Modified O'Driscoll scores at 8 weeks post-operatively showed a significant improvement in cartilage quality in the SDF-1 group relative to the empty control group (18 ± 6 *vs.* 5 ± 3; $P = 0.009$) and a trend toward improvement when compared with the gelatin-only-scaffold group (9 ± 4; $P = 0.09$); however, the difference was not statistically significant. No significant difference in O'Driscoll scores was found when comparing the empty control and gelatin-only-scaffold groups at 4 weeks ($P = 0.14$) or 8 weeks post-operatively ($P = 0.17$; **Figure 3D**).

DISCUSSION

Microfracture is one of the most widely used techniques for the repair of articular cartilage (Oussedik et al., 2015; Wylie et al., 2015). However, microfracture results in filling of the cartilage defect with fibrocartilage, which is less durable than

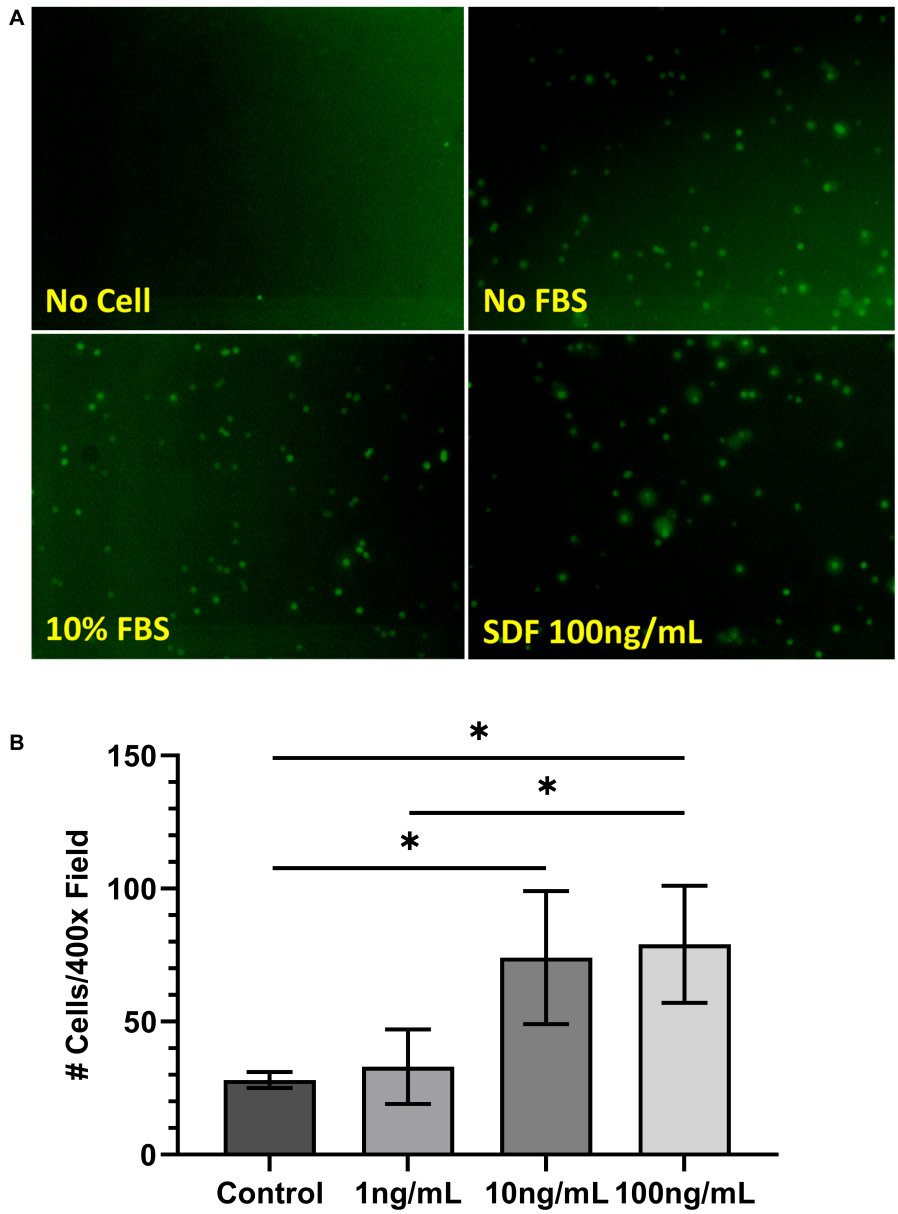

FIGURE 2 | (A) Morphology of carboxyfluorescein diacetate–succinimidyl ester-stained bone marrow-derived mesenchymal stem cells (BMSCs) following cell migration assay. **(B)** Results of cell migration assay of BMSCs treated with stromal cell-derived factor-1 (1, 10, and 100 ng/ml). Values are represented as average number of cells counted per ×400 field. $^*P < 0.05$.

native hyaline cartilage and prone to re-injury (Krych et al., 2012; Xing et al., 2013; Oussedik et al., 2015). Implantable cell-free scaffolds coated in chemoattractive factors may improve the quality of cartilage repair following microfracture (Mishima and Lotz, 2008; Chanda et al., 2010; Fong et al., 2011; Eseonu and De Bari, 2015; Truong et al., 2017; Lu et al., 2018). In this study, we determined the optimal concentration of SDF-1 for MSC chemoattraction *in vitro* and found that incorporating SDF-1 into an implantable scaffold yielded a superior quality of cartilage repair when compared with microfracture alone.

SDF-1 promotes MSC migration and homing to the bone marrow through its receptor, CXCR4 (Shi et al., 2007; Baek et al., 2011). In addition to MSCs, CXCR4 is also expressed on hematopoietic progenitor cells, chondrocytes, and fibroblasts (Kucia et al., 2005; Villalvilla et al., 2014). As the SDF-1/CXCR4 axis is not exclusive to MSC homing, determining the optimal dosage of SDF-1 for the homing of MSCs to cartilage defects is necessary. Previously, a concentration of 50–200 ng/ml was reported to enhance the chemoattraction of rat BMSCs *in vitro*. However, when the concentration of SDF-1 was increased to 400 ng/ml and above, the chemoattractant effect began to significantly

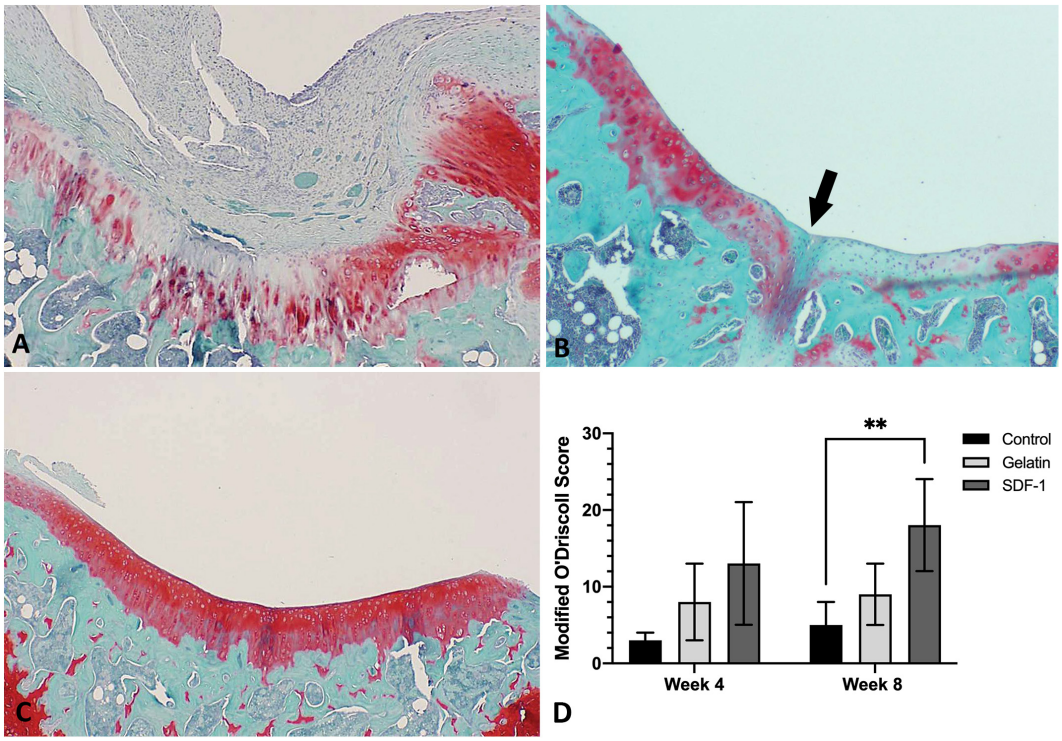

FIGURE 3 | Histological evaluation with Safranin O/Fast Green to compare the repair of microfracture defects with implantation of gelatin–collagen I scaffolds carrying stromal cell-derived factor-1 (SDF-1) (50 ng/ml) and control groups *in vivo* (×40 magnification) at 8 weeks post-operatively. Representative images were selected based upon the best quality of cartilage repair within each group. **(A)** Defect only group. **(B)** Gelatin only group. **(C)** Gelatin and SDF-1 group. **(D)** Quantitative comparison of cartilage repair quality with Modified O'Driscoll scores at 4 and 8 weeks post-operatively. $^{**}P < 0.01$.

decrease (Ji et al., 2013). In our study, we confirmed the optimal concentration of SDF-1 to be between 10 and 100 ng/ml.

To apply SDF-1 *in vivo*, we used a gelatin carrier system developed for the application of growth factors (Dines et al., 2007, 2011; Uggen et al., 2010; Cummings et al., 2012). *In vitro* testing revealed that the release of growth factors from the carrier system could be sustained at a standard rate within the first 48 h (Uggen et al., 2010; Cummings et al., 2012). After implantation, the growth factors carried by the system maintained their functional effect *in vivo* (Dines et al., 2007; Uggen et al., 2010; Cummings et al., 2012). In our study, the gelatin–SDF-1 solution was loaded on a bovine collagen I scaffold for implantation in a rat microfracture model. When assessing the compatibility of MSCs with collagen scaffolds, type I collagen scaffolds exhibited superior attachment of BMSCs and cartilage-derived MSCs than type II collagen scaffolds. Moreover, the cells attached on the type I collagen scaffold maintained their spindle shape as a monolayer, while the cells on the type II collagen scaffold were round and tightly packed (Zhang et al., 2013). In clinical application, type I collagen scaffolds combined with hydroxyapatite showed improvement in the repair of cartilage defects (Filardo et al., 2013; Delcogliano et al., 2014).

In our study, implantation of an SDF-1-coated scaffold at the site of microfracture resulted in a significant improvement in cartilage repair, with results seen as early as 4 weeks post-operatively. Similarly, using a rabbit model, Chen et al. (2015) found that type I collagen scaffolds carrying SDF-1 (100 ng/ml) enhanced the repair of cartilage defects after 12 weeks. Zhang et al. (2013) utilized collagen I scaffolds carrying SDF-1 (120 ng/ml) on a partial-thickness cartilage defect using a rabbit model and found improved repair quality in the SDF-1 treatment group at 6 weeks post-operatively. In comparison to previous studies, our SDF-1 carrier system achieved nearly complete cartilage defect filling at 8 weeks post-operatively using an SDF-1 concentration of 50 ng/ml. A subsequent elution profile of our scaffold revealed an initial bolus release of SDF-1, followed by a continuous, steady release over the following 5 days, consistent with available literature (Sun et al., 2016). This may explain why we were able to achieve significant results at a lower concentration than those of other studies. While low SDF-1 levels are tied to healing, high SDF-1 levels have been paradoxically implicated in rheumatoid arthritis and osteoarthritis (Villalvilla et al., 2014; Kanbe et al., 2015). Thus, maintaining therapeutic levels of SDF-1 in the joint space by optimizing the biomechanics of the delivery system is vital.

The limitations of our study include the small sample size and relatively short post-operative time points. We found no significant difference in the quality of cartilage repair between groups at 4 weeks post-operatively as measured by Modified O'Driscoll scores. However, significant improvement in repair

was noted at 8 weeks post-operatively in the SDF-1-treated group when compared with the empty defect group. When compared with the gelatin-dipped scaffold group, the SDF-1-treated group showed a tendency for improvement in the Modified O'Driscoll scores, but the difference did not meet statistical significance. In future studies, conducting analyses at longer time points, such as at 12- or 16-weeks post-operatively, may allow for a more appropriate length of time for mature tissue healing. Furthermore, increasing the sample size of the study would generate greater power to elucidate the difference between the gelatin- and SDF-1-treated scaffold groups. Immunohistochemical staining of healed tissue for collagen types I and II would provide definitive evidence of repair with hyaline *vs.* fibrocartilage; fibrocartilage contains a significant amount of type I collagen, while hyaline cartilage contains little to none. Based on our *in vitro* cell migration studies, a concentration of 50 ng/ml SDF-1 was chosen for the *in vivo* studies to optimize chemotaxis to the defect site with a minimal dose. However, we recognize that the kinetics of SDF-1 *in vivo* may differ significantly from the kinetics observed in *in vitro* studies. Future areas of study may include comparing a variety of SDF-1 concentrations *in vivo* to confirm the ideal concentration for cartilage repair and performing tests of durability and mechanical loading to provide evidence of clinically meaningful results. Other factors commonly implicated in cartilage repair, such as granulocyte-macrophage colony-stimulating factor transforming growth factor beta, platelet-rich plasma, and fibroblast growth factor, should be compared directly to and in combination with SDF-1 to formulate an optimal cocktail for cartilage repair (Kang et al., 2008; Huh et al., 2014; Harada et al., 2015; Truong et al., 2017).

In this study, we successfully demonstrated a cost-effective, one-step process for enhancing microfracture to improve the outcome of cartilage repair. We confirmed the chemotactic properties of SDF-1 on rat MSCs *in vitro* and found an optimized dosage range for chemotaxis between 10 and 100 ng/ml, consistent with previous literature. Furthermore, we successfully demonstrated a simple method of incorporating SDF-1 into a biocompatible scaffold at the site of osteochondral defect. SDF-1-treated defects displayed robust resurfacing with hyaline-like cartilage with minimal fibrous tissue compared with the control groups. Overall, the results suggest that scaffolds treated with SDF-1 can improve the quality of cartilage repair in an osteochondral defect.

DATA AVAILABILITY STATEMENT

The raw data supporting the conclusions of this article will be made available by the authors, without undue reservation.

ETHICS STATEMENT

The animal study was reviewed and approved by the Institutional Animal Care and Use Committee of the Feinstein Institutes for Medical Research.

AUTHOR CONTRIBUTIONS

HL, NS, and DG contributed to the concept, design, and supervision of the study. TM, JS, PP, and HL collected, analyzed, and interpreted the data. TM, HL, and DG were involved in the writing and critical review of the manuscript. TM and DG conducted the final editing and proofreading. All the authors read and approved the final manuscript.

FUNDING

This work was supported by a grant from the Department of Orthopaedic Surgery at Northwell Health.

REFERENCES

Anderson, D. D., Chubinskaya, S., Guilak, F., Martin, J. A., Oegema, T. R., Olson, S. A., et al. (2011). Post-traumatic osteoarthritis: improved understanding and opportunities for early intervention. *J. Orthop. Res.* 29, 802–809. doi: 10.1002/jor.21359

Baek, S. J., Kang, S. K., and Ra, J. C. (2011). In vitro migration capacity of human adipose tissue-derived mesenchymal stem cells reflects their expression of receptors for chemokines and growth factors. *Exp. Mol. Med.* 43, 596–603. doi: 10.3858/emm.2011.43.10.069

Chanda, D., Kumar, S., and Ponnazhagan, S. (2010). Therapeutic potential of adult bone marrow-derived mesenchymal stem cells in diseases of the skeleton. *J. Cell. Biochem.* 111, 249–257. doi: 10.1002/jcb.22701

Chen, P., Tao, J., Zhu, S., Cai, Y., Mao, Q., Yu, D., et al. (2015). Radially oriented collagen scaffold with SDF-1 promotes osteochondral repair by facilitating cell homing. *Biomaterials* 39, 114–123. doi: 10.1016/j.biomaterials.2014.10.049

Csaki, C., Schneider, P. R., and Shakibaei, M. (2008). Mesenchymal stem cells as a potential pool for cartilage tissue engineering. *Ann. Anat.* 190, 395–412. doi: 10.1016/j.aanat.2008.07.007

Cummings, S. H., Grande, D. A., Hee, C. K., Kestler, H. K., Roden, C. M., Shah, N. V., et al. (2012). Effect of recombinant human platelet-derived growth factor-BB-coated sutures on Achilles tendon healing in a rat model: a histological and biomechanical study. *J. Tissue Eng.* 3:2041731412453577. doi: 10.1177/2041731412453577

Daher, R. J., Chahine, N. O., Greenberg, A. S., Sgaglione, N. A., and Grande, D. A. (2009). New methods to diagnose and treat cartilage degeneration. *Nat. Rev. Rheumatol.* 5, 599–607. doi: 10.1038/nrrheum.2009.204

Dahlin, R. L., Kinard, L. A., Lam, J., Needham, C. J., Lu, S., Kasper, F. K., et al. (2014). Articular chondrocytes and mesenchymal stem cells seeded on biodegradable scaffolds for the repair of cartilage in a rat osteochondral defect model. *Biomaterials* 35, 7460–7469.

Delcogliano, M., de Caro, F., Scaravella, E., Ziveri, G., De Biase, C. F., Marotta, D., et al. (2014). Use of innovative biomimetic scaffold in the treatment for large osteochondral lesions of the knee. *Knee Surg. Sports Traumatol. Arthrosc.* 22, 1260–1269. doi: 10.1007/s00167-013-2717-3

Dines, J. S., Cross, M. B., Dines, D., Pantazopoulos, C., Kim, H. J., Razzano, P., et al. (2011). In vitro analysis of an rhGDF-5 suture coating process and the effects of rhGDF-5 on rat tendon fibroblasts. *Growth Factors* 29, 1–7. doi: 10.3109/08977194.2010.526605

Dines, J. S., Weber, L., Razzano, P., Prajapati, R., Timmer, M., Bowman, S., et al. (2007). The effect of growth differentiation factor-5-coated sutures on tendon repair in a rat model. *J. Shoulder Elbow Surg.* 16 (Suppl. 5), S215–S221. doi: 10.1016/j.jse.2007.03.001

Eseonu, O. I., and De Bari, C. (2015). Homing of mesenchymal stem cells: mechanistic or stochastic? Implications for targeted delivery in arthritis. *Rheumatology (Oxford)* 54, 210–218. doi: 10.1093/rheumatology/keu377

Filardo, G., Kon, E., Di Martino, A., Busacca, M., Altadonna, G., and Marcacci, M. (2013). Treatment of knee osteochondritis dissecans with a cell-free biomimetic osteochondral scaffold: clinical and imaging evaluation at 2-year follow-up. *Am. J. Sports Med.* 41, 1786–1793. doi: 10.1177/0363546513490658

Fong, E. L., Chan, C. K., and Goodman, S. B. (2011). Stem cell homing in musculoskeletal injury. *Biomaterials* 32, 395–409. doi: 10.1016/j.biomaterials.2010.08.101

Furman, B. D., Olson, S. A., and Guilak, F. (2006). The development of posttraumatic arthritis after articular fracture. *J. Orthop. Trauma* 20, 719–725. doi: 10.1097/01.bot.0000211160.05864.14

Gomoll, A. H., and Minas, T. (2014). The quality of healing: articular cartilage. *Wound Repair Regen.* 22, 30–38. doi: 10.1111/wrr.12166

Harada, Y., Nakasa, T., Mahmoud, E. E., Kamei, G., Adachi, N., Deie, M., et al. (2015). Combination therapy with intra-articular injection of mesenchymal stem cells and articulated joint distraction for repair of a chronic osteochondral defect in the rabbit. *J. Orthop. Res.* 33, 1466–1473.

Hayashi, S., Nakasa, T., Ishikawa, M., Nakamae, A., Miyaki, S., and Adachi, N. (2018). Histological evaluation of early-phase changes in the osteochondral unit after microfracture in a full-thickness cartilage defect rat model. *Am. J. Sports Med.* 46, 3032–3039. doi: 10.1177/0363546518787287

Haynesworth, S. E., Goshima, J., Goldberg, V. M., and Caplan, A. I. (1992). Characterization of cells with osteogenic potential from human marrow. *Bone* 13, 81–88.

Huh, S. W., Shetty, A. A., Kim, S. J., Kim, Y. J., Choi, N. Y., Jun, Y. J., et al. (2014). The effect of platelet rich plasma combined with microfracture for the treatment of chondral defect in a rabbit knee. *Tissue Eng. Regen. Med.* 11, 178–185.

Hwang, H. D., Lee, J. T., Koh, J. T., Jung, H. M., Lee, H. J., and Kwon, T. G. (2015). Sequential treatment with SDF-1 and BMP-2 potentiates bone formation in calvarial defects. *Tissue Eng. Part A* 21, 2125–2135. doi: 10.1089/ten.TEA.2014.0571

Ji, W., Yang, F., Ma, J., Bouma, M. J., Boerman, O. C., Chen, Z., et al. (2013). Incorporation of stromal cell-derived factor-1alpha in PCL/gelatin electrospun membranes for guided bone regeneration. *Biomaterials* 34, 735–745. doi: 10.1016/j.biomaterials.2012.10.016

Kanbe, K., Chiba, J., Inoue, Y., Taguchi, M., and Yabuki, A. (2015). SDF-1 and CXCR4 in synovium are associated with disease activity and bone and joint destruction in patients with rheumatoid arthritis treated with golimumab. *Mod. Rheumatol.* 26, 46–50. doi: 10.3109/14397595.2015.1054088

Kang, S.-W., Bada, L. P., Kang, C.-S., Lee, J.-S., Kim, C.-H., Park, J.-H., et al. (2008). Articular cartilage regeneration with microfracture and hyaluronic acid. *Biotechnol. Lett.* 30, 435–439.

Kon, E., Delcogliano, M., Filardo, G., Fini, M., Giavaresi, G., Francioli, S., et al. (2010). Orderly osteochondral regeneration in a sheep model using a novel nano-composite multilayered biomaterial. *J. Orthop. Res.* 28, 116–124. doi: 10.1002/jor.20958

Krych, A. J., Harnly, H. W., Rodeo, S. A., and Williams, R. J. III (2012). Activity levels are higher after osteochondral autograft transfer mosaicplasty than after microfracture for articular cartilage defects of the knee: a retrospective comparative study. *J. Bone Joint Surg. Am.* 94, 971–978. doi: 10.2106/JBJS.K.00815

Kucia, M., Reca, R., Miekus, K., Wanzeck, J., Wojakowski, W., Janowska-Wieczorek, A., et al. (2005). Trafficking of normal stem cells and metastasis of cancer stem cells involve similar mechanisms: pivotal role of the SDF-1-CXCR4 axis. *Stem Cells* 23, 879–894. doi: 10.1634/stemcells.2004-0342

Lee, J.-M., and Im, G.-I. (2012). SOX trio-co-transduced adipose stem cells in fibrin gel to enhance cartilage repair and delay the progression of osteoarthritis in the rat. *Biomaterials* 33, 2016–2024.

Liu, H., Li, M., Du, L., Yang, P., and Ge, S. (2015). Local administration of stromal cell-derived factor-1 promotes stem cell recruitment and bone regeneration in a rat periodontal bone defect model. *Mater. Sci. Eng. C Mater. Biol. Appl.* 53, 83–94. doi: 10.1016/j.msec.2015.04.002

Lu, J., Shen, X., Sun, X., Yin, H., Yang, S., Lu, C., et al. (2018). Increased recruitment of endogenous stem cells and chondrogenic differentiation by a composite scaffold containing bone marrow homing peptide for cartilage regeneration. *Theranostics* 8, 5039–5058. doi: 10.7150/thno.26981

Mahmoud, E. E., Kamei, N., Shimizu, R., Wakao, S., Dezawa, M., Adachi, N., et al. (2017). Therapeutic potential of multilineage-differentiating stress-enduring cells for osteochondral repair in a rat model. *Stem Cells Int.* 2017, 8154569.

Mazzetti, I., Magagnoli, G., Paoletti, S., Uguccioni, M., Olivotto, E., Vitellozzi, R., et al. (2004). A role for chemokines in the induction of chondrocyte phenotype modulation. *Arthritis Rheum.* 50, 112–122. doi: 10.1002/art.11474

Mishima, Y., and Lotz, M. (2008). Chemotaxis of human articular chondrocytes and mesenchymal stem cells. *J. Orthop. Res.* 26, 1407–1412. doi: 10.1002/jor.20668

Mithoefer, K., McAdams, T., Williams, R. J., Kreuz, P. C., and Mandelbaum, B. R. (2009). Clinical efficacy of the microfracture technique for articular cartilage repair in the knee: an evidence-based systematic analysis. *Am. J. Sports Med.* 37, 2053–2063. doi: 10.1177/0363546508328414

Murata, K., Kitaori, T., Oishi, S., Watanabe, N., Yoshitomi, H., Tanida, S., et al. (2012). Stromal cell-derived factor 1 regulates the actin organization of chondrocytes and chondrocyte hypertrophy. *PLoS One* 7:e37163. doi: 10.1371/journal.pone.0037163

Oussedik, S., Tsitskaris, K., and Parker, D. (2015). Treatment of articular cartilage lesions of the knee by microfracture or autologous chondrocyte implantation: a systematic review. *Arthroscopy* 31, 732–744. doi: 10.1016/j.arthro.2014.11.023

Qi, Y., Du, Y., Li, W., Dai, X., Zhao, T., and Yan, W. (2014). Cartilage repair using mesenchymal stem cell (MSC) sheet and MSCs-loaded bilayer PLGA scaffold in a rabbit model. *Knee Surg. Sports Traumatol. Arthrosc.* 22, 1424–1433. doi: 10.1007/s00167-012-2256-3

Richter, D. L., Schenck, R. C. Jr., Wascher, D. C., and Treme, G. (2016). Knee articular cartilage repair and restoration techniques: a review of the literature. *Sports Health* 8, 153–160. doi: 10.1177/1941738115611350

Richter, W. (2009). Mesenchymal stem cells and cartilage in situ regeneration. *J. Intern. Med.* 266, 390–405. doi: 10.1111/j.1365-2796.2009.02153.x

Shi, M., Li, J., Liao, L., Chen, B., Li, B., Chen, L., et al. (2007). Regulation of CXCR4 expression in human mesenchymal stem cells by cytokine treatment: role in homing efficiency in NOD/SCID mice. *Haematologica* 92, 897–904.

Sun, H., Wang, J., Deng, F., Liu, Y., Zhuang, X., Xu, J., et al. (2016). Co-delivery and controlled release of stromal cell-derived factor-1α chemically conjugated on collagen scaffolds enhances bone morphogenetic protein-2-driven osteogenesis in rats. *Mol. Med. Rep.* 14, 737–745. doi: 10.3892/mmr.2016.5339

Tampieri, A., Sandri, M., Landi, E., Pressato, D., Francioli, S., Quarto, R., et al. (2008). Design of graded biomimetic osteochondral composite scaffolds. *Biomaterials* 29, 3539–3546. doi: 10.1016/j.biomaterials.2008.05.008

Toupadakis, C. A., Wong, A., Genetos, D. C., Chung, D. J., Murugesh, D., Anderson, M. J., et al. (2012). Long-term administration of AMD3100, an antagonist of SDF-1/CXCR4 signaling, alters fracture repair. *J. Orthop. Res.* 30, 1853–1859. doi: 10.1002/jor.22145

Truong, M. D., Choi, B. H., Kim, Y. J., Kim, M. S., and Min, B. H. (2017). Granulocyte macrophage – colony stimulating factor (GM-CSF) significantly enhances articular cartilage repair potential by microfracture. *Osteoarthritis Cartilage* 25, 1345–1352. doi: 10.1016/j.joca.2017.03.002

Uggen, C., Dines, J., McGarry, M., Grande, D., Lee, T., and Limpisvasti, O. (2010). The effect of recombinant human platelet-derived growth factor BB-coated sutures on rotator cuff healing in a sheep model. *Arthroscopy* 26, 1456–1462. doi: 10.1016/j.arthro.2010.02.025

Villalvilla, A., Gomez, R., Roman-Blas, J. A., Largo, R., and Herrero-Beaumont, G. (2014). SDF-1 signaling: a promising target in rheumatic diseases. *Expert Opin. Ther. Targets* 18, 1077–1087. doi: 10.1517/14728222.2014.930440

Wei, L., Kanbe, K., Lee, M., Wei, X., Pei, M., Sun, X., et al. (2010). Stimulation of chondrocyte hypertrophy by chemokine stromal cell-derived factor 1 in the chondro-osseous junction during endochondral bone formation. *Dev. Biol.* 341, 236–245. doi: 10.1016/j.ydbio.2010.02.033

Wylie, J. D., Hartley, M. K., Kapron, A. L., Aoki, S. K., and Maak, T. G. (2015). What is the effect of matrices on cartilage repair? A systematic review. *Clin. Orthop. Relat. Res.* 473, 1673–1682. doi: 10.1007/s11999-015-4141-0

Xing, L., Jiang, Y., Gui, J., Lu, Y., Gao, F., and Xu, Y. (2013). Microfracture combined with osteochondral paste implantation was more effective than microfracture alone for full-thickness cartilage repair. *Knee Surg. Sports Traumatol. Arthrosc.* 21, 1770–1776. doi: 10.1007/s00167-012-2031-5

Zhang, W., Chen, J., Tao, J., Jiang, Y., Hu, C., Huang, L., et al. (2013). The use of type 1 collagen scaffold containing stromal cell-derived factor-1 to create a matrix environment conducive to partial-thickness cartilage defects repair. *Biomaterials* 34, 713–723. doi: 10.1016/j.biomaterials.2012.10.027

Conflict of Interest: The authors declare that the research was conducted in the absence of any commercial or financial relationships that could be construed as a potential conflict of interest.

frontiers in Cell and Developmental Biology

ORIGINAL RESEARCH
published: 02 March 2021
doi: 10.3389/fcell.2021.579951

MANF Produced by MRL Mouse-Derived Mesenchymal Stem Cells Is Pro-regenerative and Protects From Osteoarthritis

*Gautier Tejedor[1], Patricia Luz-Crawford[2], Audrey Barthelaix[1], Karine Toupet[1], Sébastien Roudières[3], François Autelitano[4], Christian Jorgensen[1,5] and Farida Djouad[1]**

[1] IRMB, INSERM, University of Montpellier, Montpellier, France, [2] Laboratorio de Inmunología Celular y Molecular, Facultad de Medicina, Universidad de los Andes, Santiago, Chile, [3] Sanofi, Chilly-Mazarin, France, [4] EVOTEC (France) SAS, Toulouse, France, [5] Centre Hospitalier Universitaire de Montpellier, Montpellier, France

OPEN ACCESS

Edited by:
Tiago Lazzaretti Fernandes, University of São Paulo, Brazil

Reviewed by:
Laura Iop, University of Padua, Italy
Sandra Anjo, University of Coimbra, Portugal

***Correspondence:**
Farida Djouad
farida.djouad@inserm.fr

Specialty section:
This article was submitted to Stem Cell Research, a section of the journal Frontiers in Cell and Developmental Biology

Received: *03 July 2020*
Accepted: *02 February 2021*
Published: *02 March 2021*

Citation:
Tejedor G, Luz-Crawford P, Barthelaix A, Toupet K, Roudières S, Autelitano F, Jorgensen C and Djouad F (2021) MANF Produced by MRL Mouse-Derived Mesenchymal Stem Cells Is Pro-regenerative and Protects From Osteoarthritis. Front. Cell Dev. Biol. 9:579951. doi: 10.3389/fcell.2021.579951

The super healer Murphy Roths Large (MRL) mouse represents the "holy grail" of mammalian regenerative model to decipher the key mechanisms that underlies regeneration in mammals. At a time when mesenchymal stem cell (MSC)-based therapy represents the most promising approach to treat degenerative diseases such as osteoarthritis (OA), identification of key factors responsible for the regenerative potential of MSC derived from MRL mouse would be a major step forward for regenerative medicine. In the present study, we assessed and compared MSC derived from MRL (MRL MSC) and C57BL/6 (BL6 MSC) mice. First, we compare the phenotype and the differentiation potential of MRL and BL6 MSC and did not observe any difference. Then, we evaluated the proliferation and migration potential of the cells and found that while MRL MSC proliferate at a slower rate than BL6 MSC, they migrate at a significantly higher rate. This higher migration potential is mediated, in part, by MRL MSC-secreted products since MRL MSC conditioned medium that contains a complex of released factors significantly increased the migration potential of BL6 MSC. A comparative analysis of the secretome by quantitative shotgun proteomics and Western blotting revealed that MRL MSC produce and release higher levels of mesencephalic astrocyte-derived neurotrophic factor (MANF) as compared to MSC derived from BL6, BALB/c, and DBA1 mice. MANF knockdown in MRL MSC using a specific small interfering RNA (siRNA) reduced both MRL MSC migration potential in scratch wound assay and their regenerative potential in the ear punch model in BL6 mice. Finally, injection of MRL MSC silenced for MANF did not protect mice from OA development. In conclusion, our results evidence that the enhanced regenerative potential and protection from OA of MRL mice might be, in part, attributed to their MSC, an effective reservoir of MANF.

Keywords: MRL mouse, regeneration, mesenchymal stem cells, MANF, chondroprotection, osteoarthritis

INTRODUCTION

The super healer Murphy Roths Large (MRL) mice, is an attractive model to study tissue regeneration in mammals. Indeed, MRL mice display the extraordinary capacity to regenerate several musculoskeletal tissues such as ear wounds, injured articular cartilage and amputated digits without scarring (Clark et al., 1998; Fitzgerald et al., 2008; Ward et al., 2008; Kwiatkowski et al., 2016; Deng et al., 2019; Sinha et al., 2019). Although the mechanisms underlying MRL mice regenerative capabilities are intensively studied, the exact process responsible for tissue regeneration is not fully understood.

The cartilage regenerative potential of MRL mesenchymal stem cells (MSC) have been first tested in a model of posttraumatic arthritis. In this study, the authors assessed and compared the effect of the intra-articular injection of MSC derived from the bone marrow (BM) of MRL and C57BL/6 (BL6) mice and found that both MSC exhibit a similar protective effect (Diekman et al., 2013). In line with this study, a similar cartilage repair capacity has been described for MSC derived from the synovial of MRL and C57BL/6 mice when tested in a focal cartilage defect (Mak et al., 2016). However, although MRL MSC did not exhibit superior capacity to repair the cartilage compared to BL6 MSC, only MRL MSC were found within the defect area. More recently, extracellular vesicles produced by chondrogenic progenitor cells derived from MRL and CBA mice were tested in a mouse model of osteoarthritis induced by surgical destabilization of the medial meniscus (DMM). Extracellular vesicles derived from MRL cells had a greater anti-osteoarthritic potential than extracellular vesicles derived from CBA (Wang et al., 2020). In an inflammatory environment, MSC release factors that possess potent anti-inflammatory effects and influence cartilage matrix turnover (Van Buul et al., 2012). However, the anti-osteoarthritic activity of soluble factors released by MRL MSC have never been investigated in experimental model of osteoarthritis (OA).

Mesencephalic astrocyte-derived neurotrophic factor (MANF) is a protein evolutionarily conserved (Lindholm and Saarma, 2010) that is expressed by most if not all tissues in the body (Lindholm et al., 2008). MANF expression is induced upon various stress signals and generate a cytoprotective response in different systems (Lindahl et al., 2017). *In vivo*, MANF has been described for its role on tissue regeneration and inflammation resolution (Voutilainen et al., 2009; Chen et al., 2015; Neves et al., 2016). Indeed, in damaged retina of flies and mice, MANF expression is induced in innate immune cells, activating them and inducing an enhanced neuroprotection and tissue repair (Neves et al., 2016). MANF facilitates the differentiation and migration of neural progenitor cells and thus increasing neuroblast recruitment in stroke cortex (Tseng et al., 2018). Moreover, MANF is a systemic regulator of metabolic and immune homeostasis in young individuals. Indeed, MANF supplementation improves different hallmarks of liver aging including inflammation, hepatosteatosis and metabolic dysfunction (Sousa-Victor et al., 2019). These studies give rise to the questions of whether MANF is expressed in adult MRL mouse that have retained features of embryonic metabolism (Naviaux et al., 2009) and whether MSC derived from different mouse strains release different levels of MANF that could be correlated with their pro-regenerative or/and anti-osteoarthritic potential.

In the present study, we addressed whether the regenerative potential and the anti-osteoarthritic potential of MRL mice could be attributed to the intrinsic particularities of MSC focusing on the role of MANF.

MATERIALS AND METHODS

MSC Isolation and Expansion

Mesenchymal stem cells (MSC) were isolated from the bone marrow (BM) of MRL/Mpj (MRL MSC) and C57BL/6 mice (BL6 MSC), expanded and phenotypically and functionally characterized after their spontaneous immortalization *in vitro* as previously described by our laboratory (Bouffi et al., 2010). The MSC were used between passages 15 and 20 for the present study.

MSC Immunophenotype

MRL and BL6 MSC were phenotypically characterized according to the expression levels of hematopoietic and stromal cell antigens using specific antibodies against CD73, CD90, interferon (IFN)-γR1, F4/80, CD44, stem cells antigen-1 (SCA-1), CD11b, and CD45 (BD Pharmingen) and evaluated by fluorescence-activated cell sorting (FACS). Analysis was performed using the FlowJo software (BD Pharmingen).

MSC Differentiation

Mesenchymal stem cell was induced to differentiate into chondrocytes, adipocytes and osteoblasts as previously described (Bouffi et al., 2010). Briefly, for adipogenesis, cells were seeded at 10^4 cells/cm^2 in complete Dulbecco's modified Eagle's medium (DMEM)-F12 (Invitrogen) containing 16 μM biotin, 18 μM pantothenic acid, 100 μM ascorbic acid, 5 μg/ml insulin, 0.03 μM dexamethasone, 1 μg/ml transferring, 2 ng/ml triiodothyronine (T3) and 100 nM rosiglitazone (Sigma). Formation of lipid droplets was visualized by Oil red O staining after a 1 h fixation step in 3% glutaraldehyde. For osteogenesis, cells were seeded at low confluence at 3×10^3 cells/cm^2 in proliferation media. After the cells have reached confluency, the media was replaced by osteogenic media composed of DMEM (Invitrogen) completed with 10% of fetal calf serum, 100 U/mL penicillin/streptomycin, 2 mmol/mL glutamine, 0.5 μg/ml of ascorbic acid and 3 μM NaH_2PO_4 (Sigma). The capacity of differentiated MSC to mineralize the extracellular matrix was assessed by Alizarin Red staining. The chondrogenic differentiation of MSC was induced using the micropellets protocol. To that end, cells were seeded at 2.5×10^5 cells/well in 96-Well Polypropylene (NUNC), centrifuge at 400 *g* for 5 min and cultured in DMEM (Invitrogen) completed with 100 U/mL penicillin/streptomycin, 10 μM of sodium-pyruvate, 1.7 μM of ascorbic acid-2-phosphate, insulin-transferrin-selenium (ITS, Sigma) and 1 ng/ml of human Transforming Growth Factor β3 (hTGF-β3, R&D System). After 21 days, the pellets were fixed in paraformaldehyde (PFA) and immunohistochemistry was performed on paraffin sections.

Chondrocyte Isolation, Expansion and Treatment

Chondrocytes were isolated from OA patients undergoing total knee replacement surgery as previously described (Maumus et al., 2013). Briefly, articular cartilage was harvested from the femoral condyles of 12 patients. Consent of donors was approved by the French Ministry of Research and Innovation (approvals DC2009-1052 and DC-2010-1185). Slices of knee cartilage were incubated within 2.5 mg/mL pronase (Sigma-Aldrich, Saint-Quentin-Fallavier, France) for 1 h and then at 37°C overnight within 2 mg/mL collagenase type II (Sigma). Digested slices were filtrated through cell strainer (70 μm) and the cell suspension was cultured in DMEM completed with 10% of fetal calf serum, 100 U/mL penicillin/streptomycin and 2 mmol/mL glutamine at the density of 25,000 cell/cm^2 till the end of passage 1. Chondrocytes were plated at high density and cultured alone or with MANF (50 ng/mL; R&D System) and maintained for 7 days in minimal medium composed of DMEM supplemented with proline (0.35 mmol/L), ascorbic acid (0.17 mmol/L) and sodium pyruvate (1 mmol/L). Finally, the cells were collected for the analysis by RT-qPCR.

MSC Proliferation

To evaluate the proliferation rate of MSC, the cells were culture in a proliferative medium containing DMEM supplemented with 10% of fetal calf serum, 100 U/mL penicillin/streptomycin and 2 mmol/mL glutamine during 7 days. The number of population doublings was estimated to compare the proliferation capacities of MSC populations. MSC were seeded at 5000 cells/cm^2 and counted when 80–90% of confluency was reached. For the proliferation assessment using the PrestoBlue™ assay (Life-Technologies, Courtaboeuf, France), MSC were seeded at low density (5000 cells/cm^2) in a 6 well plates in proliferative medium. After 7 days, MSC number was evaluated.

Proteome and Secretome Collection

Primary MSC derived from the bone marrow of BL6, BALB/c, DBA1, and MRL mice were cultured in a proliferative medium. Then, cells were washed three times with PBS prior to be cultured in a serum-free and phenol red-free DMEM medium overnight. MSC conditioned medium was collected (14 mL) and centrifuged at 3,000 × *g* for 5 min at 4°C to remove cells and cell debris and then filtered through 0.22 μm pore size membrane. Supernatants were adjusted to 0.025% with anionic acid labile surfactant I (AALS I, Progenta), concentrated at 4°C in VivaSpin 20 ultrafiltration units (#28-9323-58 MWCO: 3 kDa) and diafiltrated at 4°C against 50x volumes of 50 mM NH_4HCO_3 containing 0.025% AALS I. Protein concentration in the retentates was assessed using the NanoDrop 2000c Spectrophotometer (Thermo Fisher Scientific) and adjusted to 0.1 mg/mL with diafiltration buffer. Secretomes were kept frozen at −20°C until use. Cells were detached from the culture dishes by scraping into PBS on ice and lyzed by sonication in a lysis buffer containing 1% SDS in PBS supplemented with complete™ mini EDTA-free Protease Inhibitor Cocktail (Roche) and Halt™ Phosphatase Inhibitor Cocktail (Thermo Fisher Scientific) as well as 2500 units/ml of Benzonase® endonuclease (purity grade II, Merck). Lysates were centrifuged at 20,000 × *g* for 15 min at room temperature to sediment undissolved material. Supernatants were collected and their protein content was quantified by the BCA protein assay (Pierce). Cell proteomes were kept frozen at −20°C until use.

Proteolytic Digestion

Cell secretomes (15 μg protein) prepared from MRL and BL6 MSC were reduced in the presence of 10 mM dithiothreitol in 50 mM NH_4HCO_3 at 56°C for 30 min and then alkylated by adding 20 mM iodoacetamide for 30 min at room temperature in the dark. After the reduction and alkylation steps, proteins were digested with trypsin (0.75 μg) overnight at 37°C. After centrifugation, protein digests were collected, diluted twice with an equal volume of 0.2% (v/v) formic acid in H_2O, and filtered through 0.22 μm pore size membrane prior to LC-MS/MS analysis.

NanoLC-MS/MS Analysis, Proteins Identification, Quantification, and Statistical Analysis

Mass spectrometry (MS) analysis and data treatment was performed as previously described (Buzy, 2011; Autelitano et al., 2014). Briefly, peptide digests were analyzed on an Ultimate/Famos/Switchos suite of instruments (Dionex) connected to a hybrid LTQ Orbitrap mass spectrometer (Thermo Fisher Scientific) with the instruments setup and parameters described in the **Supplementary Materials**. Database searches were done using an internal MASCOT server (version 2.1, matrix Science[1]) using the UniProtKB/Swiss-Prot mouse protein knowledgebase[2] with the search parameters as described in the **Supplementary Methods**. For protein quantification, raw data were processed by an in-house label-free software, DIFFTAL (DIFferential Fourrier Transform AnaLysis) as previously published (Autelitano et al., 2014; Delcourt et al., 2015) and described in the **Supplementary Materials**. For statistical analysis, DIFFTAL data normalizations (loess normalization at sample level and median central tendency at match set level), protein ratio ("Effect size") and statistic *p*-value (ANOVA) calculations were performed using DanteR 0.0.1 software[3]. For biostatistics analysis of average differences in protein mean intensities ("Effect size"), between multiple replicate samples of MRL MSC and BL6 MSC, a one-way analysis of variance (ANOVA) was performed. "Effect size," a simple way of quantifying the size of the differences between the experimental and the reference group, was calculated. A difference of 1.5 in the Effect size was considered as a significant difference.

Bioinformatic Analysis

The identified proteins were analyzed using ProteinCenter bioinformatic tools (Proxeon Bioinformatics[4]). We made several

[1]http://www.matrixscience.com/
[2]http://www.uniprot.org/
[3]http://omics.pnl.gov/software/
[4]http://www.cbs.dtu.dk/services

protein sequences in one FASTA format file and submitted it to each program. SignalP (version 4.0[5]) was used to predict the presence of signal peptides in the identified proteins (D-cut-off values for SignalP-noTM networks > 0.45 or SignalP-TM networks > 0.5 as the default cut-off for signal peptide = 'Yes') (Petersen et al., 2011). The SecretomeP program (version 2.0[6]) was used to predict the possibility of non-classical protein secretion (SignalP signal peptide = 'No'; and SecretomeP score > 0.5 in mammal proteins) (Bendtsen et al., 2004).

Western Blot Analysis

Aliquots of cell proteomes or secretomes (20 μg protein) were mixed with 4x XT sample buffer (Bio Rad) containing 10% (v/v) 2-mercaptoethanol and heated at 60°C for 30 min before Western blot analysis. Proteins were resolved by SDS-PAGE on NuPAGE®Novex®4 – 12% Bis-Tris gels (Bio Rad) using the NuPAGE®MES SDS Running Buffer (Bio Rad) according to the manufacturer's instructions. Proteins from SDS-PAGE were transferred to nitrocellulose membranes and stained with the BLOT-FastStain™ Kit (G Biosciences) to determine transfer efficiency and reveal the protein expression profile of each sample. Blots were probed with antibodies directed against MANF (Abcam, Catalog # ab67271), growth arrest specific 6 (GAS6, R&D Systems, Catalog # MAB986), neudesin neurotrophic factor (NENF; Abcam, Catalog # ab74474), semaphorin 5A (SEMA5A, Abcam, Catalog # ab127002), or αTubulin. Immune complexes were visualized with enhanced chemiluminescence using the Amersham ECL Western blotting Detection Reagents (GE Healthcare) and X-ray films. Autoradiographs were scanned using the GS-800 Calibrated Densitometer (Bio-Rad). To quantitate the amount of protein present on the blot, signal volumes of MANF, GAS6, NENF, SEMA5A, and αTubulin were measured with Quantity One®1-D Analysis Software (Bio Rad) using volume analysis. The intensity value of each target protein band was normalized against the intensity value of αTubulin gel band used as the internal loading control for each sample.

MSC Transfection With siRNA

Mesenchymal stem cell was transfected at subconfluence (60%) with 200 nM of control siRNA (siCTL) or the siRNA against MANF (siMANF) (Silencer Select RNAi, Thermo Fisher Scientific, Illkirsch) using oligofectamine reagent (Life Technologies, Courtaboeuf) and according to the supplier's recommendations.

RT-qPCR

Total RNA was isolated from each sample using RNeasy Mini Kit (Qiagen, Courtaboeuf) and the quantity and purity of the total RNA were determined by using a NanoDrop ND-1000 spectrophotometer (NanoDrop ND, Thermo Fisher Scientific). cDNA was synthesized by reverse transcribing 500 ng RNA into cDNA using the M-MLV enzyme (Thermo Fischer Scientific). Quantitative PCR was performed using the SybrGreen PCR Master Mix (Roche) and a LightCycler®480 Detection system, following manufacturer's recommendations. Specific primers for mouse *Vimentin, Cadherin-11, N-Cadherin, E-Cadherin, ICAM-1, Integrinβ1, NCAM, MANF, RPS9* and human *TYPE 2B COLLAGEN (Col2B), AGGRECAN (AGN), LINK and SOX9* were designed using the Primer3 software (**Table 1**). Values were expressed as relative mRNA level of specific gene expression as obtained using the $2^{-\Delta\ Ct}$ method, using the RPS9 expression as housekeeping gene.

Scratch Wound Healing

In order to evaluate the migratory potential of the cells, we used the scratch wound assay. 2.5×10^5 cells were seeded in TC24 treated plates for imaging (Thermo Fischer Scientific) and

TABLE 1 | Proteins identified and quantified in MRL MSC and BL6 MSC.

Gene name	Species	Forward sequence	Reverse sequence
Vimentin	Mouse	CAG CTCACCA ACGACAAG CCG CAT	TCCTGCAAT TTCTCTCG CAGCCGCAT
Cadherin-11	Mouse	CCTTGCCTGCAT CGTCATCATTC	TTCCTCACC ACCCCCTTCAT
N-Cadherin	Mouse	TAGACGAGAGGC CTATCCATGC	CAGCAGCTTAA AGGCCCTCAT
E-Cadherin	Mouse	TCAACGATCCT GACCAGCAGT	TTGCTG CTTG GCCTCAAAA
ICAM-1	Mouse	CAATTTCTCATG CCGCACAG	AGCTGGAAGAT CGAAAGTCCG
Integrinβl	Mouse	CACGGATGCT GGGTTTCACT	TGTGCCCACT GCTGACTTAGG
NCAM	Mouse	CAGGAGTCCTT GGAATTCATCC	TGGAGAAGAC GGTGTGTCTGC
MANF	Mouse	CAGTTCCCTC TTGCCCATCC	GACACCCAGAAG CCCAAACC
RPS9	Mouse	GCTGTTGACGC TAGACGAGA	ATCTTCAGGCC CAGGATGTA
RPS9	Human	GATTACATCCTG GGCCTGAA	ATGAAGGACGG GATGTTCAC
Collagen-2	Human	CAGACGCTG GTGCTGCT	TCCTGGTTG CCGGACAT
Aggrecan	Human	TCGAGGACA GCGAGGCC	TCGAGGGTGTAG CGTGTAGAGA
LINK	Human	TTCCACAAG CACAAACTT TACACAT	GTGAAACTG AGTTTTGTATA ACCTCTCAGT
SOX9	Human	AGGTGCTCAAA GGCTACGAC	GTAATCCGGGT GGTCCTTCT

Displayed columns include the HUGO ID, UniProtKB accession number, description, type and subcellular location (annotated by UniProtKB), maximum number of unique peptide, normalized protein intensitiy (Log2 value), average differences in protein mean intensities (Effect Size) between multiple replicate samples of MRL MSC and BL6 MSC (N = 2). SignalP (version 4.0, http://www.cbs.dtu.dk/services/SignalP4.0) was used to predict the presence of signal peptides in the identified proteins (D-cut-off values for SignalP-noTM networks >0.45 or SignalP-TM networks >0.5 as the default cut-off for signal peptid = 'Yes'). The SecretomeP program (version 2.0, http://www.cbs.dtu.dk/services/SecretomeP2.0) was used to predict the possibility of nonclassical protein secretion (SignalP signal peptide = 'No'; and SecretomeP score >0.5 in mammal proteins). Proteins annotated as "secreted" in UniProtKB are indicated with "Yes".

[5]http://www.cbs.dtu.dk/services/SignalP4.0

[6]http://www.cbs.dtu.dk/services/SecretomeP2.0

the wound was performed manually once the cells adhered to the plastic. The wound closure was studied using an inverted microscope (Axiovert 200M, Zeiss) equipped with a motorized stage driven with Metamorph 7.0 software (Molecular Devices) (MRI facility). During the study, cells were maintained at 37°C with 5% of CO2. Images were taken each hour for a 24-h period. The wounded area was measured every hour using Image J Software. Area Under Curve (AUC), corresponding to the closure graph was calculated with GraphPad Prism software and normalized (percentage).

Ear Punch Model

Ten-week-old C57Bl6 female mice were used. At day 0, we performed a reproducible ear hole with a 2 mm punch through the center of the ear. For the different groups, we use five different mice that were injected either with PBS (untreated) or 2.5×10^5 MRL or BL6 MSC along the wound edge. Measurements of the ear wound area were performed at day 0 and day 44 using the ImageJ software on ear pictures.

Collagenase-Induced Osteoarthritis Model

We carried out the collagenase-induced OA (CIOA) model as previously described (Toupet et al., 2015) and according to the guidelines and regulations of the Ethical Committee for animal experimentation of the Languedoc-Roussillon (Approval 5349-2016050918198875, CEEA-LR-12117). Briefly, 1U type VII collagenase in 5 μL saline was intra-articularly (IA) administered in the knee joint of C57BL/6 mice (10 weeks old) at day 0 and 2. Groups of 10 mice received MSC IA (2.5×10^5 cells/5 μL saline), at day 7. At day 42, mice were euthanatized and paws were recovered for fixation in 4% formaldehyde and histological analysis.

Histological Analysis

Hind paws were decalcified after 2 weeks incubation within a solution of formic acid 5% and then embedded in paraffin. Tibias were sectioned frontally as previously described (Ruiz et al., 2020) and stained with safranin O fast green staining. Quantification of the degradation of cartilage was performed using the modified Pritzker OARSI score as described (Toupet et al., 2015; Cosenza et al., 2017).

Statistical Analysis

Results are expressed as the mean ± Standard Error of the Mean (SEM) and all experiments were performed at least three times. Generated *P*-values were obtained using Mann–Whitney unpaired *t*-test, two tails using GraphPad Prism 6 Software. Graphs show mean ± Standard SEM. *P*-values < 0.05 (*), $P < 0.01$ (**), or $P < 0.001$ (***) were considered statistically significant. Analysis and graphical representation were performed using Graph-Pad Prism^{TM} software (Graphpad).

RESULTS

MRL and BL6 MSC Exhibit a Similar Phenotype and Differentiation Potential

First, we studied the phenotype and the differentiation potential of MRL and BL6 MSC. After a long culture process in a medium containing fetal calf serum (Bouffi et al., 2010) to obtain a morphologically homogeneous MSC population with a spindle-shaped fibroblastic appearance, we phenotypically characterized the cells. Both MRL and BL6 MSC were positive for markers classically expressed by murine MSC (Bouffi et al., 2010) that include CD29, CD44, CD73, Sca-1 and they were negative for CD11b, CD45 and F4/80 (**Figure 1A**). Both MSC were slightly positive for IFNR1 previously demonstrated to be correlated with the immunoregulatory function of MSC (Luz-Crawford et al., 2015). Of note, the phenotypic differences observed between murine MSC derived from different strains of mice, are not related to the passage numbers but rather to do the strain of mouse they come from as we have previously reported (Bouffi et al., 2010). After induction of MSC differentiation toward the three specific lineages, both MRL and BL6 MSC gave rise to chondrocytes, adipocytes and osteoblasts as shown by the expression of aggrecan, the presence of lipid droplets in cultures and Alizarin Red S staining, respectively (**Figure 1B**). These results show that MRL and BL6 MSC display a similar phenotype and differentiation potential.

MRL MSC Exhibit a Higher Migration Potential That BL6 MSC

Since a clear relationship between MSC migration and tissue repair has been established (Fu et al., 2019), we compared the migration potential of MRL and BL6 MSC. To specifically study the migration, we first compare the proliferation rate of the two cells after a synchronization step and culture within a medium containing FCS. The number of population doublings (NPD), i.e., the total number of times MSC doubled within 7 days (in a single passage) was evaluated and we found that MRL MSC showed significantly lower NPD than BL6 MSC (**Figure 2A**). This was confirmed using the PrestoBlue assay that defined the proliferation of MSC after 2 days of culture (**Figure 2A**). Then, the non-directional migration of MRL and BL6 MSC was analyzed in a scratch wound assay by evaluating the area of the wound every 3 h during 36 h post-wounding using Image J software (National Institutes of Health, Bethesda, MD, United States). Representative images from scratch wound healing assay revealed, 36 h post-wounding, a complete resurfacing of the wound for MRL MSC but not for BL6 MSC (**Figure 2B**). The extent of healing/migration was defined as the percentage of open wound area between the original (100% at time 0) and the residual wound area at 24 h (**Figure 2B**). The curve of the percentage of open wound area over the healing period (0–24 h) and the corresponding area under curve (AUC) which reflects the migration potential of the cells revealed that MRL MSC closed faster the wound than BL6

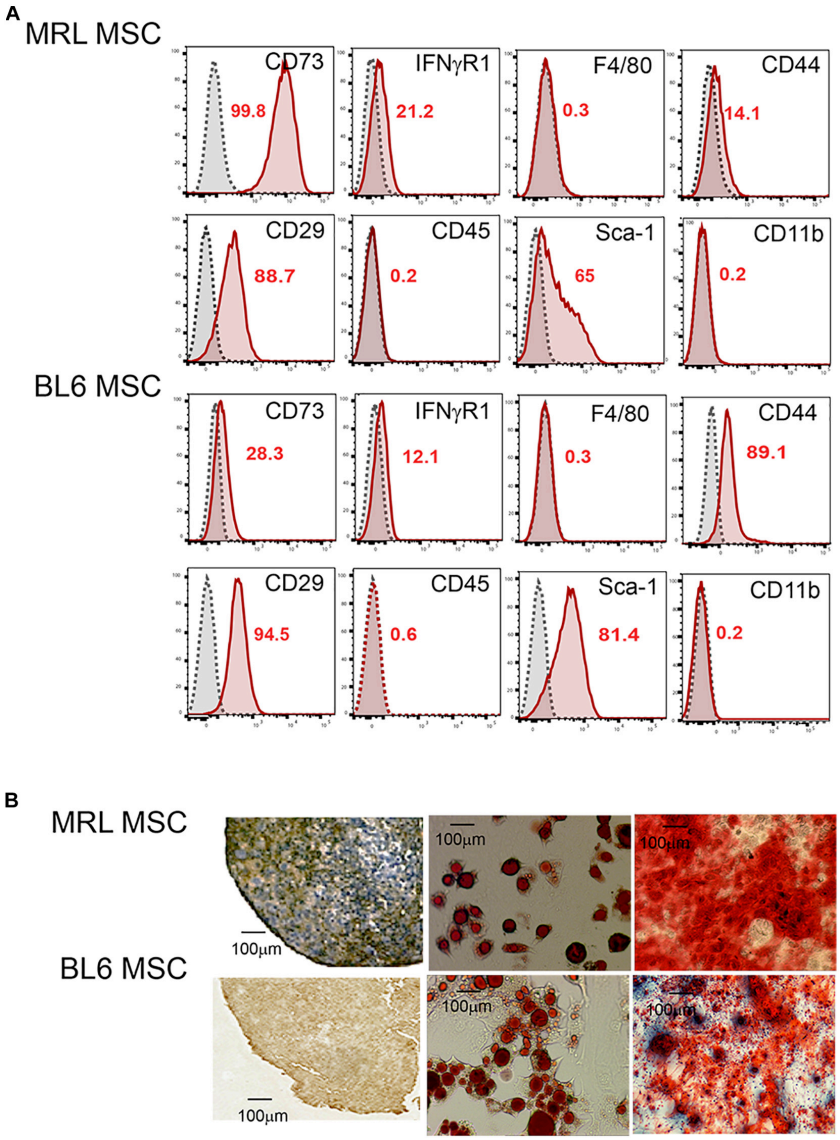

FIGURE 1 | MRL MSC and BL6 MSC have the same phenotype and differentiation potential. **(A)** Phenotype of MRL and BL6 MSC was assessed by flow cytometry using different antibodies that include CD73, IFNγR1, F4/80, CD44, CD29, CD45, SCA-1, and CD11b. The percentages of positive cells are indicated in red in the flow cytometry data. **(B)** Differentiation potential of MSC. The chondrogenic differentiation of MRL and BL6 MSC was assessed using an anti-aggrecan positive staining on pellet sections. The adipogenic potential of MSC was by the visualization of lipid droplets by phase contrast microscopy at day 21 of the differentiation process. Finally, the osteogenic differentiation potential of MSC was defined by Alizarin Red S positive staining.

MSC (**Figure 2B**). Altogether these results indicate that the slow-proliferating MRL MSC display a higher migration potential than the fast-proliferating BL6 MSC.

MRL MSC Secretome Is Responsible for Their Higher Migration Potential

Following their systemic injection, MSC migrate and accumulate at inflammation and injured sites (Rustad and Gurtner, 2012). The migration potential of MSC is controlled by several regulatory factors including adhesion molecules that also orchestrate their differentiation potential, immunoregulatory properties and their paracrine function in tissue repair (Ren et al., 2010; Fu et al., 2019). In this part of the study, we set out to examine how adhesive molecules could be correlated to the higher rate of migration of MRL MSC over BL6 MSC. Using RT-qPCR we studied the expression profiles of adhesion molecules in the two MSC. First, we found that *Vimentin*, whose expression is positively correlated with MSC migration (Huang et al., 2015), was highly expressed in MRL MSC as compared to BL6 MSC (**Figure 3A**). Similarly, ICAM-1, expressed in MSC at a low level in physiological condition and at high level in an inflammatory environment to promote MSC homing to the target and immune organs (Li et al., 2019), was expressed at

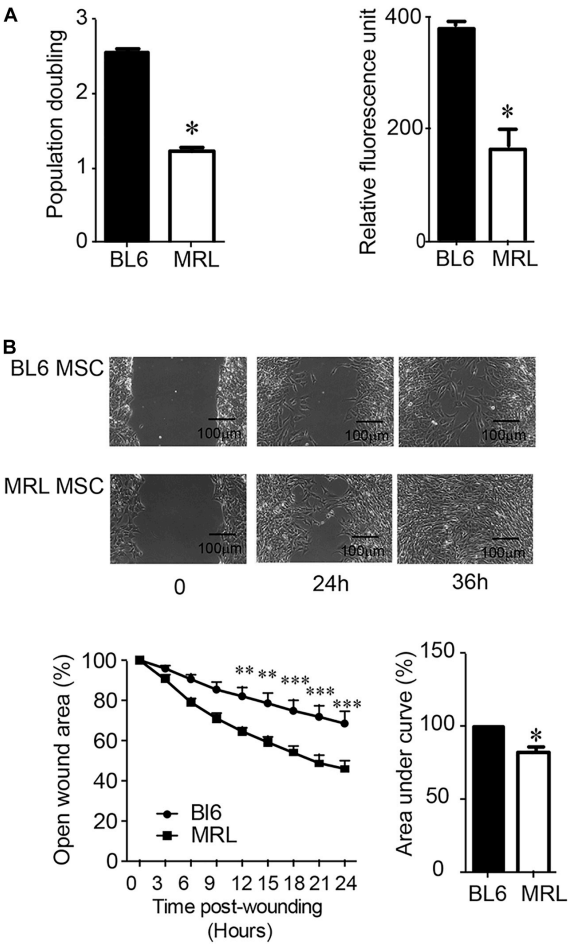

FIGURE 2 | MRL MSC exhibit a lower proliferation rate and a higher migration potential than BL6 MSC. **(A)** The proliferation potential of BL6 and MRL MSC was evaluated after an overnight synchronization in absence of serum and a 7 days culture period in complete medium by either calculating the number of population doublings, i.e., the total number of times MSC has doubled from the moment we seeded (D0) them until D7 using the formula Population Doubling = 3.33 $\log_{10}$(number of MSC at D7/number of MSC plated at D0). We also used the PrestoBlue assay (Relative fluorescence unit) to evaluate the proliferation potential of the SMC. Results represented as mean ± SEM (n = 3 replicates). **(B)** Migration of MRL and BL6 MSC were analyzed in a scratch wound assay by evaluating the area of the wound at 0, 3, 6, 9, 12, 15, 18, 21, 24, and 36 h after wounding. Representative images from scratch wound healing assay (on the top). Measure of the open wound area (bottom). 100% correspond to the highest wound area measured at 0 h using Image J software. The area under curve (AUC) was calculated from the curve of open wound area percentage over the healing period (0–24 h). Results represented as mean ± SEM (n = 5 replicates). $^{*}p \leq 0.05$, $^{**}p < 0.01$, $^{***}p < 0.001$.

a significantly higher level in MRL MSC than in BL6 MSC (**Figure 3B**). The other adhesion molecules studied such as *Cadherin-11* (**Figure 3C**), *N-Cadherin* (**Figure 3D**), *E-Cadherin* (**Figure 3E**), *Integrinβ1* (**Figure 3F**), and *NCAM* (**Figure 3G**) were expressed at a lower level in MRL MSC that in BL6 MSC. We also explored whether the higher regenerative potential of MRL MSC could be associated with soluble factors they release in culture since the regenerative potential of MSC is well-recognized to be mediated through their secretome (Menendez-Menendez et al., 2017). To that end, we cultured freshly wounded BL6 MSC with a conditioned supernatant (CM) obtained from a 24-h culture of subconfluent MRL MSC cultured in the proliferative medium (MRL CM). Scratch wounded BL6 MSC cultured with the MRL CM exhibited an enhanced capacity to resurface the wounded area as compared to BL6 MSC cultured in the proliferative medium (**Figure 3H**). This result suggests that the highest migration potential of MRL MSC compared to BL6 MSC is, in part, mediated through a paracrine mechanism.

MRL MSC Produce and Release High Amount of MANF as Compared to MSC Derived From Different Mouse Strains

In order to identify factors responsible for MRL MSC migration potential, we used label-free quantitative shotgun proteomics to identify secreted proteins that are differentially expressed between MRL MSC and BL6 MSC. Secretomes of MRL MSC and BL6 MSC were analyzed based on the protein intensities measured by LC-MS/MS (n = 2 per cell type). A total of 904 quantifiable proteins were identified with ≥2 peptides among which 127 were annotated as "Extracellular Space" in UniProtKB/Swissprot database and 411 were predicted as secretory proteins by the *in silico* bioinformatics tools SignalP (Petersen et al., 2011) and SecretomeP (Bendtsen et al., 2004) and Swissprot protein database annotation (**Supplementary Table**). We identified 810 proteins differentially expressed by at least 1.5-fold between MRL MSC and BL6 MSC. Of these, 625 proteins showed increased secretion in MRL MSC, while 185 proteins showed decreased secretion compared to BL6 MSC.

Since nerve regeneration in the MRL ear wound preceded vascularization (Buckley et al., 2011), recapitulating early mammalian development and that denervation of the ear annihilated MRL mouse regenerative ability (Buckley et al., 2012), we focused our attention on proteins with neurotrophic properties showing more than 1.5-fold increased secretion in MRL MSC compared to BL6 MSC. Among these proteins, we identified GAS6, NENF, and MANF (**Figure 4A**). Regarding the factors showing increased secretion in BL6 MSC compared to MRL MSC, we considered one member of the semaphorin family: SEMA5A. Using Western blot method, we studied the expression profiles of MANF, NENF, GAS6 and SEMA5a in MSC from different mouse strains to identify proteins specifically highly expressed in MRL-MSC (**Figure 4B**). We found that MANF was the only protein among the four tested to be overexpressed in MRL MSC as compared to MSC derived from the bone marrow of BL6, BALB/c, and DBA1 mice (**Figure 4B**). By RT-qPCR we confirmed that MANF was overexpressed in MRL MSC as compared to BL6 MSC (**Figure 4C**).

Since, the MRL CM contained factors that enhanced the migration potential of BL6 MSC, we studied the differential expression profile of the candidate factors in the conditioned medium (CM) of MSC derived from MRL, BL6, BALB/c and DBA1 mice using Western blotting. We found that while MANF was not or poorly produced in the CM of BL6, BALB/c and DBA1 it was highly released in MRL MSC cultures (**Figures 4D,E**).

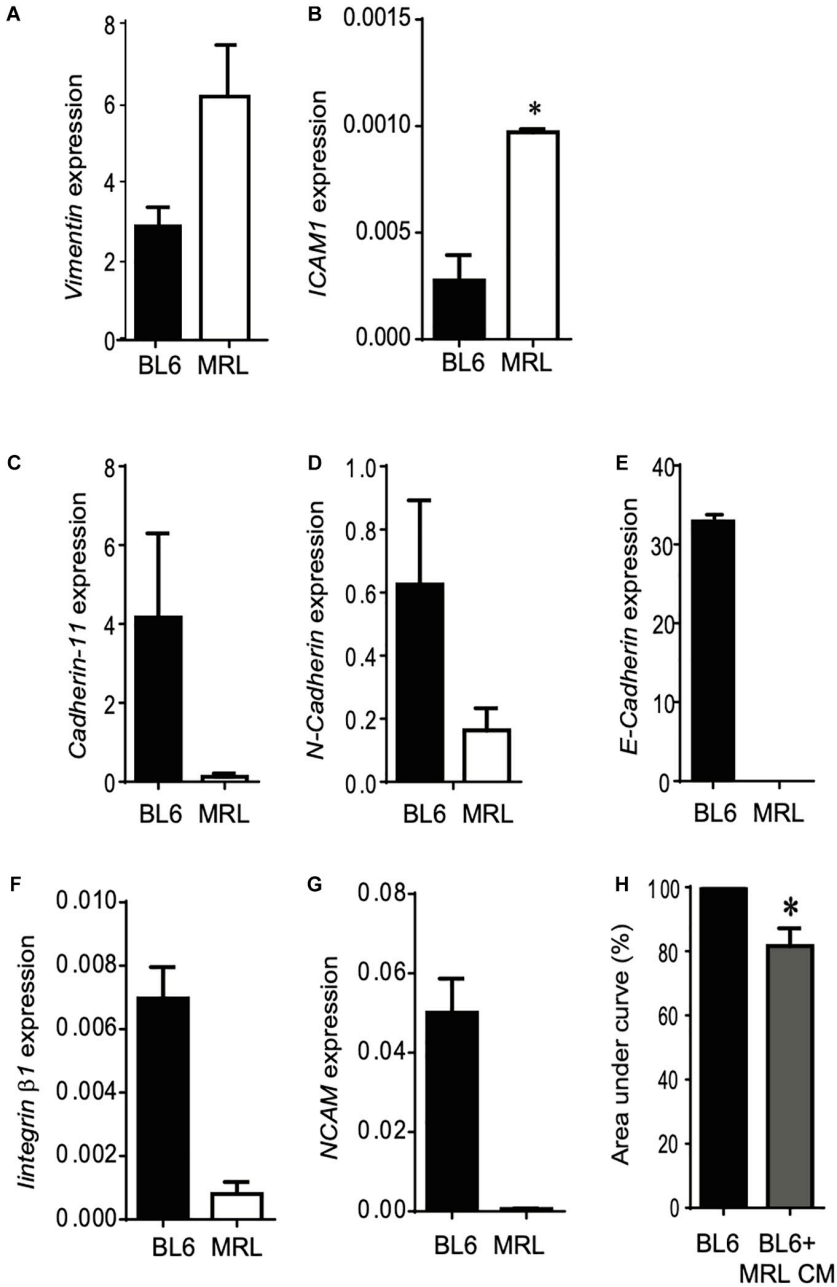

FIGURE 3 | The higher migration potential of MRL MSC is mediated through the release of soluble factors. **(A–G)** RT-qPCR analysis of *Vimentin, ICAM1, Cadherin-11, N-Cadherin, E-Cadherin, Integrinβ1, and NCAM* expression levels in MRL MSC and BL6 MSC. Results represented as mean ± SEM (n = 4 replicates). *$p \leq 0.05$. **(H)** The scratch wound was performed on BL6 MSC monolayer cultured alone or with a conditioned-medium obtained from a 24 h culture of subconfluent MRL MSC (MRL CM). The area under curve (AUC) was calculated from the curve of open wound area percentage over the healing period (0–24 h). *$p \leq 0.05$.

These results identified MANF as a factor potentially involved in the regenerative process of MRL mice.

MANF Is Necessary for the Regenerative Potential of MRL MSC *in vitro* and *in vivo*

To go further, we studied the role of MANF on the regenerative potential of MRL MSC. First, we tested the role of MANF on the non-directional migration potential of MRL MSC using the scratch wound assay. To that end, we used the small interfering RNA (siRNA) approach to knock down the expression of *MANF* in MRL MSC. 48 h post-transfection (at day 0 of the scratch wound assay) of MSC with a siRNA against *MANF* (siMANF), *MANF* expression was reduced by 30% compared with the MSC transfected with the control siRNA (siCTL) (**Figure 5A**). The percentage of open wound area over the 24-h healing

A

HUGO-ID	Accession number	Description	Unique peptide	BL6 Intensity (Log2 value)	MRL Intensity (Log2 value)	Effect size MRL/BL6
GAS6	Q61592	growth arrest- specific 6	3	11.04	17.18	18.8
MANF	Q9CXI5	mesencephalic astrocyte-derivedneurotrophicfactor	6	14.35	17.62	3.2
NENF	Q9CQ45	neuronderived neurotrophicfactor	4	18.70	19.34	1.7
SEMA5A	Q62217	Semaphorin-5A	5	18.16	14.97	0.1

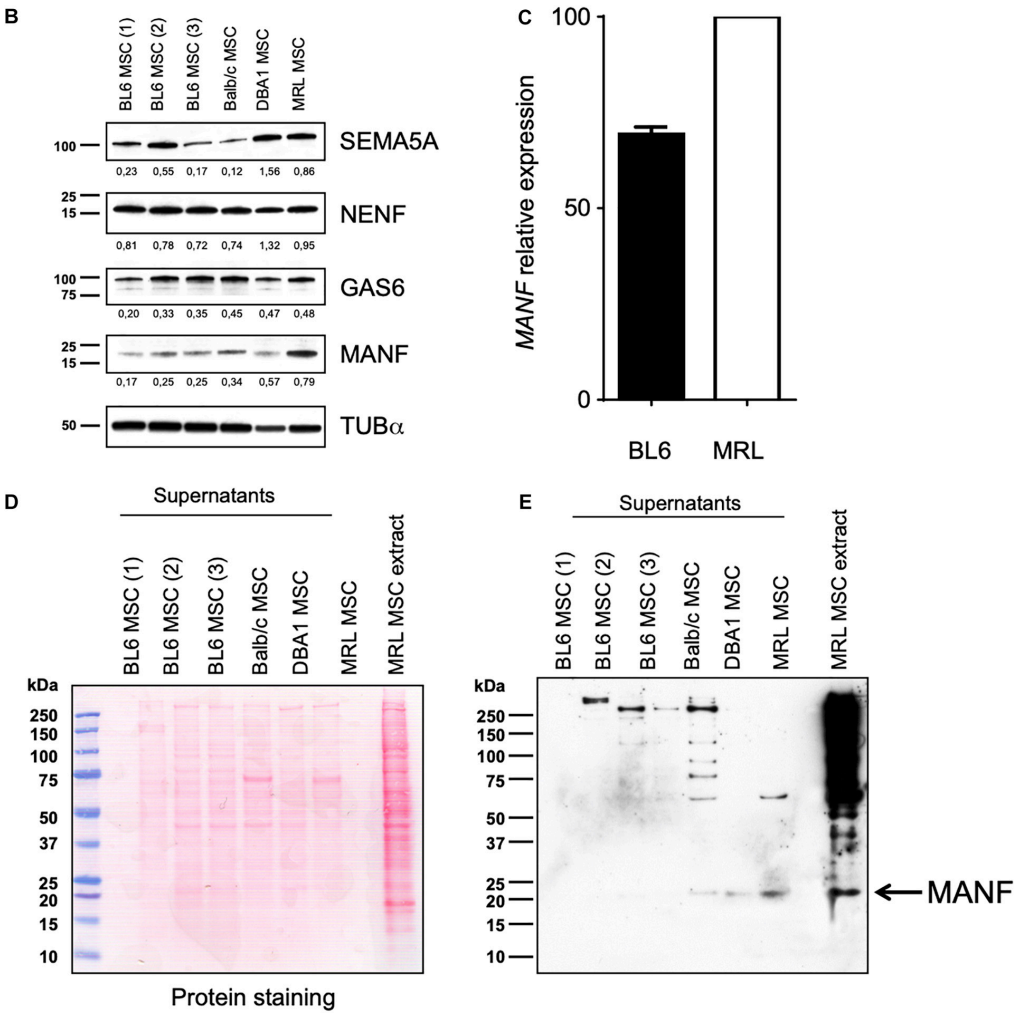

FIGURE 4 | MRL MSC produced and released higher amount of MANF than BL6, BALB/c and DBA1 MSC. **(A)** Proteomic analysis of differential expression of MANF, GAS6, NENF, and SEMA5A in MRL MSC compared to BL6 MSC secretomes. Effect size indicate the standardized mean difference in protein expression level between MRL MSC and BL6 MSC. For each protein, the median intensity levels (Log 2 value) in MRL MSC and BL6 MSC are indicated. Normalized protein intensities were used to calculate the Effect size MRL/BL6. **(B)** Western blot analysis of MANF, GAS6, NENF, and SEMA5A in whole-cell extracts from BL6, BALB/c and DBA1 MSC. The intensity value of each target protein band was normalized against the intensity value of α-Tubulin gel band used as the internal loading control for each sample. **(C)** *MANF* mRNA expression level in MRL MSC and BL6 MSC. Western blot analysis of supernatants of BL6, BALB/c, and DBA1 MSC showing blotted proteins stained with Ponceau S **(D)** and the MANF protein band revealed by the anti-MANF antibody **(E)**. MRL MSC whole cell extract was used as a positive control.

period (**Figure 5B**) and the corresponding AUC (**Figure 5C**) which reflects the migration potential of the cells revealed that *MANF* silencing reduced the capacity of MRL MSC to resurface the wound area. To define whether MANF released by MRL MSC is responsible for their migration potential, we cultured freshly wounded BL6 MSC with a conditioned supernatant (CM) obtained from a 24-h culture of subconfluent MRL MSC transfected with siMANF (MRL siMANF CM). Scratch wounded

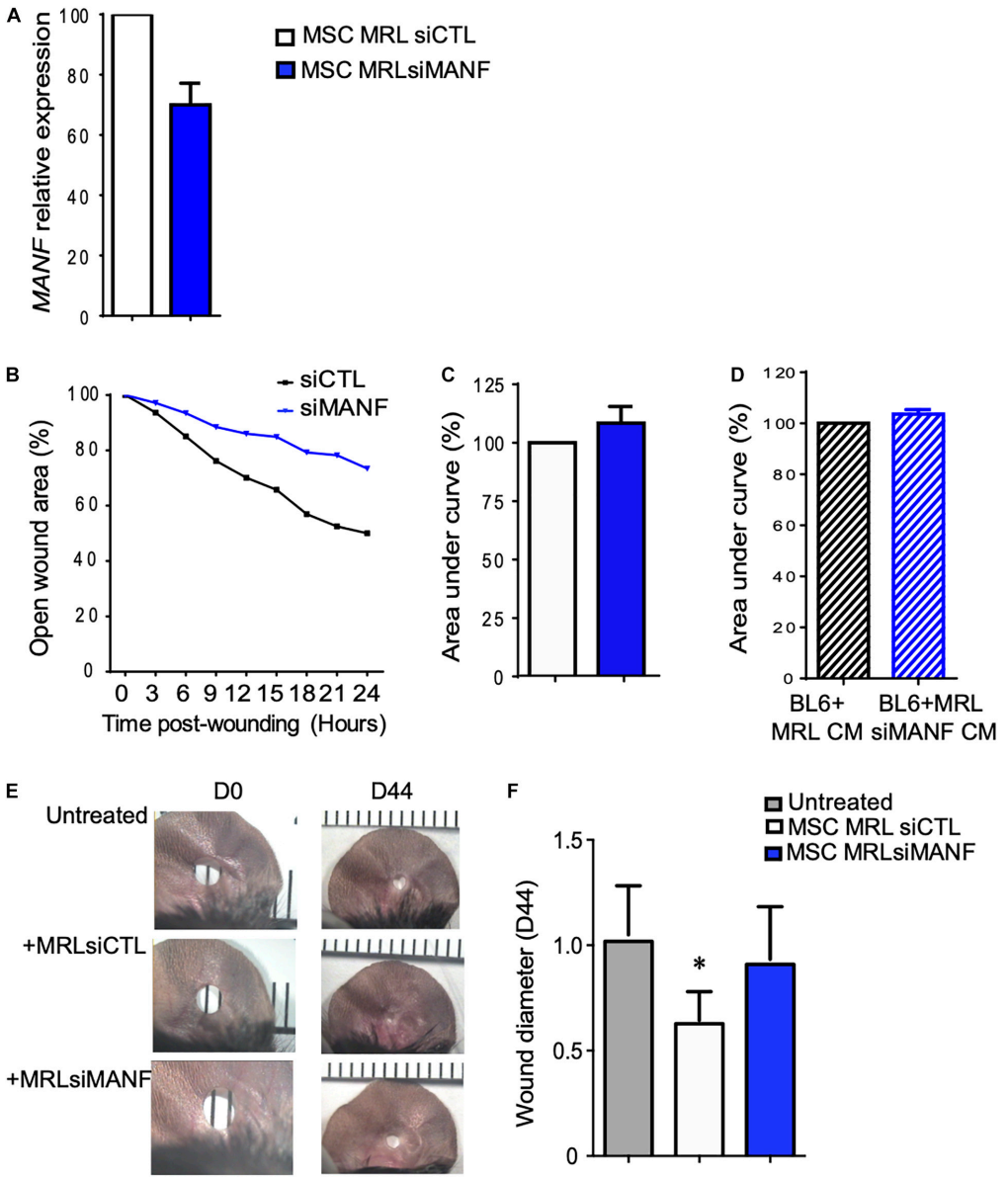

FIGURE 5 | The high migration and regenerative potential of MRL MSC depend on MANF. **(A)** *MANF* mRNA expression level in MRL MSC transfected either with a control siRNA (siRNA CTL) or a siRNA against *PYCR1* (siMANF) 48 h post-transfection (mean ± SEM, from one representative experiment). **(B)** The migration potential of MRL MSC transfected with siCTL or siMANF were analyzed in a scratch wound assay by evaluating the area of the wound at 0, 3, 6, 9, 12, 15, 18, 21, and 24 h after wounding (mean ± SEM, from one representative experiment). **(C)** The area under curve (AUC) was calculated from the curve of open wound area percentage over the healing period (0–24 h). **(D)** The scratch wound was performed on BL6 MSC monolayer cultured alone or with a conditioned-medium obtained from a 24 h culture of subconfluent MRL MSC silenced for MANF (MRL siMANF CM) (mean ± SEM, n = 3.). **(E)** Pictures of the ear holes at day 0 and day 44 after wounding. The punch-holes in the ears of MRL mice were either untreated (untreated) or treated with MSC. MRL MSC transfected either with siCTL (MRLsiCTL) or siMANF (MRLsiMANF) were injected at the wound edges. **(F)** Quantification of the ear punch hole closure at day 44 using the image J program to define the ear punch area. Results represent the mean ± SEM. N_{mice} = 10 per condition, Mann–Whitney test, two-tailed, when not indicated untreated versus MRL MSC_{siCTL}, $^{*}p \leq 0.05$.

BL6 MSC cultured with the MRL siMANF CM tend to exhibit a reduced capacity to resurface the wounded area compared to BL6 MSC cultured with the control MRL CM as revealed by the higher AUC (**Figure 5D**). Altogether these results suggest that the high migration potential of MRL MSC, *in vitro*, partly depends on their capacity to release MANF.

The MRL mouse has been well described for its remarkable capacity for cartilaginous wound closure and regeneration two decades ago (Clark et al., 1998). Indeed, 2 mm punch wounds made into MRL/MpJ mice ears closed with regeneration after 30 days, whereas they did not close in the C57BL/6 mice. Herein, we tested whether the administration of MRL MSC could

induce the regeneration in BL6 mice and whether this relies on MANF production. To that end, a 2 mm punch wounds was made into BL6 mice. Wounded mice were either untreated or treated with MSC (MRL siCTL) injected along the wound edge. Measurements of the ear punch wound area at day 44 revealed that MRL MSC induced a regenerative process leading to a significant decrease of the wound size, 40% reduction in area, as compared to the untreated mice (**Figures 5E,F**). Then, we assessed, whether this regenerative process mediated by MRL MSC was associated with their high expression level of *MANF*. The ear punch wound area of BL6 mice treated with MRL MSC deficient for *MANF* (MRL MSC siMANF) did not show any difference with the untreated mice (**Figures 5E,F**). Overall, this finding suggests that the *in vivo* regenerative potential of MRL MSC in BL6 mice depends, in part, on *MANF* expression level.

MANF Is Necessary for the Anti-osteoarthritic Properties of MRL MSC

Mesenchymal stem cell protect chondrocytes from degeneration associated with OA and protect mice from OA development (Maumus et al., 2013; Toupet et al., 2015; Cosenza et al., 2017; Ruiz et al., 2020). Since MRL mice possess an intrinsic ability to regenerate articular cartilage (Fitzgerald et al., 2008), we wondered whether MANF highly produced by MRL MSC could protect chondrocyte from a loss of anabolic markers *in vitro* and mice from OA development *in vivo*.

In order to determine the effect of MANF on human primary chondrocytes, a culture assay was designed. To that end, we used human primary chondrocytes that were isolated and cultured in proliferative medium containing 10% FCS. Then, chondrocytes were placed in a minimal medium to avoid FCS side effects and culture alone or with recombinant human MANF (50 ng/mL) during 7 days (**Figure 6A**). Then, we evaluated the phenotype of chondrocytes in the culture assay and found that while MANF tend to increase the expression of chondrocyte markers such as *Col 2B*, *Aggrecan* (*AGN*) and *LINK* its significantly increased the expression of *SOX9* (**Figure 6B**). Altogether, these data demonstrate a potent role of MANF in the protection of chondrocytes from the loss of mature chondrocyte phenotype which are characteristics of OA.

Then, we evaluated *in vivo* the effect of IA injection of BL6 and MRL MSC in CIOA mice (Toupet et al., 2015). As expected, histological analysis showed that the OA score was significantly lower in CIOA mice treated with BL6 MSC compared with untreated mice (**Figures 6C,D**). Of note, we did not observe any significant difference between the OA score of mice treated with either BL6 or MRL MSC. Conversely, the OA score was significantly higher in mice treated with MRL MSC silenced for *MANF* (MRL MSC siMANF) as compared to mice treated with MRL MSC (**Figures 6E,F**). Overall, these results indicate that MANF highly produced by MRL MSC protects chondrocytes from a loss of anabolic markers that characterizes OA-like chondrocytes and contributes to their therapeutic effect in CIOA mice.

DISCUSSION

This study provides the first evidence that MRL MSC induce ear hole regeneration and protect mice from osteoarthritis through their high capacity to release MANF.

First, we showed that the slow-proliferating MRL MSC display a higher migration potential than the fast-proliferating BL6 MSC. This is in line with the established relationship between MSC migration and tissue repair (Fu et al., 2019). Due to their paracrine ability, migration, adhesion and homing potential, MSC have been intensively studied in the field of regenerative medicine. Thus, it is tempting to believe that the identification of key factors for MRL MSC migration and regeneration potential will be of high interest for novel therapy of degenerative diseases. Thus, due to their enhanced migration potential mediated, in part, through the release of paracrine factors, we focused on the secretome of MRL MSC. We found that MANF was specifically highly produced by MRL MSC as compared to MSC derived from other mouse strains. The role of MANF in tissue regeneration has already been described. Indeed, in mice and flies, in response to retina damages retina of flies and mice, MANF was induced in innate immune cells. MANF activated innate immune cells, enhanced cytoprotection and improved tissue repair (Neves et al., 2016). In this study, MANF was shown to be necessary and sufficient to induce the *Drosophila* homolog of the mammalian anti-inflammatory macrophage marker *arginase1* in hemocytes, suggesting an association between MANF expression, resolution of inflammation and tissue repair in the retina (Neves et al., 2016).

Osteoarthritis (OA) is an inflammatory and degenerative joint disease, which mainly affects the articular cartilage and results in pain and impaired movement. It is now acknowledged that OA is a heterogeneous disease with multiple clinical phenotypes and that inflammation contributes significantly to cartilage and bone alterations during OA. However, conventional anti-inflammatory therapies have been disappointing so far for the treatment of OA. Thus the identification of a molecule that would not only control inflammation but also promote MSC migration and regeneration would be of high interest to treat most if not all degenerative diseases characterized by two main features that are inflammation and tissue degradation. Here, we demonstrate that the high migration potential of MRL MSC, *in vitro*, and the regenerative potential of MRL MSC in ear punched BL6 mice depends on *MANF*. Thus in addition to their anti-inflammatory effects described in the context of damaged retina, here, we provide the first evidence that MANF can control the migration and the regenerative properties of MSC. This is in line with the study performed in stroke cortex and that describes the neuroregenerative activity of MANF through its capacity to favor differentiation and migration of neural progenitor cells (Tseng et al., 2018). Overexpressed MANF induced STAT3 activation during subventricular zone cell migration (Tseng et al., 2018). In MSC, STAT3 silencing inhibited their migration and invasion ability while IL22 also promoted MSC migration and invasion through STAT3 signaling (Cui et al., 2019).

We also described the pro-regenerative role or MANF in the ear punch model. Indeed, while MRL MSC induced a

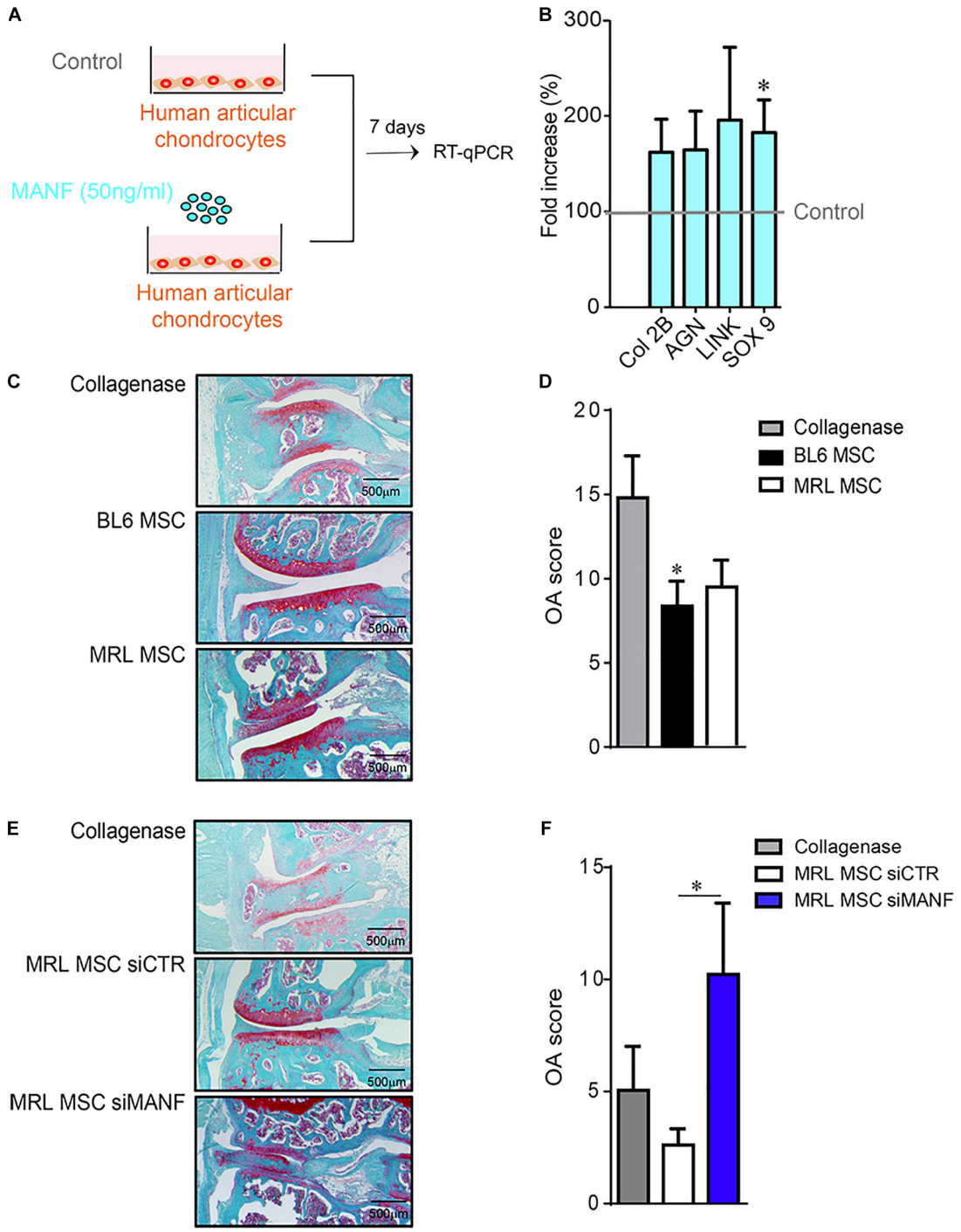

FIGURE 6 | MANF protects chondrocyte from a OA-like phenotype and mice from osteoarthritis. **(A)** Scheme showing the treatment protocol of human primary chondrocytes with MANF (50 ng/mL) during 7 days. **(B)** RT-qPCR analysis of chondrocyte anabolic markers such as *Col2B, AGN, LINK,* and *SOX9* expressed in human primary chondrocytes cultured in minimal medium or minimal medium (Control) containing MANF during 7 days. Results are expressed as fold change of gene expression compared to chondrocytes alone (Control) [mean ± SEM (n = 12 biological replicates)]. *$p \leq 0.05$. **(C)** Histological images of CIOA mice not treated (Collagenase) or treated with BL6 MSC or MRL MSC. **(D)** OA score of histological sections of knee joints of the mice described in **(C)**. **(C)** (n = 15/group). **(E)** Histological images of CIOA mice not treated (Collagenase) or treated with MRL MSC transfected with a siCTL (MRL MSC siCTL) or a siMANF (MRL MSC siMANF). **(F)** OA score of histological sections of knee joints of the mice described in **(E)**. Results are expressed as the mean ± SEM; *$p < 0.05$ (Mann–Whitney test; n = 10 mice/group).

regenerative process, MRL MSC deficient for *MANF* did not. The tissue repair potential of MANF was proposed to function through a synergistic activity as a suppressor of inflammation and apoptosis (Sousa-Victor et al., 2018). This model is in agreement with our recent findings showing the anti-apoptotic effect of MANF on human primary chondrocytes treated with camptothecin (data not shown).

Finally, we showed that MANF highly produced by MRL MSC contributes to their capacity to tend to reduce the OA score. However, although we observed a significant exacerbation of the OA score in mice treated with MRL MSC deficient for *MANF* as compared to naïve MRL MSC, we did not show an enhanced therapeutic effect of MRL MSC compared to BL6 MSC in CIOA mice. This result underlines that other factors than MANF are involved in the anti-osteoarthritic properties of MSC. Regarding the *in vivo* beneficial effect of MSC, it is still not clear whether it could be due to the immunoregulatory properties of MSC or to tissue-protective and pro-regenerative properties. Further studies should be performed to define the mechanisms underlying the anti-osteoarthritic properties of MSC.

CONCLUSION

Our findings demonstrate that the enhanced regenerative potential of MRL MSC as well as their capacity to tend to reduce OA is attributed, in part, to their capacity to release high amount of MANF.

DATA AVAILABILITY STATEMENT

The original contributions presented in the study are included in the article/**Supplementary Material**, further inquiries can be directed to the corresponding author/s.

ETHICS STATEMENT

The animal study was reviewed and approved by 5349-2016050918198875, CEEA-LR-12117.

AUTHOR CONTRIBUTIONS

FD designed the project and the experiments with the input of PL-C, FA, and CJ. GT, PL-C, AB, KT, and SR performed the experiments and analyzed the results. FD wrote the manuscript with the input of PL-C, FA, and CJ. All authors contributed to the article and approved the submitted version.

FUNDING

This work was supported by Inserm, The University of Montpellier and grant from SANOFI.

ACKNOWLEDGMENTS

We thank the MRI facility for their assistance and SMARTY platform and Network of Animal facilities of Montpellier.

SUPPLEMENTARY MATERIAL

The Supplementary Material for this article can be found online at: https://www.frontiersin.org/articles/10.3389/fcell.2021.579951/full#supplementary-material

REFERENCES

Buzy, A. (2011). *DIFFTAL : A label-free approach for absolute quantification of proteins in a complex mixture. presented at the annual meeting "6ème Journée de Spectrométrie de Masse en Midi-Pyrénées", Toulouse, France, 13 December 2011*.

Autelitano, F., Loyaux, D., Roudieres, S., Deon, C., Guette, F., Fabre, P., et al. (2014). Identification of novel tumor-associated cell surface sialoglycoproteins in human glioblastoma tumors using quantitative proteomics. *PLoS One* 9:e110316. doi: 10.1371/journal.pone.0110316

Bendtsen, J. D., Jensen, L. J., Blom, N., Von Heijne, G., and Brunak, S. (2004). Feature-based prediction of non-classical and leaderless protein secretion. *Protein Eng Des Sel* 17, 349–356. doi: 10.1093/protein/gzh037

Bouffi, C., Bony, C., Courties, G., Jorgensen, C., and Noel, D. (2010). IL-6-dependent PGE2 secretion by mesenchymal stem cells inhibits local inflammation in experimental arthritis. *PLoS One* 5:e14247. doi: 10.1371/journal.pone.0014247

Buckley, G., Metcalfe, A. D., and Ferguson, M. W. (2011). Peripheral nerve regeneration in the MRL/MpJ ear wound model. *J Anat* 218, 163–172. doi: 10.1111/j.1469-7580.2010.01313.x

Buckley, G., Wong, J., Metcalfe, A. D., and Ferguson, M. W. (2012). Denervation affects regenerative responses in MRL/MpJ and repair in C57BL/6 ear wounds. *J Anat* 220, 3–12. doi: 10.1111/j.1469-7580.2011.01452.x

Chen, L., Feng, L., Wang, X., Du, J., Chen, Y., Yang, W., et al. (2015). Mesencephalic astrocyte-derived neurotrophic factor is involved in inflammation by negatively regulating the NF-kappaB pathway. *Sci Rep* 5, 8133.

Clark, L. D., Clark, R. K., and Heber-Katz, E. (1998). A new murine model for mammalian wound repair and regeneration. *Clin Immunol Immunopathol* 88, 35–45. doi: 10.1006/clin.1998.4519

Cosenza, S., Ruiz, M., Toupet, K., Jorgensen, C., and Noel, D. (2017). Mesenchymal stem cells derived exosomes and microparticles protect cartilage and bone from degradation in osteoarthritis. *Sci Rep* 7, 16214.

Cui, X., Jing, X., Yi, Q., Xiang, Z., Tian, J., Tan, B., et al. (2019). IL22 furthers malignant transformation of rat mesenchymal stem cells, possibly in association with IL22RA1/STAT3 signaling. *Oncol Rep* 41, 2148–2158.

Delcourt, N., Quevedo, C., Nonne, C., Fons, P., O'brien, D., Loyaux, D., et al. (2015). Targeted identification of sialoglycoproteins in hypoxic endothelial cells and validation in zebrafish reveal roles for proteins in angiogenesis. *J Biol Chem* 290, 3405–3417. doi: 10.1074/jbc.m114.618611

Deng, Z., Gao, X., Sun, X., Amra, S., Lu, A., Cui, Y., et al. (2019). Characterization of articular cartilage homeostasis and the mechanism of superior cartilage regeneration of MRL/MpJ mice. *FASEB J* 2019, fj201802132RR.

Diekman, B. O., Wu, C. L., Louer, C. R., Furman, B. D., Huebner, J. L., Kraus, V. B., et al. (2013). Intra-articular delivery of purified mesenchymal stem cells from C57BL/6 or MRL/MpJ superhealer mice prevents posttraumatic arthritis. *Cell Transplant* 22, 1395–1408. doi: 10.3727/096368912x653264

Fitzgerald, J., Rich, C., Burkhardt, D., Allen, J., Herzka, A. S., and Little, C. B. (2008). Evidence for articular cartilage regeneration in MRL/MpJ mice. *Osteoarthritis Cartilage* 16, 1319–1326. doi: 10.1016/j.joca.2008.03.014

Fu, X., Liu, G., Halim, A., Ju, Y., Luo, Q., and Song, A. G. (2019). Mesenchymal Stem Cell Migration and Tissue Repair. *Cells* 2019, 8.

Huang, L., Niu, C., Willard, B., Zhao, W., Liu, L., He, W., et al. (2015). Proteomic analysis of porcine mesenchymal stem cells derived from bone marrow and umbilical cord: implication of the proteins involved in the higher migration capability of bone marrow mesenchymal stem cells. *Stem Cell Res Ther* 6, 77.

Kwiatkowski, A., Piatkowski, M., Chen, M., Kan, L., Meng, Q., Fan, H., et al. (2016). Superior angiogenesis facilitates digit regrowth in MRL/MpJ mice compared to C57BL/6 mice. *Biochem Biophys Res Commun* 473, 907–912. doi: 10.1016/j.bbrc.2016.03.149

Li, X., Wang, Q., Ding, L., Wang, Y. X., Zhao, Z. D., Mao, N., et al. (2019). Intercellular adhesion molecule-1 enhances the therapeutic effects of MSCs in a dextran sulfate sodium-induced colitis models by promoting MSCs homing to murine colons and spleens. *Stem Cell Res Ther* 10, 267.

Lindahl, M., Saarma, M., and Lindholm, P. (2017). Unconventional neurotrophic factors CDNF and MANF: Structure, physiological functions and therapeutic potential. *Neurobiol Dis* 97, 90–102. doi: 10.1016/j.nbd.2016.07.009

Lindholm, P., Peranen, J., Andressoo, J. O., Kalkkinen, N., Kokaia, Z., Lindvall, O., et al. (2008). MANF is widely expressed in mammalian tissues and differently regulated after ischemic and epileptic insults in rodent brain. *Mol Cell Neurosci* 39, 356–371. doi: 10.1016/j.mcn.2008.07.016

Lindholm, P., and Saarma, M. (2010). Novel CDNF/MANF family of neurotrophic factors. *Dev Neurobiol* 70, 360–371.

Luz-Crawford, P., Torres, M. J., Noel, D., Fernandez, A., Toupet, K., Alcayaga-Miranda, F., et al. (2015). The Immunosuppressive Signature of Menstrual Blood Mesenchymal Stem Cells Entails Opposite Effects on Experimental Arthritis and Graft Versus Host Diseases. *Stem Cells*. 34, 456-469.

Mak, J., Jablonski, C. L., Leonard, C. A., Dunn, J. F., Raharjo, E., Matyas, J. R., et al. (2016). Intra-articular injection of synovial mesenchymal stem cells improves cartilage repair in a mouse injury model. *Sci Rep* 6, 23076.

Maumus, M., Manferdini, C., Toupet, K., Peyrafitte, J. A., Ferreira, R., Facchini, A., et al. (2013). Adipose mesenchymal stem cells protect chondrocytes from degeneration associated with osteoarthritis. *Stem Cell Res* 11, 834–844. doi: 10.1016/j.scr.2013.05.008

Menendez-Menendez, Y., Otero-Hernandez, J., Vega, J. A., Perez-Basterrechea, M., Perez-Lopez, S., Alvarez-Viejo, M., et al. (2017). The role of bone marrow mononuclear cell-conditioned medium in the proliferation and migration of human dermal fibroblasts. *Cell Mol Biol Lett* 22, 29.

Naviaux, R. K., Le, T. P., Bedelbaeva, K., Leferovich, J., Gourevitch, D., Sachadyn, P., et al. (2009). Retained features of embryonic metabolism in the adult MRL mouse. *Mol Genet Metab* 96, 133–144. doi: 10.1016/j.ymgme.2008.11.164

Neves, J., Zhu, J., Sousa-Victor, P., Konjikusic, M., Riley, R., Chew, S., et al. (2016). Immune modulation by MANF promotes tissue repair and regenerative success in the retina. *Science* 353, aaf3646. doi: 10.1126/science.aaf3646

Petersen, T. N., Brunak, S., Von Heijne, G., and Nielsen, H. (2011). SignalP 4.0: discriminating signal peptides from transmembrane regions. *Nat Methods* 8, 785–786. doi: 10.1038/nmeth.1701

Ren, G., Zhao, X., Zhang, L., Zhang, J., L'huillier, A., Ling, W., et al. (2010). Inflammatory cytokine-induced intercellular adhesion molecule-1 and vascular cell adhesion molecule-1 in mesenchymal stem cells are critical for immunosuppression. *J Immunol* 184, 2321–2328. doi: 10.4049/jimmunol.0902023

Ruiz, M., Toupet, K., Maumus, M., Rozier, P., Jorgensen, C., and Noel, D. (2020). TGFBI secreted by mesenchymal stromal cells ameliorates osteoarthritis and is detected in extracellular vesicles. *Biomaterials* 226, 119544. doi: 10.1016/j.biomaterials.2019.119544

Rustad, K. C., and Gurtner, G. C. (2012). Mesenchymal Stem Cells Home to Sites of Injury and Inflammation. *Adv Wound Care* 1, 147–152. doi: 10.1089/wound.2011.0314

Sinha, K. M., Tseng, C., Guo, P., Lu, A., Pan, H., Gao, X., et al. (2019). Hypoxia-inducible factor 1alpha (HIF-1alpha) is a major determinant in the enhanced function of muscle-derived progenitors from MRL/MpJ mice. *FASEB J* 33, 8321–8334. doi: 10.1096/fj.201801794r

Sousa-Victor, P., Jasper, H., and Neves, J. (2018). Trophic Factors in Inflammation and Regeneration: The Role of MANF and CDNF. *Front Physiol* 9:1629.

Sousa-Victor, P., Neves, J., Cedron-Craft, W., Ventura, P. B., Liao, C. Y., Riley, R. R., et al. (2019). MANF regulates metabolic and immune homeostasis in ageing and protects against liver damage. *Nat Metab* 1, 276–290. doi: 10.1038/s42255-018-0023-6

Toupet, K., Maumus, M., Luz-Crawford, P., Lombardo, E., Lopez-Belmonte, J., Van Lent, P., et al. (2015). Survival and biodistribution of xenogenic adipose mesenchymal stem cells is not affected by the degree of inflammation in arthritis. *PLoS One* 10:e0114962. doi: 10.1371/journal.pone.0114962

Tseng, K. Y., Anttila, J. E., Khodosevich, K., Tuominen, R. K., Lindahl, M., Domanskyi, A., et al. (2018). MANF Promotes Differentiation and Migration of Neural Progenitor Cells with Potential Neural Regenerative Effects in Stroke. *Mol Ther* 26, 238–255. doi: 10.1016/j.ymthe.2017.09.019

Van Buul, G. M., Villafuertes, E., Bos, P. K., Waarsing, J. H., Kops, N., Narcisi, R., et al. (2012). Mesenchymal stem cells secrete factors that inhibit inflammatory processes in short-term osteoarthritic synovium and cartilage explant culture. *Osteoarthritis Cartilage* 20, 1186–1196. doi: 10.1016/j.joca.2012.06.003

Voutilainen, M. H., Back, S., Porsti, E., Toppinen, L., Lindgren, L., Lindholm, P., et al. (2009). Mesencephalic astrocyte-derived neurotrophic factor is neurorestorative in rat model of Parkinson's disease. *J Neurosci* 29, 9651–9659. doi: 10.1523/jneurosci.0833-09.2009

Wang, R., Jiang, W., Zhang, L., Xie, S., Zhang, S., Yuan, S., et al. (2020). Intra-articular delivery of extracellular vesicles secreted by chondrogenic progenitor cells from MRL/MpJ superhealer mice enhances articular cartilage repair in a mouse injury model. *Stem Cell Res Ther* 11, 93.

Ward, B. D., Furman, B. D., Huebner, J. L., Kraus, V. B., Guilak, F., and Olson, S. A. (2008). Absence of posttraumatic arthritis following intraarticular fracture in the MRL/MpJ mouse. *Arthritis Rheum* 58, 744–753. doi: 10.1002/art.23288

Conflict of Interest: FA was employed by the company Evotec France (SAS). SR was employed by the company Sanofi.

The remaining authors declare that the research was conducted in the absence of any commercial or financial relationships that could be construed as a potential conflict of interest.

frontiers in Cell and Developmental Biology

ORIGINAL RESEARCH
published: 22 March 2021
doi: 10.3389/fcell.2021.606890

Post-Adipose-Derived Stem Cells (ADSC) Stimulated by Collagen Type V (Col V) Mitigate the Progression of Osteoarthritic Rabbit Articular Cartilage

*Isabele Camargo Brindo da Cruz[1], Ana Paula Pereira Velosa[1], Solange Carrasco[1], Antonio dos Santos Filho[1], Jurandir Tomaz de Miranda[1], Eduardo Pompeu[2], Tiago Lazzaretti Fernandes[3,4], Daniela Franco Bueno[4], Camila Fanelli[5], Cláudia Goldenstein-Schainberg[1], Alexandre Todorovic Fabro[6,7], Ricardo Fuller[1], Pedro Leme Silva[8,9], Vera Luiza Capelozzi[6] and Walcy Rosolia Teodoro[1]**

[1] Rheumatology Division of the Hospital das Clinicas, Faculdade de Medicina, Universidade de São Paulo, FMUSP, São Paulo, Brazil, [2] Bioterism Center of the Hospital das Clinicas, Faculdade de Medicina, Universidade de São Paulo, FMUSP, São Paulo, Brazil, [3] Sport Medicine Division, Faculdade de Medicina, Institute of Orthopaedics and Traumatology of the Hospital das Clinicas, Universidade de Sao Paulo, FMUSP, São Paulo, Brazil, [4] Hospital Sírio-Libanês, São Paulo, Brazil, [5] Laboratory of Cellular, Genetic and Molecular Nephrology, Renal Division, University of São Paulo, São Paulo, Brazil, [6] Department of Pathology of the Hospital das Clinicas, Faculdade de Medicina, Universidade de São Paulo, FMUSP, São Paulo, Brazil, [7] Respiratory Medicine Laboratory, Department of Pathology and Legal Medicine, Ribeirão Preto Medical School, University of São Paulo (USP), São Paulo, Brazil, [8] Laboratory of Pulmonary Investigation, Centro de Ciências da Saúde, Carlos Chagas Filho Biophysics Institute, Federal University of Rio de Janeiro, Rio de Janeiro, Brazil, [9] National Institute of Science and Technology for Regenerative Medicine, Rio de Janeiro, Brazil

Collagen is essential for cartilage adhesion and formation. In the present study, histology, immunofluorescence, morphometry, and qRT-PCR suggested that adipose-derived stem cells (ADSCs) stimulated by type V collagen (Col V) induce a significant increase of type II collagen (Col II) in the degenerative area of surgical-induced osteoarthritic rabbit articular cartilage (OA). *In vitro*, the effects of Col V on the proliferation and differentiation of ADSC were investigated. The expression of the cartilage-related genes *Col2a1* and *Acan* was significantly upregulated and *Pou5f1* was downregulated post-ADSC/Col V treatment. Post-ADSC/Col V treatment, *in vivo* analyses revealed that rabbits showed typical signs of osteoarthritic articular cartilage regeneration by hematoxylin and eosin (H&E) and Safranin O/Fast Green staining. Immunohistochemical staining demonstrated that the volume of Col II fibers and the expression of Col II protein were significantly increased, and apoptosis Fas ligand positive significantly decreased post-ADSC/Col V treatment. In conclusion, the expression of Col II was higher in rabbits with surgical-induced osteoarthritic articular cartilage; hence, ADSC/Col V may be a promising therapeutic target for OA treatment.

Keywords: adipose-derived stem cells, collagen V, osteoarthritis, experimental model, cartilage treatment, therapy, hyaline cartilage

OPEN ACCESS

Edited by:
Darius Widera, University of Reading, United Kingdom

Reviewed by:
Lucienne A. Vonk, University Medical Center Utrecht, Netherlands
Jangho Kim, Chonnam National University, South Korea

****Correspondence:***
Walcy Rosolia Teodoro
walcy.teodoro@fm.usp.br

Specialty section:
This article was submitted to Stem Cell Research, a section of the journal Frontiers in Cell and Developmental Biology

Received: *15 September 2020*
Accepted: *22 February 2021*
Published: *22 March 2021*

Citation:
Brindo da Cruz IC, Velosa APP, Carrasco S, dos Santos Filho A, Tomaz de Miranda J, Pompeu E, Fernandes TL, Bueno DF, Fanelli C, Goldenstein-Schainberg C, Fabro AT, Fuller R, Silva PL, Capelozzi VL and Teodoro WR (2021) Post-Adipose-Derived Stem Cells (ADSC) Stimulated by Collagen Type V (Col V) Mitigate the Progression of Osteoarthritic Rabbit Articular Cartilage. Front. Cell Dev. Biol. 9:606890. doi: 10.3389/fcell.2021.606890

INTRODUCTION

In humans, osteoarthritis (OA), which involves the degradation of joint cartilage and underlying bone, makes the collagen matrix disorganize and decreases the proteoglycan content within the cartilage (Sanchez-Adams et al., 2014). Without the protective effects of the proteoglycans, the collagen fibers of the cartilage can become susceptible to degradation and, thus, exacerbate the degeneration (MaroudasI, 1976). Inflammation of the synovium and the surrounding joint capsule can also occur. The articular changes cause pain, joint stiffness, and limited joint motion (Gu et al., 2017), strongly impacting the patient's quality of life and the health system (Pasalini and Fuller, 2018).

Recent studies suggested that the irreparable injury of the cartilage is a major challenge in the treatment of human osteoarthritis and tissue engineering is considered to be an innovative and promising therapy for the patients (Wang et al., 2020; Kader et al., 2021; Tan et al., 2021; Xia et al., 2021). Among various cell therapies, adipose-derived stem cell (ADSC) therapy appears to hold promise (Bistolfi et al., 2021). ADSCs can differentiate into different mesenchymal cell types, including bone, cartilage, and adipose cells. Moreover, ADSCs are immune privileged due to their low immunogenicity. They can enhance the extracellular matrix microenvironment of the articulations by immune modulation of the inflammation and secreting cell growth factors, thus improving tissue repair and cartilage regeneration (Mazor et al., 2014; Wang et al., 2020). Nevertheless, the underlying mechanism is not fully understood.

Chondrocytes are specialized cells that compose the cartilage, synthesizing the collagenous extracellular matrix, an abundant ground substance that is rich in hyaluronic acid. They can be divided according to collagen types into (a) chondrocyte precursor cells (type I collagen), (b) differentiated hyaline chondrocytes (type II, IX, XI, and VI collagen), (c) hypertrophic chondrocytes (type X collagen), and (d) chondrocytes that modulate the synthesis of type I, III, and V collagen. Type II collagen (Col II) constrains the proteoglycans and the extracellular matrix responds to tensile and compressive forces that are experienced by the cartilage, with growth and remodeling of the extracellular matrix.

Type V collagen (Col V) promotes the adhesion and proliferation of chondrocytes and osteogenic cells, thus regulating cartilage adhesion. *Col Va1* mutations were detected in patients with osteoarthritis with mild chondrodysplasia (Yang et al., 2018). An interesting study suggested that targeting *Col Va2* promoted chondrocyte cell survival and extracellular matrix formation in steroid-induced necrosis of the femoral head (Yang et al., 2018). In addition, Col V is upregulated during adipogenesis and can stimulate adipocyte differentiation *in vitro* (Nakajima et al., 2002a,b). However, the stimulatory effect of Col V over ADSC proliferation and their ability to synthesize Col II in order to improve articular cartilage regeneration are unknown. Therefore, the present study evaluated the expression profiles of Col II in rabbits with surgical-induced osteoarthritic articular cartilage treated with adipose-derived stem cells (ADSCs) stimulated by Col V.

MATERIALS AND METHODS

Animals and Ethics Statement

The animal care and experimental protocols used in this study complied with the ethical principles on animal experimentation, adopted by the Brazilian College of Animal Experimentation (COBEA) of animals used for scientific purpose, and were approved by the ethics committee in the use of animals from the Medical School of the University of São Paulo (Protocol No. 123/14). Twenty-four 15-week-old male New Zealand White rabbits with a mean weight ranging from 2.1 to 2.5 kg were used. The animals were individually housed in specific cages for rabbits, with environmental and food enrichment and under controlled conditions of temperature (room temperature of 22 ± 2°C) and artificial 12-h light–dark cycles. The animals were fed *ad libitum* with stander feed and water.

Adipose-Derived Stem Cell Culture and Cell Differentiation

Sixteen rabbits were submitted to lipectomy by a longitudinal incision in the interscapular region to isolate the adipose tissue. To isolate ADSCs, adipose tissue from each animal was digested using Liberase (2.5 mg/ml) (Roche Diagnostics GmbH, Penzberg, Germany) for 40 min at 37°C and further centrifuged twice at 2,000 rpm for 5 min at 4°C. The precipitate was transferred to 25 cm^2 culture flasks containing Dulbecco's modified Eagle's medium (DMEM; Gibco Life Technologies; Invitrogen, Paisley, United Kingdom) supplemented with 10% fetal bovine serum (Gibco™) and 1% penicillin/streptomycin (Sigma Chemical Co., St. Louis, MO, United States). The culture was maintained at 37°C in an atmosphere of 5% CO_2 until confluence. All experimental assays were realized in the third culture passage (**Figure 1**). The capacity to differentiate toward adipogenic, osteogenic, and chondrogenic lineages was tested using the differentiation kits StemPro® (Gibco®, Life Technologies™) according to the manufacturer's recommendations. Cells were stained with Oil Red-O 0.5% (Sigma Chemical Co., St. Louis, MO, United States) in isopropanol 100%, Alcian Blue 1% in HCl 0.1 N, and Alizarin Red (Sigma Chemical Co., St. Louis, MO, United States) to evaluate adipogenic, chondrogenic, and osteogenic differentiation, respectively. Cell lineages were observed under a phase-contrast microscope (Nikon Eclipse TS100, Japan).

Evaluation of Col II After Col V Stimulating ADSCs

Col V from human placenta (Sigma Chemical Co., St. Louis, MO, United States) was used to stimulate ADSCs. The ideal stimulus concentration of 50 μg/ml of Col V per 72 h was determined by a dose/response curve, using 25, 50, 100, and 200 μg/mL of Col V and control without collagen. The cell cultures were maintained for a period of 1, 2, 3, 7, 14, and 21 days. These cells were cultured over coverslips in DMEM (Gibco Life Technologies, Invitrogen, Paisley, United Kingdom) supplemented with 10% fetal bovine serum (Gibco™) and 1% penicillin/streptomycin (Sigma Chemical Co., St. Louis, MO, United States) and were

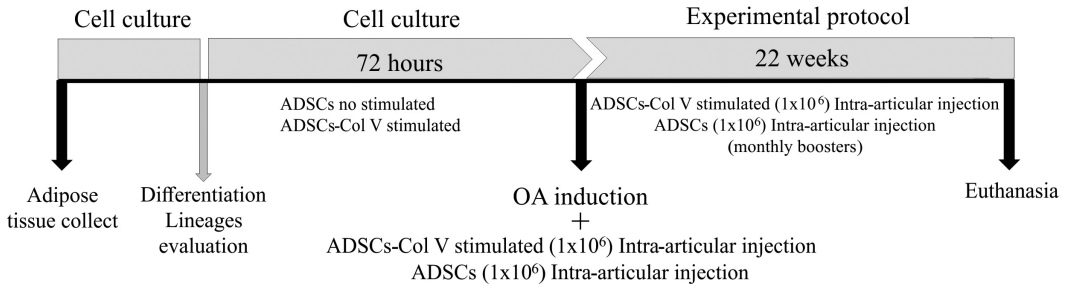

FIGURE 1 | Schematic protocol of cell culture, OA induction, and treatment with Col V-stimulated ADSCs and ADSCs (Col V-unstimulated ADSCs). ADSCs, adipose stem cells; Col V, collagen V.

maintained at 37°C in an atmosphere of 5% CO_2. The expression of Col II, a chondrogenic marker, was the criterion to determinate the ideal concentration and time of ADSC differentiation with Col V stimulus, evaluated by histomorphometry. To evaluate the potential of Col V-stimulated ADSCs, 2.5×10^5 cells in the third culture passage were treated with Col V (50 μg/ml) per 72 h in 25 cm^2 culture flasks with DMEM supplemented, in the same above conditions. After this period, cells were harvested with trypsin (Santa Cruz Biotechnology, Inc.), washed with DMEM, centrifuged at 2,000 rpm for 5 min in a conical tube (Falcon), and fixed successively in 4% paraformaldehyde and 70% alcohol. After 1 week, to evaluate Col II expression by immunofluorescence, the pellet was embedded in paraffin and 5 μm sections adhered to the slides, previously treated with 3-dimethylamino silane, dewaxed in xylene, and rehydrated with alcohol in decreasing concentrations, running and distilled water, and PBS. After blocking with 5% BSA, the sections were digested with pepsin (Sigma Chemical Co., St. Louis, MO, United States) 4 mg/ml in 0.5 N acetic acid for 30 min at 37°C. They were then washed in PBS and incubated with mouse polyclonal antibody anti-Col II (1:50, Abcam Inc., Burlingame, CA) overnight at 4°C. Afterward, the specimens were washed in PBS–$Tween_{20}$ and incubated with goat anti-mouse IgG antibody-Alexa Fluor 488 (1:200) with DAPI (1:200), a nuclear dye. The reaction was visualized utilizing confocal microscopy (ZEISS LSM 510 Meta/UV) and quantified by image analysis software (see below).

TABLE 1 | Oligonucleotide sequence.

Gene	Sense	Reverse	Base pair (bp)
Gapdh	AGGTCATCCA CGACCACTTC	GTGAGTTTCC CGTTCAGCTC	202
Pou5f1	GCCGACAACA ATGAGAACCT	ACACGGACCA CGTCTTTCTC	197
Acan	GTGACCGAGGT CAGTGGATT	CCAGGTCAGGG ATTCTGTGT	175
Col2a1	GAGACCTGAAC TGGGCAGAC	GACACGGAGT AGCACCATCG	192

Col2a1, α1 chain Col II; Acan, aggrecan; Pou5f1, POU domain, class 5, transcription factor 1; Gapdh, glyceraldehyde 3-phosphate dehydrogenase, internal control.

Col2a1, Acan, and *Pou5f1* Gene Expression

The ADSCs were seeded in 75 cm^2 culture flasks and divided into three groups: stimulated with Col V (50 μg/ml) for 72 h; TGF-β1 (10 ng/ml) for 72 h, a growth factor widely used to induce cellular differentiation; and without stimulus. Total RNA was extracted by the method of Chomczynski and Sacchi (1987) using the TRIzol reagent and RNA samples were treated with the kit RQ1 RNase-Free DNase (Promega®, Thermo Fisher Scientific, Rockford, IL), according to the manufacturer's instructions. RT-PCR reactions were performed with the primers drawn to *Col2a1* (α1 chain Col II), *Acan* (aggrecan), and *Pou5f1* (POU domain, class 5, transcription factor 1, protein transcription factor involved in the process of self-renewal and maintenance of stem cells) (**Table 1**).

Gene expression was evaluated using the Real-Time PCR System (Applied Biosystems, Foster City, CA, United States) with the kit SuperScript III Platinum SYBR® Green One-Step qRT-PCR (Life Technologies). The cycling conditions for the genes were as follows: 50°C for 10 min (for cDNA synthesis) followed by 35 cycles of 95°C for 15 s, 60°C for *Gapdh* and *Col2a1*, 59°C for *Acan*, and 57°C for the *Pou5f1* gene for 30 s and 72°C for 30 s. The analysis was performed by the $2^{-\Delta\Delta CT}$ method using *Gapdh* gene as an internal control.

Col V-Stimulated ADSC Culture to Therapeutic Assays

After Col V stimuli evaluation, ADSCs in the third culture passage were cultivated with Col V (50 μg/ml) per 72 h in 75 cm^2 culture flasks with DMEM (Gibco Life Technologies, Invitrogen, Paisley, United Kingdom), supplemented with 10% fetal bovine serum (Gibco™) and 1% penicillin/streptomycin (Sigma Chemical Co., St. Louis, MO, United States), at 37°C in an atmosphere of 5% CO_2. The Col V-stimulated ADSCs were cryopreserved in DMEM supplemented with 10% fetal bovine serum and 10% dimethyl sulfoxide (DMSO; Sigma Chemical Co., St. Louis, MO, United States) at −80°C. To therapeutic protocol, the ADSCs viability was evaluated with Trypan blue staining in Neubauer camera and 1×10^6 cells were diluted in 0.3 mL of the Physiological solution.

Induction of Osteoarthritis in Rabbits

Animals (n = 24) were anesthetized intramuscularly with xylazine (5 mg/kg) and ketamine (50 mg/kg). The procedures were performed under aseptic conditions. The induction of experimental OA was performed through a lateral parapatellar incision in the right knee followed by the removal of an anterior fourth of the lateral meniscus, preserving the ligaments, according to Moskowitz et al. (1973), with modifications. For the suture, a 4.0 mononylon wire was used at single-spaced points. All animals were given antibiotic (enrofloxacin 5 mg/kg, once daily) for 3 days and an anti-inflammatory (ketoprofen 10 mg/kg, 12/12 h), subcutaneously.

Therapeutic Protocol and Experimental Groups

Following the procedure of OA induction and antisepsis of the right knee with iodized alcohol, the OA/ADSC (n = 8) and OA/ADSC/Col V (n = 8) groups were, respectively, treated with autologous intra-articular injections of 0.3 ml of 1×10^6 ADSCs and 0.3 ml of 1×10^6 ADSCs/Col V, which were previously cultured with Col V (50 μg/ml for 72 h). After the cell administration, stretching and flexion movements were made in the knee joint in order to disperse the suspension in the intra-articular space. This treatment was performed monthly for a period of 22 weeks (**Figure 1**). The OA (n = 8) group received no treatment.

Histological Analysis

The right (operated) and the left (contralateral unoperated) knee joints of all animals were collected and fixed in 10% buffered formalin about 24 h followed by decalcification with 7% aqueous nitric acid. Then, histological procedures were made for morphological analysis and histological sections (4–5 μm thickness) were stained with H&E and Safranin O/Fast Green.

Semiquantitative Evaluation of Joint Injury

The following graduation, modified from the OARSI joint injury grade (Pritzker et al., 2006; Pearson et al., 2011; Waldstein et al., 2016), was applied to score the joint injury: *grade 0* = when the cartilage surface is smooth; the matrix and chondrocytes are organized into superficial, mid, and deep zones; and the cartilage morphology is intact; *grade 1* = when the surface is intact, but with irregularity of superficial fibrillation cluster proliferation and the mid and deep zones are unaffected; *grade 2* = when the surface is discontinuous with deep fibrillation, accompanied by cell proliferation and disparity in matrix staining or cell death; *grade 3* = when vertical fissures extended vertically until the mid-zone accompanied by cell death and cluster proliferation; *grade 4* = when the cartilage is corroded with loss of the cartilaginous matrix, cyst formation within the cartilage matrix, and cluster proliferation; *grade 5* = when the matrix is exposed and hyaline cartilage is unmineralized and completely eroded; the bone plate with microfracture and reparative fibrocartilage occupying gaps in the surface; and *grade 6* = when the matrix is deformed, with microfracture, fibrocartilaginous, and osseous repair extending above the previous surface. The resulting changes in the contour of the articular surface are illustrated in **Supplementary Figure 1**.

Immunohistochemical Analysis

The characterization of chondrocyte apoptosis and Col II expression was assessed, respectively, by immunoperoxidase (IP) and immunofluorescence (IF). Tissue sections (4 mm thick) were cut from formalin-fixed, paraffin-embedded blocks containing representative cells and tissue and processed for immunohistochemistry (IHC).

Immunoperoxidase

The chondrocyte apoptosis in the articular cartilage was evaluated by immunohistochemistry for Fas ligand using the mouse anti-FasL monoclonal antibody (1:20, Neomarkers, Fremont, CA) and the Novolink development kit (Leica Biosystems, New Castle Ltd., United Kingdom), according to the manufacturer's specifications.

Immunofluorescence

The cartilage sections on slides were deparaffinized in xylene-alcohol and rehydrated in running water, distilled water, and phosphate buffered saline. Firstly, enzymatic digestion with chondroitinase ABC 2UN (Sigma Chemical Co., St. Louis, MO, United States) in buffer containing 50 mM Tris, pH = 8.0, sodium acetate 60 mM, and 0.02% BSA at 37°C for 3 h was performed for exposure and recovery of antigenic sites. Subsequently, antigenic recovery was done with 8 mg/ml porcine pepsin (Sigma Chemical Co., St. Louis, MO, United States, 10,000 UTI/ml) diluted in acetic acid 5 N for 30 min at 37°C. For blocking non-specific sites, the sections were incubated with 5% BSA in PBS for 30 min. Polyclonal mouse anti-Col II antibody (1:20; Abcam, Burlingame, CA, United States) was incubated overnight at 4°C. After a PBS 0.05%–Tween_{20} washing cycle, goat anti-mouse IgG antibody (Alexa Fluor 488, Invitrogen, Life Technologies) diluted (1:150) in PBS and 0.006% Evans blue was incubated at room temperature for 60 min. After the sections were washed and mounted in glycerin-PBS (v/v), they were analyzed using an Olympus BX51 fluorescence microscope (Olympus Corp., Tokyo, Japan).

Morphometric Analysis

The quantification of histologic, immunoperoxidase, and immunofluorescence parameters was done by digital imaging through the Image-Pro Plus 6.0 software. Briefly, the image analysis system consisted of an Olympus camera (Olympus Corporation, St Laurent, Quebec, Canada) coupled to an Olympus microscope (Olympus BX51), from which the images were sent to an LG monitor by means of a digitizing system (Oculus TCX, Coreco Inc., St Laurent, Quebec, Canada) and downloaded to a computer (Pentium 1330 MHz). Ten images from the culture were processed with the software (Image-Pro Plus 6.0).

The histologic sections of femoral condyles and tibial plates stained with H&E were scanned at ×200 magnification to evaluate cartilage thickness. Five vertical lines were drawn from the cartilage surface to the tidemark, starting from a central

point of the tissue and 250 and 500 mm to the right and to the left. The cartilage thickness was calculated in μm^2 from the arithmetic mean of the drawn lines. The density of the chondrocyte per cartilage area was evaluated by the stereological point-counting method developed by Gundersen et al. (1988) with modifications. Using the measurement tools of the Image-Pro Plus 6.0 software, a reticulum with 100 points orthogonally distributed over the acquired image was constructed. The cells coincident with the points in the reticulum were counted and the result was given as percentage of chondrocyte cells per mm^2.

The proteoglycan levels in the cartilage were evaluated based on the quantification of the Safranin O/Fast Green staining intensity using the Image-Pro Plus 6.0 software (Pastoureau et al., 2010). Ten images in ×400 magnification were acquired and the staining intensity was measured by the software. The mean of the area stained in blue was divided by the mean of the total area analyzed, and the result expressed as percentage per mm^2.

The Col II immunofluorescence in cultures and tissue was analyzed through images acquired at ×400. The area of each field analyzed was measured in μm^2 and the mean of the immunostaining area corresponding to Col II was divided by the mean of the total area analyzed and the final result was expressed as percentage of fibers/mm^3.

Statistical Analysis

Statistical analysis was performed using GraphPad Prism 4.0 software (GraphPad Prism, Inc., San Diego, CA, United States). One-way analysis of variance (ANOVA) with Newman–Keuls post-test for comparison between groups or Kruskal–Wallis test followed by multiple Dunn's test for non-parametric data was used. Results are expressed as mean ± standard errors of the mean (SEM); a $P < 0.05$ was considered statistically significant.

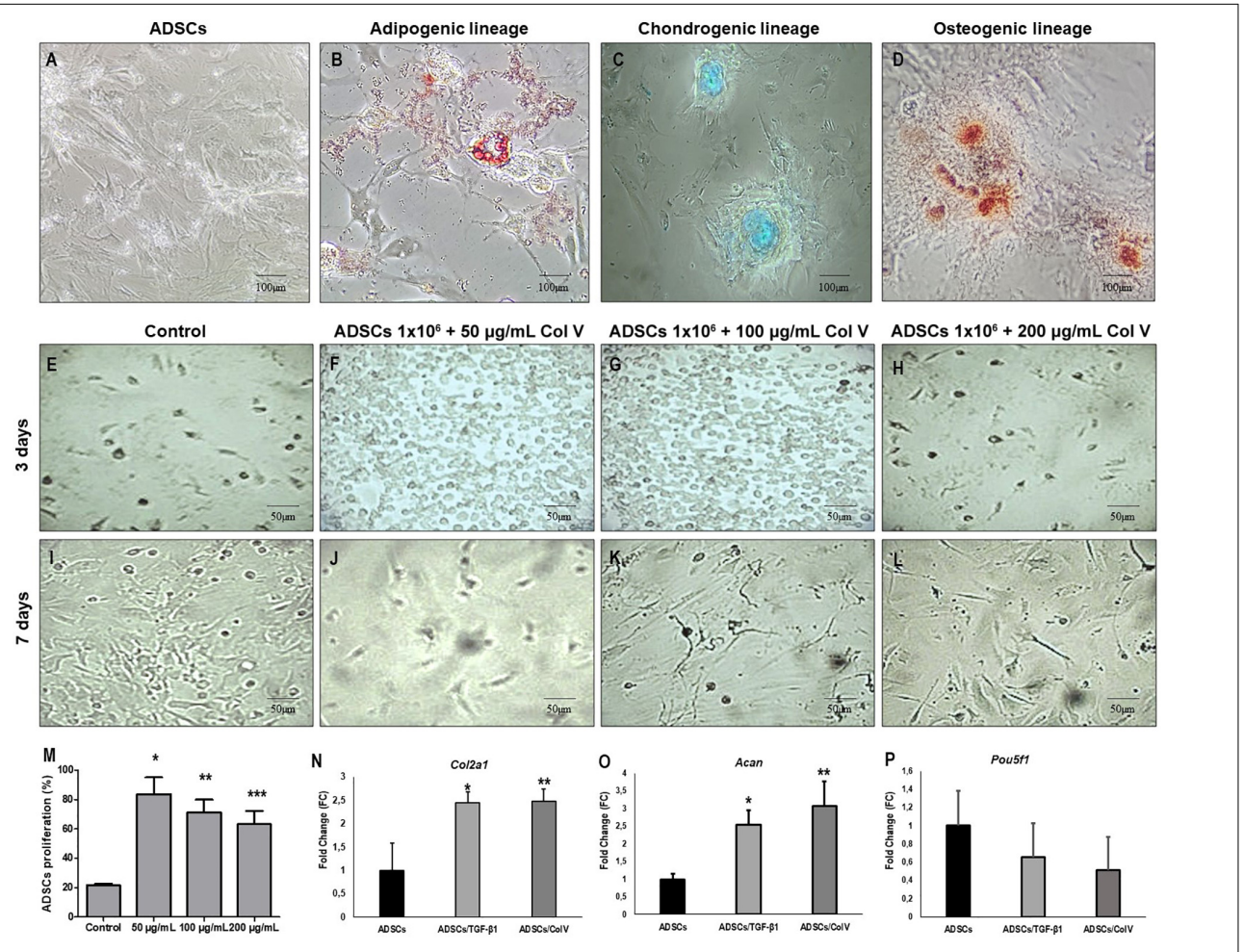

FIGURE 2 | ADSCs grown in specific medio and differentiation into adipogenic, chondrogenic and osteogenic lineages. Adipogenic lineage presents cytoplasmic lipid droplets red stained with Oil Red **(B)**, chondrogenic lineage shows matrix proteoglycans production identified by Alcian Blue staining (blue) **(C)** and osteogenic lineage exhibit calcium salts identified by Alizarin Red **(D)**. Control ADSCs grown in DMEM **(A)**. The proliferation of ADSCs **(E–M)** and expression of chondrogenic related genes and were increased post-ADSCs/Col V and TGF-β treatment. The expression of *Col2a1* **(N)**, *Acan* **(O)** and Poup5f1 **(P)** at the mRNA level was measured by RT-PCR after 3 and 7 days of incubation in the chondrogenic medium of ColV and TGF-β treated ADSCs. The cell viability of ADSCs was detected by CCK-8. ADSCs, adipose stem cells. The experiments were performed in triplicate. *$P < 0.05$; **$P < 0.001$; ***$P < 0.0001$.

RESULTS

ADSC Differentiation

ADSCs grown in specific differentiation media were able to differentiate into adipogenic, chondrogenic, and osteogenic lineages, characterized, respectively, by the presence of cytoplasmic lipid droplets (Oil Red), synthesis of proteoglycans by the presence of a proteoglycan-rich matrix (Alcian Blue), and aggregates of calcium salts with calcium deposits (Alizarin Red) (**Figures 2A–D**).

Col V Enhances ADSC Proliferation and Increases the Expression of Chondrogenic Genes *in vitro*

The impact of Col V in ADSC proliferation was assessed (**Figures 2E–L**). After incubation with Col V 50 μg/ml for 3 days, the proliferation assay revealed that Col V enhanced the proliferation of ADSCs in a dose-dependent manner (**Figure 2M**). Moreover, the expression of chondrogenic-related genes was measured by real-time qPCR. As expected, the expression of *Col2a1* and *Acan* genes was significantly upregulated post-Col V/ADSC incubation after chondrogenic differentiation at days 3 and 7 (both $P < 0.05$, **Figures 2N,O**), whereas *Pou5f1* gene expression showed a tendency to be downregulated ($P = 0.07$, **Figure 2P**). A similar expression of *Col2a1* and *Acan* genes was found with TGF-β1, a growth factor that stimulates ADSCs (**Figures 2N–P**).

The Expression of Col II Was Increased During the Process of Col V/ADSC Treatment *in vitro* and *in vivo*

Figures 3A–G show the immunofluorescence of Col II *in vitro* and *in vivo* post-ADSC treatment stimulated with Col V for 3 days (50 μg/ml). A strong and diffuse green birefringence of Col II was observed in the pellets of ADSCs/Col V (**Figure 3B**), contrasting with the weak and focal birefringence in ADSCs (**Figure 3A**). These features coincide with the significant increase of Col II expression in ADSCs/Col V when compared with ADSCs ($P < 0.01$) (**Figure 3C**). A similar strong and diffuse green birefringence of Col II was observed in osteoarthritic rabbit articular cartilage post-ADSCs stimulated with Col V intra-articular injection (**Figure 3F**). Of note is the progressive increase of Col II expression from osteoarthritis (**Figure 3D**) and OA/ADSCs (**Figure 3E**) to osteoarthritis being maximum and significant in OA/ADSCs/Col V ($P < 0.05$).

Post-ADSC/Col V Treatment Avoids the Progression of Osteoarthritic Rabbit Articular Cartilage

Figure 4A shows the gross characteristics of the femoral condyle from the OA group including thinning of the cartilage and having a pearly white color and several stretch marks of chondral erosions in the cartilage. The lesions were less severe in the OA/ADSC group presenting cartilage with superficial erosions and focal stretch marks of chondral erosions (**Figure 4B**). These gross characteristics contrast with the bright white color and regular surface of the femoral chondral cartilage in the joints of OA/ADSC/Col V animals (**Figure 4C**), similar to control (**Figure 4D**).

Histologically, the OA group coincided with severe stretch marks and thinning cartilage, osteophyte formation, subchondral sclerosis, cellular disorganization of chondrocytes and reduction of bone trabeculae, beyond complete tidemark discontinuity (**Figure 4E**), and weak Safranin O/Fast Green staining intensity of the extracellular matrix indicating reduction of glycosaminoglycans (**Figure 4I**). The OA/ADSC joints show less severe osteoarthritic histologic changes compared with those of the OA group with superficial fibrillations, moderate cellular disorganization, maintenance of the tidemark, and

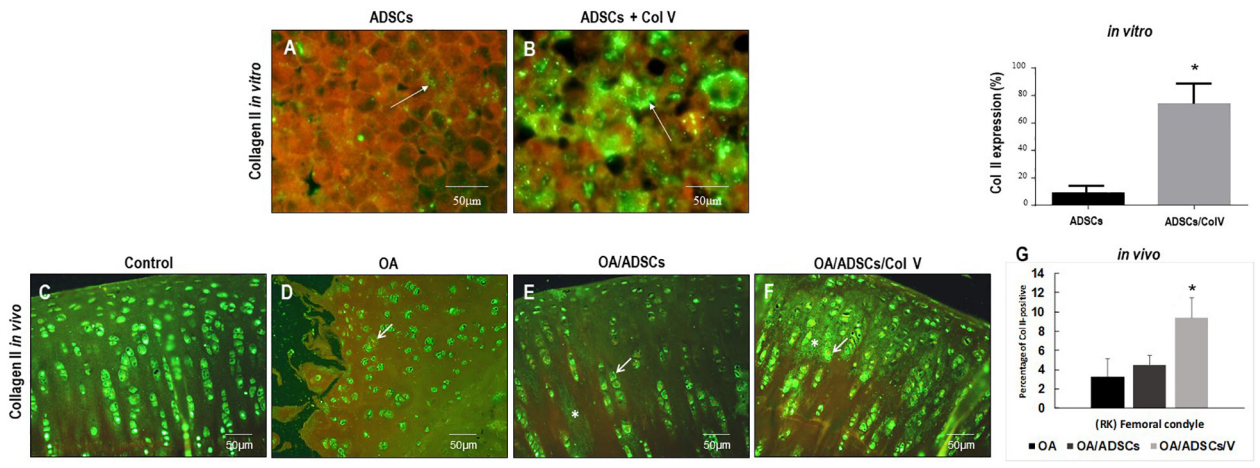

FIGURE 3 | Representative images of the strong green birefringence by immunofluorescence of Col II after 3 days with Col V (50 mg/ml) during the process of Col V/ADSC treatment *in vitro* **(A,B)** and *in vivo* **(C–F)**. The **(G)** shows the representative graphics of the amount of Col II expression *in vitro* and *in vivo* evaluated by Image-Pro Plus 6.1 software. *$P < 0.05$.

subchondral bone with less sclerotic aspect (**Figure 4F**). In this group, Safranin O/Fast Green staining intensity was moderate, indicating minor loss of proteoglycan content (**Figure 4J**). In contrast, the OA/ADSC/Col V group showed only stretch marks of the cartilaginous surface with recovery of cartilage thickness (**Figure 4G**), minor cellular disorganization, continuous tidemark, subchondral bone without sclerotic aspect (**Figure 4G**), and maintenance of proteoglycan content compared with the OA and OA/ADSCs (**Figures 4I–K**), similar to control cartilage (**Figures 4H,L**). **Supplementary Figure 1** shows the injury grades in OA, OA/ADSCs, and OA/ADSCs/Col V. The OA/ADSCs/Col V presented a significant cartilage regeneration in relation to OA (**Figure 5**; $P = 0.019$).

These histological changes in the rabbits' joints from the OA/ADSC/Col V group, which had been injected with ADSCs/Col V, coincide with the significant increase of cartilage thickness ($P < 0.05$; **Figure 4Q**), chondrocyte density ($P < 0.05$; **Figure 4R**), proteoglycans repair ($P < 0.05$; **Figure 4S**), and apoptosis reduction ($P < 0.05$; **Figures 4M–P,T**). Regarding the OA/ADSC group, intra-articular injection of ADSCs was also

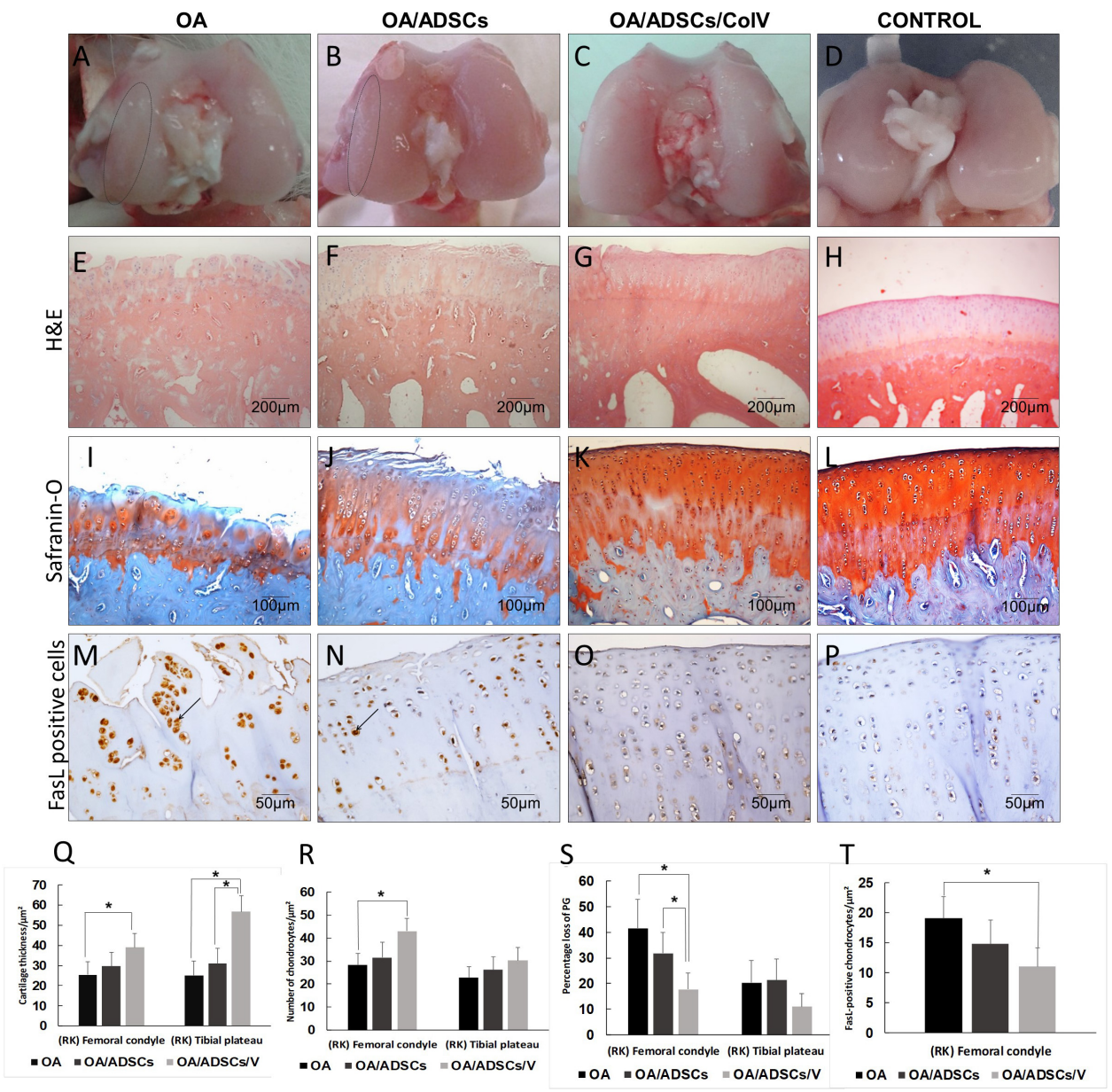

FIGURE 4 | The morphogenic changes showed typical signs of osteoarthritic rabbit articular cartilage regeneration post-ADSCs/Col V. **(A–D)** Coronal section of representative femoral heads. The circle indicates the femoral condyle cartilage degeneration. Hematoxylin and eosin **(E–H)** and Safranin O/Fast Green **(I–L)** staining. Chondrocytes apoptosis Fas ligand+(arrows) **(M–P)**. Morphometric analysis showing cartilage parameters of the upper outer subchondral bone of the femoral heads **(Q)**, chondrocytes **(R)**, proteoglycans **(S)**, and apoptosis **(T)**. *$P < 0.05$.

able to significantly increase chondrocyte density and cartilage thickness, and there was reduction of apoptosis than the amount observed in rabbits from the OA group but much less than that from the ADSC/Col V group.

DISCUSSION

Under the conditions of the present study, we found plenty of associated effects in rabbit OA. They included the following: (1) Col V enhances rabbit ADSC proliferation and differentiation and increases *in vitro* Col II expression in ADSCs; (2) in the *in vitro* expression of cartilage-related genes, *Col2a1* and *Acan* were significantly upregulated and *Pou5fl* was downregulated post-ADSC/Col V treatment; and (3) *in vivo*, the injury grades post-ADSC/Col V treatment showed typical signs of osteoarthritic articular cartilage regeneration, including decreased cartilage thickness, increased number of chondrocytes, decreased proteoglycan loss, decreased number of apoptotic chondrocytes, and increased expression of Col II protein. The current study showed that ADSCs stimulated by Col V (ADSCs/Col V) induced a significant regeneration of cartilage, indicating that ADSCs/Col V may be a therapeutic target for the treatment of osteoarthritis.

The experiments in the present study were performed in a surgical-induced osteoarthritic rabbit articular cartilage, established by Moskowitz et al. (1973) and modified by Velosa et al. (2007), which reproduces progressively the morphological changes found in human OA. The established period of 22 weeks was described equivalent to an advanced time of disease, with macroscopic lesions of the cartilage and histology features, characterized by cell disorganization, presence of cell clones, fibrillations, and fissures, in addition to loss of collagen and proteoglycans (Velosa et al., 2007).

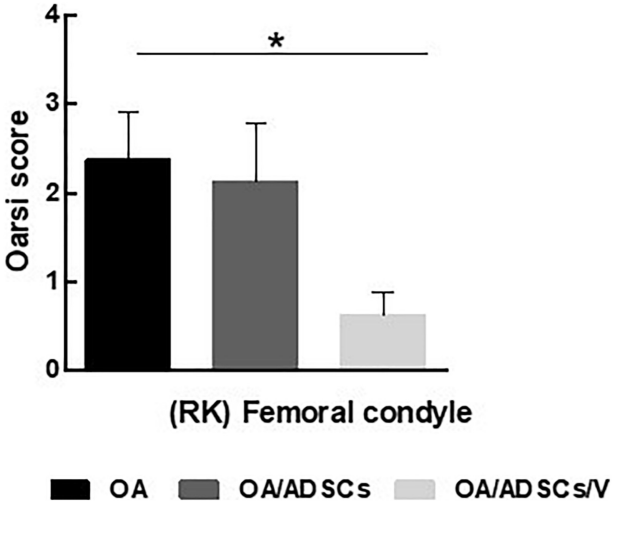

FIGURE 5 | OARSI score grading for histologic alteration in OA, OA/ADSCs, and OA/ADSCs/Col V. *$P < 0.05$.

Regarding the concentration of Col V used to stimulate ADSCs, the treatment time, the number of cells administered, and the route of administration, we employed a therapeutic protocol based on a monthly intra-articular administration of ADSCs 10^6/Col V 50 μg/ml, which is the ideal stimulus concentration based on cell culture proliferation and expression of Col II, a chondrogenic marker, during a 22-week period (Velosa et al., 2007). Intra-articular administration was chosen considering that the cells will be applied in a joint in a closed environment. Moreover, it simulates clinical practice. In addition, we decided not to perform the treatment with a shorter interval, considering that some studies detected mesenchymal stem cells (MSCs) up to 1 month after intra-articular injection (Satué et al., 2019).

The balance between the synthesis and degradation of matrix proteins in the extracellular matrix (ECM) is crucial for the dynamic stability of tissues (Humphrey et al., 2014). The interaction of chondrocytes with the cartilage ECM plays an important role for chondrocyte anchorage, proliferation, differentiation, and function (He et al., 2014). In cell culture, chondrocytes have the ability to synthesize a large variety of matrix proteins, including collagen types I, II, III, IV, and V and fibronectin (Aigner et al., 1993). Col V is synthesized and deposited in the ECM, where it cross-linked with Col I and III, to form the collagenous matrix skeleton (Mak et al., 2016). By histological and proteomic analyses, Hong et al. (2010) reported that Col V in the ECM improved cell distribution and actin fiber frame promoting adhesion in the initial stage of chondroblast differentiation. The growth and remodeling of the cartilage matrix may revert morphologic injury. Moreover, the present study showed that the gene and protein profile of Col II was significantly higher in OA rabbits, and its upregulation was confirmed both *in vitro* and *in vivo*. These findings suggest that the balance between Col V and Col II expression may revert to the pathogenesis of OA.

Chondrocytes are the only cell type composing the articular cartilage and encompass only 2–5% of its compartment, the remaining being occupied by a hydrous ECM of collagens (mostly Col II) and proteoglycans. The main function of chondrocytes is to preserve the integrity of the cartilage by reverting injury to the matrix. Nevertheless, in OA, the biomechanical and biochemical microenvironment of the cartilage is altered, as well as in the performance of chondrocytes. These collateral changes are considered in part due to repression of chondroblast differentiation from MSCs and apoptosis of chondrocytes (Hwang and Kim, 2015). At early stages, OA is mainly characterized by the apoptosis of chondrocytes, then the reparative reaction of the cartilage is initiated. The imbalance between metalloprotease-mediated cartilage resorption and chondroblast-mediated cartilage restoration led to distorted histoarchitecture and progressive breakdown of joints. As the cartilage is the main affected component in OA, molecular studies of OA have focused on the mechanism of damage to the articular cartilage (Bertrand et al., 2010). Cartilage degeneration in OA is a progressive process complemented with the gradual loss of Col II and a gradual decrease in mRNA expression of *Acan* and *Col2a1* (Buckwalter et al., 2004; Brew et al., 2010). As

expected, we found that the gene expression of the chondrocyte markers *Acan* and *Col2a1* was increased after ADSC/Col V treatment. In contrast, we found decreased expression of *Pou5f1 gene* post-ADSC/Col V treatment. Previous studies have reported that *Pou5f1* works in maintaining the cancer stem cell fate of osteosarcoma (Siclari and Qin, 2010). Guo et al. (2017) demonstrated that *Pou5f1* gene expression was downregulated by miR-335, and suggested that it could repress *Pou5f1* expression by post-translational regulation. They also found that cells expressing miR-335 possessed decreased stem cell-like properties. Although *Pou5f1* has not been reported in OA pathology, we infer that *Pou2f1* might also be a candidate gene connected with OA pathology and ADSC/Col V treatment.

The mechanism of action of Col V in the stimulation of ADSCs to synthesize Col II is unknown. However, based on our results, we infer that the biochemistry characteristics and biologic functions of Col V may induce cell proliferation and differentiation of ADSCs to produce collagen as previously reported (Ruggiero et al., 1994; Mak et al., 2016). Collagen type V works as crucial components for preserving the structural integrity of the cartilage skeleton, promoting adhesion and proliferation of several cell types including fibroblasts and chondrocytes (Fichard et al., 1995; Breuls et al., 2009; Wu et al., 2009). These properties of cell adhesion, migration, and proliferation are primarily due to tripeptide sequence consisting of arginine, glycine, and aspartic acid (RGD) sequences present in greater quantity in the α2(V) chain that bind primarily to the membrane integrins and could stimulate ADSC proliferation and differentiation (Ruggiero et al., 1994, 1996). Col V adhesion may also occur through a 30-kDa α1(V) chain fragment containing a pool of basic amino acid residues with affinity to heparin and heparin sulfate, which could enhance its interaction with anionic heparin molecules. In this way, Col V also interacts with a number of molecules in the extracellular matrix such as proteoglycans (PG), heparin sulfate, and other triggering cellular stimulus signals (Ricard-Blum et al., 2006; Symoens et al., 2011). Col V specifically decreases endothelial cell proliferation promoting cell detachment by the disassembly of F-actin filaments, and cells started to proliferate when recultured on Col I (Mak et al., 2016). Moreover, heterozygous mutation in *Col Va2* gene could lead to connective tissue hyperelasticity and joint instability (Johnston et al., 2017). In the current study, we verified that ADSCs stimulated by Col V increased Col II synthesis, the main collagenous protein of the hyaline cartilage matrix, and decreased apoptotic chondrocytes. Based on the study from Nakajima et al. (2002a,b), who demonstrated that Col V was upregulated during adipogenesis and that it can stimulate adipocyte differentiation *in vitro*, we inferred that ADSCs stimulated by Col V enhance the expression of Col II, increasing the density of cartilage tissue. Another hypothetical translational significance of this finding is that Col II deficiency may participate in the articular deterioration progress of OA. However, how ADSCs stimulated by Col V enhancement of the expression of Col II could promote the healing process of cartilage tissue in OA needs further studies using transgenic Col V ADSCs to unveil the potential role of Col V in OA.

In the present study, we also used TGF-β1, another established growth factor for *in vitro* ADSC chondrogenic differentiation (Yarak and Okamoto, 2010) and Col II synthesis (Indrawattana et al., 2004; Shirasawa et al., 2006; Kraus, 2011; Das et al., 2015; Kwon et al., 2016), to evaluate and compare the expression of *Col2a1* and *Acan* genes in ADSC stimulated by Col V. Of note, we demonstrated similar *Col2a1* and *Acan* gene expression in ADSCs stimulated with Col V and ADSCs stimulated with TGF-β1 in relation to the control culture. The similar fold change of the expression of these genes between the two stimuli suggests once again that Col V could act as a modulator of the collagen chondrogenic. In fact, recent studies showed that ADSCs stimulated with TGF-β3 and BMP-6 had increased chondrogenic gene expressions and the model of osteoarthritic knees treated with these cells had improvement of cartilage scores (Ude et al., 2018). In addition to the application of MSCs in animal models, clinical trials and meta-analytic studies have shown cartilage improvement, reduction in pain, and improvement in joint function in patients with OA after autologous MSC injections (Centeno et al., 2008; Koh et al., 2013; Robinson et al., 2018; Huang et al., 2020). Additionally, other authors have shown that a single intra-articular injection of integrin α10β1 derived from allogeneic adipose tissue was effective in treating OA in horses, showing decreased articular cartilage fibrillation (Delco et al., 2020). Since the intra-articular cavity is closed, the loss of a few stem cells is expected. Previous studies have shown that MSCs are present up to 1 month after intra-articular injection (Satué et al., 2019), and these were being done in clinical trials (Jo et al., 2014). If stem cells are still present even after 1 month of injection, this reflects a few stem cell loss. In addition, compared with intravenous injection (Eggenhofer et al., 2012), stem cells injected in the intra-articular cavity can stay longer.

CONCLUSION

In conclusion, by applying immunofluorescence, morphometry, and qRT-PCR analysis, this study demonstrated that post-ADSC stimulation by Col V treatment increased the repair process in an osteoarthritic rabbit articular cartilage model. These findings suggested that surgical-induced OA treated with ADSCs stimulated by Col V may prevent the progression of cartilage injury; nevertheless, more studies are needed in order to unveil the immunological role of ADSCs stimulated by Col V in the pathogenesis of OA.

DATA AVAILABILITY STATEMENT

The raw data supporting the conclusions of this article will be made available by the authors, without undue reservation.

ETHICS STATEMENT

The animal study was reviewed and approved by Ethics Committee in the use of animals from Medical School of the University of São Paulo (Protocol No. 123/14).

AUTHOR CONTRIBUTIONS

IB contributed the methodology, data acquisition, and original draft of the manuscript. AV contributed to the methodology, draft of the manuscript and editing the manuscript, and revising the work critically for intelectual content. SC, EP, and AS contributed to the methodology. CG-S contributed to the resources. CF contributed to the data acquisition, review of the analysis, and interpretation of the data. AG contributed to the data acquisition, review of statistical analysis, and revising the work critically for intelectual content. PS and VC contributed to the review of the analysis and interpretation of data, revising the work critically for intelectual content, and final approval of the version to be published. TF, DB, and RF critically reviewed the manuscript. WT contributed to the conceptualization, draft of the manuscript, funding acquisition, data statistic analysis, and final approval of the version to be published.

FUNDING

The research was supported by the São Paulo Research Foundation (FAPESP – Process number 2014/11419-5; FAPESP 2018/20403-6 to VC) and the National Council for Scientific and Technological Development (CNPq) (483005/2012-6 to VC).

SUPPLEMENTARY MATERIAL

The Supplementary Material for this article can be found online at: https://www.frontiersin.org/articles/10.3389/fcell.2021.606890/full#supplementary-material

REFERENCES

Aigner, T., Bertling, W., Stöss, H., Weseloh, G., and von der Mark, K. (1993). Independent expression of fibril-forming collagens I, II, and III in chondrocytes of human osteoarthritic cartilage. *J. Clin. Invest.* 91, 829–837. doi: 10.1172/jci116303

Bertrand, J., Cromme, C., Umlauf, D., Frank, S., and Pap, T. (2010). Molecular mechanisms of cartilage remodelling in osteoarthritis. *Int. J. Biochem. Cell Biol.* 42, 1594–1601. doi: 10.1016/j.biocel.2010.06.022

Bistolfi, A., Roato, I., Fornelli, G., Sabatini, L., Massč, A., and Ferracini, R. (2021). Treatment of knee osteoarthritis by intra-articular injection of concentrated autologous adipose tissue: a twenty-four-month follow-up study. *Int. Orthop.* 45, 627–633. doi: 10.1007/s00264-020-04923-0

Breuls, R. G. M., Klumpers, D. D., Everts, V., and Smit, T. H. (2009). Collagen type V modulates fibroblast behavior dependent on substrate stiffness. *Biochem. Biophys. Res. Commun.* 380, 425–429. doi: 10.1016/j.bbrc.2009.01.110

Brew, C. J., Clegg, P. D., Boot-Handford, R. P., Andrew, J. G., and Hardingham, T. (2010). Gene expression in human chondrocytes in late osteoarthritis is changed in both fibrillated and intact cartilage without evidence of generalised chondrocyte hypertrophy. *Ann. Rheum. Dis.* 69, 234–240. doi: 10.1136/ard.2008.097139

Buckwalter, J. A., Saltzman, C., and Brown, T. (2004). The impact of osteoarthritis: implications for research. *Clin. Orthop. Relat. Res.* 427, S6–S15. doi: 10.1097/01.blo.0000143938.30681.9d

Centeno, C. J., Busse, D., Kisiday, J., Keohan, C., and Freeman, M. (2008). Increased knee cartilage volume in degenerative joint disease using percutaneously implanted, autologous mesenchymal stem cells, platelet lysate and dexamethasone. *Am. J. Case Rep.* 9, 246–251.

Chomczynski, P., and Sacchi, N. (1987). Single-step method of RNA isolation by acid guanidinium thiocyanate-phenol-chloroform extraction. *Anal. Biochem.* 162, 156–159. doi: 10.1006/abio.1987.9999

Das, R., Timur, U. T., Edip, S., Haak, E., Wruck, C., Weinans, H., et al. (2015). TGF-β2 is involved in the preservation of the chondrocyte phenotype under hypoxic conditions. *Ann. Anat.* 198, 1–10. doi: 10.1016/j.aanat.2014.11.003

Delco, M. L., Goodale, M., Talts, J. F., Sarah, L., Koff, M. F., Miller, A. D., et al. (2020). Integrin α10β1-selected mesenchymal stem cells mitigate the progression of osteoarthritis in an equine talar impact model. *Am. J. Sports Med.* 48, 612–623. doi: 10.1177/0363546519899087

Eggenhofer, E., Benseler, V., Kroemer, A., Popp, F. C., Geissler, E. K., Schlitt, H. J., et al. (2012). Mesenchymal stem cells are short-lived and do not migrate beyond the lungs after intravenous infusion. *Front. Immunol.* 3:297. doi: 10.3389/fimmu.2012.00297

Fichard, A., Kleman, J. P., and Ruggiero, F. (1995). Another look at collagen V and XI molecules. *Matrix Biol.* 14, 515–531. doi: 10.1016/s0945-053x(05)80001-0

Gu, Y. T., Chen, J., Meng, Z. L., Ge, W. Y., Bian, Y. Y., Cheng, S. W., et al. (2017). Research progress on osteoarthritis treatment mechanisms. *Biomed. Pharmacother.* 93, 1246–1252.

Gundersen, H. J., Bagger, P., Bendtsen, T. F., Evans, S. M., Korbo, L., Marcussen, N., et al. (1988). The new stereological tools: disector, fractionator, nucleator and point sampled intercepts and their use in pathological research and diagnosis. *APMIS* 96, 857–881. doi: 10.1111/j.1699-0463.1988.tb00954.x

Guo, X., Yum, L., Zhang, Z., Dai, G., Gao, T., and Guo, W. (2017). miR-335 negatively regulates osteosarcoma stem cell-like properties by targeting POU5F1. *Cancer Cell Int.* 17, 29. doi: 10.1186/s12935-017-0398-6

He, F., Liu, X., Xiong, K., Chen, S., Zhou, L., and Cui, W. (2014). Extracellular matrix modulates the biological effects of melatonin in mesenchymal stem cells. *J. Endocrinol.* 223, 167–180. doi: 10.1530/joe-14-0430

Hong, D., Chen, H.-C., Yun, H.-Q., Liang, Y., Wang, C., Lian, Q.-Q., et al. (2010). Morphological and proteomic analysis of early stage of osteoblast differentiation in osteoblastic progenitor cells. *Exp. Cell Res.* 316, 2291–2300. doi: 10.1016/j.yexcr.2010.05.011

Huang, R., Li, W., Zhao, Y., Yang, F., and Xu, M. (2020). Clinical efficacy and safety of stem cell therapy for knee osteoarthritis: a meta-analysis. *Medicine* 99, e19434. doi: 10.1097/MD.0000000000019434

Humphrey, J. D., Dufresne, E. R., and Schwartz, M. A. (2014). Mechanotransduction and extracellular matrix homeostasis. *Nat. Rev. Mol. Cell Biol.* 15, 802–812. doi: 10.1038/nrm3896

Hwang, H. S., and Kim, H. A. (2015). Chondrocyte apoptosis in the pathogenesis of osteoarthritis. *Int. J. Mol. Sci.* 16, 26035–26054. doi: 10.3390/ijms161125943

Indrawattana, N., Chen, G., Tadokoro, M., Shann, L. H., Ohgushi, H., Tateishi, T., et al. (2004). Growth factor combination for chondrogenic induction from human mesenchymal stem cell. *Biochem. Biophys. Res. Commun.* 320, 914–919. doi: 10.1016/j.bbrc.2004.06.029

Jo, C. H., Lee, Y. G., Shin, W. H., Kim, H., Chai, J. W., Jeong, E. C., et al. (2014). Intra-articular injection of mesenchymal stem cells for the treatment of osteoarthritis of the knee: a proof-of-concept clinical trial. *Stem Cells* 32, 1254–1266. doi: 10.1002/stem.1634

Johnston, J. M., Connizzo, B. K., Shetye, S. S., Robinson, K. A., Huegel, J., Rodriguez, A. B., et al. (2017). Collagen V haploinsufficiency in a murine model of classic Ehlers-Danlos syndrome is associated with deficient structural and mechanical healing in tendons. *J. Orthop. Res.* 35, 2707–2715. doi: 10.1002/jor.23571

Kader, N., Asopa, V., Baryeh, K., Sochart, D., Maffulli, N., and Kader, D. (2021). Cell-based therapy in soft tissue sports injuries of the knee: a systematic review. *Expert Opin. Biol. Ther.* 19, 1–13. doi: 10.1080/14712598.2021.1872538

Koh, Y. G., Jo, S. B., Kwon, O. R., Suh, D. S., Lee, S. W., Park, S. H., et al. (2013). Mesenchymal stem cell injections improve symptoms of knee osteoarthritis. *Arthroscopy* 29, 748–755. doi: 10.1016/j.arthro.2012.11.017

Kraus, V. B. (2011). Osteoarthritis year 2010 in review: biochemical markers. *Osteoarthritis Cartilage* 19, 346–353. doi: 10.1016/j.joca.2011.02.002

Kwon, H., Paschos, N. K., Hu, J. C., and Athanasiou, K. (2016). Articular cartilage tissue engineering: the role of signaling molecules. *Cell. Mol. Life Sci.* 73, 1173–1194. doi: 10.1007/s00018-015-2115-8

Mak, K. M., Png, C. Y., and Lee, D. J. (2016). Type V collagen in health, disease, and fibrosis. *Anat. Rec.* 299, 613–629. doi: 10.1002/ar.23330

Maroudas, A. I (1976). Balance between swelling pressure and collagen tension in normal and degenerate cartilage. *Nature* 260, 808–809. doi: 10.1038/260808a0

Mazor, M., Lespessailles, E., Coursier, R., Daniellou, R., Best, T. M., and Toumi, H. (2014). Mesenchymal stem-cell potential in cartilage repair: an update. *J. Cell. Mol. Med.* 18, 2340–2350.

Moskowitz, R. W., Davis, W., Sammarco, J., Martens, M., Baker, J., Mayor, M., et al. (1973). Experimentally induced degenerative joint lesions following partial meniscectomy in the rabbit. *Arthritis Rheum.* 16, 397–405. doi: 10.1002/art.1780160317

Nakajima, I., Muroya, S., Tanabe, R., and Chikuni, K. (2002a). Extracellular matrix development during differentiation into adipocytes with a unique increase in type v and vi collagen. *Biol. Cell* 94, 197–203. doi: 10.1016/s0248-4900(02)01189-9

Nakajima, I., Muroya, S., Tanabe, R., and Chikuni, K. (2002b). Positive effect of collagen V and VI on triglyceride accumulation during differentiation in cultures of bovine intramuscular adipocytes. *Differentiation* 70, 84–91. doi: 10.1046/j.1432-0436.2002.700203.x

Pasalini, T. S. P., and Fuller, R. (2018). Public social security burden of musculoskeletal diseases in Brazil – descriptive study. *Rev. Assoc. Med. Bras.* 64, 339–345. doi: 10.1590/1806-9282.64.04.339

Pastoureau, P. C., Hunziker, E. B., and Pelletier, J. P. (2010). Cartilage, bone and synovial histomorphometry in animal models of osteoarthritis. *Osteoarthritis Cartilage* 3, S106–S112. doi: 10.1016/j.joca.2010.05.024

Pearson, R. G., Kurien, T., Shu, K. S., and Scammell, B. E. (2011). Histopathology grading systems for characterisation of human knee osteoarthritis – reproducibility, variability, reliability, correlation, and validity. *Osteoarthritis Cartilage* 19, 324–331. doi: 10.1016/j.joca.2010.12.005

Pritzker, K. P. H., Gay, S., Jimenez, S. A., Ostergaard, K., Pelletier, J. P., Revell, P. A., et al. (2006). Osteoarthritis cartilage histopathology: grading and staging. *Osteoarthritis Cartilage* 14, 13–29. doi: 10.1016/j.joca.2005.07.014

Ricard-Blum, S., Beraud, M., Raynal, N., Farndale, R. W., and Ruggiero, F. (2006). Structural requirements for heparin/heparan sulfate binding to type V collagen. *J. Biol. Chem.* 281, 25195–25204. doi: 10.1074/jbc.M603096200

Robinson, P. G., Iain, R. M., West, C. C., Goudie, E. B., Yong, L. Y., White, T. O., et al. (2018). Reporting of mesenchymal stem cell preparation protocols and composition: a systematic review of the clinical orthopaedic literature. *Am. J. Sports Med.* 47, 991–1000. doi: 10.1177/0363546518758667

Ruggiero, F., Champliaud, M. F., Garrone, R., and Aumailley, M. (1994). Interactions between cells and collagen V molecules or single chains involve distinct mechanisms. *Exp. Cell Res.* 210, 215–223. doi: 10.1006/excr.1994.1032

Ruggiero, F., Comte, J., Cabañas, C., and Garrone, R. (1996). Structural requirements for alpha 1 beta 1 and alpha 2 beta 1 integrin mediated cell adhesion to collagen V. *J. Cell Sci.* 109, 1865–1874.

Sanchez-Adams, J., Leddy, H. A., McNulty, A. L., O'Conor, C. J., and Guilak, F. (2014). The mechanobiology of articular cartilage: bearing the burden of osteoarthritis. *Curr. Rheumatol. Rep.* 16, 451. doi: 10.1007/s11926-014-0451-6

Satué, M., Schüler, C., Ginner, N., and Erben, R. G. (2019). Intra-articularly injected mesenchymal stem cells promote cartilage regeneration, but do not permanently engraft in distant organs. *Sci. Rep.* 9, 10153. doi: 10.1038/s41598-019-46554-5

Shirasawa, S., Sekiya, I., Sakaguchi, Y., Yagishita, K., Ichinose, S., and Muneta, T. (2006). In vitro chondrogenesis of human synovium-derived mesenchymal stem cells: optimal condition and comparison with bone marrow-derived cells. *J. Cell Biochem.* 97, 84–97. doi: 10.1002/jcb.20546

Siclari, V. A., and Qin, L. (2010). Targeting the osteosarcoma cancer stem cell. *J. Orthop. Surg. Res.* 5, 78. doi: 10.1186/1749-799X-5-78

Symoens, S., Renard, M., Bonod-Bidaud, C., Syx, D., Vaganay, E., Malfait, F., et al. (2011). Identification of binding partners interacting with the α1-N-propeptide of type V collagen. *Biochem. J.* 433, 371–381. doi: 10.1042/BJ20101061

Tan, S. H. S., Kwan, Y. T., Neo, W. J., Chong, J. Y., Kuek, T. Y. J., See, J. Z. F., et al. (2021). Intra-articular injections of mesenchymal stem cells without adjuvant therapies for knee osteoarthritis: a systematic review and meta-analysis. *Am. J. Sports Med.* 20, 363546520981704. doi: 10.1177/0363546520981704

Ude, C. C., Shamsul, B. S., Ng, M. H., Chen, H. C., Ohnmar, H., Amaramalar, S. N., et al. (2018). Long-term evaluation of osteoarthritis sheep knee, treated with TGF-β3 and BMP-6 induced multipotent stem cells. *Exp. Gerontol.* 104, 43–51. doi: 10.1016/j.exger.2018.01.020

Velosa, A. P. P., Oliveira, A. M., Carrasco, S., Capelozzi, V. L., Teodoro, W. R., and Yoshinari, N. H. (2007). Partial meniscectomy as an experimental model of osteoarthritis in rabbits and protector effect of chloroquine diphosphate. *Rev. Bras. Reumatol.* 47, 401–410.

Waldstein, W., Perino, G., Gilbert, S. L., Maher, S. A., Windhager, R., and Boettner, F. (2016). OARSI osteoarthritis cartilage histopathology assessment system: a biomechanical evaluation in the human knee. *J. Orthop. Res.* 34, 135–140. doi: 10.1002/jor.23010

Wang, J., Zhou, L., Zhang, Y., Huang, L., and Shi, Q. (2020). Mesenchymal stem cells – a promising strategy for treating knee osteoarthritis. *Bone Joint Res.* 9, 719–728. doi: 10.1302/2046-3758.910.bjr-2020-0031.r3

Wu, J. J., Weis, M. A., Kim, L. S., Carter, B. G., and Eyre, D. R. (2009). Differences in chain usage and cross-linking specificities of cartilage type V/XI collagen isoforms with age and tissue. *J. Biol. Chem.* 284, 5539–5545. doi: 10.1074/jbc.m806369200

Xia, P., Wang, X., Wang, Q., Wang, X., Lin, Q., Cheng, K., et al. (2021). Low-Intensity pulsed ultrasound promotes autophagy-mediated migration of mesenchymal stem cells and cartilage repair. *Cell Transplant.* 30, 963689720986142. doi: 10.1177/0963689720986142

Yang, F., Luo, P., Ding, H., Zhang, C., and Zhu, Z. (2018). Collagen type V a2 (COL5A2) is decreased in steroid-induced necrosis of the femoral head. *Am. J. Transl. Res.* 10, 2469–2479.

Yarak, S., and Okamoto, O. K. (2010). Human adipose-derived stem cells: current challenges and clinical perspectives. *Ann. Bras. Dermatol.* 85, 647–656. doi: 10.1590/s0365-05962010000500008

Conflict of Interest: The authors declare that the research was conducted in the absence of any commercial or financial relationships that could be construed as a potential conflict of interest.

frontiers in Cell and Developmental Biology

ORIGINAL RESEARCH
published: 25 March 2021
doi: 10.3389/fcell.2021.655440

Biofunctionalized Structure and Ingredient Mimicking Scaffolds Achieving Recruitment and Chondrogenesis for Staged Cartilage Regeneration

Zhen Yang[1,2†], Hao Li[1,2†], Yue Tian[1†], Liwei Fu[1,2], Cangjian Gao[1,2], Tianyuan Zhao[1,2], Fuyang Cao[1,3], Zhiyao Liao[1,2], Zhiguo Yuan[4], Shuyun Liu[1*] and Quanyi Guo[1,2*]*

[1] Institute of Orthopedics, The First Medical Center, Chinese PLA General Hospital, Beijing Key Lab of Regenerative Medicine in Orthopedics, Key Laboratory of Musculoskeletal Trauma & War Injuries PLA, Beijing, China, [2] School of Medicine, Nankai University, Tianjin, China, [3] Department of Orthopedics, The First Affiliated Hospital of Zhengzhou University, Zhengzhou, China, [4] Department of Bone and Joint Surgery, Renji Hospital, School of Medicine, Shanghai Jiao Tong University, Shanghai, China

OPEN ACCESS

Edited by:
Zhenxing Shao,
Peking University Third Hospital, China

Reviewed by:
Zigang Ge,
Peking University, China
Johannes F. W. Greiner,
Bielefeld University, Germany

***Correspondence:**
Quanyi Guo
doctorguo_301@163.com
Shuyun Liu
clear_ann@163.com
Zhiguo Yuan
yzgad@163.com

[†] These authors have contributed equally to this work

Specialty section:
This article was submitted to Stem Cell Research, a section of the journal Frontiers in Cell and Developmental Biology

Received: 18 January 2021
Accepted: 05 March 2021
Published: 25 March 2021

Citation:
Yang Z, Li H, Tian Y, Fu L, Gao C, Zhao T, Cao F, Liao Z, Yuan Z, Liu S and Guo Q (2021) Biofunctionalized Structure and Ingredient Mimicking Scaffolds Achieving Recruitment and Chondrogenesis for Staged Cartilage Regeneration. Front. Cell Dev. Biol. 9:655440. doi: 10.3389/fcell.2021.655440

It remains scientifically challenging to regenerate injured cartilage in orthopedics. Recently, an endogenous cell recruitment strategy based on a combination of acellular scaffolds and chemoattractants to specifically and effectively recruit host cells and promote chondrogenic differentiation has brought new hope for *in situ* articular cartilage regeneration. In this study, a transforming growth factor-β3 (TGF-β3)-loaded biomimetic natural scaffold based on demineralized cancellous bone (DCB) and acellular cartilage extracellular matrix (ECM) was developed and found to improve chondral repair by enhancing cell migration and chondrogenesis. The DCB/ECM scaffold has porous microstructures (pore size: 67.76 ± 8.95 μm; porosity: 71.04 ± 1.62%), allowing the prolonged release of TGF-β3 (up to 50% after 42 days *in vitro*) and infrapatellar fat pad adipose-derived stem cells (IPFSCs) that maintain high cell viability (>96%) and favorable cell distribution and phenotype after seeding onto the DCB/ECM scaffold. The DCB/ECM scaffold itself can also provide a sustained release system to effectively promote IPFSC migration (nearly twofold *in vitro*). Moreover, TGF-β3 loaded on scaffolds showed enhanced chondrogenic differentiation (such as collagen II, ACAN, and SOX9) of IPFSCs after 3 weeks of culture. After implanting the composite scaffold into the knee joints of rabbits, enhanced chondrogenic differentiation was discovered at 1, 2, and 4 weeks post-surgery, and improved repair of cartilage defects in terms of biochemical, biomechanical, radiological, and histological results was identified at 3 and 6 months post-implantation. To conclude, our study demonstrates that the growth factor (GF)-loaded scaffold can facilitate cell homing, migration, and chondrogenic differentiation and promote the reconstructive effects of *in vivo* cartilage formation, revealing that this staged regeneration strategy combined with endogenous cell recruitment and pro-chondrogenesis is promising for *in situ* articular cartilage regeneration.

Keywords: demineralized cancellous bone, extracellular matrix, transforming growth factor-β3, cell recruitment, pro-chondrogenesis, cartilage regeneration

INTRODUCTION

Articular cartilage is a connective tissue that specifically adapts to harsh biomechanical environments; however, once injured, articular cartilage presents limited self-healing potential because it is devoid of blood supply, nerves and lymphatic tissues (Sophia Fox et al., 2009; Huey et al., 2012). Articular cartilage lesions caused by trauma, severe inflammation, infection and degenerative joint diseases predispose patients to joint pain or severe osteoarthritis (Wang et al., 2020; Yan et al., 2020). Conventional surgical treatments, such as microfracture (Steadman et al., 2003), autograft (Hangody and Füles, 2003), allograft mosaicplasty (Simon and Jackson, 2018), autologous chondrocyte implantation (ACI) (Richter et al., 2016), and even arthroplasty (Qiao et al., 2020), have been commonly proposed to repair such defects but cannot generate focal hyaline cartilage (Nie et al., 2020). Moreover, undesirable complications and a second operation are not uncommon (Chen et al., 2019a; Qiao et al., 2020). Tissue engineering for cartilage research provides biomaterial-based strategies to develop therapeutics for cartilaginous tissue growth and joint function restoration.

The approach of leveraging the body's innate regenerative potential with biomaterials and bioactive cues to direct endogenous stem/progenitor cells to injured sites to assist with tissue repair is a recent trend in regenerative medicine (Gaharwar et al., 2020). Infrapatellar fat pad adipose-derived stem cells (IPFSCs), which reside in the site near articular cartilage, have attracted increasing attention due to their easy availability, rich quantity in autologous tissue, superior chondrogenic effects, less hypertrophy risk, inflammatory modulation, anti-senescence effects, cytokine secretion, and better scaffold culturing performance (Hindle et al., 2017; Zhong et al., 2020). However, the migration of IPFSCs as well as other endogenous MSCs naturally occurs during a short time window only and does not sufficiently repair the cartilage (Barry and Murphy, 2013; Yang et al., 2020). Therefore, an ideal scaffold for cartilage regeneration should provide a structural framework to facilitate endogenous MSC migration and drive the differentiation of these cells into cartilage-specific cell types.

Recently, Hakamivala et al. (2020) reported that erythropoietin (EPO)-loaded particles could effectively support cartilage regeneration by recruiting endogenous progenitor cells. However, the chondrogenic microenvironment for migrated cells is indeed. Therefore, multipotential growth factors (GFs) may be a better choice. TGF-β is a family of pleiotropic cytokines that regulate cell migration, proliferation, and differentiation, tissue repair and inflammation and are essential for cartilage formation (Makhijani et al., 2005; Qu et al., 2019). TGF-β3 has been reported to enhance stem cell migration, and a proof of concept study also showed that TGF-β3 facilitates articular cartilage formation *in vivo* on 3D-printed polycaprolactone (PCL) scaffolds (Gao et al., 2010; Lee et al., 2010). In addition, as a critical regulator of chondrogenic differentiation, TGF-β3 is also a potent GF that supports the chondrogenesis of MSCs *in vivo* and *in vitro* (Yang et al., 2017; Deng et al., 2019). TGF-β3 can also effectively induce collagen and proteoglycan synthesis by regulating the metabolism of articular cartilage and multipotent proteins in a time- and dose-dependent manner (Chen et al., 2019b). However, effective incorporation and controlled delivery of GFs remains a universal challenge for the clinical application of *in situ* tissue engineering strategies. Existing approaches rely on systemic or bolus injection and often cause administered GFs to rapidly diffuse away from the target site, leading to unwanted side effects. Given the pleiotropic effects of TGF-β3, it is vital to develop a delivery system to ensure controlled and localized release to the target tissues.

Acellular cartilage extracellular matrix (ECM) prepared by decellularization technology, which preserves active biological factors and maintains low immunogenic cellular components, has been reported to enhance cartilage regeneration and joint function recovery (Sutherland et al., 2015; Feng et al., 2020). As a biodegradable biomaterial, the ECM has been utilized to carry MSCs or chondrocytes for cartilage repair (Min et al., 2016; Li et al., 2019). Bioactive factors, such as chemokines or GFs, can also be incorporated into the ECM, which allows for continuous and local delivery of protein with the degradation of the ECM (Yang et al., 2017). Therefore, the ECM could be an excellent vehicle for GF delivery in cartilage tissue engineering. However, considering the inadequacy of the biomechanical properties of cartilage ECM-derived scaffolds, natural composite scaffolds developed for cartilage regeneration have the potential to overcome this problem (Yang et al., 2017). Demineralized cancellous bone (DCB), a natural 3D porous collagen network with excellent biocompatibility and mechanical strength, has been used as a scaffold for tissue-engineered musculoskeletal regeneration (Zhang et al., 2015; Yuan et al., 2016). Therefore, an ECM and DCB hybrid composite scaffold might be a potential construct to meet the treatment needs of cartilage defects.

In this study, we used a lyophilization method to fabricate a TGF-β3-loaded DCB/ECM composite scaffold drug delivery system, which can integrate scaffolds and GFs for *in situ* cartilage tissue engineering (**Figure 1**). TGF-β3 exerts recruitment and chondrogenic effects simultaneously when released from scaffolds. We then tested the *in vitro* physicochemical properties and biocompatibility of the DCB/ECM scaffold, and *in vitro* recruitment and chondrogenic differentiation assays were performed. Finally, we implanted the composite scaffolds in a rabbit cartilage defect model to evaluate their therapeutic ability to promote *in situ* cartilage regeneration (**Figure 1**).

MATERIALS AND METHODS

Preparation of Scaffolds

Extracellular matrix -coated porous DCB scaffolds were produced as previously reported (Yuan et al., 2016). DCB scaffolds were trimmed into a cylindrical shape (diameter: 3.5 mm; thickness: 1.2 mm) and were completely immersed in the ECM suspension accordingly (**Table 1**). After freezing and lyophilization, the DCB/ECM scaffolds were crosslinked using carbodiimide solution (14 mM 1-ethyl-3-(3-dimethylaminopropyl) carbodiimide hydrochloride [EDAC] and 5.5 mM *N*-hydroxysuccinimide [NHS]; Sigma) for 2 h and sterilized using ethylene oxide. Each DCB/ECM scaffold

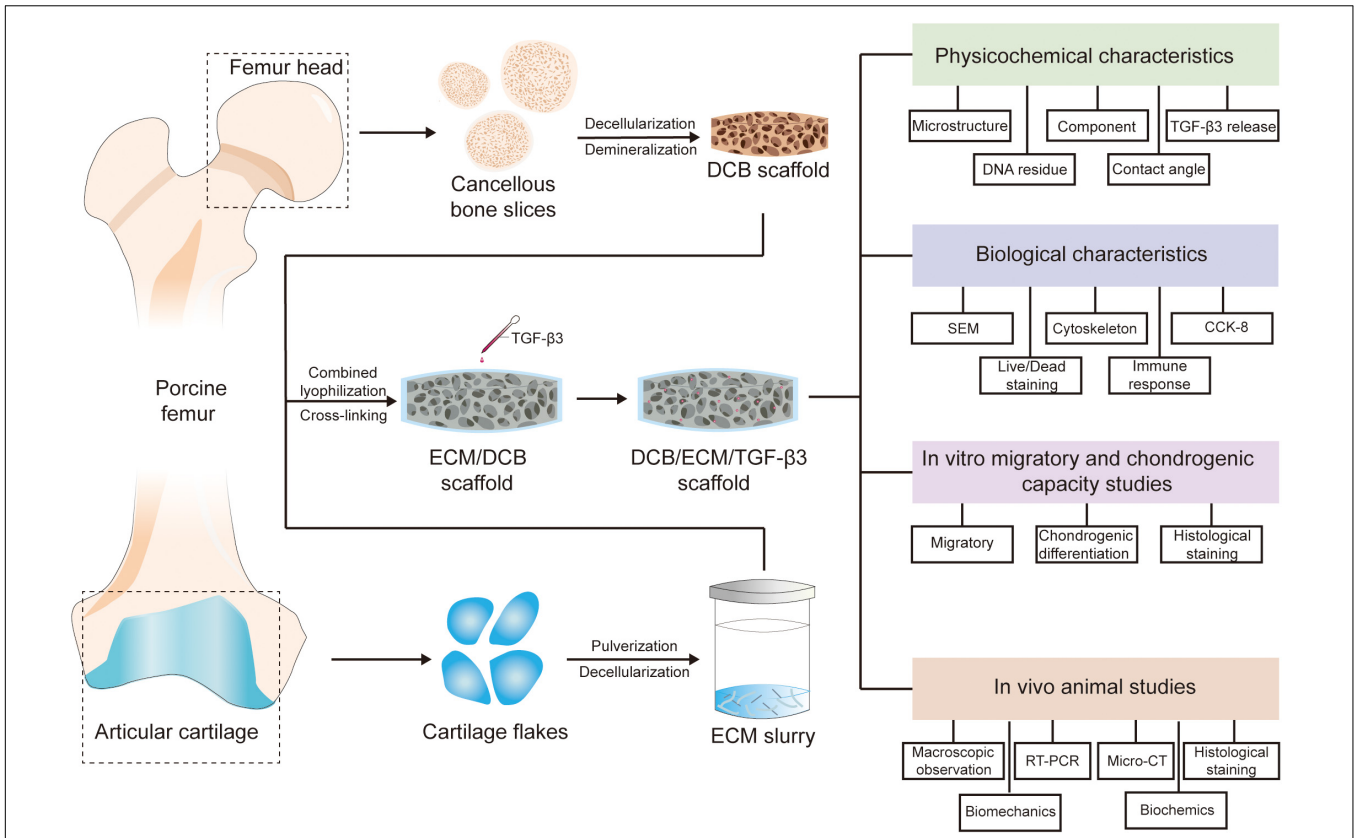

FIGURE 1 | Schematic illustration of the overall study design. DCB, demineralized cancellous bone; ECM, extracellular matrix; TGF-β3, transforming growth factor-β3.

was perfused with 20 μL of 20 μg/mL TGF-β3 and incubated subsequently at 4°C for 20 min to form the DCB/ECM/TGF-β3 scaffold according to a previous study (Huang et al., 2018) (**Figure 1**).

Physicochemical Characterization of Scaffolds

Scanning Electron Microscopy

The surfaces and interior microstructural morphologies of the DCB and DCB/ECM scaffolds were characterized by scanning electron microscopy (SEM) (S-4800 field emission scanning electron microscope; Hitachi, Tokyo, Japan) observation after putter coating with gold. Subsequently, the pore size and porosity of the different scaffolds were calculated by the software Nano Measure1.2 (China) and ImageJ (United States), respectively, according to the SEM images.

TABLE 1 | The compositions, pore size, and porosity of the scaffolds in this study.

Sample	ECM (wt%)	TGF-β3 (μg/mL)	Pore size (μm)	Porosity (%)
DCB scaffold	–	–	375.4 ± 38.52	84.93 ± 2.59
DCB/ECM scaffold	3%	–	67.76 ± 8.95****	71.04 ± 1.62*
DCB/ECM/TGF-β3 scaffold	3%	2	–	–

*n = 5, *p < 0.05, ****p < 0.0001.*

Protein Release Behaviors

The *in vitro* release of TGF-β3 was determined by adding 1.0 mL PBS buffer (pH 7.4) containing 0.5% (w/v) bovine serum albumin (BSA) to proper scaffolds in Eppendorf tubes. Tubes were incubated in a shaking water bath (37°C, 60 rpm). At determined time intervals (1, 2, 4, 7, 14, 21, 28, 35, and 42 days), the extract (1 mL) was collected for analysis and replaced by isometric fresh PBS buffer. The percentage of released TGF-β3 was measured by ELISA (R&D Systems, United States) according to the manufacturer's instructions. The ratio of cumulative release (in percent) was calculated based on the total amount of TGF-β3 obtained from the extracts.

Mechanical Testing

For compressive strength detection, approximately 5 mm cubes of the DCB and DCB/ECM scaffolds were tested using a BOSE biomechanical testing machine (BOSE 5100, United States). All scaffolds were kept moist in PBS buffer (pH 7.4) throughout these tests. The compression moduli were defined according to the slope of the linear fit to the strain-stress curves.

Cytocompatibility, Immunogenicity and Cell Recruitment Study

Cell Viability Analysis

The viability of IPFSCs in the scaffolds was evaluated using a live/dead assay and SEM. After sterilization and washing in sterile PBS buffer, the scaffolds were seeded with 5×10^5 IPFSCs in 20 μL DMEM/F12 (10% FBS) media and allowed to adhere for 2 h, during which 50 μL media was changed every 30 min; then, more media was added and refreshed every 2 days over the next 7 days.

The microstructure of the cell-scaffold composite and the growth of IPFSCs cultured *in vitro* on the scaffolds were observed by SEM. Cell-scaffold composites were harvested for 7 days after seeding. Specimens were fixed in 2.5% (v/v) glutaraldehyde and buffered with PBS. After putter coating with gold, the samples were observed using S-4800 field emission SEM (Hitachi, Tokyo, Japan).

Fluorescence staining of cells was observed by using a live/dead assay kit (Invitrogen, United States) after IPFSCs were seeded and cultured. After 4 days, scaffolds were washed with sterile PBS buffer and incubated in PBS solution with 2 mM calcein-AM and 4 mM ethidium homodimer-1 for 20 min at room temperature. Scaffolds were washed again with sterile PBS buffer, and images were acquired using a Leica TCS-SP8 confocal microscope (Leica, Germany) and analyzed with ImageJ software (United States). Cell viability was calculated as follows: (live cells/total cells) × 100% ($n = 3$).

In vivo Immune Responses Evaluation

Scaffolds were subcutaneously embedded into the back skin of SD rats to evaluate their *in vivo* biocompatibility. At 1 week after implantation, rats were euthanized, and H&E staining was performed to evaluate histological changes.

In vitro IPFSC Recruitment

To determine the cell recruitment capability of the DCB/ECM/TGF-β3 scaffold on IPFSCs, a migration assay was performed according to the protocol described in the **Supplementary Materials**. DMEM (negative control), a DCB scaffold, a DCB/ECM scaffold and a DCB/ECM/TGF-β3 scaffold were added to the lower chamber (**Figure 2A**).

In vivo Endogenous MSC Recruitment Study in Rats

Sixteen SD rats were randomly allocated into four groups as follows: (A) negative control group, (B) DCB group, (C) DCB/ECM group, and (D) DCB/ECM/TGF-β3 group. A 2.0-mm diameter and 1-mm depth cartilage defect was created on the femoral trochlea of both limbs until there was slight bleeding. The different scaffolds were implanted at the defect site and the tissue and skin were sutured. At 7 days after the operation, rats were sacrificed, all debris was removed, and the distal femurs were collected. The MSC recruitment study was assessed by immunofluorescence staining (CD73, CD105, and DAPI).

In vitro Chondrogenic Differentiation

Chondrogenic differentiation was performed according to a previously published study (Fan et al., 2008). Approximately 4×10^5 IPFSCs at passage 2 were centrifuged at 1500 rpm for 5 min in 15 mL Falcon tubes to form cell pellets. The pellets were maintained at 37°C with 5% CO_2 in basal media for 24 h, after which they were placed in Transwell plates placed in 24-well plates. The 24-well plates contained either DCB scaffolds, DCB/ECM scaffolds, DCB/ECM/TGF-β3 scaffolds or nothing. Each well of the 24-well plates containing either the scaffold or nothing was nourished with chondrogenic induction media (CIM, Cyagen Biosciences, China). TGF-β3-free CIM consisted of basal medium supplemented with chondrogenesis supplementation (dexamethasone, ascorbate, insulin-transferrin-selenium solution, sodium pyruvate, proline). Medium was replenished every third day for 3 weeks. Chondrogenesis was qualitatively evaluated through H&E, toluidine blue, safranin O and collagen II immunofluorescence staining after 21 days ($n = 4$).

In vivo Chondrogenic Differentiation Assay

Animal Surgery

An *in vivo* chondrogenic differentiation assay using a biofunctional scaffolding system was performed in a rabbit full-thickness cartilage defect model as described in our previous study (Li et al., 2019). All *in vivo* animal experiments were approved by the Institutional Animal Care and Use Committee at PLA General Hospital. This study used skeletally mature New Zealand White rabbits (male, weight 2.5–3.0 kg, 6 months old), and all animals were randomly allocated into four groups (n = 4 knees per group for each time point) as follows: (1) a negative control group, (2) a DCB group, (3) a DCB/ECM group, and (4) a DCB/ECM/TGF-β3 group (**Figure 3A**). In brief, we used a trephine to create a critical cartilage defect (3.5-mm in diameter and 1.2-mm in depth) on the patellar trochlear groove through the chondral layers. The defects of the experimental group were then implanted with three different scaffolds and adjusted to be flat against the surface of the surrounding cartilage. The negative control group received no scaffold treatment. After implantation, the joint capsule, subcutaneous tissue, and skin were closed, followed by intramuscular penicillin injections for up to 3 days. All rabbits were treated with the same dietary conditions, and none of them were excluded from this study. At different time points post-surgery, rabbits were euthanized and harvested for evaluation.

In vivo Chondrogenic Differentiation Assay

One week, 2 and 4 weeks post-implantation, a cylindrical tissue sample (3.5-mm in diameter and 1.2-mm in depth) was harvested from the defect site for further detection (n = 4 knees per group for each time point). Chondrogenic differentiation gene expression was analyzed using quantitative reverse transcription-polymerase chain reaction (RT-qPCR) as previously reported (Sun et al., 2018). Briefly, four independent cylindrical tissue specimens were snap-frozen in liquid nitrogen and then pulverized by a mortar. Total RNA was extracted using a standard TRIzol (Invitrogen, United States) procedure and quantified by a Nucleic Acid and Protein Analyzer (Microfuge18;

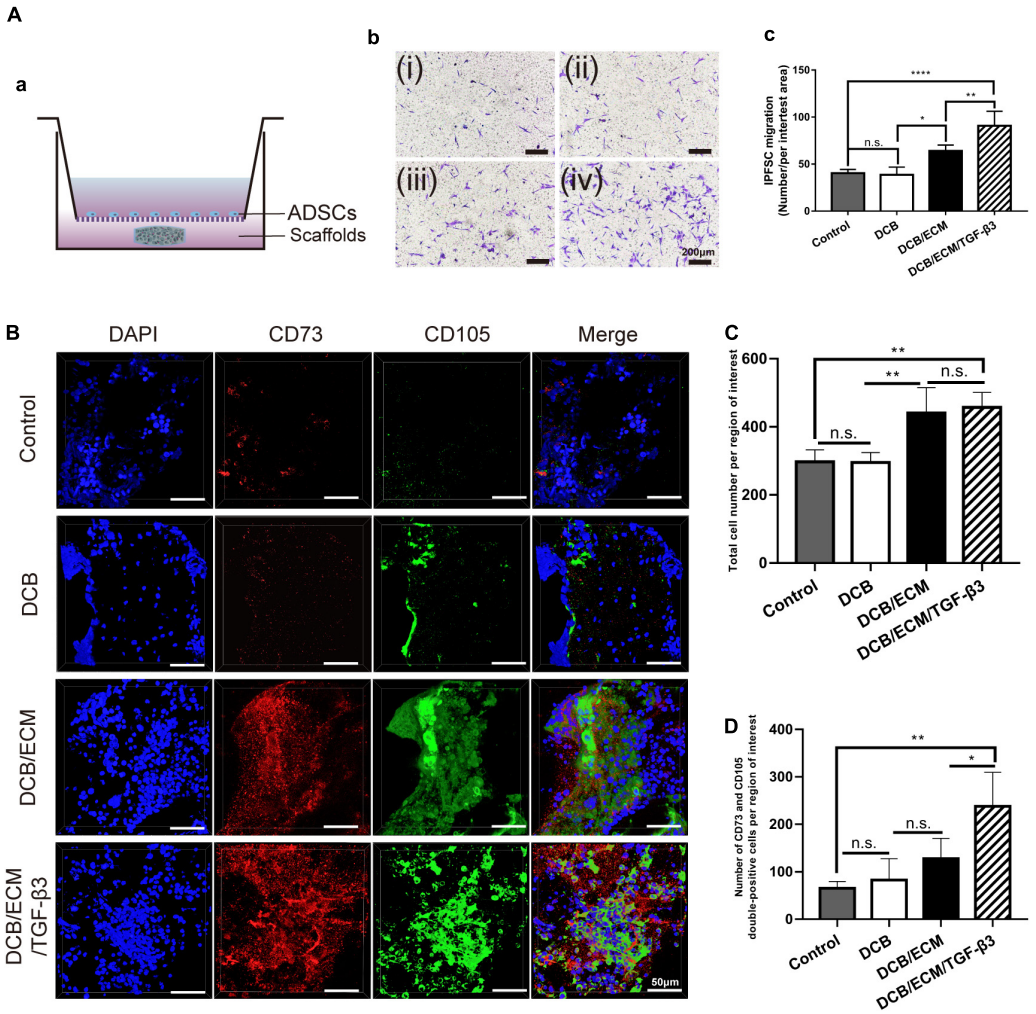

FIGURE 2 | Migratory capacity of the different scaffolds on stem cells *in vitro* and *in vivo*. **(A)** Effects of different scaffolds on the migration of IPFSCs. **(a)** Schematic illustrations of the Transwell assay. **(b)** The migratory cells were stained with crystal violet after culturing for 24 h (i: negative control group; ii: DCB group; iii: DCB/ECM group; iv: DCB/ECM/TGF-β3 group). **(c)** Statistical analysis of the average migratory cell number per region of interest from different groups at the 24-h time point; values are presented as the means ± SDs (n = 5). **(B)** Confocal images of cell migration in the different scaffold groups (n = 5). **(C)** Total cell number migrated to the rat cartilage injured sites (n = 4). **(D)** Numbers of CD73/CD105 double-positive cells migrated to the rat cartilage injured sites (n = 4).

Beckman-Coulter), followed by cDNA synthesis using a ReverTra Ace® qPCR RT Kit (FSQ-201; TOYOBO). The specific gene primers designed for qPCR are listed in **Table 2**, and the experiment was performed using the StepOne TM Real-Time PCR System (Applied Biosystems). The relative gene expression was normalized to the housekeeping gene glyceraldehyde 3-phosphate dehydrogenase (GAPDH) and presented as the fold-change relative to the negative control group using the $2^{\Delta\Delta Ct}$ method.

In vivo Cartilage Repair Study

Animal Surgery

In vivo cartilage repair using the biofunctional scaffolding system was assessed in the rabbit full-thickness cartilage defect model. All animal surgeries and groups were described above (**Figure 3A**). At 12 and 24 weeks post-surgery, all rabbits were euthanized and harvested for further detection (n = 8 knees per group for each time point).

Macroscopic Evaluation

All samples in each group of cartilage defects in the femoral condyles were observed by three independent evaluators and photographed (n = 8 knees per group for each time point). Macroscopic scoring was performed blindly by three experienced researchers specializing in musculoskeletal disease, following the ICRS scoring system guidelines.

Micro-CT Scanning

The samples were assessed using General Electric (GE) eXplorer Locus SP (GE, Boston, MA, United States) according to previous methods (Sun et al., 2018). The image data in the sagittal, frontal, and transverse planes were reconstructed and analyzed using

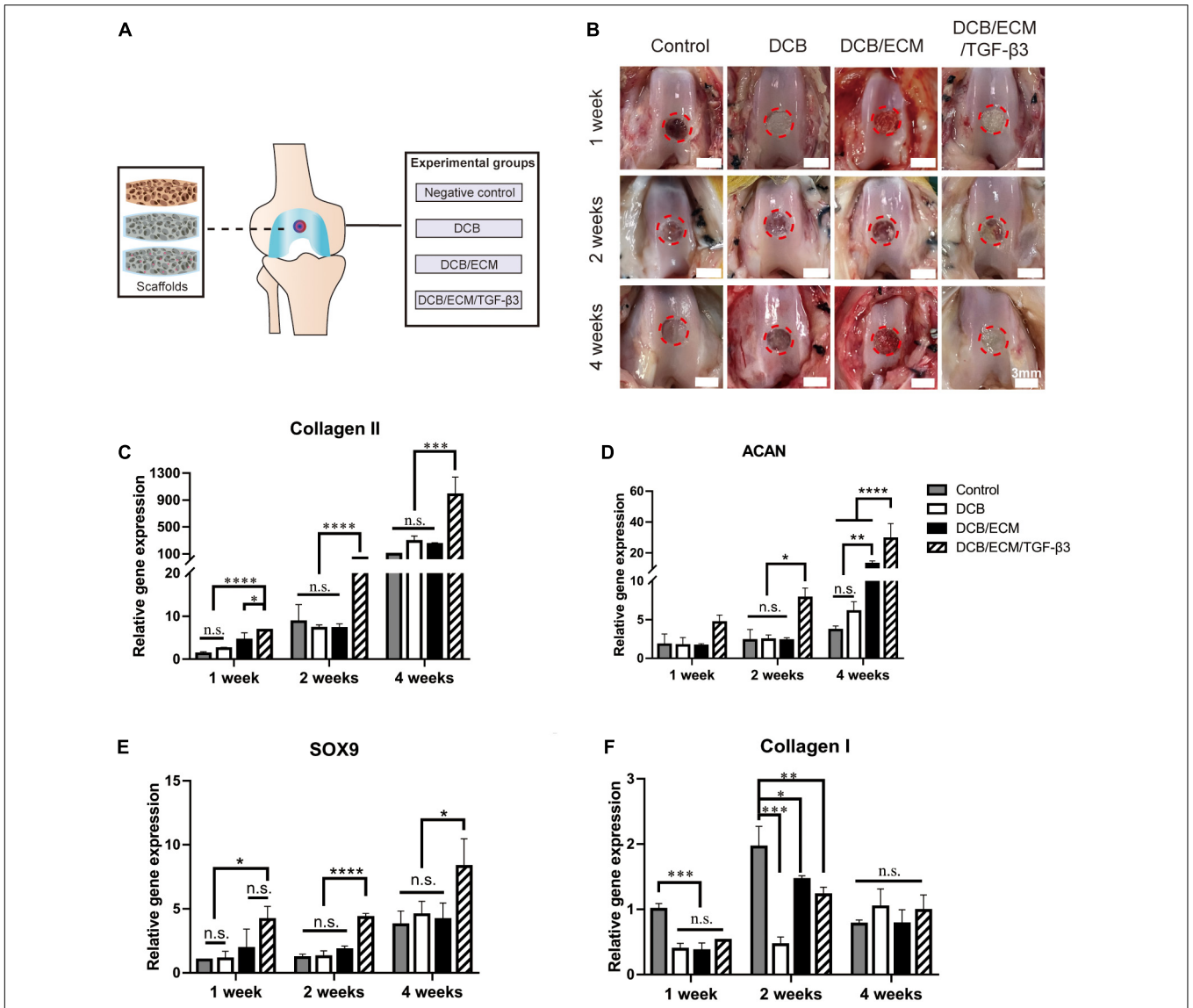

FIGURE 3 | *In vivo* chondrogenic differentiation assay. **(A)** Scaffold implantation and experimental grouping schema. **(B)** Representative macroscopy of repaired tissues at 1, 2, and 4 weeks postsurgery. The red circles indicate the repaired areas. **(C–F)** Quantitative polymerase chain reaction (qPCR) analysis for collagen II, aggrecan (ACAN), transcription factor SOX9 and collagen I. The qPCR results were repeated three times independently. Data are means ± SDs (*$p < 0.05$, **$p < 0.01$, ***$p < 0.005$, ****$p < 0.001$, n.s. represents no significant difference).

GE Health Care MicroView ABA 2.1.2 software. A cylindrical region of interest (3.5-mm in diameter and 1.2-mm in depth) corresponding to the original defect location was selected to further assay. The BMD and BV/TV were then analyzed ($n = 6$ knees per group for each time point).

Biomechanical and Biochemical Assessment of Repaired Tissue

At 3 or 6 months postoperation, compressive strength detection was conducted according to the assessment of the biomechanical properties of repaired cartilage as described above ($n = 3$).

The neotissue total collagen content assay was performed by following the procedure described in the **Supplementary Materials**, and the collagen II content assay was performed by Western blot (WB). Every sample was cut into two equal parts for the above assays ($n = 3$ knees per group for each time point).

Histology and Immunohistochemistry

After examination by micro-CT, the samples were fixed in 4% PFA and then decalcified in 10% (w/v) EDTA (pH = 7.0) for 2 months at room temperature. Next, they were dehydrated and embedded in paraffin wax, sectioned into 6-μm slices and stained with H&E, toluidine blue, safranin O/fast green, and Sirius red according to the manufacturer's protocols. Collagen II immunohistochemical staining was performed by immersing

TABLE 2 | Primer sequences used for *in vivo* chondrogenic RT-qPCR.

Target gene		Sequence
SOX9	F: 5′-3′R: 3′-5′	GCGGAGGAAGTCGGTGAAGAAT AAGATGGCGTTGGGCGAGAT
Collagen II	F: 5′-3′R: 3′-5′	CACGCTCAAGTCCCTCAACA TCTATCCAGTAGTCACCGCTCT
Collagen I	F: 5′-3′R: 3′-5′	GCCACCTGCCAGTCTTTACA CCATCATCACCATCTCTGCCT
ACAN	F: 5′-3′R: 3′-5′	GGAGGAGCAGGAGTTTGTCAA TGTCCATCCGACCAGCGAAA
GAPDH	F: 5′-3′R: 3′-5′	CAAGAAGGTGGTGAAGCAGG CACTGTTGAAGTCGCAG

the sections into 0.25% pepsin (Abcam, United States) at 37°C for 20 min and blocking them in 10% goat serum for 1 h. After antigen retrieval, the slices were incubated with primary antibodies against collagen II (1:200; Developmental Studies Hybridoma Bank, United States) at 4°C overnight. After washing with PBS, they were incubated with goat anti-mouse IgG (1:200; Cat# NB7539; Novus) for 1 h. Finally, the sections were stained with Tris-HCl buffer containing 0.05% DAB and 0.005% hydrogen peroxide, and the nuclei were stained with hematoxylin. Photomicrographs were acquired using a Nikon microscope (Japan).

To evaluate the progress of subchondral bone reconstruction and cartilage repair, sections from three knees at 3 and 6 months per group (each sample represented three tissue sections) were blindly scored by three independent observers according to an established scoring system.

Statistical Analysis

All quantitative data were analyzed using SPSS version 25.0 (SPSS, Chicago, IL, United States) and expressed as the mean ± standard deviation (SD). Student's *t*-test, one-way analysis of variance (one-way ANOVA) or two-way ANOVA, followed by the Bonferroni multiple comparison test, was performed for normally distributed data. A value of $P < 0.05$ was considered to indicate a statistically significant difference.

RESULTS

Physicochemical and Biological Characterization of Scaffolds

Scaffold Macro- and Microstructure

Macroscopic observations of DCB and DCB/ECM scaffolds are shown in **Figure 4A**, and the results showed that DCB scaffold had a larger interconnected porous structure than the DCB/ECM scaffold. The SEM photographs of the DCB scaffold in **Figure 4A** showed circular pores in the size range of 375.4 ± 38.52 μm, while the DCB/ECM scaffold exhibited smaller irregular pores in the size range of 67.76 ± 8.95 μm ($^{****}p < 0.0001$, $n = 5$, **Table 1**). The porosity of the two scaffolds was also calculated as follows: 84.93 ± 2.59% for DCB scaffold and 71.04 ± 1.62% for DCB/ECM scaffold ($^{*}p < 0.05$, $n = 5$, **Table 1**).

Protein Release Files

The TGF-β3-loaded DCB/ECM scaffolds were constructed according to the protocol (**Figure 1**). To assess the proteins released from the scaffold, total cumulative TGF-β3 release for 42 days was detected by enzyme-linked immunosorbent assay (ELISA) according to the manufacturer's instructions. The DCB/ECM/TGF-β3 scaffolds released a cumulative rate of approximately 40% after 14 days and still increased up to 50% after 42 days (**Figure 4B**). These results suggest that the DCB/ECM scaffold could be a good drug release candidate with controlled and prolonged protein release kinetics for *in situ* tissue engineering.

Mechanical Characterization

To evaluate the biomechanical properties, a compressive strength assay was conducted to compare the DCB and DCB/ECM scaffolds. The compressive moduli of the DCB/ECM scaffold were superior (90.96 ± 37.22 kPa) to that of the DCB scaffold (11.34 ± 9.64 kPa, $n = 5$) (**Figure 4C**).

Cytocompatibility and *in vivo* Immune Response of the Scaffolds

IPFSCs Attachment and Viability on the Scaffolds *in vitro*

The attachment of IPFSCs to DCB and DCB/ECM scaffolds was evaluated using SEM (**Figure 4D**). The IPFSCs attached to two scaffolds and migrated well into the interconnecting pores in DCB and DCB/ECM scaffolds over 1, 4, and 7 days culture periods. The IPFSCs were better distributed between interconnecting pores in the DCB/ECM scaffold during the three culture periods. This is probably because the pore sizes and hydrophilicity in the DCB/ECM scaffold were more suitable than those in the DCB scaffold, making it easier to attach to the interconnecting pores. To conclude, the inner walls of DCB and DCB/ECM scaffolds increase the surface area and might be suitable for IPFSC adhesion.

IPFSC viability on DCB and DCB/ECM scaffolds was observed by live/dead staining after 7 days of culture. For both scaffolds, most IPFSCs were stained with fluorescent green (living cells), with limited fluorescent red (dead) cells from 3D reconstruction images (**Figure 4E**). Quantitative cell viability analysis ($n = 3$) demonstrated that the cell viability rates on both the DCB and DCB/ECM scaffolds were higher than 96% but did not show any significant differences. The above results demonstrate that DCB and DCB/ECM scaffolds had good cytocompatibility and were suitable for cells to adhere and proliferate.

Scaffolds' Immune Response in Rats

Acute inflammatory and immune responses of DCB and DCB/ECM scaffolds were evaluated at 1 week after rat subcutaneous implantation. No obvious scar tissues formation was found around the two scaffolds in the macroscopic observations and H&E staining images (**Figure 4F**). We observed some neutrophil and monocyte infiltration around the DCB/ECM scaffold, but only a small amount of immune cells were observed around the DCB scaffold, suggesting that the

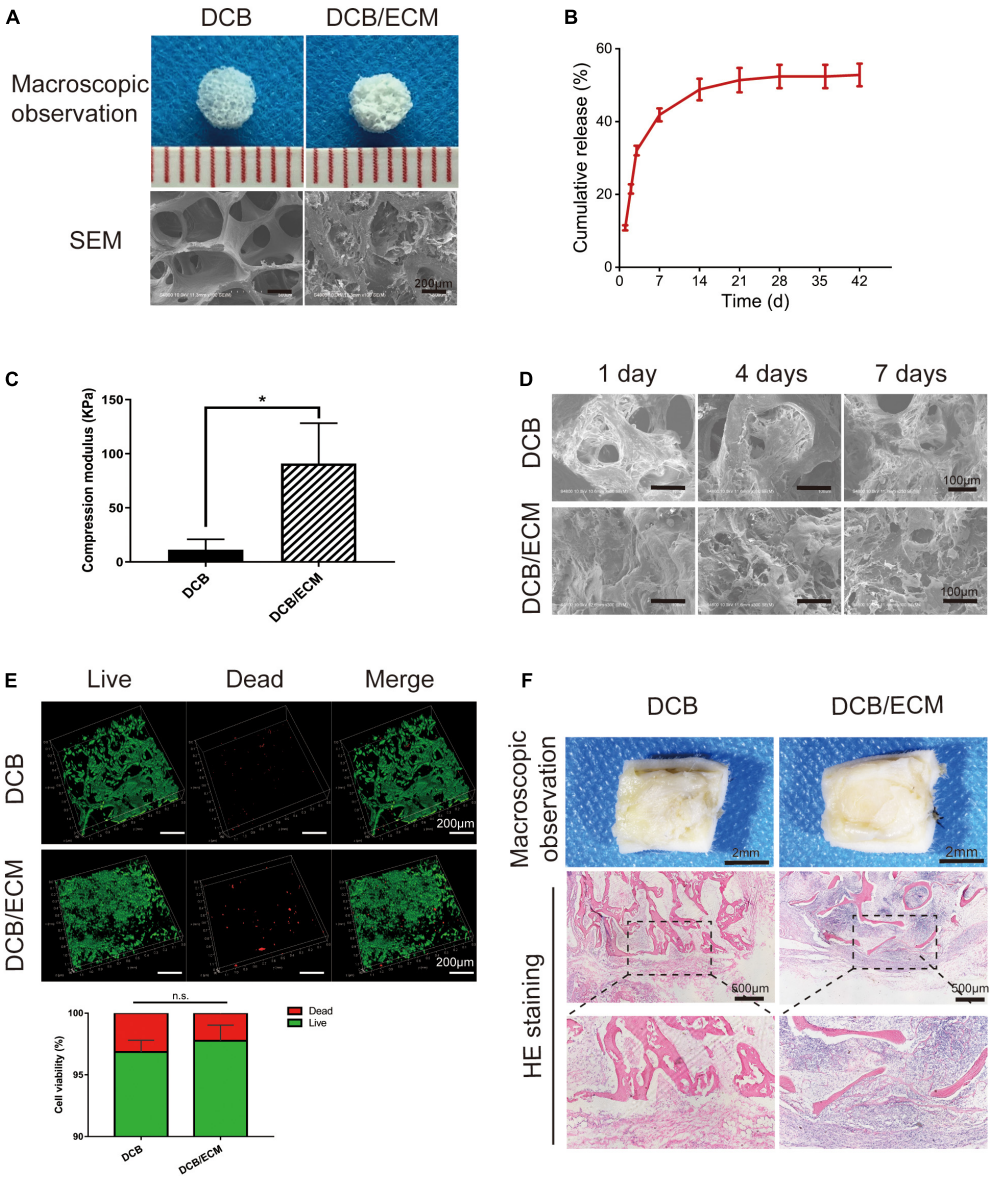

FIGURE 4 | The physicochemical, biocompatibility, and immunogenicity properties of DCB and DCB/ECM scaffolds. **(A)** Macroscopic features and SEM of DCB and DCB/ECM scaffolds. **(B)** TGF-β3 release kinetics of the DCB/ECM/TGF-β3 scaffold. Values are presented as the means ± SDs (n = 3). **(C)** Compression modulus of DCB and DCB/ECM (scaffolds; values are presented as the means ± SD, n = 5). **(D)** SEM of DCB and DCB/ECM scaffolds on which IPFSCs were seeded for 1, 4, and 7 days. **(E)** Live/dead staining analysis of IPFSCs cultured in DCB and DCB/ECM scaffolds for 7 days. Representative 3D reconstruction images show live (green) cells and dead (red) cells. Values are presented as the means ± SDs (n = 3). (*$p < 0.05$, n.s. represents no significant difference). **(F)** Macroscopic observations and H&E staining of the immune responses of DCB and DCB/ECM scaffolds at 1-week postimplantation in rats.

pure DCB scaffold had lower immunogenic properties than the DCB/ECM scaffold.

In vitro Cell Recruitment and Chondrogenic Differentiation Assays

In vitro and *in vivo* Stem Cell Migration Assay

To determine the effect of different scaffolds on IPFSC mobility, we performed Transwell system assays *in vitro*. Twenty-four hours after stimulation with different scaffolds, the cell numbers were 40.25 ± 4.03 for the negative control group, 38.5 ± 8.35 for the DCB group, 64 ± 6.22 for the DCB/ECM group, and 90.75 ± 15.39 for the DCB/ECM/TGF-β3 group, among which the DCB/ECM/TGF-β3 group showed the best cell recruitment capacity (**Figure 2A**). To conclude, the above results indicate that the DCB/ECM and DCB/ECM/TGF-β3 scaffolds could promote IPFSC migration *in vitro* (n = 5, *$p < 0.05$, **$p < 0.01$, ****$p < 0.001$).

Moreover, *in vivo* MSC recruitment by TGF-β3 was further assessed by comparing the migrated MSCs in different groups

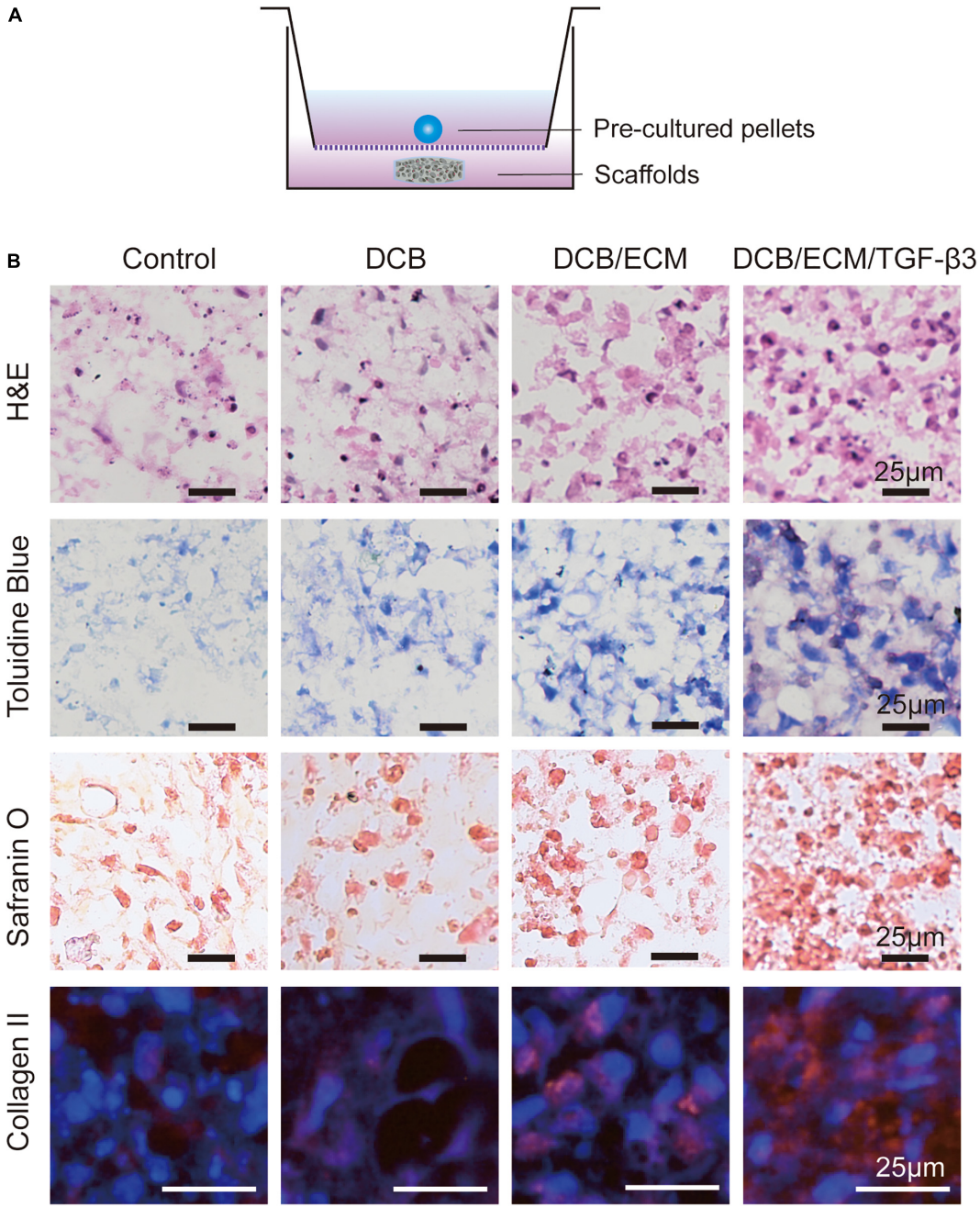

FIGURE 5 | Chondrogenic capacity of the different scaffolds *in vitro*. **(A)** Schematic illustrations of the coculture systems between pre-cultured pellets and the different scaffolds. **(B)** Histological and immunofluorescence analyses of chondrogenic pellets performed in a coculture system with different scaffolds. H&E, toluidine blue, safranin O, and collagen II immunofluorescence staining were used.

at 1 week postoperation (**Figure 2B**). The results demonstrated that compared with the control and DCB groups, total cell numbers were higher in the DCB/ECM and DCB/ECM/TGF-β3 groups, while there were no dramatic differences between these two groups (**Figure 2C**). In addition, CD73 and CD105 double-positive cells were dramatically more concentrated in the DCB/ECM/TGF-β3 group than in the other groups (**Figure 2D**). These results also suggested that the TGF-β3 effectively enriched surrounding MSCs to the defect site and improved the regeneration of damaged cartilage.

In vitro Chondrogenic Differentiation Assay

To observe the bioactivity of TGF-β3 released from the scaffold, a 3D pellet coculture system experiment was performed according to previous studies (**Figure 5A**) (Chen et al., 2020). As shown in **Figure 5B**, H&E staining indicated that the 3D pellets

were successfully cultured. Toluidine blue and safranin O staining, which stains synthesized proteoglycans, demonstrated the greatest intensity of pellets in the DCB/ECM/TGF-β3 scaffold group. In addition, collagen II immunofluorescence staining also showed that TGF-β3 released from scaffolds significantly promoted the secretion of collagen II.

In vivo Chondrogenic Differentiation

After 1 week of *in vivo* implantation, gross observation demonstrated that cartilage defects were unrepaired in the control group and that scaffolds were still not completely degraded in the other three groups (control, DCB scaffold, and DCB/ECM scaffold). At 2 weeks, neocartilaginous tissue barely formed around the edge of the defects in the control, DCB and DCB/ECM groups. Moreover, cartilage defects in the DCB/ECM/TGF-β3 group were filled by a certain amount of repaired tissue (**Figure 3B**). After 4 weeks of implantation, cartilage defects were partially filled in the control group, but the cartilage did not regrow well. In the DCB and DCB/ECM groups, the defect was filled with regrown cartilage, but the surface was still rough. The regenerated cartilage in the DCB/ECM/TGF-β3 group was similar to the surrounding native cartilage tissue. However, obvious uneven edges between the surrounding cartilage still existed.

To demonstrate chondrogenic differentiation capabilities in different scaffolds, chondrogenic relative gene expression (collagen II, ACAN, SOX9 and collagen I) was assessed in the four groups at 1, 2, and 4 weeks postsurgery *in vivo* for the first time (**Figures 3C–F**). The results show that with time, the expression level of cartilage-related genes increased gradually, which indicates that chondrogenic differentiation occurs during the natural repair process and may play an important role in tissue regeneration. Furthermore, the expression levels of cartilage-related genes (collagen II, ACAN, and SOX9) were significantly upregulated in the TGF-β3-loaded DCB/ECM group; however, there were no significant differences among the control, DCB and DCB/ECM groups. This shows that supplementation with TGF-β3 could significantly stimulate chondrogenic differentiation of MSCs in defects compared with that in pure DCB scaffolds or DCB/ECM scaffolds. In terms of osteogenic differentiation, we did not find any regular trend of the related gene COL1 throughout the three different times *in vivo*. These results show that the scaffolds loaded with TGF-β3 could effectively enhance chondrogenic differentiation at the defect site and consequently enhance tissue repair and regeneration.

In vivo Cartilage Repair Study

Gross Observation and Biomechanical Assessment of the Repaired Tissue

The rabbit cartilage defect model was used to evaluate the therapeutic value of the scaffold. Three months postsurgery, gross observation demonstrated that cartilage defects were unrepaired in the control group (**Figure 6A**). In the DCB group, neocartilaginous tissue was partly formed surrounding the edge of the defects and showed irregular surface regularity with structural damage and fissures. Moreover, the cartilage defects in the DCB/ECM and DCB/ECM/TGF-β3 groups were filled with granulation tissue with uneven surfaces. We found that the regenerated cartilage of the DCB/ECM/TGF-β3 group was more similar to native cartilage than to that of the DCB/ECM group (**Figure 6A**). At 6 months, defects in the control group were characterized by incomplete filling of neotissue, surface irregularity, and distinct boundary areas. In the DCB group, the defect was filled with regrew cartilage, and cracks were observed in the center. In addition, cartilage defects were mostly filled in the DCB/ECM group. However, the surface was still rough, and the edges next to the surrounding cartilage were obviously uneven. The regenerated cartilage in the DCB/ECM/TGF-β3 group was similar to the surrounding native cartilage tissue, with a neat surface and complete fusion with the surrounding cartilage.

Consistent with the gross observation, the International Cartilage Research Society (ICRS) macroscopic scores of DCB/ECM/TGF-β3 (8.00 ± 1.31 at 3 months and 10.125 ± 0.84 at 6 months) were apparently better than those of the other groups: the control group (3.25 ± 1.04 at 3 months and 4.00 ± 1.31 at 6 months), DCB group (3.75 ± 1.04 at 3 months and 7.50 ± 1.20 at 6 months), and DCB/ECM group (6.25 ± 0.89 at 3 months and 8.38 ± 0.74 at 6 months) at both time points ($^{*}p < 0.05$, $^{**}p < 0.01$, $^{***}p < 0.005$, $^{****}p < 0.001$) (**Figure 6B**).

Microcomputed Tomography (Micro-CT) Analysis of the Repaired Tissue

For all groups, the growth pattern of the subchondral bone reconstruction at 3 and 6 months after surgery was evaluated by micro-CT imaging (**Figure 6C**). The quantitative bone mineral density (BMD) data were plotted (**Figure 6D**) and revealed that the value of the DCB/ECM/TGF-β3 group was significantly higher than that of the other three groups. Furthermore, no other significant differences within the control, DCB and DCB/ECM groups were found at any other time point. In addition, the bone volume-to-tissue volume ratio (BV/TV) values in the DCB/ECM/TGF-β3 group were dramatically higher than those in the other three groups at both time points (**Figure 6E**). In addition, only non-significant differences in BV/TV were found at 6-month time points between the DCB/ECM and DCB/ECM/TGF-β3 groups.

Biomechanical and Biochemical Assessment of Repaired Tissue

To evaluate the biomechanical properties of repaired tissue, compressive strength testing was conducted to compare the different groups. The 6-month repaired tissue generally had higher compressive moduli than the 3-month regenerated cartilage tissue. At 3 months postoperation, the compressive modulus was approximately 0.81 ± 0.36 MPa for the negative control group, 1.16 ± 0.49 MPa for the DCB group, 1.44 ± 0.32 MPa for the DCB/ECM group, and 1.51 ± 0.32 MPa for the DCB/ECM/TGF-β3 group (**Figure 6F**), whereas there was no significant difference among them. The compressive moduli of the repaired tissue (2.91 ± 0.45 MPa) in the DCB/ECM/TGF-β3 group were significantly higher than those in the other three groups (**Figure 6F**, $n = 3$, $^{*}p < 0.05$).

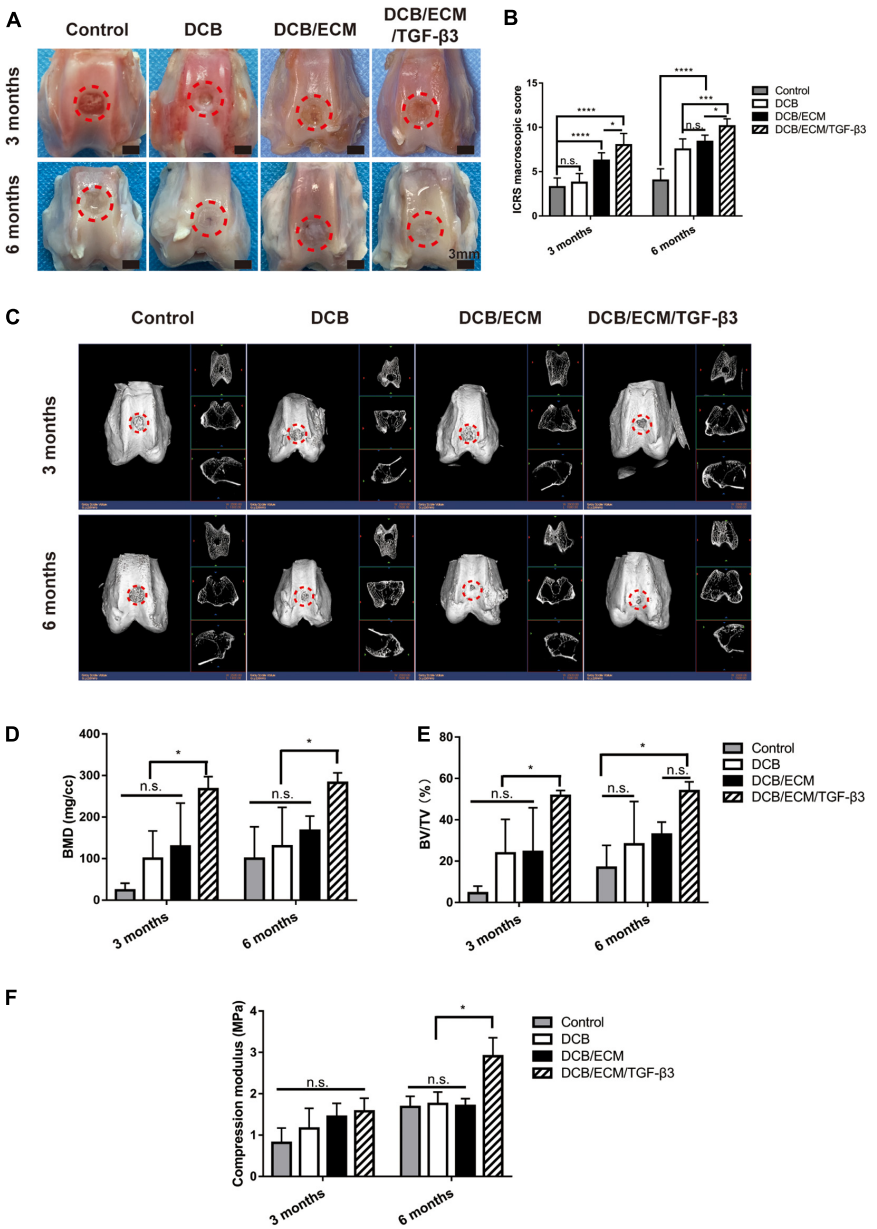

FIGURE 6 | Representative macroscopic, radiological and biomechanical properties of repaired tissues at 3 and 6 months postoperation. **(A)** Representative macroscopy. **(B)** ICRS scores at 3 and 6 months. **(C)** Representative 3D and 2D micro-CT images at each time point. Quantitative analysis of **(D)** BMD and **(E)** BV/TV (n = 6 knees). The repaired sites were indicated by red circles. **(F)** Compression modulus of repaired tissues at 3 and 6 months (n = 3 knees). The red circles indicate the repaired areas. Data are means ± SDs (*$p < 0.05$, ***$p < 0.005$, ****$p < 0.001$, n.s. represents no significant difference).

Biochemical assays for total collagen (**Figure 7D**) revealed that the total collagen content in the DCB/ECM/TGF-β3 group (142.90 ± 11.68 μg/mg at 3 months and 165.58 ± 10.92 μg/mg at 6 months) was significantly higher than that in the negative control group (79.61 ± 13.10 μg/mg at 3 months and 78.59 ± 9.66 μg/mg at 6 months), DCB group (81.59 ± 8.00 μg/mg at 3 months and 103.67 ± 5.80 μg/mg at 6 months), and DCB/ECM group (94.68 ± 12.87 μg/mg at 3 months and 124.21 ± 9.66 μg/mg at 6 months), among which the DCB/ECM group showed superior total collagen deposition than the negative control group (**$p < 0.01$). In addition, the protein expression of collagen II (**Figure 7E**) in repaired tissue of the DCB/ECM/TGF-β3 group was also higher than that of the control group, DCB group and DCB/ECM group.

Histomorphometry of the Repaired Tissue

At 3 months, the histological staining results showed that the non-treated control group was insufficient to induce cartilage formation, the defect border remained, and fibrous tissues were filled (**Figure 7A**). In the DCB and DCB/ECM groups, distinct

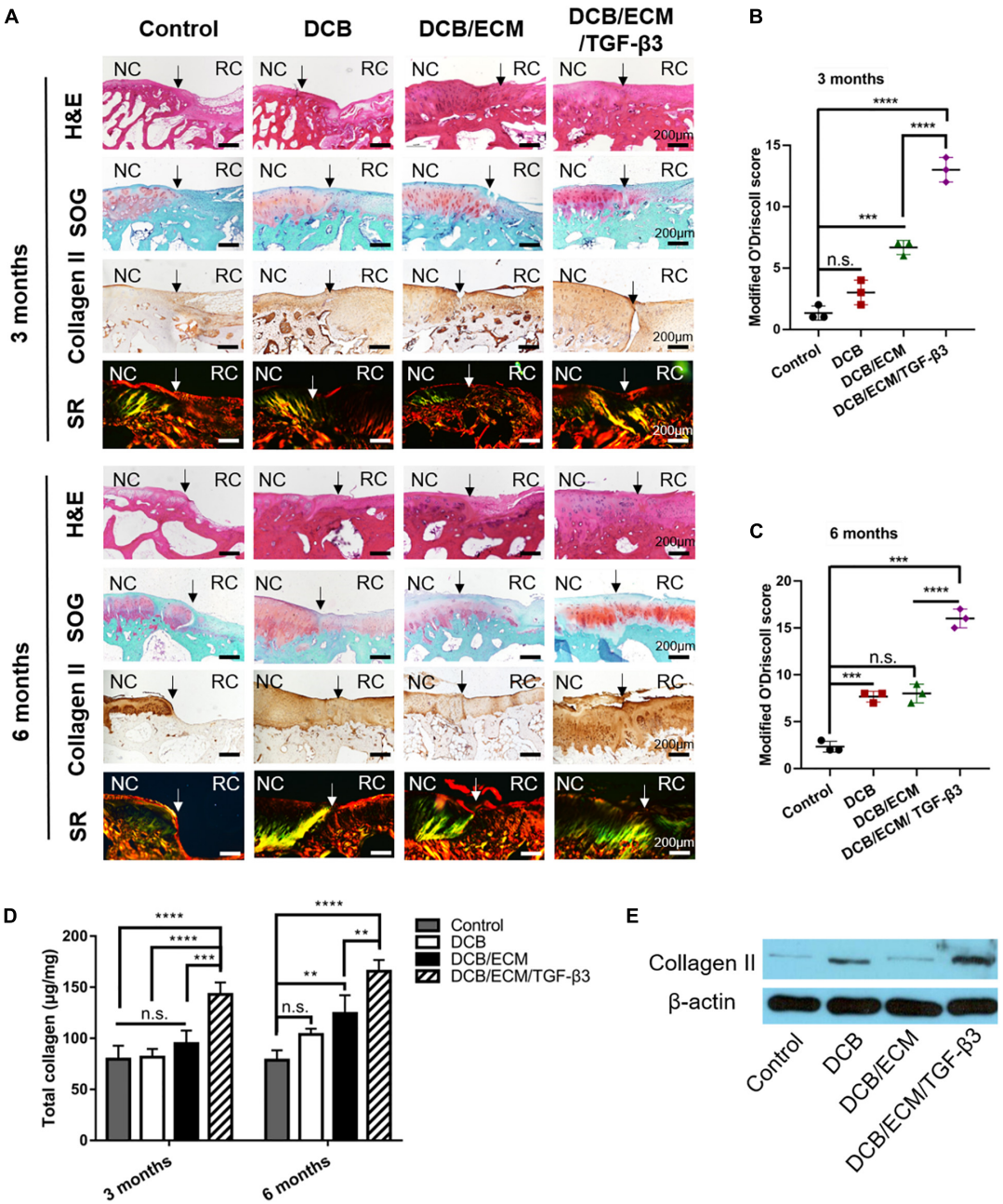

FIGURE 7 | Histological and biochemical evaluation of repaired tissue. **(A)** Representative H&E, safranin O/fast green (SOG), collagen II and picrosirius red (SR) staining of repaired knees at 3 and 6 months (n = 6 knees). Staining was repeated twice or more independently. Modified O'Driscoll scoring for cartilage evaluation at 3 months **(B)** and 6 months **(C)** (n = 3 knees). **(D)** Total collagen contents of repaired knees at 3 and 6 months (n = 3 knees). **(E)** WB analysis of collagen II in repaired tissues at 6 months. NC, normal cartilage; RC, regenerated cartilage. Data are means ± SDs (**$p < 0.01$, ***$p < 0.005$, ****$p < 0.001$, n.s. represents no significant difference).

repaired tissue filled in the cartilage defect area, but these tissues were not properly integrated with adjacent cartilage. The deposition of proteoglycan and collagen II was also limited in this group. In contrast, the repaired tissue merged with the surrounding cartilage in DCB/ECM/TGF-β3 with abundant cartilaginous extracellular matrix deposition, which was strongly stained by an anti-collagen II antibody.

At 6 months, the defect area of the control group was not fully filled, and the repaired tissues were more likely fibrous tissue with poor proteoglycan content (**Figure 7A**). Compared to that at 3 months, the DCB and DCB/ECM groups produced more proteoglycan deposition and enhanced positive type II collagen on the surface of the defective joint. Indeed, the regenerated tissue in the DCB/ECM/TGF-β3 group presented with more type II

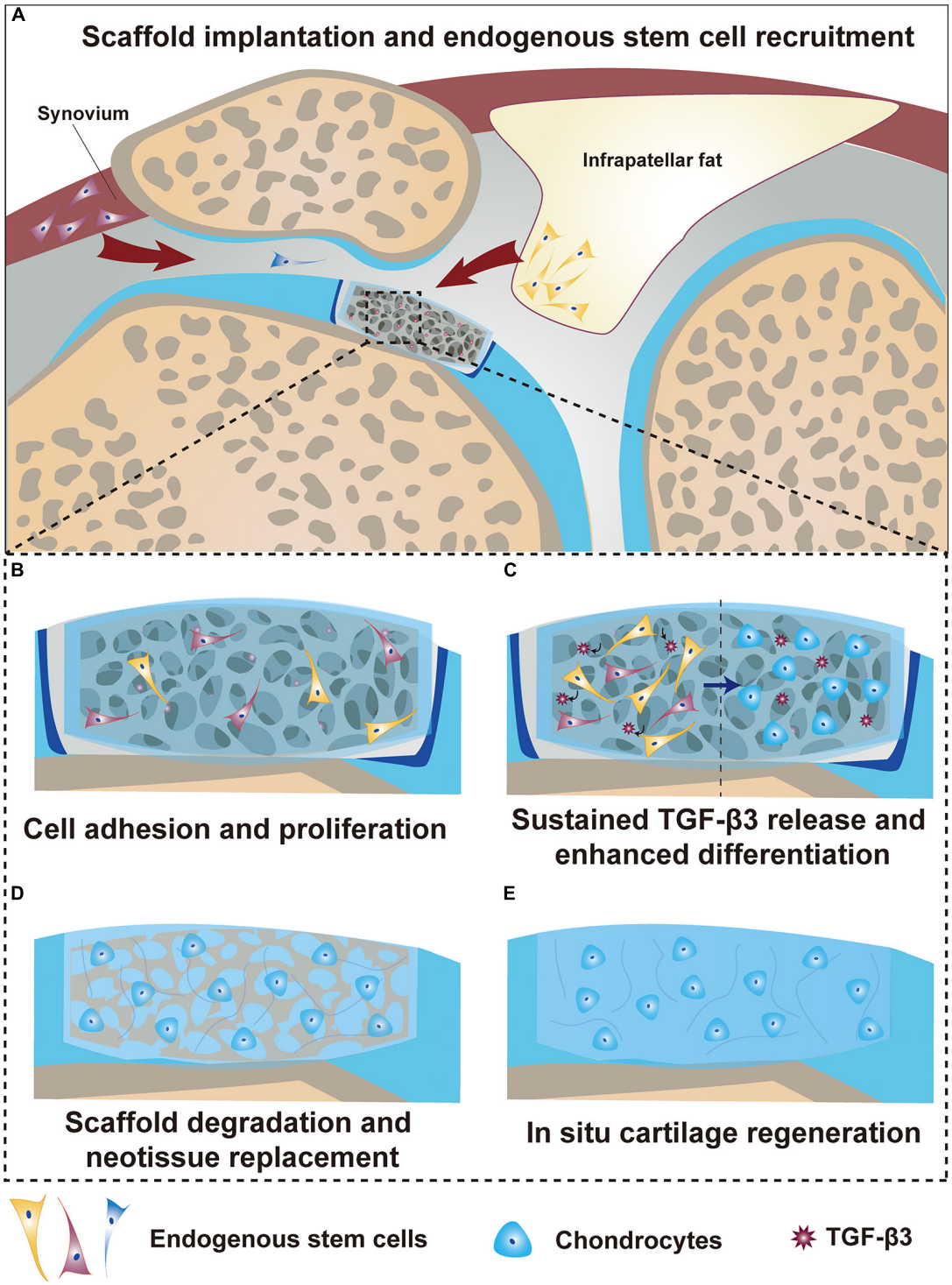

FIGURE 8 | Summarized schematic of the mechanism of *in situ* cartilage regeneration. **(A)** Scaffold implantation and endogenous stem cell recruitment. **(B)** Stem cell adhesion and proliferation. **(C)** Sustained TGF-β3 release and enhanced stem cell differentiation. **(D)** Scaffold degradation and neotissue replacement. **(E)** *In situ* articular cartilage regeneration.

collagen-enriched hyaline cartilaginous tissue retaining similarity to native cartilage. In addition, the deposition and organization of type II collagen in the defective site of each group were also assessed by Sirius red staining. The regenerated tissue in the DCB/ECM/TGF-β3 group showed higher collagen II expression, whereas other groups (control, DCB and DCB/ECM) tended to

exhibit lower collagen II expression. Moreover, more organized collagen fibers were observed in the DCB/ECM/TGF-β3 group, presenting a more oriented pattern similar to hyaline cartilage.

After 3 and 6 months of treatment, a trend toward an elevated modified O'Driscoll score was noted in the DCB/ECM/TGF-β3 group (13 ± 1 at 3 months and 16 ± 1 at 6 months) compared to the other three treatment groups (control: 1.33 ± 0.58 at 3 months and 2.33 ± 0.58 at 6 months; DCB: 3 ± 1 at 3 months and 7.67 ± 0.58 at 6 months; DCB/ECM: 6.67 ± 0.58 at 3 months and 8 ± 1 at 6 months), particularly in the control group and DCB group (**Figures 7B,C**).

DISCUSSION AND CONCLUSION

Recent advances in methods and materials have led to the development of suitable constructs for the clinical repair of injured cartilage (Cheng et al., 2019). However, the complex and multiple functions and limited self-healing capacity of native cartilage still hamper successful reconstruction of adult cartilage tissue restoration (Huey et al., 2012). Recently, *in situ* tissue engineering approaches that rely on recruiting endogenous cells to damaged sites avoid many drawbacks based on cell-seeded scaffolds and have offered great promise for *in situ* cartilage regeneration (Lee et al., 2010; Shi et al., 2017; Yang et al., 2020). To more effectively utilize the host's own regenerative potential, a biofunctionalized scaffold with interconnecting and complex microchannels can serve as a platform for endogenous cell immobilization, infiltration and chondrogenesis (Lee et al., 2010). Lee et al. (2010) reported that TGF-β3-loaded 3D printed PCL/collagen composite scaffolds successfully regenerated the entire synovial articular cartilage surface of rabbits through host cell homing, diffusion, histogenesis, and angiogenesis. Another study conducted by Sun et al. (2018) proved that the cell-free scaffolding system DCM-RAD/SKP, which was produced by the integration of decellularized cartilage matrix (DCM) scaffold and self-assembly Ac-(RADA)4-CONH2/Ac-(RADA)4GGSKPPGTSS-CONH2 (RAD/SKP) peptide nanofiber hydrogel, enhanced bone marrow-derived cell recruitment when combined with microfracture, thus facilitating articular cartilage regeneration.

Endogenous joint-resident cells play a critical role in joint pathophysiology, especially in cartilage injury (Yang et al., 2020). After cartilage damage, activated stem cells migrate and exert reparative effects via biochemical signals and finally differentiate into specialized cell types (Im, 2016; McGonagle et al., 2017). Notably, various subpopulations of endogenous stem/progenitor cells are critical for cartilage homeostasis and repair but may possess different potentials for chondrogenesis (Yang et al., 2020). Evidently, intraarticular fat pad-derived stem cells and synovium-derived MSCs were proven to be potent cell source reservoirs that contribute to chondrogenic differentiation and are less likely to lead to chondrocyte hypertrophy (Chen et al., 2015; Hindle et al., 2017). Therefore, it is necessary to introduce a bioactive factor to effectively recruit these cells to the injury site. However, rapid and uncontrolled release of GFs from biofunctionalized scaffolds at damage sites is probably unable to recruit a sufficient number of stem cells and has some unwanted side effects (Patel et al., 2019). This motivates tissue engineering researchers and clinicians to develop a multifunctional scaffold that can effectively carry and deliver GFs for sustained release. In this study, we aimed to test the reparative effects of a TGF-β3-loaded scaffold that combines articular cartilage ECM and DCB in cartilage regeneration. The results of the biochemical assays of residual DNA, total collagen and GAG (**Supplementary Figures 2–4**) and the histological and immunohistochemical staining (**Supplementary Figure 5**) indicated that the DCB/ECM scaffold showed a bionic structure and ingredients of native cartilage. In addition, *in vitro* cell migration experiments confirmed that TGF-β3- and TGF-β3-loaded scaffolds can facilitate IPFSC mobilization, which is in line with the results of previous studies (Lee et al., 2010) (**Figure 3A** and **Supplementary Figure 9**). The DCB/ECM scaffold showed a higher percentage water absorption (**Supplementary Figure 1**) and better surface hydrophilicity than the DCB scaffold (**Supplementary Figure 6**), and provided an optimal porous microenvironment for cell proliferation, infiltration and ECM production (**Figures 4D,E** and **Supplementary Figures 7**, **8**). Moreover, *in vitro* and *in vivo* and chondrogenic experiments showed that the TGF-β3-loaded DCB/ECM scaffold exhibited superior chondrogenic capacity than the other scaffold without TGF-β3 (DCB scaffold and DCB/ECM scaffold) (**Figures 3C–F**, 5B).

An important point regarding the *in situ* tissue engineering strategies for cartilage regeneration involves a functional scaffold that can serve as a temporary "home" to (i) provide appropriate 3D structural and biomechanical support, (ii) facilitate resident stem cell migration, infiltration and proliferation, and (iii) initiate chondrogenic differentiation and stimulate ideal matrix deposition for functional cartilage regeneration. The natural microenvironment of the cartilaginous ECM plays an essential role in instructing cell fate, mainly owing to its microstructures and bioactive contents (Sun et al., 2018; Kim et al., 2019). Hence, cartilage ECM-based materials can act as a more suitable microenvironment to better mimic natural cell-ECM interactions and further improve cartilage repair outcomes. Previous studies have shown that DCBs contain a natural 3D porous structure and exert excellent biocompatibility and promising mechanical properties, thus ideally combining with the cartilage ECM to spontaneously mimic the 3D microenvironment and provide biomechanical support (Yuan et al., 2016; Kim et al., 2019). In our study, both SEM, live/dead and DAPI/phalloidin staining confirmed that DCBs and DCB/ECM possess proper microstructure and biocompatibility (**Figures 4D,E** and **Supplementary Figure 8**). The introduced GF TGF-β3 has been shown to be capable of recruiting approximately 130% more endogenous stem cells to cartilage regenerated sites (Lee et al., 2010). However, bolus injection of GFs tends to induce rapid diffusion and inflammatory side effects. When absorbed and released from the DCB/ECM delivery platform, *in vitro* release experiments demonstrated prolonged release profiles (**Figure 4B**) and could also significantly modulate and facilitate IPFSC mobilization (**Figure 2A** and **Supplementary Figure 9**). Considering the above, the DCM/ECM scaffold acts as a biofunctional "home" for

stem cell resistance and delivery of bioactive factors that improve cell recruitment and chondrogenesis.

To validate the biodegradability and chondrogenic effects of the biofunction-composited scaffold, *in vivo* degradability and chondrogenic experiments were performed (**Figure 3**). After 1, 2, and 4 weeks of *in vivo* implantation, we harvested and captured the *in situ* degradation and repair performance of each group and demonstrated that DCB/ECM/TGF-β3 had excellent biodegradability to orchestrate neotissue ingrowth (**Figure 3B**). Next, we demonstrated that the TGF-β3-loaded DCB/ECM scaffold exhibited more chondrogenic-related gene expression than the scaffold without additional GFs. Significantly, in the DCB/ECM/TGF-β3 group, more collagen II, ACAN and SOX9 expression at all time points was demonstrated (**Figures 3C–F**). Additionally, collagen I expression in the control group was highest at 1 and 2 weeks after implantation, which means that the repaired tissue was more fibrous-like. These results suggest that the GF-functionalized DCM/ECM scaffold possesses favorable biodegradability and provides a suitable and inductive host microenvironment for chondrogenesis of migrated cells. On the basis of our cartilage layer defect animal model, the recruited MSCs might be mainly derived from intraarticular fat pats, synovial tissue, synovial fluid, or even the vascular system. However, the lack of evidence from *in vivo* recruitment experiments and limited knowledge of cell markers hampered our understanding of certain participants; thus, further studies need to be conducted to understand the subpopulations of these cells in cartilage regeneration.

In terms of *in vivo* cartilage repair studies, DCB, DCM/ECM, and DCB/ECM/TGF-β3 scaffolds can promote cartilage repair to different extents. Histomorphometry (**Figure 7**), radiographic (**Figures 6C–E**), and biomechanical assessment (**Figure 6F**) analyses confirmed that the DCB/ECM/TGF-β3 scaffold showed superior repair results in terms of histological structure, biochemical contents, biomechanical performance and subchondral bone reconstruction. Although neocartilage could be observed in the control groups, it was quite inferior to that in the TGF-β3-loaded group. This may be because the natural composite scaffold could only provide structural support but was not inductive enough for cell infiltration and chondrogenesis.

We proposed a possible mechanism of cartilage regeneration based on the findings of the present study (**Figure 8**). First, when a biofunctionalized scaffold was implanted into the cartilage defect, the fast released TGF-β3 acted as a signaling molecule to recruit resident stem cells within the joint to infiltrate into the scaffold (**Figure 8A**). Then, various adhesion proteins, GFs and the hydrophilic surface of this composite decellularized constructure enabled cells to adhere and proliferate well around every corner within the scaffold and interface (**Figure 8B**). Additionally, the prolonged release of TGF-β3 cooperated with biomechanical stimuli to induce chondrogenic differentiation of recruited and proliferated cells in the targeted space (**Figure 8C**). Finally, scaffold degradation was orchestrated with neotissue replacement and achieved optimal remodeling, mutation and regeneration of the cartilage (**Figures 8D,E**).

We must admit that there are some limitations to this study. First, the *in vitro* release of TGF-β3 lasted for only 6 weeks, which falls short of the *in vivo* repair requirement. On the other hand, investigations of this DCB/ECM/TGF-β3 scaffold in larger animals at a longer time point may be more clinically relevant. Although this study presents promising results in cartilage regeneration, there still remains a significant challenge for clinical translation. Briefly, our study provides a potential scaffolding system with many advantages for one-step surgical implantation such as availability, low immunogenicity and biodegradability. Therefore, our scaffolds and related regeneration strategies may not only provide new curative options for articular cartilage regeneration but also avoid laborious effort in contrast to *in vitro* cell culture prior to *in vivo* implantation.

In conclusion, the present study developed a staged regeneration strategy that combines endogenous cell recruitment and pro-chondrogenesis approaches for *in situ* articular cartilage regeneration. As a proof of concept, we created a 3D hybrid DCB/ECM/TGF-β3 scaffold with biomimetic microarchitecture and bioactivity through a combination of dual-functional TGF-β3 enhancing reparative cell recruitment and chondrogenic differentiation and a DCB/ECM scaffold with biomimetic microarchitecture facilitating reparative cell settlement and proliferation. The biofunctionalized scaffold has been proven to recruit IPFSCs *in vitro* and support the cell settlement and chondrogenic differentiation of migratory cells. Our *in vivo* analysis also demonstrated that the functional scaffold could promote superior cartilage regeneration and subchondral bone protection in a rabbit full-thickness cartilage defect model. In conclusion, with the help of controlled and prolonged drug delivery, this staged regeneration strategy, which leverages the body's innate regenerative potential, holds great promise for clinically effective *in situ* articular cartilage regeneration.

DATA AVAILABILITY STATEMENT

The raw data supporting the conclusions of this article will be made available by the authors, without undue reservation.

ETHICS STATEMENT

The animal study was reviewed and approved by Institutional Animal Care and Use Committee at PLA General Hospital.

AUTHOR CONTRIBUTIONS

ZY: writing original draft, investigation, data curation, formal analysis, and visualization. HL: investigation and data curation. YT: investigation and visualization. LF: data curation and formal analysis. CG: data curation. TZ: formal analysis. FC: methodology. ZL: software. ZY: conceptualization and supervision. SL: supervision and project administration. QG: supervision. All authors contributed to the article and approved the submitted version.

FUNDING

This work was supported by the National Key R&D Program of China (2019YFA0110600) and the National Natural Science Foundation of China (81772319).

SUPPLEMENTARY MATERIAL

The Supplementary Material for this article can be found online at: https://www.frontiersin.org/articles/10.3389/fcell.2021.655440/full#supplementary-material

REFERENCES

Barry, F., and Murphy, M. (2013). Mesenchymal stem cells in joint disease and repair. *Nat. Rev. Rheumatol.* 9, 584–594. doi: 10.1038/nrrheum.2013.109

Chen, C.a, Huang, K., Zhu, J., Bi, Y., Wang, L., Jiang, J., et al. (2020). A novel elastic and controlled-release poly (ether-ester-urethane) urea scaffold for cartilage regeneration. *J. Mater. Chem. B* 8, 4106–4121. doi: 10.1039/c9tb02754h

Chen, S., Fu, P., Cong, R., Wu, H., and Pei, M. (2015). Strategies to minimize hypertrophy in cartilage engineering and regeneration. *Genes Dis.* 2, 76–95. doi: 10.1016/j.gendis.2014.12.003

Chen, Y., Wu, T., Huang, S., Suen, C.-W. W., Cheng, X., Li, J., et al. (2019a). Sustained release SDF-1α/TGF-β1-loaded silk fibroin-porous gelatin scaffold promotes cartilage repair. *ACS Appl. Mater. Interfaces* 11, 14608–14618. doi: 10.1021/acsami.9b01532

Chen, Y.-R., Zhou, Z.-X., Zhang, J.-Y., Yuan, F.-Z., Xu, B.-B., Guan, J., et al. (2019b). Low-molecular-weight heparin-functionalized chitosan-chondroitin sulfate hydrogels for controlled release of TGF-β3 and in vitro neocartilage formation. *Front. Chem.* 7:745. doi: 10.3389/fchem.2019.00745

Cheng, A., Schwartz, Z., Kahn, A., Li, X., Shao, Z., Sun, M., et al. (2019). Advances in porous scaffold design for bone and cartilage tissue engineering and regeneration. *Tissue Eng. Part B Rev.* 25, 14–29. doi: 10.1089/ten.teb.2018.0119

Deng, Y., Sun, A. X., Overholt, K. J., Gary, Z. Y., Fritch, M. R., Alexander, P. G., et al. (2019). Enhancing chondrogenesis and mechanical strength retention in physiologically relevant hydrogels with incorporation of hyaluronic acid and direct loading of TGF-β. *Acta Biomater.* 83, 167–176. doi: 10.1016/j.actbio.2018.11.022

Fan, H., Zhang, C., Li, J., Bi, L., Qin, L., Wu, H., et al. (2008). Gelatin microspheres containing TGF-β3 enhance the chondrogenesis of mesenchymal stem cells in modified pellet culture. *Biomacromolecules* 9, 927–934. doi: 10.1021/bm7013203

Feng, B., Ji, T., Wang, X., Fu, W., Ye, L., Zhang, H., et al. (2020). Engineering cartilage tissue based on cartilage-derived extracellular matrix cECM/PCL hybrid nanofibrous scaffold. *Mater. Des.* 193:108773. doi: 10.1016/j.matdes.2020.108773

Gaharwar, A. K., Singh, I., and Khademhosseini, A. (2020). Engineered biomaterials for in situ tissue regeneration. *Nat. Rev. Mater.* 5, 686–705. doi: 10.1038/s41578-020-0209-x

Gao, J., Yan, X.-L., Li, R., Liu, Y., He, W., Sun, S., et al. (2010). Characterization of OP9 as authentic mesenchymal stem cell line. *J. Genet. Genomics* 37, 475–482. doi: 10.1016/s1673-8527(09)60067-9

Hakamivala, A., Robinson, K., Huang, Y., Yu, S., Yuan, B., Borrelli, J. Jr., et al. (2020). Recruitment of endogenous progenitor cells by erythropoietin loaded particles for in situ cartilage regeneration. *Bioact. Mater.* 5, 142–152. doi: 10.1016/j.bioactmat.2020.01.007

Hangody, L., and Füles, P. (2003). Autologous osteochondral mosaicplasty for the treatment of full-thickness defects of weight-bearing joints: ten years of experimental and clinical experience. *J. Bone Joint Surg. Am.* 85, 25–32. doi: 10.2106/00004623-200300002-00004

Hindle, P., Khan, N., Biant, L., and Péault, B. (2017). The infrapatellar fat pad as a source of perivascular stem cells with increased chondrogenic potential for regenerative medicine. *Stem Cells Transl. Med.* 6, 77–87. doi: 10.5966/sctm.2016-0040

Huang, H., Hu, X., Zhang, X., Duan, X., Zhang, J., Fu, X., et al. (2018). Codelivery of synovium-derived mesenchymal stem cells and TGF-β by a hybrid scaffold for cartilage regeneration. *ACS Biomater. Sci. Eng.* 5, 805–816. doi: 10.1021/acsbiomaterials.8b00483

Huey, D. J., Hu, J. C., and Athanasiou, K. A. (2012). Unlike bone, cartilage regeneration remains elusive. *Science* 338, 917–921. doi: 10.1126/science.1222454

Im, G.-I. (2016). Endogenous cartilage repair by recruitment of stem cells. *Tissue Eng. Part B Rev.* 22, 160–171. doi: 10.1089/ten.teb.2015.0438

Kim, Y. S., Majid, M., Melchiorri, A. J., and Mikos, A. G. (2019). Applications of decellularized extracellular matrix in bone and cartilage tissue engineering. *Bioeng. Transl. Med.* 4, 83–95. doi: 10.1002/btm2.10110

Lee, C. H., Cook, J. L., Mendelson, A., Moioli, E. K., Yao, H., and Mao, J. J. (2010). Regeneration of the articular surface of the rabbit synovial joint by cell homing: a proof of concept study. *Lancet* 376, 440–448. doi: 10.1016/s0140-6736(10)60668-x

Li, X., Guo, W., Zha, K., Jing, X., Wang, M., Zhang, Y., et al. (2019). Enrichment of CD146+ adipose-derived stem cells in combination with articular cartilage extracellular matrix scaffold promotes cartilage regeneration. *Theranostics* 9, 5105–5121. doi: 10.7150/thno.33904

Makhijani, N. S., Bischoff, D. S., and Yamaguchi, D. T. (2005). Regulation of proliferation and migration in retinoic acid treated C3H10T1/2 cells by TGF−β isoforms. *J. Cell. Physiol.* 202, 304–313. doi: 10.1002/jcp.20128

McGonagle, D., Baboolal, T. G., and Jones, E. (2017). Native joint-resident mesenchymal stem cells for cartilage repair in osteoarthritis. *Nat. Rev. Rheumatol.* 13, 719–730. doi: 10.1038/nrrheum.2017.182

Min, B.-H., Lee, H. J., Kim, Y. J., and Choi, B. H. (2016). Repair of partial thickness cartilage defects using cartilage extracellular matrix membrane-based chondrocyte delivery system in human Ex Vivo model. *Tissue Eng. Regenerative Med.* 13, 182–190. doi: 10.1007/s13770-016-9043-z

Nie, X., Chuah, Y. J., Zhu, W., He, P., Peck, Y., and Wang, D.-A. (2020). Decellularized tissue engineered hyaline cartilage graft for articular cartilage repair. *Biomaterials* 235:119821. doi: 10.1016/j.biomaterials.2020.119821

Patel, J. M., Saleh, K. S., Burdick, J. A., and Mauck, R. L. (2019). Bioactive factors for cartilage repair and regeneration: improving delivery, retention, and activity. *Acta Biomater.* 93, 222–238. doi: 10.1016/j.actbio.2019.01.061

Qiao, Z., Lian, M., Han, Y., Sun, B., Zhang, X., Jiang, W., et al. (2020). Bioinspired stratified electrowritten fiber-reinforced hydrogel constructs with layer-specific induction capacity for functional osteochondral regeneration. *Biomaterials* 266:120385. doi: 10.1016/j.biomaterials.2020.120385

Qu, D., Zhu, J. P., Childs, H. R., and Lu, H. H. (2019). Nanofiber-based transforming growth factor-β3 release induces fibrochondrogenic differentiation of stem cells. *Acta Biomater.* 93, 111–122. doi: 10.1016/j.actbio.2019.03.019

Richter, D. L., Schenck, R. C. Jr., Wascher, D. C., and Treme, G. (2016). Knee articular cartilage repair and restoration techniques: a review of the literature. *Sports Health* 8, 153–160. doi: 10.1177/1941738115611350

Shi, W., Sun, M., Hu, X., Ren, B., Cheng, J., Li, C., et al. (2017). Structurally and functionally optimized silk-fibroin–gelatin scaffold using 3D printing to repair cartilage injury in vitro and in vivo. *Adv. Materials* 29:1701089. doi: 10.1002/adma.201701089

Simon, T. M., and Jackson, D. W. (2018). Articular cartilage: injury pathways and treatment options. *Sports Med. Arthrosc. Rev.* 26, 31–39. doi: 10.1097/jsa.0000000000000182

Sophia Fox, A. J., Bedi, A., and Rodeo, S. A. (2009). The basic science of articular cartilage: structure, composition, and function. *Sports Health* 1, 461–468. doi: 10.1177/1941738109350438

Steadman, J. R., Briggs, K. K., Rodrigo, J. J., Kocher, M. S., Gill, T. J., and Rodkey, W. G. (2003). Outcomes of microfracture for traumatic chondral defects of the knee: average 11-year follow-up. *Arthroscopy* 19, 477–484. doi: 10.1053/jars.2003.50112

Sun, X., Yin, H., Wang, Y., Lu, J., Shen, X., Lu, C., et al. (2018). In situ articular cartilage regeneration through endogenous reparative cell homing

using a functional bone marrow-specific scaffolding system. *ACS Appl. Mater. Interfaces* 10, 38715–38728. doi: 10.1021/acsami.8b11687

Sutherland, A. J., Converse, G. L., Hopkins, R. A., and Detamore, M. S. (2015). The bioactivity of cartilage extracellular matrix in articular cartilage regeneration. *Adv. Healthc. Mater.* 4, 29–39. doi: 10.1002/adhm.201400165

Wang, Z., Han, L., Sun, T., Ma, J., Sun, S., Ma, L., et al. (2020). Extracellular matrix derived from allogenic decellularized bone marrow mesenchymal stem cell sheets for the reconstruction of osteochondral defects in rabbits. *Acta Biomater.* 118, 54–68. doi: 10.1016/j.actbio.2020.10.022

Yan, W., Xu, X., Xu, Q., Sun, Z., Lv, Z., Wu, R., et al. (2020). An injectable hydrogel scaffold with kartogenin-encapsulated nanoparticles for porcine cartilage regeneration: a 12-month follow-up study. *Am. J. Sports Med.* 48, 3233–3244. doi: 10.1177/0363546520957346

Yang, Q., Teng, B.-H., Wang, L.-N., Li, K., Xu, C., Ma, X.-L., et al. (2017). Silk fibroin/cartilage extracellular matrix scaffolds with sequential delivery of TGF-β3 for chondrogenic differentiation of adipose-derived stem cells. *Int. J. Nanomed.* 12, 6721–6733. doi: 10.2147/ijn.s141888

Yang, Z., Li, H., Yuan, Z., Fu, L., Jiang, S., Gao, C., et al. (2020). Endogenous cell recruitment strategy for articular cartilage regeneration. *Acta Biomater.* 114, 31–52. doi: 10.1016/j.actbio.2020.07.008

Yuan, Z., Liu, S., Hao, C., Guo, W., Gao, S., Wang, M., et al. (2016). AMECM/DCB scaffold prompts successful total meniscus reconstruction in a rabbit total meniscectomy model. *Biomaterials* 111, 13–26. doi: 10.1016/j.biomaterials.2016.09.017

Zhang, Z.-Z., Jiang, D., Wang, S.-J., Qi, Y.-S., Zhang, J.-Y., and Yu, J.-K. (2015). Potential of centrifugal seeding method in improving cells distribution and proliferation on demineralized cancellous bone scaffolds for tissue-engineered meniscus. *ACS Appl. Mater. Interfaces* 7, 15294–15302. doi: 10.1021/acsami.5b03129

Zhong, Y.-C., Wang, S.-C., Han, Y.-H., and Wen, Y. (2020). Recent advance in source, property, differentiation, and applications of infrapatellar fat pad adipose-derived stem cells. *Stem Cells Int.* 2020:2560174.

Conflict of Interest: The authors declare that the research was conducted in the absence of any commercial or financial relationships that could be construed as a potential conflict of interest.

frontiers in Cell and Developmental Biology

ORIGINAL RESEARCH
published: 01 April 2021
doi: 10.3389/fcell.2021.656153

BMSC-Derived Small Extracellular Vesicles Induce Cartilage Reconstruction of Temporomandibular Joint Osteoarthritis *via* Autotaxin–YAP Signaling Axis

*Yingnan Wang†, Miaomiao Zhao†, Wen Li, Yuzhi Yang, Zhenliang Zhang, Ruijie Ma and Mengjie Wu**

The Affiliated Hospital of Stomatology, School of Stomatology, Zhejiang University School of Medicine, Key Laboratory of Oral Biomedical Research of Zhejiang Province, Hangzhou, China

OPEN ACCESS

Edited by:
Zhenxing Shao, Peking University Third Hospital, China

Reviewed by:
Wei Seong Toh, National University of Singapore, Singapore
Xiaoqing Hu, Peking University Third Hospital, China

***Correspondence:**
Mengjie Wu
wumengjie@zju.edu.cn

† These authors have contributed equally to this work

Specialty section:
This article was submitted to Stem Cell Research, a section of the journal Frontiers in Cell and Developmental Biology

Received: *20 January 2021*
Accepted: *03 March 2021*
Published: *01 April 2021*

Citation:
Wang Y, Zhao M, Li W, Yang Y, Zhang Z, Ma R and Wu M (2021) BMSC-Derived Small Extracellular Vesicles Induce Cartilage Reconstruction of Temporomandibular Joint Osteoarthritis via Autotaxin–YAP Signaling Axis. Front. Cell Dev. Biol. 9:656153. doi: 10.3389/fcell.2021.656153

Background: Temporomandibular joint osteoarthritis (TMJOA) seriously affects the health of patients, and the current treatments are invasive and only used for advanced cases. Bone marrow mesenchymal stem cell (BMSC)-derived small extracellular vesicles (BMSC-sEVs) may represent a safer and more effective treatment, but their role in TMJOA has not been elucidated. This study attempted to analyze the cartilage reconstruction effect of BMSC-sEVs on TMJOA and the mechanism underlying this effect.

Methods: BMSC-sEVs were isolated and purified by microfiltration and ultrafiltration and were subsequently characterized by nanoparticle tracking analysis, electron microscopy, and immunoblotting. TMJOA models were established *in vivo* and *in vitro*, and hematoxylin–eosin staining, immunohistochemistry, and histological scoring were performed to analyze the histological changes in TMJOA cartilage tissues treated with BMSC-sEVs. The proliferation, migratory capacity, and cell cycle distribution of TMJOA cartilage cells treated with BMSC-sEVs were detected. Furthermore, the related mechanisms were studied by bioinformatic analysis, immunoblotting, and quantitative PCR, and they were further analyzed by knockdown and inhibitor techniques.

Results: The acquisition and identification of BMSC-sEVs were efficient and satisfactory. Compared with the osteoarthritis (OA) group, the condylar tissue of the OA group treated with BMSC-sEV (OA^{sEV}) showed an increase in cartilage lacuna and hypertrophic cartilage cells in the deep area of the bone under the cartilage. Significantly upregulated expression of proliferating cell nuclear antigen and cartilage-forming factors and downregulated expression of cartilage inflammation-related factors in OA^{sEV} were observed. In addition, we found higher rates of cell proliferation and migratory activity and alleviated G1 stagnation of the cell cycle of OA^{sEV}. Autotaxin was found in the

BMSC-sEVs, and key factors of the Hippo pathway, Yes-associated protein (YAP), phosphorylated Yes-associated protein (p-YAP), etc. were upregulated in the OA^{sEV} group. Treatment with BMSC-sEVs after autotaxin knockdown or inhibition no longer resulted in expression changes in cartilage-forming and inflammation-related factors and key factors of the Hippo pathway.

Conclusions: These results suggest that the autotaxin–YAP signaling axis plays an important role in the mechanism by which BMSC-sEVs promote cartilage reconstruction in TMJOA, which may provide guidance regarding their therapeutic applications as early and minimally invasive therapies for TMJOA, and provide insight into the internal mechanisms of TMJOA.

Keywords: temporomandibular joint osteoarthritis (TMJ-OA), bone marrow mesenchymal stem cell (bMSC), autotaxin (ATX), hippo signaling pathway, cartilage reconstruction, small extracellular vesicles (sEVs), yes-associated protein (YAP)

BACKGROUND

Temporomandibular joint osteoarthritis (TMJOA) is when the temporomandibular joint disorder (TMD) progresses to a condition marked by severe histological damage, with early signs of hard tissue changes such as cartilage absorption on the surface of the joint, osteophyte formation, shifting or perforation of the joint disc, and even facial asymmetry or mandibular retrognathism (Kim et al., 2019). The current treatment methods for TMJOA are mostly focused on treating advanced stages of the condition by applying invasive treatments, so how to achieve early and minimally invasive treatment for TMJOA needs to be addressed. In recent years, treatments such as tissue engineering therapy, immunology, and gene therapy have emerged (Abouelhuda et al., 2018; Wu et al., 2021). These biotherapies are a good attempt, but their efficacy needs to be further explored, and their mechanisms of action are not yet clear.

Currently, novel treatments for TMJOA are mostly focused on the application of cells, such as mesenchymal stem cells (MSCs), which can reduce cell apoptosis and participate in immune regulation. This approach has become a new potential treatment for joint defects and osteoarthritis (OA)-related damage. Among them, bone marrow MSCs (BMSCs) play an important role in the repair of OA and bone fractures. Compared with extraskeletal MSCs, BMSCs are superior in phenotype, morphology, function, and potential therapeutic applications (García-García et al., 2015). It has been found that BMSCs implanted in TMJOA inhibit cartilage degradation and repair diseased tissues (Chen et al., 2013; Lu et al., 2015). Thus, BMSCs have a therapeutic effect on TMJOA and can promote the reconstruction of the cartilage. However, there are some limitations to the treatment of TMJOA with MSCs, such as unevenness and a tumorous tendency, and it is reported that MSCs exert their effects mainly through secretion function (Yu et al., 2014). Given all these, more stable and reliable methods to treat TMJOA with MSCs are necessary.

Extracellular vesicle (EV) is a kind of vesicle secreted by all cell types, with diameters of approximately 50–1,000 nm that contain and transport functional contents. Among them, vesicles with diameters of roughly 50–100 nm are defined as small extracellular vesicles (sEVs), frequently classified as "exosomes," "microvesicles," etc. (Théry et al., 2018). They are considered to be important regulatory factors for intercellular communication and are involved in multiple pathological processes (Wang et al., 2018). Considering their small size, good targeting, satisfactory stability, and capability of crossing barriers, avoiding degradation and transporting their cargos into the cytoplasm, sEVs have become a new treatment approach to many kinds of diseases. Although it is known that MSC-derived sEVs (MSC-sEVs) exert many therapeutic applications (Witwer et al., 2019), the role of BMSC-sEVs in TMJOA has been rarely reported, which still remains unclear.

Therefore, the purpose of this study was to explore the role and molecular mechanism of BMSC-sEVs in enhancing cartilage reconstruction in TMJOA and to provide theoretical support for the clinical applications and further mechanistic interpretations of MSC-derived sEV therapy for TMJOA in the future.

MATERIALS AND METHODS

Cell Culture

Human BMSCs were kindly provided by the Stem Cell Bank, Chinese Academy of Sciences, harvested from healthy people and cultured in Dulbecco's minimum essential medium (DMEM; BasalMedia, China). Mandibular condylar chondrocytes (MCCs) were extracted from the condyles of the temporomandibular joints (TMJs) of New Zealand rabbits and cultured in DMEM. All media were supplemented with 10% fetal bovine serum (FBS, Yeasen, China) and 1% penicillin-streptomycin (BasalMedia, China), and all cells were cultured in a humidified incubator (Thermo Fisher Scientific, United States) with 5% CO_2 at 37°C.

Abbreviations: TMJOA, temporomandibular joint osteoarthritis; BMSC-sEVs, bone marrow mesenchymal stem cell-derived small extracellular vesicles; ATX, autotaxin; YAP, Yes-associated protein; PCNA, proliferating cell nuclear antigen; Col-II/I, type II/I collagen; ACAN, aggrecan; SOX9, SRY-related high-mobility group box 9; MMP13, matrix metalloproteinase 13; RUNX2, RUNX family transcription factor 2; RhoA, ras homolog family member A; IB, immunoblotting; IHC, immunohistochemistry; qPCR, quantitative polymerase chain reaction.

Small Extracellular Vesicle Isolation and Purification

First, sEVs were isolated from the medium supernatant of BMSCs without FBS or penicillin-streptomycin, which was harvested after 48 h of culture. After centrifugation (4,000 rpm, 10 min), the supernatant was sequentially minifilter through polyvinylidene fluoride (PVDF) membrane filters at 450 nm (Merck Millipore, Germany) and then 200 nm (PALL, United States). Then, the flow-through was ultrafiltered by 100-kD centrifugal filter devices (Merck Millipore, Germany). A 15-ml device is usually used, and a 0.5-ml device can be used to further concentrate the sEVs, which can then be harvested by reverse centrifugation. Finally, sEVs isolated from approximately 80-ml medium supernatant were suspended in 1 × phosphate buffer saline (PBS) buffer or culture medium through the use of 0.5-ml centrifugal filter devices (Merck Millipore, Germany) for further experiments.

Nanoparticle Tracking Analysis

For particle size and concentration determination, nanoparticle tracking analysis (NTA) was performed with a NanoSight NS300 (Malvern, United Kingdom) equipped with fast video capture and NTA analytical software. Nanoparticles were illuminated by the laser, and their movements under Brownian motion were captured for 60 s. Videos were analyzed by the software to provide the nanoparticle concentration and size distribution profiles.

Transmission Electron Microscopy

The BMSC-sEV samples were added onto a piece of copper grid for 1 min. Then, a drop of 2% uranyl acetate was added onto the copper grid for 1 min. After drying for 10 min, the cells were examined under a transmission electron microscope (Thermo Fisher Scientific, United States).

Immunoblotting

BMSC-sEVs and cells were lysed with radioimmunoprecipitation assay (RIPA) lysis buffer (Yeasen, China) containing protease inhibitors. The lysates were boiled with Protein SDS-PAGE Loading Buffer (GenScript, China), electrophoresed through 4–20% polyacrylamide gels (GenScript, China) and transferred onto 0.45-μm PVDF membranes (Absin, China). The membranes were blocked using 5% skim milk (Yeasen, China) in PBS. Antibodies against the following proteins were used for immunoblotting (IB) analysis: CD81 (SBI, Japan), CD63 (SBI, Japan), Ras-related protein 5 (Rab5; Biovision, United States), ALG2-interacting protein (Alix; Thermo Fisher Scientific, United States), glucose-regulated protein 94 (GRP94; Thermo Fisher Scientific, United States), aggrecan (ACAN; Bioss, China), SRY-related high-mobility group box 9 (SOX9; Bioss, China), matrix metalloproteinase 13 (MMP13; Bioss, China), RUNX family transcription factor 2 (RUNX2; Bioss, China), Collagen I (Bioss, China), proliferating cell nuclear antigen (PCNA; Proteintech, United States), cartilage-forming factors-type II collagen (Col-II; Novus, United States), Autotaxin (Abcam, China), Yes-associated protein (YAP; Absinthe, China), phosphorylated Yes-associated protein (p-YAP; LifeSpan BioSciences, United States), RhoA (Absinthe, China), large tumor suppressor kinase 1 (LATS1; Absinthe, China), large tumor suppressor kinase 2 (LATS2; Absinthe, China), and glyceraldehyde 3-phosphate dehydrogenase (GAPDH; Proteintech, United States). Horseradish peroxidase (HRP)-conjugated goat anti-rabbit IgG and anti-mouse IgG (Proteintech, United States) were used as secondary antibodies. Detection was performed using Chemiluminescent HRP Substrate (Merck Millipore, Germany), and signals were captured and observed using Molecular Imager® ChemiDoc™ XRS + (Bio-Rad, United States).

Temporomandibular Joint Osteoarthritis Model Establishment

By using chemical method modeling-collagenase injection, a TMJOA animal model was established. The posterior pole of the TMJ condyle can be found behind the outer canthus of 12- to 18-week-old New Zealand rabbits. In its mouth opening position, with left forefinger tip pressing on the area of joint space, the syringe needle held in the right hand was thrust into the joint space inward, forward, and downward, parallel to the infraorbital margin. If the needle entered approximately 0.5 cm and was withdrawn without blood, approximately 0.25 ml of 4 mg/ml collagenase II (Yeasen, China) was injected into the TMJ, and this group was named OA group (the control group was injected with approximately 0.25 ml normal saline). 4 weeks later, the TMJOA rabbit model was identified by morphological evaluation and histological and molecular biological examination. All protocol and procedures employed *in vivo* were ethically reviewed and approved by the Institutional Animal Care and Use Committee at Zhejiang Laboratory Animal Center (Approval No. ZJCLA-IACUC-20050012) for the rational care and use of laboratory animals.

Under sterile conditions, the condyles of 12- to 18-week-old New Zealand rabbits were excised, and surrounding soft tissues were removed. Cartilage tissues on the condyles were separated and cut into 1-mm^3 size; and after rinsing with PBS, 0.25% trypsin was added and treated for 30 min. Then, high-glucose DMEM containing 10% FBS was added to terminate dissociation. After discarding supernatant, 2 ml 0.3% collagenase (Yeasen, China) and 4 ml high-glucose DMEM containing 10% FBS were added and placed in 37°C. After 12 h, the MCCs were collected and cultured in six-well plates. When MCCs grew to 80–90% confluency, 10 ng/ml recombinant human interleukin-1 beta (IL-1β; Novoprotein, China) was added into the MCC medium and cultured in 37°C for 24 h, and then identification of TMJOA cell model, such as expression of OA-related factors, was launched.

Small Extracellular Vesicle Treatment of Temporomandibular Joint Osteoarthritis Model

In vivo, normal and TMJOA model rabbits were randomly assigned into control groups and experimental groups, separately, and there were 6–8 TMJs of rabbits (i.e., 3–4 rabbits) in each group (one rabbit died in the OA group, which means that there were six TMJs of rabbits in that OA group), half male and half female. In the first *in vivo* experiment, the animals

were divided into four groups: control group (rabbits in the former control group treated with PBS), OA group (rabbits in the former OA group treated with PBS), sEV group (rabbits in the former control group treated with sEVs), and OA^{sEV} group (rabbits in the former OA group treated with sEVs). This experiment was launched three times, for 4-week, 6–week, and 8-week observation, separately. In the second *in vivo* experiment, the animals were divided into four groups: OA group (rabbits in the former OA group treated with PBS), OA + sEV group (rabbits in the former OA group treated with sEV), OA + $sEV^{-/-ATX}$ group (rabbits in the former OA group treated with $sEV^{-/-ATX}$), and OA + $sEV^{Ziritaxestat}$ group (rabbits in the former OA group treated with $sEV^{Ziritaxestat}$). This experiment was launched three times, for 4 weeks, 6 weeks, and 8 weeks of observation, separately. In each *in vivo* experiment, approximately 200 μl (4–8) × 10^8 BMSC-sEVs extracted from about 5.5 × 10^7 BMSCs were injected into each TMJ in the experimental groups, once per side *per capita*. *In vitro*, approximately (2–4) × 10^8 BMSC-sEVs aforementioned were used in the experimental groups (the control group was added with normal saline).

Micro-Computed Tomography

Condyle specimens were scanned and analyzed by the high-resolution micro-computed tomography (micro-CT) scanner U-CT-XUHR (Milabs, Netherlands) and Imalytics Preclinical 2.1 software. Scanning parameters were 0.24 μA current, 50 kV voltage, 15-ms exposure time, and 30 deg/s angle speed. Subchondral cancellous bone was defined as the cancellous bone region 0.5 mm beneath the calcified cartilage–bone junction. The cylinder with volume of ($\pi \times 1.5^2 \times 1$) mm^3 was selected for each specimen to calculate the parameters, including bone volume fraction (BVF, BV/TV), bone surface/bone volume ratio (BS/BV), bone mineral density (BMD), trabecular thickness (Tb.Th), and trabecular spacing (Tb.Sp).

Histology and Immunohistochemistry

Hematoxylin–eosin (HE) staining and specific staining for condylar cartilage (such as safranine O/fast green and Alcian blue) were adopted to identify the successful establishment of the TMJOA animal model.

Immunohistochemistry (IHC) for PCNA, Col-I, Col-II, ACAN, SOX9, MMP13, and RUNX2 was adopted to analyze the changes in the cartilage tissue of the condyle in the normal and TMJOA states with or without BMSC-sEV treatment.

Scoring of Histology

The histologic observations of normal and TMJOA animal tissues were scored using the International Cartilage Regeneration & Joint Preservation Society (ICRS) Visual Histological Assessment Scale (**Supplementary Table 1**) and Wakitani Histological Grading Scale (**Supplementary Table 2**). The ICRS Visual Histological Assessment Scale contains six features (surface, matrix, cell distribution, cell population viability, subchondral bone, and cartilage mineralization), scored from 0 to 3, and the Wakitani Histological Grading Scale contains five categories (cell morphology, matrix staining, surface regularity, thickness of cartilage, and integration of donor with host adjacent cartilage), scored from 4 to 0, total maximum 14. Three independent blinded technicians from the Department of Pathology in our hospital were recruited to score, respectively.

Laser Scanning Confocal Microscopy

Stem cell-derived small extracellular vesicles were dyed with Exo-Glow Exosome Labeling Kit (SBI, Japan). Single-stranded RNAs in the sEVs were fluorescently labeled in red by acridine orange (AO). F-actin was stained green with Actin-stain 488 fluorescent phalloidin (Cytoskeleton Inc., United States). Finally, the cell nucleus was stained blue with 4′,6-diamidino-2-phenylindole (DAPI; Thermo Fisher Scientific, United States). Fluorescence images were acquired on a TCS SP2 laser scanning confocal microscope (Leica Microsystems, Germany).

Proliferation Assay

Cell proliferation of the MCCs was determined by the Cell Counting Kit-8 (CCK-8; Yeasen, China). MCCs were seeded in a 96-well plate in triplicate. They were treated with BMSC-sEVs for 24 h. During the next few days, the proliferation of the MCCs was detected at a wavelength of 450 nm, as measured by SpectraMax i3 (Molecular Devices, United States).

Migration Assay

MCCs were cultured at 37°C until they were in the logarithmic phase and then treated with DMEM without FBS containing BMSC-sEVs for 24 h. The medium with the cells was then placed in the top chamber of a Transwell (Corning, United States) inserted into a 24-well plate. DMEM with 10% FBS was added to the bottom chamber, and the cells were cultured for approximately 24 h. Then, the cells that had migrated into the bottom chamber were fixed with 4% paraformaldehyde, dyed with 0.1% crystal violet, and observed by microscopy (Olympus, Japan).

Cell Cycle Distribution Assay

The cell cycle distribution of the MCCs was determined by a Cell Cycle and Apoptosis Analysis Kit (Yeasen, China). Cell sediments were washed with PBS and resuspended in binding buffer. Propidium iodide (PI) was added to the solution and incubated for 15 min at room temperature in the dark. Then, the samples were analyzed by flow cytometry (FCM; CytoFLEX LX, Beckman, United States).

Real-Time Quantitative PCR

Total RNA of the BMSCs and MCCs was extracted by TRIeasy™ Total RNA Extraction Reagent (Yeasen, China) and reverse transcribed into cDNA using Hifair® II 1st Strand cDNA Synthesis SuperMix for qPCR (Yeasen, China) and a Mastercycler instrument (Eppendorf, Germany). All qPCR programs were performed using Hieff UNICON® Power qPCR SYBR Green Master Mix (Yeasen, China) and the CFX384™ Real-Time System (Bio-Rad, United States). mRNA expression was quantified by quantitative PCR (qPCR) using the $2^{-\Delta\Delta CT}$ relative quantitation method, and GAPDH served as the internal control. The primers are listed in **Table 1**.

Knockdown and Inhibition of Autotaxin

To knock down the expression of autotaxin, three gene-specific short interfering RNAs (siRNAs) (**Table 2**) were synthesized (GenePharma, China) and used. The cells were transfected with these siRNAs using Lipofectamine RNAiMAX Transfection Reagent (Thermo Fisher Scientific, United States). After 48 h, the knockdown efficacy was confirmed by qPCR and immunoblotting to quantitate the expression of the genes at both the transcription and translation levels in the cells and in their sEVs. To inhibit the expression of autotaxin, a specific inhibitor, ziritaxestat (GLPG1690) (Selleck, United States), was used.

Statistical Analysis

Statistical analyses were performed with SPSS 19.0 (IBM Corp., United States), and the figures were made with GraphPad Prism 8 software (GraphPad Software, United States). Both parametric and non-parametric inferential statistics were used depending on whether the data were normally distributed tested by Kolmogorov–Smirnov test. Two-tailed *t*-test and Mann–Whitney *U* test were used to identify differences between groups. One-way analysis of variance (ANOVA) and Kruskal–Wallis tests were carried out for multiple group comparisons. Three replicates were set for each treatment. The data are presented as the mean ± standard error of the mean (SEM). *P* value less than 0.05 was considered statistically significant.

TABLE 1 | The primer sequences of target genes.

Primer	Sequence (5′–3′)
PCNA-F	GCTCCATCCTGAAGAAGGTGCTG
PCNA-R	CGTGGGACGAGTCCATGCTTTG
COL2A1-F	GTCCTGTGCGACGACATAATCT
COL2A1-R	GGCAGTGGCGAGGTCAGTAG
ACAN-F	GCTACGACGCCATCTGCTACAC
ACAN-R	GTCCTCCTCACCGCCCACTC
SOX9-F	GAAGCTCTGGAGACTGCTGAA
SOX9-R	CCCATTCTTCACCGACTTCCT
MMP13-F	TCCAGTTTGCAGAGAGCTACC
MMP13-R	GACTGCATTTCTCGGAGCCT
RUNX2-F	GAACCCAGAAGGCACAGACAGAAG
RUNX2-R	GAGGCGGGACACCTACTCTCATAC
ATX-F	TGTCCTCCTTCATCCTGCCTCAC
ATX-R	TGTTCAATGTCACGCACCCTAGC
RHOA-F	ATTGTCGGTGATGGTGCTTGTGG
RHOA-R	TGGGGACATACACCTCTGGGAAC
LATS1-F	GTGACCATCCACGGCAAGATAGC
LATS1-R	GTGCTAGACATCGCTGGTGCTG
LATS2-F	CCAACTCCTTCAACAGCCAGCAG
LATS2-R	CAGCACCCGCACACTCTTCAC
AKT2-F	GGTCGCCAACAGCCTCAAGC
AKT2-R	ACCGCCACTTCCATCTCCTCAG
AKT3-F	ACAGATGCAGCCACCATGAAGAC
AKT3-R	GAACGGCAACCTCCCACACATC
GAPDH-F	AGGTCGGAGTGAACGGATTT
GAPDH-R	GATCTCGCTCCTGGAAGATGG

PCNA, proliferating cell nuclear antigen; COL2A1, type II collagen; ACAN, aggrecan; SOX9, SRY-related high-mobility group box 9; MMP13, matrix metalloproteinase 13; RUNX2, RUNX family transcription factor 2; ATX, autotaxin; RhoA, ras homolog family member; ALATS 1/2, large tumor suppressor kinase 1/2; GAPDH, glyceraldehyde 3-phosphate dehydrogenase.

RESULTS

Acquisition and Identification of the Bone Marrow Mesenchymal Stem Cell-Derived Small Extracellular Vesicles

Human BMSCs were harvested from the healthy human iliac bone marrow. Viewed by optical microscopy, their cell form was fibroblast-like, with a long barracuda, fish, vortex, or reticular arrangement (**Figure 1A**). By FCM, the BMSC markers CD105, CD29, and CD44 were identified (whose counts were 96.1, 98.7, and 99.4%, respectively), and the results complied with the BMSC identification criteria (**Figures 1B–D**).

By centrifugation, microfiltration (0.45 and 0.20 μm) and ultrafiltration (100 kD), BMSC-sEVs were obtained (**Figure 1E**). Through transmission electron microscopy (TEM), many "cup-shaped" and "tea saucer-shaped" vesicles with membrane structures could be seen, with diameters of approximately 30–120 nm. The size and morphology of the BMSC-sEV samples observed under the microscope conformed to the relevant definitions and characteristics of sEVs (**Figure 1F**). The NTA results showed that the particle size distribution of the BMSC-sEV samples obtained in this experiment was concentrated at approximately 106 nm. Each 1 ml BMSC-sEV sample contained approximately 1.05×10^7 particles, derived from approximately 5.5×10^7 BMSCs (**Figure 1G**). The NTA results suggested that the BMSC-sEV samples obtained in this experiment conformed to the relevant definitions and characteristics of sEVs, consistent with the TEM results mentioned above. In addition, the results showed that the concentration and purity of the sEV samples from the BMSC sources were satisfactory.

sEVs can also be identified by positive and negative markers. Positive markers of sEVs, such as CD63, CD81, Rab5, and Alix, were clearly detected in the BMSC-sEVs and their donor cells, whereas the negative marker GRP94 was only detected in the BMSCs (**Figure 1H**).

TABLE 2 | The siRNA sequences targeting the autotaxin gene.

siRNA		Sequence (5′–3′)
Negative control	Sense	UUCUCCGAACGUGUCACGUTT
	Anti-sense	ACGUGACACGUUCGGAGAATT
siAutotaxin-1	Sense	GCAGCAAAGUCAUGCCUAATT
	Anti-sense	UUAGGCAUGACUUUGCUGCTT
siAutotaxin-2	Sense	GCAGUGCUUUAUCGGACUATT
	Anti-sense	UAGUCCGAUAAAGCACUGCTT
siAutotaxin-3	Sense	GGUCUGGAAUUAUUUCCAATT
	Anti-sense	UUGGAAAUAAUUCCAGACCTT

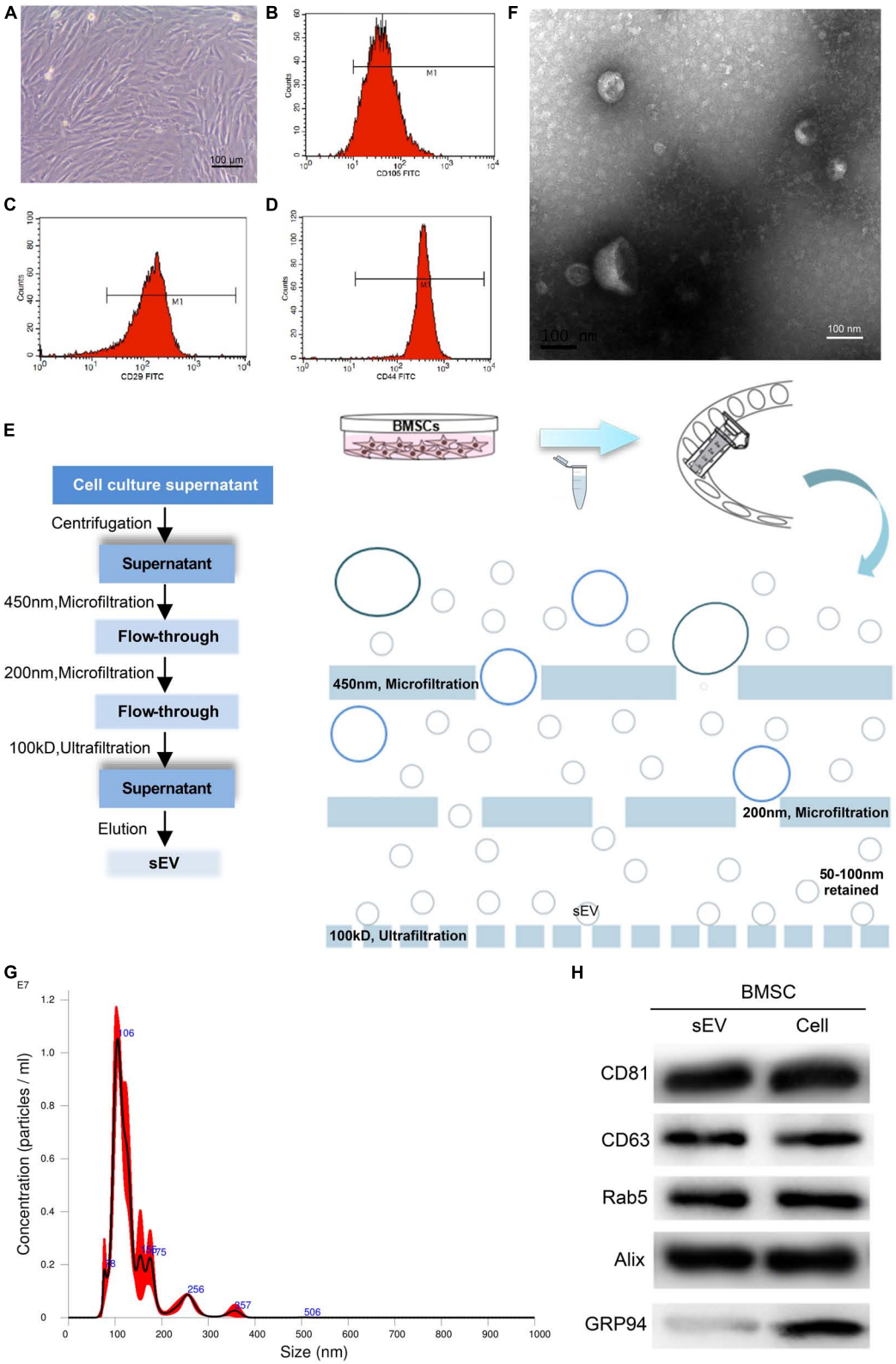

FIGURE 1 | Acquisition and identification of bone marrow mesenchymal stem cell-derived small extracellular vesicles (BMSC-sEVs). **(A)** Morphologic observation of BMSCs under an optical microscope (100×). **(B–D)** Identification of BMSCs by CD105, CD29, and CD44 using flow cytometry (FCM). **(E)** Flow and schematic diagram of sEV isolation and purification. **(F)** Electron microscopy analysis of BMSC-sEVs. **(G)** Nanoparticle tracking analysis of BMSC-sEVs. **(H)** Immunoblotting analysis of exosomal positive and negative markers in BMSC-sEVs (left) and in donor whole-cell lysates (right).

These results show that the sEV separation and purification technology used in this study is reliable and effective; the BMSC-sEV samples are in line with the recognized definition and identification standards of sEVs, with satisfactory concentration and purity.

Bone Marrow Mesenchymal Stem Cell-Derived Small Extracellular Vesicles Contributed to Temporomandibular Joint Osteoarthritis Reconstruction *in vivo*

Histologic Assessment of Temporomandibular Joint Osteoarthritis Condylar Cartilage Treated With Bone Marrow Mesenchymal Stem Cell-Derived Small Extracellular Vesicles

The rabbit TMJOA model was established according to the method described above (**Figure 2A**). During the operation, the injection point and depth were accurate; the needle entered the supra-fissure of the TMJ capsule between the condyle and the joint disc (**Figure 2B**). Gross observation results showed that the condyles in OA group relatively lacked integrity (**Supplementary Figure 1A**). Micro-CT results suggested that BVF, BMD, and Tb.Th were significantly reduced and that BS/BV and Tb.Sp were increased in the OA group (**Supplementary Figures 1B–G**). The results of HE and Alcian blue staining for cartilage showed that each layer of the OA group's cartilage (fiber layer, proliferation layer, mature cartilage layer, and calcified cartilage layer) was thin compared to the control group, and the cartilage structure and level were not well organized (**Figures 2C,D**). The above results showed that the rabbit TMJOA model was successfully established.

The histological scores of the OA group were worse than those of the control group. Better histological scores were not observed in the sEV group than in the control group. Compared with the OA group, however, the histology scores of the OA^{sEV} group were better (**Figures 2E–H**). These results suggested that BMSC-sEVs could induce histologic repair of TMJOA condylar cartilage.

Expression of Osteoarthritis-Related Factors in Temporomandibular Joint Osteoarthritis Condylar Cartilage Treated With Bone Marrow Mesenchymal Stem Cell-Derived Small Extracellular Vesicles

The HE staining results showed that compared with the untreated OA group, the condylar tissue of the OA^{sEV} exhibited an increase in cartilage lacuna. The cartilage cell proliferation was obvious. Hypertrophic cartilage cells (with larger cartilage lacuna) could also be seen in the deep area of the bone under the cartilage, which suggested more obvious hyaline cartilage formation (**Figure 3A**). The IHC results showed that compared with the untreated OA group, the condylar tissue of the OA^{sEV} exhibited significantly upregulated expression of cell proliferation-related factor-PCNA, Col-II, ACAN, SOX9 (with no significant difference in the expression of Col-I), and the downregulated expression of cartilage inflammation-related factor-MMP13 and RUNX2 (**Figures 3A,B**).

Combined with the above results, the *in vivo* experiments confirmed that BMSC-sEVs played an important role in promoting cartilage reconstruction in TMJOA.

Bone Marrow Mesenchymal Stem Cell-Derived Small Extracellular Vesicles Upregulated Cartilage Cell Activity and Cartilage Reconstruction Factor Expression in Temporomandibular Joint Osteoarthritis *in vitro*

Acquisition and Identification of Mandibular Condylar Cartilage Cells

MCCs were extracted from healthy New Zealand rabbit TMJ condyles and identified by specific staining and immunocytochemistry (ICC). The results showed that the MCCs were irregularly distributed in the polygon or strip, similar to short fibroblasts, and the MCCs stained with toluene blue (TB) and Col-II using the ICC technique met the identification criteria (**Figures 4A–C**).

Bone Marrow Mesenchymal Stem Cell-Derived Small Extracellular Vesicles Could Be Internalized by Mandibular Condylar Chondrocytes

Then, BMSC-sEVs were analyzed using fluorescent dyes and laser scanning confocal microscopy (**Figure 4D**). BMSC-sEVs harboring red dye-labeled RNAs were internalized in the MCCs, which showed that BMSC-sEVs could be internalized by MCCs.

Enhancement of the Biological Activity of Mandibular Condylar Chondrocytes Treated With Bone Marrow Mesenchymal Stem Cell-Derived Small Extracellular Vesicles

The migration test using Transwell assays showed that compared with the control group, the migratory ability of the MCCs in the OA group (established by the aforementioned IL-1β) was weakened; in contrast, the migration of the MCCs in the sEV group was enhanced. Furthermore, the migratory ability of the MCCs in the OA^{sEV} group was increased compared with that in the OA group. In addition, the treatment duration (12, 24, and 48 h) did not change the results (**Figure 4E**).

The proliferation of TMJOA MCCs was enhanced by BMSC-sEVs compared with their corresponding control group (**Figure 4F**). In addition, the FCM results showed that compared with the control group, the cell cycle of the MCCs in the OA group was stagnated in the G1 stage relative to the control group; in contrast, stagnation of the cell cycle of the MCCs in the OA^{sEV} group was alleviated to some degree (**Figures 4G,H**).

Expression of the Relevant Factors of Mandibular Condylar Chondrocyte Cartilage Reconstruction Treated With Bone Marrow Mesenchymal Stem Cell-Derived Small Extracellular Vesicles

Compared with the OA group, in the OA^{sEV} group, the expression of PCNA, Col-II, ACAN, and SOX9 was upregulated (Col-I expression did not show a significant difference), while

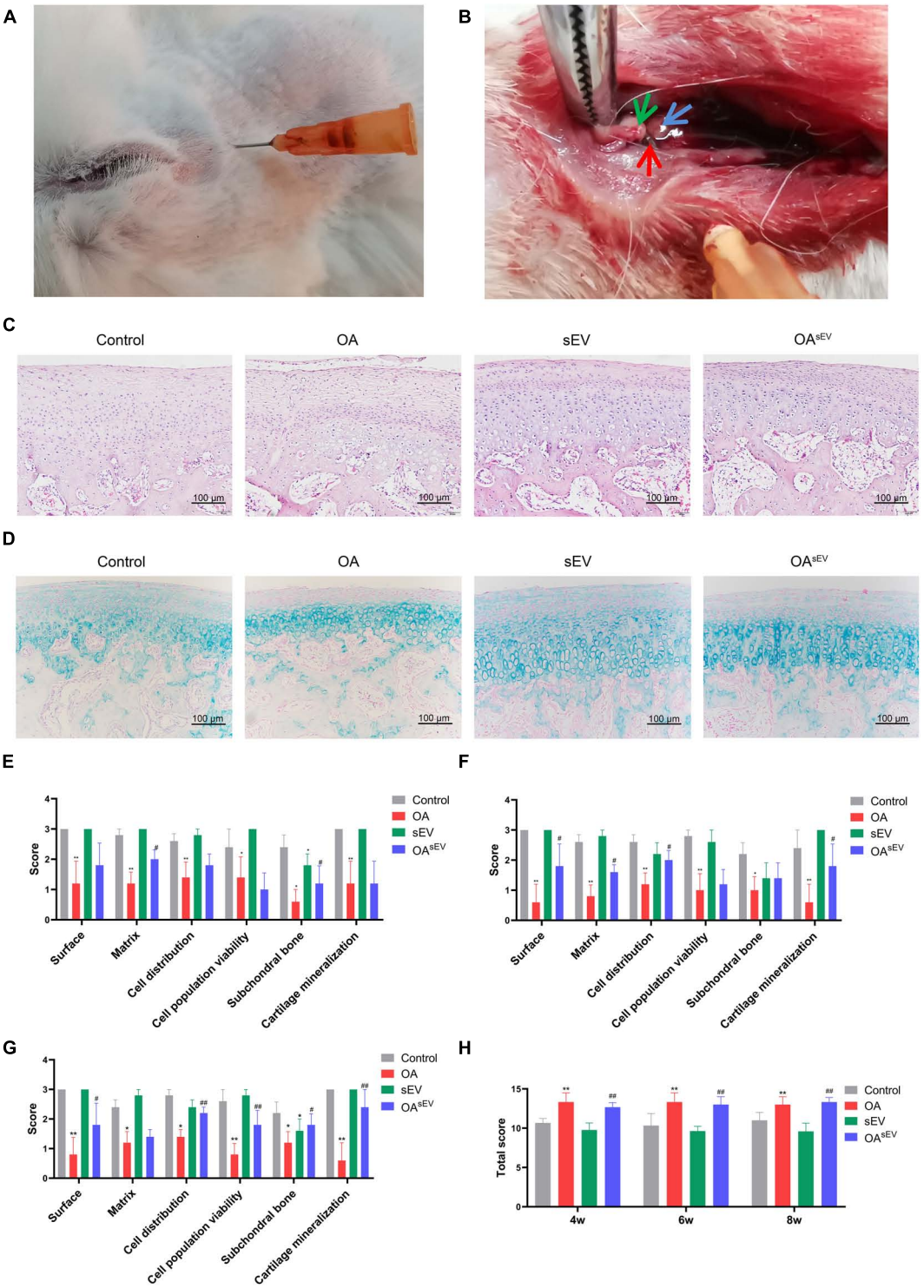

FIGURE 2 | Histologic assessment of temporomandibular joint osteoarthritis (TMJOA) condylar cartilage treated with bone marrow mesenchymal stem cell-derived small extracellular vesicles (BMSC-sEVs). **(A)** Needle insertion site to establish the rabbit TMJOA model using the chemical injection method. **(B)** Anatomy of the establishment of the TMJOA model by the chemical injection method (green arrow pointing to the TMJ disc, blue arrow pointing to the condylar cartilage, and red arrow pointing to the needle tip). **(C)** Hematoxylin–eosin (HE) staining observation of the establishment of the TMJOA model (200×). **(D)** Alcian blue staining observation of the establishment of the TMJOA model (200×). **(E–G)** Histologic scoring of the condyle of normal and the TMJOA model group (treated with BMSC-sEVs for 4, 6, and 8 weeks, respectively) by the ICRS Grading Scale. **(H)** Histologic scoring of the condyle of the normal and TMJOA model groups by the Wakitani Grading Scale. *: Compared with the control group, #: Compared with the OA group. */#$P < 0.05$, **/##$P < 0.01$.

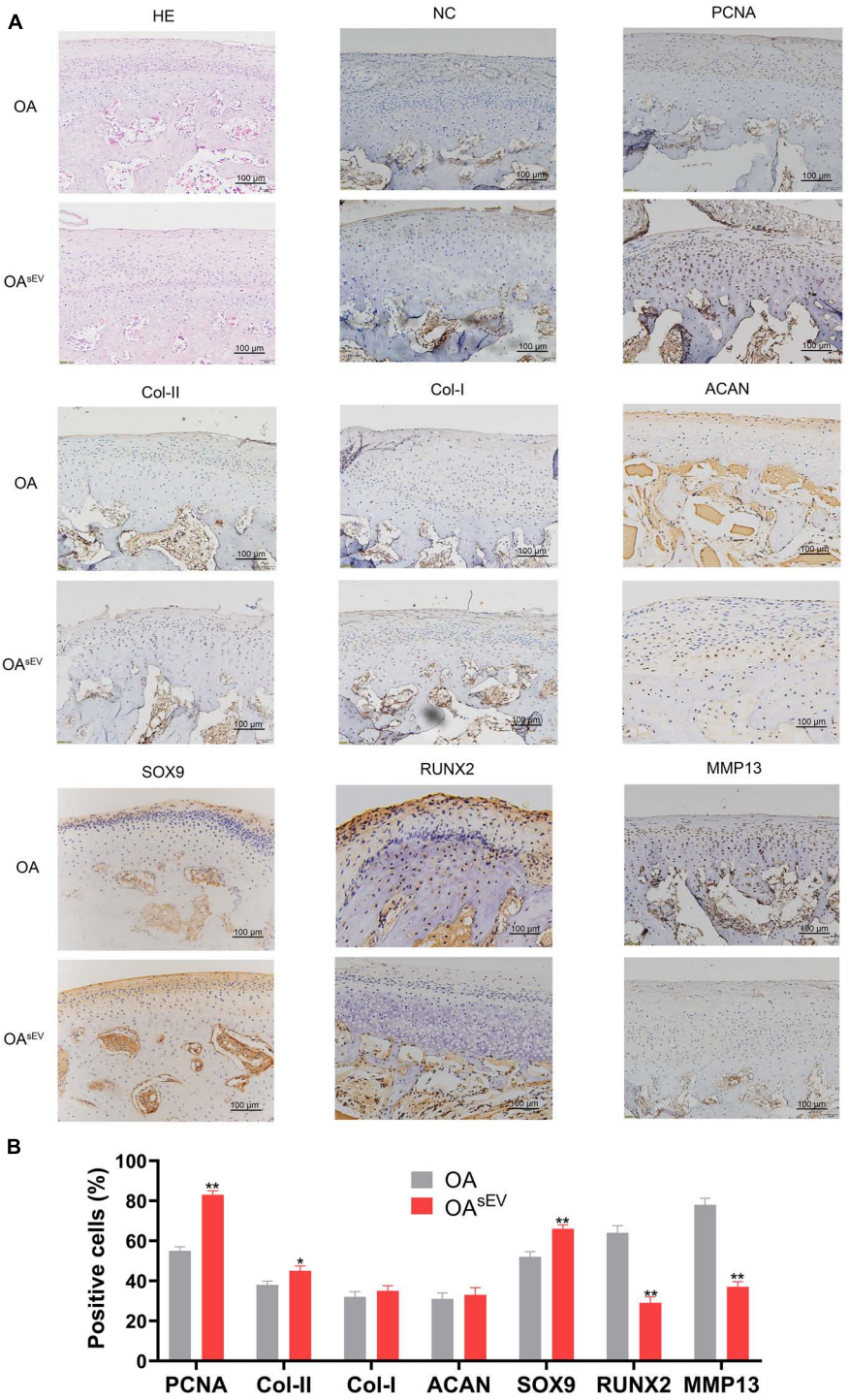

FIGURE 3 | Histologic expression of osteoarthritis (OA)-related factors in temporomandibular joint osteoarthritis (TMJOA) condylar cartilage treated with bone marrow mesenchymal stem cell-derived small extracellular vesicles (BMSC-sEVs). **(A)** Hematoxylin–eosin (HE) and immunohistochemistry (IHC) analysis of the expression of proliferating cell nuclear antigen (PCNA), cartilage-forming factors, and cartilage inflammation-related factors in the OA control group and the OA treated with BMSC-sEV group (OA^{sEV}) (200×). NC, negative control. **(B)** Semiquantitative analysis of IHC. $^{*}P < 0.05$, $^{**}P < 0.01$.

the expression of RUNX2 and MMP13 was decreased, indicating that BMSC-sEVs could promote TMJOA cartilage reconstruction (**Figures 4I,J**).

Combining the above results, the *in vitro* experiments confirmed that BMSC-sEVs significantly promoted cartilage reconstruction in TMJOA.

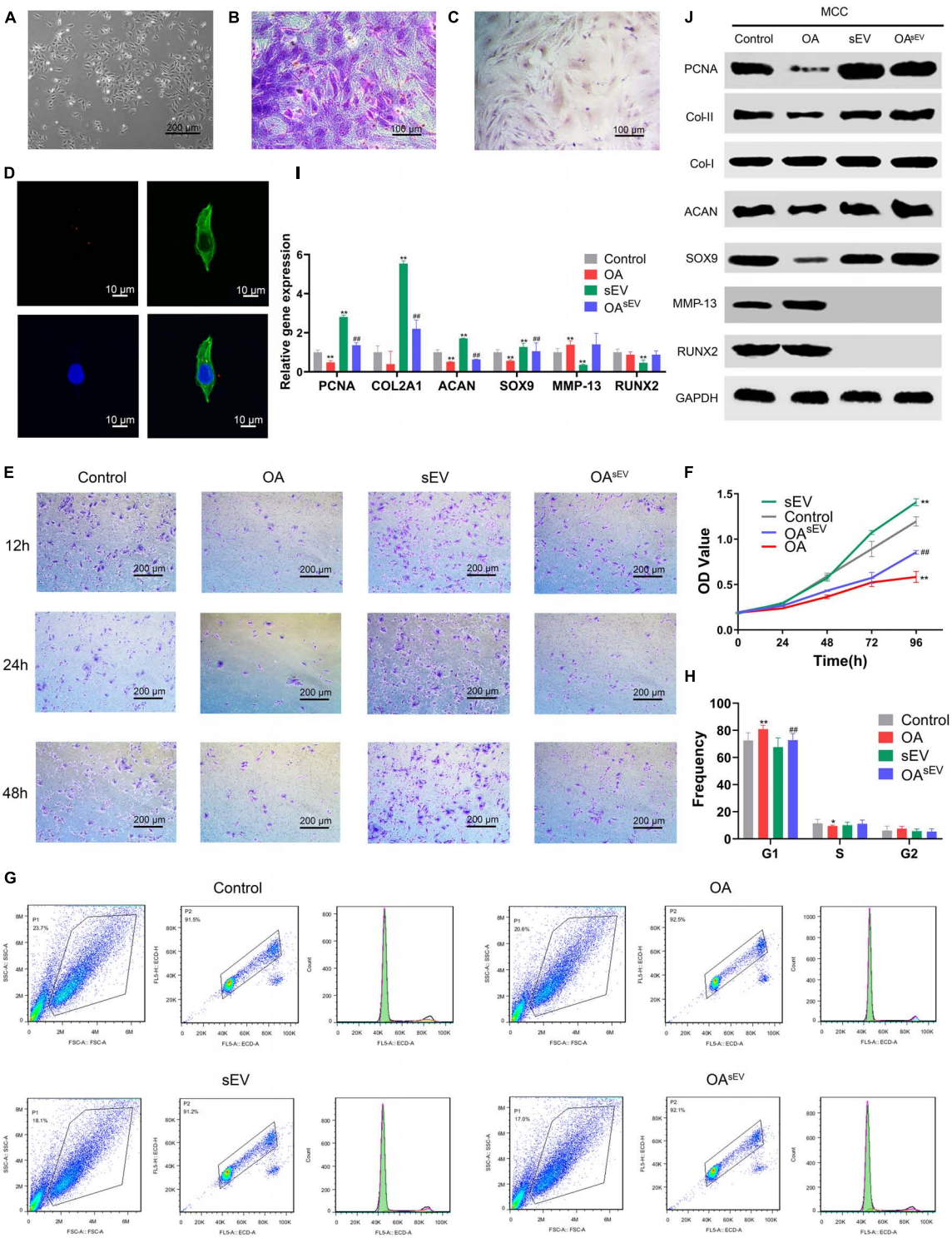

FIGURE 4 | Bone marrow mesenchymal stem cell-derived small extracellular vesicles (BMSC-sEVs) promoted cartilage reconstruction of temporomandibular joint osteoarthritis (TMJOA) *in vitro*. **(A)** Morphologic observation of mandibular condylar chondrocytes (MCCs) under an optical microscope (100×). **(B)** Identification of MCCs using toluene blue staining (200×). **(C)** Immunohistochemistry (IHC) identification of MCCs targeting type II collagen (Col-II) (200×). **(D)** Laser scanning confocal microscopy analysis of BMSC-sEV (red) internalization by MCCs. **(E)** Analysis of the cell migration activity of MCCs by Transwell assays at 12, 24, and 48 h (100×). **(F)** Analysis of the cell proliferation activity of MCCs by Cell Counting Kit-8 (CCK-8). **(G,H)** Detection of the cell cycle distribution of MCCs by flow cytometry (FCM) and statistical analysis. **(I,J)** The expression of PCNA, cartilage-forming factors, and cartilage inflammation-related factors at the transcriptional and translational levels by quantitative polymerase chain reaction (qPCR) and immunoblotting, respectively. *: Compared with the control group, #: Compared with the OA group. */#$P < 0.05$, **/##$P < 0.01$.

The Mechanism of the Effect of Bone Marrow Mesenchymal Stem Cell-Derived Small Extracellular Vesicles on the Acceleration of Cartilage Reconstruction in Temporomandibular Joint Osteoarthritis

The Important Role of the Autotaxin and Hippo Pathways in Temporomandibular Joint Osteoarthritis Using Bioinformatic Analysis

Based on the Gene Expression Omnibus (GEO) database, the gene expression chips of normal humans and OA patients, GSE6119, GSE19664, GSE27357, etc., were obtained. Using GEO2R[1], KOBAS 3.0[2], DAVID 6.8[3] and other analysis methods, functional Gene Ontology (GO) analysis and Kyoto Encyclopedia of Genes and Genomes (KEGG) signaling pathway analysis were adopted to determine the differentially expressed factors and signaling pathways involved in TMJOA.

Take the GSE6119 data in the GEO database as an example. Among the differentially expressed genes, many Hippo pathway-related factors, such as Bmp7, Bmp6, Tgfb2, Bmp4, Bmp2, Ccnd1, Id1, Tgfb3, Wnt9a, Fgf1, and Dlg4, were present. In addition, the Hippo pathway was ranked at the top 1% among the large number of signaling pathways involved. These results suggested that the Hippo pathway was differentially expressed between OA tissue and healthy tissue and played a more important role than the other signaling pathways in TMJOA.

Upregulation of Key Factors of the Hippo Pathway in Mandibular Condylar Chondrocytes Treated With Bone Marrow Mesenchymal Stem Cell-Derived Small Extracellular Vesicles

Compared with the untreated OA group, MCCs in the OA^{sEV} group had upregulated expression of YAP, key factors of the Hippo pathway, and its upstream molecules, such as ras homolog family member A (RhoA), and downstream molecules, such as LATS 1/2. Conversely, the expression trend of p-YAP (S127) was contrary to the above factors, indicating that the BMSC-sEVs inhibited YAP phosphorylation in MCCs, thereby inhibiting the Hippo pathway, and played a role in promoting proliferation and cartilage regeneration in TMJOA (**Figures 5A,B**).

No Upregulated Expression of Key Factors of the Hippo Pathway in Mandibular Condylar Chondrocytes Treated With Bone Marrow Mesenchymal Stem Cell-Derived Small Extracellular Vesicles When Autotaxin Was Inhibited or Knocked Down

The IB results showed that BMSCs and their secreted sEVs expressed autotaxin (**Figure 5C**). In MCCs treated with BMSC-sEVs, in which autotaxin was inhibited or knocked down (**Figures 5D,E**), key factors of the Hippo pathway, such as RhoA and YAP, were no longer upregulated. These results preliminarily revealed that MSC-sEVs promoted cartilage reconstruction of TMJOA *via* the autotaxin–YAP signaling axis (**Figures 5F–H**).

No Cartilage Reconstruction of Mandibular Condylar Chondrocytes Treated With Bone Marrow Mesenchymal Stem Cell-Derived Small Extracellular Vesicles When Autotaxin Was Inhibited or Knocked Down

Gross observation results showed that compared with the other OA groups, the OA^{sEV} group had better integrity of condyles (**Figure 6A**). Micro-CT results suggested that BVF, BMD, and Tb.Th were significantly increased in the OA^{sEV} group and that BS/BV and Tb.Sp were reduced in this group (**Figures 6C–G**). These data proved that damage in the surface of condyle cartilage and subchondral bone in TMJOA could be reversed by sEV-autotaxin derived from BMSCs (**Figures 6C–G**).

HE and safranin O/fast green staining results showed that compared with the untreated OA group, the condylar tissue of the OA^{sEV} group exhibited an increase in cartilage lacuna (**Figure 6**), which is consistent with the results above (**Figure 3A**). In contrast, the condylar tissue of the OA^{sEV}, in which autotaxin had been knocked down or inhibited ($OA + sEV^{-/-ATX}$, $OA + sEV^{Ziritaxestat}$), no longer exhibited an increase in cartilage lacuna (**Figure 6**). The IHC results showed that compared with the untreated OA group, the condylar tissue of the OA^{sEV} group showed upregulated expression of PCNA, Col-II, and SOX9 and downregulated the expression of RUNX2 and MMP13 (**Figures 6H,I** and **Supplementary Figure 2**), which is consistent with the results above (**Figures 3A,B**). In contrast, the condylar tissue of the OA^{sEV}, in which autotaxin had been knocked down or inhibited ($OA + sEV^{-/-ATX}$, $OA + sEV^{Ziritaxestat}$), did not show changes in the expression of these factors (**Figures 6H,I** and **Supplementary Figure 2**).

DISCUSSION

BMSCs have been widely used in many occasions, such as defect repairing and tissue regeneration, which are based on several experimental and clinical studies. A recent study reported that BMSC implantation appeared to be an effective and safe treatment for chondral defects at up to 10 years (Teo et al., 2019). Nevertheless, there are some problems with the treatment of TMJOA with MSCs, one of which is their inefficiency. To improve their transplantation and survival, some studies have placed MSCs into advanced carrier systems to improve their retention, vitality, growth, and differentiation. MSCs can be loaded into the material, such as by inoculation into a macroporous scaffold or into hydrogel (Armiento et al., 2018). Bio-hydrogels developed by the research team at our university, with fast light curing and long degradation cycles, can be loaded with BMSCs to promote cell migration, a nutritional supply, and cell survival.

Nevertheless, in clinical applications, the number of MSCs required to achieve the desired therapeutic results is still very large. This leads to another problem: forcing MSCs to multiply in large quantities to increase their yields can induce MSCs to

[1]http://www.ncbi.nlm.nih.gov/geo/geo2r

[2]http://kobas.cbi.pku.edu.cn/kobas3

[3]https://david.ncifcrf.gov

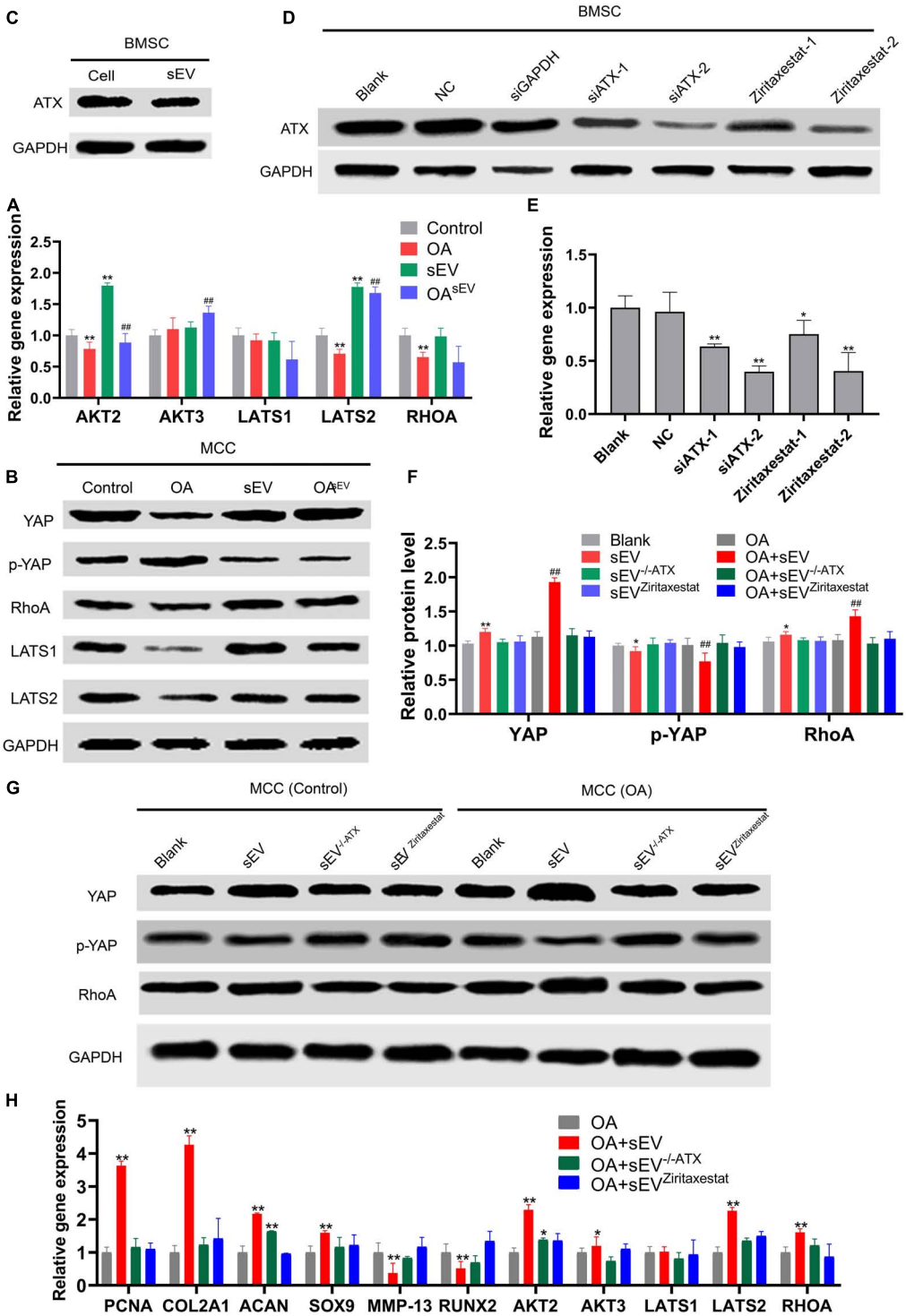

FIGURE 5 | Effect of autotaxin on the mechanism by which bone marrow mesenchymal stem cell-derived small extracellular vesicles (BMSC-sEVs) accelerated cartilage reconstruction in temporomandibular joint osteoarthritis (TMJOA). **(A,B)** Expression of key factors [such as Yes-associated protein (YAP), ras homolog family member (RhoA), etc.] of the Hippo pathway in mandibular condylar chondrocytes (MCCs) at the transcriptional and translational levels by quantitative polymerase chain reaction (qPCR) and immunoblotting (IB), respectively. **(C)** Expression of autotaxin in BMSCs and their secreted sEVs by immunoblotting. **(D,E)** Efficiency of knockdown and inhibition of BMSCs targeting autotaxin at the translation and transcription levels by immunoblotting and qPCR, respectively (NC, negative control; siGAPDH, positive control; siATX-1/2, two siRNAs targeting autotaxin; ziritaxestat-1/2, autotaxin inhibitors at concentrations of 2 and 10 μM, respectively). $^{*}P < 0.05$, $^{**}P < 0.01$. **(F,G)** Expression of key factors (such as YAP, RhoA, etc.) of the Hippo pathway in normal MCCs or those with autotaxin knockdown or inhibition at the translation level by immunoblotting and statistical analysis. **(H)** Expression of key factors (such as YAP, RhoA, etc.) of Hippo pathway in normal MCCs and those with autotaxin knockdown or inhibition at the transcription level by qPCR. *: Compared with the control group, #: Compared with the OA group. $^{*}/\#P < 0.05$, $^{**}/\#\#P < 0.01$.

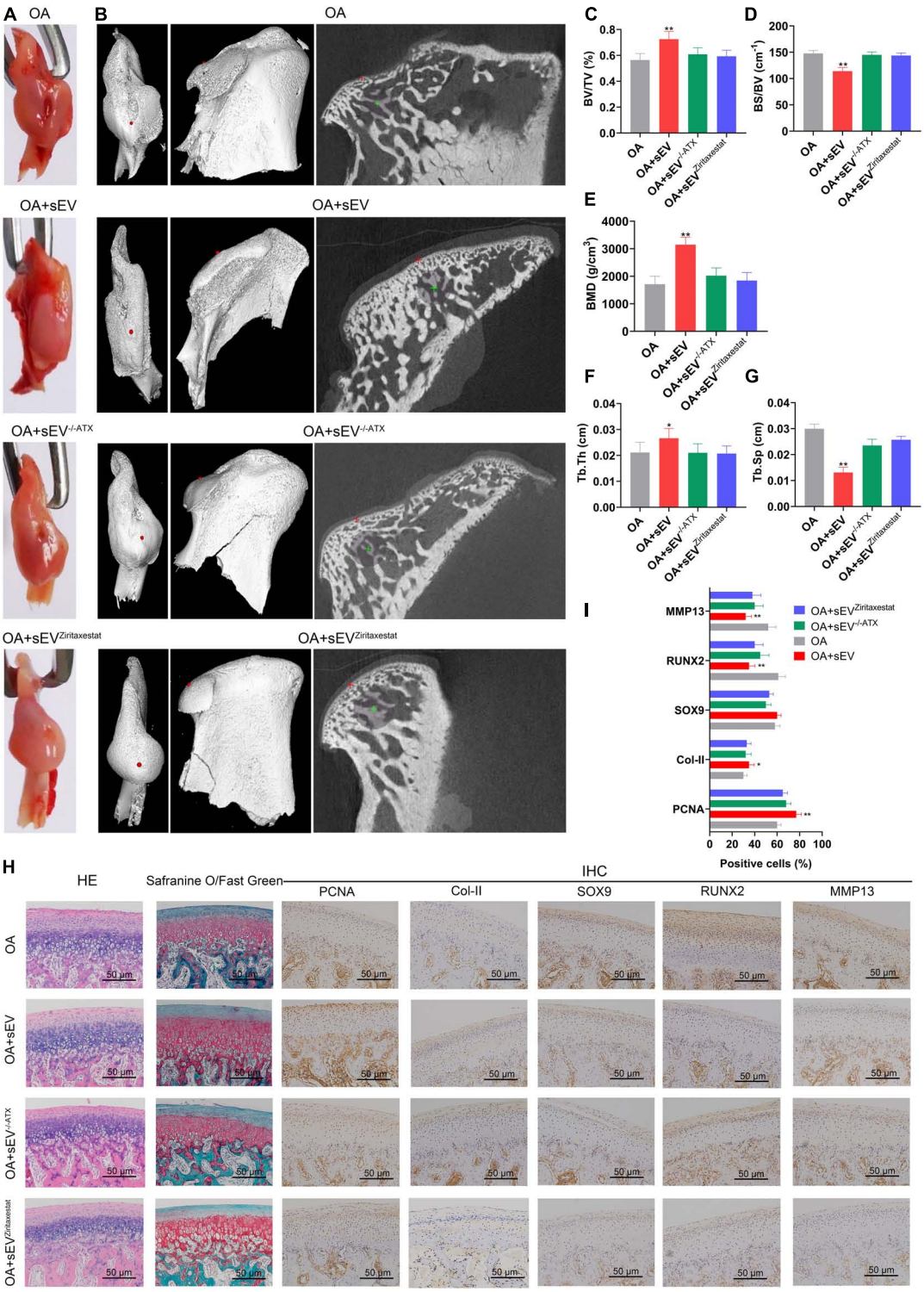

FIGURE 6 | No cartilage reconstruction of mandibular condylar chondrocytes (MCCs) treated with bone marrow mesenchymal stem cell-derived small extracellular vesicles (BMSC-sEVs) was observed when autotaxin was inhibited or knocked down. **(A)** Gross observation of condyles of temporomandibular joint osteoarthritis (TMJOA) animal model treated with BMSC-sEVs, normal and autotaxin knockdown or inhibition. **(B)** Micro-CT images of condyles of TMJOA animal model treated with BMSC-sEVs, normal and autotaxin knockdown or inhibition. **(C–G)** Parameters of micro-CT analysis of these groups, including bone volume fraction (BVF), bone surface/bone volume ratio (BS/BV), bone mineral density (BMD), trabecular thickness (Tb.Th), and trabecular spacing (Tb.Sp). **(H)** Hematoxylin–eosin (HE), safranin O/fast green, and immunohistochemistry (IHC) analysis of condyles of TMJOA animal model treated with BMSC-sEVs, normal and autotaxin knockdown or inhibition for 4 weeks (200×). **(I)** Semiquantitative analysis of IHC. $^{*}P < 0.05$, $^{**}P < 0.01$.

show a tumorous tendency. In addition, there is unevenness in the expanded MSC population, which leads to less stable and reliable treatment by MSCs from different sources and batches, limiting further clinical applications of MSCs. Currently, it is widely proposed that MSCs may play their multiple biological roles by producing extracellular vesicles of varying sizes (Phinney and Pittenger, 2017). Considering this, using BMSC-sEVs instead could be a reliable and effective treatment for TMJOA, which is supported by the results of this study.

BMSC-sEVs can overcome problems arising from direct applications of MSCs, and in recent years, they have been found to have a therapeutic effect on OA. BMSC-sEVs can promote the repair of cartilage defects by promoting cell proliferation and infiltration, and they can also regulate cell proliferation, migration, and vascular formation through a variety of miRNAs (Qin et al., 2016; Cosenza et al., 2017; Zhang et al., 2018). When co-cultured with OA chondrocytes, BMSC-sEVs highly expressed cyclooxygenase-2 (COX-2) and pro-inflammatory interleukin, inhibited the activity of tumor necrosis factor (TNF)-alpha-induced collagen, and promoted the synthesis of ACAN and type II collagen (Vonk et al., 2018). In addition, embryo-derived sEVs could reduce matrix degradation and cartilage destruction in mice and promote cartilage regeneration (Guo et al., 2016; Wang et al., 2017). A recent study indicated that human BMSC-sEVs overexpressing miRNA-26a-5p could alleviate OA by reducing prostaglandin endoperoxide synthase 2 (PTGS2) (Jin et al., 2020).

However, the role of BMSC-sEVs in TMJOA is still unclear. The TMJ has two motor patterns, sliding and rotation with a disc inside, which means that its function and mechanism are complex. In addition, unlike other joints of the body derived from the mesoderm, the TMJ is derived from the ectoderm, which means that there are many differences in its histogenesis, inflammation, and immunity. Therefore, determining whether MSC-sEVs have a similar effect on TMJOA is necessary because relevant research is very limited. Recent studies have suggested that MSC-sEVs can promote cartilage repair in rats and reduce TMJOA-related pain (Zhang et al., 2019; Lee et al., 2020). The results of this article showed that human BMSC-sEVs could promote cartilage reconstruction in rabbit TMJOA and increase cell proliferation activity. Cartilage cell proliferation-, formation-, and matrix regeneration-related factors were all enhanced (**Figures 3**, **6**).

Regarding the mechanism by which MSC-sEVs promote OA cartilage cell proliferation, migratory activity, and cartilage regeneration, some studies have pointed to the Hippo signaling pathway, which plays an important role in cell proliferation, tissue regeneration, and stem cell function. Based on the GEO database, gene chips from OA patients and a normal human population were obtained and analyzed. The Hippo signaling pathway was significantly differentially expressed in the OA tissues, and the role of the pathway was more important than the other signaling pathways involved. Previous studies have shown that synovial MSC-sEVs activate the key factor of the

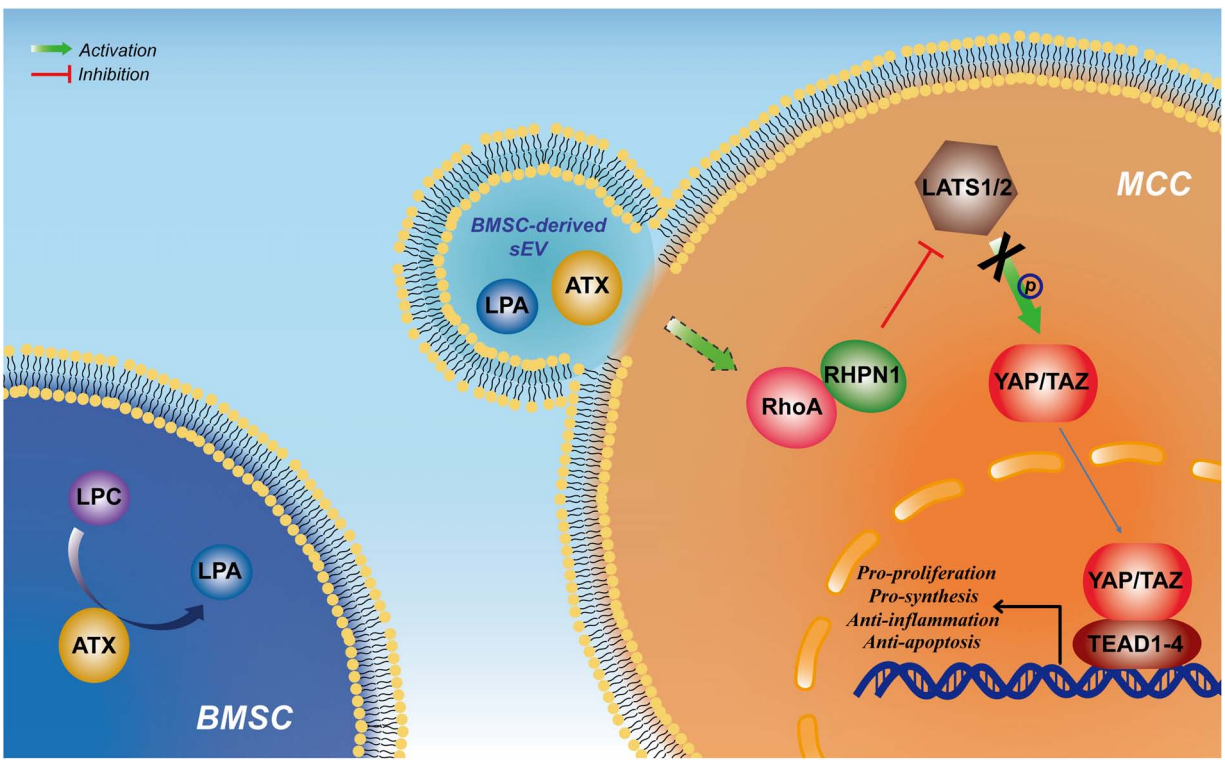

FIGURE 7 | Schematic suggesting that bone marrow mesenchymal stem cell-derived small extracellular vesicles (BMSC-sEVs) induce cartilage reconstruction of temporomandibular joint osteoarthritis (TMJOA) *via* the autotaxin–Yes-associated protein (YAP) signaling axis.

Hippo signaling pathway, YAP, which increases the proliferation and migratory activity of chondrocytes in an OA model in mice (Tao et al., 2017). In addition, YAP can also phosphorylate Akt and thus promote cell survival. After TMJOA rats were treated with MSC-sEVs, Akt expression was increased, which in turn promoted cartilage regeneration (Zhang et al., 2019).

Nevertheless, the role of YAP in cartilage regeneration is not clear. The YAP-TEA domain (TEAD) complex can increase cell proliferation potential by activating the SOX6 promoter. However, YAP can activate the Wnt/β-catenin pathway, reducing the ability of cells to differentiate into cartilage, and YAP also reduces the expression of the RUNX2-mediated COL10A1 gene, which hinders the maturation of chondrocytes (Li et al., 2017). Therefore, the role and mechanisms of the Hippo pathway in OA with YAP as the key factor are worth exploring in further detail. The results from this study showed that BMSC-sEVs can promote an increase in YAP expression in TMJOA chondrocytes and that the level of YAP phosphorylation is downregulated, indicating that the Hippo pathway is inhibited, and this promotes cell survival and proliferation (**Figure 5**). Nevertheless, further mass spectrometry and sequencing of proteins and miRNAs are required for further study of the role of the Hippo pathway and the relationships among other pathways in this mechanism.

The upstream factors of the Hippo signaling pathway have not been explained thoroughly. A recent study revealed the role of the RhoA-striatin-interacting phosphatase and kinase (STRIPAK) signaling axis in the Hippo pathway (Chen et al., 2019). After stimulation by serum or lysophosphatidic acid (LPA), active RhoA binds to STRIPAK, which induces the binding and dephosphorylation of mammalian STE20-like protein kinase (MST1/2) and mitogen-activated protein kinase kinase kinase kinases (MAP4Ks). This results in YAP dephosphorylation, Hippo pathway inhibition, and the expression of cell proliferation- and cartilage regeneration-related factors. Autotaxin plays a role in the process of wound healing, angiogenesis factor formation, chemotaxis and the cell cycle (Knowlden and Georas, 2014). Studies have shown that autotaxin promotes MSC migration and cytoskeletal rearrangement (Ryu and Han, 2015). It has also been found that autotaxin binds to sEVs, which in turn transport LPA to target cells (Jethwa et al., 2016).

The results of this study showed that the BMSC-sEVs could carry autotaxin and that sEV-autotaxin could induce condylar cartilage repair and upregulate the expression of the aforementioned key factors of the Hippo pathway (**Figures 5**, **6**). Nevertheless, further study of the mechanism is still needed by using a knockout animal model and by analyzing the detailed interaction between autotaxin and the Hippo signaling pathway. Finally, clinical trials of BMSC-sEVs in TMJOA patients are expected in the near future.

CONCLUSION

Our study reveals that BMSC-derived sEVs could induce cartilage reconstruction in TMJOA *via* the autotaxin–YAP signaling axis (**Figure 7**), which could be expected to play an important role in the clinical application of sEVs in TMJOA and increase comprehension of the underlying mechanism.

DATA AVAILABILITY STATEMENT

The original contributions presented in the study are included in the article/**Supplementary Material**, further inquiries can be directed to the corresponding author/s.

ETHICS STATEMENT

The animal study was reviewed and approved by Institutional Animal Care and Use Committee at Laboratory Animal Center of Zhejiang University. Written informed consent was obtained from the owners for the participation of their animals in this study.

AUTHOR CONTRIBUTIONS

YW and MW conceived and designed the research. YW and MZ performed the main experiments and wrote the manuscript. WL performed the data statistics and interpretation. YY and RM involved in data validation. ZZ and MW reviewed and revised the manuscript. All authors read and approved the final manuscript.

FUNDING

This study was supported by grants from the National Natural Science Foundation of China (grant no. 81970956), Medical Science and Technology Project of Zhejiang Province (grant no. 2021418901), and the Fundamental Research Funds for the Central Universities (grant no. 2020FZZX008-06).

ACKNOWLEDGMENTS

We wish to thank Chenyu Wang and Cunyi Wang for assisting in establishing the TMJOA animal model and Zhuangjie Yu and Yidan Zhang for their assisting in IHC and histological scoring.

SUPPLEMENTARY MATERIAL

The Supplementary Material for this article can be found online at: https://www.frontiersin.org/articles/10.3389/fcell.2021.656153/full#supplementary-material

Supplementary Figure 1 | Gross observation and Micro-CT of condyles of TMJOA animal model. **(A)** Gross observation of condyles of TMJOA animal model. **(B)** Micro-CT images of condyles of TMJOA animal model. **(C–G)**. Parameters of micro-CT analysis of TMJOA animal model, including BVF, BS/BV, BMD, Tb.Th and Tb.Sp. $^{*}P < 0.05$, $^{**}P < 0.01$.

Supplementary Figure 2 | Histologic and IHC analysis of condyles of TMJOA model treated with multiple kinds of BMSC-sEVs. HE, safranin O/fast green and IHC analysis of condyles of TMJOA animal model treated with BMSC-sEVs, normal and autotaxin knockdown or inhibition for 6 w and 8 w, respectively (200×).

REFERENCES

Abouelhuda, A. M., Khalifa, A. K., Kim, Y. K., and Hegazy, S. A. (2018). Non-invasive different modalities of treatment for temporomandibular disorders: review of literature. *Korean Assoc. Oral Maxillofac. Surg.* 44, 43–51. doi: 10.5125/jkaoms.2018.44.2.43

Armiento, A. R., Stoddart, M. J., Alini, M., and Eglin, D. (2018). Biomaterials for articular cartilage tissue engineering: learning from biology. *Acta Biomater.* 65, 1–20. doi: 10.1016/j.actbio.2017.11.021

Chen, K., Man, C., Zhang, B., Hu, J., and Zhu, S. S. (2013). Effect of in vitro chondrogenic differentiation of autologous mesenchymal stem cells on cartilage and subchondral cancellous bone repair in osteoarthritis of temporomandibular joint. *Int. J Oral Maxillofac. Surg.* 42, 240–248. doi: 10.1016/j.ijom.2012.05.030

Chen, R., Xie, R., Meng, Z., Ma, S., and Guan, K. L. (2019). STRIPAK integrates upstream signals to initiate the Hippo kinase cascade. *Nat. Cell Biol.* 21, 1565–1577. doi: 10.1038/s41556-019-0426-y

Cosenza, S., Ruiz, M., Toupet, K., Jorgensen, C., and Noël, D. (2017). Mesenchymal stem cells derived exosomes and microparticles protect cartilage and bone from degradation in osteoarthritis. *Sci. Rep.* 7:16214.

García-García, A., de Castillejo, C. L., and Méndez-Ferrer, S. (2015). BMSCs and hematopoiesis. *Immunol. Lett.* 168, 129–135. doi: 10.1016/j.imlet.2015.06.020

Guo, S., Tao, S., Yin, W., Qi, X., Sheng, J., and Zhang, C. (2016). Exosomes from human synovial-derived mesenchymal stem cells prevent glucocorticoid-induced osteonecrosis of the femoral head in the rat. *Int. J Biol. Sci.* 12, 1262–1271. doi: 10.7150/ijbs.16150

Jethwa, S. A., Leah, E. J., Zhang, Q., Bright, N. A., Oxley, D., Bootman, M. D., et al. (2016). Exosomes bind autotaxin and act as a physiological delivery mechanism to stimulate LPA receptor signalling in cells. *J Cell Sci.* 129, 3948–3957. doi: 10.1242/jcs.184424

Jin, Z., Ren, J., and Qi, S. (2020). Human bone mesenchymal stem cells-derived exosomes overexpressing microRNA-26a-5p alleviate osteoarthritis via down-regulation of PTGS2. *Int. Immunopharmacol.* 78:105946. doi: 10.1016/j.intimp.2019.105946

Kim, H., Yang, G., Park, J., Choi, J., Kang, E., and Lee, B. K. (2019). Therapeutic effect of mesenchymal stem cells derived from human umbilical cord in rabbit temporomandibular joint model of osteoarthritis. *Sci. Rep.* 9:13854.

Knowlden, S., and Georas, S. N. (2014). The autotaxin-LPA axis emerges as a novel regulator of lymphocyte homing and inflammation. *J Immunol.* 192, 851–857. doi: 10.4049/jimmunol.1302831

Lee, Y. H., Park, H. K., Auh, Q. S., Nah, H., Lee, J. S., Moon, H. J., et al. (2020). Emerging potential of exosomes in regenerative medicine for temporomandibular joint Osteoarthritis. *Int. J Mol. Sci.* 21:1541. doi: 10.3390/ijms21041541

Li, C., Wang, S., Xing, Z., Lin, A., Liang, K., Song, J., et al. (2017). A ROR1-HER3-lncRNA signaling axis modulates the Hippo-YAP pathway to regulate bone metastasis. *Nat. Cell Biol.* 19, 106–119. doi: 10.1038/ncb3464

Lu, L., Zhang, X., Zhang, M., Zhang, H., Liao, L., Yang, T., et al. (2015). RANTES and SDF-1 are keys in cell-based therapy of TMJ osteoarthritis. *J Dent. Res.* 94, 1601–1609. doi: 10.1177/0022034515604621

Phinney, D. G., and Pittenger, M. F. (2017). Concise review: MSC-derived exosomes for cell-free therapy. *Stem Cells* 35, 851–858. doi: 10.1002/stem.2575

Qin, Y., Sun, R., Wu, C., Wang, L., and Zhang, C. (2016). Exosome: a novel approach to stimulate bone regeneration through regulation of osteogenesis and angiogenesis. *Int. J Mol. Sci.* 17:712. doi: 10.3390/ijms17050712

Ryu, J. M., and Han, H. J. (2015). Autotaxin-LPA axis regulates hMSC migration by adherent junction disruption and cytoskeletal rearrangement via LPAR1/3–dependent PKC/GSK3β/β–catenin and PKC/Rho GTPase pathways. *Stem Cells* 33, 819–832. doi: 10.1002/stem.1882

Tao, S., Yuan, T., Zhang, Y., Yin, W., Guo, S., and Zhang, C. (2017). Exosomes derived from miR-140-5p-overexpressing human synovial mesenchymal stem cells enhance cartilage tissue regeneration and prevent osteoarthritis of the knee in a rat model. *Theranostics* 7, 180–195. doi: 10.7150/thno.17133

Teo, A. Q. A., Wong, K. L., Shen, L., Lim, J. Y., Toh, W. S., Lee, E. H., et al. (2019). Equivalent 10-year outcomes after implantation of autologous bone marrow-derived mesenchymal stem cells versus autologous chondrocyte implantation for chondral defects of the knee. *Am. J Sports Med.* 47, 2881–2887. doi: 10.1177/0363546519867933

Théry, C., Witwer, K. W., Aikawa, E., Alcaraz, M. J., Anderson, J. D., Andriantsitohaina, R., et al. (2018). Minimal information for studies of extracellular vesicles 2018 (MISEV2018), a position statement of the international society for extracellular vesicles and update of the MISEV2014 guidelines. *J. Extracell Vesicles* 7:1535750.

Vonk, L. A., van Dooremalen, S. F. J., Liv, N., Klumperman, J., Coffer, P. J., Saris, D. B. F., et al. (2018). Mesenchymal stromal/stem cell-derived extracellular vesicles promote human cartilage regeneration in vitro. *Theranostics* 8, 906–920. doi: 10.7150/thno.20746

Wang, Y., Qin, X., Zhu, X., Chen, W., Zhang, J., and Chen, W. (2018). Oral Cancer-derived exosomal NAP1 enhances cytotoxicity of natural killer cells via the IRF-3 pathway. *Oral Oncol.* 76, 34–41. doi: 10.1016/j.oraloncology.2017.11.024

Wang, Y., Yu, D., Liu, Z., Zhou, F., Dai, J., Wu, B., et al. (2017). Exosomes from embryonic mesenchymal stem cells alleviate osteoarthritis through balancing synthesis and degradation of cartilage extracellular matrix. *Stem Cell Res.* 8:189.

Witwer, K. W., Van Balkom, B. W. M., Bruno, S., Choo, A., Dominici, M., Gimona, M., et al. (2019). Defining mesenchymal stromal cell (MSC)-derived small extracellular vesicles for therapeutic applications. *J. Extracell Vesicles* 8:1609206. doi: 10.1080/20013078.2019.1609206

Wu, M., Cai, J., Yu, Y., Hu, S., Wang, Y., and Wu, M. (2021). Therapeutic agents for the treatment of temporomandibular joint disorders: progress and perspective. *Front. Pharmacol.* 11:596099. doi: 10.3389/fphar.2020.596099

Yu, B., Zhang, X., and Li, X. (2014). Exosomes derived from mesenchymal stem cells. *Int. J Mol. Sci.* 15, 4142–4157.

Zhang, S., Chuah, S. J., Lai, R. C., Hui, J. H. P., Lim, S. K., and Toh, W. S. (2018). MSC exosomes mediate cartilage repair by enhancing proliferation, attenuating apoptosis and modulating immune reactivity. *Biomaterials* 156, 16–27. doi: 10.1016/j.biomaterials.2017.11.028

Zhang, S., Teo, K. Y. W., Chuah, S. J., Lai, R. C., Lim, S. K., and Toh, W. S. (2019). MSC exosomes alleviate temporomandibular joint osteoarthritis by attenuating inflammation and restoring matrix homeostasis. *Biomaterials* 200, 35–47. doi: 10.1016/j.biomaterials.2019.02.006

Conflict of Interest: The authors declare that the research was conducted in the absence of any commercial or financial relationships that could be construed as a potential conflict of interest.

frontiers in Cell and Developmental Biology

ORIGINAL RESEARCH
published: 02 July 2021
doi: 10.3389/fcell.2021.604756

Pyrroline-5-Carboxylate Reductase 1 Directs the Cartilage Protective and Regenerative Potential of Murphy Roths Large Mouse Mesenchymal Stem Cells

*Gautier Tejedor[1], Rafael Contreras-Lopez[1], Audrey Barthelaix[1], Maxime Ruiz[1], Danièle Noël[1,2], Frédéric De Ceuninck[3], Philippe Pastoureau[3], Patricia Luz-Crawford[4], Christian Jorgensen[1,2] and Farida Djouad[1]**

[1] IRMB, INSERM, University Montpellier, Montpellier, France, [2] CHU Montpellier, Montpellier, France, [3] Center for Therapeutic Innovation, Immuno-Inflammatory Disease, Institut de Recherches Servier, Croissy-sur-Seine, France, [4] Laboratorio de Inmunología Celular y Molecular, Facultad de Medicina, Universidad de los Andes, Santiago, Chile

OPEN ACCESS

Edited by:
Kazunori Shimomura, Osaka University, Japan

Reviewed by:
Camila Oliveira Rodini, University of São Paulo, Brazil
Ali Mobasheri, University of Oulu, Finland
Lucienne A. Vonk, University Medical Center Utrecht, Netherlands
Ran Xiao, Institute of Plastic Surgery (CAMS), China

***Correspondence:**
Farida Djouad
farida.djouad@inserm.fr

Specialty section:
This article was submitted to Stem Cell Research, a section of the journal Frontiers in Cell and Developmental Biology

Received: *10 September 2020*
Accepted: *03 June 2021*
Published: *02 July 2021*

Citation:
Tejedor G, Contreras-Lopez R, Barthelaix A, Ruiz M, Noël D, De Ceuninck F, Pastoureau P, Luz-Crawford P, Jorgensen C and Djouad F (2021) Pyrroline-5-Carboxylate Reductase 1 Directs the Cartilage Protective and Regenerative Potential of Murphy Roths Large Mouse Mesenchymal Stem Cells. Front. Cell Dev. Biol. 9:604756. doi: 10.3389/fcell.2021.604756

Murphy Roths Large (MRL) mice possess outstanding capacity to regenerate several tissues. In the present study, we investigated whether this regenerative potential could be associated with the intrinsic particularities possessed by their mesenchymal stem cells (MSCs). We demonstrated that MSCs derived from MRL mice (MRL MSCs) display a superior chondrogenic potential than do C57BL/6 MSC (BL6 MSCs). This higher chondrogenic potential of MRL MSCs was associated with a higher expression level of pyrroline-5-carboxylate reductase 1 (PYCR1), an enzyme that catalyzes the biosynthesis of proline, in MRL MSCs compared with BL6 MSCs. The knockdown of PYCR1 in MRL MSCs, using a specific small interfering RNA (siRNA), abolishes their chondrogenic potential. Moreover, we showed that PYCR1 silencing in MRL MSCs induced a metabolic switch from glycolysis to oxidative phosphorylation. In two *in vitro* chondrocyte models that reproduce the main features of osteoarthritis (OA) chondrocytes including a downregulation of chondrocyte markers, a significant decrease of PYCR1 was observed. A downregulation of chondrocyte markers was also observed by silencing PYCR1 in freshly isolated healthy chondrocytes. Regarding MSC chondroprotective properties on chondrocytes with OA features, we showed that MSCs silenced for PYCR1 failed to protect chondrocytes from a reduced expression of anabolic markers, while MSCs overexpressing PYCR1 exhibited an increased chondroprotective potential. Finally, using the ear punch model, we demonstrated that MRL MSCs induced a regenerative response in non-regenerating BL6 mice, while BL6 and MRL MSCs deficient for PYCR1 did not. In conclusion, our results provide evidence that MRL mouse regenerative potential is, in part, attributed to its MSCs that exhibit higher PYCR1-dependent glycolytic potential, differentiation capacities, chondroprotective abilities, and regenerative potential than BL6 MSCs.

Keywords: MRL mouse, regeneration, mesenchymal stem cells, PYCR1, metabolism, chondrogenesis, chondrocyte, chondroprotection

INTRODUCTION

The superhealer Murphy Roths Large (MRL) mice possess remarkable capacity to regenerate several musculoskeletal tissues such as ear wounds, amputated digits, and injured articular cartilage with no evidence of scarring (Clark et al., 1998; Fitzgerald et al., 2008; Ward et al., 2008; Kwiatkowski et al., 2016; Deng et al., 2019; Sinha et al., 2019). Although the mechanisms that underlie MRL mice regenerative potential have been intensively studied during the two last decades, the exact process involved is still poorly understood.

Cartilage regeneration requires an extensive tissue remodeling; and in this context, the capacity of MRL mice to induce a breakdown in the basement membrane, which permits the formation of a blastema and ear-hole closure, has been shown (Gourevitch et al., 2003). This process relies on an inflammatory response characterized by the recruitment and the activation of neutrophils and macrophages positive for MMP-2, MMP-9, TIMP-2, and TIMP-3 in the ear after injury (Gourevitch et al., 2003). Thus, during the regenerative healing, an inflammatory regenerative environment with an increased number of pro-inflammatory cells in the MRL mice compared with the non-regenerating C57BL/6 mice was observed (Gourevitch et al., 2014). Moreover, the high regenerative potential of MRL mice has been attributed, in part, to their mesenchymal stem cells (MSCs) or their secretome (Diekman et al., 2013; Wang et al., 2020). The intra-articular injection of MSCs derived either from C57BL/6 mouse (B6 MSCs) or MRL mouse (MRL MSCs) prevents the development of post-traumatic arthritis after fracture at a similar extent, although MRL MSCs exhibit a higher capacity for bone volume increase during repair (Diekman et al., 2013).

Thus, MSCs and in particular MRL MSCs, described for their capacity to promote tissue repair/regeneration based on their trophic functions, should be further deciphered to identify promising therapeutic factors for degenerative diseases such as osteoarthritis (OA). Indeed, MSCs regulate the inflammatory response and provide a regenerative environment either by releasing bioactive molecules that will promote the functions of endogenous stem cells or by repressing the function and proliferation of abnormally activated immune cells (Djouad et al., 2009; Maumus et al., 2013a; Pers et al., 2015, 2018). MSC functions rely on their metabolic status. MSCs, when undifferentiated, rely on glycolysis for energy such as most types of stem cells. Then, MSCs activate the mitochondrial process of oxidative phosphorylation (OXPHOS) when induced to differentiate into osteoblasts (Shum et al., 2016). During the early phase of adipogenesis, MSCs exhibit an increased oxygen consumption and mitochondrial activity indicating a metabolic switch from glycolysis to OXPHOS (Drehmer et al., 2016). In contrast to MSCs induced to differentiate into osteoblasts or adipocytes, MSCs that differentiate into chondrocytes present reduced O_2 consumption and OXPHOS, indicating an increased glycolysis (Pattappa et al., 2011). Therefore, given the pivotal role of MSC metabolic status on its functions, it is reasonable to hypothesize that the phenotypic and functional differences reported between MSCs from different sources (Elahi et al., 2016), species (Ren et al., 2009), or strain of mice (Peister et al., 2004; Bouffi et al., 2010) might be associated with metabolic differences. Moreover, the metabolic signature of MSCs is dynamic and changes with aging. Compared with rapid-aging MSCs, which display low regenerative capabilities, slow-aging MSCs exhibit a significantly higher glycolytic capacity and a higher potential for glucose uptake and reserve (Macrin et al., 2019).

In MRL mice, regeneration proceeds through the formation of a wound epithelium and a blastema-like structure, a heterogeneous cell mass that transiently forms adjacent to a specialized wound epithelium through migration and proliferation of local progenitor cells to give rise to distinct cell types organizing into the exact copy of the lost entity (for review, see Kumar and Brockes, 2012). Thus, regeneration such as tumorigenesis is characterized by a massive cell proliferation, tightly controlled in the case of regeneration and anarchic during tumorigenesis. Proline biosynthesis and metabolism play a central role in the metabolic reprogramming observed during tumorigenesis as well as during development (Phang and Liu, 2012; Phang et al., 2015; Phang, 2019). Pyrroline-5-carboxylate reductase 1 (PYCR1), a key enzyme for proline biosynthesis, is required for normal development. Indeed, PYCR1 mutation has been described in patients with multisystem disorders such as autosomal-recessive cutis laxa type 2 (ARCL2) characterized by premature aging, general developmental delay, and skin and joint laxity (Guernsey et al., 2009). Moreover, PYCR1 has been described to promote tumorigenesis. Indeed, PYCR1 inhibition using gene interference technology represses cell proliferation while promoting cell apoptosis in hepatocellular carcinoma (Zhuang et al., 2019). Similarly, PYCR1 silencing using small interfering RNA (siRNA) significantly inhibited cell proliferation and increased apoptosis of non-small cell lung cancer (Cai et al., 2018). PYCR1-dependent proline biosynthesis is pivotal for tumorigenesis by promoting cell proliferation and connecting the cycle of proline to glycolysis (Liu et al., 2015). However, the role of PYCR1 on MRL MSC regenerative process and metabolic status has never been investigated.

In this study, we addressed whether the regenerative potential of MRL mice could be attributed to the intrinsic properties of MSCs focusing on the role of PYCR1 in their therapeutic potential.

MATERIALS AND METHODS

Bioethics

Mice were housed and cared for in accordance with the Ethics Committee on Animal Research and Care of the Languedoc-Roussillon. We obtained the approval from the Ethical Committee for animal experimentation of the Languedoc-Roussillon before initiating the study (approval CEEA-LR-12117).

Mesenchymal Stem Cell Isolation and Expansion

Mesenchymal Stem Cells (MSCs) were isolated from MRL/Mpj and C57BL/6 mice bone marrow. Their expansion as well as

their phenotypic and functional characterization was performed as previously described after their spontaneous immortalization *in vitro* (Bouffi et al., 2010; Tejedor et al., 2021). The immortalized MSCs used in the present study between passages 15 and 20 exhibited the minimal criteria for defining MSCs (Dominici et al., 2006).

Chondrogenic Differentiation of Mesenchymal Stem Cell

Mesenchymal Stem Cell differentiation into chondrocytes was performed as previously described (Bouffi et al., 2010). Briefly, MSCs were induced to differentiate using the protocol of micropellets, which consist in seeding the MSCs at 2.5×10^5 cells/well in 96-Well Polypropylene, centrifuged during 5 min at 400 *g*. The micropellets were cultured during 21 days in a medium containing DMEM (Invitrogen), 100 U/ml of penicillin/streptomycin, 10 μM of sodium-pyruvate, 1.7 μM of ascorbic acid-2-phosphate, insulin-transferrin-selenium (ITS; Sigma-Aldrich Corp., St. Louis, MO, United States), and 1 ng/ml of human Transforming Growth Factor β3 (hTGF-β3; R&D Systems, Minneapolis, MN, United States) prior to being recovered for RT-qPCR analysis.

Chondrocyte Isolation and Expansion

Articular chondrocytes were isolated from femoral heads and knees of 3-day-old C57BL/6 mice and seeded at 25,000 cells/cm^2 in 12-well TPP culture plates (TPP Techno Plastic Products, Trasadingen, Switzerland) in culture medium for 5 days as previously described (Gosset et al., 2008). The chondrocytes were treated with IL-1β (1 ng/ml, R&D Systems) during 24 h to reproduce the main features of OA chondrocytes. Then, IL-1β was removed, and IL-1β-induced chondrocytes were cocultured during another 24 h with MSCs seeded in culture inserts and recovered to be analyzed by RT-qPCR.

Mesenchymal Stem Cell and Chondrocyte Transfection With Small Interfering RNA and Plasmids

Chondrocytes and MSCs were transfected at subconfluence (60%) with 200 nM of control siRNA (siCTL) or the siRNA against *Pycr1* (si*Pycr1*) (Silencer Select RNAi, Thermo Fisher Scientific, Illkirch, France) using oligofectamine reagent (Life Technologies, Courtaboeuf, France) according to the supplier's recommendations.

Mesenchymal Stem Cells were transfected at 60% of confluence with control or PYCR1-expressing plasmids (pCMV6 Entry; OriGene Technologies, Rockville, MD, United States) using lipofectamine reagent (Life Technologies, Courtaboeuf) according to the supplier's recommendations.

Proliferation Assay

Murphy Roths Large MSC proliferation rate was assessed using the PrestoBlue assay (Promega, Charbonnières-les-Bains, France) and following the manufacturer's recommendations. Briefly, MSCs were seeded at the density of 3,500 cells/cm^2 in a 6-well plate 48 h after transfection, in a proliferative medium containing DMEM supplemented with 10% of fetal calf serum, 100 U/ml of penicillin/streptomycin, and 2 mmol/ml of glutamine. After 3 days of culture, MRL MSCs were collected, and the number of viable cells was quantified.

RT-qPCR

Total RNA was isolated from each sample using RNeasy Mini Kit (Qiagen, Courtaboeuf, France), and the quantity and purity of the total RNA were determined by using a NanoDrop ND-1000 spectrophotometer (NanoDrop ND, Thermo Fisher Scientific). cDNA was synthesized by reverse transcribing 500 ng of RNA into cDNA using the SensiFAST cDNA synthesis kit (Bioline, Memphis, TN, United States). Quantitative PCR was performed using the SensiFAST^{TM} SYBR (Bioline) and a LightCycler® 480 Detection system, following the manufacturer's recommendations. Specific primers for *Acan*, *Adamts5*, *Col2B*, *Mmp13*, and *Pycr1* were designed using the Primer3 software (*Acan* F: GCGAGTCCAACTCTTCAAGC-R: GAAGTAGCAGGGGATGGTGA; *Adamts5* F: CTGCC TTCAAGGCAAATGTGTGG-R: CAATGGCGGTAGGCAAAC TGC; *Col2B* F: CTGGTGCTGCTGACGCT-R: GCCCT AATTTTCGGGCAT; *Mmp13* F: TCTGGATCACTCCAAGGAC C-R: ATCAGGAAGCATGAAATGGC; *Pycr1* F: GAAGAT GGCAGGCTTGTGGA-R: CTGGGAAGCCCCATTTTCAC. Data were normalized to the housekeeping gene ribosomal protein S9 (RPS9). Values were expressed as relative mRNA level of specific gene expression as obtained using the $2^{-\Delta Ct}$ method.

Oxygen Consumption Rate and Extracellular Acidification Rate Measurement

Oxygen consumption rate (OCR) and extracellular acidification rate (ECAR) were measured using the XFe96 analyzer (Seahorse Bioscience, North Billerica, MA, United States). Murine MSCs (20,000 cells/well) were plated on 96-well plates, in XF media (non-buffered DMEM medium, without glucose, 2 mM of L-glutamine, and 1 mM of sodium pyruvate) and analyzed according to the manufacturer's recommended protocol. Three independent readings were taken after each sequential injection. Instrumental background was measured in separate control wells using the same conditions without biologic material. ECAR/OCR ratio was calculated with the glycolytic rate and basal OCR.

Lactate Quantification

Lactate was measured in the supernatants of MSCs using the Lactate assay kit II (Sigma Aldrich) following manufacturer's instruction.

Ear Punch Model

C57BL/6 female mice with an age of 10 weeks were used for the model. At day 0, we performed a reproducible ear hole with a 2-mm punch through the center of the ear. For the different groups, we injected either 20 μl of phosphate-buffered saline (PBS) (untreated) or 3×10^5 MSCs/20 μl of PBS along the wound edge using a 10-μl Hamilton syringe connected with a 25-gauge needle (two injections were performed to inject a final

volume of 20 μl). Measurements of the ear wound area were performed at day 0 and day 35 from using the ImageJ software on ear pictures. For the untreated condition, we injected PBS.

Statistical Analysis

Generated *p*-values were obtained using the Mann–Whitney unpaired t-test, two-tailed, using GraphPad Prism 6 Software. Graphs show mean ± SEM. $p < 0.05$ (*), $p < 0.01$ (**), or $p < 0.001$ (***) was considered statistically significant.

RESULTS

Pycr1 Is Highly Expressed in Murphy Roths Large Mesenchymal Stem Cell and Progressively Increased During Chondrogenesis

We first studied the expression level of *Pycr1* in adult MRL MSCs as compared with MSCs derived from BL6 mice by RT-qPCR. We found that *Pycr1* mRNA expression was significantly higher in MRL MSCs than in BL6 MSCs (**Figure 1A**). Then, since MSCs undergoing chondrogenesis rely on proline addition in the chondrogenic media and exhibit a metabolic shift toward glycolysis (Pattappa et al., 2011), we investigated whether *Pycr1* expression could be modulated during the induction of MSC differentiation into chondrocytes. *Pycr1* expression level was progressively increased during MSC chondrogenesis to reach a significantly higher level from D14 than undifferentiated MSCs (**Figure 1B**). This increased expression level of *Pycr1* paralleled the well-described increased expression level of the chondrocyte markers such as type IIB collagen (*Col2B*) and aggrecan (*Acan*) during MSC differentiation into chondrocytes (**Figure 1C**). Moreover, at day 21, we found that MRL MSCs induced to differentiate into chondrocytes express a higher level of *Col2B* and *Acan* than BL6 MSCs. This suggests that MRL MSCs exhibit a higher chondrogenic potential than BL6 MSCs (**Figure 1C**).

Pycr1 Is Necessary for Mesenchymal Stem Cell Chondrogenic Potential

With regard to the increased expression of *Pycr1* during chondrogenesis, in particular for MRL MSCs, we next asked whether MSC chondrogenic differentiation could be regulated by a cell-autonomous function of *PYCR1*. To address that question, we used the siRNA approach to knock down the expression of *Pycr1* in MRL MSCs. Forty-eight hours post-transfection (at day 0 of MSC chondrogenesis) of MSCs with a siRNA against *Pycr1* (siPycr1), *Pycr1* expression was reduced by 70% compared with the MSCs transfected with the control siRNA (siCTL) (**Figure 2A**). The silencing of *Pycr1* in MRL MSCs did not modify their proliferation rate (**Figure 2B**). Then, MSC chondrogenic differentiation was induced by culture in micropellet in the presence of TGFβ3 for 21 days. While we observed a significant increase of *Pycr1* during chondrogenesis in MSCs transfected with the siCTL, *Pycr1* expression level did not change within differentiating MSCs transfected with si*Pycr1* (**Figure 2A**). Moreover, we assessed whether the downregulation of *Pycr1* altered the chondrogenic differentiation of MSCs; and we found, at early stages, that si*Pycr1*-transfected MSCs formed flat micropellets with a reduced density as compared with the micropellets formed with MSCs transfected with the si*Ctl* (data not shown). Moreover, *Pycr1* knockdown significantly reduced the expression, *Col2B*, a mature chondrocyte marker, by day 21 (**Figure 2C**).

Pycr1 Is Necessary for Murphy Roths Large Mesenchymal Stem Cell Glycolytic Metabolism

PYCR1 activity has been linked to the glycolytic pathway through the production of NAD^+ (Liu et al., 2015). Therefore, we wondered whether the high expression of *Pycr1* in MRL MSCs could regulate MRL MSC metabolism. We quantified, in both BL6 MSCs and MRL MSC, the OCR (**Figure 3A**) and their ECAR (**Figure 3B**), which are associated with OXPHOS and glycolysis, respectively. Overall, MRL MSCs showed an active glycolysis, which was partially controlled by *Pycr1* expression (**Figures 3A,B**). Indeed, the knockdown of *Pycr1* in MRL MSCs induces a switch from glycolysis to OXPHOS as revealed by the ratio of ECAR to OCR, which was also significantly lower in MRL MSCs deficient for *Pycr1* than in MSCs transfected with siCTL (**Figure 3C**). Then, we evaluated the lactate production (**Figure 3D**). In contrast, the knockdown of *Pycr1* in BL6 MSCs did not modify their metabolism (**Figure 3E**). Our results showed *Pycr1* downregulation induces a reprogramming of MRL MSC metabolism specifically associated with a decreased lactate concentration in the extracellular media of MRL MSCs deficient for *Pycr1* (**Figure 3D**). Altogether, these results provide evidence for the role of *Pycr1* in the cytosolic glycolytic activity in MRL MSCs.

Pycr1 Is Necessary for the Maintenance of Chondrocyte Phenotype

Articular chondrocytes are exposed to low O_2 microenvironment *in vivo* and generate ATP by glycolysis (Lane et al., 2015). Under physiological conditions, chondrocytes rely on glycolysis to meet the cellular energy requirements, but when challenged with a stress or in OA, chondrocytes modify their mitochondrial respiration. This metabolic flexibility of chondrocytes is critical for their survival when stressed (Lane et al., 2015). We thus wondered whether the expression level of *Pycr1*, critical for cell glycolytic metabolism and function, could be modulated in chondrocytes exposed to different stresses. First, we assessed the modulation of *Pycr1* expression level in an *in vitro* model of chondrocyte inflammation that consists in treating freshly isolated chondrocytes with IL-1β (Ruiz et al., 2020). IL-1β treatment induced a chondrocyte model that reproduces the main OA chondrocyte features, namely, decreased expression of anabolic markers and increased expression of catabolic and inflammatory markers. In this model, IL-1β-treated chondrocytes exhibit a reduced expression of *Col2B* and *Acan* and increased expression of *Mmp13* and *Adamts5* (Ruiz et al., 2020). We found that the treatment of chondrocytes with IL-1β induced a significant downregulation of *Pycr1* (**Figure 4A**) similar to the

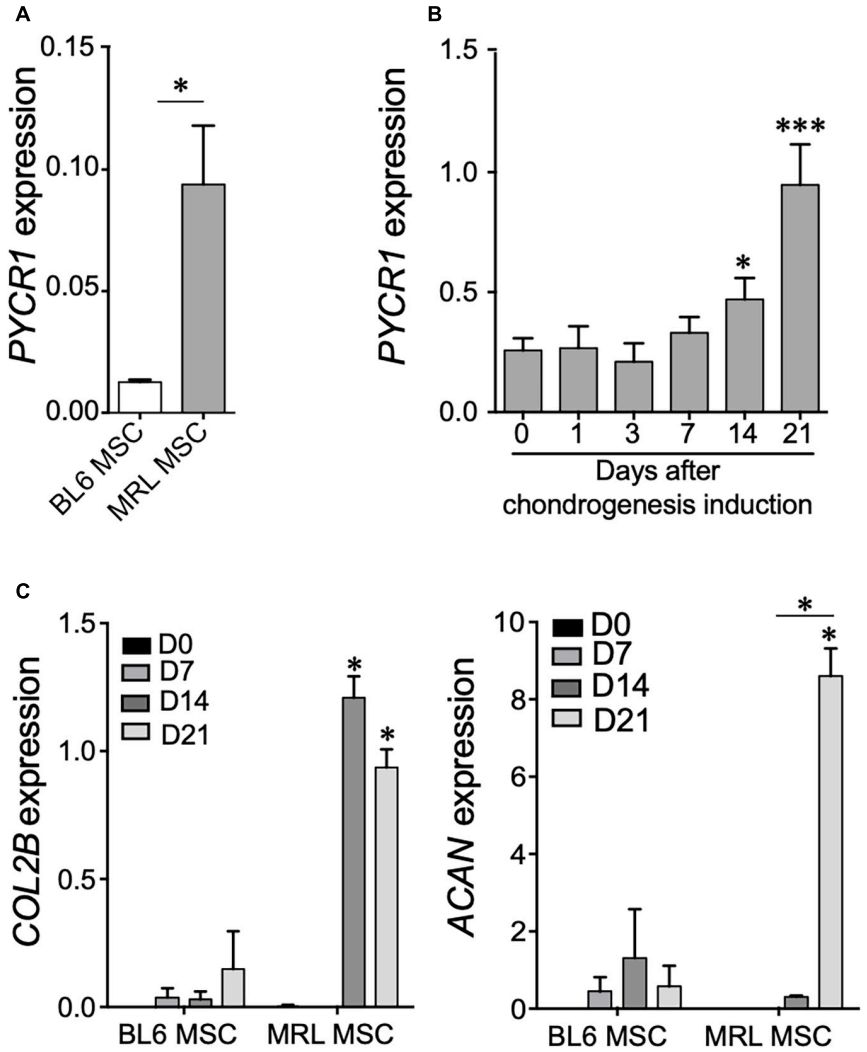

FIGURE 1 | *Pycr1* is highly expressed in MRL MSCs and in MSC-derived chondrocytes. **(A)** *Pycr1* mRNA expression level in MRL MSCs and BL6 MSCs assessed by RT-qPCR. **(B)** *Pycr1* mRNA expression level in MRL MSCs at different time points of the chondrogenic differentiation of MRL MSCs induced in pellets by TGFβ3 assessed by RT-qPCR. **(C)** mRNA expression levels of chondrocyte markers, *Col2B* and *Acan*, in BL6 and MRL MSCs at different time points of the chondrogenic differentiation. Results represent the mean ± SEM of three independent experiments. Results represent the mean ± SEM of three independent experiments. Statistics: Mann–Whitney test, two-tailed. When not indicated day 0 (0) versus day 14 (14) or 21 (21), p-values < 0.05 (*) or $p < 0.001$ (***). MRL, Murphy Roths Large; MSCs, mesenchymal stem cells.

one observed after the transfection of the chondrocytes with si*Pycr1* (**Figure 4B**). *Pycr1* silencing in articular chondrocytes using the si*Pycr1* resulted in a downregulation of the chondrocyte anabolic marker *Acan* (**Figure 4C**). No effect was observed on chondrocyte catabolic markers *Mmp13* and *Adamts5* (**Figure 4D**). This result suggests that *Pycr1* is essential to maintain chondrocyte phenotype. To confirm a correlation between the decreased expression level of *Pycr1* and the loss of chondrocyte phenotype, we then used the model of dedifferentiated chondrocytes (Monteagudo et al., 2017). In this model, chondrocytes progressively dedifferentiate upon serial passages in culture as revealed by the reduced expression level of chondrocyte anabolic markers (Monteagudo et al., 2017). Here, we found that in parallel to the progressive downregulation of *Col2B* and *Acan* in chondrocytes undergoing serial passages (**Figure 4E**), *Pycr1* was also progressively lost (**Figure 4F**).

Altogether, these results reveal that *Pycr1* loss parallels the loss of chondrocyte anabolic markers that characterize chondrocytes with OA features.

Pycr1 Is Necessary for the Chondroprotective Potential of Murphy Roths Large Mesenchymal Stem Cell on the *in vitro* Model of Chondrocyte Inflammation

We then asked whether *PYCR1* could be required for the chondroprotective properties of MSCs (Maumus et al., 2013b;

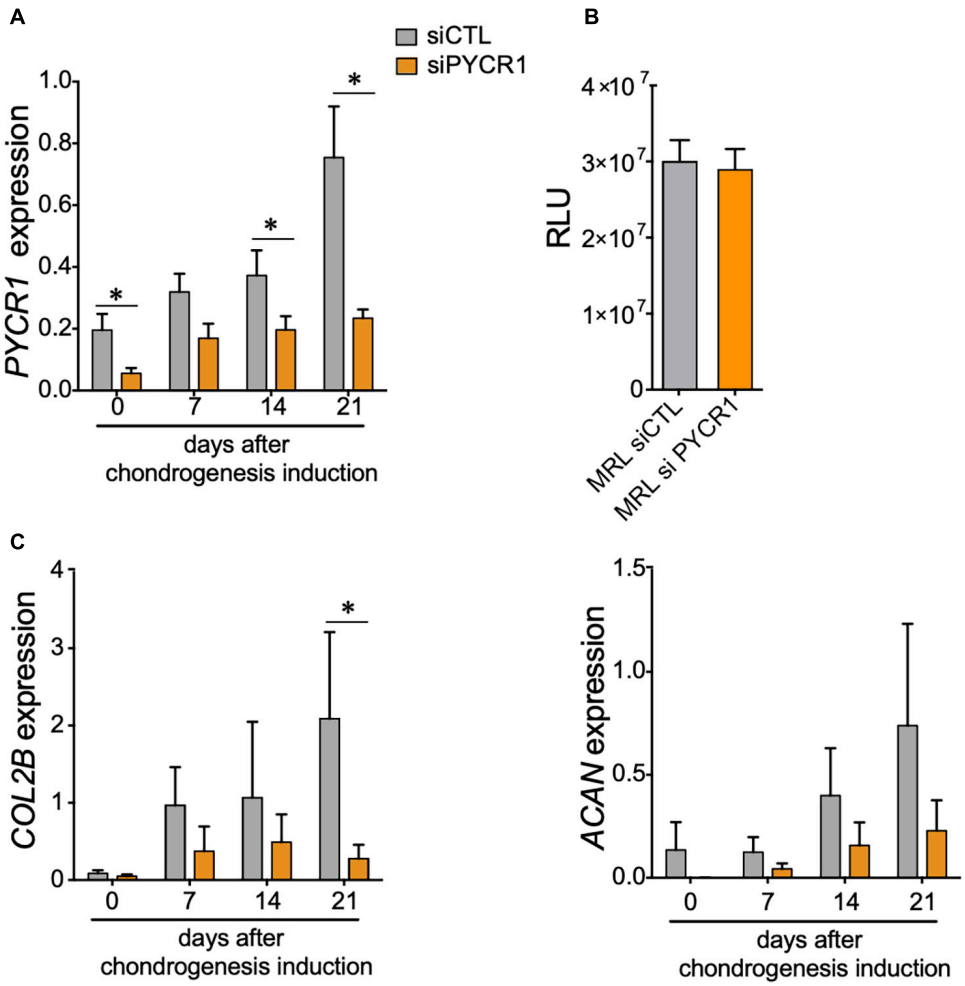

FIGURE 2 | *Pycr1* is required for the chondrogenic potential of MRL MSCs. **(A)** *Pycr1* mRNA expression level in MRL MSCs transfected with either a control siRNA (siCTL) or a siRNA against *Pycr1* (siPYCR1) at different time points of the chondrogenic differentiation induced in pellets by TGFβ3. **(B)** Proliferation rate of MRL MSCs transfected with either a control siRNA (siCTL) or a siRNA against *Pycr1* (siPYCR1). **(C)** mRNA expression levels of chondrocyte markers, *Col2B* and *Acan*, in MRL MSCs transfected with either siCTL or siPYCR1 at different time points of the chondrogenic differentiation induced in pellets by TGFβ3. Results represent the mean ± SEM of three independent experiments. Statistics: Mann–Whitney test, two-tailed. p-Values < 0.05 (*). MRL, Murphy Roths Large; MSCs, mesenchymal stem cells; siRNA, small interfering RNA.

Ruiz et al., 2020). To that end, we tested the effect of *Pycr1* silencing on MRL MSC chondroprotective effects on the IL-1β-induced chondrocyte model. While coculture of IL-1β-treated chondrocytes with MRL MSCs transfected with a si*Ctl* (MRL MSC_{siCTL}) significantly upregulated the expression of chondrocyte anabolic markers including *Col2B* and *Acan*, MRL MSCs silenced for *Pycr1* (MRL $MSC_{siPYCR1}$) did not (**Figures 5A,B**). Conversely, we asked whether *Pycr1* overexpression on MRL MSCs would further enhance their chondroprotective properties on IL-1β-treated chondrocytes. To that end, MRL MSCs were transfected with either a plasmid encoding *Pycr1* (MRL $MSC_{plPYCR1}$) or an empty vector control (MRL MSC_{plCTL}) prior to being cocultured with OA-like chondrocytes (**Figure 5A**). *Pycr1* was expressed 80-fold more in MRL $MSC_{plPYCR1}$ than in MRL MSC_{plCTL} (**Figure 5C**). Coculture of IL-1β-treated chondrocytes with MRL MSCs overexpressing *Pycr1* significantly upregulated the expression of chondrocyte anabolic markers *Col2B* and *Acan* (**Figure 5C**) as compared with the cocultures with MRL MSC_{plCTL}. Altogether, these results indicate that *Pycr1* contributes to MRL MSC pro-anabolic function on chondrocytes.

Pycr1 Is Necessary for the Regenerative Potential of Murphy Roths Large Mesenchymal Stem Cell in an Ear Punch Model

The MRL mouse has been well described for its remarkable capacity for cartilaginous wound closure and regeneration (Clark et al., 1998). Two−millimeter punch wounds made into MRL/MpJ mice ears closed with regeneration after 30 days, whereas they did not close in the C57BL/6 mice. Histological analysis revealed a normal angiogenesis and chondrogenesis of the ear in contrast to control BL6 mice, which have unclosed ear

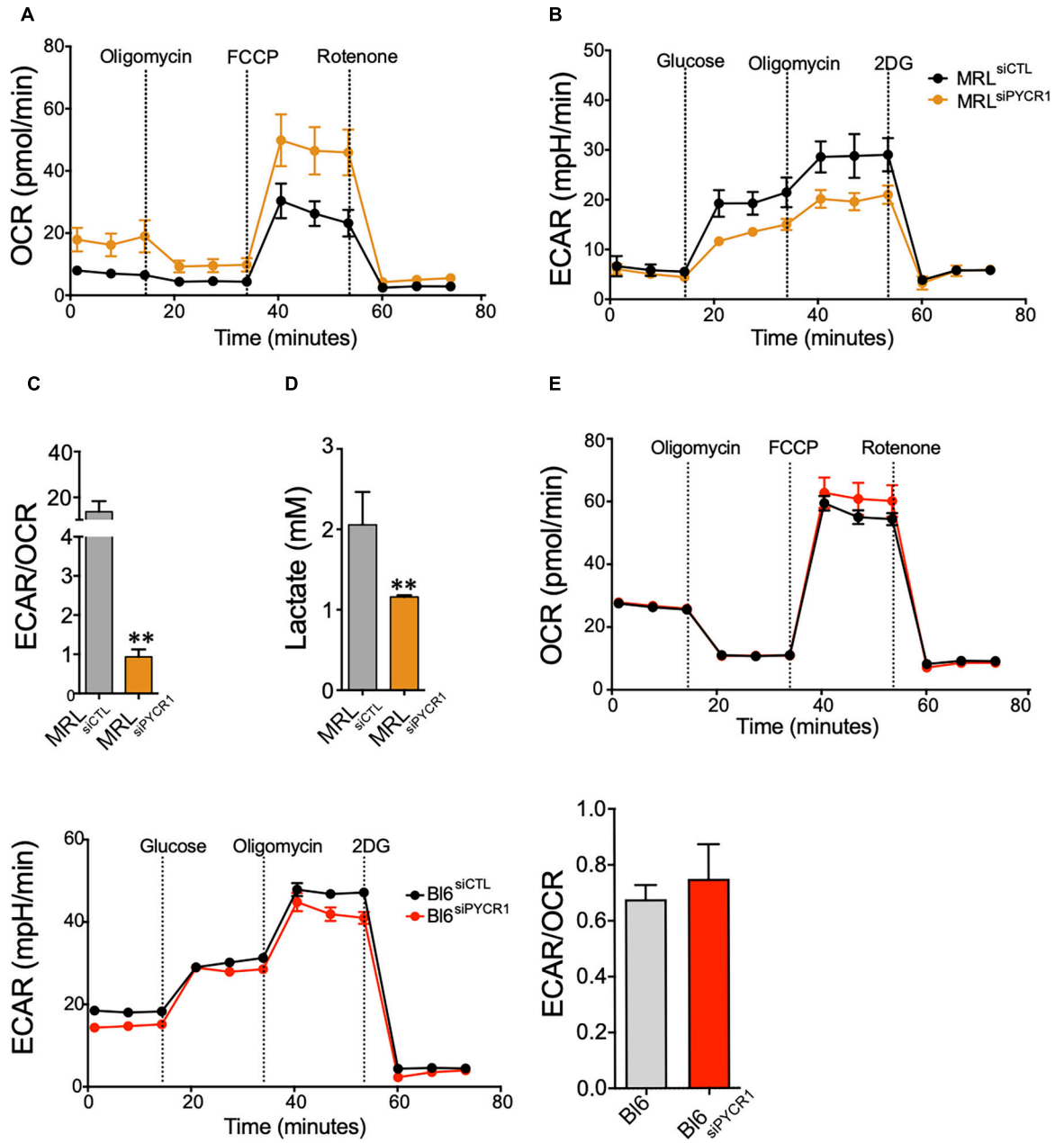

FIGURE 3 | *Pycr1* induces a glycolytic metabolism on MRL MSCs. **(A,B)** The metabolic activity of MRL MSC siCTL (MRL MSCs transfected with the siCTL siRNA) control (black line) and siPYCR1 (orange line) was evaluated by measuring the OCR **(A)** or the ECAR **(B)** with Seahorse analyzer. The knockdown of *Pycr1* affects both the OCR and ECAR profiles, which translates to a preferentially oxidative metabolism. **(C)** The ratio between glycolytic rate and basal OCR confirms a significant decline in the glycolytic metabolism of MRL siPYCR1. **(D)** Similarly, we observed a significant decrease in lactate concentration in the extracellular media, as a result of the diminished glycolytic activity on MRL siPYCR1, compared with MRL siCTL. Results represent the mean ± SEM of three independent experiments with five different replicates each time. Statistics: Mann–Whitney unpaired *t*-test. **: $p < 0.01$. **(E)** The metabolic activity of BL6 MSC siCTL and BL6 MSC siPYCR1 was evaluated by measuring the OCR, ECAR and the ratio ECAR/OCR with Seahorse analyzer. MRL, Murphy Roths Large; MSCs, mesenchymal stem cell; siRNA, small interfering RNA.

holes (Clark et al., 1998). Going further, other studies have shown that the ear holes regenerate by the formation of a blastema−like structure, a highly proliferative structure composed of progenitor cells, leading to a scar-free vascularized tissue made of collagen, hair follicles, sebaceous glands, and even cartilage (Gawriluk et al., 2016). Since MRL MSCs have enhanced chondrogenic and chondroprotective properties as compared with BL6 MSCs, we investigated, *in vivo*, whether the regenerative potential of MRL mice was due to the intrinsic regenerative properties of their MSCs. To that end, non-regenerating BL6 mice were subjected

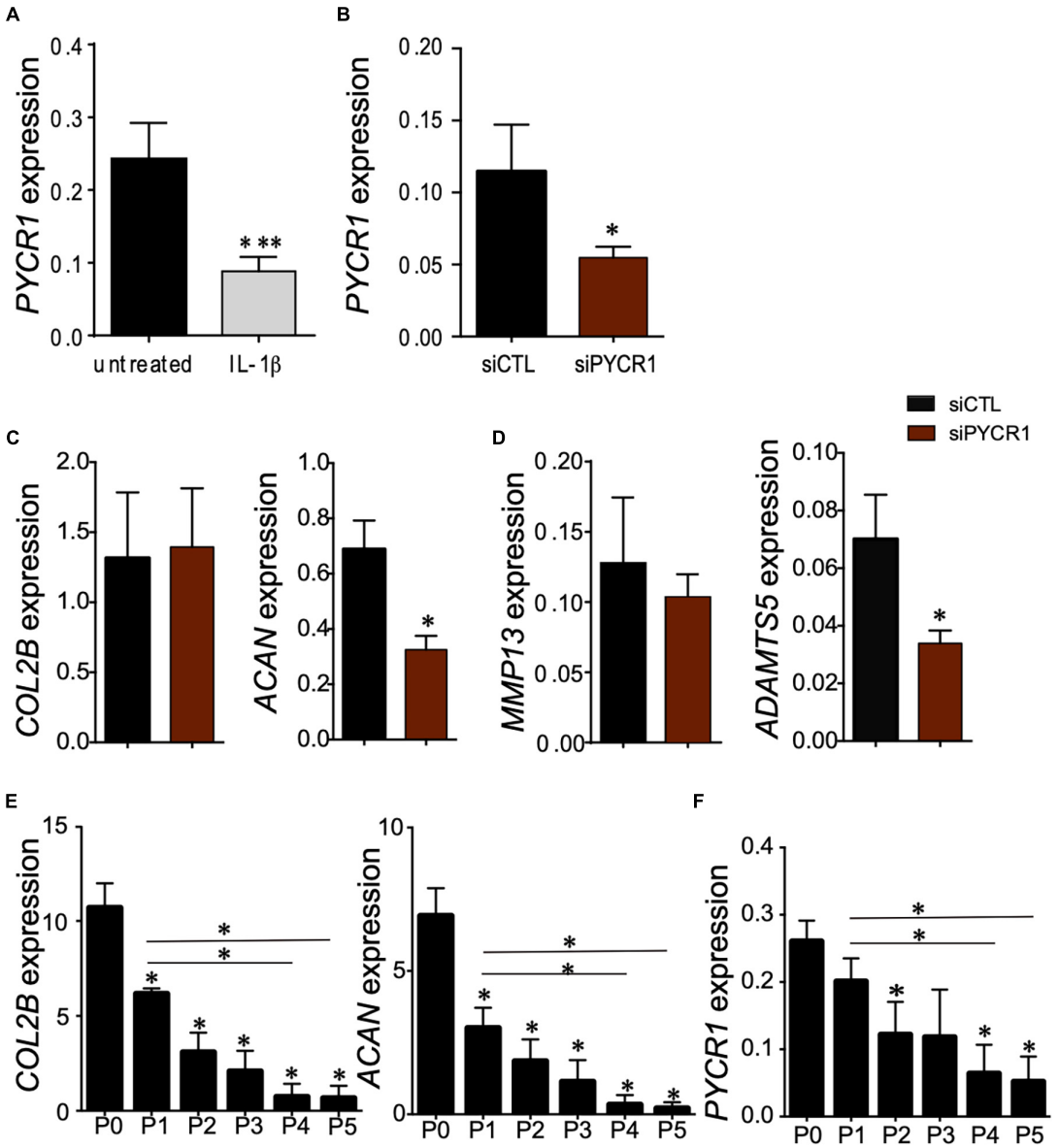

FIGURE 4 | *Pycr1* silencing, a novel method to generate mouse IL-1β-treated chondrocytes. **(A)** Scheme showing the generation of chondrocytes with OA features with IL-1β treatment of freshly isolated chondrocytes. RT-qPCR analysis of *Pycr1* expression level in untreated healthy chondrocytes (untreated) and in IL-1β-treated chondrocytes (IL-1β). **(B)** RT-qPCR analysis of *Pycr1* expression level in chondrocytes transfected with a siRNA against PCYR1 (siPYCR1). **(C)** RT-qPCR analysis of the chondrocyte anabolic markers *Col2B* and *Acan* and **(D)** chondrocyte catabolic markers *Mmp13* and *Adamts5* in chondrocytes transfected with a control siRNA (siCTL) or a siRNA against *Pycr1* (siPYCR1). **(E)** RT-qPCR analysis of the chondrocyte anabolic markers *Col2B* and *Acan* and **(F)** *Pycr1* in mouse chondrocytes induced differently after serial passages in culture [from passage 0 (P0) to passage 5 (P5)]. Results represent the mean ± SEM of three independent experiments. Statistics: Mann–Whitney test, two-tailed. When not indicated P0 versus P1, P2, P3, P4, and P5. p-values < 0.05 (*). OA, osteoarthritis; siRNA, small interfering RNA.

to a through-and-through hole generated in the ear pinna using a 2-mm biopsy punch. Then, the wounded mice were either untreated or treated with MSCs injected along the wound edge. Measurements of the ear punch wound area at day 35 revealed that MRL MSCs induced a regenerative process leading to a significant decrease of the wound size, 37% or 36% reduction in area, as compared with the untreated mice (PBS injected) or mice treated with BL6 MSCs, respectively (**Figures 6A,B**). Then, we assessed, whether this regenerative process mediated by MRL MSCs was associated with their high expression level of *Pycr1*. The ear punch wound area of BL6 mice treated with MRL MSCs deficient for *Pycr1* (MRL MSC si_{PYCR1}) did not show any difference with the untreated or BL6 MSCs treated mice (**Figures 6A,B**). Overall, this finding suggests that the *in vivo* regenerative potential of MRL MSCs that we showed in BL6 mice depends on *Pycr1* expression level.

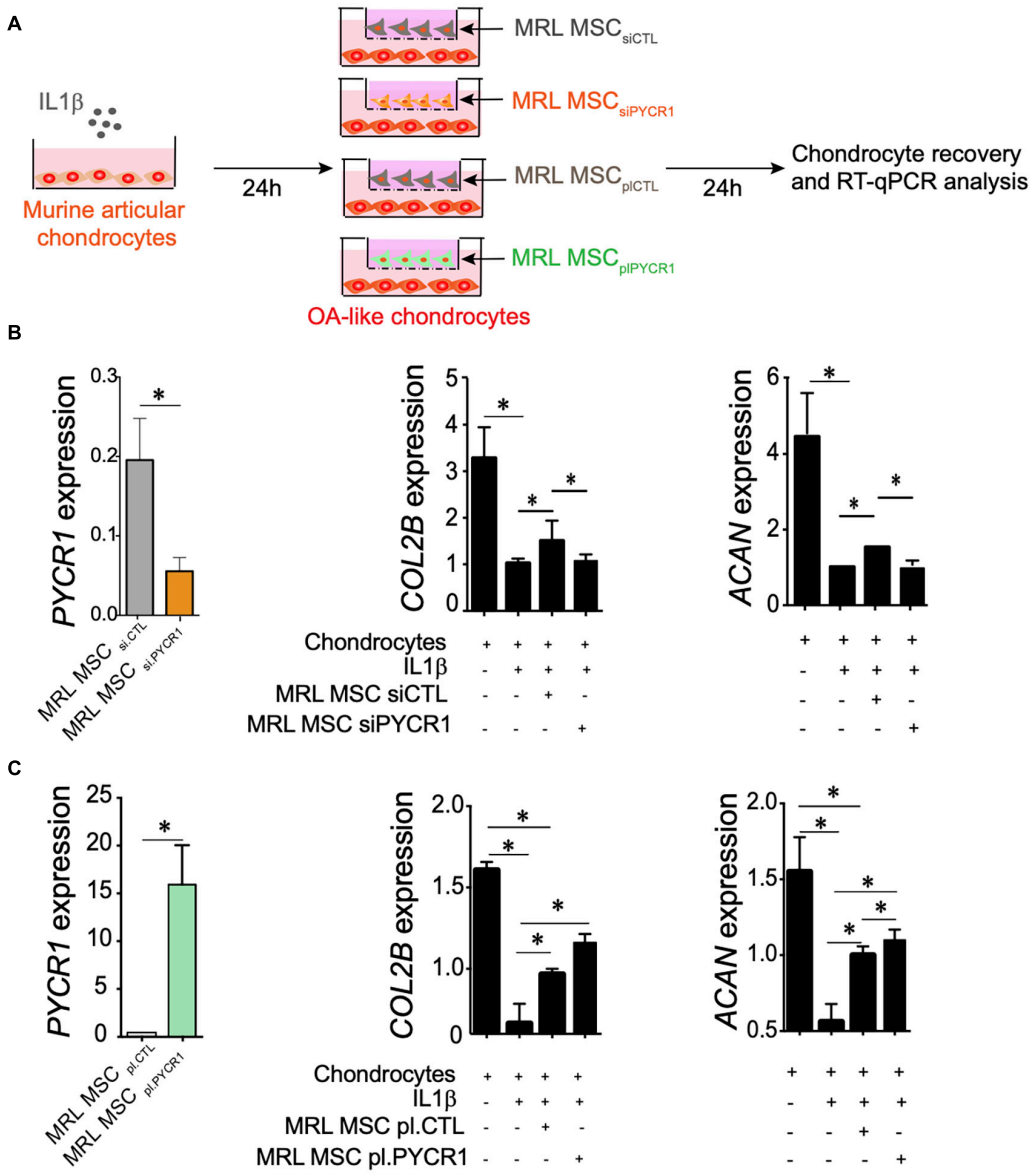

FIGURE 5 | *Pycr1* regulates the chondroprotective abilities of MRL MSCs. **(A)** Scheme illustrating the different coculture conditions using chondrocytes with OA features induced by a 24-h incubation of freshly isolated chondrocytes with IL-1β and MRL MSCs. MRL MSCs were either transfected with a control siRNA (MRL MSC_{siCTL}), a siRNA against *Pycr1* (MRL $MSC_{siPYCR1}$), an empty vector control (MRL MSC_{plCTL}), or a plasmid encoding *Pycr1* (MRL$MSC_{plPYCR1}$). IL-1β-treated chondrocytes and MRL MSCs were cultured during 24 h before to be collected for RT-qPCR analysis. **(B)** RT-qPCR analysis of different chondrocyte markers, *Col2B* and *Acan*, in healthy chondrocytes and IL-1β-treated chondrocytes cultured alone or with either MRL MSC_{siCTL} or MRL $MSC_{siPYCR1}$. **(C)** RT-qPCR analysis of different chondrocyte markers, *Col2B* and *Acan*, in healthy chondrocytes and IL-1β-treated chondrocytes cultured alone or with either MRL MSC_{plCTL} or MRL $MSC_{plPYCR1}$. Results represent the mean ± SEM obtained with three biological replicates. Statistics: Mann–Whitney test, two-tailed. *p*-Values < 0.05 (*). MRL, Murphy Roths Large; MSC, mesenchymal stem cell; OA, osteoarthritis.

DISCUSSION

This study provides the first evidence that MRL MSCs exhibit enhanced chondrogenic, chondroprotective, and regenerative properties as compared with BL6 MSCs in a *Pycr1*-dependent manner.

We found that MRL MSCs induce toward the chondrogenic lineage differentiate faster and better than BL6 MSCs as revealed by the high expression level of chondrocyte markers as soon as day 14 of the MSC differentiation process that takes normally 21 days for MSCs. Herein, we evidenced a progressive increase in the expression level of *Pycr1* during the course of chondrogenic differentiation of MSCs and that the loss of *Pycr1* in MRL MSCs abolishes their chondrogenic potential as revealed by the decreased expression levels of chondrogenic markers that we studied at the mRNA expression level since we have

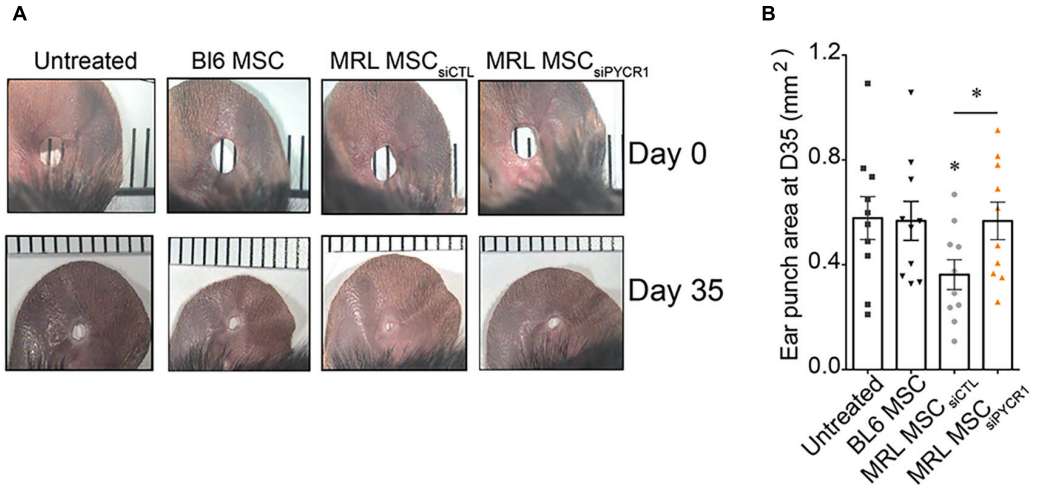

FIGURE 6 | MRL MSCs induce tissue regeneration in BL6 mice in a *Pycr1*-dependent manner. **(A)** Pictures of the ear holes at day 0 and day 35 after wounding. The punch holes in the ears of BL6 mice were either untreated (untreated) or treated with MSCs. BL6 MSCs and MRL MSCs transfected with either siCTL (MRL MSC_{siCTL}) or siPYCR1 (MRL $MSC_{siPYCR1}$) were injected at the wound edges. **(B)** Quantification of the ear punch hole closure at day 35 (D35) using the ImageJ program to define the ear punch area. Results represent the mean ± SEM. N_{mice} = 10 per condition, Mann–Whitney test, two-tailed, when not indicated untreated versus MRL MSC_{siCTL}, p-values < 0.05 (*). MRL, Murphy Roths Large; MSC, mesenchymal stem cell.

previously shown a nice correlation between mRNA and protein of chondrogenic markers (Bouffi et al., 2010). This latter effect might be due, in part, to the fact that PYCR1 is the final enzyme in the biosynthesis of proline that makes up approximately 15% of collagen accounting for about two-thirds of articular cartilage dry weight. Proline, with also the post-translational modifications, are necessary for appropriate collagen synthesis, folding, and secretion (Guzy and Redente, 2021; Stum et al., 2021). Thus, further research is needed to determine the effect of *Pycr1* downregulation on the capacity of MSCs undergoing chondrogenesis to produce reduced level of PYCR1 and collagen. Of note, since a similar regulation between mRNA and protein levels of PYCR1 has been previously described (Huang et al., 2018; Weijin et al., 2019; Xiao et al., 2020), we mainly relied on the mRNA expression level of *Pycr1* to confirm *Pycr1* silencing and overexpression in the present study. Moreover, *PYCR1* mutations are deleterious for mitochondrial function and responsible for progeroid changes in connective tissues (Reversade et al., 2009). Thus, *Pycr1* silencing in MRL MSCs might have antagonized the intrinsic properties of MRL mouse cells that have retained some features of embryonic cells including their metabolism and the expression of stem cell markers such as *Nanog*, *Islet-1*, and *Sox2* (Naviaux et al., 2009). The retention of such embryonic features in adulthood is rare in mammals and might confer to MRL MSCs their enhanced differentiation potential in a *Pycr1*-dependent manner.

Moreover, PYCR1 participates to the upregulation of glycolysis through proline biosynthesis (Liu et al., 2015). We therefore studied the metabolism of MSCs derived from the superhealer MRL mice (MRL MSCs) and found a high glycolytic metabolism in those cells. Moreover, in loss-of-function experiments, we demonstrated that the glycolytic status of MRL MSCs is associated with a high expression level of *Pycr1*. Indeed, *Pycr1* silencing significantly reduces the ratios of ECAR to OCR that indicates a preference for OXPHOS over glycolysis in MRL MSCs deficient for *Pycr1*. Moreover, the lactate production by MRL MSCs silenced for *Pycr1* was also significantly reduced. This is in accordance with the capacity of PYCR1 to increase glycolysis (Liu et al., 2015) and the reduced O_2 consumption and OXPHOS in MSCs during chondrogenesis, indicating a shift toward increased glycolysis (for review, see Shyh-Chang et al., 2013; Mobasheri et al., 2017; Zheng et al., 2021). During chondrogenesis, a rapid and significative reduction in oxygen consumption has been reported in MSCs not due to the chondrogenic differentiation *per se* but rather to the 3D pellet culture conditions. The expression levels of genes associated with glycolysis increased in MSCs that adopt a glycolytic metabolism and differentiate into chondrocytes (Pattappa et al., 2011). Moreover, under hypoxia that induces a high glycolytic metabolism, chondrogenesis is enhanced (Lennon et al., 2001; Wang et al., 2005; Xu et al., 2007; Markway et al., 2010). Altogether, these results suggest that MRL MSCs are more prone to differentiate into chondrocytes presumably due to their PYCR1-dependent glycolytic status.

Mature chondrocytes are highly glycolytic with a minimal oxygen consumption (Rajpurohit et al., 1996; Heywood and Lee, 2008). Downregulation of the chondrocyte markers such as *Col2B* and *Acan* in chondrocytes undergoing serial passages is correlated with *Pycr1* expression progressive loss. This was confirmed using another model of chondrocyte inflammation that induces their osteoarthritic-like dedifferentiation characterized by a loss of chondrocyte marker expression (Benya et al., 1978; Monteagudo et al., 2017), increasing their oxygen consumption and their OXPHOS metabolism (Heywood and Lee, 2008). Indeed, we demonstrated that in parallel to the progressive acquisition of an OA-like phenotype upon

IL-1β exposure, chondrocytes exhibit a reduced expression of *Pycr1*. Going further, we showed that *Pycr1* silencing led to a significant decrease of chondrocyte markers confirming that *Pycr1* expression in articular chondrocytes is required for a functional phenotype. Altogether, our results show that PCYR1, pivotal for cell glycolytic metabolism, is required for healthy and functional articular chondrocytes. These results are in line with the effect induced by the treatment of chondrocytes with 2-deoxyglucose (2-DG), a chemical inhibitor of glycolysis, that highly reduces *Col2B* expression levels supporting the pivotal role of glycolytic energy production for cartilage matrix synthesis (Pfander et al., 2003, 2006).

Knockdown of *Pycr1* in MSCs also altered MSC chondroprotective properties on IL-1β-treated chondrocytes. We showed that while MRL MSCs protect IL-1β-treated chondrocytes from a loss of anabolic markers (*Acan* and *Col2B*), MRL MSCs silenced *Pycr1* did not. Moreover, we showed that *Pycr1* enhances the chondroprotective potential of MSCs as revealed by higher expression levels of anabolic markers in IL-1β-treated chondrocytes cocultured with MSCs overexpressing *Pycr1* as compared with IL-1β-treated chondrocyte coculture with control MSCs. Thus, we evidenced that the chondroprotective effect of MRL MSCs relies on *Pycr1* expression. The cytoprotective effect of MSCs has been associated with their glycolytic phenotype. Enhancement of glycolysis promotes MSC survival (Yang et al., 2019). The glycolytic metabolic state maintains MSC homeostasis by limiting reactive oxygen species (ROS) production through the cytoprotective effect of high glycolytic flux that enhances generation of antioxidant precursors (Galluzzi et al., 2013; Yuan et al., 2019). Our results suggest that *Pycr1* is pivotal for the chondroprotective high glycolytic flux mediated by MRL MSC.

The activation of glycolysis has been shown to play a pivotal role in regeneration (Magadum and Engel, 2018). The regenerative abilities of MRL mice have been associated with an increased glycolysis and a reduced OXPHOS (Naviaux et al., 2009). Moreover, during planarian tissue regeneration, the activation of glycolysis has been reported (Osuma et al., 2018). Glycolysis inhibition repressed regeneration of mouse neonatal hearts (Wang et al., 2018) and adult skeletal muscle (Fu et al., 2015). However, although regeneration is associated with glycolysis, the underlying mechanisms are poorly understood. Here, we show that MRL MSCs have enhanced regenerative properties and that their injection at the wound edges stimulates the regenerative process in non-regenerating BL6 mice. This regenerative potential exhibited by MRL MSCs required the expression of *Pycr1*, previously described to play a critical role in energy metabolism.

In conclusion, our findings demonstrate that the enhanced regenerative potential of MRL mice is attributed, in part, to their MSCs that exhibit PYCR1-dependent higher glycolytic potential, differentiation capacities, chondroprotective abilities, and regenerative properties than BL6 MSCs.

DATA AVAILABILITY STATEMENT

The original contributions presented in the study are included in the article/supplementary material, further inquiries can be directed to the corresponding author/s.

ETHICS STATEMENT

The animal study was reviewed and approved by Ethical Committee for animal experimentation of the Languedoc-Roussillon before to initiate the study (approval CEEA−LR−12117).

AUTHOR CONTRIBUTIONS

FD designed the all project and the experiments. DN, FDC, PP, PL-C, and CJ contributed to design and interpreted the data for the work. GT, RC-L, AB, PL-C, and MR performed the experiments and analyzed the results. FD wrote the manuscript with the input of PL-C and CJ. All authors revised and gave final approval of the manuscript.

FUNDING

This work was supported by INSERM, the University of Montpellier. We thank Servier for financial support of this project.

ACKNOWLEDGMENTS

We thank the MRI facility for their assistance and SMARTY platform and Network of Animal Facilities of Montpellier.

REFERENCES

Benya, P. D., Padilla, S. R., and Nimni, M. E. (1978). Independent regulation of collagen types by chondrocytes during the loss of differentiated function in culture. *Cell* 15, 1313–1321. doi: 10.1016/0092-8674(78)90056-9

Bouffi, C., Bony, C., Courties, G., Jorgensen, C., and Noel, D. (2010). IL-6-dependent PGE2 secretion by mesenchymal stem cells inhibits local inflammation in experimental arthritis. *PLoS One* 5:e14247. doi: 10.1371/journal.pone.0014247

Cai, F., Miao, Y., Liu, C., Wu, T., Shen, S., Su, X., et al. (2018). Pyrroline-5-carboxylate reductase 1 promotes proliferation and inhibits apoptosis in non-small cell lung cancer. *Oncol. Lett.* 15, 731–740.

Clark, L. D., Clark, R. K., and Heber-Katz, E. (1998). A new murine model for mammalian wound repair and regeneration. *Clin. Immunol. Immunopathol.* 88, 35–45. doi: 10.1006/clin.1998.4519

Deng, Z., Gao, X., Sun, X., Amra, S., Lu, A., Cui, Y., et al. (2019). Characterization of articular cartilage homeostasis and the mechanism of superior cartilage regeneration of MRL/MpJ mice. *FASEB J.* 33, 8809–8821. doi: 10.1096/fj.201802132rr

Diekman, B. O., Wu, C. L., Louer, C. R., Furman, B. D., Huebner, J. L., Kraus, V. B., et al. (2013). Intra-articular delivery of purified mesenchymal stem cells from C57BL/6 or MRL/MpJ superhealer mice prevents posttraumatic arthritis. *Cell Transplant.* 22, 1395–1408. doi: 10.3727/096368912x653264

Djouad, F., Bouffi, C., Ghannam, S., Noel, D., and Jorgensen, C. (2009). Mesenchymal stem cells: innovative therapeutic tools for rheumatic diseases. *Nat. Rev. Rheumatol.* 5, 392–399. doi: 10.1038/nrrheum.2009.104

Dominici, M., Le Blanc, K., Mueller, I., Slaper-Cortenbach, I., Marini, F., Krause, D., et al. (2006). Minimal criteria for defining multipotent mesenchymal stromal cells. The International Society for Cellular Therapy position statement. *Cytotherapy* 8, 315–317. doi: 10.1080/14653240600855905

Drehmer, D. L., De Aguiar, A. M., Brandt, A. P., Petiz, L., Cadena, S. M., Rebelatto, C. K., et al. (2016). Metabolic switches during the first steps of adipogenic stem cells differentiation. *Stem Cell Res.* 17, 413–421. doi: 10.1016/j.scr.2016.09.001

Elahi, K. C., Klein, G., Avci-Adali, M., Sievert, K. D., Macneil, S., and Aicher, W. K. (2016). Human mesenchymal stromal cells from different sources diverge in their expression of cell surface proteins and display distinct differentiation patterns. *Stem Cells Int.* 2016:5646384.

Fitzgerald, J., Rich, C., Burkhardt, D., Allen, J., Herzka, A. S., and Little, C. B. (2008). Evidence for articular cartilage regeneration in MRL/MpJ mice. *Osteoarthritis Cartilage* 16, 1319–1326. doi: 10.1016/j.joca.2008.03.014

Fu, X., Zhu, M. J., Dodson, M. V., and Du, M. (2015). AMP-activated protein kinase stimulates Warburg-like glycolysis and activation of satellite cells during muscle regeneration. *J. Biol. Chem.* 290, 26445–26456. doi: 10.1074/jbc.m115.665232

Galluzzi, L., Kepp, O., Vander Heiden, M. G., and Kroemer, G. (2013). Metabolic targets for cancer therapy. *Nat. Rev. Drug Discov.* 12, 829–846.

Gawriluk, T. R., Simkin, J., Thompson, K. L., Biswas, S. K., Clare-Salzler, Z., Kimani, J. M., et al. (2016). Comparative analysis of ear-hole closure identifies epimorphic regeneration as a discrete trait in mammals. *Nat. Commun.* 7:11164.

Gosset, M., Berenbaum, F., Thirion, S., and Jacques, C. (2008). Primary culture and phenotyping of murine chondrocytes. *Nat. Protoc.* 3, 1253–1260. doi: 10.1038/nprot.2008.95

Gourevitch, D., Clark, L., Chen, P., Seitz, A., Samulewicz, S. J., and Heber-Katz, E. (2003). Matrix metalloproteinase activity correlates with blastema formation in the regenerating MRL mouse ear hole model. *Dev. Dyn.* 226, 377–387. doi: 10.1002/dvdy.10243

Gourevitch, D., Kossenkov, A. V., Zhang, Y., Clark, L., Chang, C., Showe, L. C., et al. (2014). Inflammation and its correlates in regenerative wound healing: an alternate perspective. *Adv. Wound Care* 3, 592–603. doi: 10.1089/wound.2014.0528

Guernsey, D. L., Jiang, H., Evans, S. C., Ferguson, M., Matsuoka, M., Nightingale, M., et al. (2009). Mutation in pyrroline-5-carboxylate reductase 1 gene in families with cutis laxa type 2. *Am. J. Hum. Genet.* 85, 120–129. doi: 10.1016/j.ajhg.2009.06.008

Guzy, R., and Redente, E. F. (2021). Kindlin for the fire: targeting proline synthesis to extinguish matrix production in pulmonary fibrosis. *Am. J. Respir. Cell Mol. Biol.* doi: 10.1165/rcmb.2021-0137ED Online ahead of print

Heywood, H. K., and Lee, D. A. (2008). Monolayer expansion induces an oxidative metabolism and ROS in chondrocytes. *Biochem. Biophys. Res. Commun.* 373, 224–229. doi: 10.1016/j.bbrc.2008.06.011

Huang, Y. W., Chiang, M. F., Ho, C. S., Hung, P. L., Hsu, M. H., Lee, T. H., et al. (2018). A transcriptome study of progeroid neurocutaneous syndrome reveals POSTN as a new element in proline metabolic disorder. *Aging Dis.* 9, 1043–1057. doi: 10.14336/ad.2018.0222

Kumar, A., and Brockes, J. P. (2012). Nerve dependence in tissue, organ, and appendage regeneration. *Trends Neurosci.* 35, 691–699. doi: 10.1016/j.tins.2012.08.003

Kwiatkowski, A., Piatkowski, M., Chen, M., Kan, L., Meng, Q., Fan, H., et al. (2016). Superior angiogenesis facilitates digit regrowth in MRL/MpJ mice compared to C57BL/6 mice. *Biochem. Biophys. Res. Commun.* 473, 907–912. doi: 10.1016/j.bbrc.2016.03.149

Lane, R. S., Fu, Y., Matsuzaki, S., Kinter, M., Humphries, K. M., and Griffin, T. M. (2015). Mitochondrial respiration and redox coupling in articular chondrocytes. *Arthritis Res. Ther.* 17:54.

Lennon, D. P., Edmison, J. M., and Caplan, A. I. (2001). Cultivation of rat marrow-derived mesenchymal stem cells in reduced oxygen tension: effects on in vitro and in vivo osteochondrogenesis. *J. Cell. Physiol.* 187, 345–355. doi: 10.1002/jcp.1081

Liu, W., Hancock, C. N., Fischer, J. W., Harman, M., and Phang, J. M. (2015). Proline biosynthesis augments tumor cell growth and aerobic glycolysis: involvement of pyridine nucleotides. *Sci. Rep.* 5:17206.

Macrin, D., Alghadeer, A., Zhao, Y. T., Miklas, J. W., Hussein, A. M., Detraux, D., et al. (2019). Metabolism as an early predictor of DPSCs aging. *Sci. Rep.* 9:2195.

Magadum, A., and Engel, F. B. (2018). PPARbeta/delta: linking metabolism to regeneration. *Int. J. Mol. Sci.* 19:2013. doi: 10.3390/ijms19072013

Markway, B. D., Tan, G. K., Brooke, G., Hudson, J. E., Cooper-White, J. J., and Doran, M. R. (2010). Enhanced chondrogenic differentiation of human bone marrow-derived mesenchymal stem cells in low oxygen environment micropellet cultures. *Cell Transplant.* 19, 29–42. doi: 10.3727/096368909x478560

Maumus, M., Jorgensen, C., and Noel, D. (2013a). Mesenchymal stem cells in regenerative medicine applied to rheumatic diseases: role of secretome and exosomes. *Biochimie* 95, 2229–2234. doi: 10.1016/j.biochi.2013.04.017

Maumus, M., Manferdini, C., Toupet, K., Peyrafitte, J. A., Ferreira, R., Facchini, A., et al. (2013b). Adipose mesenchymal stem cells protect chondrocytes from degeneration associated with osteoarthritis. *Stem Cell Res.* 11, 834–844. doi: 10.1016/j.scr.2013.05.008

Mobasheri, A., Rayman, M. P., Gualillo, O., Sellam, J., Van Der Kraan, P., and Fearon, U. (2017). The role of metabolism in the pathogenesis of osteoarthritis. *Nat. Rev. Rheumatol.* 13, 302–311. doi: 10.1038/nrrheum.2017.50

Monteagudo, S., Cornelis, F. M. F., Aznar-Lopez, C., Yibmantasiri, P., Guns, L. A., Carmeliet, P., et al. (2017). DOT1L safeguards cartilage homeostasis and protects against osteoarthritis. *Nat. Commun.* 8:15889.

Naviaux, R. K., Le, T. P., Bedelbaeva, K., Leferovich, J., Gourevitch, D., Sachadyn, P., et al. (2009). Retained features of embryonic metabolism in the adult MRL mouse. *Mol. Genet. Metab.* 96, 133–144. doi: 10.1016/j.ymgme.2008.11.164

Osuma, E. A., Riggs, D. W., Gibb, A. A., and Hill, B. G. (2018). High throughput measurement of metabolism in planarians reveals activation of glycolysis during regeneration. *Regeneration* 5, 78–86. doi: 10.1002/reg2.95

Pattappa, G., Heywood, H. K., De Bruijn, J. D., and Lee, D. A. (2011). The metabolism of human mesenchymal stem cells during proliferation and differentiation. *J. Cell. Physiol.* 226, 2562–2570. doi: 10.1002/jcp.22605

Peister, A., Mellad, J. A., Larson, B. L., Hall, B. M., Gibson, L. F., and Prockop, D. J. (2004). Adult stem cells from bone marrow (MSCs) isolated from different strains of inbred mice vary in surface epitopes, rates of proliferation, and differentiation potential. *Blood* 103, 1662–1668. doi: 10.1182/blood-2003-09-3070

Pers, Y. M., Quentin, J., Feirreira, R., Espinoza, F., Abdellaoui, N., Erkilic, N., et al. (2018). Injection of adipose-derived stromal cells in the knee of patients with severe osteoarthritis has a systemic effect and promotes an anti-inflammatory phenotype of circulating immune cells. *Theranostics* 8, 5519–5528. doi: 10.7150/thno.27674

Pers, Y. M., Ruiz, M., Noel, D., and Jorgensen, C. (2015). Mesenchymal stem cells for the management of inflammation in osteoarthritis: state of the art and perspectives. *Osteoarthritis Cartilage* 23, 2027–2035. doi: 10.1016/j.joca.2015.07.004

Pfander, D., Cramer, T., Schipani, E., and Johnson, R. S. (2003). HIF-1alpha controls extracellular matrix synthesis by epiphyseal chondrocytes. *J. Cell Sci.* 116, 1819–1826. doi: 10.1242/jcs.00385

Pfander, D., Swoboda, B., and Cramer, T. (2006). The role of HIF-1alpha in maintaining cartilage homeostasis and during the pathogenesis of osteoarthritis. *Arthritis Res. Ther.* 8:104.

Phang, J. M. (2019). Proline Metabolism in Cell Regulation and cancer biology: recent advances and hypotheses. *Antioxid. Redox. Signal.* 30, 635–649. doi: 10.1089/ars.2017.7350

Phang, J. M., and Liu, W. (2012). Proline metabolism and cancer. *Front. Biosci.* 17:1835–1845. doi: 10.2741/4022

Phang, J. M., Liu, W., Hancock, C. N., and Fischer, J. W. (2015). Proline metabolism and cancer: emerging links to glutamine and collagen. *Curr. Opin. Clin. Nutr. Metab. Care* 18, 71–77. doi: 10.1097/mco.0000000000000121

Rajpurohit, R., Koch, C. J., Tao, Z., Teixeira, C. M., and Shapiro, I. M. (1996). Adaptation of chondrocytes to low oxygen tension: relationship between hypoxia and cellular metabolism. *J. Cell. Physiol.* 168, 424–432. doi: 10.1002/(sici)1097-4652(199608)168:2<424::aid-jcp21>3.0.co;2-1

Ren, G., Su, J., Zhang, L., Zhao, X., Ling, W., L'huillie, A., et al. (2009). Species variation in the mechanisms of mesenchymal stem cell-mediated immunosuppression. *Stem Cells* 27, 1954–1962. doi: 10.1002/stem.118

Reversade, B., Escande-Beillard, N., Dimopoulou, A., Fischer, B., Chng, S. C., Li, Y., et al. (2009). Mutations in PYCR1 cause cutis laxa with progeroid features. *Nat. Genet.* 41, 1016–1021.

Ruiz, M., Toupet, K., Maumus, M., Rozier, P., Jorgensen, C., and Noel, D. (2020). TGFBI secreted by mesenchymal stromal cells ameliorates osteoarthritis and is detected in extracellular vesicles. *Biomaterials* 226:119544. doi: 10.1016/j.biomaterials.2019.119544

Shum, L. C., White, N. S., Mills, B. N., Bentley, K. L., and Eliseev, R. A. (2016). Energy metabolism in mesenchymal stem cells during osteogenic differentiation. *Stem Cells Dev.* 25, 114–122.

Shyh-Chang, N., Daley, G. Q., and Cantley, L. C. (2013). Stem cell metabolism in tissue development and aging. *Development* 140, 2535–2547. doi: 10.1242/dev.091777

Sinha, K. M., Tseng, C., Guo, P., Lu, A., Pan, H., Gao, X., et al. (2019). Hypoxia-inducible factor 1alpha (HIF-1alpha) is a major determinant in the enhanced function of muscle-derived progenitors from MRL/MpJ mice. *FASEB J.* 33, 8321–8334. doi: 10.1096/fj.201801794r

Stum, M. G., Tadenev, A. L. D., Seburn, K. L., Miers, K. E., Poon, P. P., Mcmaster, C. R., et al. (2021). Genetic analysis of Pycr1 and Pycr2 in mice. *Genetics* 218:iyab048.

Tejedor, G., Luz-Crawford, P., Barthelaix, A., Toupet, K., Roudieres, S., Autelitano, F., et al. (2021). MANF produced by MRL mouse-derived mesenchymal stem cells is pro-regenerative and protects from osteoarthritis. *Front. Cell Dev. Biol.* 9:579951. doi: 10.3389/fcell.2021.579951

Wang, D. W., Fermor, B., Gimble, J. M., Awad, H. A., and Guilak, F. (2005). Influence of oxygen on the proliferation and metabolism of adipose derived adult stem cells. *J. Cell. Physiol.* 204, 184–191. doi: 10.1002/jcp.20324

Wang, R., Jiang, W., Zhang, L., Xie, S., Zhang, S., Yuan, S., et al. (2020). Intra-articular delivery of extracellular vesicles secreted by chondrogenic progenitor cells from MRL/MpJ superhealer mice enhances articular cartilage repair in a mouse injury model. *Stem Cell Res. Ther.* 11:93.

Wang, X., Ha, T., Liu, L., Hu, Y., Kao, R., Kalbfleisch, J., et al. (2018). TLR3 mediates repair and regeneration of damaged neonatal heart through glycolysis dependent YAP1 regulated miR-152 expression. *Cell Death. Differ.* 25, 966–982. doi: 10.1038/s41418-017-0036-9

Ward, B. D., Furman, B. D., Huebner, J. L., Kraus, V. B., Guilak, F., and Olson, S. A. (2008). Absence of posttraumatic arthritis following intraarticular fracture in the MRL/MpJ mouse. *Arthritis Rheum.* 58, 744–753. doi: 10.1002/art.23288

Weijin, F., Zhibin, X., Shengfeng, Z., Xiaoli, Y., Qijian, D., Jiayi, L., et al. (2019). The clinical significance of PYCR1 expression in renal cell carcinoma. *Medicine* 98:e16384. doi: 10.1097/md.0000000000016384

Xiao, S., Li, S., Yuan, Z., and Zhou, L. (2020). Pyrroline-5-carboxylate reductase 1 (PYCR1) upregulation contributes to gastric cancer progression and indicates poor survival outcome. *Ann. Transl. Med.* 8:937. doi: 10.21037/atm-19-4402

Xu, Y., Malladi, P., Chiou, M., Bekerman, E., Giaccia, A. J., and Longaker, M. T. (2007). In vitro expansion of adipose-derived adult stromal cells in hypoxia enhances early chondrogenesis. *Tissue Eng.* 13, 2981–2993. doi: 10.1089/ten.2007.0050

Yang, F., Li, B., Yang, Y., Huang, M., Liu, X., Zhang, Y., et al. (2019). Leptin enhances glycolysis via OPA1-mediated mitochondrial fusion to promote mesenchymal stem cell survival. *Int. J. Mol. Med.* 44, 301–312.

Yuan, X., Logan, T. M., and Ma, T. (2019). Metabolism in human mesenchymal stromal cells: a missing link between hMSC biomanufacturing and therapy? *Front. Immunol* 10:977. doi: 10.3389/fimmu.2019.00977

Zheng, L., Zhang, Z., Sheng, P., and Mobasheri, A. (2021). The role of metabolism in chondrocyte dysfunction and the progression of osteoarthritis. *Ageing Res. Rev.* 66:101249. doi: 10.1016/j.arr.2020.101249

Zhuang, J., Song, Y., Ye, Y., He, S., Ma, X., Zhang, M., et al. (2019). PYCR1 interference inhibits cell growth and survival via c-Jun N-terminal kinase/insulin receptor substrate 1 (JNK/IRS1) pathway in hepatocellular cancer. *J. Transl. Med.* 17:343.

Conflict of Interest: FDC and PP were employed by the Institut de Recherches Servier.

The authors declare that this study received funding from Servier. The funder was not involved in the study design, collection, analysis, interpretation of data and the writing of this article for publication.

frontiers in Cell and Developmental Biology

REVIEW
published: 03 August 2021
doi: 10.3389/fcell.2021.720477

Cell Interplay in Osteoarthritis

*Zihao Li[1], Ziyu Huang[2] and Lunhao Bai[1]**

[1] Department of Orthopedics, Shengjing Hospital of China Medical University, Shenyang, China, [2] Foreign Languages College, Shanghai Normal University, Shanghai, China

Osteoarthritis (OA) is a common chronic disease and a significant health concern that needs to be urgently solved. OA affects the cartilage and entire joint tissues, including the subchondral bone, synovium, and infrapatellar fat pads. The physiological and pathological changes in these tissues affect the occurrence and development of OA. Understanding complex crosstalk among different joint tissues and their roles in OA initiation and progression is critical in elucidating the pathogenic mechanism of OA. In this review, we begin with an overview of the role of chondrocytes, synovial cells (synovial fibroblasts and macrophages), mast cells, osteoblasts, osteoclasts, various stem cells, and engineered cells (induced pluripotent stem cells) in OA pathogenesis. Then, we discuss the various mechanisms by which these cells communicate, including paracrine signaling, local microenvironment, co-culture, extracellular vesicles (exosomes), and cell tissue engineering. We particularly focus on the therapeutic potential and clinical applications of stem cell-derived extracellular vesicles, which serve as modulators of cell-to-cell communication, in the field of regenerative medicine, such as cartilage repair. Finally, the challenges and limitations related to exosome-based treatment for OA are discussed. This article provides a comprehensive summary of key cells that might be targets of future therapies for OA.

Keywords: cartilage, subchondral bone, synovium, infrapatellar fat pad, stem cell, exosome, osteoarthritis

OPEN ACCESS

Edited by:
Kazunori Shimomura, Osaka University, Japan

Reviewed by:
Csaba Matta, University of Debrecen, Hungary
Janos Kanczler, University of Southampton, United Kingdom

****Correspondence:***
Lunhao Bai
lunhaobai_ace@163.com

Specialty section:
This article was submitted to Stem Cell Research, a section of the journal Frontiers in Cell and Developmental Biology

Received: *04 June 2021*
Accepted: *14 July 2021*
Published: *03 August 2021*

Citation:
Li Z, Huang Z and Bai L (2021) Cell Interplay in Osteoarthritis. Front. Cell Dev. Biol. 9:720477. doi: 10.3389/fcell.2021.720477

INTRODUCTION

Osteoarthritis (OA) is a common degenerative disease of the joints that causes chronic pain and motor dysfunction and affects the quality of life of more than 300 million people worldwide (GBD 2017 Risk Factor Collaborators, 2018). OA also poses a considerable economic burden on patients and is a major public health problem. OA's current treatment strategies include non-drug treatment (e.g., exercise, weight reduction, and physiotherapy), drug treatment, and surgery (Bannuru et al., 2019; Kloppenburg and Berenbaum, 2020). Non-pharmacological therapies are used for patients in the early stages of OA to delay its development. However, the effects of these approaches on early symptoms are limited, particularly on structural diseases (Cutolo et al., 2015). On the other hand, medications, including pain relievers and non-steroidal anti-inflammatory drugs, are prescribed to control the pain, preserve functional capacity, and improve the quality of daily life. However, because patients with OA are prone to complications, inappropriate drug treatment and multi-drug therapy can increase the risk of side effects (Gore et al., 2011). Meanwhile, surgical treatment is considered for patients with advanced OA; however, this modality is associated with high failure rates and complications, and additional costs. Because the molecular mechanisms underlying OA initiation and progression remain poorly understood, there are no current interventions with

satisfactory curative effects that can delay disease progression (Dieppe et al., 2011; Bannuru et al., 2019). Therefore, new insights into the mechanism of OA pathogenesis are required to promote the development of new therapies that meet future clinical needs.

Osteoarthritis was previously considered to be caused by mechanical damage or the habitual overuse of a joint that is an inevitable part of aging. However, it has become increasingly clear that OA is much more complex than a wear-and-tear disease, and various factors such as inflammation, metabolism, and biochemical machinery play an important role in its pathogenesis (Brandt et al., 2006; Martel-Pelletier et al., 2016). Furthermore, aging, obesity, joint damage, and high-intensity activities have been identified as risk factors leading to OA development (Zhang and Jordan, 2008; Silverwood et al., 2015; Martel-Pelletier et al., 2016). Hence, OA is now viewed as a multifactorial disease that involves local and systemic factors and has multiple pathogenetic mechanisms. Therefore, these factors must be considered when exploring new treatment methods for OA.

In addition, rather than merely involving the destruction of articular cartilage, OA is now more accurately thought of as a disease of the whole joint and is characterized by the partial loss of cartilage, thickening of the synovial sac, subchondral bone sclerosis and osteophyte formation, and changes in the structure of joints, ligaments, and surrounding muscles (Pereira et al., 2011; Hunter and Bierma-Zeinstra, 2019). During its development, different tissues within the joint and their interactions contribute to the pathology and clinical symptoms of OA (Burr, 1998; de Lange-Brokaar et al., 2012). Recently, the role of the subchondral bone, which refers to the cortical bone layer under the articular cartilage and the trabecular bone in the lower part of the joint, in OA pathogenesis has attracted increasing attention. Studies have shown that the subchondral bone may affect cartilage degeneration through changes in mechanical stress or paracrine-mediated interaction between the bone and cartilage (Sharma et al., 2013; Zhen et al., 2013; Lin et al., 2019). In an inflammatory environment, synovial fibroblasts (SFB) may affect the formation of osteophytes and the degradation of the cartilage matrix by releasing bone regulatory factors (including BMP-2) and pro-inflammatory factors (such as IL-1β) (Mathiessen and Conaghan, 2017). Infrapatellar fat pad (IPFP) and synovium can also release various pro-inflammatory mediators during inflammation. These mediators not only result in the abnormal structure and function of synovial tissue but also aggravate cartilage damage and the development of OA (Clockaerts et al., 2010; Mathiessen and Conaghan, 2017; Kuang et al., 2020). Therefore, new insights into the interaction and communication among the different cells in the joint may lead to a greater understanding of the disease mechanism of OA and provide new perspectives for the development of OA treatment strategies.

In this review, we first introduce the cells found in joint tissues and their role in OA pathogenesis. Then, we discuss the various ways by which these cells communicate, including paracrine signaling, local microenvironment, co-culture, extracellular vesicles (EVs), and exosomes. Finally, we summarize the recent studies on the therapeutic potential and clinical applications of stem cell-derived EVs for OA treatment. This article provides a comprehensive summary of key cells that might be targets of future therapies for OA.

JOINT CELLS AND TISSUES

Cartilage and Chondrocytes

Articular cartilage is the connective tissue located on the surface of the synovial joint and plays a role in lubrication and weight-bearing during joint activities. Due to the lack of a vascular system and limited oxygen and nutrient supply, articular cartilage has low regenerative potential (Sophia Fox et al., 2009; Chen et al., 2017; Singh et al., 2019). In addition to the chondrocytes, which were long considered to be the only cell type within articular cartilage, cartilage stem/progenitor cells (CSPC) have been recently identified in OA cartilage (Williams et al., 2010), representing approximately 10% of the total cells (Alsalameh et al., 2004; Bosserhoff et al., 2014; Riegger et al., 2018). Moreover, single-cell RNA-seq analysis revealed various chondrocyte populations in advanced OA, including homeostatic chondrocytes, proliferative chondrocytes, effector chondrocytes, regulatory chondrocytes, pre-hypertrophic chondrocytes, hypertrophic chondrocytes, and fibrocartilage chondrocytes (Ji et al., 2019).

As the resident cell type in tissues, chondrocytes can form an extracellular matrix mainly composed of aggrecan and type II collagen. However, chondrocytes only account for 1–5% of the total volume of cartilage tissue (Bhosale and Richardson, 2008). Owing to the limited number of cells and their pyknotic nature, damage caused by various risk factors, such as abnormal mechanical load, trauma, and inflammation, can lead to changes in the structure and function of cartilage. Joint degenerative diseases are prone to occur without timely and adequate treatment (Palazzo et al., 2016; Vina and Kwoh, 2018; Li et al., 2019; Singh et al., 2019). Although the composition of articular cartilage is simple, its horizontal-layered structure containing chondrocytes with various morphologies and different distribution and secretion characteristics remains well-organized.

Changes in the metabolic state of chondrocytes lead to the imbalance of collagen synthesis and degradation, cartilage degeneration, chondrosenescence, and an intra-articular inflammatory environment, ultimately leading to OA (Martin and Buckwalter, 2002). The metabolic changes in chondrocytes may exhibit distinct characteristics and have been described in four clinical OA phenotypes. First, the inflammation-associated OA phenotype is characterized by a low degree of inflammation (Scanzello, 2017). The continuous accumulation of pro-inflammatory mediators leads to the excessive production of reactive oxygen species and mtDNA damage and drives the catabolic reaction in the chondrocytes, subsequently disrupting the balance between cartilage repair and damage. The second phenotype is the mechanical overload-associated OA phenotype. Normal physiological load is important to maintain chondrocyte function and ECM metabolic balance. Mechanical overloading is thus harmful to chondrocytes and results in a weakened anabolic response, decreased extracellular matrix (ECM) synthesis, and

enhanced catabolic response, thereby stimulating the synthesis of matrix metalloproteinases (MMPs) (Loeser et al., 2012). Metabolic syndrome-associated OA phenotype is characterized by increased fasting plasma glucose concentration, increased triglyceride level, decreased high-density lipoprotein level, and/or hypertension (Dickson et al., 2019). The occurrence and development of OA can be positively affected by increasing the production of fat-derived pro-inflammatory mediators, such as advanced glycation end-products (Oren et al., 2011). The last is the aging-associated OA phenotype. The catabolism of aging chondrocytes is active, and disruption of the interplay between autophagy and the inflammasome is observed in an inflammatory environment (Salminen et al., 2012). In addition, the decline in chondrocyte mitochondrial function is accompanied by decreased chondrocyte autophagy and increased apoptosis (Blanco et al., 2018). The proliferation and synthesis ability of chondrocytes in aging articular cartilage also decreases; however, their ability to produce pro-inflammatory mediators and MMPs remains unchanged (Loeser, 2009). Overall, the initiation and progression of OA are closely related to the phenotypic changes in chondrocytes.

Synovium and Synovial Cells

Increasing evidence has shown that the mutual communication between different tissues in the joint is essential for maintaining joint homeostasis. The communication between synovium and cartilage not only contributes to OA symptoms but is also a key factor in disease pathogenesis. The morphology and cell composition of the synovium are often used as biomarkers for the development of OA. Although the synovial tissue may not be affected in the early-stage of OA, many patients with advanced OA suffer from severe synovitis (Wenham and Conaghan, 2010).

In healthy joints, the synovium is mainly composed of two types of synovial cells. Type A macrophage-like synovial cells, which are relatively small, mainly have a phagocytic function and produce pro-inflammatory cytokines. Meanwhile, type B fibroblast-like synovial cells provide structure, nutrition, and lubrication and represent approximately 75% of the cells in the synovium (Firestein and McInnes, 2017). In addition, fibroblasts-like synovial cells can migrate to the site of tissue remodeling and interact with ECM molecules via specific surface receptors (Pap and Bertrand, 2012). They can perceive and respond to the changes in the composition and structure of the surrounding synovial tissue by adjusting their interaction with and the production of ECM components. In the initiation of OA, the intimal lining layer becomes hypertrophic and is infiltrated by macrophages, fibroblasts, mast cells, T cells, B cells, dendritic cells, and neutrophils, leading to a 5- to 10-fold increase in cell density (Culemann et al., 2019). These infiltrating cells promote the production of pro-inflammatory cytokines and catabolites, thereby changing the composition of synovial fluid, an important source of these pro-inflammatory mediators in OA (Falconer et al., 2018). In the synovial fluid of OA patients, the proportion of macrophages is relatively low, whereas that of mast cells is relatively high (de Lange-Brokaar et al., 2012; Robinson et al., 2016; Xie et al., 2019).

Macrophages

Synovitis can occur at both the early and late stages of OA (Sellam and Berenbaum, 2010) and is characterized by the accumulation of macrophages in the intimal lining layer (Sun A. R. et al., 2016). Macrophages are heterogeneous and plastic immune cells that produce chemokines and cytokines in inflamed joints. Macrophages can be activated by various stimuli, including pro-inflammatory (IL-1β, TNF-α, and IL-6) and immunomodulatory cytokines (IL-4 and IL-10) (Wang et al., 2014; Dutta et al., 2020) and abnormal mechanical forces, which are mostly produced during stress or cell damage (Liu et al., 2018). Activated macrophages are generally classified into two distinct phenotypes, namely, classically activated/inflammatory (M1) type and alternatively activated/immunomodulatory (M2) type.

Polarized M1 macrophages can generate a large amount of pro-inflammatory cytokines, nitric oxide (NO), and reactive oxygen species, thereby enhancing host defense response (Mosser, 2003; Genin et al., 2015). However, excessive activation of M1 macrophages can lead to autoimmune diseases and tissue damage (Mosser and Edwards, 2008). M2 macrophages are mainly present in the subsiding phase of inflammation and are responsible for producing anti-inflammatory cytokines and eliminating apoptotic cells. In addition, M2 macrophages can produce osteogenic growth factors, such as bone morphogenetic protein 2 (BMP-2; an effective promoter of osteogenic differentiation of MSCs belonging to a subclass of the TGF-β family), (Champagne et al., 2002; Li C. J. et al., 2018) TGF-β, (Assoian et al., 1987) 1,25-dihydroxy vitamin D3, (Kreutz et al., 1993) and osteopontin (Takahashi et al., 2004).

Therefore, the imbalance in the ratio between these two kinds of cells in OA may be related to the initiation and progression of OA (Xue et al., 2019). The significantly increased number of M1 macrophages in synovial tissues (Sun et al., 2017) and the high proportion of M2 macrophages have clinical diagnostic significance for OA (Chen et al., 2020). However, it is difficult to assess the polarization state of synovial macrophages before OA occurs or even in its early stages. In late-stage OA, M1- and M2-like macrophages can coexist in the joint synovium and adjacent adipose tissues. However, the role of macrophages in OA initiation and progression is unquestionable. Macrophages play an important role in the occurrence of OA through inflammatory factors, cytokines, and proteins, whether it is inflammatory or mechanical injury (Bondeson et al., 2010).

Mast Cells

Mast cells (MCs), a type of immune cells that reside in tissues, play a pivotal role in allergic reactions (Galli and Tsai, 2012). The synovial fluid of patients with OA showed an increased number of MCs and increased concentration of certain MC mediators, such as histamine and tryptase (Bridges et al., 1991) (Buckley et al., 1997). The role of MCs in bone metabolism remains controversial (Urist and McLean, 1957). In MC-deficient mouse models, MCs were involved in the occurrence and development of OA (Schubert et al., 2015; Kroner et al., 2017) and fracture healing and may also be involved in regulating the production of osteoclasts (Behrends et al., 2014; Kroner et al., 2017). Many MC mediators can regulate or

induce bone metabolism by inhibiting osteoblast activity (such as IL-1, TNF) and/or promoting osteoclastogenesis (such as histamine, TNF, IL-6) (Biosse-Duplan et al., 2009; Pietschmann et al., 2016). MCs can also play a role in maintaining bone homeostasis. For instance, the transforming growth factor-β (TGF-β) can stimulate the production of osteoblasts, while IL-12 and interferon-γ (IFN-γ) can inhibit the formation of osteoclasts (Pietschmann et al., 2016).

Several clinical studies have reported the increased expression of genes involved in MC differentiation and activity in the synovial tissues of OA patients (Wang et al., 2019). MC-deficient mice were protected from inflammation and cartilage destruction of OA; however, MC implantation in engraftment reversed this protection (Wang et al., 2019). In addition, the inhibition of tryptase activity in wild-type mice reduced the concentration of pro-inflammatory mediators, such as IL-6, IL-1β, IL-8, and MMP-3. Furthermore, the synovial MCs of patients with OA can secrete TNF-α following stimulation with the high-affinity receptor of IgG (Lee et al., 2013). In a cross-sectional cohort study, H1 antihistamine treatment was associated with decreased prevalence of OA (Shirinsky and Shirinsky, 2018). These results confirm the critical role of MC in the occurrence and development of OA and indicate that MCs may be a potential therapeutic target for OA.

Subchondral Bone and Osteoblasts and Osteoclasts

The degeneration and degradation of articular cartilage had long been considered the leading cause of OA, and many treatment strategies have been developed to protect the cartilage. Although the relationship between cartilage degeneration and subchondral bone destruction is close (Thielen et al., 2019), not all patients with OA exhibit abnormalities in the articular cartilage bone. In addition, in the aging OA phenotype, the imbalance in chondrocyte metabolism occurs before abnormal subchondral bone remodeling (Peffers et al., 2020). In contrast, in the trauma-induced OA phenotype, the early micro-injury in subchondral bone is detected first (Barton et al., 2017).

However, increasing evidence demonstrates that maintaining the integrity and remodeling balance of the articular subchondral bone can combat cartilage degeneration to restore homeostasis in joint tissues (Castañeda et al., 2012; Hoshi et al., 2017). Thus, exploring the mechanism underlying subchondral bone remodeling in OA can provide new insights for developing treatments for early-stage OA. The microstructural changes in articular subchondral bone in OA include the formation of subchondral bone cysts, bone marrow edema-like lesions, and osteophytes caused by early bone loss, late bone sclerosis, and histopathological changes (Li et al., 2013). These changes are caused by chondrocytes, osteoblasts, osteoclasts, endothelial cells, and the subchondral bone microenvironment (Henrotin et al., 2012).

Osteoblasts differentiate from mesenchymal cells and undergo four stages of maturation, namely, preosteoblasts, osteoblasts, bone-lining cells, and bone cells (Clarke, 2008; Katsimbri, 2017). The phenotype and activity of OA osteoblasts in subchondral bone are altered. For example, the levels of OCN, RANKL, (Kwan Tat et al., 2008) insulin-like growth factor 1, (Hilal et al., 1998) transforming growth factor β1, (Abed et al., 2017) vascular endothelial growth factor (Corrado et al., 2013), and alkaline phosphatase activity are elevated in OA, which subsequently lead to osteoclastogenesis, sclerosis (Wang et al., 2013) and angiogenesis. Osteoclasts are multinucleated cells derived from bone marrow myeloid progenitor cells and are mainly responsible for bone resorption and formation (Teitelbaum, 2000; Katsimbri, 2017). During osteoclast formation, progenitor cells are recruited to specific parts of the bone surface to differentiate into osteoclasts (monocytes) and fuse, thereby forming multinucleated mature osteoclasts. Mature osteoclasts adhere to the old bone area and release hydrogen ions and catalytic enzymes to dissolve the bone.

Mesenchymal Stem Cells

Mesenchymal stem cells (MSCs) are multipotent progenitor cells that originate from the mesoderm. MSCs by default can't regenerate bona fide articular hyaline cartilage (it's primarily fibrous cartilage and hypertrophy) (Buhrmann et al., 2010). However, MSCs can contribute to cartilage and bone repair, and their function in immune regulation and organ regeneration has been extensively studied (Levy et al., 2020). MSCs can be roughly divided into three types: embryonic stem cells, pluripotent stem cells, and adult stem cells (Vizoso et al., 2017).

Pluripotent stem cells are found in bone-related tissues, such as the bone marrow, synovium, infrapatellar fat pad, and adipose tissues (Pers et al., 2015). Bone marrow-derived MSCs (BMSCs) are the most well-characterized pluripotent stem cells. As early as 2002, stem cell therapy based on the *in vitro* expansion of autologous BMSCs has been used to treat OA. Although there was no significant difference in clinical results, improvement in symptoms was observed from arthroscopic and histological findings (Wakitani et al., 2002). *In vitro*, synovial MSCs (SMSCs) exhibit a particularly high capacity for cartilage differentiation (Shirasawa et al., 2006; Kurth et al., 2007). Studies have shown that SMSCs from OA patients can repair cartilage through allogenic tissue-engineered constructs in both *in vitro* and *in vivo* models. In experimental animal models, the injection of SMSCs into the joint cavity achieved a similar effect (Kondo et al., 2019; Enomoto et al., 2020; Dragoo et al., 2012). Infrapatellar fat pad (IPFP), a column of fat tissue located behind the patella, and synovium are involved in the occurrence and development of intra-articular diseases, such as OA (Favero et al., 2017). As the MSCs/stromal cells derived from IPFP (Kouroupis et al., 2019) are similar to SMSCs, (To et al., 2019) IPFP MSCs are speculated to have the ability for tissue repair (Galipeau et al., 2016), indicating IPFP as a potential target for joint diseases (Attur et al., 2010). Its potential in chondrogenic, osteogenic, and adipogenic lineages has been reported (Sun et al., 2018). *In vitro*, the chondrogenic differentiation ability of IPFP MSCs was greater than that of BMSCs, adipose tissue MSC (AMSCs), and UC-MSCs (Ding et al., 2015). AMSCs can promote cartilage regeneration and regulate inflammation. Because they are versatile and readily available, AMSCs are an excellent source of cells for OA treatment (Kim and Koh, 2018;

Lee et al., 2019). However, the mechanism by which AMSCs induce cartilage regeneration remains unclear. Current evidence indicates that AMSCs regulate the local microenvironment through paracrine nutritional factors, thereby making it more favorable for regeneration and repair and subsequently delaying cartilage degradation and improving joint function (Damia et al., 2018). Previously, a small number of MSC-like progenitor cells-chondrogenic stem cells/progenitor cells (CSPCs) were detected in cartilage tissues (Alsalameh et al., 2004; Fickert et al., 2004; Koelling et al., 2009). Because they share similar properties with BMSCs, CSPCs are speculated to be involved in cartilage regeneration. CSPC migration occurs upon cartilage damage, and their proliferation and immune regulation capabilities are enhanced (Seol et al., 2012; Riegger et al., 2018).

Induced Pluripotent Stem Cells and Tissue-Engineered Cells

Induced pluripotent stem cells (iPSCs) can provide an unlimited cell source for tissue engineering and are an attractive substitute for primary cells. iPSCs are characterized by a high degree of plasticity and promising differentiation potential and have promising potential in cell therapy. Patient-specific iPSCs can be engineered to minimize the autoimmune response, making them an almost ideal cell source for cell-based therapy. Studies on cartilage tissue engineering of iPSCs have demonstrated their utility for functional cartilage repair and as models for studying cartilage pathology (Diekman et al., 2012; Willard et al., 2014). iPSCs provide a platform for identifying candidate, patient-specific OA therapeutic agents (Lietman, 2016). For example, iPSCs reprogrammed from somatic cells (Takahashi et al., 2007; Yu et al., 2007) could generate endless OA patient-specific stem cells for drug research. Moreover, iPSCs isolated from the tissues of OA patients could differentiate into the cartilage, which provides opportunities for cartilage tissue research (Wei et al., 2012; Lach et al., 2014; Nam et al., 2018). However, there are no clinical studies published about cartilage cell therapy using iPSCs. iPSCs not only have excellent proliferation and differentiation capabilities similar to other stem cells but also do not cause immune rejection and ethical issues (Moradi et al., 2019). Therefore, more studies are required to improve the future applications of iPSC-derived chondrocytes in OA replacement therapy.

VARIOUS MECHANISMS OF CELLULAR CROSSTALK IN OA PATHOGENESIS

Microenvironment, Paracrine Signals, and Co-culture Method

Cartilage and Subchondral Bone

In joints with OA, some blood vessels of the subchondral bone can penetrate calcified cartilage and even invade non-calcified cartilage (Chen et al., 2015). Osteoclast precursors invade the area of hypertrophic cartilage and interact with its cells to reshape the cartilage matrix and form an ossification center (Tonna et al., 2016). In addition, mature osteoclasts could regulate nearby chondrocytes, which destroys the connection between the bone and cartilage and degrade articular cartilage via cysteine proteases and matrix metalloproteinases (Löfvall et al., 2018). Osteoclasts could aggravate cartilage damage by regulating chondrocytes. The expression level of TGF-β1 in osteoclasts was upregulated in a time-dependent and dose-dependent manner under mechanical stimulation. Upon co-culture with osteoclasts, chondrocytes showed aggravated apoptosis. The injection of TGF-β1R inhibitor into the abdominal cavity of rats with OA effectively reduced chondrocyte apoptosis and cartilage degradation (Zhang R. K. et al., 2018). TGF-β1 was not derived from osteoclastic bone resorption but was transported from the subchondral bone to the cartilage layer via diffusion or blood circulation to adversely affect chondrocytes. The cartilage can also obtain calcium–phosphate complexes from subchondral bone via p38, ERK1/2, nuclear factor- kappa B (NF-κB), signal transducer, and activator of transcription 3 (STAT3) to increase the production of MMP-13 in chondrocytes (Jung et al., 2018).

Chondrocytes can also promote the loss of subchondral bone by regulating osteoclasts. Abnormal mechanical stress could induce IL-1β production in primary chondrocytes (Fujisawa et al., 1999). IL-1β increased the expression of receptor activator of NF-κB ligand (RANKL) through osteoblasts, thereby indirectly inducing the generation and maturation of osteoclasts (Cao et al., 2016). In an OA model induced by destabilization of the medial meniscus (DMM), chondrocytes produced large amounts of TNF-α and IL-6 (Pearson et al., 2017). TNF-α activates NF-κB and c-Jun NH2-terminal protein kinase (JNK) in a RANKL-independent manner to directly induce osteoclast differentiation (Kobayashi et al., 2000) and indirectly induce its production (Tanaka et al., 2005). In an *in vivo* OA model, the expression of high-mobility group box 1 (HMGB1) was detected in chondrocytes (Aulin et al., 2020). As demonstrated by the bone development of $HMGB1^{-/-}$ hypertrophic chondrocytes in the mouse growth plate, endochondral bone formation was disrupted due to the delayed invasion of osteoclast precursors into the primary ossification center (Taniguchi et al., 2007). In addition, senescent chondrocytes and hypertrophic chondrocytes produced pro-inflammatory mediators, catabolic enzymes, and chemokines, collectively known as the senescence-associated secretory phenotype (SASP), (Rim et al., 2020) to affect subchondral osteoclast lineage cells.

Infrapatellar Fat Pad and Synovium

In OA, IPFP and nearby synovium also experience inflammatory infiltration and hyperplasia (Favero et al., 2017). IPFP releases IL-6, IL-8, prostaglandin F2a (PGF2α), and TNFα, which subsequently causes fibrosis of the synovium (Bastiaansen-Jenniskens et al., 2013; Eymard et al., 2014). *In vitro*, fibroblast-like synovial cells of OA patients pre-treated with TGFβ or PGF2α inhibitors were cultured in the conditioned medium derived from IPFP tissues for 4 days and exhibited different migration and proliferation abilities. Hyperplasia and fibrosis also occurred (Bastiaansen-Jenniskens et al., 2013). In addition, adipocytes derived from IPFP could regulate macrophages and CD4 + T cells infiltrating into the synovium by secreting lipids (Ioan-Facsinay et al., 2013; Klein-Wieringa et al., 2013).

The free fatty acids found in the conditioned medium derived from IPFP adipocytes improved the proliferation of CD4 + T cells and their ability to produce IFN-γ. These free fatty acids could also reduce the secretion of IL-12p40 cytokine by macrophages (Klein-Wieringa et al., 2013); IL-12p40 is a chemoattractant that can induce macrophage inflammation and fibrosis (Cooper and Khader, 2007).

Macrophages have been used as potential therapeutic targets, and their pharmacological depletion and phenotypic changes in IPFP and synovium have been explored (Fernandes et al., 2020; Wu et al., 2020). Macrophages can be induced to polarize back to another anti-inflammatory M2 phenotype. Although there are no reports on the MSC-mediated direct regulation of the phenotype of synovial macrophages in patients with OA, MSCs have been demonstrated to block the activation of M1 macrophages and promote the polarization of M2 macrophages to inhibit inflammation *in vitro* (Harrell et al., 2019). MSCs first migrate to the tissue injury site and promote the polarization of M2 macrophages by secreting a large number of cytokines, chemokines, and growth factors (Fernandes et al., 2020), thereby enhancing the repair of damaged tissues. The intra-articular injection of MSCs could downregulate the level of iNOS in macrophages and reduce the formation of M1 macrophages (Hamilton et al., 2019). Interestingly, in OA joints, M1 macrophages subsequently inhibited the proliferation and viability of MSCs, enhanced the immune response, and ultimately aggravated cartilage degradation.

Infrapatellar fat pad can also interact with the cartilage. The main limitation of MSC-based cartilage constructs is the induction of a hypertrophic phenotype during *in vivo* differentiation, which leads to endochondral ossification (Scotti et al., 2013; Correa et al., 2015; Feng et al., 2018). However, 8 weeks after implementing hybrid structures in which IPFP MSCs and articular chondrocytes were co-cultured in nude mice, cartilage mineralization was reduced, and the phenotype was stable (Mesallati et al., 2015). IPFP MSCs could accumulate a large amount of sGAG on articular cartilage agarose gels, thereby improving the mechanical properties of tissue-engineered articular cartilage constructs (Mesallati et al., 2017).

Cell Co-culture

Co-culture of chondrocytes and synovial cells has been used in cartilage research as an *in vitro* model for OA. Co-cultured chondrocytes and synovial cells stimulated by pro-inflammatory cytokines interact via calcium signaling and paracrine pathway to maintain the homeostasis of chondrocytes. This co-culture method allows for the accurate evaluation of the role of anti-inflammatory or chondroprotective molecules in the articular cartilage (Beekhuizen et al., 2011). The co-culture of osteoblasts and chondrocytes can also be used to study the role of chondroprotection (via delaying the onset of cartilage degradation) in bone remodeling. Paracrine signals are also used to maintain the physiological state and phenotype of the cells (Thysen et al., 2015). MSCs promote specific dedifferentiation due to their pluripotency. When co-cultured with other cells, different cell pathways can be analyzed together with articular chondrocytes with cell secretion markers (Hendriks et al., 2007). However, the co-cultivation method also has certain limitations, including restricted growth of cells and high cost.

Intercellular Signaling by EVs

Extracellular vesicles (EVs) are nano-sized communication messengers secreted by cells that transmit biological signals between cells and are mainly divided into three categories, namely, exosomes, microvesicles, and apoptotic bodies. EVs have received increasing research attention in the field of regenerative medicine. Increasing studies have demonstrated potential value for alleviating inflammation and promoting tissue repair and regeneration (Bjørge et al., 2017).

Extracellular vesicles are small double lipid membrane vesicles with a diameter of approximately 30–2000 nm that can carry various biologically active molecules, such as RNA subtypes (mRNA, microRNA, and lncRNA), DNA fragments, lipids, proteins, and enzymes (Lamichhane et al., 2015). Most cells, such as those in connective tissues and MSCs, can produce and secrete EVs into various biological fluids, such as the blood and synovial fluid (Rani et al., 2015). Once released, EVs can take effect immediately or be transported to a distant place. EVs communicate with the recipient cell by producing the same effect as their donor cell.

Exosomes are small vesicles with a diameter of approximately 30–150 nm derived from the endosomal compartment. They are the most widely studied type of EVs (Théry et al., 2002). Endosomal membrane invaginates to form multivesicular bodies containing intraluminal vesicles. When multivesicular bodies fuse with the plasma membrane, intraluminal vesicles are secreted as exosomes into the extracellular space. Microvesicles are slightly larger than exosomes, with a diameter ranging between 50 and 1000 nm (De Jong et al., 2014). Because microvesicles are directly shed from the plasma membrane, their markers on the membrane surface are also the same as the donor cells. Similar to exosomes, microvesicles can transport biologically active molecules to recipient cells. Apoptotic bodies are the largest type of EVs, with a diameter of $\geq$1000 nm, and are formed in the late-stage of apoptosis (De Jong et al., 2014). Apoptotic bodies may function as biomarkers. However, at present, the connection between regenerative medicine and cells remains unclear.

Extracellular vesicles serve as mediators of intercellular communication (Raposo and Stoorvogel, 2013; De Jong et al., 2014). EVs interact with the surface receptors of recipient cells through their transmembrane proteins to activate downstream intracellular signaling pathways. EVs can also be directly endocytosed by recipient cells to release their contents (Jaiswal et al., 2014). The type of donor cells and the environment in which they are located, such as being in a state of stress, can affect EVs' function and contents (de Jong et al., 2012). The biological functions of EVs and their biogenesis require more studies. Increasing studies in regenerative medicine have focused on the production of protective and pro-regenerative EVs, particularly in cartilage repair.

Studies have revealed the role of EVs in OA pathogenesis, inflammation, and cartilage regeneration and have demonstrated their potential implications for joint disease therapy

(Zhang S. et al., 2018). EVs derived from different types of joint cells participate in maintaining joint homeostasis and can initiate and promote the progression of OA (Murphy et al., 2018). Macrophages and leukocytes infiltrating the synovium could interact with fibroblast-like synovial cells through EVs (Malda et al., 2016). The activated fibroblast-like synovial cells then transmit inflammatory signals, such as cytokines and enzymes, to the macrophages and leukocytes, thus forming a feedback loop that further aggravates OA. These EVs could also cause the degradation of the extracellular matrix and result in changes in the subchondral bone. In an *in vitro* OA model, EVs enhanced cartilage anabolism and relieved inflammation (Wang et al., 2017), thereby delaying cartilage degradation and the progression of OA (Zhu et al., 2017). In addition, EVs protected chondrocytes (Headland et al., 2015) and regulated the physiological activities of various types of immune cells (Lo Sicco et al., 2017), indicating their anti-inflammatory effects. The induction of a regenerative immune phenotype and enhanced metabolic level of chondrocytes promote the formation of type II collagen-rich cartilage that can repair cartilage defects in rat and rabbit OA models (Zhang et al., 2016; Zhang S. et al., 2018). Hydrogel encapsulation delivers EVs at more accurate positions and higher doses, thereby significantly enhancing repair ability (Liu et al., 2017).

Recently, the application of stem cell-derived EVs in the treatment of joint damage and OA has received increasing attention. They have been derived from the bone marrow (Cosenza et al., 2018; Vonk et al., 2018), adipose tissue (Lo Sicco et al., 2017), synovium (Zhu et al., 2017), or pluripotent cells, including embryonic stem cells (Zhang et al., 2016; Zhang S. et al., 2018) and iPSCs (Liu et al., 2017; Zhu et al., 2017). Exosomes are the main research target in EVs. The difference between exosomes and microvesicles derived from the same cell has been investigated (Cosenza et al., 2017, 2018). Moreover, EVs containing both exosomes and microvesicles have been analyzed (Headland et al., 2015; Lo Sicco et al., 2017). In addition to sharing similar biological functions with stem cells, stem cell-derived EVs offer significant advantages due to their small size and low immunogenicity. Issues associated with direct cell injection can also be avoided. EVs do not pose the risk of antigen presentation due to differentiation into specific cell types such as MSCs, which allows them to be used in allogeneic therapy. In addition, the biologically active cargoes inside MSC-derived EVs are more stable, and problems such as senescence following expansion or cartilage calcification following induction are eliminated.

Exosomes Derived From Joint Tissues

Exosomes maintain homeostasis (Gao et al., 2018) and facilitate cell-to-cell communication in diseases (Li Z. et al., 2018). The source and content of exosomes determine their functions and biological characteristics. Exosomes secreted by therapeutic cells help treat diseases, while those released by cells in the pathological microenvironment accelerate the disease process. In this section, we discuss the various kinds of exosomes derived from joint tissues and their biological effects in OA.

Cartilage-Derived Exosomes

Osteoarthritis chondrocytes release extracellular articular cartilage matrix vesicles with a diameter of 100 nm and participate in the pathologic mineralization of articular cartilage (Anderson, 2003; Jubeck et al., 2008). Exosomes and articular cartilage matrix vesicles share similar features, including size, morphology, and lipid and protein content (Shapiro et al., 2015), suggesting that they exhibit homologous functions with respect to cell communication (Ni et al., 2019). Exosomes derived from normal primary chondrocytes (D0 exosomes) could restore mitochondrial function and enhance immune infiltration by increasing the ratio of M2/M1 macrophages. The intra-articular injection of D0 exosomes effectively suppressed the occurrence and development of OA (Zheng et al., 2019). OA chondrocyte-derived exosomes stimulated the activation of inflammasomes in macrophages and released mature IL-1β via the miR-449a-5p/ATG4B/autophagy pathway, thereby inducing synovitis and exacerbating OA (Ni et al., 2019). In addition, exosomes derived from chondrocytes could achieve efficient ectopic chondrogenesis of cartilage progenitor cell (CPC) constructs, representing a novel cell-free therapeutic approach for cartilage regeneration (Chen et al., 2018).

Synovial-Derived Exosomes

Microvesicles derived from neutrophils have been shown to penetrate cartilage, implying that EVs from the synovium could meditate the crosstalk between the synovium and cartilage (Headland et al., 2015). Kato et al. employed IL-1β to stimulate normal SFB, isolated the secreted exosomes, and co-cultured them with chondrocytes. They found that the expression of catabolic-related genes, such as *MMP13* and *ADAMTS-5*, significantly increased, whereas that of anabolic-related genes, such as *COL2A1* and *ACAN*, significantly decreased. In addition, these exosomes promoted the production of proteoglycan from cartilage explants (Kato et al., 2014). These findings indicate that synovial-derived exosomes could induce OA-like phenotype both *in vivo* and *in vitro*.

Exosomes derived from other synovial cells, such as macrophages, have also been studied. For instance, the effects of salazosulfapyridine and methotrexate on the proteome of exosomes produced by a human synovial sarcoma cell line (SW982) have been investigated. Tsuno et al. observed that these anti-rheumatic drugs altered the protein profiles of SW982-derived exosomes and inhibited the effect of IL-1β on the exosomal proteome (Tsuno et al., 2016).

Subchondral Bone-Derived Exosomes

Exosomes derived from cells in the subchondral bone, including osteoblasts, osteoclasts, and bone marrow mesenchymal stem cells, regulate the microenvironment of subchondral bone (Li et al., 2016; Sun W. et al., 2016). Osteoblasts in the subchondral bone of patients with different degrees of OA secreted exosomes positive for HSP70, CD9, and flotillin-1 (exosomal markers) and a diameter ranging between 30–150 nm. In addition, these exosomes contained a large number of miRNAs, such as miR-135a-3p, miR-210-5p, miR-885-3p, and

miR-1225-5p. Exosomes derived from cells in other subchondral bones also have diagnostic value.

Therapeutic Potential of Stem Cell-Derived Exosomes in OA

Stem cells, such as BMSCs and AMSCs, promote cartilage regeneration and have been used in clinical trials for OA treatment (Lee and Wang, 2017; De Bari and Roelofs, 2018). The safety and feasibility of intra-articular injection of MSC have been confirmed (Di Matteo et al., 2019), which can partially relieve knee joint pain (Yokota et al., 2019) and improve the knee society clinical rating system (KSS) and the outcome score of OA (Jo et al., 2017; Kim et al., 2020). Stem cells exert therapeutic effects mainly through their paracrine functions, such as the secretion of EVs (Phinney and Pittenger, 2017). In this section, we summarize the recent studies on exosomes derived from different types of stem cells, focusing on their roles in the occurrence and development of OA and their therapeutic potential.

BMSC-derived exosomes

Exosomes derived from BMSCs (BMSC-Exos) can promote the regeneration and repair of damaged cartilage and subchondral bone (Mianehsaz et al., 2019; Asghar et al., 2020). The exosomes and microvesicles from TGFβ3-pre-treated BMSCs increased the expression of anabolic markers and decreased the levels of catabolic marker genes in osteoarthritic chondrocytes. In addition, these BMSC-derived exosomes could prevent osteoarthritic chondrocytes from undergoing apoptosis (Cosenza et al., 2017). BMSC-Exos could be taken up by chondrocytes to abolish damage to the mitochondrial membrane potential and IL-1β-induced apoptosis (Qi et al., 2019). BMSC-Exos could also affect the phenotype of other cells in OA joints by inhibiting the activity of osteoclasts in subchondral bone and activating macrophages in the synovium (Li et al., 2020), and suppressing the proliferative activity of SFB pre-treated with IL-1β and increasing its apoptosis. In an *in vivo* OA model, the injection of BMSC-Exos into the joint cavity abrogated the damage and degradation of cartilage and subchondral bone and decreased synovial tissue proliferation and inflammatory cell infiltration, thereby alleviating the symptoms of OA (Jin et al., 2020).

Genetic modification or drug intervention can influence the effect of exosomes on recipient cells by regulating the secretion and contents of exosomes (Ma et al., 2017; Liu and Su, 2019). Exosomes secreted by BMSCs overexpressing miR-92a-3p were collected and applied to chondrocytes. The expression levels of SOX9, COL2A1, and aggrecan increased, whereas those of RUNX2 and MMP13 decreased, indicating that modified BMSC-Exos greatly enhance cartilage repair (Mao et al., 2018). In addition, *in vivo*, and *in vitro* experiments showed that kartogenin-pre-treated BMSC-Exos more significantly enhanced cartilage formation and damage repair than normal BMSC-Exos (Liu et al., 2020).

BMSC-derived exosomes

In vitro synovial mesenchymal stem cells (SMSCs) possess an exceptionally high capacity for cartilage differentiation (Kurth et al., 2007). One study using allogenic tissue-engineered constructs reported that SMSCs from OA patients effectively enhanced cartilage repair (Koizumi et al., 2016). In animal OA models, the injection of SMSC into the joint cavity inhibited the occurrence and development of OA (Ozeki et al., 2016; Kondo et al., 2019). Exosomes derived from SMSC (SMSC-Exos) could not only induce the proliferation and migration of chondrocytes but also reduce the secretion of ECM. Interestingly, SMSC-Exos transfected with miR-140-5p blocked damage to ECM, effectively reduced joint damage, lowered the OARSI score, and delayed the occurrence and development of OA (Tao et al., 2017). In addition to maintaining cartilage homeostasis, SMSC-Exos can regulate bone remodeling (including subchondral bone changes and osteophyte formation) by reducing glucocorticoid-induced fat cell accumulation, trabecular bone loss, and bone marrow necrosis. In addition, SMSC-Exos could partially reverse proliferation arrest and glucocorticoid-induced apoptosis of BMSCs (Guo et al., 2016).

IPFP MSC-derived exosomes

Infrapatellar fat pad plays a key role in knee joint function and pathology. IPFP-derived MSCs (IPFP MSCs) have been suggested as promising cell sources for OA treatment owing to their potent capability for cartilage regeneration (Buckley et al., 2010; Koh and Choi, 2012). In a DMM-induced OA mouse model, exosomes derived from IPFP MSCs effectively reduced cartilage damage and improved abnormal gait. RNA sequencing analysis of the exosomes revealed high miR-100-5p levels, indicating that exosomal IPFP MSCs may inhibit the mTOR pathway via miR-100-5p to regulate chondrocyte phenotype (Wu et al., 2019). The physiological and pathological effects of other exosomes in the IPFP, such as those secreted by adipocytes, also have research value.

AMSC-derived exosomes

Although the mechanism by which AMSCs induce cartilage regeneration is unclear, mounting evidence suggests that AMSCs regulate the cartilage microenvironment by secreting paracrine growth factors (Damia et al., 2018). EVs, including exosomes and microvesicles, mainly mediate the paracrine effects of osteoblasts in OA. AMSC-derived exosomes (AMSC-Exos) reduced the accumulation of senescence-associated β-galactosidase and γH2AX foci in osteoblasts pre-treated with IL-1β, decreased the levels of PGE2 and IL-6, increased that of IL-10, and downregulated the mitochondrial membrane potential (Tofiño-Vian et al., 2017). In addition, AMSC-Exos could inhibit the production of pro-inflammatory mediators, such as TNF-α and NO, and suppress the activity of MMP while enhancing that of anti-inflammatory cytokines, such as IL-10 and type II collagen. These findings indicate the anti-inflammatory and chondroprotective effects of AMSC-Exos (Tofiño-Vian et al., 2018). AMSC-derived EVs (86.46 nm in diameter) promoted the proliferation and migration of OA chondrocytes and maintained the metabolic balance of ECM. In monosodium iodoacetate (MIA) rat and DMM mouse models, the injection of AMSC-derived EVs into the joint cavity effectively delayed OA progression and showed protective effects against cartilage degeneration (Woo et al., 2020). ADSCs-Exos could downregulate the expression of pro-inflammatory genes

in SFB and increase anti-inflammatory cytokines, promoting the proliferation and cartilage formation of periosteal cells via miR-145 and miR-221 (Zhao C. et al., 2020). Overall, AMSC-Exos has great therapeutic potential for the treatment of OA.

Embryonic mesenchymal stem cell (EMSC)-derived exosomes

Embryonic mesenchymal stem cells are another potential candidate for cartilage regeneration and OA treatment (Mamidi et al., 2016; Gibson et al., 2017). Recently, exosomes derived from embryonic MSCs (EMSC-Exos) have been reported to regulate the phenotype of chondrocytes and delayed OA progression (Zhang S. et al., 2018; Zhang et al., 2019). After successfully isolating and identifying EMSC-Exos, Zhang et al. (2016) injected them into osteochondral defects in rats. After 6 weeks, cartilage and subchondral bone damage were largely reversed, and complete recovery was achieved at 12 weeks. Similarly, exosomes derived from the E1-MYC 16.3 human embryonic stem cell line reduced the production of M1 macrophages and pro-inflammatory cytokines and increased the infiltration of M2 macrophages. In addition, this study observed that EMSC-Exos could be endocytosed by chondrocytes to regulate their chondrocyte proliferation, migration, and matrix synthesis (Zhang S. et al., 2018). In an OA model of the temporomandibular joint in rats, EMSC-Exos reduced inflammation, alleviated early pain, and promoted cartilage repair and subchondral bone healing. The activation of AKT, ERK, and AMPK pathways can also reverse IL-1β-induced production of MMP13 and NO and inhibit sGAG synthesis (Zhang et al., 2019). TGF-β1 increases miR-135b levels in EMSC-Exos, thereby reducing the expression of Sp1 to promote the proliferation of chondrocytes and accelerate cartilage repair (Wang et al., 2018).

Exosomes derived from other stem cells

Exosomes derived from amniotic fluid stem cells (AFSC-Exos) in an MIA-induced OA model improved the pain tolerance, induced the restoration of regular hyaline cartilage, and inhibited the polarization of M1 macrophages, suggesting that AFSC-Exos can regulate inflammation (Zavatti et al., 2020). Meanwhile, those derived from umbilical mesenchymal stem cells (UMSC-Exos) induced chondroprotective effects, including increased proliferation and migration of chondrocytes, increased ECM synthesis, and reduced cell apoptosis. UMSC-Exos produced from 3D culture enhanced cartilage repair compared to those from 2D culture (Yan and Wu, 2020). Exosomes secreted by MSCs derived from pluripotent stem cells (with a diameter of approximately 50–150 nm; iMSC-Exos) significantly promoted the proliferation and migration of chondrocytes and had improved efficacy for OA treatment compared with SMSC-Exos (Zhu et al., 2017).

However, how the exosomes in joint tissues and cells participate in OA initiation remains unclear. In addition to their positive therapeutic effects, exosomes in the OA microenvironment may exert unwanted effects, including promotion of inflammation and inhibition of cartilage repair. Therefore, it is also imperative to explore the mechanism of "negative" exosomes in OA. A recent study on exosomes in the plasma and synovial fluid reported their diagnostic value in patients with OA (Zhao and Xu, 2018). However, the exosomes shared by these two tissues could not distinguish between early-stage and late-stage OA. Notably, the expression level of exosomal lncRNA PCGEM1 in synovial fluid was significantly higher in patients with advanced OA than in those with early OA and was higher in early OA, indicating that exosomal lncRNA PCGEM1 from synovial fluid may be a powerful indicator for distinguishing early-stage and late-stage OA. lncRNA PCGEM1 acts as sponge lncRNA targeting miR-770 and promotes the proliferation of synovial cells (Kang et al., 2016). In general, the clinical utility of exosomes as diagnostic biomarkers for OA diagnosis is in its preliminary stages.

Cell Tissue Engineering

Recent attempts to differentiate iPSCs derived from OA patients into chondrocytes have been conducted. Generally, the addition of growth factors, such as TGF-β, FGF-2, BMP, and WNT3A, and paracrine factors, such as Ihh and Runx, to the culture medium is necessary to drive iPSCs to the chondrogenic lineage (Yamashita et al., 2018; Zhao Y. et al., 2020). Currently, four main methods are available: (1) transformation of iPSCs into MSC-like cells and their differentiation into chondrocytes (Nejadnik et al., 2015); (2) co-culture of MSCs derived from iPSCs with primary chondrocytes (Qu et al., 2013); (3) formation of embryoid bodies (EBs) (Nakagawa et al., 2009); (4) cultivation of iPSCs in a medium that mimics the physiological environment during development (Diekman et al., 2012). Studies aiming to form iPSCs through EB and co-culture them with chondrocytes have been conducted (Wei et al., 2012). First, the chondrocytes of OA patients were reprogrammed into OA-iPSCs by lentivirus induction. After the formation of EB, they were continually cultured in the chondrogenic medium for 14 days. Subsequently, the iPSCs were transfected with a lentivirus carrying TGF-1β and inoculated on alginate matrix-coated dishes. After culturing for another 14 days, TGF-1β/iPSCs were subcutaneously injected into the back of mice. Ectopic cartilage tissue was observed at 6 weeks after transplantation.

Engineered cartilage tissue from chondrocytes, when transiently transfected circuits activate the *PTGS2* gene, immunomodulatory IL-4 is produced, thereby representing a new immunomodulatory method (Nims et al., 2021). Autologous articular chondrocytes are an established cell-based tissue engineering strategy for treating knee cartilage or osteochondral defects (Brittberg et al., 1994). Most of the current scaffolds or biomaterials contain MSCs that can undergo chondrogenic differentiation and are used as clinically relevant chondrogenic implants to repair cartilage defects. However, after their implantation in the body, differentiated chondrocytes showed a hypertrophic phenotype (collagen X, MMP13) and induced ectopic bone formation (Pelttari et al., 2006). Therefore, the production of articular chondrocytes with stable, extracellular matrix and phenotype is the main goal of *in vitro* cartilage tissue engineering.

Macrophages are among the main types of cells that affect joint homeostasis and have been applied for the development of related cell engineering technologies. In addition

to using biomaterial scaffolds to regulate macrophage-induced inflammation, macrophages themselves have been utilized for drug delivery or treatment. The intrinsic homing ability of macrophages allows their migration to the site of inflammation or injury in OA. Using this feature, autologous M1 macrophages are used to deliver nanoparticle-encapsulated drugs to induce transient phagosome maturation arrest (Visser et al., 2019). The regular use of clustered interspaced short palindromic repeats (CRISPR)-Cas9 genome editing to create a cell-autonomous system ("SMART" cell), which is derived from mouse induced pluripotent stem cells (miPSCs), has also been attempted. Chondrocytes can automatically regulate inflammation in both *in vivo* and *in vitro* OA models. When "SMART" chondrocytes receive specific targeting signals (such as inflammatory cytokines IL-1 or TNF-α), they released corresponding biological drugs, such as IL-1Ra and or soluble TNFR1, to relieve inflammation (Brunger et al., 2017; Pferdehirt et al., 2019). In the same way, the design of self-regulating "SMART" macrophages enables these cells to not only automatically home to the inflammation/injury site but also to have cytokine-activated feedback-controlled capabilities. Thus, targeted drugs can be effectively delivered to treat joint diseases (Adkar et al., 2017). Overall, cell tissue engineering is a powerful tool to develop new modalities for OA treatment.

CONCLUSION AND PROSPECTS

This review discusses the functions of different types of cells in the joints and their roles in OA, the interaction among various joint cells and tissues, and the latest cell tissue engineering techniques. Our article provides a comprehensive summary of the complex mechanisms underlying the occurrence and development of OA and potential targets of future therapies for OA (**Figure 1**). Among the various cell types, MSCs and their secreted products (EVs) are the focus of future research (**Figure 2**).

Increasing studies have demonstrated the clinical applications of MSCs (Mendicino et al., 2014), such as their role in promoting cartilage repair and delaying the progression of OA (Lee and Wang, 2017). In phase I and II clinical trials, the injection of MSCs into the joint cavity is reportedly reliable and safe. A 5-year follow-up survey demonstrated the efficacy of MSCs in improving cartilage quality and joint function (Yubo et al., 2017; McIntyre et al., 2018). However, the use of MSCs for OA treatment has certain limitations. For example, cell survival and long-term cell behavior after injection are difficult to predict, and the maintenance of cell banks is also a major challenge (Heldring et al., 2015). The quality of MSCs from different donors varies, particularly from elderly or deceased donors who have reduced proliferation capacity and physiological function. In addition, the *in vitro* expansion of MSCs causes senescence, proliferation decline, and even dedifferentiation (Siddappa et al., 2007). MSCs are also "environmentally responsive," and changes in the microenvironment can cause drastic changes in cell behavior (Murphy et al., 2013). For example, the stimulation of AMSCs by TNF changed the phenotype and resulted in the secretion of pro-inflammatory proteins, which aggravated the inflammatory response (Lee et al., 2010).

Immunotherapy and nanotechnology can help overcome these limitations. At present, genetic engineering techniques, including the use of viral vectors and CRISPR-Cas9 genome

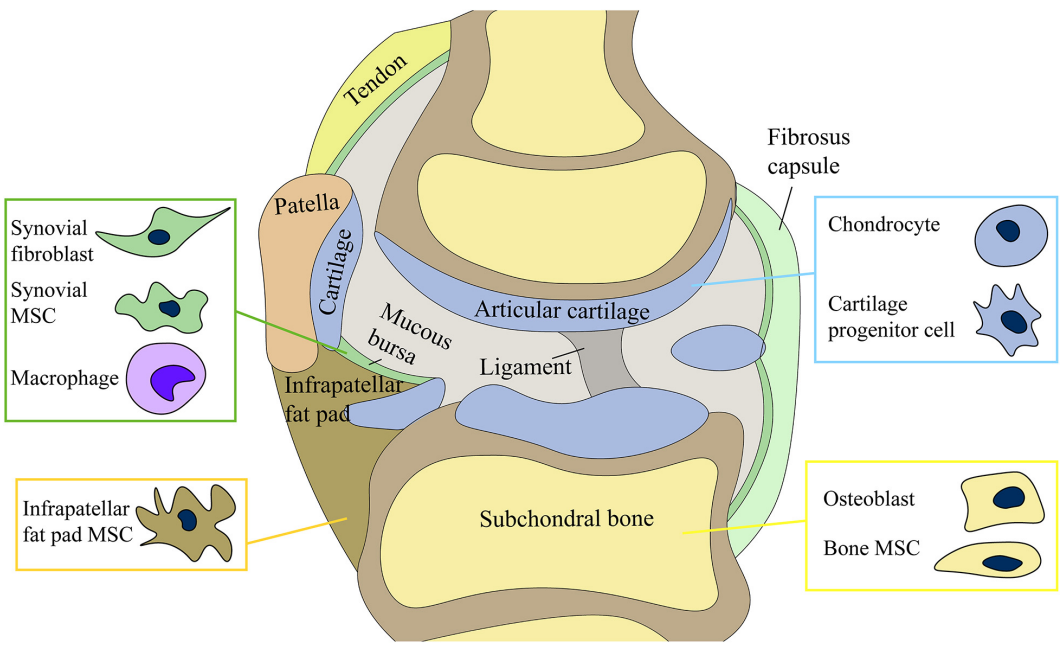

FIGURE 1 | Joint cells) include chondrocytes, osteoblasts of subchondral bone, synovial mesenchymal stem cells (MSCs) and fibroblasts, and infrapatellar fat pad MSCs. The production and release of exosomes by stem cells may be involved in the regulation of joint homeostasis.

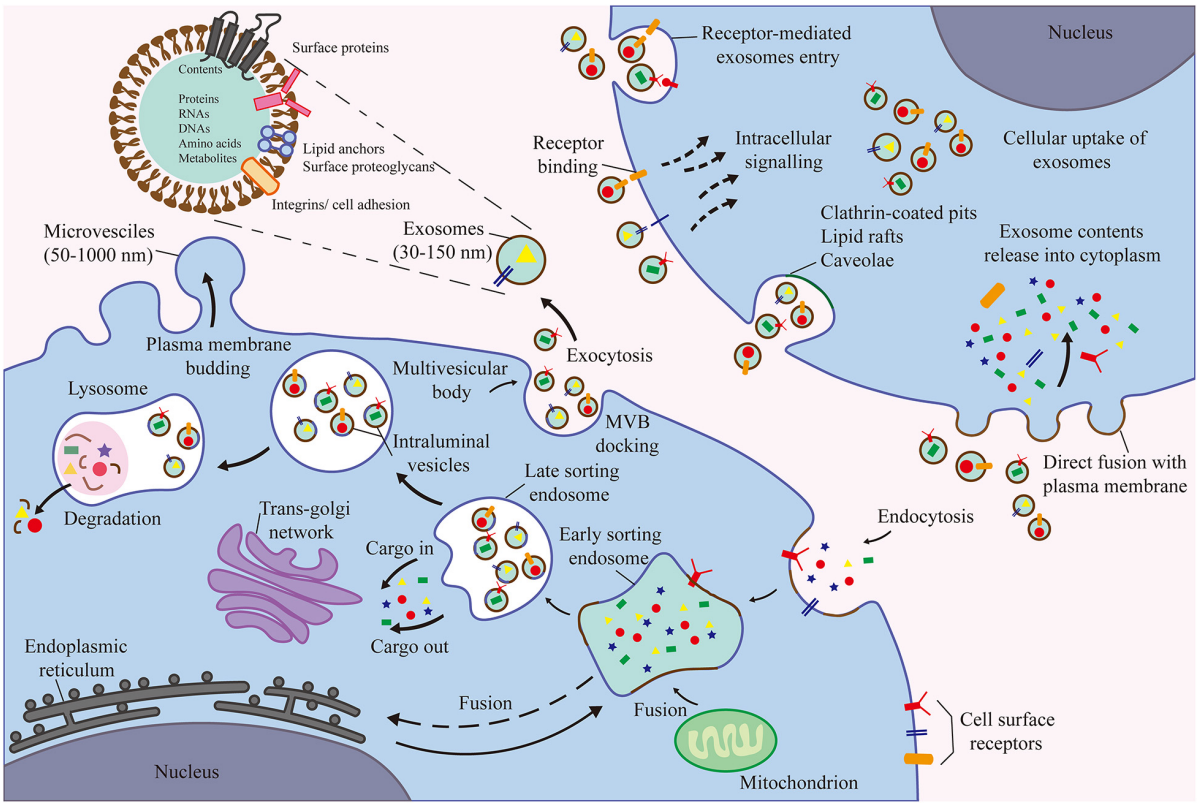

FIGURE 2 | The contents of exosomes are proteins, nucleic acids, amino acids, and metabolites. Extracellular components enter the cell through endocytosis and plasma membrane invagination. Plasma membrane buds are formed on the cavity side and fuse with the components of the endoplasmic reticulum, trans-Golgi network, and mitochondria to form early sorting endosomes. Then, the late sorting endosomes modify the cargo and produce and form various intraluminal vesicles and multivesicular bodies (MVB). Among them, some MVBs degrade after fusion with lysosomes. Other MVB can be transported to the plasma membrane to release intraluminal vesicles as exosomes outside the cell through exocytosis.

editing (Gerace et al., 2017; Pawitan et al., 2020), have been proposed to improve the immune regulation of MSCs. The biological scaffold carrying MSCs expressed IL-1Ra under the influence of exogenous doxycycline, which induces inflammation resistance, contributing to the recovery of degenerative articular cartilage, indicating that cell engineering combined with biological materials can enhance the immunomodulatory ability of MSCs (Glass et al., 2014).

Exploring the function of the products secreted by MSCs, such as EVs, is an alternate direction for OA treatment. The application of stem cell-derived EVs in OA treatment is an emerging field in regenerative medicine. The cargoes delivered by EVs are the same as those of donor cells; however, the former is simpler, more practical, and safer than direct cell transplantation. Exosomes serve as an important mediator of cellular interaction during OA development and have tremendous therapeutic potential. However, this research area has some challenges. At present, there is no direct evidence for the delivery and transfer of endogenous exosomes between cells, which makes identifying the recipient cells of exosomes difficult. The mechanism of exosome production and release in joints also remains unclear, limiting the development of cell therapies that target exosomes. Because cartilage destruction is not severe in early-stage OA, exosomes cannot effectively penetrate the cartilage matrix to interact with cartilage cells. Therefore, current studies on MSC-Exos cell engineering mainly focus on surface chondrocytes, cartilage matrix, synovial cells, and other joint cells that can easily communicate with exosomes.

Future studies on EVs should explore their cell sources, optimized conditions for the production of EVs, their content and biodistribution in the joints, the type of recipient cells or tissues, and their therapeutic mechanisms in OA. Engineered products based on EVs are expected to further promote the interaction between cells, and the intersection between biology and engineering technology can further optimize the function and production of EVs. Finally, it can represent a relatively complete treatment strategy to reduce the burden of OA patients.

A better understanding of the various interactions among cells and tissues in the joint in OA pathogenesis paves the development of future cell-based therapies for OA treatment.

AUTHOR CONTRIBUTIONS

ZL conducted the literature review, drafted the manuscript, and prepared the figures. ZH and LB edited and revised the

manuscript. All authors have substantially contributed to the article and approved the submitted version.

FUNDING

This work was supported by the National Natural Science Foundation of China (grant numbers 81772420, 81272050, and 31900847); the China Postdoctoral Fund (grant number 2019M66169); and the Liaoning Provincial Doctor Start-up Fund (grant number 2019JH3/10100299).

ACKNOWLEDGMENTS

We thank the laboratory affiliated to the China Medical University for the core support.

REFERENCES

Abed, É, Delalandre, A., and Lajeunesse, D. (2017). Beneficial effect of resveratrol on phenotypic features and activity of osteoarthritic osteoblasts. *Arthritis Res. Ther.* 19:151.

Adkar, S. S., Brunger, J. M., Willard, V. P., Wu, C. L., Gersbach, C. A., and Guilak, F. (2017). Genome engineering for personalized arthritis therapeutics. *Trends Mol. Med.* 23, 917–931. doi: 10.1016/j.molmed.2017.08.002

Alsalameh, S., Amin, R., Gemba, T., and Lotz, M. (2004). Identification of mesenchymal progenitor cells in normal and osteoarthritic human articular cartilage. *Arthritis Rheum.* 50, 1522–1532. doi: 10.1002/art.20269

Anderson, H. C. (2003). Matrix vesicles and calcification. *Curr. Rheumatol. Rep.* 5, 222–226.

Asghar, S., Litherland, G. J., Lockhart, J. C., Goodyear, C. S., and Crilly, A. (2020). Exosomes in intercellular communication and implications for osteoarthritis. *Rheumatology (Oxford)* 59, 57–68.

Assoian, R. K., Fleurdelys, B. E., Stevenson, H. C., Miller, P. J., Madtes, D. K., Raines, E. W., et al. (1987). Expression and secretion of type beta transforming growth factor by activated human macrophages. *Proc. Natl. Acad. Sci. U.S.A.* 84, 6020–6024. doi: 10.1073/pnas.84.17.6020

Attur, M., Samuels, J., Krasnokutsky, S., and Abramson, S. B. (2010). Targeting the synovial tissue for treating osteoarthritis (OA): where is the evidence? *Best Pract. Res. Clin. Rheumatol.* 24, 71–79. doi: 10.1016/j.berh.2009.08.011

Aulin, C., Lassacher, T., Palmblad, K., and Erlandsson Harris, H. (2020). Early stage blockade of the alarmin HMGB1 reduces cartilage destruction in experimental OA. *Osteoarthritis Cartilage* 28, 698–707. doi: 10.1016/j.joca.2020.01.003

Bannuru, R. R., Osani, M. C., Vaysbrot, E. E., Arden, N. K., Bennell, K., Bierma-Zeinstra, S. M. A., et al. (2019). OARSI guidelines for the non-surgical management of knee, hip, and polyarticular osteoarthritis. *Osteoarthritis Cartilage* 27, 1578–1589. doi: 10.1016/j.joca.2019.06.011

Barton, K. I., Shekarforoush, M., Heard, B. J., Sevick, J. L., Vakil, P., Atarod, M., et al. (2017). Use of pre-clinical surgically induced models to understand biomechanical and biological consequences of PTOA development. *J. Orthop. Res.* 35, 454–465. doi: 10.1002/jor.23322

Bastiaansen-Jenniskens, Y. M., Wei, W., Feijt, C., Waarsing, J. H., Verhaar, J. A., Zuurmond, A. M., et al. (2013). Stimulation of fibrotic processes by the infrapatellar fat pad in cultured synoviocytes from patients with osteoarthritis: a possible role for prostaglandin f2α. *Arthritis Rheum.* 65, 2070–2080. doi: 10.1002/art.37996

Beekhuizen, M., Bastiaansen-Jenniskens, Y. M., Koevoet, W., Saris, D. B., Dhert, W. J., Creemers, L. B., et al. (2011). Osteoarthritic synovial tissue inhibition of proteoglycan production in human osteoarthritic knee cartilage: establishment and characterization of a long-term cartilage-synovium coculture. *Arthritis Rheum.* 63, 1918–1927. doi: 10.1002/art.30364

Behrends, D. A., Cheng, L., Sullivan, M. B., Wang, M. H., Roby, G. B., Zayed, N., et al. (2014). Defective bone repair in mast cell deficient mice with c-Kit loss of function. *Eur. Cells Mater.* 28, 209–221; discussion 21–22.

Bhosale, A. M., and Richardson, J. B. (2008). Articular cartilage: structure, injuries and review of management. *Br. Med. Bull.* 87, 77–95. doi: 10.1093/bmb/ldn025

Biosse-Duplan, M., Baroukh, B., Dy, M., de Vernejoul, M. C., and Saffar, J. L. (2009). Histamine promotes osteoclastogenesis through the differential expression of histamine receptors on osteoclasts and osteoblasts. *Am. J. Pathol.* 174, 1426–1434. doi: 10.2353/ajpath.2009.080871

Bjørge, I. M., Kim, S. Y., Mano, J. F., Kalionis, B., and Chrzanowski, W. (2017). Extracellular vesicles, exosomes and shedding vesicles in regenerative medicine - a new paradigm for tissue repair. *Biomater. Sci.* 6, 60–78. doi: 10.1039/c7bm00479f

Blanco, F. J., Valdes, A. M., and Rego-Pérez, I. (2018). Mitochondrial DNA variation and the pathogenesis of osteoarthritis phenotypes. *Nat. Rev. Rheumatol.* 14, 327–340. doi: 10.1038/s41584-018-0001-0

Bondeson, J., Blom, A. B., Wainwright, S., Hughes, C., Caterson, B., and van den Berg, W. B. (2010). The role of synovial macrophages and macrophage-produced mediators in driving inflammatory and destructive responses in osteoarthritis. *Arthritis Rheum.* 62, 647–657. doi: 10.1002/art.27290

Bosserhoff, A. K., Hofmeister, S., Ruedel, A., and Schubert, T. (2014). DCC is expressed in a CD166-positive subpopulation of chondrocytes in human osteoarthritic cartilage and modulates CRE activity. *Int. J. Clin. Exp. Pathol.* 7, 1947–1956.

Brandt, K. D., Radin, E. L., Dieppe, P. A., and van de Putte, L. (2006). Yet more evidence that osteoarthritis is not a cartilage disease. *Ann. Rheum. Dis.* 65, 1261–1264. doi: 10.1136/ard.2006.058347

Bridges, A. J., Malone, D. G., Jicinsky, J., Chen, M., Ory, P., Engber, W., et al. (1991). Human synovial mast cell involvement in rheumatoid arthritis and osteoarthritis. Relationship to disease type, clinical activity, and antirheumatic therapy. *Arthritis Rheum.* 34, 1116–1124. doi: 10.1002/art.1780340907

Brittberg, M., Lindahl, A., Nilsson, A., Ohlsson, C., Isaksson, O., and Peterson, L. (1994). Treatment of deep cartilage defects in the knee with autologous chondrocyte transplantation. *N. Engl. J. Med.* 331, 889–895.

Brunger, J. M., Zutshi, A., Willard, V. P., Gersbach, C. A., and Guilak, F. (2017). Genome engineering of stem cells for autonomously regulated, closed-loop delivery of biologic drugs. *Stem Cell Rep.* 8, 1202–1213. doi: 10.1016/j.stemcr.2017.03.022

Buckley, C. T., Vinardell, T., and Kelly, D. J. (2010). Oxygen tension differentially regulates the functional properties of cartilaginous tissues engineered from infrapatellar fat pad derived MSCs and articular chondrocytes. *Osteoarthritis Cartilage* 18, 1345–1354. doi: 10.1016/j.joca.2010.07.004

Buckley, M. G., Walters, C., Wong, W. M., Cawley, M. I., Ren, S., Schwartz, L. B., et al. (1997). Mast cell activation in arthritis: detection of alpha- and beta-tryptase, histamine and eosinophil cationic protein in synovial fluid. *Clin. Sci. (Lond. Engl. 1979)* 93, 363–370. doi: 10.1042/cs0930363

Buhrmann, C., Mobasheri, A., Matis, U., and Shakibaei, M. (2010). Curcumin mediated suppression of nuclear factor-κB promotes chondrogenic differentiation of mesenchymal stem cells in a high-density co-culture microenvironment. *Arthritis Res. Ther.* 12:R127.

Burr, D. B. (1998). The importance of subchondral bone in osteoarthrosis. *Curr. Opin. Rheumatol.* 10, 256–262. doi: 10.1097/00002281-199805000-00017

Cao, Y., Jansen, I. D., Sprangers, S., Stap, J., Leenen, P. J., Everts, V., et al. (2016). IL-1β differently stimulates proliferation and multinucleation of distinct mouse bone marrow osteoclast precursor subsets. *J. Leukoc. Biol.* 100, 513–523. doi: 10.1189/jlb.1a1215-543r

Castañeda, S., Roman-Blas, J. A., Largo, R., and Herrero-Beaumont, G. (2012). Subchondral bone as a key target for osteoarthritis treatment. *Biochem. Pharmacol.* 83, 315–323. doi: 10.1016/j.bcp.2011.09.018

Champagne, C. M., Takebe, J., Offenbacher, S., and Cooper, L. F. (2002). Macrophage cell lines produce osteoinductive signals that include bone morphogenetic protein-2. *Bone* 30, 26–31. doi: 10.1016/s8756-3282(01)00638-x

Chen, S., Fu, P., Wu, H., and Pei, M. (2017). Meniscus, articular cartilage and nucleus pulposus: a comparative review of cartilage-like tissues in anatomy, development and function. *Cell Tissue Res.* 370, 53–70. doi: 10.1007/s00441-017-2613-0

Chen, Y., Wang, T., Guan, M., Zhao, W., Leung, F. K., Pan, H., et al. (2015). Bone turnover and articular cartilage differences localized to subchondral cysts in knees with advanced osteoarthritis. *Osteoarthritis Cartilage* 23, 2174–2183. doi: 10.1016/j.joca.2015.07.012

Chen, Y., Xue, K., Zhang, X., Zheng, Z., and Liu, K. (2018). Exosomes derived from mature chondrocytes facilitate subcutaneous stable ectopic chondrogenesis of cartilage progenitor cells. *Stem Cell Res. Ther.* 9:318.

Chen, Z., Ma, Y., Li, X., Deng, Z., Zheng, M., and Zheng, Q. (2020). the immune cell landscape in different anatomical structures of knee in osteoarthritis: a gene expression-based study. *Biomed. Res. Int.* 2020:9647072.

Clarke, B. (2008). Normal bone anatomy and physiology. *Clin. J. Am. Soc. Nephrol. CJASN* 3 (Suppl. 3), S131–S139.

Clockaerts, S., Bastiaansen-Jenniskens, Y. M., Runhaar, J., Van Osch, G. J., Van Offel, J. F., Verhaar, J. A., et al. (2010). The infrapatellar fat pad should be considered as an active osteoarthritic joint tissue: a narrative review. *Osteoarthritis Cartilage* 18, 876–882. doi: 10.1016/j.joca.2010.03.014

Cooper, A. M., and Khader, S. A. (2007). IL-12p40: an inherently agonistic cytokine. *Trends Immunol.* 28, 33–38. doi: 10.1016/j.it.2006.11.002

Corrado, A., Neve, A., and Cantatore, F. P. (2013). Expression of vascular endothelial growth factor in normal, osteoarthritic and osteoporotic osteoblasts. *Clin. Exp. Med.* 13, 81–84. doi: 10.1007/s10238-011-0170-5

Correa, D., Somoza, R. A., Lin, P., Greenberg, S., Rom, E., Duesler, L., et al. (2015). Sequential exposure to fibroblast growth factors (FGF) 2, 9 and 18 enhances hMSC chondrogenic differentiation. *Osteoarthritis Cartilage* 23, 443–453. doi: 10.1016/j.joca.2014.11.013

Cosenza, S., Ruiz, M., Toupet, K., Jorgensen, C., and Noël, D. (2017). Mesenchymal stem cells derived exosomes and microparticles protect cartilage and bone from degradation in osteoarthritis. *Sci. Rep.* 7:16214.

Cosenza, S., Toupet, K., Maumus, M., Luz-Crawford, P., Blanc-Brude, O., Jorgensen, C., et al. (2018). Mesenchymal stem cells-derived exosomes are more immunosuppressive than microparticles in inflammatory arthritis. *Theranostics* 8, 1399–1410. doi: 10.7150/thno.21072

Culemann, S., Grüneboom, A., Nicolás-Ávila, J., Weidner, D., Lämmle, K. F., Rothe, T., et al. (2019). Locally renewing resident synovial macrophages provide a protective barrier for the joint. *Nature* 572, 670–675. doi: 10.1038/s41586-019-1471-1

Cutolo, M., Berenbaum, F., Hochberg, M., Punzi, L., and Reginster, J. Y. (2015). Commentary on recent therapeutic guidelines for osteoarthritis. *Semin. Arthritis Rheum.* 44, 611–617. doi: 10.1016/j.semarthrit.2014.12.003

Damia, E., Chicharro, D., Lopez, S., Cuervo, B., Rubio, M., Sopena, J. J., et al. (2018). Adipose-Derived mesenchymal stem cells: are they a good therapeutic strategy for osteoarthritis? *Int. J. Mol. Sci.* 19:1926. doi: 10.3390/ijms19071926

De Bari, C., and Roelofs, A. J. (2018). Stem cell-based therapeutic strategies for cartilage defects and osteoarthritis. *Curr. Opin. Pharmacol.* 40, 74–80. doi: 10.1016/j.coph.2018.03.009

De Jong, O. G., Van Balkom, B. W., Schiffelers, R. M., Bouten, C. V., and Verhaar, M. C. (2014). Extracellular vesicles: potential roles in regenerative medicine. *Front. Immunol.* 5:608. doi: 10.3389/fimmu.2014.00608

de Jong, O. G., Verhaar, M. C., Chen, Y., Vader, P., Gremmels, H., Posthuma, G., et al. (2012). Cellular stress conditions are reflected in the protein and RNA content of endothelial cell-derived exosomes. *J. Extracell. Vesicles* 1:18396. doi: 10.3402/jev.v1i0.18396

de Lange-Brokaar, B. J., Ioan-Facsinay, A., van Osch, G. J., Zuurmond, A. M., Schoones, J., Toes, R. E., et al. (2012). Synovial inflammation, immune cells and their cytokines in osteoarthritis: a review. *Osteoarthritis Cartilage* 20, 1484–1499. doi: 10.1016/j.joca.2012.08.027

Di Matteo, B., Vandenbulcke, F., Vitale, N. D., Iacono, F., Ashmore, K., Marcacci, M., et al. (2019). Minimally manipulated mesenchymal stem cells for the treatment of knee osteoarthritis: a systematic review of clinical evidence. *Stem Cells Int.* 2019:1735242.

Dickson, B. M., Roelofs, A. J., Rochford, J. J., Wilson, H. M., and De Bari, C. (2019). The burden of metabolic syndrome on osteoarthritic joints. *Arthritis Res. Ther.* 21:289.

Diekman, B. O., Christoforou, N., Willard, V. P., Sun, H., Sanchez-Adams, J., Leong, K. W., et al. (2012). Cartilage tissue engineering using differentiated and purified induced pluripotent stem cells. *Proc. Natl. Acad. Sci. U.S.A.* 109, 19172–19177. doi: 10.1073/pnas.1210422109

Dieppe, P., Lim, K., and Lohmander, S. (2011). Who should have knee joint replacement surgery for osteoarthritis? *Int. J. Rheum. Dis.* 14, 175–180. doi: 10.1111/j.1756-185x.2011.01611.x

Ding, D. C., Wu, K. C., Chou, H. L., Hung, W. T., Liu, H. W., and Chu, T. Y. (2015). Human infrapatellar fat pad-derived stromal cells have more potent differentiation capacity than other mesenchymal cells and can be enhanced by hyaluronan. *Cell Transplant.* 24, 1221–1232. doi: 10.3727/096368914x681937

Dragoo, J. L., Johnson, C., and McConnell, J. (2012). Evaluation and treatment of disorders of the infrapatellar fat pad. *Sports Med. (Auckland, NZ)* 42, 51–67. doi: 10.2165/11595680-000000000-00000

Dutta, B., Arya, R. K., Goswami, R., Alharbi, M. O., Sharma, S., and Rahaman, S. O. (2020). Role of macrophage TRPV4 in inflammation. *Lab. Invest. J. Tech. Methods Pathol.* 100, 178–185. doi: 10.1038/s41374-019-0334-6

Enomoto, T., Akagi, R., Ogawa, Y., Yamaguchi, S., Hoshi, H., Sasaki, T., et al. (2020). Timing of intra-articular injection of synovial mesenchymal stem cells affects cartilage restoration in a partial thickness cartilage defect model in rats. *Cartilage* 11, 122–129. doi: 10.1177/1947603518786542

Eymard, F., Pigenet, A., Citadelle, D., Flouzat-Lachaniette, C. H., Poignard, A., Benelli, C., et al. (2014). Induction of an inflammatory and prodegradative phenotype in autologous fibroblast-like synoviocytes by the infrapatellar fat pad from patients with knee osteoarthritis. *Arthritis Rheumatol.* 66, 2165–2174. doi: 10.1002/art.38657

Falconer, J., Murphy, A. N., Young, S. P., Clark, A. R., Tiziani, S., Guma, M., et al. (2018). Review: synovial cell metabolism and chronic inflammation in rheumatoid arthritis. *Arthritis Rheumatol.* 70, 984–999. doi: 10.1002/art.40504

Favero, M., El-Hadi, H., Belluzzi, E., Granzotto, M., Porzionato, A., Sarasin, G., et al. (2017). Infrapatellar fat pad features in osteoarthritis: a histopathological and molecular study. *Rheumatology (Oxford)* 56, 1784–1793. doi: 10.1093/rheumatology/kex287

Feng, X., Li, Z., Wei, J., Feng, Z., Wu, W., and Zhao, Y. (2018). Injectable cartilaginous template transformed BMSCs into vascularized bone. *Sci. Rep.* 8:8244.

Fernandes, T. L., Gomoll, A. H., Lattermann, C., Hernandez, A. J., Bueno, D. F., and Amano, M. T. (2020). Macrophage: a potential target on cartilage regeneration. *Front. Immunol.* 11:111. doi: 10.3389/fimmu.2020.00111

Fickert, S., Fiedler, J., and Brenner, R. E. (2004). Identification of subpopulations with characteristics of mesenchymal progenitor cells from human osteoarthritic cartilage using triple staining for cell surface markers. *Arthritis Res. Ther.* 6, R422–R432.

Firestein, G. S., and McInnes, I. B. (2017). Immunopathogenesis of rheumatoid arthritis. *Immunity* 46, 183–196. doi: 10.1016/j.immuni.2017.02.006

Fujisawa, T., Hattori, T., Takahashi, K., Kuboki, T., Yamashita, A., and Takigawa, M. (1999). Cyclic mechanical stress induces extracellular matrix degradation in cultured chondrocytes via gene expression of matrix metalloproteinases and interleukin-1. *J. Biochem.* 125, 966–975. doi: 10.1093/oxfordjournals.jbchem.a022376

Galipeau, J., Krampera, M., Barrett, J., Dazzi, F., Deans, R. J., DeBruijn, J., et al. (2016). International Society for Cellular Therapy perspective on immune functional assays for mesenchymal stromal cells as potency release criterion for advanced phase clinical trials. *Cytotherapy* 18, 151–159. doi: 10.1016/j.jcyt.2015.11.008

Galli, S. J., and Tsai, M. (2012). IgE and mast cells in allergic disease. *Nat. Med.* 18, 693–704. doi: 10.1038/nm.2755

Gao, M., Gao, W., Papadimitriou, J. M., Zhang, C., Gao, J., and Zheng, M. (2018). Exosomes-the enigmatic regulators of bone homeostasis. *Bone Res.* 6:36.

GBD 2017 Risk Factor Collaborators (2018). Global, regional, and national comparative risk assessment of 84 behavioural, environmental and occupational, and metabolic risks or clusters of risks for 195 countries and territories, 1990-2017: a systematic analysis for the Global Burden of Disease Study 2017. *Lancet* 392, 1923–1994.

Genin, M., Clement, F., Fattaccioli, A., Raes, M., and Michiels, C. (2015). M1 and M2 macrophages derived from THP-1 cells differentially modulate the response of cancer cells to etoposide. *BMC Cancer* 15:577. doi: 10.1186/s12885-015-1546-9

Gerace, D., Martiniello-Wilks, R., Nassif, N. T., Lal, S., Steptoe, R., and Simpson, A. M. (2017). CRISPR-targeted genome editing of mesenchymal stem cell-derived therapies for type 1 diabetes: a path to clinical success? *Stem Cell Res. Ther.* 8:62.

Gibson, J. D., O'Sullivan, M. B., Alaee, F., Paglia, D. N., Yoshida, R., Guzzo, R. M., et al. (2017). Regeneration of articular cartilage by human ESC-Derived mesenchymal progenitors treated sequentially with BMP-2 and Wnt5a. *Stem Cells Transl. Med.* 6, 40–50. doi: 10.5966/sctm.2016-0020

Glass, K. A., Link, J. M., Brunger, J. M., Moutos, F. T., Gersbach, C. A., and Guilak, F. (2014). Tissue-engineered cartilage with inducible and tunable immunomodulatory properties. *Biomaterials* 35, 5921–5931. doi: 10.1016/j.biomaterials.2014.03.073

Gore, M., Tai, K. S., Sadosky, A., Leslie, D., and Stacey, B. R. (2011). Clinical comorbidities, treatment patterns, and direct medical costs of patients with osteoarthritis in usual care: a retrospective claims database analysis. *J. Med. Econ.* 14, 497–507. doi: 10.3111/13696998.2011.594347

Guo, S. C., Tao, S. C., Yin, W. J., Qi, X., Sheng, J. G., and Zhang, C. Q. (2016). Exosomes from human synovial-derived mesenchymal stem cells prevent glucocorticoid-induced osteonecrosis of the femoral head in the rat. *Int. J. Biol. Sci.* 12, 1262–1272. doi: 10.7150/ijbs.16150

Hamilton, A. M., Cheung, W. Y., Gómez-Aristizábal, A., Sharma, A., Nakamura, S., Chaboureau, A., et al. (2019). Iron nanoparticle-labeled murine mesenchymal stromal cells in an osteoarthritic model persists and suggests anti-inflammatory mechanism of action. *PLoS One* 14:e0214107. doi: 10.1371/journal.pone.0214107

Harrell, C. R., Markovic, B. S., Fellabaum, C., Arsenijevic, A., and Volarevic, V. (2019). Mesenchymal stem cell-based therapy of osteoarthritis: current knowledge and future perspectives. *Biomed. Pharmacother.* 109, 2318–2326. doi: 10.1016/j.biopha.2018.11.099

Headland, S. E., Jones, H. R., Norling, L. V., Kim, A., Souza, P. R., Corsiero, E., et al. (2015). Neutrophil-derived microvesicles enter cartilage and protect the joint in inflammatory arthritis. *Sci. Transl. Med.* 7:315ra190. doi: 10.1126/scitranslmed.aac5608

Heldring, N., Mäger, I., Wood, M. J., Le Blanc, K., and Andaloussi, S. E. (2015). Therapeutic potential of multipotent mesenchymal stromal cells and their extracellular vesicles. *Human Gene Ther.* 26, 506–517. doi: 10.1089/hum.2015.072

Hendriks, J., Riesle, J., and van Blitterswijk, C. A. (2007). Co-culture in cartilage tissue engineering. *J. Tissue Eng. Regen. Med.* 1, 170–178. doi: 10.1002/term.19

Henrotin, Y., Pesesse, L., and Sanchez, C. (2012). Subchondral bone and osteoarthritis: biological and cellular aspects. *Osteoporos. Int.* 23(Suppl. 8), S847–S851.

Hilal, G., Martel-Pelletier, J., Pelletier, J. P., Ranger, P., and Lajeunesse, D. (1998). Osteoblast-like cells from human subchondral osteoarthritic bone demonstrate an altered phenotype in vitro: possible role in subchondral bone sclerosis. *Arthritis Rheum.* 41, 891–899. doi: 10.1002/1529-0131(199805)41:5<891::aid-art17>3.0.co;2-x

Hoshi, H., Akagi, R., Yamaguchi, S., Muramatsu, Y., Akatsu, Y., Yamamoto, Y., et al. (2017). Effect of inhibiting MMP13 and ADAMTS5 by intra-articular injection of small interfering RNA in a surgically induced osteoarthritis model of mice. *Cell Tissue Res.* 368, 379–387. doi: 10.1007/s00441-016-2563-y

Hunter, D. J., and Bierma-Zeinstra, S. (2019). Osteoarthritis. *Lancet* 393, 1745–1759.

Ioan-Facsinay, A., Kwekkeboom, J. C., Westhoff, S., Giera, M., Rombouts, Y., van Harmelen, V., et al. (2013). Adipocyte-derived lipids modulate CD4+ T-cell function. *Eur. J. Immunol.* 43, 1578–1587. doi: 10.1002/eji.201243096

Jaiswal, R., Raymond Grau, G. E., and Bebawy, M. (2014). Cellular communication via microparticles: role in transfer of multidrug resistance in cancer. *Future Oncol. (Lond. Engl.)* 10, 655–669. doi: 10.2217/fon.13.230

Ji, Q., Zheng, Y., Zhang, G., Hu, Y., Fan, X., Hou, Y., et al. (2019). Single-cell RNA-seq analysis reveals the progression of human osteoarthritis. *Ann. Rheum. Dis.* 78, 100–110. doi: 10.1136/annrheumdis-2017-212863

Jin, Z., Ren, J., and Qi, S. (2020). Human bone mesenchymal stem cells-derived exosomes overexpressing microRNA-26a-5p alleviate osteoarthritis via down-regulation of PTGS2. *Int. Immunopharmacol.* 78:105946. doi: 10.1016/j.intimp.2019.105946

Jo, C. H., Chai, J. W., Jeong, E. C., Oh, S., Shin, J. S., Shim, H., et al. (2017). Intra-articular injection of mesenchymal stem cells for the treatment of osteoarthritis of the knee: a 2-Year follow-up study. *Am. J. Sports Med.* 45, 2774–2783. doi: 10.1177/0363546517716641

Jubeck, B., Gohr, C., Fahey, M., Muth, E., Matthews, M., Mattson, E., et al. (2008). Promotion of articular cartilage matrix vesicle mineralization by type I collagen. *Arthritis Rheum.* 58, 2809–2817. doi: 10.1002/art.23762

Jung, Y. K., Han, M. S., Park, H. R., Lee, E. J., Jang, J. A., Kim, G. W., et al. (2018). Calcium-phosphate complex increased during subchondral bone remodeling affects earlystage osteoarthritis. *Sci. Rep.* 8:487.

Kang, Y., Song, J., Kim, D., Ahn, C., Park, S., Chun, C. H., et al. (2016). PCGEM1 stimulates proliferation of osteoarthritic synoviocytes by acting as a sponge for miR-770. *J. Orthop. Res.* 34, 412–418. doi: 10.1002/jor.23046

Kato, T., Miyaki, S., Ishitobi, H., Nakamura, Y., Nakasa, T., Lotz, M. K., et al. (2014). Exosomes from IL-1β stimulated synovial fibroblasts induce osteoarthritic changes in articular chondrocytes. *Arthritis Res. Ther.* 16:R163.

Katsimbri, P. (2017). The biology of normal bone remodelling. *Eur. J. Cancer Care* 26:e12740. doi: 10.1111/ecc.12740

Kim, S. H., Djaja, Y. P., Park, Y. B., Park, J. G., Ko, Y. B., and Ha, C. W. (2020). Intra-articular injection of culture-expanded mesenchymal stem cells without adjuvant surgery in knee osteoarthritis: a systematic review and meta-analysis. *Am. J. Sports Med.* 48, 2839–2849. doi: 10.1177/0363546519892278

Kim, Y. S., and Koh, Y. G. (2018). Comparative matched-pair analysis of open-wedge high tibial osteotomy with versus without an injection of adipose-derived mesenchymal stem cells for varus knee osteoarthritis: clinical and second-look arthroscopic results. *Am. J. Sports Med.* 46, 2669–2677. doi: 10.1177/0363546518785973

Klein-Wieringa, I. R., Andersen, S. N., Kwekkeboom, J. C., Giera, M., de Lange-Brokaar, B. J., van Osch, G. J., et al. (2013). Adipocytes modulate the phenotype of human macrophages through secreted lipids. *J. Immunol.* 191, 1356–1363. doi: 10.4049/jimmunol.1203074

Kloppenburg, M., and Berenbaum, F. (2020). Osteoarthritis year in review 2019: epidemiology and therapy. *Osteoarthritis Cartilage* 28, 242–248. doi: 10.1016/j.joca.2020.01.002

Kobayashi, K., Takahashi, N., Jimi, E., Udagawa, N., Takami, M., Kotake, S., et al. (2000). Tumor necrosis factor alpha stimulates osteoclast differentiation by a mechanism independent of the ODF/RANKL-RANK interaction. *J. Exp. Med.* 191, 275–286. doi: 10.1084/jem.191.2.275

Koelling, S., Kruegel, J., Irmer, M., Path, J. R., Sadowski, B., Miro, X., et al. (2009). Migratory chondrogenic progenitor cells from repair tissue during the later stages of human osteoarthritis. *Cell Stem Cell* 4, 324–335. doi: 10.1016/j.stem.2009.01.015

Koh, Y. G., and Choi, Y. J. (2012). Infrapatellar fat pad-derived mesenchymal stem cell therapy for knee osteoarthritis. *Knee* 19, 902–907. doi: 10.1016/j.knee.2012.04.001

Koizumi, K., Ebina, K., Hart, D. A., Hirao, M., Noguchi, T., Sugita, N., et al. (2016). Synovial mesenchymal stem cells from osteo- or rheumatoid arthritis joints exhibit good potential for cartilage repair using a scaffold-free tissue engineering approach. *Osteoarthritis Cartilage* 24, 1413–1422. doi: 10.1016/j.joca.2016.03.006

Kondo, S., Nakagawa, Y., Mizuno, M., Katagiri, K., Tsuji, K., Kiuchi, S., et al. (2019). Transplantation of aggregates of autologous synovial mesenchymal stem cells for treatment of cartilage defects in the femoral condyle and the femoral groove in microminipigs. *Am. J. Sports Med.* 47, 2338–2347. doi: 10.1177/0363546519859855

Kouroupis, D., Bowles, A. C., Willman, M. A., Perucca Orfei, C., Colombini, A., Best, T. M., et al. (2019). Infrapatellar fat pad-derived MSC response to inflammation and fibrosis induces an immunomodulatory phenotype involving CD10-mediated Substance P degradation. *Sci. Rep.* 9:10864.

Kreutz, M., Andreesen, R., Krause, S. W., Szabo, A., Ritz, E., and Reichel, H. (1993). 1,25-dihydroxyvitamin D3 production and vitamin D3 receptor expression are developmentally regulated during differentiation of human monocytes into macrophages. *Blood* 82, 1300–1307. doi: 10.1182/blood.v82.4.1300.1300

Kroner, J., Kovtun, A., Kemmler, J., Messmann, J. J., Strauss, G., Seitz, S., et al. (2017). Mast cells are critical regulators of bone fracture-induced inflammation and osteoclast formation and activity. *J. Bone Min. Res.* 32, 2431–2444. doi: 10.1002/jbmr.3234

Kuang, L., Wu, J., Su, N., Qi, H., Chen, H., Zhou, S., et al. (2020). FGFR3 deficiency enhances CXCL12-dependent chemotaxis of macrophages via upregulating CXCR7 and aggravates joint destruction in mice. *Ann. Rheum. Dis.* 79, 112–122. doi: 10.1136/annrheumdis-2019-215696

Kurth, T., Hedbom, E., Shintani, N., Sugimoto, M., Chen, F. H., Haspl, M., et al. (2007). Chondrogenic potential of human synovial mesenchymal stem cells in alginate. *Osteoarthritis Cartilage* 15, 1178–1189. doi: 10.1016/j.joca.2007.03.015

Kwan Tat, S., Pelletier, J. P., Lajeunesse, D., Fahmi, H., Lavigne, M., and Martel-Pelletier, J. (2008). The differential expression of osteoprotegerin (OPG) and receptor activator of nuclear factor kappaB ligand (RANKL) in human osteoarthritic subchondral bone osteoblasts is an indicator of the metabolic state of these disease cells. *Clin. Exp. Rheumatol.* 26, 295–304.

Lach, M., Trzeciak, T., Richter, M., Pawlicz, J., and Suchorska, W. M. (2014). Directed differentiation of induced pluripotent stem cells into chondrogenic lineages for articular cartilage treatment. *J. Tissue Eng.* 5:2041731414552701.

Lamichhane, T. N., Sokic, S., Schardt, J. S., Raiker, R. S., Lin, J. W., and Jay, S. M. (2015). Emerging roles for extracellular vesicles in tissue engineering and regenerative medicine. *Tissue Eng. Part B Rev.* 21, 45–54. doi: 10.1089/ten.teb.2014.0300

Lee, H., Kashiwakura, J., Matsuda, A., Watanabe, Y., Sakamoto-Sasaki, T., Matsumoto, K., et al. (2013). Activation of human synovial mast cells from rheumatoid arthritis or osteoarthritis patients in response to aggregated IgG through Fcγ receptor I and Fcγ receptor II. *Arthritis Rheum.* 65, 109–119. doi: 10.1002/art.37741

Lee, M. J., Kim, J., Kim, M. Y., Bae, Y. S., Ryu, S. H., Lee, T. G., et al. (2010). Proteomic analysis of tumor necrosis factor-alpha-induced secretome of human adipose tissue-derived mesenchymal stem cells. *J. Proteome Res.* 9, 1754–1762. doi: 10.1021/pr900898n

Lee, W. S., Kim, H. J., Kim, K. I., Kim, G. B., and Jin, W. (2019). Intra-Articular injection of autologous adipose tissue-derived mesenchymal stem cells for the treatment of knee osteoarthritis: a phase IIB, randomized, placebo-controlled clinical trial. *Stem Cells Transl. Med.* 8, 504–511. doi: 10.1002/sctm.18-0122

Lee, W. Y., and Wang, B. (2017). Cartilage repair by mesenchymal stem cells: clinical trial update and perspectives. *J. Orthop. Transl.* 9, 76–88. doi: 10.1016/j.jot.2017.03.005

Levy, O., Kuai, R., Siren, E. M. J., Bhere, D., Milton, Y., Nissar, N., et al. (2020). Shattering barriers toward clinically meaningful MSC therapies. *Sci. Adv.* 6:eaba6884. doi: 10.1126/sciadv.aba6884

Li, C. J., Xiao, Y., Yang, M., Su, T., Sun, X., Guo, Q., et al. (2018). Long noncoding RNA Bmncr regulates mesenchymal stem cell fate during skeletal aging. *J. Clin. Invest.* 128, 5251–5266. doi: 10.1172/jci99044

Li, D., Liu, J., Guo, B., Liang, C., Dang, L., Lu, C., et al. (2016). Osteoclast-derived exosomal miR-214-3p inhibits osteoblastic bone formation. *Nat. Commun.* 7:10872.

Li, G., Yin, J., Gao, J., Cheng, T. S., Pavlos, N. J., Zhang, C., et al. (2013). Subchondral bone in osteoarthritis: insight into risk factors and microstructural changes. *Arthritis Res. Ther.* 15:223. doi: 10.1186/ar4405

Li, J., Ding, Z., Li, Y., Wang, W., Wang, J., Yu, H., et al. (2020). BMSCs-Derived exosomes ameliorate pain via abrogation of aberrant nerve invasion in subchondral bone in lumbar facet joint osteoarthritis. *J. Orthop. Res.* 38, 670–679. doi: 10.1002/jor.24497

Li, X., Guo, W., Zha, K., Jing, X., Wang, M., Zhang, Y., et al. (2019). Enrichment of CD146(+) adipose-derived stem cells in combination with articular cartilage extracellular matrix scaffold promotes cartilage regeneration. *Theranostics* 9, 5105–5121. doi: 10.7150/thno.33904

Li, Z., Wang, Y., Xiao, K., Xiang, S., Li, Z., and Weng, X. (2018). Emerging role of exosomes in the joint diseases. *Cell. Physiol. Biochem.* 47, 2008–2017. doi: 10.1159/000491469

Lietman, S. A. (2016). Induced pluripotent stem cells in cartilage repair. *World J. Orthop.* 7, 149–155. doi: 10.5312/wjo.v7.i3.149

Lin, C., Liu, L., Zeng, C., Cui, Z. K., Chen, Y., Lai, P., et al. (2019). Activation of mTORC1 in subchondral bone preosteoblasts promotes osteoarthritis by stimulating bone sclerosis and secretion of CXCL12. *Bone Res.* 7:5.

Liu, B., Zhang, M., Zhao, J., Zheng, M., and Yang, H. (2018). Imbalance of M1/M2 macrophages is linked to severity level of knee osteoarthritis. *Exp. Ther. Med.* 16, 5009–5014.

Liu, C., and Su, C. (2019). Design strategies and application progress of therapeutic exosomes. *Theranostics* 9, 1015–1028. doi: 10.7150/thno.30853

Liu, C., Li, Y., Yang, Z., Zhou, Z., Lou, Z., and Zhang, Q. (2020). Kartogenin enhances the therapeutic effect of bone marrow mesenchymal stem cells derived exosomes in cartilage repair. *Nanomedicine (Lond. Engl.)* 15, 273–288. doi: 10.2217/nnm-2019-0208

Liu, X., Yang, Y., Li, Y., Niu, X., Zhao, B., Wang, Y., et al. (2017). Integration of stem cell-derived exosomes with in situ hydrogel glue as a promising tissue patch for articular cartilage regeneration. *Nanoscale* 9, 4430–4438. doi: 10.1039/c7nr00352h

Lo Sicco, C., Reverberi, D., Balbi, C., Ulivi, V., Principi, E., Pascucci, L., et al. (2017). Mesenchymal stem cell-derived extracellular vesicles as mediators of anti-inflammatory effects: endorsement of macrophage polarization. *Stem Cells Transl. Med.* 6, 1018–1028. doi: 10.1002/sctm.16-0363

Loeser, R. F. (2009). Aging and osteoarthritis: the role of chondrocyte senescence and aging changes in the cartilage matrix. *Osteoarthritis Cartilage* 17, 971–979. doi: 10.1016/j.joca.2009.03.002

Loeser, R. F., Olex, A. L., McNulty, M. A., Carlson, C. S., Callahan, M. F., Ferguson, C. M., et al. (2012). Microarray analysis reveals age-related differences in gene expression during the development of osteoarthritis in mice. *Arthritis Rheum.* 64, 705–717. doi: 10.1002/art.33388

Löfvall, H., Newbould, H., Karsdal, M. A., Dziegiel, M. H., Richter, J., Henriksen, K., et al. (2018). Osteoclasts degrade bone and cartilage knee joint compartments through different resorption processes. *Arthritis Res. Ther.* 20:67.

Ma, J., Zhao, Y., Sun, L., Sun, X., Zhao, X., Sun, X., et al. (2017). Exosomes derived from Akt-modified human umbilical cord mesenchymal stem cells improve cardiac regeneration and promote angiogenesis via activating platelet-derived growth factor D. *Stem Cells Transl. Med.* 6, 51–59. doi: 10.5966/sctm.2016-0038

Malda, J., Boere, J., van de Lest, C. H., van Weeren, P., and Wauben, M. H. (2016). Extracellular vesicles — new tool for joint repair and regeneration. *Nat. Rev. Rheumatol.* 12, 243–249. doi: 10.1038/nrrheum.2015.170

Mamidi, M. K., Das, A. K., Zakaria, Z., and Bhonde, R. (2016). Mesenchymal stromal cells for cartilage repair in osteoarthritis. *Osteoarthritis Cartilage* 24, 1307–1316. doi: 10.1016/j.joca.2016.03.003

Mao, G., Zhang, Z., Hu, S., Zhang, Z., Chang, Z., Huang, Z., et al. (2018). Exosomes derived from miR-92a-3p-overexpressing human mesenchymal stem cells enhance chondrogenesis and suppress cartilage degradation via targeting WNT5A. *Stem Cell Res. Ther.* 9:247.

Martel-Pelletier, J., Barr, A. J., Cicuttini, F. M., Conaghan, P. G., Cooper, C., Goldring, M. B., et al. (2016). Osteoarthritis. *Nat. Rev. Dis. Primers* 2:16072.

Martin, J. A., and Buckwalter, J. A. (2002). Aging, articular cartilage chondrocyte senescence and osteoarthritis. *Biogerontology* 3, 257–264.

Mathiessen, A., and Conaghan, P. G. (2017). Synovitis in osteoarthritis: current understanding with therapeutic implications. *Arthritis Res. Ther.* 19:18.

McIntyre, J. A., Jones, I. A., Han, B., and Vangsness, C. T. Jr. (2018). Intra-articular mesenchymal stem cell therapy for the human joint: a systematic review. *Am. J. Sports Med.* 46, 3550–3563. doi: 10.1177/0363546517735844

Mendicino, M., Bailey, A. M., Wonnacott, K., Puri, R. K., and Bauer, S. R. (2014). MSC-based product characterization for clinical trials: an FDA perspective. *Cell Stem Cell* 14, 141–145. doi: 10.1016/j.stem.2014.01.013

Mesallati, T., Buckley, C. T., and Kelly, D. J. (2017). Engineering cartilaginous grafts using chondrocyte-laden hydrogels supported by a superficial layer of stem cells. *J. Tissue Eng. Regen. Med.* 11, 1343–1353. doi: 10.1002/term.2033

Mesallati, T., Sheehy, E. J., Vinardell, T., Buckley, C. T., and Kelly, D. J. (2015). Tissue engineering scaled-up, anatomically shaped osteochondral constructs for joint resurfacing. *Eur. Cells Mater.* 30, 163–185; discussion 85–86.

Mianehsaz, E., Mirzaei, H. R., Mahjoubin-Tehran, M., Rezaee, A., Sahebnasagh, R., Pourhanifeh, M. H., et al. (2019). Mesenchymal stem cell-derived exosomes: a new therapeutic approach to osteoarthritis? *Stem Cell Res. Ther.* 10:340.

Moradi, S., Mahdizadeh, H., Šarić, T., Kim, J., Harati, J., Shahsavarani, H., et al. (2019). Research and therapy with induced pluripotent stem cells (iPSCs): social, legal, and ethical considerations. *Stem Cell Res. Ther.* 10:341.

Mosser, D. M. (2003). The many faces of macrophage activation. *J. Leukoc. Biol.* 73, 209–212. doi: 10.1189/jlb.0602325

Mosser, D. M., and Edwards, J. P. (2008). Exploring the full spectrum of macrophage activation. *Nat. Rev. Immunol.* 8, 958–969. doi: 10.1038/nri2448

Murphy, C., Withrow, J., Hunter, M., Liu, Y., Tang, Y. L., Fulzele, S., et al. (2018). Emerging role of extracellular vesicles in musculoskeletal diseases. *Mol. Aspects Med.* 60, 123–128. doi: 10.1016/j.mam.2017.09.006

Murphy, M. B., Moncivais, K., and Caplan, A. I. (2013). Mesenchymal stem cells: environmentally responsive therapeutics for regenerative medicine. *Exp. Mol. Med.* 45:e54. doi: 10.1038/emm.2013.94

Nakagawa, T., Lee, S. Y., and Reddi, A. H. (2009). Induction of chondrogenesis from human embryonic stem cells without embryoid body formation by

bone morphogenetic protein 7 and transforming growth factor beta1. *Arthritis Rheum.* 60, 3686–3692. doi: 10.1002/art.27229

Nam, Y., Rim, Y. A., Lee, J., and Ju, J. H. (2018). Current therapeutic strategies for stem cell-based cartilage regeneration. *Stem Cells Int.* 2018:8490489.

Nejadnik, H., Diecke, S., Lenkov, O. D., Chapelin, F., Donig, J., Tong, X., et al. (2015). Improved approach for chondrogenic differentiation of human induced pluripotent stem cells. *Stem Cell Rev. Rep.* 11, 242–253. doi: 10.1007/s12015-014-9581-5

Ni, Z., Kuang, L., Chen, H., Xie, Y., Zhang, B., Ouyang, J., et al. (2019). The exosome-like vesicles from osteoarthritic chondrocyte enhanced mature IL-1β production of macrophages and aggravated synovitis in osteoarthritis. *Cell Death Dis.* 10:522.

Nims, R. J., Pferdehirt, L., Ho, N. B., Savadipour, A., Lorentz, J., Sohi, S., et al. (2021). A synthetic mechanogenetic gene circuit for autonomous drug delivery in engineered tissues. *Sci. Adv.* 7:eabd9858. doi: 10.1126/sciadv.abd9858

Oren, T. W., Botolin, S., Williams, A., Bucknell, A., and King, K. B. (2011). Arthroplasty in veterans: analysis of cartilage, bone, serum, and synovial fluid reveals differences and similarities in osteoarthritis with and without comorbid diabetes. *J. Rehabil. Res. Dev.* 48, 1195–1210. doi: 10.1682/jrrd.2010.09.0186

Ozeki, N., Muneta, T., Koga, H., Nakagawa, Y., Mizuno, M., Tsuji, K., et al. (2016). Not single but periodic injections of synovial mesenchymal stem cells maintain viable cells in knees and inhibit osteoarthritis progression in rats. *Osteoarthritis Cartilage* 24, 1061–1070. doi: 10.1016/j.joca.2015.12.018

Palazzo, C., Nguyen, C., Lefevre-Colau, M. M., Rannou, F., and Poiraudeau, S. (2016). Risk factors and burden of osteoarthritis. *Ann. Phys. Rehabil. Med.* 59, 134–138. doi: 10.1016/j.rehab.2016.01.006

Pap, T. K. A., and Bertrand, M. H. J. (2012). "Joint biochemistry," in *Oxford Textbook of Rheumatology*, 4th Edn, eds R. A. Watts, P. G. Conaghan, C. Denton, H. Foster, J. Isaacs, and U. Müller-Ladner (Oxford: Oxford University Press)

Pawitan, J. A., Bui, T. A., Mubarok, W., Antarianto, R. D., Nurhayati, R. W., Dilogo, I. H., et al. (2020). Enhancement of the therapeutic capacity of mesenchymal stem cells by genetic modification: a systematic review. *Front. Cell Dev. Biol.* 8:587776. doi: 10.3389/fcell.2020.587776

Pearson, M. J., Herndler-Brandstetter, D., Tariq, M. A., Nicholson, T. A., Philp, A. M., Smith, H. L., et al. (2017). IL-6 secretion in osteoarthritis patients is mediated by chondrocyte-synovial fibroblast cross-talk and is enhanced by obesity. *Sci. Rep.* 7:3451.

Peffers, M. J., Chabronova, A., Balaskas, P., Fang, Y., Dyer, P., Cremers, A., et al. (2020). SnoRNA signatures in cartilage ageing and osteoarthritis. *Sci. Rep.* 10:10641.

Pelttari, K., Winter, A., Steck, E., Goetzke, K., Hennig, T., Ochs, B. G., et al. (2006). Premature induction of hypertrophy during in vitro chondrogenesis of human mesenchymal stem cells correlates with calcification and vascular invasion after ectopic transplantation in SCID mice. *Arthritis Rheum.* 54, 3254–3266. doi: 10.1002/art.22136

Pereira, D., Peleteiro, B., Araújo, J., Branco, J., Santos, R. A., and Ramos, E. (2011). The effect of osteoarthritis definition on prevalence and incidence estimates: a systematic review. *Osteoarthritis Cartilage* 19, 1270–1285. doi: 10.1016/j.joca.2011.08.009

Pers, Y. M., Ruiz, M., Noël, D., and Jorgensen, C. (2015). Mesenchymal stem cells for the management of inflammation in osteoarthritis: state of the art and perspectives. *Osteoarthritis Cartilage* 23, 2027–2035. doi: 10.1016/j.joca.2015.07.004

Pferdehirt, L., Ross, A. K., Brunger, J. M., and Guilak, F. (2019). A synthetic gene circuit for self-regulating delivery of biologic drugs in engineered tissues. *Tissue Eng. Part A* 25, 809–820. doi: 10.1089/ten.tea.2019.0027

Phinney, D. G., and Pittenger, M. F. (2017). Concise review: MSC-derived exosomes for cell-free therapy. *Stem Cells (Dayton Ohio)* 35, 851–858. doi: 10.1002/stem.2575

Pietschmann, P., Mechtcheriakova, D., Meshcheryakova, A., Föger-Samwald, U., and Ellinger, I. (2016). Immunology of Osteoporosis: a mini-review. *Gerontology* 62, 128–137. doi: 10.1159/000431091

Qi, H., Liu, D. P., Xiao, D. W., Tian, D. C., Su, Y. W., and Jin, S. F. (2019). Exosomes derived from mesenchymal stem cells inhibit mitochondrial dysfunction-induced apoptosis of chondrocytes via p38, ERK, and Akt pathways. *In Vitro Cell. Dev. Biol. Anim.* 55, 203–210. doi: 10.1007/s11626-019-00330-x

Qu, C., Puttonen, K. A., Lindeberg, H., Ruponen, M., Hovatta, O., Koistinaho, J., et al. (2013). Chondrogenic differentiation of human pluripotent stem cells in chondrocyte co-culture. *Int. J. Biochem. Cell Biol.* 45, 1802–1812. doi: 10.1016/j.biocel.2013.05.029

Rani, S., Ryan, A. E., Griffin, M. D., and Ritter, T. (2015). Mesenchymal stem cell-derived extracellular vesicles: toward cell-free therapeutic applications. *Mol. Ther.* 23, 812–823. doi: 10.1038/mt.2015.44

Raposo, G., and Stoorvogel, W. (2013). Extracellular vesicles: exosomes, microvesicles, and friends. *J. Cell Biol.* 200, 373–383. doi: 10.1083/jcb.201211138

Riegger, J., Palm, H. G., and Brenner, R. E. (2018). The functional role of chondrogenic stem/progenitor cells: novel evidence for immunomodulatory properties and regenerative potential after cartilage injury. *Eur. Cells Mater.* 36, 110–127. doi: 10.22203/ecm.v036a09

Rim, Y. A., Nam, Y., and Ju, J. H. (2020). The role of chondrocyte hypertrophy and senescence in osteoarthritis initiation and progression. *Int. J. Mol. Sci.* 21:2358. doi: 10.3390/ijms21072358

Robinson, W. H., Lepus, C. M., Wang, Q., Raghu, H., Mao, R., Lindstrom, T. M., et al. (2016). Low-grade inflammation as a key mediator of the pathogenesis of osteoarthritis. *Nat. Rev. Rheumatol.* 12, 580–592. doi: 10.1038/nrrheum.2016.136

Salminen, A., Kaarniranta, K., and Kauppinen, A. (2012). Inflammaging: disturbed interplay between autophagy and inflammasomes. *Aging (Albany NY)* 4, 166–175. doi: 10.18632/aging.100444

Scanzello, C. R. (2017). Role of low-grade inflammation in osteoarthritis. *Curr. Opin. Rheumatol.* 29, 79–85. doi: 10.1097/bor.0000000000000353

Schubert, N., Dudeck, J., Liu, P., Karutz, A., Speier, S., Maurer, M., et al. (2015). Mast cell promotion of T cell-driven antigen-induced arthritis despite being dispensable for antibody-induced arthritis in which T cells are bypassed. *Arthritis Rheumatol.* 67, 903–913. doi: 10.1002/art.38996

Scotti, C., Piccinini, E., Takizawa, H., Todorov, A., Bourgine, P., Papadimitropoulos, A., et al. (2013). Engineering of a functional bone organ through endochondral ossification. *Proc. Natl. Acad. Sci. U.S.A.* 110, 3997–4002. doi: 10.1073/pnas.1220108110

Sellam, J., and Berenbaum, F. (2010). The role of synovitis in pathophysiology and clinical symptoms of osteoarthritis. *Nat. Rev. Rheumatol.* 6, 625–635. doi: 10.1038/nrrheum.2010.159

Seol, D., McCabe, D. J., Choe, H., Zheng, H., Yu, Y., Jang, K., et al. (2012). Chondrogenic progenitor cells respond to cartilage injury. *Arthritis Rheum.* 64, 3626–3637. doi: 10.1002/art.34613

Shapiro, I. M., Landis, W. J., and Risbud, M. V. (2015). Matrix vesicles: are they anchored exosomes? *Bone* 79, 29–36. doi: 10.1016/j.bone.2015.05.013

Sharma, A. R., Jagga, S., Lee, S. S., and Nam, J. S. (2013). Interplay between cartilage and subchondral bone contributing to pathogenesis of osteoarthritis. *Int. J. Mol. Sci.* 14, 19805–19830. doi: 10.3390/ijms141019805

Shirasawa, S., Sekiya, I., Sakaguchi, Y., Yagishita, K., Ichinose, S., and Muneta, T. (2006). In vitro chondrogenesis of human synovium-derived mesenchymal stem cells: optimal condition and comparison with bone marrow-derived cells. *J. Cell. Biochem.* 97, 84–97. doi: 10.1002/jcb.20546

Shirinsky, I., and Shirinsky, V. (2018). H(1)-antihistamines are associated with lower prevalence of radiographic knee osteoarthritis: a cross-sectional analysis of the Osteoarthritis Initiative data. *Arthritis Res. Ther.* 20:116.

Siddappa, R., Licht, R., van Blitterswijk, C., and de Boer, J. (2007). Donor variation and loss of multipotency during in vitro expansion of human mesenchymal stem cells for bone tissue engineering. *J. Orthop. Res.* 25, 1029–1041. doi: 10.1002/jor.20402

Silverwood, V., Blagojevic-Bucknall, M., Jinks, C., Jordan, J. L., Protheroe, J., and Jordan, K. P. (2015). Current evidence on risk factors for knee osteoarthritis in older adults: a systematic review and meta-analysis. *Osteoarthritis Cartilage* 23, 507–515. doi: 10.1016/j.joca.2014.11.019

Singh, Y. P., Bandyopadhyay, A., and Mandal, B. B. (2019). 3D bioprinting using cross-linker-free silk-gelatin bioink for cartilage tissue engineering. *ACS Appl. Mater. Interfaces* 11, 33684–33696. doi: 10.1021/acsami.9b11644

Sophia Fox, A. J., Bedi, A., and Rodeo, S. A. (2009). The basic science of articular cartilage: structure, composition, and function. *Sports Health* 1, 461–468. doi: 10.1177/1941738109350438

Sun, A. R., Friis, T., Sekar, S., Crawford, R., Xiao, Y., and Prasadam, I. (2016). Is synovial macrophage activation the inflammatory link between obesity and osteoarthritis? *Curr. Rheumatol. Rep.* 18:57.

Sun, A. R., Panchal, S. K., Friis, T., Sekar, S., Crawford, R., Brown, L., et al. (2017). Obesity-associated metabolic syndrome spontaneously induces infiltration of pro-inflammatory macrophage in synovium and promotes osteoarthritis. *PLoS One* 12:e0183693. doi: 10.1371/journal.pone.0183693

Sun, W., Zhao, C., Li, Y., Wang, L., Nie, G., Peng, J., et al. (2016). Osteoclast-derived microRNA-containing exosomes selectively inhibit osteoblast activity. *Cell Discov.* 2:16015.

Sun, Y., Chen, S., and Pei, M. (2018). Comparative advantages of infrapatellar fat pad: an emerging stem cell source for regenerative medicine. *Rheumatology (Oxford)* 57, 2072–2086. doi: 10.1093/rheumatology/kex487

Takahashi, F., Takahashi, K., Shimizu, K., Cui, R., Tada, N., Takahashi, H., et al. (2004). Osteopontin is strongly expressed by alveolar macrophages in the lungs of acute respiratory distress syndrome. *Lung* 182, 173–185.

Takahashi, K., Tanabe, K., Ohnuki, M., Narita, M., Ichisaka, T., Tomoda, K., et al. (2007). Induction of pluripotent stem cells from adult human fibroblasts by defined factors. *Cell* 131, 861–872. doi: 10.1016/j.cell.2007.11.019

Tanaka, E., Aoyama, J., Miyauchi, M., Takata, T., Hanaoka, K., Iwabe, T., et al. (2005). Vascular endothelial growth factor plays an important autocrine/paracrine role in the progression of osteoarthritis. *Histochem. Cell Biol.* 123, 275–281. doi: 10.1007/s00418-005-0773-6

Taniguchi, N., Yoshida, K., Ito, T., Tsuda, M., Mishima, Y., Furumatsu, T., et al. (2007). Stage-specific secretion of HMGB1 in cartilage regulates endochondral ossification. *Mol. Cell. Biol.* 27, 5650–5663. doi: 10.1128/mcb.00130-07

Tao, S. C., Yuan, T., Zhang, Y. L., Yin, W. J., Guo, S. C., and Zhang, C. Q. (2017). Exosomes derived from miR-140-5p-overexpressing human synovial mesenchymal stem cells enhance cartilage tissue regeneration and prevent osteoarthritis of the knee in a rat model. *Theranostics* 7, 180–195. doi: 10.7150/thno.17133

Teitelbaum, S. L. (2000). Bone resorption by osteoclasts. *Science* 289, 1504–1508. doi: 10.1126/science.289.5484.1504

Théry, C., Zitvogel, L., and Amigorena, S. (2002). Exosomes: composition, biogenesis and function. *Nat. Rev. Immunol.* 2, 569–579. doi: 10.1038/nri855

Thielen, N. G. M., van der Kraan, P. M., and van Caam, A. P. M. (2019). TGFβ/BMP signaling pathway in cartilage homeostasis. *Cells* 8:969. doi: 10.3390/cells8090969

Thysen, S., Luyten, F. P., and Lories, R. J. (2015). Targets, models and challenges in osteoarthritis research. *Dis. Models Mech.* 8, 17–30. doi: 10.1242/dmm.016881

To, K., Zhang, B., Romain, K., Mak, C., and Khan, W. (2019). Synovium-Derived mesenchymal stem cell transplantation in cartilage regeneration: a PRISMA review of in vivo studies. *Front. Bioeng. Biotechnol.* 7:314. doi: 10.3389/fbioe.2019.00314

Tofiño-Vian, M., Guillén, M. I., Pérez Del Caz, M. D., Castejón, M. A., and Alcaraz, M. J. (2017). Extracellular vesicles from adipose-derived mesenchymal stem cells downregulate senescence features in osteoarthritic osteoblasts. *Oxid. Med. Cell. Longev.* 2017:7197598.

Tofiño-Vian, M., Guillén, M. I., Pérez Del Caz, M. D., Silvestre, A., and Alcaraz, M. J. (2018). Microvesicles from human adipose tissue-derived mesenchymal stem cells as a new protective strategy in osteoarthritic chondrocytes. *Cell. Physiol. Biochem.* 47, 11–25. doi: 10.1159/000489739

Tonna, S., Poulton, I. J., Taykar, F., Ho, P. W., Tonkin, B., Crimeen-Irwin, B., et al. (2016). Chondrocytic ephrin B2 promotes cartilage destruction by osteoclasts in endochondral ossification. *Development (Cambridge Engl.)* 143, 648–657.

Tsuno, H., Suematsu, N., Sato, T., Arito, M., Matsui, T., Iizuka, N., et al. (2016). Effects of methotrexate and salazosulfapyridine on protein profiles of exosomes derived from a human synovial sarcoma cell line of SW982. *Proteomics Clin. Appl.* 10, 164–171. doi: 10.1002/prca.201500064

Urist, M. R., and McLean, F. C. (1957). Accumulation of mast cells in endosteum of bones of calcium-deficient rats. *AMA Arch. Pathol.* 63, 239–251.

Vina, E. R., and Kwoh, C. K. (2018). Epidemiology of osteoarthritis: literature update. *Curr. Opin. Rheumatol.* 30, 160–167. doi: 10.1097/bor.0000000000000479

Visser, J. G., Van Staden, A. D. P., and Smith, C. (2019). Harnessing macrophages for controlled-release drug delivery: lessons from microbes. *Front. Pharmacol.* 10:22. doi: 10.3389/fphar.2019.00022

Vizoso, F. J., Eiro, N., Cid, S., Schneider, J., and Perez-Fernandez, R. (2017). Mesenchymal stem cell secretome: toward cell-free therapeutic strategies in regenerative medicine. *Int. J. Mol. Sci.* 18:1852. doi: 10.3390/ijms18091852

Vonk, L. A., van Dooremalen, S. F. J., Liv, N., Klumperman, J., Coffer, P. J., Saris, D. B. F., et al. (2018). Mesenchymal stromal/stem cell-derived extracellular vesicles promote human cartilage regeneration in vitro. *Theranostics* 8, 906–920. doi: 10.7150/thno.20746

Wakitani, S., Imoto, K., Yamamoto, T., Saito, M., Murata, N., and Yoneda, M. (2002). Human autologous culture expanded bone marrow mesenchymal cell transplantation for repair of cartilage defects in osteoarthritic knees. *Osteoarthritis Cartilage* 10, 199–206. doi: 10.1053/joca.2001.0504

Wang, N., Liang, H., and Zen, K. (2014). Molecular mechanisms that influence the macrophage m1-m2 polarization balance. *Front. Immunol.* 5:614. doi: 10.3389/fimmu.2014.00614

Wang, Q., Lepus, C. M., Raghu, H., Reber, L. L., Tsai, M. M., Wong, H. H., et al. (2019). IgE-mediated mast cell activation promotes inflammation and cartilage destruction in osteoarthritis. *Elife* 8:e39905.

Wang, R., Xu, B., and Xu, H. (2018). TGF-β1 promoted chondrocyte proliferation by regulating Sp1 through MSC-exosomes derived miR-135b. *Cell Cycle (Georgetown Tex)* 17, 2756–2765. doi: 10.1080/15384101.2018.1556063

Wang, T., Wen, C. Y., Yan, C. H., Lu, W. W., and Chiu, K. Y. (2013). Spatial and temporal changes of subchondral bone proceed to microscopic articular cartilage degeneration in guinea pigs with spontaneous osteoarthritis. *Osteoarthritis Cartilage* 21, 574–581. doi: 10.1016/j.joca.2013.01.002

Wang, Y., Yu, D., Liu, Z., Zhou, F., Dai, J., Wu, B., et al. (2017). Exosomes from embryonic mesenchymal stem cells alleviate osteoarthritis through balancing synthesis and degradation of cartilage extracellular matrix. *Stem Cell Res. Ther.* 8:189.

Wei, Y., Zeng, W., Wan, R., Wang, J., Zhou, Q., Qiu, S., et al. (2012). Chondrogenic differentiation of induced pluripotent stem cells from osteoarthritic chondrocytes in alginate matrix. *Eur. Cells Mater.* 23, 1–12. doi: 10.22203/ecm.v023a01

Wenham, C. Y., and Conaghan, P. G. (2010). The role of synovitis in osteoarthritis. *Ther. Adv. Musculoskelet. Dis.* 2, 349–359.

Willard, V. P., Diekman, B. O., Sanchez-Adams, J., Christoforou, N., Leong, K. W., and Guilak, F. (2014). Use of cartilage derived from murine induced pluripotent stem cells for osteoarthritis drug screening. *Arthritis Rheumatol.* 66, 3062–3072. doi: 10.1002/art.38780

Williams, R., Khan, I. M., Richardson, K., Nelson, L., McCarthy, H. E., Analbelsi, T., et al. (2010). Identification and clonal characterisation of a progenitor cell sub-population in normal human articular cartilage. *PLoS One* 5:e13246. doi: 10.1371/journal.pone.0013246

Woo, C. H., Kim, H. K., Jung, G. Y., Jung, Y. J., Lee, K. S., Yun, Y. E., et al. (2020). Small extracellular vesicles from human adipose-derived stem cells attenuate cartilage degeneration. *J. Extracell. Vesicles* 9:1735249. doi: 10.1080/20013078.2020.1735249

Wu, C. L., Harasymowicz, N. S., Klimak, M. A., Collins, K. H., and Guilak, F. (2020). The role of macrophages in osteoarthritis and cartilage repair. *Osteoarthritis Cartilage* 28, 544–554. doi: 10.1016/j.joca.2019.12.007

Wu, J., Kuang, L., Chen, C., Yang, J., Zeng, W. N., Li, T., et al. (2019). miR-100-5p-abundant exosomes derived from infrapatellar fat pad MSCs protect articular cartilage and ameliorate gait abnormalities via inhibition of mTOR in osteoarthritis. *Biomaterials* 206, 87–100. doi: 10.1016/j.biomaterials.2019.03.022

Xie, J., Huang, Z., Yu, X., Zhou, L., and Pei, F. (2019). Clinical implications of macrophage dysfunction in the development of osteoarthritis of the knee. *Cytokine Growth Factor Rev.* 46, 36–44. doi: 10.1016/j.cytogfr.2019.03.004

Xue, Y. Z. B., Niu, Y. M., Tang, B., and Wang, C. M. (2019). PCL/EUG scaffolds with tunable stiffness can regulate macrophage secretion behavior. *Prog. Biophys. Mol. Biol.* 148, 4–11. doi: 10.1016/j.pbiomolbio.2019.05.006

Yamashita, A., Tamamura, Y., Morioka, M., Karagiannis, P., Shima, N., and Tsumaki, N. (2018). Considerations in hiPSC-derived cartilage for articular cartilage repair. *Inflamm. Regen.* 38:17.

Yan, L., and Wu, X. (2020). Exosomes produced from 3D cultures of umbilical cord mesenchymal stem cells in a hollow-fiber bioreactor show improved osteochondral regeneration activity. *Cell Biol. Toxicol.* 36, 165–178. doi: 10.1007/s10565-019-09504-5

Yokota, N., Hattori, M., Ohtsuru, T., Otsuji, M., Lyman, S., Shimomura, K., et al. (2019). Comparative clinical outcomes after intra-articular injection with adipose-derived cultured stem cells or noncultured stromal vascular fraction for the treatment of knee osteoarthritis. *Am. J. Sports Med.* 47, 2577–2583. doi: 10.1177/0363546519864359

Yu, J., Vodyanik, M. A., Smuga-Otto, K., Antosiewicz-Bourget, J., Frane, J. L., Tian, S., et al. (2007). Induced pluripotent stem cell lines derived from human somatic cells. *Science* 318, 1917–1920.

Yubo, M., Yanyan, L., Li, L., Tao, S., Bo, L., and Lin, C. (2017). Clinical efficacy and safety of mesenchymal stem cell transplantation for osteoarthritis treatment: a meta-analysis. *PLoS One* 12:e0175449. doi: 10.1371/journal.pone.0175449

Zavatti, M., Beretti, F., Casciaro, F., Bertucci, E., and Maraldi, T. (2020). Comparison of the therapeutic effect of amniotic fluid stem cells and their exosomes on monoiodoacetate-induced animal model of osteoarthritis. *BioFactors (Oxford Engl.)* 46, 106–117. doi: 10.1002/biof.1576

Zhang, R. K., Li, G. W., Zeng, C., Lin, C. X., Huang, L. S., Huang, G. X., et al. (2018). Mechanical stress contributes to osteoarthritis development through the activation of transforming growth factor beta 1 (TGF-β1). *Bone Joint Res.* 7, 587–594. doi: 10.1302/2046-3758.711.bjr-2018-0057.r1

Zhang, S., Chu, W. C., Lai, R. C., Lim, S. K., Hui, J. H., and Toh, W. S. (2016). Exosomes derived from human embryonic mesenchymal stem cells promote osteochondral regeneration. *Osteoarthritis Cartilage* 24, 2135–2140. doi: 10.1016/j.joca.2016.06.022

Zhang, S., Chuah, S. J., Lai, R. C., Hui, J. H. P., Lim, S. K., and Toh, W. S. (2018). MSC exosomes mediate cartilage repair by enhancing proliferation, attenuating apoptosis and modulating immune reactivity. *Biomaterials* 156, 16–27. doi: 10.1016/j.biomaterials.2017.11.028

Zhang, S., Teo, K. Y. W., Chuah, S. J., Lai, R. C., Lim, S. K., and Toh, W. S. (2019). MSC exosomes alleviate temporomandibular joint osteoarthritis by attenuating inflammation and restoring matrix homeostasis. *Biomaterials* 200, 35–47. doi: 10.1016/j.biomaterials.2019.02.006

Zhang, Y., and Jordan, J. M. (2008). Epidemiology of osteoarthritis. *Rheum. Dis. Clin. North Am.* 34, 515–529.

Zhao, C., Chen, J. Y., Peng, W. M., Yuan, B., Bi, Q., and Xu, Y. J. (2020). Exosomes from adipose-derived stem cells promote chondrogenesis and suppress inflammation by upregulating miR-145 and miR-221. *Mol. Med. Rep.* 21, 1881–1889.

Zhao, Y., and Xu, J. (2018). Synovial fluid-derived exosomal lncRNA PCGEM1 as biomarker for the different stages of osteoarthritis. *Int. Orthop.* 42, 2865–2872. doi: 10.1007/s00264-018-4093-6

Zhao, Y., Liu, H., Zhao, C., Dang, P., Li, H., and Farzaneh, M. (2020). Paracrine interactions involved in human induced pluripotent stem cells differentiation into chondrocytes. *Curr. Stem Cell Res. Ther.* 15, 233–242. doi: 10.2174/1574888x15666191224122058

Zhen, G., Wen, C., Jia, X., Li, Y., Crane, J. L., Mears, S. C., et al. (2013). Inhibition of TGF-β signaling in mesenchymal stem cells of subchondral bone attenuates osteoarthritis. *Nat. Med.* 19, 704–712. doi: 10.1038/nm.3143

Zheng, L., Wang, Y., Qiu, P., Xia, C., Fang, Y., Mei, S., et al. (2019). Primary chondrocyte exosomes mediate osteoarthritis progression by regulating mitochondrion and immune reactivity. *Nanomedicine (Lond. Engl.)* 14, 3193–3212. doi: 10.2217/nnm-2018-0498

Zhu, Y., Wang, Y., Zhao, B., Niu, X., Hu, B., Li, Q., et al. (2017). Comparison of exosomes secreted by induced pluripotent stem cell-derived mesenchymal stem cells and synovial membrane-derived mesenchymal stem cells for the treatment of osteoarthritis. *Stem Cell Res. Ther.* 8:64.

Conflict of Interest: The authors declare that the research was conducted in the absence of any commercial or financial relationships that could be construed as a potential conflict of interest.

Publisher's Note: All claims expressed in this article are solely those of the authors and do not necessarily represent those of their affiliated organizations, or those of the publisher, the editors and the reviewers. Any product that may be evaluated in this article, or claim that may be made by its manufacturer, is not guaranteed or endorsed by the publisher.

Advantages of publishing in Frontiers

OPEN ACCESS
Articles are free to read for greatest visibility and readership

FAST PUBLICATION
Around 90 days from submission to decision

HIGH QUALITY PEER-REVIEW
Rigorous, collaborative, and constructive peer-review

TRANSPARENT PEER-REVIEW
Editors and reviewers acknowledged by name on published articles

Frontiers
Avenue du Tribunal-Fédéral 34
1005 Lausanne | Switzerland

Visit us: www.frontiersin.org
Contact us: frontiersin.org/about/contact

REPRODUCIBILITY OF RESEARCH
Support open data and methods to enhance research reproducibility

DIGITAL PUBLISHING
Articles designed for optimal readership across devices

FOLLOW US
@frontiersin

IMPACT METRICS
Advanced article metrics track visibility across digital media

EXTENSIVE PROMOTION
Marketing and promotion of impactful research

LOOP RESEARCH NETWORK
Our network increases your article's readership